SPATIAL GENOME ORGANIZATION

EDITED BY: Karim Mekhail and Evi Soutoglou

PUBLISHED IN: Frontiers in Genetics and Frontiers in Cell and Developmental Biology

frontiers Research Topics

ISSN 1664-8714
ISBN 978-2-88974-504-3
DOI 10.3389/978-2-88974-504-3

About Frontiers

Frontiers is more than just an open-access publisher of scholarly articles: it is a pioneering approach to the world of academia, radically improving the way scholarly research is managed. The grand vision of Frontiers is a world where all people have an equal opportunity to seek, share and generate knowledge. Frontiers provides immediate and permanent online open access to all its publications, but this alone is not enough to realize our grand goals.

Frontiers Journal Series

The Frontiers Journal Series is a multi-tier and interdisciplinary set of open-access, online journals, promising a paradigm shift from the current review, selection and dissemination processes in academic publishing. All Frontiers journals are driven by researchers for researchers; therefore, they constitute a service to the scholarly community. At the same time, the Frontiers Journal Series operates on a revolutionary invention, the tiered publishing system, initially addressing specific communities of scholars, and gradually climbing up to broader public understanding, thus serving the interests of the lay society, too.

Dedication to Quality

Each Frontiers article is a landmark of the highest quality, thanks to genuinely collaborative interactions between authors and review editors, who include some of the world's best academicians. Research must be certified by peers before entering a stream of knowledge that may eventually reach the public - and shape society; therefore, Frontiers only applies the most rigorous and unbiased reviews.
Frontiers revolutionizes research publishing by freely delivering the most outstanding research, evaluated with no bias from both the academic and social point of view. By applying the most advanced information technologies, Frontiers is catapulting scholarly publishing into a new generation.

What are Frontiers Research Topics?

Frontiers Research Topics are very popular trademarks of the Frontiers Journals Series: they are collections of at least ten articles, all centered on a particular subject. With their unique mix of varied contributions from Original Research to Review Articles, Frontiers Research Topics unify the most influential researchers, the latest key findings and historical advances in a hot research area! Find out more on how to host your own Frontiers Research Topic or contribute to one as an author by contacting the Frontiers Editorial Office: frontiersin.org/about/contact

SPATIAL GENOME ORGANIZATION

Topic Editors:
Karim Mekhail, University of Toronto, Canada
Evi Soutoglou, INSERM U964 Institut de Génétique et de Biologie Moléculaire et Cellulaire (IGBMC), France

Citation: Mekhail, K., Soutoglou, E., eds. (2022). Spatial Genome Organization. Lausanne: Frontiers Media SA. doi: 10.3389/978-2-88974-504-3

Table of Contents

frontiers in Genetics

MINI REVIEW
published: 19 June 2019
doi: 10.3389/fgene.2019.00602

Finding Friends in the Crowd: Three-Dimensional Cliques of Topological Genomic Domains

Philippe Collas[1,2], Tharvesh M. Liyakat Ali[1], Annaël Brunet[1] and Thomas Germier[1]*

[1] Department of Molecular Medicine, Faculty of Medicine, Institute of Basic Medical Sciences, University of Oslo, Oslo, Norway, [2] Department of Immunology and Transfusion Medicine, Oslo University Hospital, Oslo, Norway

The mammalian genome is intricately folded in a three-dimensional topology believed to be important for the orchestration of gene expression regulating development, differentiation and tissue homeostasis. Important features of spatial genome conformation in the nucleus are promoter-enhancer contacts regulating gene expression within topologically-associated domains (TADs), short- and long-range interactions between TADs and associations of chromatin with nucleoli and nuclear speckles. In addition, anchoring of chromosomes to the nuclear lamina via lamina-associated domains (LADs) at the nuclear periphery is a key regulator of the radial distribution of chromatin. To what extent TADs and LADs act in concert as genomic organizers to shape the three-dimensional topology of chromatin has long remained unknown. A new study addressing this key question provides evidence of (i) preferred long-range associations between TADs forming TAD "cliques" which organize large heterochromatin domains, and (ii) stabilization of TAD cliques by LADs at the nuclear periphery after induction of terminal differentiation. Here, we review these findings, address the issue of whether TAD cliques exist in single cells and discuss the extent of cell-to-cell heterogeneity in higher-order chromatin conformation. The recent observations provide a first appreciation of changes in 4-dimensional higher-order genome topologies during differentiation.

Keywords: 4D nucleome, genome structural modeling, Hi-C, LAD, TAD clique, TAD-TAD interaction

OPEN ACCESS

Edited by:
Karim Mekhail,
University of Toronto, Canada

Reviewed by:
Roland Foisner,
Medical University of Vienna, Austria
Jose Luis Gomez-Skarmeta,
Centro Andaluz de Biología del Desarrollo (CABD), Spain

****Correspondence:***
Philippe Collas
philc@medisin.uio.no;
philippe.collas@medisin.uio.no

Specialty section:
This article was submitted to Epigenomics and Epigenetics, a section of the journal Frontiers in Genetics

Received: *25 April 2019*
Accepted: *05 June 2019*
Published: *19 June 2019*

Citation:
Collas P, Liyakat Ali TM, Brunet A and Germier T (2019) Finding Friends in the Crowd: Three-Dimensional Cliques of Topological Genomic Domains. Front. Genet. 10:602. doi: 10.3389/fgene.2019.00602

INTRODUCTION

Three-dimensional (3D) genome topology is important for the orchestration of gene expression governing development and tissue homeostasis. In mammalian nuclei, individual chromosomes occupy well-defined territories and adopt a radial (nuclear center-to-periphery) position which is overall conserved between cell types (Cremer and Cremer, 2010). At the nucleus scale, radial placement of chromosome territories generates topological conformations enabling a spatio-temporal regulation of processes such as DNA replication and gene expression (Bickmore and van Steensel, 2013).

A wealth of data combining high-throughput genomics, microscopy and bioinformatics has in the past decade enabled significant advancements in our understanding of spatial genome conformation at a range of scales (from gene locus to nucleus level) and resolutions (from kilobase to megabase). Comparisons between cell types and developmental studies combined with single-cell data convey an unprecedented view of common features of genome conformations and of heterogeneity in chromatin topologies at all scales. These studies also start to provide an appreciation of 4-dimensional (4D) changes in genome configuration, where the 4th dimension is time. Here, we highlight recent accounts of dynamic chromatin topologies in mammalian nuclei and address the heterogeneity of higher-order chromatin conformations in light of results from ensemble data and single-cell analyses.

A MODULAR 3-DIMENSIONAL LAYOUT OF THE GENOME

Genomic Interactions

The combination of chromosome conformation capture techniques with high-throughput sequencing makes it possible to map 3D chromosomal interactions in entire genomes using methods such as Hi-C (Dekker et al., 2013). Hi-C is based on a chemical crosslinking of chromatin segments in close proximity (or "interacting") in the nucleus, ligation and sequencing of these interacting segments, and mapping to a reference genome to provide a snap-shot of interacting genomic regions. The result is a matrix of interaction frequencies, often shown as a heat map, between all regions of the genome in the cell population analyzed. Hi-C data consistently show that proximal interactions, along or close to the matrix diagonal, are statistically more frequent than long-range interactions (away from the matrix diagonal) and that intrachromosomal contacts vastly dominate over contacts between chromosomes.

Analysis of Hi-C data, corroborated by microscopy approaches (Boettiger et al., 2016; Beagrie et al., 2017; Bintu et al., 2018; Szabo et al., 2018; Finn et al., 2019), suggests a segregation of the genome into multi-megabase (Mb) "open"/active A compartments and "closed"/repressed B compartments (Rao et al., 2014). Within compartments, at the 0.5–1 Mb scale, topologically associated domains (TADs) are defined as regions with a high frequency of intrachromosomal contacts, whereas contacts are much less frequent between adjacent TADs (Dixon et al., 2012; Nora et al., 2012; **Figure 1A**). Within TADs, the number and nature of contacts can vary, partially specifying gene regulatory interactions (Kragesteen et al., 2018). Along the linear (1-dimensional) genome, TAD borders are overall conserved between cell types (Rao et al., 2014) and disrupting or weakening of TAD borders, for example by mutations in DNA binding motifs for structural proteins, can cause disease (Guo et al., 2015; Lupianez et al., 2015, 2016; Ren and Dixon, 2015) or be oncogenic (Hnisz et al., 2016; Valton and Dekker, 2016). Nevertheless, interactions between TADs (Olivares-Chauvet et al., 2016; Beagrie et al., 2017; Niskanen et al., 2018; Quinodoz et al., 2018; Szabo et al., 2018) and positioning of TADs in the nucleus space (Li et al., 2015; Paulsen et al., 2019) can vary between cells, conveying the idea that spatial genome topology displays cell-to-cell heterogeneity in a population and is therefore not static.

The Nuclear Lamina Provides Anchors for Chromatin at the Nuclear Periphery

3D genome conformation is also under the influence of interactions of chromosomes with the nuclear envelope, at the nuclear periphery (Zuleger et al., 2013; Lund et al., 2014; Czapiewski et al., 2016; van Steensel and Belmont, 2017; Buchwalter et al., 2019). Subjacent to the nuclear membranes lays the nuclear lamina, a meshwork of intermediate filament proteins called lamins; these consist of lamins A and C (also referred to as lamins A/C or indiscriminately here as "lamin A" because they are splice variants of the *LMNA* gene) and lamins B1 and B2, products of the *LMNB1* and *LMNB2* genes (de Leeuw et al., 2018). Genomics and microscopy studies show that nuclear lamins interact with chromatin via lamina-associated domains (LADs) (Guelen et al., 2008; Buchwalter et al., 2019; **Figure 1A**). While lamin B1-chromatin interactions (lamin B1 LADs) are predominantly detected at the nuclear periphery, lamin A-associated regions have been shown to occur both at the nuclear periphery (lamin A LADs) and in the nuclear interior (Kind et al., 2013; Lund et al., 2013; Lund et al., 2015), in agreement with the existence of a nucleoplasmic pool of chromatin-bound lamin A (Naetar et al., 2017). Overall, peripheral LADs are gene-poor, heterochromatic and transcriptionally silent, however intranuclear lamin A-associated regions tend to be more gene-rich and euchromatic, and contain expressed genes (Lund et al., 2015; Gesson et al., 2016). This supports the view that nuclear lamin A in particular is able to associate with genomic regions harboring distinct chromatin features. This property may underline the broad impact of lamin A on the radial positioning of chromatin (Solovei et al., 2013; Thanisch et al., 2017), higher-order and locus-level chromatin conformation (Cesarini et al., 2015; Rønningen et al., 2015; Gesson et al., 2016; Oldenburg et al., 2017; Paulsen et al., 2017; Briand et al., 2018; Grigoryan et al., 2018; Forsberg et al., 2019; Ulianov et al., 2019) and chromatin mobility (Bronshtein et al., 2015, 2016; Vivante et al., 2018). It is important to mention, however, that although A-type lamins are able to bind DNA and nucleosomes *in vitro* (as do B-type lamins) (Bruston et al., 2010), they are not sufficient to anchor heterochromatin at the nuclear periphery, and rather do so via lamin-associated protein complexes containing integral proteins of the inner nuclear membrane (Solovei et al., 2013; Buchwalter et al., 2019).

Mapping of LADs during cell differentiation suggests that a proportion of lamin-chromatin interactions are developmentally regulated (Peric-Hupkes et al., 2010; Lund et al., 2013; Rønningen et al., 2015; Robson et al., 2016, 2017). In mesenchymal stem cells (MSCs) from human adipose tissue, promoters of

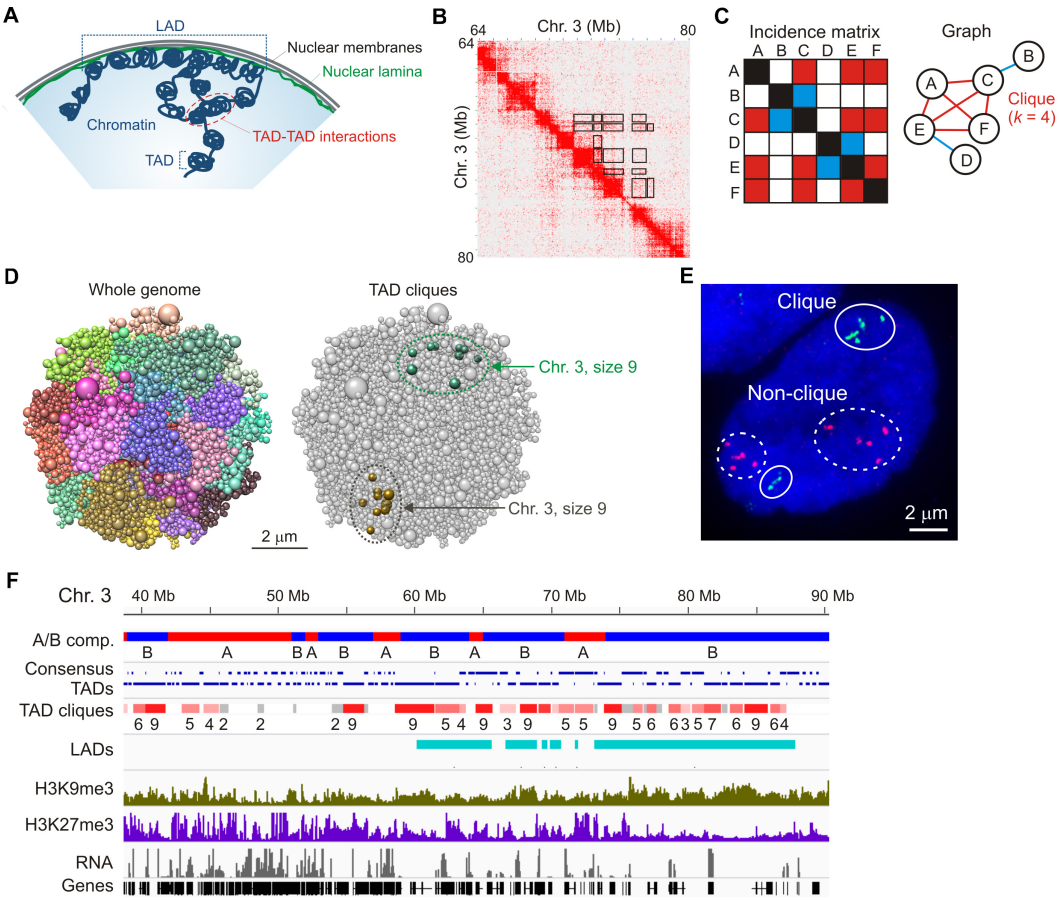

FIGURE 1 | TAD cliques represent spatial assemblies of heterochromatic TADs from Hi-C data. **(A)** Higher-order chromatin topology in a mammalian nucleus, highlighting a lamina-associated domain (LAD), topologically-associated domains (TADs) and TAD-TAD interactions. **(B)** Hi-C contact matrix showing TADs along the diagonal and highlighting some of the long-range TAD-TAD interactions, away from the diagonal (black frames); shown here for a region of chromosome 3 in human adipose MSCs. **(C)** Graph representation of a clique where four vertices (or TADs; **A,C,E,F**) all interact pair-wise in the fictive incidence matrix (red cells in the matrix, red edges in the graph). Vertices B and D, respectively, interact with vertices C and E only (blue cells in the matrix, blue edges in the graph) and do not belong to the clique. The clique shown here is of size $k = 4$. **(D)** Chrom3D structural models of an MSC nucleus. Models show all chromosomes as a continuous chain of beads (TADs) labeled differently (*left*) and highlight TAD cliques of size 9 on both chromosome 3 homologs (*right*). Note the variation in TAD proximity in both modeled chromosomes. **(E)** Representative FISH image of six TADs in a clique (green probes; chromosome 1) and five TADs not in clique (red probes; chromosome 5) (see Paulsen et al., 2019 for details). Note the absence of strict physical contact between all TADs even when they belong to a clique in the Hi-C data (green probes). Also note the variation in relative TAD distributions between the two sets of homologous chromosomes. Bar, 2 μm. **(F)** Browser view of A and B compartments, consensus TADs (shown over two lines for clarity), TAD cliques with clique size (number of TADs), LADs, H3K9me3, H3K27me3 and gene expression in undifferentiated adipose MSCs. Sequence data can be accessed at NCBI GEO GSE109924 (compartments, TADs, cliques and LADs), GSM621398 (H3K9me3), GSM621420 (H3K27me3), and GSE60237 (RNA).

genes that control adipogenesis and that are bound to lamin A in undifferentiated cells, have been shown to dissociate from lamin A after induction of adipogenesis (while genes regulating other lineages do not), in a manner that could prime these genes for activation (Lund et al., 2013). Variable lamin A-chromatin interactions are detectable not only at individual loci but also encompass entire regions (Rønningen et al., 2015; Gesson et al., 2016). An additional level of complexity of chromatin association with nuclear lamins are occurrences of exchangeable interactions of chromatin with lamins A and B1 in an *in vitro* steatosis cell model (Forsberg et al., 2019). Computational models of 3D genome structure corroborated by fluorescence *in situ* hybridization (FISH) illustrate, based on these lamin-chromatin interaction data, a radial repositioning of TADs as a function of whether or not they contain lamin B1 LADs (Forsberg et al., 2019). Dynamic interactions of chromatin with the nuclear lamina, and lamina-associated protein complexes, thus provide a means of radially (re)positioning chromatin in the nucleus (Reddy et al., 2008; Kind et al., 2013; Solovei et al., 2013; Harr et al., 2015; Kind et al., 2015).

How TADs and LADs as genomic organizers together orchestrate spatial genome topology has recently been investigated in a controlled differentiation system (Paulsen et al., 2019). The findings, discussed below, provide evidence of multiple long-range TAD-TAD interactions which, together

with associations with the nuclear lamina through LADs, contribute to shaping the 4-dimensional genome during terminal differentiation.

A GET-TOGETHER OF TADS INTO CLIQUES

How Are TAD Cliques Recognizable?

Hi-C matrices typically reveal interactions within TADs, between linearly consecutive TADs (along the matrix diagonal), and between linearly non-contiguous TADs – that is, away from the matrix diagonal (**Figure 1B**, exemplified in boxed areas). Such long-range TAD-TAD interactions involve only two TADs (TAD pairs) or multiple TADs. In addition, when multiple TADs interact in the Hi-C data, all TADs can interact with one another in this "network," or only a subset of TADs does. Identifying multiple TAD-TAD interactions in a Hi-C matrix can therefore constitute a real challenge. One way to overcome this is to turn to the mathematical area of graph theory and cliques. In graph theory, a clique is a subset of k vertices (or nodes) which are all connected pair-wise by an edge (**Figure 1C**). In a recent interrogation of changes in long-range TAD-TAD interactions during differentiation, we defined a "TAD clique" as a subset of k TADs (with $k \geq 3$) which are fully connected – that is, which all interact pair-wise in the Hi-C data (Paulsen et al., 2019; **Figure 1C**).

A key step in the identification of TAD cliques is mapping statistically significant pair-wise TAD-TAD interactions. This has been achieved using a non-central hypergeometric distribution to calculate the probability of observing a given number of Hi-C contacts dependent on the number of contacts involved between the two TADs, the total number of contacts the two TADs are involved in, and the genomic distance between the TADs (Paulsen et al., 2018). A P-value is then computed to identify statistically significant contacts – i.e., contacts that occur more frequently than what would be expected by chance. TAD cliques are subsequently identified by representing all significant inter-TAD contacts as a graph (**Figure 1C**) and searching for maximal clique sizes (Paulsen et al., 2019). Using this approach, we found that TAD cliques represent a prominent feature of higher-order genome organization: from ∼15,000 significant pair-wise inter-TAD contacts mapped in human adipose MSCs, we found more than 3,000 cliques of 3–11 TADs which altogether make up ∼50% of the genome.

Three-dimensional structural models of the genome (Paulsen et al., 2017) predict long-range inter-TAD interactions for TADs in cliques that are more frequent than that of TADs in a randomized topology (**Figure 1D**; Paulsen et al., 2019). Dual-color FISH using probes against TADs in cliques and outside cliques supports the modeling predictions and illustrates that TADs in cliques can form close associations, as exemplified in **Figure 1E**. However, as discussed later, variations in how physically close to one another TADs in a clique are, demonstrate the heterogeneity in chromatin configurations between cells and challenges the interpretation of ensemble Hi-C data.

TAD Cliques Form Higher-Order Chromatin Assemblies Identifiable in the Hi-C Data

TAD cliques are enriched in B compartments and accordingly, genes in cliques are overall repressed or lowly expressed (**Figure 1F**). TAD cliques are enriched in trimethylated histone H3 lysine 9 (H3K9me3) usually throughout the TADs, and to a greater extent than in the Polycomb mark H3K27me3 (**Figure 1F**). Thus TAD cliques exhibit characteristics of constitutive heterochromatin and may harbor Polycomb domains. H3K9me3/H3K27me3 enrichment profiles in TAD cliques suggest that they represent a subtype of B compartment previously unrecognized (Rao et al., 2014), containing H3K9me3 with variegated H3K27me3 and, as discussed later in this article, variable LADs.

TAD cliques are also found in A compartments, yet in lower proportions than in B compartments (Paulsen et al., 2019). Intriguingly, TAD cliques in A compartments include active genes interspersed with H3K27me3-marked genes, but overall harbor no LADs (**Figure 1F**). In undifferentiated cells, such cliques may represent associations of facultative heterochromatin containing genes that can be activated during differentiation.

TAD Cliques Represent Dynamic Topological Assemblies

TAD cliques are not static entities and following their fate during differentiation reveals the dynamics of higher-order chromatin topologies. Supporting this idea, using an alluvial graph representation, TAD cliques have been shown to expand or shrink during adipose differentiation, by gaining or losing TADs, and some cliques also exhibit adipose versus neuronal lineage-specificity (Paulsen et al., 2019). In line with the repressed nature of TAD cliques, clique expansion is associated with downregulation of expression of genes within the clique, and conversely, down-sizing of a clique coincides with upregulation of gene expression. Changes in clique size do not correspond to changes in B compartment size or to A/B compartment switching, suggesting that TAD clique dynamics constitutes yet another level of higher-order chromatin conformation changes.

Temporal changes in inter-TAD contacts characterize not only mesenchymal and embryonic stem cell differentiation (Bonev et al., 2017; Paulsen et al., 2019), but also dedifferentiation, as shown during the reprogramming of mouse B cells toward pluripotency (Stadhouders et al., 2018). Remarkably, during cell reprogramming, a striking reduction in the number of TAD cliques detected in B cells (Paulsen et al., 2019) likely reflects a loosening of higher-order chromatin structure as cells acquire a pluripotent state. Inter-TAD contacts also appear to be prone to environmental conditions. The heat shock response in *Drosophila* cells is topologically manifested by a decrease in contacts within TADs (perhaps reflecting gene expression changes) and an increase in long-range inter-TAD interactions (Li et al., 2015). This implies a spatial rearrangement of TADs and a large-scale reorganization of chromatin which may be important for gene silencing after temperature stress. How long-range TAD-TAD interactions are promoted in this system remains unknown but

could implicate a decrease in the strength of TAD borders (Li et al., 2015). These studies exemplify how dynamic long-range interactions between topological domains, such as a gain or loss of TADs in cliques, emerge as functionally important processes shaping the 4D nucleome.

TAD CLIQUES AND OTHER LONG-RANGE ASSOCIATIONS BETWEEN TADS

Cliques and SPRITE Hubs

Chromatin is anchored to intranuclear bodies, including nucleoli (Nemeth et al., 2010) and nuclear speckles (Baudement et al., 2018; Chen et al., 2018). The split-pool recognition of interactions by tag extension (SPRITE) method was developed to detect higher-order multi-way chromosomal interactions (Quinodoz et al., 2018). Over 300,000 so-called SPRITE clusters of 3–14 "*k*-mers" (or associations) have been reported. These associations were interpreted to form "chromosomal hubs" arising from long-range interactions including either gene-dense, active and RNA-polymerase II-marked regions at nuclear speckles, or inactive centromere-proximal regions at the nucleolus (Quinodoz et al., 2018). Since unlike Hi-C, SPRITE does not depend on proximity ligation, the method enables detection of genomic interactions over longer distances than those detectable by Hi-C (Quinodoz et al., 2018). The heterochromatic nature of cliques and of nucleolus-associated domains (Nemeth et al., 2010; Sen Gupta and Sengupta, 2017) raises the possibility that a fraction of repressed SPRITE clusters could reside in TAD cliques or encompass several cliques at the periphery of nucleoli.

TAD Cliques and Long-Range Inter-TAD Interactions in Other Systems

Heterochromatic TAD cliques resemble H3K9me3-rich "TAD hubs" reported in B compartments as a result of long-range inter-TAD contacts in the Hi-C data in endothelial cells, and similarly to cliques, these "hubs" are enriched in LADs (Niskanen et al., 2018). Interestingly, analyses of TAD cliques and of the "hubs" of Niskanen et al. concur in that despite the clique rearrangements discussed above, most chromatin domains seem to fall within a pre-established overarching conformation (such as TAD cliques or absence thereof) that is overall maintained during terminal differentiation (Niskanen et al., 2018; Paulsen et al., 2019).

TAD assemblies have also been reported in *Drosophila* using Hi-C and 3D FISH. The data interestingly reveal higher-order dynamic interactions between TADs, where repressed TADs are organized as a succession of "nanocompartments" interspersed by active regions (Szabo et al., 2018). Some of these nanocompartments involve linearly non-adjacent TADs (as suggested by FISH and inferences from 3D models of these configurations), supporting the idea of TAD cliques. The TAD assemblies of Szabo et al. also resemble TAD cliques in A compartments harboring H3K27me3 and similarly to these particular cliques, they seldom occur (Szabo et al., 2018). The Paulsen and Szabo studies also concur in that changes in inter-TAD interactions reflect discrete chromosomal contacts and not a fusion or splitting of TADs.

Other studies also provide evidence of inter-TAD interactions, but properties of these interactions distinguish them from TAD cliques. (i) "Meta-TADs" have been reported as interactions between multiple neighboring TADs and thus do not encompass strictly long-range TAD-TAD interactions that define cliques. Meta-TADs are enriched in H3K27me3 and RNA polymerase II (Fraser et al., 2015) but are devoid of H3K9me3, which again segregates them from TAD cliques. (ii) A variation of Hi-C using "chromosome walks" (C-walks) captures associations between two to four TADs, the occurrence of which is enhanced by Polycomb group proteins (Olivares-Chauvet et al., 2016). Interestingly however, the C-walk data favor a view of pair-wise TAD-TAD contacts over a hub-like topology, and random associations between active loci rather than a regulated process. (iii) Genome architecture mapping, a method that measures genomic contacts based on the sequencing a large number of thin slices through nuclei, has been shown to identify three-way TAD interactions (Beagrie et al., 2017). These multivalent interactions regroup active genes and enhancers (Beagrie et al., 2017) and may constitute supra-TAD gene regulation units.

WHEN TAD CLIQUES BECOME PERIPHERAL MATTER

A feature of TAD cliques in human and mouse cells is their enrichment in LADs, however, this relationship seems to depend on clique size and cell state (Paulsen et al., 2019). Accordingly, the proportion of linear clique coverage by LADs increases with clique size (up to 50% in large cliques), and adipogenic induction coincides with an increase in the LAD content of cliques irrespectively of clique size. This implies that large cliques tend to associate with the nuclear lamina and that this association is exacerbated in terminally differentiated cells. Nevertheless, lamina association appears to be dispensable for TAD clique formation because many cliques exist in the absence of LADs (**Figure 1F**; see region 40–60 Mb in chromosome 3), and there are several instances of LADs emerging within already established cliques during adipose differentiation (**Figure 2A**; *de novo* LADs). Interestingly, nuclear lamina anchoring of TADs in cliques may further compact chromatin in these TADs (Ulianov et al., 2019).

Three-dimensional genome structural models corroborate these features and predict a nuclear peripheral localization of TAD cliques in relation to clique size, with larger cliques more frequently found at the nuclear periphery, and differentiation (Paulsen et al., 2019; **Figure 2B**). Given their heterochromatic nature, it is reasonable to speculate that TAD cliques may strengthen a repressive state of gene expression by stabilizing peripheral heterochromatin at the nuclear lamina. To achieve this, our data argue that only a subset of TADs would be sufficient to anchor a clique at the nuclear lamina since within a clique containing LADs, not all TADs necessarily harbor LADs. Thus, a peripheral localization of TADs in a clique may not directly

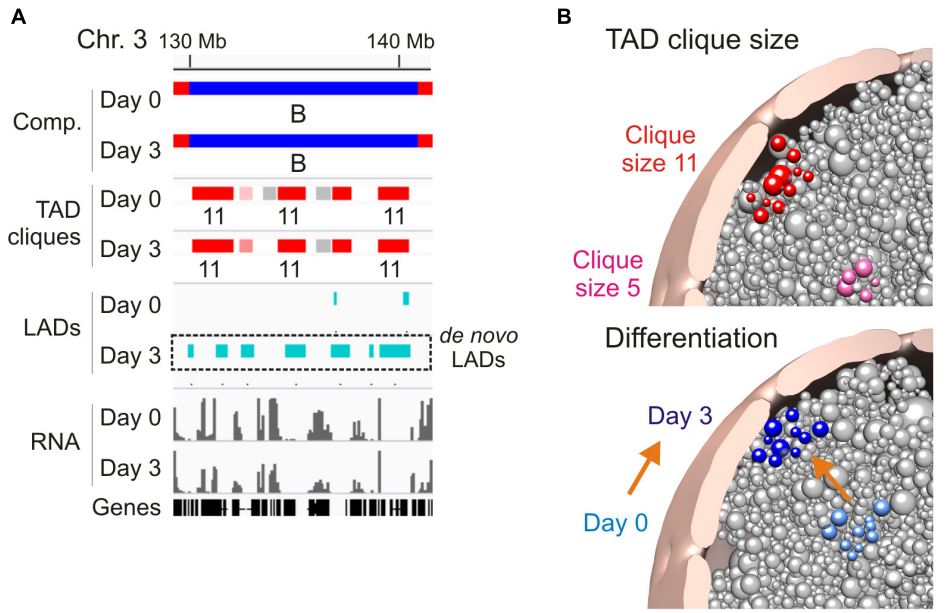

FIGURE 2 | Association of TAD cliques with the nuclear periphery. **(A)** Browser view showing *de novo* LADs appearing in pre-existing TAD cliques in a B compartment on day 3 of adipose differentiation. Sequence data can be accessed at NCBI GEO GSE109924 and GSE60237. **(B)** Radial positioning of TAD cliques in the nucleus: model views. *Top*, differential preferred radial position of a small (pink) and a large (red) TAD clique. *Bottom*, differentiation repositions a TAD clique toward the nuclear periphery; orange arrow symbolizes differentiation.

require LADs if this localization implicates LADs in neighboring TADs. The clique concept further argues that these neighboring TADs need not be linearly contiguous as long as they remain spatially close in a 3D environment.

ARE THERE TAD CLIQUES IN SINGLE CELLS?

TAD cliques are currently identified from Hi-C data generated from millions of cells, so Hi-C data reflect averages of chromosomal interactions across a cell population and do not reflect genomic interactions in individual cells. This knowledge gap has prompted the advent of single-cell Hi-C as a technical *tour-de-force* (Nagano et al., 2013, 2017; Flyamer et al., 2017; Stevens et al., 2017). Single-cell Hi-C captures snapshots of chromosomal interactions in individual cells, and although contacts are sparser than in ensemble Hi-C matrices, it is possible to detect statistically significant pair-wise TAD-TAD contacts (Paulsen et al., 2019). Nevertheless, this sparsity of contacts makes identification of TAD cliques virtually impossible.

To circumvent this problem, we have proposed a five-step proxy strategy which enables an estimation of TAD-TAD contacts within projected TAD cliques identified from ensemble Hi-C data:

- Determine significant pair-wise TAD-TAD interactions in single-cell Hi-C contact matrices;
- Map TAD cliques in ensemble Hi-C data for the same cell type;
- Project these cliques onto individual single-cell Hi-C matrices;
- Calculate TAD contact frequencies within the projected cliques and outside the cliques;
- Calculate TAD contact densities in the projected cliques.

Using this approach, we found in mouse embryonic stem cells an enrichment of TAD-TAD interactions in projected cliques compared to randomized controls (Paulsen et al., 2019). Further, most single cells analyzed display clique-like TAD assemblies with at least 50% TAD connectivity within them (that is, with more than 50% of TADs connected pair-wise within the projected cliques in the single-cell Hi-C data). Thus, although this does not demonstrate the existence of TAD cliques in single cells, the subsets of TADs may display statistically significant long-range associations also in single-cell Hi-C data.

HETEROGENEITY IN HIGHER-ORDER CHROMATIN TOPOLOGIES

FISH and Hi-C: Variations in Locus Proximities

At the level of the nucleus, pair-wise TAD-TAD contacts can be highly variable between cells in a population. Single-cell Hi-C data show variability in the number and genomic coordinates of chromosomal interactions (Nagano et al., 2013, 2017; Flyamer et al., 2017; Stevens et al., 2017) and in significant inter-TAD contacts. This is also seen in the number and nature of TADs involved in projected TAD cliques using the approach outlined

above. FISH analysis corroborates the Hi-C data and reveals heterogeneity in spatial TAD proximity (Szabo et al., 2018; Finn et al., 2019; Paulsen et al., 2019; see **Figure 1E**). Therefore, sets of TADs may preferably be in proximity at the single-cell level but not necessarily in physical contact in all cells. Stochastic interactions within this proximal neighborhood, which has led to the view of "stochastic clusters" (Flyamer et al., 2017), can still be statistically more frequent than stochastic interactions between TADs in a spatial random configuration.

Heterogeneity in FISH configurations is also detected for homotypic TADs that exhibit "statistical preference" (Boettiger et al., 2016; Szabo et al., 2018). Corroborating this view, C-walks favor the idea of stochastic TAD-TAD interactions rather than functional interaction hubs (Olivares-Chauvet et al., 2016). Similarly, analysis of chromosome conformation by high-throughput FISH shows that even neighboring TADs do not necessarily cluster, and concurs in that cell populations display a wide array of genome configurations (Finn et al., 2019). Some of this variation can be caused by inter-allelic variation within single nuclei (Oldenburg et al., 2017; Finn et al., 2019; Paulsen et al., 2019; see also **Figures 1D,E**), which adds to the challenge of interpreting Hi-C data in the absence of sufficient polymorphism. These observations altogether illustrate the variegated higher-order topologies of chromatin between cells and between homologous chromosomes in a given cell.

Cell-to-Cell Variability in Genome Conformation Estimated From Structural 3D Models of the Genome

With recent developments in computational approaches to model genome structure in 3D, it is now possible to make powerful estimations of the spatial arrangement of chromatin domains, including their radial positioning and their spatial proximity (Paulsen et al., 2018). Several frameworks and pipelines can model 3D genome structures (Imakaev et al., 2012; Dekker et al., 2013; Serra et al., 2015; Szalaj et al., 2016; Tjong et al., 2016; Li et al., 2017; Paulsen et al., 2017), and some can incorporate locus positional constraints in the modeled nuclei. Integrated Modeling Platform (IMP) is a framework initially developed to model 3D protein structure, and can in principle integrate spatial restraints for chromatin (Kalhor et al., 2011; Bau and Marti-Renom, 2012; Russel et al., 2012; Tjong et al., 2016; Li et al., 2017). Other methods enable integration of non-Hi-C data in the modeling, such as nucleolus constraints and centromere position in yeast (Duan et al., 2010), or interactions with the nuclear lamina (LADs) (Li et al., 2017; Paulsen et al., 2017). We have recently introduced Chrom3D (Paulsen et al., 2017, 2018), a platform designed to incorporate Hi-C and lamin ChIP-seq data as positional constraints for TADs (or any other genomic unit); these provide respective information on inter-domain interactions and on the radial positioning of loci in the modeled nuclei (Briand et al., 2018; Forsberg et al., 2019). Analyses of 3D genome models enable statistically robust estimates of variations in 3D genome structures between cells in the population under study (Paulsen et al., 2017). Using deconvolution techniques, IMP-based approaches estimate an ensemble of structures as part of a single simulation (Dai et al., 2016; Tjong et al., 2016; Li et al., 2017). In contrast, Chrom3D generates a single structure per simulation, and hundreds of simulations allows for statistical estimates of the position of domains across a large number of models (Paulsen et al., 2017).

The modeling exercises predict that heterogeneity in 3D genome structures exist between cells in a population, both in terms of spatial proximity of given domains (Paulsen et al., 2019) and in their positioning relative to the nuclear periphery (Dai et al., 2016; Tjong et al., 2016; Li et al., 2017; Paulsen et al., 2017; Briand et al., 2018; Forsberg et al., 2019). This variation, visualized by FISH (Kind et al., 2015; Paulsen et al., 2017; Briand et al., 2018; Finn et al., 2019; Forsberg et al., 2019), emerges as a significant factor impacting higher-order genome topologies. Chrom3D modeling reveals that TADs in cliques show closer proximity than TADs outside cliques in a control random configuration (Paulsen et al., 2019). Importantly however, TADs in cliques (as seen in Hi-C data) are rarely, if at all, all closely associated in a given modeled nucleus (or in FISH experiments) (see **Figures 1D,E**), in line with the interpretation of ensemble versus single-cell observations. At present, we do not know whether population-based modeling provides more information than statistical estimates from multiple simulations. Despite validations of predicted 3D genome structures by FISH (Tjong et al., 2016; Li et al., 2017; Paulsen et al., 2017, 2019; Forsberg et al., 2019), more work is required to determine whether variations in chromatin topologies can also be reliably predicted by computational modeling.

CONCLUDING REMARKS AND FUTURE DIRECTIONS

A role of TADs and LADs in spatially organizing the genome has been established through their respective purpose in confining gene regulatory interactions and anchoring chromatin at the nuclear periphery. The nuclear lamina has been shown to anchor subsets of TADs at the nuclear envelope through LADs in a differentiation-dependent manner (Robson et al., 2016; Paulsen et al., 2019), providing a radial relationship between these genomic organizers. The recent results presented here highlight a new level of 4D genome organization involving long-range TAD-TAD associations into TAD cliques and a radial positioning of cliques related to their LAD content. Of note, TAD cliques can exist in the nuclear interior without LADs, making LADs unlikely to be required for cliques to assemble. LADs may, however, be necessary to stabilize cliques containing long-term repressed developmental genes at the nuclear periphery. Following the dynamics and spatial (re)positioning of TAD cliques during development, lineage commitment and terminal differentiation, in relation to the evolution of epigenetic components, including chromatin accessibility and DNA methylation, is expected to provide new insights on higher-order genome topologies in a 4-dimensional context.

A key question remains of how TAD cliques are formed and disassembled. TAD cliques in B compartments are primarily heterochromatic. So mechanistically, proteins promoting

the formation or spreading of heterochromatin, such as heterochromatin protein 1 (HP1) isoforms (CBX1, CBX3, or CBX5) (Canzio et al., 2014) are interesting candidates as mediators of clique assembly. Physically, TAD clique formation could involve a phase separation process, which has been shown to be implicated in the formation of heterochromatin and in driving the segregation of heterochromatin from euchromatin (Larson et al., 2017; Strom et al., 2017). If TADs in a clique do not physically contact each other at the single-cell level, but are rather in a close neighborhood, proximity of TADs in cliques could be mediated by liquid condensates aggregating and constraining specific homotypic chromatin domains in a confined space (Shin et al., 2018). Supporting this idea are demonstrations of clustering of enhancers (Sabari et al., 2018) and formation of Polycomb condensates by phase separation (Tatavosian et al., 2019). The latter could potentially explain a subset of H3K27me3-rich TAD cliques in A compartments (Paulsen et al., 2019) and other Polycomb domains (Fraser et al., 2015; Olivares-Chauvet et al., 2016).

Loss-of-function experiments should provide clues on factors involved in the gain or loss of TADs in cliques. What is currently missing is a robust method to assay TAD clique formation or breakdown, which would not depend on costly and labor-intensive Hi-C experiments. High-throughput FISH assays (Finn et al., 2019), TAD visualization in living cells using CRISPR/Cas9-EGFP marking of domains (Wang and Qi, 2016) or using genetic tagging with the ANCHOR system (Bystricky, 2015; Germier et al., 2017), may be tools worthy of investigation to monitor TAD clique expansion, shrinking and spatial distribution in the nucleus. Live-cell chromatin imaging methods would also enable visualization of TAD clique dynamics and spatial tracking in real time.

Variability in spatial genome conformations highlighted in single-cell experiments raises the issue of to whether TAD clique dynamics represents a deterministic or stochastic process (Bystricky, 2015). The current lack of demonstration that TAD clique assembly and disassembly is a regulated process opens for possibilities that stochasticity plays a significant role in spatial genome configurations (Flyamer et al., 2017). Inasmuch as stochasticity in gene expression emerges as an important contributor to regulated gene expression patterns (Dessalles et al., 2017; Horowitz and Kulkarni, 2017), stochasticity in genome conformation may favor preferred topologies that direct gene expression programs. Such deterministic view of genome structure-function relationships at higher-order level remains to be examined in 4D contexts using matched topological and transcriptome datasets. Along these lines, more detailed analyses of the links between differentiation- and lineage-specific TAD clique formation and expression control of genes within TAD cliques will in the future help gaining further insights into the significant of these higher-order long-range domain associations.

Are TAD cliques deregulated in disease contexts? TAD cliques harbor a large number of disease-associated genes in normal cultured MSCs. Lamin A modulates large-scale chromatin dynamics (Bronshtein et al., 2015) and contributes to the peripheral anchoring of heterochromatin at the nuclear envelope (Solovei et al., 2013). So the role of A-type lamins in the regulation of TAD cliques, and whether they are differentially affected in B versus A compartments, will be important to investigate in the context of lamin A mutations causing laminopathies (Worman, 2012) – in particular mutations that affect lamin-chromatin interactions and gene positioning (Mewborn et al., 2010; Perovanovic et al., 2016; Paulsen et al., 2017; Briand and Collas, 2018; Briand et al., 2018). In the near future, the combination of strategies including high-throughput genome editing and genomics (Leemans et al., 2019), high-throughput FISH (Finn et al., 2019), live-cell imaging of chromatin (Germier et al., 2017), biophysical approaches and computational modeling methods will enhance our knowledge of the functional relationship between genome organizers in a 4D nucleome perspective.

AUTHOR CONTRIBUTIONS

All authors have contributed to the conception of this article and approved it for publication.

FUNDING

This work was supported by EU Scientia Fellowship FP7-PEOPLE-2013-COFUND (No. 609020 to AB), the Research Council of Norway (No. 249734), the University of Oslo, the Norwegian Cancer Society (No. 190299-2017), and South-East Health Norway (No. 2018082).

REFERENCES

Bau, D., and Marti-Renom, M. A. (2012). Genome structure determination via 3C-based data integration by the integrative modeling platform. *Methods* 58, 300–306. doi: 10.1016/j.ymeth.2012.04.004

Baudement, M. O., Cournac, A., Court, F., Seveno, M., Parrinello, H., Reynes, C., et al. (2018). High-salt-recovered sequences are associated with the active chromosomal compartment and with large ribonucleoprotein complexes including nuclear bodies. *Genome Res.* 28, 1733–1746. doi: 10.1101/gr.237073.118

Beagrie, R. A., Scialdone, A., Schueler, M., Kraemer, D. C., Chotalia, M., Xie, S. Q., et al. (2017). Complex multi-enhancer contacts captured by genome architecture mapping. *Nature* 543, 519–524. doi: 10.1038/nature21411

Bickmore, W. A., and van Steensel, B. (2013). Genome architecture: domain organization of interphase chromosomes. *Cell* 152, 1270–1284. doi: 10.1016/j.cell.2013.02.001

Bintu, B., Mateo, L. J., Su, J. H., Sinnott-Armstrong, N. A., Parker, M., Kinrot, S., et al. (2018). Super-resolution chromatin tracing reveals domains and cooperative interactions in single cells. *Science* 362:eaau1783. doi: 10.1126/science.aau1783

Boettiger, A. N., Bintu, B., Moffitt, J. R., Wang, S., Beliveau, B. J., Fudenberg, G., et al. (2016). Super-resolution imaging reveals distinct chromatin folding for different epigenetic states. *Nature* 529, 418–422. doi: 10.1038/nature16496

Bonev, B., Mendelson Cohen, N., Szabo, Q., Fritsch, L., Papadopoulos, G. L., Lubling, Y., et al. (2017). Multiscale 3D genome rewiring during mouse neural development. *Cell* 171, 557–572. doi: 10.1016/j.cell.2017.09.043

Briand, N., and Collas, P. (2018). Laminopathy-causing lamin A mutations reconfigure lamina-associated domains and local spatial chromatin conformation. *Nucleus* 9, 216–226. doi: 10.1080/19491034.2018.1449498

Briand, N., Guenantin, A. C., Jeziorowska, D., Shah, A., Mantecon, M., Capel, E., et al. (2018). The lipodystrophic hotspot lamin A p.R482W mutation deregulates the mesodermal inducer T/Brachyury and early vascular differentiation gene networks. *Hum. Mol. Genet.* 27, 1447–1459. doi: 10.1093/hmg/ddy055

Bronshtein, I., Kanter, I., Kepten, E., Lindner, M., Berezin, S., Shav-Tal, Y., et al. (2016). Exploring chromatin organization mechanisms through its dynamic properties. *Nucleus* 7, 27–33. doi: 10.1080/19491034.2016.1139272

Bronshtein, I., Kepten, E., Kanter, I., Berezin, S., Lindner, M., Redwood, A. B., et al. (2015). Loss of lamin A function increases chromatin dynamics in the nuclear interior. *Nat. Commun.* 6:8044. doi: 10.1038/ncomms9044

Bruston, F., Delbarre, E., Ostlund, C., Worman, H. J., Buendia, B., and Duband-Goulet, I. (2010). Loss of a DNA binding site within the tail of prelamin A contributes to altered heterochromatin anchorage by progerin. *FEBS Lett.* 584, 2999–3004. doi: 10.1016/j.febslet.2010.05.032

Buchwalter, A., Kaneshiro, J. M., and Hetzer, M. W. (2019). Coaching from the sidelines: the nuclear periphery in genome regulation. *Nat. Rev. Genet.* 20, 39–50. doi: 10.1038/s41576-018-0063-5

Bystricky, K. (2015). Chromosome dynamics and folding in eukaryotes: insights from live cell microscopy. *FEBS Lett.* 589, 3014–3022. doi: 10.1016/j.febslet.2015.07.012

Canzio, D., Larson, A., and Narlikar, G. J. (2014). Mechanisms of functional promiscuity by HP1 proteins. *Trends Cell Biol.* 24, 377–386. doi: 10.1016/j.tcb.2014.01.002

Cesarini, E., Mozzetta, C., Marullo, F., Gregoretti, F., Gargiulo, A., Columbaro, M., et al. (2015). Lamin A/C sustains PcG protein architecture, maintaining transcriptional repression at target genes. *J. Cell Biol.* 211, 533–551. doi: 10.1083/jcb.201504035

Chen, Y., Zhang, Y., Wang, Y., Zhang, L., Brinkman, E. K., Adam, S. A., et al. (2018). Mapping 3D genome organization relative to nuclear compartments using TSA-Seq as a cytological ruler. *J Cell Biol.* 217, 4025–4048. doi: 10.1083/jcb.201807108

Cremer, T., and Cremer, M. (2010). Chromosome territories. *Cold Spring Harb. Perspect. Biol.* 2:a003889. doi: 10.1101/cshperspect.a003889

Czapiewski, R., Robson, M. I., and Schirmer, E. C. (2016). Anchoring a leviathan: how the nuclear membrane tethers the genome. *Front. Genet.* 7:82. doi: 10.3389/fgene.2016.00082

Dai, C., Li, W., Tjong, H., Hao, S., Zhou, Y., Li, Q., et al. (2016). Mining 3D genome structure populations identifies major factors governing the stability of regulatory communities. *Nat. Commun.* 7:11549. doi: 10.1038/ncomms11549

de Leeuw, R., Gruenbaum, Y., and Medalia, O. (2018). Nuclear lamins: thin filaments with major functions. *Trends Cell Biol.* 28, 34–45. doi: 10.1016/j.tcb.2017.08.004

Dekker, J., Marti-Renom, M. A., and Mirny, L. A. (2013). Exploring the three-dimensional organization of genomes: interpreting chromatin interaction data. *Nat. Rev. Genet.* 14, 390–403. doi: 10.1038/nrg3454

Dessalles, R., Fromion, V., and Robert, P. (2017). A stochastic analysis of autoregulation of gene expression. *J. Math. Biol.* 75, 1253–1283. doi: 10.1007/s00285-017-1116-7

Dixon, J. R., Selvaraj, S., Yue, F., Kim, A., Li, Y., Shen, Y., et al. (2012). Topological domains in mammalian genomes identified by analysis of chromatin interactions. *Nature* 485, 376–380. doi: 10.1038/nature11082

Duan, Z., Andronescu, M., Schutz, K., McIlwain, S., Kim, Y. J., Lee, C., et al. (2010). A three-dimensional model of the yeast genome. *Nature* 465, 363–367. doi: 10.1038/nature08973

Finn, E. H., Pegoraro, G., Brandao, H. B., Valton, A. L., Oomen, M. E., Dekker, J., et al. (2019). Extensive heterogeneity and intrinsic variation in spatial genome organization. *Cell* 176:e1510. doi: 10.1016/j.cell.2019.01.020

Flyamer, I. M., Gassler, J., Imakaev, M., Brandao, H. B., Ulianov, S. V., Abdennur, N., et al. (2017). Single-nucleus Hi-C reveals unique chromatin reorganization at oocyte-to-zygote transition. *Nature* 544, 110–114. doi: 10.1038/nature21711

Forsberg, F., Brunet, A., Ali, T. M. L., and Collas, P. (2019). Interplay of lamin A and lamin B LADs on the radial positioning of chromatin. *Nucleus* 10, 7–20. doi: 10.1080/19491034.2019.1570810

Fraser, J., Ferrai, C., Chiariello, A. M., Schueler, M., Rito, T., Laudanno, G., et al. (2015). Hierarchical folding and reorganization of chromosomes are linked to transcriptional changes in cellular differentiation. *Mol. Syst. Biol.* 11:852. doi: 10.15252/msb.20156492

Germier, T., Kocanova, S., Walther, N., Bancaud, A., Shaban, H. A., Sellou, H., et al. (2017). Real-time imaging of a single gene reveals transcription-initiated local confinement. *Biophys. J.* 113, 1383–1394. doi: 10.1016/j.bpj.2017.08.014

Gesson, K., Rescheneder, P., Skoruppa, M. P., von, H. A., Dechat, T., and Foisner, R. (2016). A-type lamins bind both hetero- and euchromatin, the latter being regulated by lamina-associated polypeptide 2 alpha. *Genome Res.* 26, 462–473. doi: 10.1101/gr.196220.115

Grigoryan, A., Guidi, N., Senger, K., Liehr, T., Soller, K., Marka, G., et al. (2018). LaminA/C regulates epigenetic and chromatin architecture changes upon aging of hematopoietic stem cells. *Genome Biol.* 19:189. doi: 10.1186/s13059-018-1557-3

Guelen, L., Pagie, L., Brasset, E., Meuleman, W., Faza, M. B., Talhout, W., et al. (2008). Domain organization of human chromosomes revealed by mapping of nuclear lamina interactions. *Nature* 453, 948–951. doi: 10.1038/nature06947

Guo, Y., Xu, Q., Canzio, D., Shou, J., Li, J., Gorkin, D. U., et al. (2015). CRISPR inversion of CTCF sites alters genome topology and enhancer/promoter function. *Cell* 162, 900–910. doi: 10.1016/j.cell.2015.07.038

Harr, J. C., Luperchio, T. R., Wong, X., Cohen, E., Wheelan, S. J., and Reddy, K. L. (2015). Directed targeting of chromatin to the nuclear lamina is mediated by chromatin state and A-type lamins. *J. Cell Biol.* 208, 33–52. doi: 10.1083/jcb.201405110

Hnisz, D., Weintraub, A. S., Day, D. S., Valton, A. L., Bak, R. O., Li, C. H., et al. (2016). Activation of proto-oncogenes by disruption of chromosome neighborhoods. *Science* 351, 1454–1458. doi: 10.1126/science.aad9024

Horowitz, J. M., and Kulkarni, R. V. (2017). Stochastic gene expression conditioned on large deviations. *Phys. Biol.* 14:03LT01. doi: 10.1088/1478-3975/aa6d89

Imakaev, M., Fudenberg, G., McCord, R. P., Naumova, N., Goloborodko, A., Lajoie, B. R., et al. (2012). Iterative correction of Hi-C data reveals hallmarks of chromosome organization. *Nat. Methods* 9, 999–1003. doi: 10.1038/nmeth.2148

Kalhor, R., Tjong, H., Jayathilaka, N., Alber, F., and Chen, L. (2011). Genome architectures revealed by tethered chromosome conformation capture and population-based modeling. *Nat. Biotechnol.* 30, 90–98. doi: 10.1038/nbt.2057

Kind, J., Pagie, L., de Vries, S. S., Nahidiazar, L., Dey, S. S., Bienko, M., et al. (2015). Genome-wide maps of nuclear lamina interactions in single human cells. *Cell* 163, 134–147. doi: 10.1016/j.cell.2015.08.040

Kind, J., Pagie, L., Ortabozkoyun, H., Boyle, S., de Vries, S. S., Janssen, H., et al. (2013). Single-cell dynamics of genome-nuclear lamina interactions. *Cell* 153, 178–192. doi: 10.1016/j.cell.2013.02.028

Kragesteen, B. K., Spielmann, M., Paliou, C., Heinrich, V., Schopflin, R., Esposito, A., et al. (2018). Dynamic 3D chromatin architecture contributes to enhancer specificity and limb morphogenesis. *Nat. Genet.* 50, 1463–1473. doi: 10.1038/s41588-018-0221-x

Larson, A. G., Elnatan, D., Keenen, M. M., Trnka, M. J., Johnston, J. B., Burlingame, A. L., et al. (2017). Liquid droplet formation by HP1alpha suggests a role for phase separation in heterochromatin. *Nature* 547, 236–240. doi: 10.1038/nature22822

Leemans, C., van der Zwalm, M. C. H., Brueckner, L., Comoglio, F., van Schaik, T., Pagie, L., et al. (2019). Promoter-intrinsic and local chromatin features determine gene repression in LADs. *Cell* 177:e814. doi: 10.1016/j.cell.2019.03.009

Li, L., Lyu, X., Hou, C., Takenaka, N., Nguyen, H. Q., Ong, C. T., et al. (2015). Widespread rearrangement of 3D chromatin organization underlies polycomb-mediated stress-induced silencing. *Mol. Cell* 58, 216–231. doi: 10.1016/j.molcel.2015.02.023

Li, Q., Tjong, H., Li, X., Gong, K., Zhou, X. J., Chiolo, I., et al. (2017). The three-dimensional genome organization of *Drosophila* melanogaster through data integration. *Genome Biol.* 18:145. doi: 10.1186/s13059-017-1264-5

Lund, E., Oldenburg, A., Delbarre, E., Freberg, C., Duband-Goulet, I., Eskeland, R., et al. (2013). Lamin A/C-promoter interactions specify chromatin state-dependent transcription outcomes. *Genome Res.* 23, 1580–1589. doi: 10.1101/gr.159400.113

Lund, E. G., Duband-Goulet, I., Oldenburg, A., Buendia, B., and Collas, P. (2015). Distinct features of lamin A-interacting chromatin domains mapped by

ChIP-sequencing from sonicated or micrococcal nuclease-digested chromatin. *Nucleus* 6, 30–38. doi: 10.4161/19491034.2014.990855

Lund, E. G., Oldenburg, A. R., and Collas, P. (2014). Enriched domain detector: a program for detection of wide genomic enrichment domains robust against local variations. *Nucleic Acids Res.* 42:e92. doi: 10.1093/nar/gku324

Lupianez, D. G., Kraft, K., Heinrich, V., Krawitz, P., Brancati, F., Klopocki, E., et al. (2015). Disruptions of topological chromatin domains cause pathogenic rewiring of gene-enhancer interactions. *Cell* 161, 1012–1025. doi: 10.1016/j.cell.2015.04.004

Lupianez, D. G., Spielmann, M., and Mundlos, S. (2016). Breaking TADs: how alterations of chromatin domains result in disease. *Trends Genet.* 32, 225–237. doi: 10.1016/j.tig.2016.01.003

Mewborn, S. K., Puckelwartz, M. J., Abuisneineh, F., Fahrenbach, J. P., Zhang, Y., MacLeod, H., et al. (2010). Altered chromosomal positioning, compaction, and gene expression with a lamin A/C gene mutation. *PLoS One* 5:e14342. doi: 10.1371/journal.pone.0014342

Naetar, N., Ferraioli, S., and Foisner, R. (2017). Lamins in the nuclear interior - life outside the lamina. *J. Cell Sci.* 130, 2087–2096. doi: 10.1242/jcs.203430

Nagano, T., Lubling, Y., Stevens, T. J., Schoenfelder, S., Yaffe, E., Dean, W., et al. (2013). Single-cell Hi-C reveals cell-to-cell variability in chromosome structure. *Nature* 502, 59–64. doi: 10.1038/nature12593

Nagano, T., Lubling, Y., Varnai, C., Dudley, C., Leung, W., Baran, Y., et al. (2017). Cell-cycle dynamics of chromosomal organization at single-cell resolution. *Nature* 547, 61–67. doi: 10.1038/nature23001

Nemeth, A., Conesa, A., Santoyo-Lopez, J., Medina, I., Montaner, D., Peterfia, B., et al. (2010). Initial genomics of the human nucleolus. *PLoS Genet.* 6:e1000889. doi: 10.1371/journal.pgen.1000889

Niskanen, H., Tuszynska, I., Zaborowski, R., Heinaniemi, M., Yla-Herttuala, S., Wilczynski, B., et al. (2018). Endothelial cell differentiation is encompassed by changes in long range interactions between inactive chromatin regions. *Nucleic Acids Res.* 46, 1724–1740. doi: 10.1093/nar/gkx1214

Nora, E. P., Lajoie, B. R., Schulz, E. G., Giorgetti, L., Okamoto, I., Servant, N., et al. (2012). Spatial partitioning of the regulatory landscape of the X-inactivation centre. *Nature* 485, 381–385. doi: 10.1038/nature11049

Oldenburg, A., Briand, N., Sorensen, A. L., Cahyani, I., Shah, A., Moskaug, J. O., et al. (2017). A lipodystrophy-causing lamin A mutant alters conformation and epigenetic regulation of the anti-adipogenic MIR335 locus. *J. Cell Biol.* 216, 2731–2743. doi: 10.1083/jcb.201701043

Olivares-Chauvet, P., Mukamel, Z., Lifshitz, A., Schwartzman, O., Elkayam, N. O., Lubling, Y., et al. (2016). Capturing pairwise and multi-way chromosomal conformations using chromosomal walks. *Nature* 540, 296–300. doi: 10.1038/nature20158

Paulsen, J., Liyakat Ali, T. M., and Collas, P. (2018). Computational 3D genome modeling using Chrom3D. *Nat. Protoc.* 13, 1137–1152. doi: 10.1038/nprot.2018.009

Paulsen, J., Liyakat Ali, T. M., Nekrasov, M., Delbarre, E., Baudement, M. O., Kurscheid, S., et al. (2019). Long-range interactions between topologically associating domains shape the four-dimensional genome during differentiation. *Nat. Genet.* 51, 835–843. doi: 10.1038/s41588-019-0392-0

Paulsen, J., Sekelja, M., Oldenburg, A. R., Barateau, A., Briand, N., Delbarre, E., et al. (2017). Chrom3D: three-dimensional genome modeling from Hi-C and lamin-genome contacts. *Genome Biol.* 18:21. doi: 10.1186/s13059-016-1146-2

Peric-Hupkes, D., Meuleman, W., Pagie, L., Bruggeman, S. W., Solovei, I., Brugman, W., et al. (2010). Molecular maps of the reorganization of genome-nuclear lamina interactions during differentiation. *Mol. Cell* 38, 603–613. doi: 10.1016/j.molcel.2010.03.016

Perovanovic, J., Dell'Orso, S., Gnochi, V. F., Jaiswal, J. K., Sartorelli, V., Vigouroux, C., et al. (2016). Laminopathies disrupt epigenomic developmental programs and cell fate. *Sci. Transl. Med.* 8:335ra358. doi: 10.1126/scitranslmed.aad4991

Quinodoz, S. A., Ollikainen, N., Tabak, B., Palla, A., Schmidt, J. M., Detmar, E., et al. (2018). Higher-order inter-chromosomal hubs shape 3D genome organization in the nucleus. *Cell* 174, 744–757e724. doi: 10.1016/j.cell.2018.05.024

Rao, S. S., Huntley, M. H., Durand, N. C., Stamenova, E. K., Bochkov, I. D., Robinson, J. T., et al. (2014). A 3D map of the human genome at kilobase resolution reveals principles of chromatin looping. *Cell* 159, 1665–1680. doi: 10.1016/j.cell.2014.11.021

Reddy, K. L., Zullo, J. M., Bertolino, E., and Singh, H. (2008). Transcriptional repression mediated by repositioning of genes to the nuclear lamina. *Nature* 452, 243–247. doi: 10.1038/nature06727

Ren, B., and Dixon, J. R. (2015). A CRISPR connection between chromatin topology and genetic disorders. *Cell* 161, 955–957. doi: 10.1016/j.cell.2015.04.047

Robson, M. I., de Las Heras, J. I., Czapiewski, R., Le Thanh, P., Booth, D. G., Kelly, D. A., et al. (2016). Tissue-specific gene repositioning by muscle nuclear membrane proteins enhances repression of critical developmental genes during myogenesis. *Mol. Cell* 62, 834–847. doi: 10.1016/j.molcel.2016.04.035

Robson, M. I., de Las Heras, J. I., Czapiewski, R., Sivakumar, A., Kerr, A. R. W., and Schirmer, E. C. (2017). Constrained release of lamina-associated enhancers and genes from the nuclear envelope during T-cell activation facilitates their association in chromosome compartments. *Genome Res.* 27, 1126–1138. doi: 10.1101/gr.212308.116

Rønningen, T., Shah, A., Oldenburg, A. R., Vekterud, K., Delbarre, E., Moskaug, J. O., et al. (2015). Prepatterning of differentiation-driven nuclear lamin A/C-associated chromatin domains by GlcNAcylated histone H2B. *Genome Res.* 25, 1825–1835. doi: 10.1101/gr.193748.115

Russel, D., Lasker, K., Webb, B., Velazquez-Muriel, J., Tjioe, E., Schneidman-Duhovny, D., et al. (2012). Putting the pieces together: integrative modeling platform software for structure determination of macromolecular assemblies. *PLoS Biol.* 10:e1001244. doi: 10.1371/journal.pbio.1001244

Sabari, B. R., Dall'Agnese, A., Boija, A., Klein, I. A., Coffey, E. L., Shrinivas, K., et al. (2018). Coactivator condensation at super-enhancers links phase separation and gene control. *Science* 361:eaar3958. doi: 10.1126/science.aar3958

Sen Gupta, A., and Sengupta, K. (2017). Lamin B2 modulates nucleolar morphology, dynamics, and function. *Mol. Cell Biol.* 37, e274–e217. doi: 10.1128/MCB.00274-17

Serra, F., Di Stefano, M., Spill, Y. G., Cuartero, Y., Goodstadt, M., Bau, D., et al. (2015). Restraint-based three-dimensional modeling of genomes and genomic domains. *FEBS Lett.* 589, 2987–2995. doi: 10.1016/j.febslet.2015.05.012

Shin, Y., Chang, Y. C., Lee, D. S. W., Berry, J., Sanders, D. W., Ronceray, P., et al. (2018). Liquid nuclear condensates mechanically sense and restructure the genome. *Cell* 175, 1481–1491. doi: 10.1016/j.cell.2018.10.057

Solovei, I., Wang, A. S., Thanisch, K., Schmidt, C. S., Krebs, S., Zwerger, M., et al. (2013). LBR and lamin A/C sequentially tether peripheral heterochromatin and inversely regulate differentiation. *Cell* 152, 584–598. doi: 10.1016/j.cell.2013.01.009

Stadhouders, R., Vidal, E., Serra, F., Di Stefano, B., Le Dily, F., Quilez, J., et al. (2018). Transcription factors orchestrate dynamic interplay between genome topology and gene regulation during cell reprogramming. *Nat. Genet.* 50, 238–249. doi: 10.1038/s41588-017-0030-7

Stevens, T. J., Lando, D., Basu, S., Atkinson, L. P., Cao, Y., Lee, S. F., et al. (2017). 3D structures of individual mammalian genomes studied by single-cell Hi-C. *Nature* 544, 59–64. doi: 10.1038/nature21429

Strom, A. R., Emelyanov, A. V., Mir, M., Fyodorov, D. V., Darzacq, X., and Karpen, G. H. (2017). Phase separation drives heterochromatin domain formation. *Nature* 547, 241–245. doi: 10.1038/nature22989

Szabo, Q., Jost, D., Chang, J. M., Cattoni, D. I., Papadopoulos, G. L., Bonev, B., et al. (2018). TADs are 3D structural units of higher-order chromosome organization in *Drosophila*. *Sci. Adv.* 4:eaar8082. doi: 10.1126/sciadv.aar8082

Szalaj, P., Tang, Z., Michalski, P., Pietal, M. J., Luo, O. J., Sadowski, M., et al. (2016). An integrated 3-Dimensional genome modeling engine for data-driven simulation of spatial genome organization. *Genome Res.* 26, 1697–1709. doi: 10.1101/gr.205062.116

Tatavosian, R., Kent, S., Brown, K., Yao, T., Duc, H. N., Huynh, T. N., et al. (2019). Nuclear condensates of the Polycomb protein chromobox 2 (CBX2) assemble through phase separation. *J. Biol. Chem.* 294, 1451–1463. doi: 10.1074/jbc.RA118.006620

Thanisch, K., Song, C., Engelkamp, D., Koch, J., Wang, A., Hallberg, E., et al. (2017). Nuclear envelope localization of LEMD2 is developmentally dynamic and lamin A/C dependent yet insufficient for heterochromatin tethering. *Differentiation* 94, 58–70. doi: 10.1016/j.diff.2016.12.002

Tjong, H., Li, W., Kalhor, R., Dai, C., Hao, S., Gong, K., et al. (2016). Population-based 3D genome structure analysis reveals driving forces in spatial genome organization. *Proc. Natl. Acad. Sci. U.S.A.* 113, E1663–E1672. doi: 10.1073/pnas.1512577113

Ulianov, S. V., Doronin, S. A., Khrameeva, E. E., Kos, P. I., Luzhin, A. V., Starikov, S. S., et al. (2019). Nuclear lamina integrity is required for proper spatial organization of chromatin in *Drosophila*. *Nat. Commun.* 10:1176. doi: 10.1038/s41467-019-09185-y

Valton, A. L., and Dekker, J. (2016). TAD disruption as oncogenic driver. *Curr. Opin. Genet. Dev.* 36, 34–40. doi: 10.1016/j.gde.2016.03.008

van Steensel, B., and Belmont, A. S. (2017). Lamina-associated domains: links with chromosome architecture. heterochromatin, and gene repression. *Cell* 169, 780–791. doi: 10.1016/j.cell.2017.04.022

Vivante, A., Brozgol, E., Bronshtein, I., Levi, V., and Garini, Y. (2018). Chromatin dynamics governed by a set of nuclear structural proteins. *Genes Chromosomes Cancer* 58, 437–451. doi: 10.1002/gcc.22719

Wang, F., and Qi, L. S. (2016). Applications of CRISPR genome engineering in cell biology. *Trends Cell Biol.* 26, 875–888. doi: 10.1016/j.tcb.2016.08.004

Worman, H. J. (2012). Nuclear lamins and laminopathies. *J. Pathol.* 226, 316–325. doi: 10.1002/path.2999

Zuleger, N., Boyle, S., Kelly, D. A., de Las Heras, J. I., Lazou, V., Korfali, N., et al. (2013). Specific nuclear envelope transmembrane proteins can promote the location of chromosomes to and from the nuclear periphery. *Genome Biol.* 14:R14. doi: 10.1186/gb-2013-14-2-r14

Conflict of Interest Statement: The authors declare that the research was conducted in the absence of any commercial or financial relationships that could be construed as a potential conflict of interest.

frontiers in Genetics

ORIGINAL RESEARCH
published: 03 October 2019
doi: 10.3389/fgene.2019.00917

Nuclear Lamin B1 Interactions With Chromatin During the Circadian Cycle Are Uncoupled From Periodic Gene Expression

Annaël Brunet[1†], Frida Forsberg[1†], Qiong Fan[1], Thomas Sæther[1] and Philippe Collas[1,2]*

[1] Department of Molecular Medicine, Institute of Basic Medical Sciences, Faculty of Medicine, University of Oslo, Oslo, Norway, [2] Department of Immunology and Transfusion Medicine, Oslo University Hospital, Oslo, Norway

Many mammalian genes exhibit circadian expression patterns concordant with periodic binding of transcription factors, chromatin modifications, and chromosomal interactions. Here we investigate whether chromatin periodically associates with nuclear lamins. Entrainment of the circadian clock is accompanied, in mouse liver, by a net gain of lamin B1–chromatin interactions genome-wide, after which the majority of lamina-associated domains (LADs) are conserved during the circadian cycle. By tailoring a bioinformatics pipeline designed to identify periodic gene expression patterns, we also observe hundreds of variable lamin B1–chromatin interactions among which oscillations occur at 64 LADs, affecting one or both LAD extremities or entire LADs. Only a small subset of these oscillations however exhibit highly significant 12, 18, 24, or 30 h periodicity. These periodic LADs display oscillation asynchrony between their 5′ and 3′ borders, and are uncoupled from periodic gene expression within or in the vicinity of these LADs. Periodic gene expression is also unrelated to variations in gene-to-nearest LAD distances detected during the circadian cycle. Accordingly, periodic genes, including central clock-control genes, are located megabases away from LADs throughout circadian time, suggesting stable residence in a transcriptionally permissive chromatin environment. We conclude that periodic LADs are not a dominant feature of variable lamin B1–chromatin interactions during the circadian cycle in mouse liver. Our results also suggest that periodic hepatic gene expression is not regulated by rhythmic chromatin associations with the nuclear lamina.

Keywords: circadian rhythm, lamin B, lamina-associated domain, oscillation, period

OPEN ACCESS

Edited by:
Karim Mekhail,
University of Toronto, Canada

Reviewed by:
Richard Alan Katz,
Fox Chase Cancer Center, United States
Andrei V. Chernov,
University of California, United States

****Correspondence:***
Philippe Collas
philc@medisin.uio.no

†These authors contributed equally to this work

Specialty section:
This article was submitted to Epigenomics and Epigenetics, a section of the journal Frontiers in Genetics

Received: *26 June 2019*
Accepted: *30 August 2019*
Published: *03 October 2019*

Citation:
Brunet A, Forsberg F, Fan Q, Sæther T and Collas P (2019) Nuclear Lamin B1 Interactions With Chromatin During the Circadian Cycle Are Uncoupled From Periodic Gene Expression. Front. Genet. 10:917. doi: 10.3389/fgene.2019.00917

INTRODUCTION

Thousands of mammalian genes exhibit autonomous oscillatory patterns of expression concordant with the circadian (24 h) rhythm (Hastings et al., 2018). The circadian rhythm is governed by central and peripheral clocks, respectively in the nervous system and in individual organs including adipose tissue, lungs and liver, controlled by transcriptional and translational negative feedback loops (Takahashi, 2017). The core clock is regulated by the CLOCK and BMAL1 transcription factors

Abbreviations: ChIP-seq, chromatin immunoprecipitation sequencing; CT, circadian time; LAD, lamina-associated domain; NS, non-synchronized; PBS, phosphate buffered saline; PMSF, phenylmethylsulfonyl fluoride; RNA-seq, RNA-sequencing; RT-qPCR, reverse transcription quantitative polymerase chain reaction; TF, transcription factor.

(TFs) which drive expression of clock-controlled genes including *Per*, *Cry*, *Nr1d1/Nr1d2* (encoding REV-ERB alpha/beta proteins, respectively), and *Ror* genes (encoding ROR alpha/beta/gamma), by binding to E-boxes in their promoters. The PER-CRY repressor complex inhibits activity of CLOCK–BMAL1, lowering transcription of *Per* and *Cry* and generating a negative feedback loop. RORs and REV-ERBs act as activators and repressors, respectively, of *Arntl* (also called *Bmal1*) and other clock genes, driving their rhythmic transcription. Stability of PER and CRY proteins is regulated by post-translational modifications leading to their time-dependent degradation, enabling a new cycle of CLOCK–BMAL1-driven gene expression.

Circadian binding of TFs and chromatin modifiers to promoters and enhancers generates rhythmic chromatin modifications and remodeling (Koike et al., 2012; Masri et al., 2014; Zhang et al., 2015; Kim et al., 2018). In mouse liver, histone H3 lysine 4 trimethylation (H3K4me3) levels oscillate at promoters of circadian genes (Vollmers et al., 2012; Aguilar-Arnal et al., 2015), while rhythmic H3K4me1 and H3K27 acetylation (H3K27ac) levels define oscillating enhancers (Koike et al., 2012; Vollmers et al., 2012; Fang et al., 2014; Takahashi, 2017). Recruitment to chromatin of the sirtuin SIRT1, a histone deacetylase (HDAC) involved in circadian control of metabolism (Nakahata et al., 2008; Masri et al., 2014), is under influence of oscillatory levels of metabolites (Aguilar-Arnal et al., 2015) and provides a molecular link between metabolism, chromatin and circadian rhythms. Periodic recruitment of HDAC3 to chromatin also regulates circadian rhythms (Feng et al., 2011). These oscillatory cistromes and chromatin modifications raise the possibility that other chromatin-linked processes also show rhythmic patterns. Indeed, periodic promoter–enhancer interactions regulate and connect circadian liver gene expression networks (Aguilar-Arnal et al., 2013; Xu et al., 2016; Kim et al., 2018; Mermet et al., 2018). Thus, circadian-dependent changes in chromatin topology contribute to shaping the nuclear landscape (Yeung and Naef, 2018).

Dynamic interactions of chromatin with the nuclear lamina, a meshwork of A-type lamins [lamins A and C (LMNA and LMNC)], products of the *Lmna* gene, and B-type lamins [lamins B1 and B2 (LMNB1 and LMNB2)], encoded by the *Lmnb1* and *Lmnb2* genes respectively, at the nuclear periphery (Burke and Stewart, 2013) also constitute one mechanism of regulation of gene expression (van Steensel and Belmont, 2017). Interestingly, A- and B-type lamins are not only found at the nuclear periphery, where the nuclear lamina is located, but also in the nucleoplasm where interactions with chromatin have been reported to also occur (Naetar et al., 2017; Pascual-Reguant et al., 2018). Regions of chromatin interacting with lamins, so-called lamina-associated domains (LADs), are typically heterochromatic and relatively well conserved between cell types (Peric-Hupkes et al., 2010). However, other LADs are variable and altered during differentiation (Peric-Hupkes et al., 2010; Rønningen et al., 2015; Poleshko et al., 2017; Paulsen et al., 2019). It remains however unclear to what extent variable LADs arise and disappear as a consequence of regulatory mechanisms or through random interactions of chromatin with nuclear lamins. Whether individual loci or broader domains such as LADs display oscillatory interactions with nuclear lamins has also to our knowledge not been addressed.

Scarce evidence links the nuclear envelope to circadian gene expression. HDAC3, a component of the clock negative feedback loop (Shi et al., 2016) and a regulator of lamina-associated genes (Demmerle et al., 2013), interacts with the inner nuclear membrane proteins TMPO/lamina-associated polypeptide 2β (Somech et al., 2005) and emerin (Demmerle et al., 2013). The clock regulators SIRT1 and SIRT6 deacetylases interact with LMNA (Liu et al., 2012; Ghosh et al., 2015) at the nuclear lamina, where they modulate histone acetylation and gene expression. *In vitro*, BMAL1 expression seems to be modulated by MAN1, another protein of the inner nuclear membrane, through MAN1 binding to the *ARNTL* (also called *BMAL1*) promoter (Lin et al., 2014). Lastly, in a human colon cancer cell line, a handful of circadian genes have been shown to rhythmically interact with the nuclear lamina, regulating their transcription (Zhao et al., 2015). These observations suggest that nuclear lamins may contribute to the regulation of circadian gene expression. However, whether chromatin exhibits genome-scale periodic associations with the lamina has not been examined.

Here, we determined whether chromatin exhibits periodic interactions with LMNB1 after entrainment of the circadian clock in mouse liver. We opted to examine this feature of genome organization in the liver because it is highly responsive to entrainment of the circadian clock at the metabolic level and as such is the most studied organ in investigations of circadian control of transcriptional regulation (Takahashi, 2017) and spatial chromatin conformation (Aguilar-Arnal et al., 2013; Kim et al., 2018). We show that periodic lamin B1–chromatin interactions are not a dominant feature of LADs during the circadian cycle and are uncoupled from periodic gene expression. Our data strongly suggest that periodic gene expression is not under direct regulation of rhythmic association of chromatin with the nuclear lamina.

MATERIALS AND METHODS

Mice

Wild-type C57Bl/6 male mice (Jackson Laboratories) were housed in 12 h light/12 h dark cycles with lights on at 6 am and lights off at 6 pm. Mice were kept off chow for 24 h, refed *ad libitum* at circadian time CT0 (6 am) and sacrificed at CT6, 12, 18, 24, and 30 h (n = 7 mice per CT). Non-synchronized (NS) mice (n = 7) were sacrificed at 12:00 noon on the day prior to food restriction. Livers were collected from all mice, partitioned and snap-frozen in liquid nitrogen. Procedures were approved by the University of Oslo and Norwegian Regulatory Authorities (approval No. 8565).

RNA-Sequencing and Gene Expression Analysis

Total RNA was isolated from livers of five mice at each CT using the RNeasy Mini Kit (Qiagen). RNA (1 μg) was reverse-transcribed (BioRad Laboratories) and analyzed by qPCR using IQ SYBR green (BioRad Laboratories), *Eif2a* as reference and

primers listed in **Supplementary Table S1** (n = 5 mice per CT). RNA was also processed to prepare RNA-sequencing (RNA-seq) libraries (TruSeq Stranded mRNA Library Prep Kit; Illumina; n = 3 mice per CT) which were sequenced on an Illumina HiSeq2500. RNA-seq reads were processed with Tuxedo (Trapnell et al., 2010). TopHat v2.10 was used to align reads with no mismatch against the mm10 genome (Langmead and Salzberg, 2012). Transcript level was estimated using cufflinks v2.2.1 and differential gene expression determined using cuffdiff v2.2.1 (Trapnell et al., 2010). Gene expression plots show mean ± SD relative expression levels (for RT-qPCR data) or FPKM (fragments per kilobase of exon model per million reads mapped; RNA-seq data) at each CT, as indicated, with single data points. A gene was ascribed to a LAD if its transcription start site overlapped with the LAD.

MetaCycle Analysis

We used MetaCycle (Wu et al., 2016) to identify genes with periodic expression patterns. MetaCycle measures the goodness-of-fit between RNA-seq, FPKM, and theoretical cosine curves with varying periods and phases. The extrapolated periodic function best fitting the RNA-seq data is selected and the significance of a given periodicity is determined by assigning *P* values after scrambling FPKM values. MetaCycle was applied to the entire range of CTs in the study (30 h). To fit RNA-seq data with periodic functions, MetaCycle normalizes FPKM values by computing z-scores. Our time series data are integer intervals with even sampling and do not include missing values. Given the features of our time series data, MetaCycle incorporated both the JTK_CYCLE (JTK) and the Lomb-Scargle (LS) methods for periodic signal detection. Based on our data and time resolution, available period values are integers (0, 6, 12, 18, 24, 30, and 36 h) for JTK and real numbers ranging from 12 to 48 h for LS. Periods are the mean of JTK and LS period values. Thus we focused our analyses on oscillations with 12, 18, 24, and 30 h periods, each ± 3 h, i.e. half the time resolution in our study. Moreover, the restricted 12 ± 3 h period group was not able to distinguish groups of 12 h periodic genes oscillating in positive ($\Phi\_\pi/2$) or negative ($\Phi\_-\pi/2$) quadrature of phase, but only those oscillating in phase or opposition of phase. MetaCycle was also applied to identify periodicity in LAD coverage (see below).

Liver Extracts and Immunoblotting

Mouse liver samples were homogenized in ice-cold phosphate buffered saline (PBS) with 1× protease inhibitor cocktail (Sigma-Aldrich) and 1 mM phenylmethylsulfonide fluoride (PMSF; Sigma-Aldrich), using a Dounce tissue grinder with an A-type glass pestle, followed by centrifugation at 200 g for 5 min at 4°C. Supernatants were discarded, and pellets washed once in ice-cold PBS with 1× protease inhibitor cocktail and 1 mM PMSF and centrifuged at 200 g for 5 min at 4°C. Cells were lysed in RIPA buffer (140 mM NaCl, 10 mM Tris–HCl pH 8.0, 1 mM EDTA, 0.5 mM EGTA, 1% Triton X-100, 0.1% SDS, 0.1% sodium deoxycholate, 1 mM PMSF, protease inhibitors) with 1× protease inhibitor cocktail and 1 mM PMSF, sonicated twice with 30 s on/off in a Bioruptor (Diagenode), and incubated under rotation at 25 rpm for 30 min at 4°C. Lysates were centrifuged at 10,000 g for 10 min at 4°C and supernatants collected for immunoblotting analysis. Proteins were separated by 7.5% SDS-PAGE, transferred onto an Immobilon-FL membrane (Millipore) and membranes blocked with 3% BSA in TBST (0.15 M NaCl, 50 mM Tris–HCl pH 7.6, 0.05% Tween®20). Membranes were incubated with antibodies against CLOCK (1:500; Abcam ab3517), LMNB1 (1:1,000; Santa Cruz Biotechnology sc6216), and β-actin (1:2,000; Sigma-Aldrich A5441) in TBST with 3% BSA. Secondary horseradish peroxidase-conjugated anti-mouse (Jackson ImmunoResearch #115-035-174) and anti-goat (Rockland #605-4302) antibodies were used at 1:10,000 dilutions in TBST with 3% BSA.

Chromatin Immunoprecipitation (ChIP)

ChIP of LMNB1 was done as described earlier (Rønningen et al., 2015) and adapted for liver pieces. Snap-frozen liver tissue pieces (40–50 mg, in liquid nitrogen) were thawed on ice and minced on ice for 30 s. Minced tissue was resuspended in PBS containing 1 mM PMSF and protease inhibitors, and homogenized by 7–10 strokes in a 2-ml Dounce homogenizer using a pestle B (tight-fitting). Samples were centrifuged at 400 g and supernatants discarded. Pellets were resuspended in PBS containing 1% formaldehyde (Sigma-Aldrich) and cross-linking was allowed to occur for 10 min at room temperature. Cross-linked samples were sedimented and lysed in RIPA buffer. Chromatin was fragmented by sonication (4 times 10 min) in a Bioruptor (Diagenode). After sedimentation, the supernatant was diluted 10-fold in RIPA buffer and incubated with anti-LMNB1 antibodies (10 µg; Abcam ab16048) coupled to Dynabeads Protein G (Invitrogen) overnight at 4 °C. ChIP samples were washed 3 times in ice-cold RIPA buffer. Cross-links were reversed and DNA eluted for 6 h at 68°C in 50 mM NaCl, 20 mM Tris–HCl pH 7.5, 5 mM EDTA, 1% SDS and 50 ng/µl proteinase K. DNA was purified by phenol-chloroform-isoamylalcohol extraction and used for qPCR (see **Supplementary Table S1** for primer information) or to prepare libraries (Illumina) for sequencing on an Illumina HiSeq2500. Input ChIP DNA consisted of fragmented chromatin aliquots (as above) incubated overnight at 4 °C with no antibodies or beads and subsequently processed as, and in parallel with, the ChIP samples.

LMNB1 ChIP-Seq Data Processing

LMNB1 ChIP-seq and input reads were mapped to the mm10 genome using Bowtie v2.25.0 (Langmead et al., 2009) with default parameters after removing duplicates using Picard's MarkDuplicates. To avoid normalization bias, we ensured that each pair of mapped ChIP and input read files had the same read depth by down-sampling reads for each chromosome individually. Mapped reads were used to call LADs using Enriched Domain Detector (EDD) (Lund et al., 2014) with the following alterations (Forsberg et al., 2019) as described here. To account for technical variation occurring in LAD calling, we first ran EDD 10 times on each LMNB1 ChIP-seq dataset in auto-estimation mode for GapPenalty (GP) and BinSize (BS). Average GP standard deviation was ≤ 1.6 units while BS did not vary (**Supplementary Table S2**). GP variations elicited minimal alterations in LAD calls, allowing estimation of technical variability. For all LADs, median length of these variations was 0.32 Mb; this is < 1% of total LAD coverage, and 3–15 times smaller than median LAD sizes for each CT and replicate. Thus intrinsic EDD variability did not significantly impact LAD calling. Average GP and BS

values from the 10 runs were used to set GP and BS before a final EDD run with each ChIP-seq dataset (**Supplementary Table S2**). Intersects between LADs and genes were determined using BEDTools v2.21.0 (Quinlan and Hall, 2010) and BEDOPS v2.4.27 (Neph et al., 2012). Scripts were written in Bash, Perl, or R and ggplot2 in R was used for plots. Browser files were generated by calculating ChIP/input ratios in 10-kb bins with input normalized to the ratio of total ChIP reads over total input reads.

Determination of Periodic Lads With MetaCycle

To quantify the genomic coverage of variation in the length of LADs during the circadian cycle, we determined for each LAD its "maximal coverage" (cov_{max}) as the union of LAD coverage across all replicates and CTs, and attributed to this cov_{max} a reference value of 1. The cov_{max} 5′ and 3′ limits provided genomic coordinates for measures of variations in LAD length within cov_{max}. For each CT and replicate, variable 5′ and 3′ genomic lengths (in base pairs) were extracted and standardized from 0 to 1, 0 referring to the complete disappearance of a LAD and 1 being the cov_{max} value of the LAD. MetaCycle was applied to determine the periodicity of LAD extensions and shortenings at the 5′ and 3′ borders. Period groups were defined as for RNA-seq analysis (12, 18, 24, and 30 h, each ± 3 h). The method is described in more detail as part of the *Results* section.

Randomization to Validate Periodic LAD Significance

A randomization test was done as additional validation of extrapolated MetaCycle LAD periodicity. To this end, we shuffled the measured experimental variations in 5′ and 3′ LAD lengths within the cov_{max} area for all datasets across CTs and replicates; this was done 3 times. MetaCycle was applied to each randomized order of CTs to identify any periodicity in the variations in LAD lengths across these randomized CTs. The extrapolated periodicity given by MetaCycle was compared with the periodicity found for the experimental order of CTs. If experimental LAD periodicity was different from at least two randomized CTs, it was considered as imposed by the order of CT and not due to random lamin–chromatin interactions.

Determination of Gene-LAD Distance

Gene-to-nearest LAD distance was calculated as the distance from the 5′ and 3′ end of a gene to, respectively, the nearest 3′ and 5′ LAD border. Gene strand was respected and LAD intersects were used at each CT. If a gene was entirely in a LAD, gene-to-nearest LAD distance was the distance from the 5′ and 3′ end of the gene to the first neighboring LAD, both upstream and downstream. In our approach, internal LAD configuration within the cov_{max} area, such as a LAD split or fusion, was not considered in the determination of periodicity at the 5′ and 3′ borders.

Data Viewing

Genome browser views were produced with the Integrated Genomics Viewer (Robinson et al., 2011) using the mm10 genome annotation to illustrate LADs in regions of interest.

Statistics

MetaCycle used its built-in statistical method to assign *P* values from Fisher's exact tests. The JTK and LS methods used in MetaCycle assign a *P* value for each fitted data type, i.e. gene expression variation for RNA-seq and RT-qPCR, protein expression level for Western blot quantification or LAD size variation for LMNB1 ChIP-seq data. These multiple *P* values are combined into a one-test Chi-square statistics assuming a Chi-squared distribution with 2 k degrees of freedom (where k is the number of *P* values; here k = 3 for RNA-seq data, k = 5 for RT-qPCR, k = 3 for Western blot data and k = 2 for LAD data), when all null-hypotheses are true and each *P* value is independent. The combined *P* value was determined by the Chi-square *P* value and was used to determine the significance of oscillating patterns. Protein levels in Western blots were compared pair-wise between time-points using paired t-tests generating two-tailed *P* values; $P < 0.01$ was considered significant.

RESULTS

Hepatic Genes Exhibit Distinct Periodic Transcript Levels in Liver

To entrain the circadian clock, mice were subjected to 24 h fasting and refed *ad libitum* from circadian time CT0 (Tahara et al., 2011). Livers were collected every 6 h until CT30, and from non-synchronized (NS) mice 18 h before the fasting period (**Figure 1A**). Entrainment of the clock was confirmed by periodic expression of the core clock genes *Clock*, *Arntl* (*Bmal1*), *Cry1*, *Per1*, and *Nr1d1*, assessed by RT-qPCR and analysis of their periodicity using MetaCycle (**Supplementary Figure 1**; **Supplementary Table S3**). We used MetaCycle to identify genes with periodic expression patterns from RNA-seq data generated in biological triplicates at each CT. MetaCycle measures the goodness-of-fit between RNA-seq FPKM and cosine curves with varying periods and phases. The extrapolated periodic function best fitting the data is selected and significance is determined (Fisher's exact tests) after scrambling FPKM values. From the period distribution for all 17,330 expressed genes in liver (expressed at least at one time point), we focused on oscillations with 12, 18, 24, and 30 h periods (each ± 3 h, half the time resolution in our study) (**Supplementary Figure S2A**). We find that nearly 20% of oscillations are circadian (24 h period; 3,046 genes), and thousands of genes oscillate with periods within the circadian rhythm and beyond (**Figure 1B**), in line with previous reports (Hughes et al., 2009; Korencic et al., 2014; Zhu et al., 2017). Among these, a subset displays highly significantly oscillating transcripts ($P < 0.005$; **Figures 1B** and **C**). Within a given period, mRNA oscillations occurred with distinct phases (**Supplementary Figure S2B**): oscillations are in phase ($\Phi = 0$, time at first maxima) and opposition of phase ($\Phi = \pi$), and for 18, 24, and 30 h periods, are also offset by one-quarter cycle ($\Phi = ½\ \pi$ and $\Phi = -½\ \pi$) (**Figure 1C**; **Supplementary Figures S2C** and **D**). Significantly periodic genes include the core clock genes (**Figure 1D**; **Supplementary Figure S2E**), confirming entrainment of the clock. Genes (644) also display significant ($P < 0.005$) mRNA oscillations with periods outside 12, 18, 24, or 30 h. We also defined a set of 204 "non-periodic" genes with mRNA

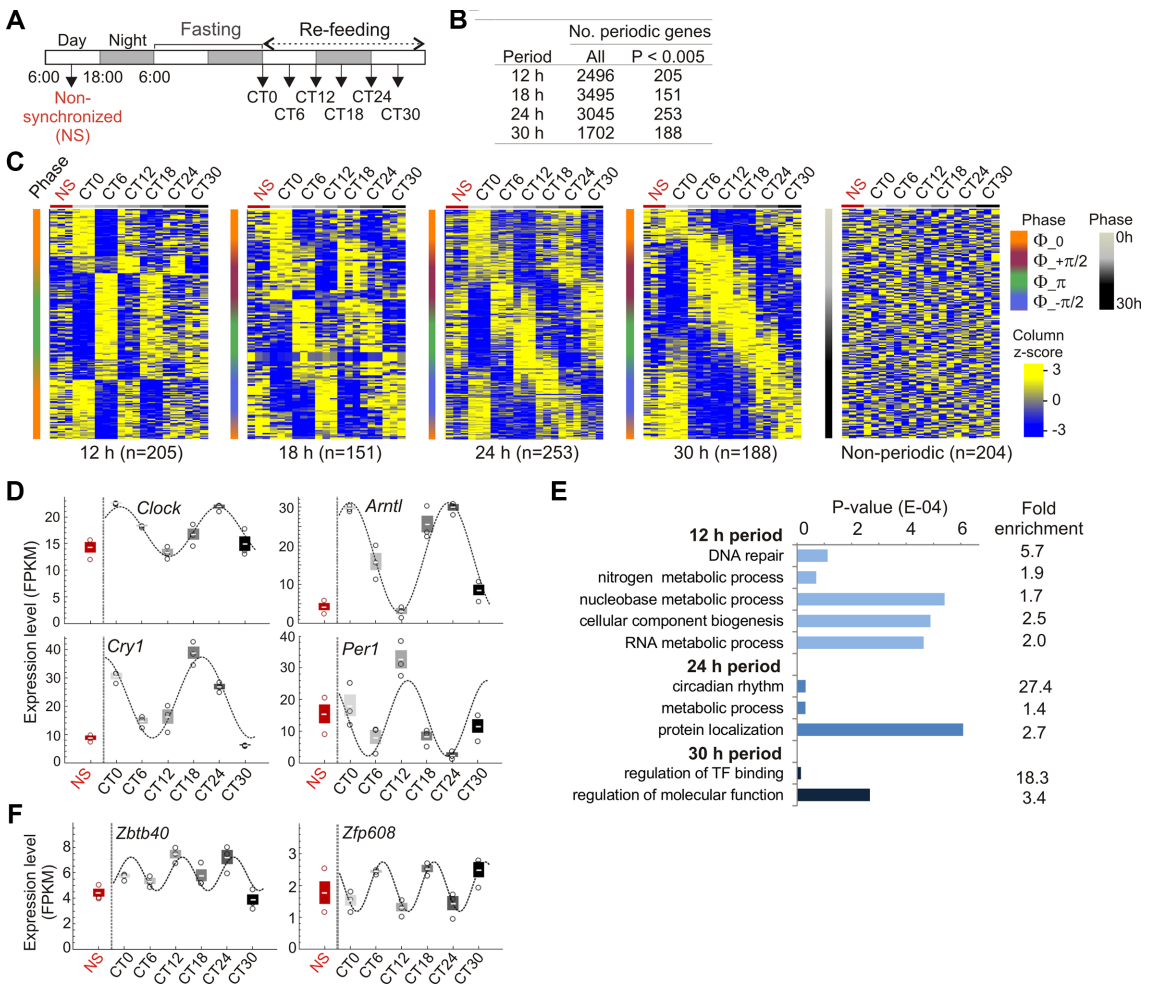

FIGURE 1 | Fasting and refeeding entrains circadian gene expression in liver. **(A)** Circadian clock entrainment schedule used in this study. **(B)** Numbers of periodic genes. **(C)** Expression profiles (FPKM z-scores) of periodic and non-periodic genes in non-synchronized (NS) mice and from CT0 to CT30 (3 mice per CT). Genes are ranked by increasing phase value (y axis; scale on the right). **(D)** RNA-seq analysis of circadian expression patterns of central clock control genes (mean ± SD, individual values). **(E)** Enriched GO terms for periodic genes. **(F)** Circadian expression patterns of the BTB/POZ domain transcription factor gene *Zbtb40* and of the zinc-finger transcription factor gene *Zfp608* (FPKM z-scores; mean ± SD, individual values). In **(D)** and **(F)** cosine curves are MetaCycle best-fits; see **Supplementary Table S3** for details.

levels discordant ($1 > P > 0.9999$) with any cosine curve tentatively fitted by MetaCycle (**Figure 1B**). Lists of periodic and non-periodic genes are provided in **Supplementary Tables S4** and **S5**.

Gene ontology analysis confirms enrichment of 24 h periodic genes in rhythmic and circadian processes, including key metabolic functions (**Figure 1E**; **Supplementary Table S6**). A number of periodic genes encode BTB/POZ domain TFs, some of which are involved in targeting chromatin to the nuclear lamina (Zullo et al., 2012) (**Supplementary Table S4**). Some of these genes are CLOCK or BMAL1 targets (e.g. *Zbtb40*, *Zbtb7b/cKrox*, and *Zfp608*; **Figure 1F**) and could tentatively be involved in associations of chromatin with the nuclear envelope.

Entrainment of the Circadian Clock Resets LMNB1–Chromatin Interactions

We therefore examined chromatin association with nuclear lamins in liver during the circadian cycle. We first established that LMNB1 protein levels vary moderately over time but do not significantly oscillate ($P = 0.61$; Fisher's exact test), and that *Lmnb1* transcripts analyzed by RNA-seq and verified by RT-qPCR do not periodically oscillate (**Figures 2A–C**; **Supplementary Figure S3A**). Moreover, chromatin immunoprecipitation (ChIP)-qPCR of LMNB1 from liver confirmed LMNB1 enrichment in LADs found in several other mouse cell types (constitutive LADs; cLADs) (Meuleman et al., 2013) (**Figure 2D**).

Thus, we determined to what extent LADs varied during the circadian cycle. We performed a ChIP-seq analysis of LMNB1 from livers of NS mice and at each CT in biological replicates (i.e. two mice per CT) and mapped LADs (**Figure 3A**; see **Supplementary Table S2**). We find that LAD sizes are overall constant and LADs display low gene density (**Supplementary Figures S3B** and **C**). LADs also show robust overlap between replicates (**Figure 3A** and **B**), as shown by Jaccard indices (**Figure 3C**) and by minimal variations between intersect coverage and

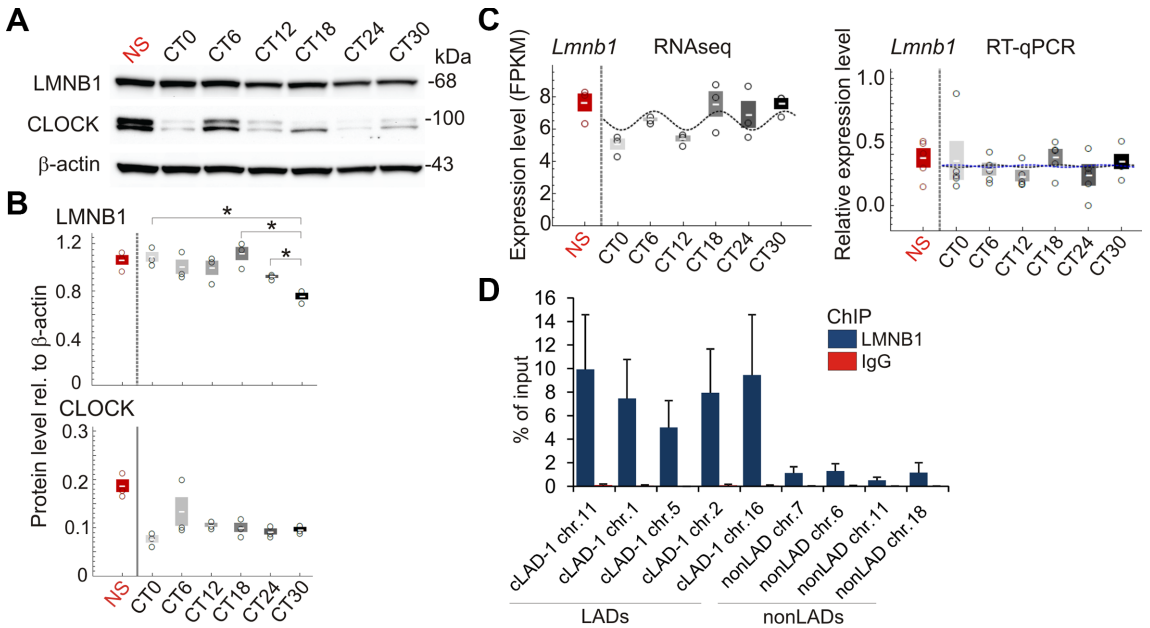

FIGURE 2 | Expression of LMNB1 protein and transcripts during the circadian cycle. **(A)** Western blots of LMNB1 and CLOCK expression; β-actin was used as loading control; see **Supplementary Figure S3A** for all biological replicates. **(B)** Quantification of Western blots from biological triplicates, relative to β-actin; mean ± SD, individual values; *P < 0.01 (paired t-tests, two tailed *P* values). Note the difference in variation of expression of CLOCK protein and *Clock* transcripts expected from the regulation of protein expression at the transcriptional and protein degradation levels). **(C)** Levels of *Lmnb1* transcripts determined by RNA-seq (FPKM; n = 3) and RT-qPCR (n = 5; expression relative to *Eif2a* levels); means ± SD, individual values. Cosine curves are MetaCycle best-fits. *Lmnb1* is not significantly periodic (RNA-seq *P* = 0.16; RT-qPCR *P* = 0.98; MetaCycle Fisher's exact tests). RT-qPCR graph: blue line, MetaCycle best-fit from RT-qPCR data; black line, MetaCycle best-fit from RNA-seq data; note the overlap between the two, indicating strong concordance between the two datasets. Amplitude and base values used for both fits are from RT-qPCR MetaCycle analysis. **(D)** ChIP-qPCR analysis of LMNB1 occupancy in constitutive LADs and in non-LAD regions (mean ± SD of % of input chromatin analyzed by qPCR; n = 3 NS mice); ChIP using an irrelevant IgG was done as negative control.

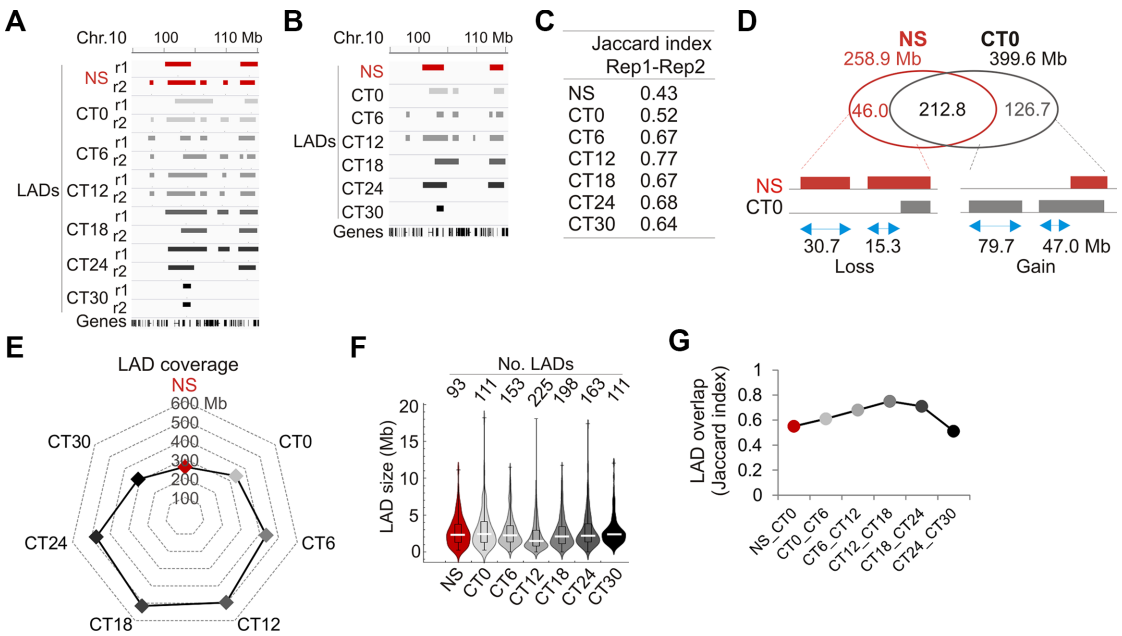

FIGURE 3 | Characterization of LADs during the circadian cycle. **(A)** Genome browser view of LADs in biological replicate (r1, r2) and at each CT for the indicated region on chromosome 10. **(B)** Genome browser view of LAD intersects between replicates for each CT in the same region as in **(A)**. **(C)** Jaccard indices of LAD overlap between replicates. **(D)** Venn diagram of LAD overlap between NS mice and CT0 (intersect of replicates); bottom, schematic representation of genome coverage by LADs gained or lost at CT0 relative to NS, for stand-alone LADs and LAD extension or shortening. **(E)** Radar plot of genome coverage by LADs. **(F)** Distribution and median of LAD size. **(G)** Jaccard indices of LAD overlap between consecutive CTs.

replicates (< 1 Mb, or 0.05–0.21% of LAD coverage per replicate; **Supplementary Table S7**). Thus unless specified otherwise, LADs were subsequently analyzed at each time point as intersects between replicates.

We next assessed to what extent entrainment of the circadian clock did reset LADs. We find that entrainment of the clock is manifested by a LAD gain of 126.7 Mb at CT0 relative to NS, as stand-alone LADs or as extensions of existing LADs (**Figure 3D**). This increase in LMNB1–chromatin interactions was confirmed by ChIP-qPCR (**Supplementary Figures S3D** and **E**). We also note a LAD loss of 46 Mb at CT0 relative to NS, mostly as stand-alone LADs (**Figure 3D**). Thus, entrainment of the clock is associated with a net gain of LMNB1–chromatin interactions.

Comparison of LAD coverage over time reveals an increase from CT0 (339 Mb) to CT12 (496 Mb), followed by a decrease to CT30 (312 Mb) (**Figure 3E**), likely resulting from variations in LAD numbers rather than LAD size (**Figure 3F**). LADs nevertheless display robust overlap across CTs (**Figure 3G; Supplementary Figure S3F**), indicating that they are overall conserved in liver during the circadian cycle. However, the data also indicate that some changes in LMNB1–chromatin interactions do occur, and underline the detection of variable LADs. Of note, although LMMB1 is predominantly found at the nuclear lamina at the nuclear periphery, a fraction of LMNB1 has also been reported in the nucleoplasm, in association with nucleoli in heterochromatin domains (Sen Gupta and Sengupta, 2017) and with domains of euchromatin (Pascual-Reguant et al., 2018). Moreover, our ChIP approach to identify LMNB1 LADs does not *a priori* discriminate between the nuclear peripheral and internal pools of LMNB1. Thus we do not at present exclude that a subset of LMNB1–chromatin interactions detected during the circadian cycle in our study potentially involves a nucleoplasmic LMNB1 pool.

Periodic Oscillations in LMNB1–Chromatin Interactions Constitute a Minor Proportion of LADs

We next examined variations in LADs more closely during the circadian cycle. These occur by LAD extension or shortening, sometimes resulting in a fusion or splitting of LADs, or by formation and dissociation of entire LADs (see **Figures 3A** and **B**). We therefore devised a strategy to quantitatively characterize the genomic coverage of these variable LADs over time. We determined for each LAD the maximal genome coverage (cov_{max}) in the CT0–CT30 time course as the union of LAD coverage across all replicates and CTs, and ascribed to cov_{max} a reference value of 1 (**Figure 4A**, left panel). The 5′ and 3′ boundaries of this cov_{max} area provided genomic coordinates for measures of variations in LAD length within this area. For each CT and replicate, variable 5′ and 3′ LAD lengths were extracted and standardized from 0 to 1 (cov_{max}), 0 referring to the complete disappearance of a LAD, and 1 corresponding to the entire LAD being present over the whole cov_{max} area (**Figure 4A**, middle panel). We then used MetaCycle to identify any periodicity in the extension or shortening of LADs within the cov_{max} area (**Figure 4A**, right panel), where MetaCycle applied a cosine curve best-fitting genome coverage variations at the 5′ and 3′ end of LADs.

We applied MetaCycle to 626 variable LAD borders (at 313 LADs) to identify periodically oscillating lengths of these LADs over the CT0–CT30 time course (**Figure 4B**). Among these, MetaCycle tentatively identifies 5′ and/or 3′ end oscillations with 12, 18, 24, or 30 h (± 3 h) periods in 420 LAD borders (among 240 LADs; **Figure 4B**; **Supplementary Table S8**). Ascribing a stringent P value of < 0.005 (Fisher's exact test; as in our MetaCycle RNA-seq analysis) returns 10 highly significantly periodic LADs with periods distributed throughout the circadian cycle (**Figure 4B**; **Table 1**; **Supplementary Table S8**). Relaxing the P value to $P < 0.05$ expectedly increases the number of periodic LAD borders to 77 (30 5′-periodic, 47 3′-periodic, and 13 both 5′- and 3′-periodic) among 64 distinct LADs (**Figure 4B**; **Supplementary Table S8**). However, inspection of the profiles of these LADs revealed, for some of them, discrepancy with the best curve fitted by MetaCycle. This led us to focus our subsequent analysis on the 10 LADs identified above at $P < 0.005$, which we henceforth refer to as "periodic LADs" (**Figures 4C** and **D**). Periodic LADs therefore constitute a subset of variable LADs with highly significant periodic oscillations in the genomic coverage in their 5′ or 3′ ends. These LADs withstand a randomization test of all replicates and CTs (see Materials and Methods section), suggesting that LAD periodicity observed in our data is imposed by the order of CTs. Periodic LADs include LADs with a stable core and variable borders, and LADs that entirely appear or disappear (**Figures 4C** and **D**). Altogether, our data indicate that significant periodicity in LAD border interactions with LMNB1 only concerns a minor set of LADs. Thus, the majority of LMNB1–chromatin interactions are conserved during the circadian cycle.

Periodic Gene Expression Is Uncoupled From Rhythmic LMNB1–Chromatin Interactions

We then examined the relationship between periodic LADs and gene expression. Out of 430 genes found in periodic LADs, only 68 genes are expressed, albeit with no periodicity (**Figures 5A** and **B**; **Supplementary Figure S4A**). Moreover, we find that the vast majority of periodic genes are outside LADs at any time point during the circadian cycle (only < 2% are in LADs; **Figure 5C**). We then examined genes located within 2.5 Mb of the 5′ or 3′ end of periodic LADs (523 genes). Most of these genes are expressed (437genes), among which ~10% are periodic, yet again with no dominant period and no temporal relationship to LAD periodicity (**Figure 5A**). Thus, since most genes reside outside LADs during the circadian cycle and no specific feature was identified in periodic LADs, we then determined at each CT the relationship between genes, and in particular periodic genes, and gene distance to the nearest LAD (see Materials and Methods). We find that the minimal distance occurred at CT12 while the maximal distance was detected at CT0 and CT24/30 (**Supplementary Figure S4B**). We thus examined the magnitude of variations in gene-to-nearest-LAD distance occurring between CT0 and CT12 and between CT12 and CT24 (to maintain 12-h intervals in both cases during a 24 h circadian time). Consistent with this transient gain in LAD coverage (see **Figure 3E**) and with the gene-poor content of LADs, we observe

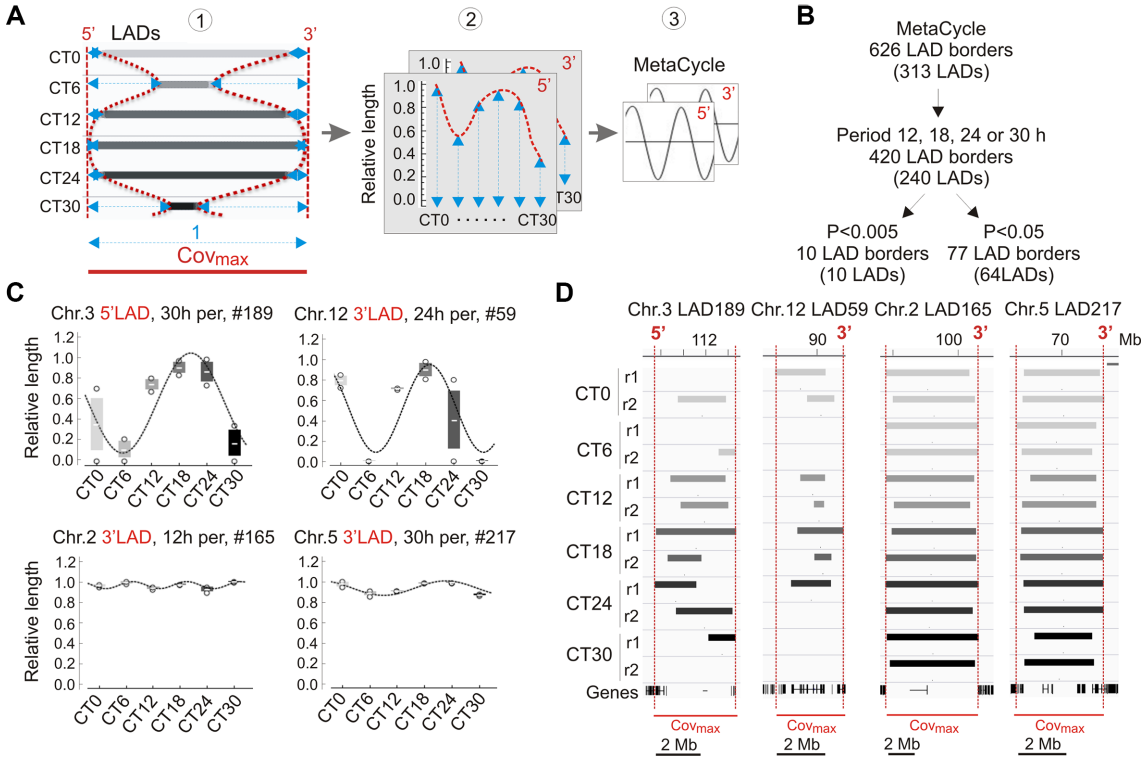

FIGURE 4 | Analysis of periodicity in genome coverage by LADs. **(A)** Approach to the identification of periodic LADs. (1) A variable LAD area is identified, for each LAD, across CTs and replicates (not shown here for clarity); the maximal merged area of these LADs is defined as Cov_{max} and distances from the 5′ and 3′ end of each LAD to the Cov_{max} limits are measured (blue arrows); (2) relative lengths are calculated at both the 5′ and 3′ end of LADs (1 = Cov_{max} length; 0 = no LAD); (3) MetaCycle is applied to identify periods at the 5′ and 3′ ends of LADs. **(B)** Identification of periodic LADs using MetaCycle. **(C)** Examples of periodic oscillations ($P < 0.005$; MetaCycle Fisher's exact test) in LAD 5′ and 3′ length during the circadian cycle among the 10 LADs identified by MetaCycle (see also **Table 1**); mean ± SD, individual data points and MetaCycle best-fit cosine curves are shown. **(D)** Genome browser views of periodic LADs shown in **(C)**. Red lines delimit Cov_{max} and the 5′/3′ numbering denotes the periodic LAD border shown in **(C)**.

an overall decrease in gene-to-nearest LAD distance between CT0 and CT12 (**Figure 5D**; data points in quadrants 1 and 2 and along the y axis, negative values), and for most genes, an increase thereafter, between CT12 and CT24 (data points in quadrant 2). These changes concern both periodic genes (*left panel*, green data points) and all other genes (*right panel*) regardless of the magnitude of this variation (**Figure 5D**; y axis negative values). Of note, the magnitude of this variation (**Figure 5E**) is larger than that of the intrinsic cumulated EDD error at each CT involved (see **Supplementary Table S2**, EDD error) and larger than the LAD variation between LAD intersects and replicates (see **Supplementary Table S7**, LAD variation).

We conclude that there is no correlation between periodicity in gene expression and variation in gene-to-nearest LAD distance. This variation appears to be caused by a transient gain in the number of LADs, the functional significance of which remains to be examined. Similarly, the central clock-regulating genes are typically megabases away from the nearest LAD (**Supplementary Table S9**; **Supplementary Figure S4C**), and promoter regions of these genes are also essentially devoid of LMNB1 interaction at any CT (**Supplementary Figure S4D**).

Altogether, our results argue for a constitutive localization of circadian genes, including clock regulators, in a chromatin environment essentially devoid of B-type lamin interactions, providing permissiveness for periodic transcriptional activation during the circadian cycle (Koike et al., 2012; Kim et al., 2018). Our findings argue that oscillatory expression of periodic genes, including central clock-control genes, is uncoupled from a direct association with the nuclear lamina or from their localization in the vicinity of periodic LADs.

TABLE 1 | Period of 5′ and 3′ significantly periodic LAD borders.

LAD no.	Chr.	5′ period (h)	3′ period (h)
15	1	–	12
165	2	–	12
167	2	24	–
189	3	30	–
194	3	–	12
217	5	–	30
239	7	–	18
262	8	12	–
36	10	18	–
59	12	24	–

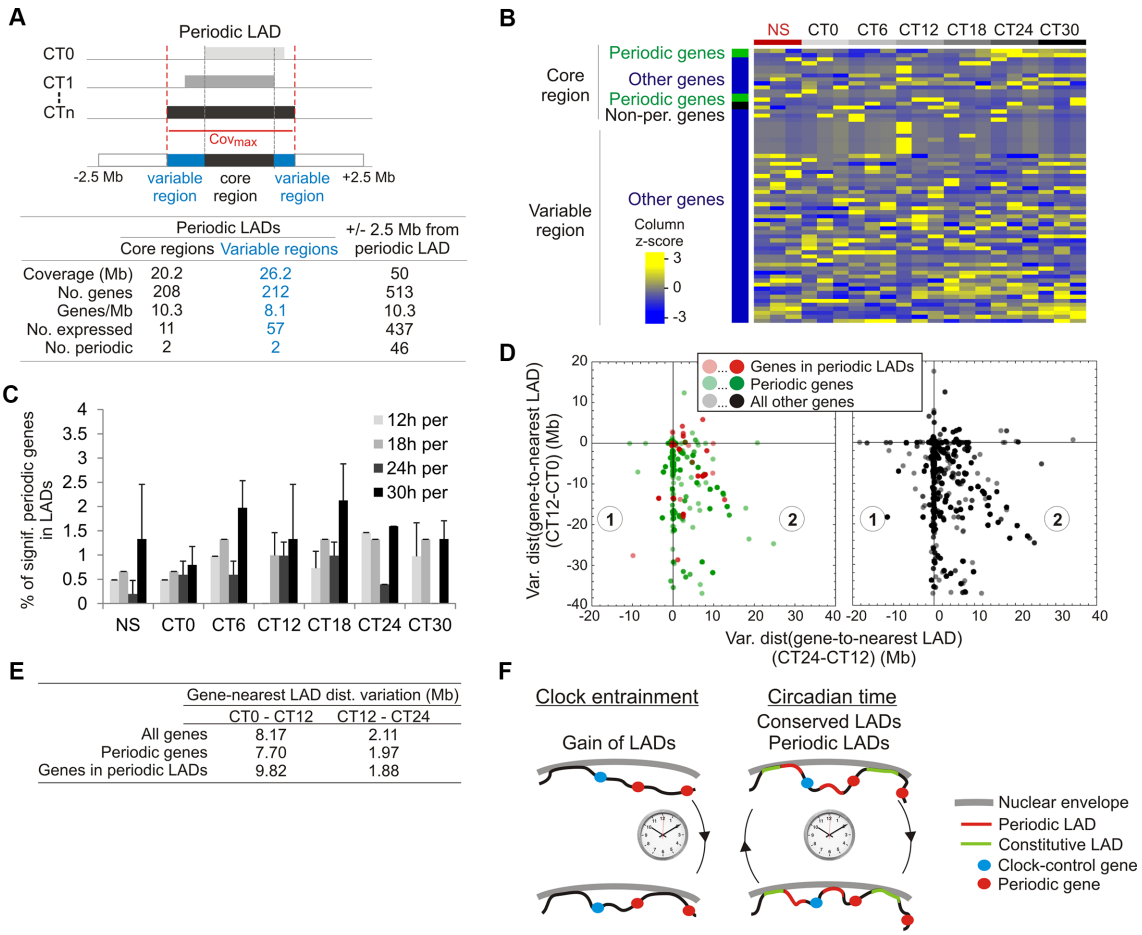

	Periodic LADs		+/- 2.5 Mb from periodic LAD
	Core regions	Variable regions	
Coverage (Mb)	20.2	26.2	50
No. genes	208	212	513
Genes/Mb	10.3	8.1	10.3
No. expressed	11	57	437
No. periodic	2	2	46

	Gene-nearest LAD dist. variation (Mb)	
	CT0 - CT12	CT12 - CT24
All genes	8.17	2.11
Periodic genes	7.70	1.97
Genes in periodic LADs	9.82	1.88

FIGURE 5 | Genes in or near periodic LADs do not display periodic expression. **(A)** Representation and gene statistics of the core and variable regions of the significantly periodic LADs. **(B)** Gene expression z-score of expressed genes (n = 63) localized in significantly periodic LADs, for each CT and replicate (n = 3). Genes are sorted by groups (indicated on the left) and within groups, by phase. **(C)** Percentages of significantly periodic genes ($P < 0.005$, MetaCycle Fisher's exact test) found in LADs at each CT. **(D)** Scatter plots of variations in gene-to-nearest LAD distances between CT0 and CT12 (y axis) and between CT12 and CT24 (x axis). One data-point represents a single gene or multiple genes at a particular coordinate on the graph, with color intensity reflecting the number of genes at that point. **(E)** Mean gene-to-nearest LAD distance variation. **(F)** Summary and model of oscillatory LAD patterns after entrainment of the circadian clock. Entrainment of the clock is accompanied by a net gain of LMNB1 LADs (bottom). During circadian time, most LADs are conserved (constitutive LADs) while a small number is periodic. Typical genomic positions of clock-control genes and periodic genes relative to these LADs are shown.

DISCUSSION

Oscillations in chromatin conformation mediated by rhythmic chromosomal interactions contribute to the regulation of circadian gene expression (Aguilar-Arnal et al., 2013; Xu et al., 2016; Kim et al., 2018; Mermet et al., 2018; Yeung et al., 2018). We now provide evidence of a net gain of lamin–chromatin interactions following entrainment of the circadian clock (NS-CT0 transition), which speculatively may reinforce the robustness of segregation of chromatin domains in the nucleus space.

Given the overall repressive chromatin environment at the nuclear periphery (van Steensel and Belmont, 2017), and evidence of cyclic recruitment and silencing of specific genes at the nuclear envelope in a human cancer cell line (Zhao et al., 2015), we reasoned that periodic gene expression could at least in part be regulated by periodic interactions with the nuclear lamina. We applied MetaCycle, a tool designed to identify periodic transcript oscillations (Wu et al., 2016), to identify periodic changes in genome coverage by LMNB1. Our approach distinguishes 5′ and 3′ LAD extension or shortening from entire LAD emergence or disappearance (**Figure 5F**). The gain of lamin–chromatin interactions between NS to CT0 is followed by periodic interactions of specific genomic regions with LMNB1, suggestive of discrete rhythmic associations with the nuclear lamina. Our ChIP approach would notably detect interactions of chromatin with nucleoplasmic LMNB1, which appear to be more euchromatic than peripheral LADs (Pascual-Reguant et al., 2018), suggesting that periodic LADs may also be nucleoplasmic. The detection of periodic LADs in our study adds to mounting evidence that chromatin is able to display oscillations in its 3-dimensional conformation (Kim et al., 2018).

Counterintuitively however, several points in our data argue that in the mouse liver, periodic gene expression is not directly

coupled to oscillating or periodic chromatin associations with the nuclear lamina. (1) Genes with periodic transcript levels reside outside LADs at any time point during the circadian cycle. This notably includes *Pard3*, which has been found to be periodically recruited to the nuclear envelope in human colon cancer cells (Zhao et al., 2015), but in mouse liver is localized 15 Mb away from the nearest (and conserved) LAD. (2) Similarly, our analysis reveals that central clock-control genes reside megabases away from the nearest LAD and show no promoter association with LMNB1. This configuration may keep these genes in a transcriptionally permissive ("lamin-free") environment throughout the circadian cycle, compatible with a regulation of circadian transcription by rhythmic TF binding and activity (Koike et al., 2012; Masri et al., 2014; Zhang et al., 2015). Our results also suggest that rhythmic chromatin looping activity which may regulate gene expression within TADs (Kim et al., 2018) take place in an environment where chromatin is not restrained by nuclear lamins (Bronshtein et al., 2015). (3) Periodic genes can also flank constitutive LADs and conversely, genes with stable (high or low) expression levels may flank periodic LADs. (4) Lastly, there is no relationship between periodic gene expression and gene-nearest LAD distance during the circadian cycle. We find that periodic genes are primarily involved in chromatin regulation, transcription regulation and several metabolic functions. Our data strongly suggest therefore that the periodic LAD patterns identified here in liver cannot readily explain these oscillatory gene expression patterns. In fact, periodic hepatic gene expression as a whole appears to be uncoupled from periodic chromatin association with the nuclear lamina.

Concurring with our results, other chromatin-linked processes are uncoupled from gene expression patterns. For example, many oscillatory genes display stable chromosomal interactions (Kim et al., 2018), including promoter–enhancer contacts (Beytebiere et al., 2019) during the circadian cycle. Conversely, many expressed genes display circadian oscillations in promoter and enhancer histone modification patterns that are irrespective of whether or not these genes are periodic or not (Koike et al., 2012). These observations highlight a complex and in some instances enigmatic cross-talk between circadian transcription and rhythmic changes in chromatin states.

Our findings raise several important issues. First, periodic LADs are not a prominent feature of LMNB1–chromatin interactions during the circadian cycle. Sixty-four LADs display variations in their 5′ and/or 3′ end coverage, but we only find, using our stringent approach, ten highly significantly periodic LADs, with asynchronous oscillations between their 5′ and 3′ borders. Yet, these variations withstand a randomization test, suggesting that rhythmicity is elicited by the underlying order of CTs (i.e. circadian time) rather than by random lamin–chromatin interactions. Our findings suggest therefore that the periodic LMNB1–chromatin interactions identified here represent a small subset of all variable interactions. Nevertheless, although we find no evidence of punctual interactions of LMNB1 with individual clock-control genes or promoters, it remains possible that a subset of genes, including periodic genes, display discrete circadian interactions with LMNB1 reminiscent of those shown in cancer cells (Zhao et al., 2015). In addition, periodic LADs do not seem to harbor any evident functional properties. This contrasts with developmentally regulated B-type lamin–chromatin interactions which have been reported during differentiation of mouse embryonic stem cells (Peric-Hupkes et al., 2010). On the other hand, differential LMNB1 LADs have also been reported in hepatocarcinoma cells treated with cyclosporin, albeit with no significant changes in gene expression (Forsberg et al., 2019), akin to what we observe in the liver. It remains to be examined whether LADs, and periodic LADs in particular, described here involve a level of regulation which currently remains unappreciated.

Second, how could periodic lamin–chromatin interactions be regulated? The cistrome of circadian genes can oscillate in a manner concordant with circadian gene expression (Feng et al., 2011; Fang et al., 2014; Zhang et al., 2015), thus factors mediating lamin–chromatin interactions may also be periodically recruited to target loci. Our transcriptome data indicate that several genes encoding BTB/POZ domain proteins oscillate during the circadian cycle. These proteins share DNA binding motifs enriched in LADs (Guelen et al., 2008) and in lamin-associated sequences (Zullo et al., 2012; Lund et al., 2013), and are found in sequences able to re-localize chromatin to the nuclear lamina (Harr et al., 2015). Thus, oscillating LADs could potentially be regulated through the periodic recruitment of factors important for chromatin localization at the nuclear periphery (Shachar et al., 2015). A search for protein binding motifs in the core and variable regions of periodic LADs using several tools including HOMER (Heinz et al., 2010) and the MEME suite (Bailey et al., 2009), however, revealed no significant enrichment in known motifs which could point to protein candidates mediating these periodic lamin–chromatin interactions. Speculatively, proteins of the inner nuclear membrane or bound to the nuclear lamina, through rhythmic post-translational modifications or through their periodic recruitment to these nuclear domains, could also mediate periodic interactions by direct or indirect interactions with chromatin. A discovery of the proteome of the nuclear periphery or of interactome of nuclear lamins during the circadian cycle would be valuable in the identification of periodic association of chromatin with the nuclear lamina.

Third, what would be the significance of oscillating, or taken more broadly, variable lamin–chromatin interactions and their impact on genome architecture? Resetting of LADs immediately after entrainment of the circadian clock may strengthen the robustness of liver-specific gene expression, possibly through a marked segregation of heterochromatin from euchromatin (Solovei et al., 2013; Falk et al., 2019). Oscillations of subsets of LADs, regardless of periodicity, may alter the radial positioning of chromatin and/or confer dynamic changes in chromatin states in regions that are in 3-dimensional proximity, but not necessarily in linear proximity. These changes altogether may affect gene expression in some of these regions (Robson et al., 2016; Paulsen et al., 2019), but not necessarily in all (Forsberg et al., 2019). LAD displacement may also result in radial repositioning of topological chromatin domains (Robson et al., 2016), or of regulatory elements (Robson et al., 2017).

Assessment of periodic LADs in a 3-dimensional context should shed light on the putative long-range impact of LAD dynamics on genome architecture and function.

DATA AVAILABILITY STATEMENT

Lamin B1 ChIP-seq and RNA-seq data have been deposited to the NCBI GEO database and are available under GEO accession No. GSE128675.

ETHICS STATEMENT

Animal procedures were approved by the Norwegian Regulatory Authorities (Approval No. 8565).

AUTHOR CONTRIBUTIONS

FF, AB and PC designed the study. FF and QF did wet-lab experiments. TS supervised parts of these experiments. AB did the bioinformatics analyses. AB and PC supervised the work and wrote the manuscript.

ACKNOWLEDGMENTS

We thank Dr. Nolwenn Briand and our missed colleague Professor Jan Øivind Moskaug for fruitful discussions. This work was funded by EU Marie Curie Scientia Fellowship FP7-PEOPLE-2013-COFUND No. 609020 (A.B.), the Research Council of Norway and South-East Health Norway. An earlier version of this manuscript has been released as a pre-print at: bioRxiv 584011; doi: https://doi.org/10.1101/584011 (Brunet et al., 2019).

SUPPLEMENTARY MATERIAL

The Supplementary Material for this article can be found online at: https://www.frontiersin.org/articles/10.3389/fgene.2019.00917/full#supplementary-material

REFERENCES

Aguilar-Arnal, L., Hakim, O., Patel, V. R., Baldi, P., Hager, G. L., and Sassone-Corsi, P. (2013). Cycles in spatial and temporal chromosomal organization driven by the circadian clock. *Nat. Struct. Mol. Biol.* 20, 1206–1213. doi: 10.1038/nsmb.2667

Aguilar-Arnal, L., Katada, S., Orozco-Solis, R., and Sassone-Corsi, P. (2015). NAD(+)-SIRT1 control of H3K4 trimethylation through circadian deacetylation of MLL1. *Nat. Struct. Mol. Biol.* 22, 312–318. doi: 10.1038/nsmb.2990

Bailey, T. L., Boden, M., Buske, F. A., Frith, M., Grant, C. E., Clementi, L., et al. (2009). MEME Suite: tools for motif discovery and searching. *Nucl. Acids Res.* 37, W202–W208. doi: 10.1093/nar/gkp335

Beytebiere, J. R., Trott, A. J., Greenwell, B. J., Osborne, C. A., Vitet, H., Spence, J., et al. (2019). Tissue-specific BMAL1 cistromes reveal that rhythmic transcription is associated with rhythmic enhancer–enhancer interactions. *Genes Dev.* 33, 294–309. doi: 10.1101/gad.322198.118

Bronshtein, I., Kepten, E., Kanter, I., Berezin, S., Lindner, M., Redwood, A. B., et al. (2015). Loss of lamin A function increases chromatin dynamics in the nuclear interior. *Nat. Commun.* 6, 8044. doi: 10.1038/ncomms9044

Brunet, A., Forsberg, F., and Collas, P. (2019). Rhythmic chromatin interactions with lamin B1 reflect stochasticity in variable lamina-associated domains during the circadian cycle. *bioRxiv*, 584011. doi: 10.1101/584011

Burke, B., and Stewart, C. L. (2013). The nuclear lamins: flexibility in function. *Nat. Rev. Mol. Cell Biol.* 14, 13–24. doi: 10.1038/nrm3488

Demmerle, J., Koch, A. J., and Holaska, J. M. (2013). Emerin and histone deacetylase 3 (HDAC3) cooperatively regulate expression and nuclear positions of MyoD, Myf5, and Pax7 genes during myogenesis. *Chromosome Res.* 21, 765–779. doi: 10.1007/s10577-013-9381-9

Falk, M., Feodorova, Y., Naumova, N., Imakaev, M., Lajoie, B. R., Leonhardt, H., et al. (2019). Heterochromatin drives compartmentalization of inverted and conventional nuclei. *Nature* 570, 395–399. doi: 10.1038/s41586-019-1275-3

Fang, B., Everett, L. J., Jager, J., Briggs, E., Armour, S. M., Feng, D., et al. (2014). Circadian enhancers coordinate multiple phases of rhythmic gene transcription *in vivo*. *Cell* 159, 1140–1152. doi: 10.1016/j.cell.2014.10.022

Feng, D., Liu, T., Sun, Z., Bugge, A., Mullican, S. E., Alenghat, T., et al. (2011). A circadian rhythm orchestrated by histone deacetylase 3 controls hepatic lipid metabolism. *Science* 331, 1315–1319. doi: 10.1126/science.1198125

Forsberg, F., Brunet, A., Ali, T. M. L., and Collas, P. (2019). Interplay of lamin A and lamin B LADs on the radial positioning of chromatin. *Nucleus* 10, 7–20. doi: 10.1080/19491034.2019.1570810

Ghosh, S., Liu, B., Wang, Y., Hao, Q., and Zhou, Z. (2015). Lamin A Is an Endogenous SIRT6 Activator and Promotes SIRT6-Mediated DNA Repair. *Cell Rep.* 13, 1396–1406. doi: 10.1016/j.celrep.2015.10.006

Guelen, L., Pagie, L., Brasset, E., Meuleman, W., Faza, M. B., Talhout, W., et al. (2008). Domain organization of human chromosomes revealed by mapping of nuclear lamina interactions. *Nature* 453, 948–951. doi: 10.1038/nature06947

Harr, J. C., Luperchio, T. R., Wong, X., Cohen, E., Wheelan, S. J., and Reddy, K. L. (2015). Directed targeting of chromatin to the nuclear lamina is mediated by chromatin state and A-type lamins. *J. Cell Biol.* 208, 33–52. doi: 10.1083/jcb.201405110

Hastings, M. H., Maywood, E. S., and Brancaccio, M. (2018). Generation of circadian rhythms in the suprachiasmatic nucleus. *Nat. Rev. Neurosci.* 19, 453–469. doi: 10.1038/s41583-018-0026-z

Heinz, S., Benner, C., Spann, N., Bertolino, E., Lin, Y. C., Laslo, P., et al. (2010). Simple combinations of lineage-determining transcription factors prime cis-regulatory elements required for macrophage and B cell identities. *Mol. Cell* 38, 576–589. doi: 10.1016/j.molcel.2010.05.004

Hughes, M. E., DiTacchio, L., Hayes, K. R., Vollmers, C., Pulivarthy, S., Baggs, J. E., et al. (2009). Harmonics of circadian gene transcription in mammals. *PLoS Genet.* 5, e1000442. doi: 10.1371/journal.pgen.1000442

Kim, Y. H., Marhon, S. A., Zhang, Y., Steger, D. J., Won, K. J., and Lazar, M. A. (2018). Rev-erbalpha dynamically modulates chromatin looping to control circadian gene transcription. *Science* 359, 1274–1277. doi: 10.1126/science.aao6891

Koike, N., Yoo, S. H., Huang, H. C., Kumar, V., Lee, C., Kim, T. K., et al. (2012). Transcriptional architecture and chromatin landscape of the core circadian clock in mammals. *Science* 338, 349–354. doi: 10.1126/science.1226339

Korencic, A., Kosir, R., Bordyugov, G., Lehmann, R., Rozman, D., and Herzel, H. (2014). Timing of circadian genes in mammalian tissues. *Sci. Rep.* 4, 5782. doi: 10.1038/srep05782

Langmead, B., and Salzberg, S. L. (2012). Fast gapped-read alignment with Bowtie 2. *Nat. Methods* 9, 357–359. doi: 10.1038/nmeth.1923

Langmead, B., Trapnell, C., Pop, M., and Salzberg, S. L. (2009). Ultrafast and memory-efficient alignment of short DNA sequences to the human genome. *Genome Biol.* 10, R25. doi: 10.1186/gb-2009-10-3-r25

Lin, S. T., Zhang, L., Lin, X., Zhang, L. C., Garcia, V. E., Tsai, C. W., et al. (2014). Nuclear envelope protein MAN1 regulates clock through BMAL1. *Elife* 3, e02981. doi: 10.7554/eLife.02981

Liu, B., Ghosh, S., Yang, X., Zheng, H., Liu, X., Wang, Z., et al. (2012). Resveratrol rescues SIRT1-dependent adult stem cell decline and alleviates progeroid features in laminopathy-based progeria. *Cell Metab.* 16, 738–750. doi: 10.1016/j.cmet.2012.11.007

Lund, E., Oldenburg, A., Delbarre, E., Freberg, C., Duband-Goulet, I., Eskeland, R., et al. (2013). Lamin A/C-promoter interactions specify chromatin state-dependent transcription outcomes. *Genome Res.* 23, 1580–1589. doi: 10.1101/gr.159400.113

Lund, E. G., Oldenburg, A. R., and Collas, P. (2014). Enriched Domain Detector: a program for detection of wide genomic enrichment domains robust against local variations. *Nucleic Acids Res.* 42, e92. doi: 10.1093/nar/gku324

Masri, S., Rigor, P., Cervantes, M., Ceglia, N., Sebastian, C., Xiao, C., et al. (2014). Partitioning circadian transcription by SIRT6 leads to segregated control of cellular metabolism. *Cell* 158, 659–672. doi: 10.1016/j.cell.2014.06.050

Mermet, J., Yeung, J., Hurni, C., Mauvoisin, D., Gustafson, K., Jouffe, C., et al. (2018). Clock-dependent chromatin topology modulates circadian transcription and behavior. *Genes Dev.* 32, 347–358. doi: 10.1101/gad.312397.118

Meuleman, W., Peric-Hupkes, D., Kind, J., Beaudry, J. B., Pagie, L., Kellis, M., et al. (2013). Constitutive nuclear lamina–genome interactions are highly conserved and associated with A/T-rich sequence. *Genome Res.* 23, 270–280. doi: 10.1101/gr.141028.112

Naetar, N., Ferraioli, S., and Foisner, R. (2017). Lamins in the nuclear interior — life outside the lamina. *J. Cell Sci.* 130, 2087–2096. doi: 10.1242/jcs.203430

Nakahata, Y., Kaluzova, M., Grimaldi, B., Sahar, S., Hirayama, J., Chen, D., et al. (2008). The NAD+-dependent deacetylase SIRT1 modulates CLOCK-mediated chromatin remodeling and circadian control. *Cell* 134, 329–340. doi: 10.1016/j.cell.2008.07.002

Neph, S., Kuehn, M. S., Reynolds, A. P., Haugen, E., Thurman, R. E., Johnson, A. K., et al. (2012). BEDOPS: high-performance genomic feature operations. *Bioinformatics* 28, 1919–1920. doi: 10.1093/bioinformatics/bts277

Pascual-Reguant, L., Blanco, E., Galan, S., Le Dily, F., Cuartero, Y., Serra-Bardenys, G., et al. (2018). Lamin B1 mapping reveals the existence of dynamic and functional euchromatin lamin B1 domains. *Nat. Commun.* 9, 3420. doi: 10.1038/s41467-018-05912-z

Paulsen, J., Liyakat Ali, T. M., Nekrasov, M., Delbarre, E., Baudement, M. O., Kurscheid, S., et al. (2019). Long-range interactions between topologically associating domains shape the four-dimensional genome during differentiation. *Nat. Genet.* 51, 835–843. doi: 10.1038/s41588-019-0392-0

Peric-Hupkes, D., Meuleman, W., Pagie, L., Bruggeman, S. W., Solovei, I., Brugman, W., et al. (2010). Molecular maps of the reorganization of genome–nuclear lamina interactions during differentiation. *Mol. Cell* 38, 603–613. doi: 10.1016/j.molcel.2010.03.016

Poleshko, A., Shah, P. P., Gupta, M., Babu, A., Morley, M. P., Manderfield, L. J., et al. (2017). Genome–nuclear lamina interactions regulate cardiac stem cell lineage restriction. *Cell* 171, 573–587. doi: 10.1016/j.cell.2017.09.018

Quinlan, A. R., and Hall, I. M. (2010). BEDTools: a flexible suite of utilities for comparing genomic features. *Bioinformatics* 26, 841–842. doi: 10.1093/bioinformatics/btq033

Robinson, J. T., Thorvaldsdottir, H., Winckler, W., Guttman, M., Lander, E. S., Getz, G., et al. (2011). Integrative genomics viewer. *Nat. Biotechnol.* 29, 24–26. doi: 10.1038/nbt.1754

Robson, M. I., de Las Heras, J. I., Czapiewski, R., Le Thanh, P., Booth, D. G., Kelly, D. A., et al. (2016). Tissue-specific gene repositioning by muscle nuclear membrane proteins enhances repression of critical developmental genes during myogenesis. *Mol. Cell* 62, 834–847. doi: 10.1016/j.molcel.2016.04.035

Robson, M. I., de Las Heras, J. I., Czapiewski, R., Sivakumar, A., Kerr, A. R. W., and Schirmer, E. C. (2017). Constrained release of lamina-associated enhancers and genes from the nuclear envelope during T-cell activation facilitates their association in chromosome compartments. *Genome Res.* 27, 1126–1138. doi: 10.1101/gr.212308.116

Rønningen, T., Shah, A., Oldenburg, A. R., Vekterud, K., Delbarre, E., Moskaug, J. O., et al. (2015). Prepatterning of differentiation-driven nuclear lamin A/C-associated chromatin domains by GlcNAcylated histone H2B. *Genome Res.* 25, 1825–1835. doi: 10.1101/gr.193748.115

Sen Gupta, A., and Sengupta, K. (2017). Lamin B2 Modulates Nucleolar Morphology, Dynamics, and Function. *Mol. Cell Biol.* 37, e00274–e00217. doi: 10.1128/MCB.00274-17

Shachar, S., Voss, T. C., Pegoraro, G., Sciascia, N., and Misteli, T. (2015). Identification of gene positioning factors using high-throughput imaging mapping. *Cell* 162, 911–923. doi: 10.1016/j.cell.2015.07.035

Shi, G., Xie, P., Qu, Z., Zhang, Z., Dong, Z., An, Y., et al. (2016). Distinct roles of HDAC3 in the core circadian negative feedback loop are critical for clock function. *Cell Rep.* 14, 823–834. doi: 10.1016/j.celrep.2015.12.076

Solovei, I., Wang, A. S., Thanisch, K., Schmidt, C. S., Krebs, S., Zwerger, M., et al. (2013). LBR and lamin A/C sequentially tether peripheral heterochromatin and inversely regulate differentiation. *Cell* 152, 584–598. doi: 10.1016/j.cell.2013.01.009

Somech, R., Shaklai, S., Geller, O., Amariglio, N., Simon, A. J., Rechavi, G., et al. (2005). The nuclear-envelope protein and transcriptional repressor LAP2beta interacts with HDAC3 at the nuclear periphery, and induces histone H4 deacetylation. *J. Cell Sci.* 118, 4017–4025. doi: 10.1242/jcs.02521

Tahara, Y., Otsuka, M., Fuse, Y., Hirao, A., and Shibata, S. (2011). Refeeding after fasting elicits insulin-dependent regulation of Per2 and Rev-erbalpha with shifts in the liver clock. *J. Biol. Rhythms* 26, 230–240. doi: 10.1177/0748730411405958

Takahashi, J. S. (2017). Transcriptional architecture of the mammalian circadian clock. *Nat. Rev. Genet.* 18, 164–179. doi: 10.1038/nrg.2016.150

Trapnell, C., Williams, B. A., Pertea, G., Mortazavi, A., Kwan, G., van Baren, M. J., et al. (2010). Transcript assembly and quantification by RNA-Seq reveals unannotated transcripts and isoform switching during cell differentiation. *Nat. Biotechnol.* 28, 511–515. doi: 10.1038/nbt.1621

van Steensel, B., and Belmont, A. S. (2017). Lamina-associated domains: links with chromosome architecture, heterochromatin, and gene repression. *Cell* 169, 780–791. doi: 10.1016/j.cell.2017.04.022

Vollmers, C., Schmitz, R. J., Nathanson, J., Yeo, G., Ecker, J. R., and Panda, S. (2012). Circadian oscillations of protein-coding and regulatory RNAs in a highly dynamic mammalian liver epigenome. *Cell Metab.* 16, 833–845. doi: 10.1016/j.cmet.2012.11.004

Wu, G., Anafi, R. C., Hughes, M. E., Kornacker, K., and Hogenesch, J. B. (2016). MetaCycle: an integrated R package to evaluate periodicity in large scale data. *Bioinformatics* 32, 3351–3353. doi: 10.1093/bioinformatics/btw405

Xu, Y., Guo, W., Li, P., Zhang, Y., Zhao, M., Fan, Z., et al. (2016). Long-range chromosome interactions mediated by cohesin shape circadian gene expression. *PLoS Genet.* 12, e1005992. doi: 10.1371/journal.pgen.1005992

Yeung, J., Mermet, J., Jouffe, C., Marquis, J., Charpagne, A., Gachon, F., et al. (2018). Transcription factor activity rhythms and tissue-specific chromatin interactions explain circadian gene expression across organs. *Genome Res.* 28, 182–191. doi: 10.1101/gr.222430.117

Yeung, J., and Naef, F. (2018). Rhythms of the Genome: Circadian dynamics from chromatin topology, tissue-specific gene expression, to behavior. *Trends Genet.* 34, 915–926. doi: 10.1016/j.tig.2018.09.005

Zhang, Y., Fang, B., Emmett, M. J., Damle, M., Sun, Z., Feng, D., et al. (2015). Discrete functions of nuclear receptor Rev-erbalpha couple metabolism to the clock. *Science* 348, 1488–1492. doi: 10.1126/science.aab3021

Zhao, H., Sifakis, E. G., Sumida, N., Millan-Arino, L., Scholz, B. A., Svensson, J. P., et al. (2015). PARP1- and CTCF-mediated interactions between active and repressed chromatin at the lamina promote oscillating transcription. *Mol. Cell* 59, 984–997. doi: 10.1016/j.molcel.2015.07.019

Zhu, B., Zhang, Q., Pan, Y., Mace, E. M., York, B., Antoulas, A. C., et al. (2017). A Cell-autonomous mammalian 12 hr clock coordinates metabolic and stress rhythms. *Cell Metab.* 25, 1305–1319 e1309. doi: 10.1016/j.cmet.2017.05.004

Zullo, J. M., Demarco, I. A., Pique-Regi, R., Gaffney, D. J., Epstein, C. B., Spooner, C. J., et al. (2012). DNA sequence-dependent compartmentalization and silencing of chromatin at the nuclear lamina. *Cell* 149, 1474–1487. doi: 10.1016/j.cell.2012.04.035

Conflict of Interest: The authors declare that the research was conducted in the absence of any commercial or financial relationships that could be construed as a potential conflict of interest.

frontiers in Genetics

ORIGINAL RESEARCH
published: 17 October 2019
doi: 10.3389/fgene.2019.01029

Assessment of the Utility of Gene Positioning Biomarkers in the Stratification of Prostate Cancers

Karen J. Meaburn and Tom Misteli**

Cell Biology of Genomes Group, National Cancer Institute, NIH, Bethesda, MD, United States

There is a pressing need for additional clinical biomarkers to predict the aggressiveness of individual cancers. Here, we examine the potential usefulness of spatial genome organization as a prognostic tool for prostate cancer. Using fluorescence *in situ* hybridization on formalin-fixed, paraffin embedded human prostate tissue specimens, we compared the nuclear positions of four genes between clinically relevant subgroups of prostate tissues. We find that directional repositioning of *SP100* and *TGFB3* gene loci stratifies prostate cancers of differing Gleason scores. A more peripheral position of *SP100* and *TGFB3* in the nucleus, compared to benign tissues, is associated with low Gleason score cancers, whereas more internal positioning correlates with higher Gleason scores. Conversely, *LMNA* is more internally positioned in many non-metastatic prostate cancers, while its position is indistinguishable from benign tissue in metastatic cancer. The false positive rates were relatively low, whereas, the false negative rates of single or combinations of genes were high, limiting the clinical utility of this assay in its current form. Nevertheless, our findings of subtype-specific gene positioning patterns in prostate cancer provides proof-of-concept for the potential usefulness of spatial gene positioning for prognostic applications, and encourage further exploration of spatial gene positioning patterns to identify novel clinically relevant molecular biomarkers, which may aid treatment decisions for cancer patients.

Keywords: spatial genome organization, spatial gene positioning, gene positioning biomarkers, prostate cancer, cancer stratification

OPEN ACCESS

Edited by:
Evi Soutoglou, INSERM U964 Institut de Génétique et de Biologie Moléculaire et Cellulaire (IGBMC), France

Reviewed by:
Janine M. LaSalle, University of California, Davis, United States
Alexander Kouzmenko, Tokiwa Foundation, Japan

****Correspondence***
Karen J. Meaburn
meaburnk@mail.nih.gov; kmeaburn@hotmail.com
Tom Misteli
mistelit@mail.nih.gov

Specialty section:
This article was submitted to Epigenomics and Epigenetics, a section of the journal Frontiers in Genetics

Received: *01 August 2019*
Accepted: *25 September 2019*
Published: *17 October 2019*

Citation:
Meaburn KJ and Misteli T (2019) Assessment of the Utility of Gene Positioning Biomarkers in the Stratification of Prostate Cancers. Front. Genet. 10:1029. doi: 10.3389/fgene.2019.01029

INTRODUCTION

The genome is highly spatially organized within the interphase nucleus (Cremer and Cremer, 2001; Bickmore, 2013). Most chromosomes, genes, and individual non-coding regions of the genome occupy preferred nuclear positions relative to the center of the nucleus or to other nuclear landmarks, such as associations with other genomic loci or nuclear bodies (Takizawa et al., 2008b; Bickmore and van Steensel, 2013; Meaburn, 2016). Some loci alter their position under different physiological conditions, for example, between cell/tissue types (Boyle et al., 2001; Parada et al., 2004; Peric-Hupkes et al., 2010; Meaburn et al., 2016) or between different proliferation states (Bridger et al., 2000; Meaburn and Misteli, 2008; Chandra et al., 2015). Spatial reorganization of the genome is also

Abbreviations: BAC, bacterial artificial chromosome; EDT, Euclidean distance transform; FISH, fluorescence *in situ* hybridization; FFPE, formalin-fixed, paraffin embedded; GPB, gene positioning biomarker; HSA, human chromosome; KS test, Kolmogorov-Smirnov test; NAT, normal adjacent to tumor; PND, pooled normal distribution; PSA, serum prostate specific antigen; RRD, relative radial distribution; TMA, tissue microarray.

a common feature of disease, and has been documented in a wide range of pathologies, including epilepsy (Borden and Manuelidis, 1988), Down syndrome (Paz et al., 2015), laminopathies (Meaburn et al., 2007; Mewborn et al., 2010), viral and parasitic infections (Li et al., 2010; Knight et al., 2011), and cancer (Meaburn, 2016; Mai, 2018). Repositioning events are loci-specific and do not reflect global genome reorganization events (Meaburn, 2016).

Although the spatial organization of the genome has been studied for decades, how gene positioning patterns are established and maintained remains largely elusive. It is also unclear if the nuclear position of a locus is important for function or is largely a consequence of nuclear activities (Meaburn, 2016). Most often, a functional link is drawn between spatial genome organization and gene expression (Brown et al., 1997; Brickner and Walter, 2004; Williams et al., 2006; Takizawa et al., 2008a; Peric-Hupkes et al., 2010), however, there are also many instances where changes in gene expression and nuclear position of a locus are unrelated (Scheuermann et al., 2004; Williams et al., 2006; Kumaran and Spector, 2008; Meaburn and Misteli, 2008; Harewood et al., 2010; Meaburn, 2016). Most likely, there are multiple mechanisms in play to determine the spatial organization of the genome (Shachar et al., 2015; Meaburn, 2016; Randise-Hinchliff et al., 2016). In addition to gene expression, chromatin modifications, even in the absence of changes in gene expression (Towbin et al., 2012; Therizols et al., 2014; Harr et al., 2016; Cabianca et al., 2019; Falk et al., 2019), replication timing (Hiratani et al., 2008) and a variety of structural nuclear proteins (Dundr et al., 2007; Meaburn et al., 2007; Solovei et al., 2013; Zuleger et al., 2013; Shachar et al., 2015) have be implicated in the positioning of genomic loci.

While the mechanisms governing spatial positioning patterns are unclear, the fact that the genome is spatially reorganized in disease begs the question of whether spatial positioning patterns can be exploited for clinical purposes (Meaburn, 2016; Mai, 2018). We have previously demonstrated that the positioning patterns of some genes can be used to reproducibly and accurately discriminate benign breast and prostate tissues from cancerous ones (Meaburn et al., 2009; Leshner et al., 2016; Meaburn et al., 2016). For instance, the positioning patterns of *HES5* and *FLI1* are highly indicative of cancer, with both *HES5* and *FLI1* repositioned in 100% of breast cancers and *FLI1* repositioned in 92.9% of prostate cancers, compared to benign tissue controls (Meaburn et al., 2009; Leshner et al., 2016; Meaburn et al., 2016). High repositioning rates result in low false negative detection rates. Crucially for diagnostic applications, many of the genes that reproducibly reposition in cancer show limited variability between morphologically normal tissues and do not reposition in benign disease, yielding low false positive detection rates (Meaburn et al., 2009; Leshner et al., 2016; Meaburn et al., 2016). Given the sensitivity and specificity for the positioning patterns of several genes in detecting cancer, these small-scale studies suggest gene positioning biomarkers (GPBs) could be a useful addition to cancer diagnostics.

Prostate cancer is a leading cause of cancer and cancer-related deaths (Bray et al., 2018). As with most cancers, while there is value in additional diagnostic biomarkers, there is also a critical need for additional prognostic biomarkers, to predict best treatment options, including to reduce overtreatment in patients whose cancer would have remained asymptomatic during their lifetime without treatment (Welch and Black, 2010; Sandhu and Andriole, 2012). Currently, the cornerstone of predicating a patient's outcome is the Gleason grading system, which is based on histological assessment (Epstein et al., 2005; Brimo et al., 2013). In this system the architectural structure of the prostate tissue is graded from Gleason grade 1, which represents a well differentiated tissue morphology, to the very poorly differentiated Gleason grade 5. The two most prominent Gleason grades in a given tumor/biopsy are summed to give a Gleason score (Epstein et al., 2005; Epstein, 2018). Low Gleason score cancers are more likely to be indolent, whereas higher Gleason scores correlates with poor outcomes (Albertsen et al., 1998; Pound et al., 1999; Brimo et al., 2013). However, further markers are required as there is a range in outcomes for patients with the same Gleason score.

To improve on the Gleason system, additional clinical factors, most commonly serum prostate-specific antigen (PSA) levels, T stage (size of tumor/spread to nearby tissues), percentage of cancer positive biopsy cores, and patient age are taken into account (D'Amico et al., 1998; Thompson et al., 2007; Cooperberg et al., 2009; Chang et al., 2014). ~15% of patients are diagnosed with high-risk (likely to cause morbidity, recur, metastasize and/or be lethal) prostate cancer, based on PSA levels of >20ng/ml and/or Gleason score of 8-10 and/or T stage of either T2c-T4 or T3a-T4, depending on the classification system (Thompson et al., 2007; Cooperberg et al., 2009; Chang et al., 2014). Low-risk cancers (PSA <10ng/ml, Gleason score 2-6, and T stage T1-T2a) are generally predicted to remain asymptomatic during the patient's lifetime and the use of active surveillance/watchful waiting is often recommended, as opposed to active treatment (Thompson et al., 2007; Cooperberg et al., 2009). Conversely, intermediate risk (Gleason score 7 or T stage T2b/c) patients generally receive treatment (Thompson et al., 2007; Cooperberg et al., 2010). Gleason scores can be subject to inter- and intra-observer variability, usually of just a single Gleason score (Montironi et al., 2005), but for patients at the border of low and intermediate risk this may make the difference of receiving treatment or not. Moreover, with the current clinical criteria to stratify risk, both over- and under-treatment remains a concern for all prostate cancer risk groups (Cooperberg et al., 2010; Punnen and Cooperberg, 2013). Improved markers are needed to better distinguish indolent from high-risk prostate cancers and to aid classification of intermediate-risk cancers, to reduce overtreatment and optimize therapeutic strategies.

There is a growing number of genomic prognostic biomarkers for prostate cancer, including several commercial assays based on the DNA methylation status of a small number of genes or on gene expression (Kornberg et al., 2018). Additionally, changes to nuclear size and shape and gross chromatin texture, which are not considered in Gleason scoring, provide additional predictive power to detect aggressive prostate cancers (Veltri and Christudass, 2014; Hveem et al., 2016). Few studies have assessed the prognostic potential of the spatial organization of the genome. The most compelling evidence for prognostic GPBs comes from telomeres, where increased telomeric aggregation correlates with progression and risk in several types of cancers (Mai, 2018). Similarly, in a single acute myeloid leukemia patient, HSA8 and 21 became more proximal to each other while the patient was in

remission, prior to a disease relapse and re-emergence of t(8;21) in the patient's bone marrow (Tian et al., 2015).

Here, we explore the utility of spatial gene positioning patterns to identify clinically distinct subgroups of prostate cancer. We find subtype-specific positioning for *SP100*, *TGFB3* and *LMNA*. The direction in which *SP100* and *TGFB3* reposition, compared to benign tissue, distinguishes low and intermediate/high Gleason score cancers, whereas *LMNA* repositions in many non-metastatic cancers but not in metastatic cancers. Although the sensitivity of this assay is currently too low to be clinically useful, our findings of subtype-specific gene positioning patterns in prostate cancer provides additional evidence for the potential of spatial genome organization as a novel prognostic biomarker.

MATERIALS AND METHODS

Tissue Fluorescence *In Situ* Hybridization (FISH)

4-5μm thick normal, benign disease (hyperplasia and chronic prostatitis), and cancerous formalin-fixed, paraffin embedded (FFPE) human prostate tissues were obtained from US Biomax Inc, Imgenex Corporation, BioChain Institute, or the University of Washington (Prof. Lawrence True) under the guidelines and approval of the Institutional Review Board of the University of Washington (#00-3449) (**Supplementary Table 1**). Patient tissues were de-identified before receipt.

To generate probe DNA for FISH, bacterial artificial chromosome (BAC) clones were labeled with biotin- (Roche), digoxigenin- (Roche) or DY-547P1- (Dyomics GmbH) conjugated dUTPs by nick translation (Meaburn, 2010). The following BACs were used: RP11-727M18 (to position *SP100*, chromosome location: 2q37.1); RP11-270M14 (*TGFB3,* 14q24.3); RP11-1021J5 (*SATB1*, 3p24.3); RP11-35P22 (*LMNA*, 1q22) (BACPAC resource center). Single- or dual-probe FISH experiments were performed as previously described (Meaburn et al., 2009; Leshner et al., 2016; Meaburn et al., 2016), with the following modifications: for most tissues a 1 hour 60°C bake step was performed, prior to the xylenes (Macron Fine Chemicals) deparaffinization step; 40μg yeast RNA (Life Technologies) was used in place of tRNA; DyLight 488 labeled anti-digoxigenin (Vector Laboratories) was occasionally used to detect digoxigenin-labeled probe DNA; and no probe detection steps were required for the fluorescently labeled DY-547P1-dUTP FISH probes.

Image Acquisition

Epithelial nuclei were randomly imaged throughout the tissue, unless benign and malignant glands were present in the same tissue section. In such cases, care was taken to image and analyze the different morphologies separately, whilst still acquiring epithelial cell nuclei randomly within the benign or malignant regions to capture as much diversity within the cancer (or benign tissue) as possible. Image accusation was performed as previously described, using an IX70 (Olympus) Deltavision (Applied Precision) system, with a 60x 1.42N oil objective lens (Olympus), an auxiliary magnification of 1.6, and a X-Y pixel size of 67.25nm (Meaburn et al., 2009; Leshner et al., 2016; Meaburn et al., 2016) or with a similar imaging regime using an IX71 (Olympus) Deltavision (Applied Precision) system, 100x 1.40N oil objective lens (Olympus), with an X-Y pixel size of 64.6nm. Image stacks were acquired to cover the thickness of the tissue section, with a 0.5μm or 0.25μm step interval along the Z axis, respectively. All image stacks were deconvolved and converted to maximum intensity projections using SoftWoRx (Applied Precision). The change in acquisition approach did not affect the resulting positioning data from the image datasets. We obtained similarly statistically identical distributions for the position of a gene in a given tissue using the two different acquisition methods (P = 0.79-0.86, Kolmogorov-Smirnov (KS) test), as from repeat analysis of tissues using an identical acquisition method (P = 0.65-0.99 (Meaburn et al., 2009), unpublished data).

Image Analysis

Image analysis to determine the radial position of a gene within a tissue was performed as previously described (Meaburn et al., 2009; Leshner et al., 2016; Meaburn et al., 2016). Briefly, 96-167 interphase epithelial nuclei were manually segmented in Photoshop (Adobe) for each gene in each tissue, except for *TGFB3* in tissue C10 where 88 nuclei were segmented. To map the radial position of the gene loci, nuclei were run though custom image analysis software scripts, using MATLAB (The Mathsworks Inc.), with DIPImage and PRTools toolboxes [Deft University, P. Gudla and S Lockett (NCI/NIH); (Meaburn et al., 2009)]. Euclidean distance transform (EDT) was computed for each nucleus, to assign every pixel within the nucleus its distance to the nearest nuclear boundary. The software then determined the nuclear EDT position of the geometric gravity center of the automatically detected FISH signals. To normalize for variations in nuclear size and shape between specimens, the EDT of a FISH signal was normalized to the maximal nuclear EDT for that nucleus, with 0 denoting the nuclear periphery and 1 the nuclear center. The normalized FISH signal EDTs for a given gene in each specimen was then combined to produce a relative radial distribution (RRD), and a cumulative frequency distribution was generated. All detected alleles in a nucleus were included, regardless of the number present. In the case of the pooled normal distributions (PNDs), the normalized FISH EDTs from all allele in all the normal tissues analyzed, for a given gene, were combined into a single dataset (**Supplementary Figure 1**). The number of nuclei and tissues used in each PND were as follows: the *SP100* PND contained 845 nuclei from 7 normal tissues; *TGFB3*, 996 nuclei from 8 normal tissues; *SATB1*, 874 nuclei from 7 normal tissues; and *LMNA*, 725 nuclei from 6 normal tissues. Finally, to statistically compare a gene's positioning patterns, RRDs between tissues, or between specimens and the PND, were cross-compared using the nonparametric two-sample 1D KS test, where $P < 0.01$ was considered significant.

Some previously reported RRDs were included in the current analysis [**Supplementary Table 1**; (Leshner et al., 2016; Meaburn et al., 2016)], which were compared to an update PND. The four PNDs used in this study included normal tissues N6 and N7, in addition to the normal tissues previously reported, which did not affect the RRDs (P = 0.83-1, 1D KS test). RRDs for *TGFB3* in tissues C25, C27, B9, N3, N4, N11-14 were previously reported in

(Meaburn et al., 2016), and the RRDs of *SP100* in C11, C12, C13, C25, N1, N2, N6-10, *SATB1* in C11, C12, C13, C25, B9, N1, N2, N6-10, and *LMNA* in C11, C18, C19, N5, N10 and N15-16 were reported in (Leshner et al., 2016).

RESULTS

Mapping of Candidate Genes in Prostate Tissues

We have previously identified genes that radially reposition in breast and/or prostate cancer and have demonstrated their potential as diagnostic biomarkers (Meaburn et al., 2009; Leshner et al., 2016; Meaburn et al., 2016). Here, we sought to extend these studies to determine if candidate genes occupied distinct nuclear positions between different subgroups of prostate cancer, with the goal of assessing their utility for cancer prognostics. To identify prognostic candidate genes we took advantage of our previous studies, in which we had screened the radial positions of 47 genes in a panel of prostate cancers (Leshner et al., 2016; Meaburn et al., 2016). From that gene set we chose two genes, *SATB1* and *LMNA*, for further assessment as potential biomarkers of high-risk prostate cancer because both genes repositioned in a single high-risk T3 stage cancer, but not in two intermediate risk T2 cancers, or a low risk T2 cancer (Leshner et al., 2016). We also selected *SP100* to test its potential as a marker of low risk, since we previously found it to reposition in a low risk Gleason score 6 prostate cancer, but not in three intermediate or high-risk Gleason score 7 cancers (Leshner et al., 2016). Finally, we selected *TGFB3* for further analysis since it repositioned in one of two low risk Gleason score 6 prostate cancers, but not in two prostate cancers of unknown Gleason score and TNM stage (Meaburn et al., 2016), representing a potential low-risk/indolent prostate cancer biomarker.

To determine whether the positioning patterns of these genes were able to stratify prostate cancers into clinically relevant subgroups, we performed FISH on a panel of 4-5μm thick FFPE human prostate tissues, which included a diverse group of 32 prostate cancer specimens covering a range of Gleason scores and T stages, with and without known metastases, and 25 benign prostate tissues (for details see **Supplementary Table 1**). To map the spatial positioning pattern of a gene in a given tissue, we measured the radial position, normalized for nuclear size and shape, of each locus in ~120 epithelial interphase nuclei as previously described (see Materials and Methods; (Meaburn et al., 2009; Leshner et al., 2016; Meaburn et al., 2016). The normalized radial position of each gene was determined and the cumulative RRDs were statistically compared to a PND, a standardized normal distribution created by pooling all nuclei from normal tissues for a given gene, or individual tissues using the 1D KS test, with $P < 0.01$ considered significant (see Materials and Methods, (Meaburn et al., 2009; Leshner et al., 2016; Meaburn et al., 2016), **Supplementary Figure 1**).

We initially assessed the repositioning rates for the candidate genes in the assorted set of prostate cancer samples. Compared to the PND, *SP100* was in a statistically significantly different radial position in 44.4% (12/27) prostate cancer specimens (**Figure 1**, **Table 1**, **Supplementary Table 2**). Similarly, *LMNA*

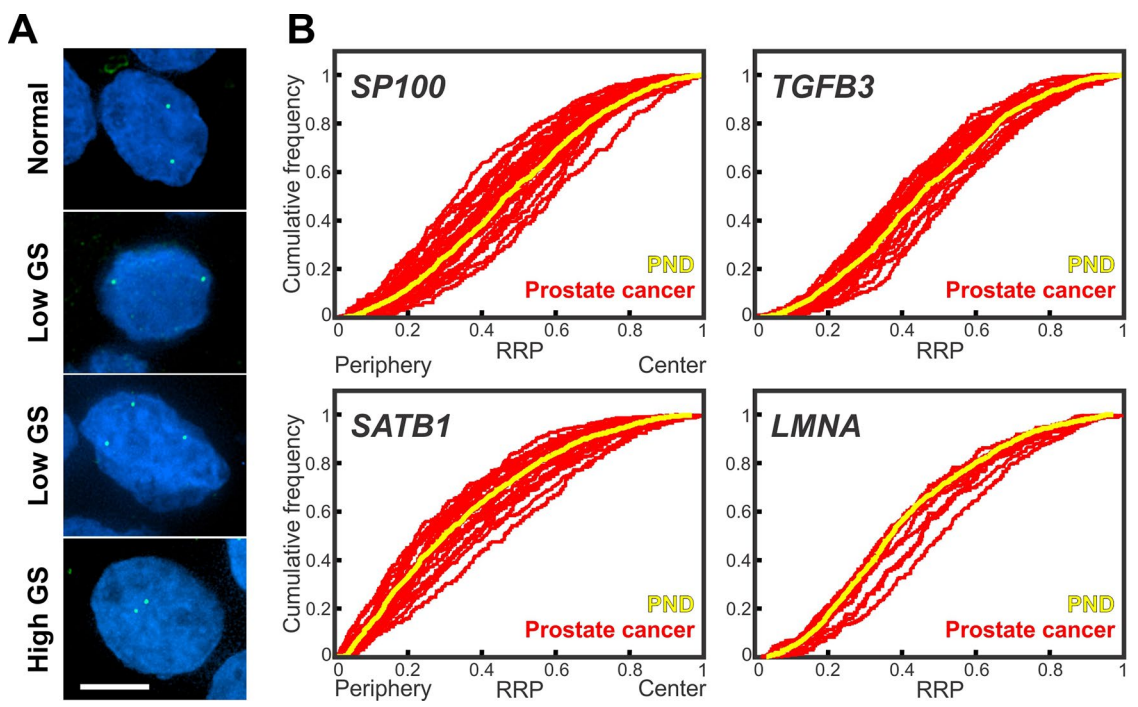

FIGURE 1 | Gene positioning in prostate cancer tissues **(A)** Gene loci were detected by FISH in FFPE prostate tissue sections. *SP100* gene loci (green) in normal and cancerous prostate tissues. GS, Gleason score. Projected image stacks shown. Nuclei were counterstain with DAPI (blue). Scale bar, 5μm. **(B)** Cumulative RRDs for the indicated genes in prostate cancer (red) and the pooled normal distribution (PND; Yellow). RRP, relative radial position.

TABLE 1 | Spatial repositioning of target genes in prostate cancer.

Tissue	*SP100*	*TGFB3*	*SATB1*	*LMNA*	Gleason score	Gleason Grade	TNM	Risk
C1	I				9 (4 + 5)	4	T3N0M1	High
C2					9 (5 + 4)	4-5	T2N1M1c	High
C3			I		9 (5 + 4)	5	T3aN0M0	High
C4	I				8 (4 + 4)	4	T3N0M0	High
C5				I	9 (4 + 5)		T2N0M0	High
C6	P	I	P		9 (4 + 5)		T2N0M0	High
C7		I			9 (4 + 5)		T2N0M0	High
C8		P	P		8 (4 + 4)	4	Unknown	High
C9					7 (3 + 4)	4	T3N0M1b	High
C10					7 (3 + 4)	3	T4N1M1c	High
C11			I	I	7	3	T3N0	High
C12					7	3	T2N0	Intermediate
C13					7	3	T2N0	Intermediate
C14		I	P		7 (3 + 4)		T2N0M0	Intermediate
C15	I		I		7 (3 + 4)	4	T2N0M0	Intermediate
C16	I				7 (3 + 4)	4	T2N0M0	Intermediate
C17	I				7 (3 + 4)		T1N0M0	Intermediate
C18					7		T2N0	Intermediate
C19					7		T2N0	Intermediate
C20	P		I		4 (2 + 2)	2	T4N1M1	High
C21	P	P			3 (1 + 2)	2	T3N1M1	High
C22					6 (2 + 4)	4	T3N0M1b	High
C23					6 (3 + 3)	3	T3N1M0	High
C24	P				6 (3 + 3)	3	T3N0M0	High
C25	P	P			6 (3 + 3)	3	T2N0M0	Low
C26	P	P		I	6 (3 + 3)	3	T2N0M0	Low
C27					6		T2N0	Low
C28	P			I	5 (1 + 4)		T2N0M0	Low
C29					5 (2 + 3)	3	T2N0M0	Low
C30					5 (2 + 3)	3	T2N0M0	Low
C31			I		4 (2 + 2)	2	T2N0M0	Low
C32					3 (1 + 2)	1	T1N0M0	Low

Statistical comparisons of the RRD of a gene in individual cancer tissues to the PND, using the two-sample 1D KS test. Red, significantly different (P < 0.01); Blue, statistically similar position (P > 0.01). I, a more internal position in the cancer, compared to the PND; P, a more peripheral positioned in the cancer tissue; Red text: mark of aggressive/high risk cancer; blue text: mark of low risk cancer; purple text, intermediate Gleason score. Low risk, Gleason score 2-6 and T1/2 and N0M0; intermediate risk, Gleason score 7 and T1/2 and N0M0; high risk, Gleason score 8-10 and/or T3/4 and/or N1 and/or M1.

repositioned in 36.4% (4/11), *SATB1* in 34.8% (8/23), and *TGFB3* in 31.8% (7/22) of prostate cancer tissues (**Figure 1**, **Table 1**, **Supplementary Tables 3–5**). The repositioning rates are slightly higher than in the previous smaller scale studies (25-33.3%) (Leshner et al., 2016; Meaburn et al., 2016). However, in keeping with previous findings, all four genes repositioned in too few cancers to be of use as prostate cancer diagnostic GPBs since detecting cancer based on the repositioning of the gene would misclassify 55.6-68.2% of the tumors as not cancerous, depending on the gene. The likelihood of a gene repositioning in a cancer did not correlated with gene copy number (**Figure 1**, **Supplementary Table 6**).

In addition to whether a gene was repositioned, the direction of its repositioning was also determined (**Figure 1**, **Table 1**). Of the 12 prostate cancers in which *SP100* was repositioned, the gene was more internally positioned compare to the PND in five cancer tissues (5/12; 41.7%) and more peripherally positioned in seven (58.3%). Similarly, *TGFB3* was more internally positioned in three (3/7; 42.9%) cancers and more peripherally positioned in four (57.1%). *SATB1* was more internally positioned in five of the eight cancers where the gene was repositioned (62.5%) and more peripherally positioned in three cancers (37.5%). Conversely, *LMNA* repositioned to a more internal nuclear location in all four cancer specimens in which the gene was repositioned (**Figure 1**, **Table 1**). The direction of repositioning accounted for most of the differences in the positioning patterns for a given gene between the cancer tissues in which repositioning occurred. There was little variation between the RRDs of a gene between the cancers in which the gene was more internally positioned. Similarly, there was little statistical variation in RRDs among cancers in which the gene was more peripherally positioned, with the exception of *SATB1* (**Table 2**, **Supplementary Tables 2–5**). Taken together, we find heterogeneity in the radial positioning patterns for all four candidate genes between prostate cancers.

SP100 and *TGFB3* Exhibit Differential Positioning Patterns Between Low and Intermediate/High Gleason Score Cancers

Next, we sought to determine if the differences in gene repositioning patterns between prostate cancers correlated with clinicopathological features. Comparing RRDs between individual cancer tissues was not useful for subgrouping cancers. For the most part, there was a similar proportion of

TABLE 2 | Cross-comparisons between individual tissues % (number) of significantly different cross-comparison among.

	SP100	*TGFB3*	*SATB1*	*LMNA*
Individual cancer tissues	46.7% (164/351)	33.8% (78/231)	42.3% (107/253)	32.7% (18/55)
More I cancers	0% (0/10)	0% (0/3)	0% (0/10)	N/A
More P cancers	9.5% (2/21)	0% (0/6)	66.7% (2/3)	33.3% (2/6)
Individual normal vs cancer tissues	33.3% (63/189)	28.4% (50/176)	22.4% (36/161)	24.2% (16/66)
Individual normal tissues	0.0% (0/21)	21.4% (6/28)	19.0% (4/21)	26.7% (4/15)
Individual benign disease tissues	20% (2/10)	10.0% (1/10)	0.0% (0/10)	0.0% (0/1)
Individual normal vs benign disease	14.3% (5/35)	10.0% (4/40)	5.7% (2/35)	25.0% (3/12)
Individual benign tissues	10.6% (7/66)	14.1% (11/78)	9.1% (6/66)	25.0% (7/28)

Significantly different, based on a KS test, P < 0.01; More I cancers, cancers in which the gene is more internally positioned than the PND (P < 0.01); More P cancers, cancers in which the gene is more peripherally positioned than the PND (P < 0.01); N/A, not applicable.

cross-comparisons between cancers that were significantly different to each other within clinically relevant subgroups as there was between subgroups (for *P*-values see **Supplementary Tables 2-5**). For example, *SP100* was in a significantly different position in 49.1% (27/55) of cross-comparisons amongst Gleason score 2-6 prostate cancers, and 53.4% (47/88) of cross-comparisons when Gleason score 2-6 cancers were compared to Gleason score 7 cancers, and 50% (44/88) of cross-comparisons between Gleason score 2-6 and Gleason score 8-10 cancers (**Supplementary Table 2**).

In contrast, the behavior of a gene in a cancerous tissue compared to the PND was a better indicator to detect differential positioning between subgroups (**Figure 1**, **Supplementary Figure 2**, **Tables 1**, **3** and **4**, **Supplementary Tables 2–5**). We first compared positioning patterns to Gleason score. In line with the clinical risk assessment of prostate cancers (Thompson et al., 2007), we classified Gleason scores of 2-6 as a low Gleason score, Gleason score 7 as intermediate, and scores of 8-10 as a high Gleason score. There was a modest increase in the proportion of cancer specimens with either *SATB1* or *LMNA* repositioned, compared to the PND, with increasing Gleason score, however, in the case of *LMNA* this may be due to the small sample size (**Table 3**). *SATB1* was in a statistically different nuclear position in 25% (2/8) of low Gleason score cancers, 33.3% (3/9) Gleason score 7 cancers and 50% (3/6) high Gleason score cancers. Similarly, *LMNA* repositioned in 33.3% of low (2/6) and intermediate

TABLE 3 | Positioning patterns for *SATB1* and *LMNA* by prostate cancer subgroups.

Direction of repositioning:	***SATB1* % (number) of cancers SD to the PND**			***LMNA* % (number) of cancers SD to the PND**		
	Any	**Internal**	**Peripheral**	**Any**	**Internal**	**Peripheral**
All cancers	34.8% (8/23)	62.5% (5/8)	37.5% (3/8)	36.4% (4/11)	100% (4/4)	0% (0/4)
GS 2-6	25.0% (2/8)	100% (2/2)	0% (0/2)	33.3% (2/6)	100% (2/2)	0% (0/2)
GS 7-10	40.0% (6/15)	50.0% (3/6)	50.0% (3/6)	40.0% (2/5)	100% (2/2)	0% (0/2)
GS 7	33.3% (3/9)	66.7% (2/3)	33.3% (1/3)	33.3% (1/3)	100% (1/1)	0% (0/1)
GS 8-10	50.0% (3/6)	33.3% (1/3)	66.7% (2/3)	50.0% (1/2)	100% (1/1)	0% (0/1)
GG1/GG2	66.7% (2/3)	100% (2/2)	0% (0/2)	0% (0/3)		
GG3	12.5% (1/8)	100% (1/1)	0% (0/1)	100% (2/2)	100% (2/2)	0% (0/2)
GG4/GG5	44.4% (4/9)	50.0% (2/4)	50.0% (2/4)	33.3% (1/3)	100% (1/1)	0% (0/1)
Unknown GG	33.3% (1/3)	0% (0/1)	100% (1/1)	33.3% (1/3)	100% (1/1)	0% (0/1)
T1/T2	30.8% (4/13)	50.0% (2/4)	50.0% (2/4)	42.9% (3/7)	100% (3/3)	0% (0/3)
T3/T4	33.3% (3/9)	100% (3/3)	0% (0/3)	25.0% (1/4)	100% (1/1)	0% (0/1)
Unknown T stage	100% (1/1)	0% (0/1)	100% (1/1)	0% (0/0)		
N0M0	37.5% (6/16)	50.0% (3/6)	50.0% (3/6)	57.1% (4/7)	100% (4/4)	0% (0/4)
N1/M1	16.7% (1/6)	100% (1/1)	0% (0/1)	0% (0/4)		
Unknown N/M status	100% (1/1)	0% (0/1)	100% (1/1)	0% (0/0)		
T1/T2 N0M0	30.8% (4/13)	50.0% (2/4)	50.0% (2/4)	50.0% (3/6)	100% (3/3)	0% (0/3)
T3N0M0	66.7% (2/3)	100% (2/2)	0% (0/2)	100% (1/1)	100% (1/1)	0% (0/1)
T4/N1/M1	16.7% (1/6)	100% (1/1)	0% (0/1)	0% (0/4)		
Unknown T/N/M	100% (1/1)	0% (0/1)	100% (1/1)	0% (0/0)		
Low risk	25.0% (1/4)	100% (1/1)	0% (0/1)	66.7% (2/3)	100% (2/2)	0% (0/2)
Int. risk	33.3% (2/6)	50.0% (1/2)	50.0% (1/2)	0% (0/2)		
High risk	38.5% (5/13)	60.0% (3/5)	40.0% (2/5)	33.3% (2/6)	100% (2/2)	0% (0/2)

SD, significantly different, based on 1D KS test (P < 0.01); GS, Gleason score; GG, Gleason grade; low risk, Gleason score 2-6 and T1/2 and N0M0; int. risk, intermediate risk (Gleason score 7 and T1/2 and N0M0); high risk, Gleason score 8-10 and/or T3/4 and/or N1 and/or M1.

(1/3) Gleason score cancers, and 50% (1/2) of high Gleason score cancers. Inclusion of the direction of repositioning did little to aid stratification (**Table 3**). Thus, we concluded that neither *SATB1* nor *LMNA* are biomarkers of Gleason score. The proportion of cancers in which *SP100* and *TGFB3* repositioned also did not stratify Gleason score groups. *SP100* was slightly more frequently repositioned in low Gleason score cancers specimens, repositioning in 54.5% (6/11) of low Gleason score cancers, 37.5% (3/8) of intermediate Gleason score cancers, and 37.5% (3/8) of high Gleason score cancers. *TGFB3* repositioned in 30% (3/10) low Gleason score cancer tissues, 20% (1/5) of intermediate Gleason score cancers, and 42.9% (3/7) of high Gleason score cancers. On the other hand, in cancer specimens in which either gene repositioned, the direction of repositioning correlated with Gleason score (**Supplementary Figure 2A**, **Table 4**). Both *SP100* and *TGFB3* shifted to a more peripheral position in 100% of the low Gleason score cancers in which these genes showed an altered radial position. In contrast, *SP100* and *TGFB3* were in a more internal position in 83.3% (5/6) and 75.0% (3/4), respectively, of the Gleason score 7 and higher cancers in which they repositioned. Intermediate/high Gleason score cancer tissue repositioning is not exclusively more internal, since for both genes a more peripheral positioning was detected in a Gleason score 9 prostate cancer (**Supplementary Figure 2A**, **Tables 1** and **4**). The positioning patterns of *SP100* and *TGFB3* could not distinguish intermediate Gleason score cancer tissues from high Gleason score cancer tissues (**Supplementary Figure 2A**, **Tables 1** and **4**).

We also assessed if positioning patterns correlated with Gleason grade. For all four genes, increasing Gleason grade did not correlate with the percentage of cancer specimens in which the genes repositioned (**Tables 3** and **4**). Consistent with Gleason score, the direction that *SATB1* and *LMNA* repositioned did not aid in stratifying cancers by Gleason grade (**Table 3**), but the direction of repositioning did correlate with Gleason grade for *SP100* and *TGFB3* (**Table 4**). As with Gleason score, in the more highly differentiated cancers (Gleason grades 1-3) *SP100* and *TGFB3* repositioned towards the nuclear periphery in 100% (5 and 3 cancers, respectively) of the cancers in which these genes repositioned. Yet, in the poorly differentiated cancers (Gleason grade 4 and 5) both genes preferentially repositioned towards the nuclear interior. *SP100* was more internally positioned in 80% (4/5) of Gleason grade 4 and 5 cancer in which *SP100* repositioned and *TGFB3* was more internally positioned in 66.7% (2/3) of the Gleason grade 4 and 5 cancers in which *TGFB3* was repositioned, compared to the PND (**Table 4**). The similarity between Gleason grade and Gleason score positioning patterns are not surprising given that Gleason score is the sum of the two most prominent Gleason grades (Epstein et al., 2005; Epstein, 2018). An important caveat to be noted is that while the subgrouping of the cancers was based on the most predominant Gleason grade of the tissue, it is not necessarily the predominant Gleason grade of the nuclei analyzed from each specimen.

Collectively, these observations demonstrate that while positioning patterns performed less well than the Gleason system

TABLE 4 | Positioning patterns for *SP100* and *TGFB3* by prostate cancer subgroups.

Direction of repositioning:	*SP100* % (number) of cancers SD to the PND			*TGFB3* % (number) of cancers SD to the PND		
	Any	Internal	Peripheral	Any	Internal	Peripheral
All cancers	44.4% (12/27)	41.7% (5/12)	58.3% (7/12)	31.8% (7/22)	42.9% (3/7)	57.1% (4/7)
GS 2-6	54.5% (6/11)	0% (0/6)	100% (6/6)	30.0% (3/10)	0% (0/3)	100% (3/3)
GS 7-10	37.5% (6/16)	83.3% (5/6)	16.7% (1/6)	33.3% (4/12)	75.0% (3/4)	25.0% (1/4)
GS 7	37.5% (3/8)	100% (3/3)	0% (0/3)	20.0% (1/5)	100% (1/1)	0% (0/1)
GS 8-10	37.5% (3/8)	66.7% (2/3)	33.3% (1/3)	42.9% (3/7)	66.7% (2/3)	33.3% (1/3)
GG1/GG2	50.0% (2/4)	0% (0/2)	100% (2/2)	33.3% (1/3)	0% (0/1)	100% (1/1)
GG3	33.3% (3/9)	0% (0/3)	100% (3/3)	28.6% (2/7)	0% (0/2)	100% (2/2)
GG4/GG5	45.5% (5/11)	80.0% (4/5)	20.0% (1/5)	30.0% (3/10)	66.7% (2/3)	33.3% (1/3)
Unknown GG	66.7% (2/3)	50.0% (1/2)	50.0% (1/2)	50.0% (1/2)	100% (1/1)	0% (0/1)
T1/T2	43.8% (7/16)	42.9% (3/7)	57.1% (4/7)	41.7% (5/12)	60.0% (3/5)	40.0% (2/5)
T3/T4	50.0% (5/10)	40.0% (2/5)	60.0% (3/5)	11.1% (1/9)	0% (0/1)	100% (1/1)
Unknown T stage	0% (0/1)			100% (1/1)	0% (0/1)	100% (1/1)
N0M0	47.4% (9/19)	44.4% (4/9)	55.6% (5/9)	33.3% (5/15)	60.% (3/5)	20.0% (2/5)
N1/M1	42.9% (3/7)	33.3% (1/3)	66.7% (2/3)	16.7% (1/6)	0% (0/0)	100% (1/1)
Unknown N/M status	0% (0/1)			100% (1/1)	0% (0/1)	100% (1/1)
T1/T2 N0M0	46.7% (7/15)	42.9% (3/7)	57.1% (4/7)	41.7% (5/12)	60.0% (3/5)	40.0% (2/5)
T3N0M0	50.0% (2/4)	50% (1/2)	50.0% (1/2)	0% (0/3)		
T4/N1/M1	42.9% (3/7)	33.3% (1/3)	66.7% (2/3)	16.7% (1/6)	0% (0/1)	100% (1/1)
Unknown T/N/M status	0% (0/1)			100% (1/1)	0% (0/1)	100% (1/1)
Low risk	50.0% (3/6)	0% (0/3)	100% (3/3)	33.3% (2/6)	0% (0/2)	100% (2/2)
Int. risk	50.0% (3/6)	100% (3/3)	0% (0/3)	33.3% (1/3)	100% (1/1)	0% (0/1)
High risk	40.0% (6/15)	33.3% (2/6)	66.7% (4/6)	30.8% (4/13)	50% (2/4)	50% (2/4)

SD, significantly different, based on 1D KS test ($P < 0.01$); GS, Gleason score; GG, Gleason grade; low risk, Gleason score 2-6 and T1/2 and N0M0; int. risk, intermediate risk (Gleason score 7 and T1/2 and N0M0); high risk, Gleason score 8-10 and/or T3/4 and/or N1 and/or M1.

at stratifying cancers, we identify differential gene positioning patterns between subgroups of prostate cancers.

Multiplexing *SP100 and TGFB3* Improves Detecting Intermediate and High Gleason Score Cancers

Although both *SP100* and *TGFB3* displayed differential positioning patterns between low and intermediate/high Gleason score cancer specimens, the sensitivity for subgrouping prostate cancers by Gleason score based on positioning patterns is low. Using a more peripheral positioning of *SP100* compared to the PND as a marker of low Gleason score cancers, the false negative rate (percentage of cancers without a more peripheral positioning) is 45.4% (5/11 low Gleason score cancers; **Table 1**). For *TGFB3* the false negative rate is even higher at 70% (7/10; **Table 1**). Additionally, using this criterion, false positive cancers were identified for both genes. More peripheral positioning was detected in one high Gleason score specimen for both *SP100* and *TGFB3*, resulting in a false positive rate of 6.3% (1/16) and 8.3% (1/12), respectively, for intermediate and high Gleason score cancers (**Table 1**). Neither gene was more internally positioned in low Gleason score cancers (**Table 1**). Using a more internal positioning pattern as a biomarker of intermediate and high Gleason score cancers resulted in a false negative rate of 62.5% (10/16) and 66.7% (8/12) for *SP100* and *TGFB3*, respectively (**Table 1**).

We have previously demonstrated that the sensitivity of diagnostic GPBs can be improved by multiplexing (Meaburn et al., 2009; Leshner et al., 2016). We therefore evaluated if combining positioning data from *SP100* and *TGFB3* would increase the number of cancers classified as low or intermediate/high Gleason score based on gene positioning patterns. Importantly for multiplexing to improve the sensitivity, *SP100* and *TGFB3* would need to be frequently repositioned in different cancer specimens. Of a subset of 19 cancer tissues in which both genes were positioned, 10 (52.6%) had differential repositioning patterns for *SP100* to that of *TGFB3* (**Table 1**, **Supplementary Table 7**). For six of these cancers *SP100* was repositioned but *TGFB3* was not, whereas in three cancers only *TGFB3* was repositioned. For one cancer sample, both genes were repositioned, compared to their PND, but they relocated in opposite directions, with *SP100* being more peripherally positioned, while *TGFB3* was more internally positioned (**Table 1**, **Supplementary Table 7**). However, multiplexing the two genes did not improve the sensitivity to detect low Gleason score cancers above using *SP100* alone. *SP100* was more peripherally positioned in all five cancers where at least one of the two genes repositioned (**Table 1**, **Supplementary Table 7**). Nevertheless, multiplexing increased the sensitivity of detecting intermediate/high Gleason score cancers (**Table 1**, **Supplementary Table 7**). At least one gene repositioned in eight of the 11 (72.7%) Gleason score 7 and higher cancers. Both *SP100* and *TGFB3* contributed to the increased proportion of cancer specimens with repositioning events. Of the seven cancers with only one of the two genes more internally repositioned, *SP100* was more internally repositioned in four and *TGFB3* more internally positioned in three cancers (**Table 1**, **Supplementary Table 7**). Using a more internal position of at least one of *SP100* or *TGFB3* the false negative rate for detecting intermediate or high Gleason score cancers was reduced to 36.4% (4/11). While most of the repositioning events in intermediate/high Gleason score cancers were to a more internal position, in one cancer the only repositioning event resulted in a more peripheral location of *TGFB3* and in another cancer tissue, there was both a more peripheral and more internal repositioning events, with *SP100* more peripherally position and *TGFB3* more internally located (**Table 1**, **Supplementary Table 7**).

Gleason score is not a perfect measure of risk. Given the variability in positioning patterns within the same Gleason group, we asked if the positioning patterns could be useful to distinguish aggressive low Gleason core cancers from non-aggressive low Gleason score cancers. Such a marker would aid treatment decisions. However, *SP100* and *TGFB3* were repositioned in a similar proportion of low Gleason score cancers with or without metastasis (**Table 1**). *SP100* repositioned in 50% (2/4) of low Gleason score cancers that had metastasized and 57.1% (4/7) of low Gleason score cancers without metastases. Likewise, *TGFB3* repositioned in 33.3% (1/3) of metastatic low Gleason score cancer specimens and 28.8% (2/7) of non-metastatic low Gleason score cancer specimens (**Table 1**). Thus, in addition to the high false negative rate for Gleason score, *SP100* and *TGFB3* can not distinguish aggressive low Gleason score cancers from non-aggressive low Gleason score cancers, limiting their clinical potential.

Low Gleason Score Cancer Gene Positioning Patterns Are Distinct From Benign Disease

Given the fact that low Gleason score cancers are fairly well differentiated tissues, it is possible that low Gleason score cancers have a similar genome organization to benign disease. We therefore sought to determine the cancer-specificity of the repositioning events. We positioned *SP100*, *TGFB3*, *SATB1* and *LMNA* in non-cancerous prostate tissues (**Figure 2**, **Supplementary Figure 1**, **Tables 5** and **6**, **Supplementary Tables 2–5**). For all four genes we found that the positioning patterns were highly similar between benign tissues. For *SP100, TGFB3* and *SATB1*, only 9.1%-14.1% of comparisons between the individual non-cancerous tissues reached significance. There was a little more variability between benign tissues for *LMNA*, where 25% of cross-comparisons between benign tissues were significantly different (**Figure 2**, **Table 2**, **Supplementary Table 2–5**).There was also little repositioning of the four genes in benign tissues when compared to the PND, with repositioning in 7.7%-16.7% of benign tissues, depending on the gene (**Figure 2**, **Tables 5** and **6**). *SP100* was statistically similarly positioned in all seven normal tissues, compared to the PND, but was significantly repositioned in 40% (2/5) of benign disease tissue (**Figure 2**, **Tables 5** and **6**). However, the positioning patterns of *SP100* were distinct in benign disease and low Gleason score cancer, since it was more internally localized in the two benign disease tissues, yet more peripherally located in low Gleason score cancers (**Tables 1** and **5**).

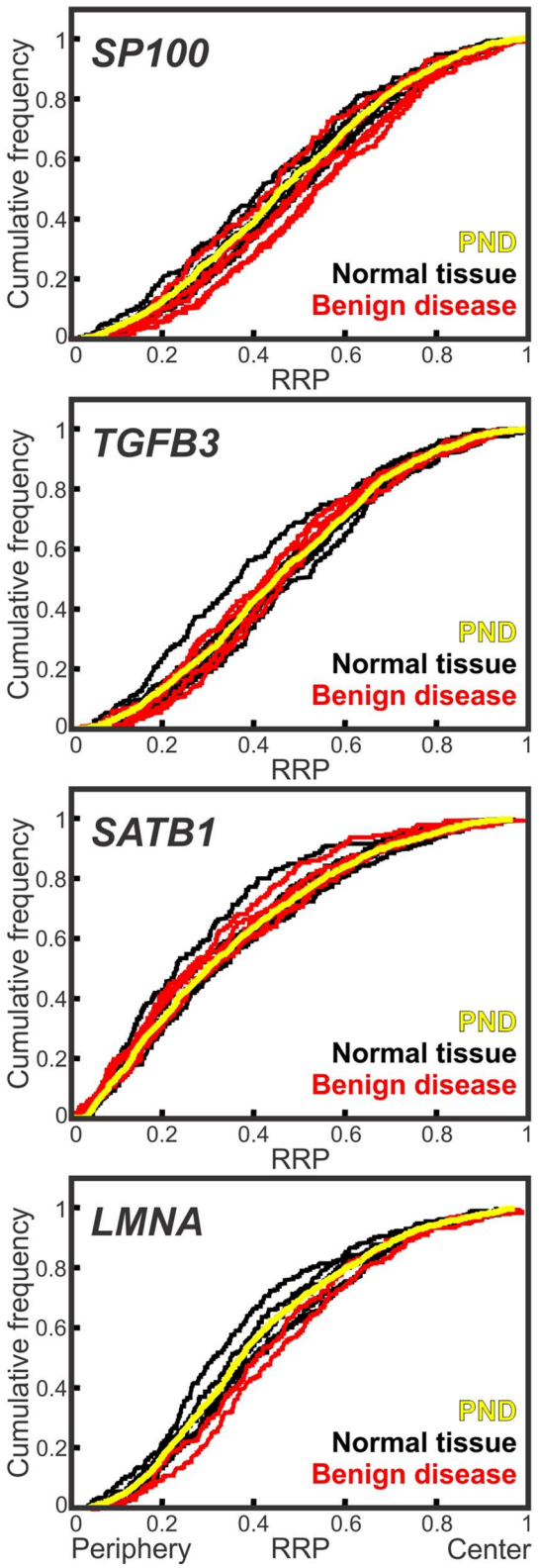

FIGURE 2 | Conserved spatial organization of the genome in benign tissues. Cumulative RRDs for the indicated genes in normal prostate tissue (black), benign disease (red) and the pooled normal distribution (PND; yellow). RRP, relative radial position.

TABLE 5 | Conservation of positioning between normal prostate tissues and in benign disease.

Tissue	*SP100*	*TGFB3*	*SATB1*	*LMNA*
N1				
N2			P	
N3		P		
N4				
N5				
N6				
N7				
N8				
N9				
N10				
N11				
N12				
N13				
N14				
N15				
N16				
B1	I			
B2				
B3	I			I
B4				
B5				
B6				
B7				
B8				
B9				

Statistical comparisons of the RRD of a gene in individual benign tissues and to the PND, using the two-sample 1D KS test. Red, significantly different ($P < 0.01$); Blue, statistically similar position ($P > 0.01$). N1-16, normal prostate tissue; B1-9, benign disease tissues; I, a more internal position in the benign, compared to the PND; P, a more peripheral positioning in the benign tissue.

Inclusion of the direction of repositioning in the analysis further confirmed the specificity of the repositioning events to the different Gleason score subgroups. When using more peripheral positioning, compared to the PND, as a marker of low Gleason score prostate cancer, the false positive rate for *SP100* is very low, at 3.6%, since it is more peripherally positioned in only one of 28 normal, benign disease and higher Gleason score cancer tissues (**Tables 1** and **5**). Similarly, *TGFB3* was repositioned in a single normal tissue (12.5%; 1/8) and in none of the benign disease tissues (0/5), compared to the PND (**Figure 2**, **Tables 5** and **6**). Unlike *SP100*, the direction *TGFB3* reposition in the normal tissue was the same as in low Gleason score cancer. However, the false positive rate for using a more peripheral positioning of *TGFB3* was relatively low at 8%, because it was more peripherally positioned in two of the 25 benign tissues and higher Gleason score cancers (**Tables 1** and **5**). The false positive rate of using a more internal position of *SP100* or *TGFB3* to detect intermediate/high Gleason score cancers is also low, at 8.7% and 0%, respectively, since *SP100* was more internally repositioned in only two of the 23 benign tissues and low Gleason score cancer specimens and *TGFB3* was not more internally repositioned in these groups of tissues ($N = 23$; **Table 1** and **5**). Taken together, we find the spatial organization of the genome is generally conserved between benign tissues, and benign disease tissue have a distinct genome organization to both low and intermediate/high Gleason score cancers.

TABLE 6 | Comparison of individual benign tissue to the pooled normal.

	SP100	*TGFB3*	*SATB1*	*LMNA*
Normal tissues	0.0% (0/7)	12.5% (1/8)	14.3% (1/7)	0.0% (0/6)
Benign disease	40.0 (2/5)	0.0% (0/5)	0.0% (0/5)	50.0% (1/2)
Total benign tissues	16.7% (2/12)	7.7% (1/13)	8.3% (1/12)	12.5% (1/8)

% (number) of benign tissues where the RRD is significantly different to the PND (P < 0.01; KS test).

LMNA Repositions in Low Risk and Non-Metastatic Cancers

Having determined the biomarker potential of the candidate genes for subgrouping prostate cancers by Gleason score, we compared their positioning patterns to other clinical markers of poor patient outcome. The TNM staging system is commonly used to aid the prediction of the aggressiveness of the cancer and the risk of poor patient outcome (Thompson et al., 2007). In stage T1 and T2 prostate cancers the tumor is contained within the prostate, whereas in stages T3 and T4 the cancer has spread from the prostate into the surrounding tissue. T1 and T2 cancers are lower risk cancers and respond better to treatment than T3 and T4 prostate cancers (Thompson et al., 2007; Chang et al., 2014). The N and M score indicates whether the cancer has spread beyond the surrounding tissue. In N0 cancers, no cancer cells are detected in the regional lymph nodes, whereas N1 denotes that the cancer has spread into the regional lymph nodes. For M0 cancers, no distant metastasis are detected, while distant metastases, to non-regional lymph nodes or organs, have occurred in M1 cancers (Thompson et al., 2007).

Positioning patterns for *SP100* and *SATB1* were similar in low and high T stage cancer specimens and could not be used to distinguish the different T stage group cancers from each other (**Tables 3** and **4**). *TGFB3* and *LMNA* were both more frequently repositioned in low T stage cancers to that of high T stage cancers, but with high false positive rates (**Tables 3** and **4**). *TGFB3* repositioned in 41.7% (5/12) of T1/2 cancers, 11.1% (1/9) of T3/4 cancers, and 7.7% (1/13) of benign tissues, compared to the PND (**Tables 1**, **4** and **6**). This equates to a false negative rate of 58.3% (7/12) and a false positive rate of 9.1% (2/22) for using the reposition of *TGFB3* to detect low T stage prostate cancer. Similarly, *LMNA* repositioned in 42.9% (3/7) of low T stage cancer, 25% (1/4) of high T stage cancers and 12.5% (1/8) of benign tissues (**Tables 3** and **6**), making the false negative and positive rates of using the repositioning of *LMNA* to demark low T stage cancers 57.1% (4/7) and 16.7% (2/12), respectively.

Clinically, multiple factors are combined to determine risk of poor outcome. Therefore, we also compared gene positioning patterns with a multifactorial determinant of risk using standard clinical risk assessment criteria (Thompson et al., 2007; Chang et al., 2014) with the exception of PSA levels, since no information on serum PSA were available for our specimens. Moreover, we included N1 and/or M1 cancers in the high-risk group, since they are known aggressive cancers. We classified low risk cancer as Gleason score 2-6 and T1/2 and N0M0 cancers; intermediate risk cancers as Gleason score 7 and T1/2 and N0M0; high risk as Gleason score 8-10 and/or T3/4 and/or N1 and/or M1 prostate cancers. The positioning patterns of *SP100*, *TGFB3* and *SATB1* were similar in all three risk groups, and thus could not be used as markers of risk (**Tables 3** and **4**). Conversely, *LMNA* was more frequently repositioned in low risk prostate cancer, since it repositioned in 66.7% (2/3) of low risk cancers, 0% (0/2) of intermediate risk and 33.3% (2/6) of high-risk groups (**Table 3**).

Finally, as a more direct measure of the aggressiveness of a cancer we compared non-metastatic cancers (N0M0) and metastatic (N1/M1) prostate cancers (**Supplementary Figure 2B**, **Table 1**, **3** and **4**). *SP100* repositioned, compared to the PND, in a similar proportion of N0M0 (47.4%; 9/19) and metastatic (42.9%; 3/7) cancer specimens. Furthermore, the direction of repositioning was similarly mixed in both groups of cancer (**Table 4**). The remaining three genes repositioned more frequently in non-metastatic cancers. For *TGFB3* and *SATB1* this difference is small, with the genes repositioned in ~33.3% (5/15 and 6/16 respectively; false negative rate ~66.7%) of non-metastatic cancers and 16.7% (1/6) of metastatic cancers (**Table 3** and **4**). *LMNA* was the best marker of non-metastatic cancers. *LMNA* repositioned in 57.1% (4/7) of non-metastatic prostate cancer specimens and was not repositioned in metastatic (0/4) cancer tissues (**Supplementary Figure 2B**, **Table 3**). As with *SP100* and *TGFB3* as markers of Gleason score, the false negative rate for using *LMNA* positioning as a marker of non-metastatic cancer was high at 42.9% (3/7), and the false positive rate is relatively low at 8.3% (1/12) (**Tables 1**, **3** and **5**).

Taken together, our data suggest that there are distinct spatial gene positioning patterns between some subgroups of prostate cancers, although the false negative rates were generally high, limiting their potential for clinical use.

DISCUSSION

To reduce overtreatment in cancer patients that receive no benefit from medical intervention, there is an urgent need for biomarkers that predict the aggressiveness of a cancer. Here, we assess the feasibility of utilizing the spatial positioning patterns of genes in interphase nuclei for prognostic purposes in prostate cancer. We find a differential enrichment of specific positioning patterns for multiple genes between clinically relevant subgroups of prostate cancers. While the false positive rates for prognostic evaluation are low, the false negative rates are generally high, limiting clinical usefulness. Our results of subtype-specific genome organization patterns suggest that it should be possible to find clinically valuable prognostic GPB by screening additional genes and combinations of genes.

The spatial organization of the genome is altered in diseased cells, and at least some of the changes to genomic spatial positioning

patterns are disease-specific (Meaburn, 2016). For instance, *HES5* repositions in breast cancer, but not in benign breast disease nor prostate cancer (Meaburn et al., 2009; Meaburn et al., 2016). Alternative spatial positioning patterns are not only found in cancers formed in different organs, but there is also heterogeneity in the spatial organization of the genome between individual cancers of the same type (Meaburn et al., 2009; Knecht et al., 2012; Leshner et al., 2016; Meaburn et al., 2016). We hypothesized that heterogeneity within a cancer type may reflect the aggressiveness of a cancer and therefore be of prognostic value. Prognosis-related repositioning of genomic regions in several types of cancer has previously been reported, with increased clustering of telomeres linked to poorer patient outcomes (Mai, 2018). For example, at the time of diagnosis telomeres were more likely to cluster in Hodgkin lymphoma patients whose disease later relapsed or progressed compared to patients who responded well to treatment (Knecht et al., 2012). Currently, Gleason score and the presence or absence of metastasis are key clinicopathological tumor features for predicting the aggressiveness of a prostate cancer. We find that *SP100* and *TGFB3* occupy alterative positions in low Gleason score cancers compared to higher Gleason scored cancers, and that *LMNA* repositions more internally in many non-metastatic and low risk prostate cancers, but infrequently reposition in high risk/aggressive cancers.

Our previous identification of diagnostic GPBs was based on the percentage of cancer specimens in which a gene had an alternative radial position, compared to its distribution in normal tissues (Meaburn, 2016). Interestingly, for *SP100* and *TGFB3* it was not the repositioning itself, but the direction of repositioning that was useful for stratification of prostate cancers. Repositioning of either *SP100* or *TGFB3* towards the nuclear periphery was associated with low Gleason score whereas repositioning towards the interior was a marker of higher Gleason score cancers. The repositioning patterns of *SP100* and *TGFB3* could not distinguish intermediate from high Gleason score cancers. Nevertheless, this does not necessarily rule them out as useful clinical markers since low Gleason score cancers are less likely to receive treatment than intermediate or high Gleason score cancers (Thompson et al., 2007; Cooperberg et al., 2010; Leshner et al., 2016). Given that there is inter-and intra-observer variability when scoring cancers (Montironi et al., 2005), additional markers that can clarify if a cancer is Gleason score 6 (low) or 7 (intermediate) would be useful in guiding therapeutic choices. However, because the positioning patterns of our genes could not separate aggressive, metastatic low Gleason score cancers from non-metastatic low Gleason score cancers, they are unlikely to aid the decision of whether to treat a cancer or not. In keeping with a differential spatial genome organization in cancers above and below the treatment threshold, we previously found *MMP9* to reposition in 20% of low Gleason score cancers compared to 82% of intermediate/high Gleason score cancers (Leshner et al., 2016). Unlike *SP100* and *TGFB3*, the direction *MMP9* repositioned did not aid stratification (Leshner et al., 2016), unpublished data). *MMP9* was positioned predominantly in Gleason score 6 and 7 prostate cancers, making it unclear how specific these positioning patterns are more generally to the different Gleason scores subgroups. *SP100*, *TGFB3* and *MMP9* each map to different chromosomes (HSA 2, 14 and 20, respectively) and therefore represent independent repositioning events within the subgroups of different Gleason score cancers.

In our analysis we find low false positive rates for distinguishing low from intermediate/high Gleason score cancers. In keeping with previous studies (Borden and Manuelidis, 1988; Meaburn et al., 2009; Leshner et al., 2016; Meaburn et al., 2016), we find similar positioning patterns for both *SP100* and *TGFB3* amongst normal tissues and between normal and benign disease tissues, highlighting that the gene repositioning in cancer tissues were specific to cancer. Despite the fact that low Gleason score cancers represents fairly well differentiated tissues there were distinct positioning patterns for *SP100* and *TGFB3* between low Gleason score cancers and benign disease, which are considered differentiated tissues. *TGFB3* did not reposition in benign disease and *SP100* was repositioned in only 20% of the benign disease tissues. However, unlike low Gleason score cancers, *SP100* was more internally positioned in benign disease tissues, and therefore does not contribute to the false positive rate when using more peripheral positioning of these genes to detect low Gleason score cancers. Unlike biomarkers used to diagnose cancer, the false positive rate of detecting a subtype of cancer for prognostic purposes is not only generated from non-cancerous tissues, it needs to also include cancers from the alternative subgroups. Even so, the false positive rates of detecting low Gleason score prostate cancers were low because the direction of repositioning for *SP100* and *TGFB3* was mostly specific to the subgroups. In contrast to the false positive rates, the false negative rates for *SP100* and *TGFB3* were high, at 45-70%. We have previously found that for some genes multiplexing reduces the false negative rate and thus increases the sensitivity of detecting cancer (Meaburn et al., 2009; Leshner et al., 2016). Constant with this, we find that multiplexing *SP100* and *TGFB3* reduces the false negative rate of detecting intermediate and higher Gleason score cancers. However, multiplexing with a more peripheral position of either *SP100* or *TGFB3* did not reduce the false negative rate for low Gleason score cancers from that of using *SP100* alone. We conclude that the observed high false negative rates reduce marker strength and the utility of these genes for prognostic purposes.

Even though the positioning patterns of *SP100* and *TGFB3* are inferior to the Gleason system at stratifying cancers, our results reveal subtype-specific genome organization. Similarly, the repositioning of *LMNA* is also subtype-specific, but in this case the repositioning occurs only in non-metastatic cancers, although also with a high false negative rate. Interestingly, the reorganization events between the different subtypes of prostate cancer appear to be gene-specific. *LMNA* and *SATB1* positioning patterns were not able to stratify prostate cancers by Gleason score and *SP100*, *TGFB3* and *SATB1* were not accurate markers of risk or aggressiveness of the cancer. Consistently, the radial repositioning patterns of *FLI1*, *MMP9* and *MMP2* also do not correlate with the risk/aggressiveness of prostate cancer (Leshner et al., 2016). Given that it can take many years after the initial diagnosis of prostate cancer to progress to recurrence, metastasis and/or lethality (Albertsen et al., 1998; D'Amico et al., 1998; Pound et al., 1999; Cooperberg et al., 2009), it will be necessary to analyze specimens with long-term (15+ years) follow-up to accurately assess the potential of spatial positioning for assessment of risk or aggressiveness.

It is unknown what mechanisms lead to the reorganization of the genome in disease, and many processes have been implicated in regulating spatial positioning patterns, including changes in

gene expression, replication timing, chromatin modifications, altered amounts of nuclear proteins, making it likely that the mis-regulations of these cellular functions in cancer cells is related to the spatial mis-organization of the genome (Zink et al., 2004; Meaburn, 2016; Flavahan et al., 2017). The four genes we studied have all been associated with carcinogenesis and have a range of functions. SP100 is a major component of the PML nuclear body and has been implicated in transcription regulation, cellular stress, oxidative stress, telomere length and stability, senescence, apoptosis and DNA damage repair (Lallemand-Breitenbach and de The, 2010). However, most of the evidence for PML bodies role in cancer relates to the PML protein, not SP100, which has not been implicated in prostate cancer. TGFB3 is a cytokine, with important roles in development, wound healing, the immune response and acts as a tumor suppresser in early cancers but can switch to promoting cancer progression in later stages (Massague, 2008; Laverty et al., 2009). *TGFB3* gene expression levels have been identified as a potential biomarker for prostate cancer, being expressed at lower levels in prostate cancer than normal tissue (Wang et al., 2017). Moreover, *TGFB3* expression levels correlated weakly with both progression-free survival and Gleason score (Wang et al., 2017). SATB1, a nuclear architectural protein that facilitates DNA loop formation and chromatin remodeling (Kohwi-Shigematsu et al., 2013), promotes the progression of many cancers, including prostate cancer, and is overexpressed in high Gleason score cancers compared to low Gleason score cancers and in metastatic compared to non-metastatic prostate cancers (Mao et al., 2013; Shukla et al., 2013; Naik and Galande, 2019). *LMNA* encodes for A-type lamins, proteins that reside predominantly at the nuclear envelope, and have a variety of roles including in nuclear structure, transcription regulation, and spatial genome organization (Dittmer and Misteli, 2011). A-type lamins levels are altered in many types of cancer, with reduced levels often, but not always, linked to a tendency for a poorer prognostic outcome (Meaburn, 2016). It is not currently clear what effect prostate cancer has on A-type lamin protein levels. On the one hand, levels of A-type lamins in prostate cancer have been correlated with poor outcome, with reduced levels associated with an increased risk of lymph node metastasis, and poor outcome in Gleason score 7 and higher prostate cancers (Saarinen et al., 2015). On the other hand, reduced A-type lamin levels in Gleason score 6 cancer compared to high Gleason score cancer, increased A-type lamin levels in cells at the invasive leading edge of prostate cancers, and enhanced migration and invasion in the presence of high A-type lamin levels have been also been reported (Skvortsov et al., 2011; Kong et al., 2012).

Increased cell proliferation is associated with a poor outcome for prostate cancer patients (Berlin et al., 2017), and several genomic loci are differentially positioned between proliferating and non-proliferating cells (Bridger et al., 2000; Meaburn and Misteli, 2008). However, variations in proliferation rate is unlikely to be a major determinant in the gene repositioning we detect. In fact, the vast majority of cells in a prostate cancer tumor are non-proliferating, with a mean of just 6.1% proliferating cells per cancer (Berlin et al., 2017). Furthermore, in a cell culture model of breast cancer, there were distinct genome spatial rearrangements associated with proliferation status to that of carcinogenesis (Meaburn and Misteli, 2008). Similarly, although we find that changes in copy number did not correlated with propensity to reposition (**Supplementary Table 6**; (Meaburn et al., 2009; Leshner et al., 2016; Meaburn et al., 2016), we can not fully rule out that structural genomic alterations have not influenced the spatial position of any of the genes in the tissues analyzed since, in some cases, genomic instability can lead to spatial reorganization of the genome (Croft et al., 1999; Taslerova et al., 2003; Harewood et al., 2010; Federico et al., 2019). Regardless, importantly for a clinical test, we find that even in the background of genomic instability it is still possible to use gene positioning to distinguish normal tissue from cancer (Meaburn et al., 2009; Leshner et al., 2016; Meaburn et al., 2016) and to stratify cancers into clinically distinct subgroups, as demonstrated in this study.

Taken together, this study assesses the utility of spatial gene positioning in the stratification of prostate cancers. Our results reveal correlations between gene location and the aggressiveness of a tumor, which may serve as the foundation for prognostic usage of gene positioning. While the genes analyzed here have a relatively high false negative rate of detecting cancer subgroups, our results encourage the exploration of additional candidate genes in larger sample sets for the discovery of spatial genome positioning patterns as prognostic biomarkers.

DATA AVAILABILITY STATEMENT

All datasets generated for this study are included in the article/ **Supplementary Files**.

AUTHOR CONTRIBUTIONS

KM and TM conceived the study and wrote the manuscript. KM designed the study, performed the experiments, analyzed and interpreted data, and made the figures.

FUNDING

This work was supported by a Department of Defense Idea Award (W81XWH-15-1-0322) and the Intramural Research Program of the NIH, NCI, Center for Cancer Research.

ACKNOWLEDGMENTS

We thank Lawrence True for invaluable and insightful prostate pathology discussions, Prabhakar Gudla and Stephen Lockett for the FISH positioning analysis software; Delft University (Netherlands) for providing the DIPImage and PRTools toolboxes and Tatiana Karpova for microscopy support. Fluorescence imaging was performed at the National Cancer Institute (NCI) Fluorescence Imaging Facility.

SUPPLEMENTARY MATERIAL

The Supplementary Material for this article can be found online at: https://www.frontiersin.org/articles/10.3389/fgene.2019.01029/full#supplementary-material.

REFERENCES

Albertsen, P. C., Hanley, J. A., Gleason, D. F., and Barry, M. J. (1998). Competing risk analysis of men aged 55 to 74 years at diagnosis managed conservatively for clinically localized prostate cancer. *JAMA* 280, 975–980. doi: 10.1001/jama.280.11.975

Berlin, A., Castro-Mesta, J. F., Rodriguez-Romo, L., Hernandez-Barajas, D., Gonzalez-Guerrero, J. F., Rodriguez-Fernandez, I. A., et al. (2017). Prognostic role of Ki-67 score in localized prostate cancer: A systematic review and meta-analysis. *Urol. Oncol.* 35, 499–506. doi: 10.1016/j.urolonc.2017.05.004

Bickmore, W. A. (2013). The spatial organization of the human genome. *Annu. Rev. Genomics Hum. Genet.* 14, 67–84. doi: 10.1146/annurev-genom-091212-153515

Bickmore, W. A., and van Steensel, B. (2013). Genome architecture: domain organization of interphase chromosomes. *Cell* 152, 1270–1284. doi: 10.1016/j.cell.2013.02.001

Borden, J., and Manuelidis, L. (1988). Movement of the X chromosome in epilepsy. *Science* 242, 1687–1691. doi: 10.1126/science.3201257

Boyle, S., Gilchrist, S., Bridger, J. M., Mahy, N. L., Ellis, J. A., and Bickmore, W. A. (2001). The spatial organization of human chromosomes within the nuclei of normal and emerin-mutant cells. *Hum. Mol. Genet.* 10, 211–219. doi: 10.1093/hmg/10.3.211

Bray, F., Ferlay, J., Soerjomataram, I., Siegel, R. L., Torre, L. A., and Jemal, A. (2018). Global cancer statistics 2018: GLOBOCAN estimates of incidence and mortality worldwide for 36 cancers in 185 countries. *CA Cancer J. Clin.* 68, 394–424. doi: 10.3322/caac.21492

Brickner, J. H., and Walter, P. (2004). Gene recruitment of the activated INO1 locus to the nuclear membrane. *PLoS Biol.* 2, e342. doi: 10.1371/journal.pbio.0020342

Bridger, J. M., Boyle, S., Kill, I. R., and Bickmore, W. A. (2000). Re-modelling of nuclear architecture in quiescent and senescent human fibroblasts. *Curr. Biol.* 10, 149–152. doi: 10.1016/S0960-9822(00)00312-2

Brimo, F., Montironi, R., Egevad, L., Erbersdobler, A., Lin, D. W., Nelson, J. B., et al. (2013). Contemporary grading for prostate cancer: implications for patient care. *Eur. Urol.* 63, 892–901. doi: 10.1016/j.eururo.2012.10.015

Brown, K. E., Guest, S. S., Smale, S. T., Hahm, K., Merkenschlager, M., and Fisher, A. G. (1997). Association of transcriptionally silent genes with Ikaros complexes at centromeric heterochromatin. *Cell* 91, 845–854. doi: 10.1016/S0092-8674(00)80472-9

Cabianca, D. S., Munoz-Jimenez, C., Kalck, V., Gaidatzis, D., Padeken, J., Seeber, A., et al. (2019). Active chromatin marks drive spatial sequestration of heterochromatin in C. elegans nuclei. *Nature* 569, 734–739. doi: 10.1038/s41586-019-1243-y

Chandra, T., Ewels, P. A., Schoenfelder, S., Furlan-Magaril, M., Wingett, S. W., Kirschner, K., et al. (2015). Global reorganization of the nuclear landscape in senescent cells. *Cell Rep.* 10, 471–483. doi: 10.1016/j.celrep.2014.12.055

Chang, A. J., Autio, K. A., Roach, M., 3rd, and Scher, H. I. (2014). High-risk prostate cancer-classification and therapy. *Nat. Rev. Clin. Oncol.* 11, 308–323. doi: 10.1038/nrclinonc.2014.68

Cooperberg, M. R., Broering, J. M., and Carroll, P. R. (2009). Risk assessment for prostate cancer metastasis and mortality at the time of diagnosis. *J. Natl. Cancer Inst.* 101, 878–887. doi: 10.1093/jnci/djp122

Cooperberg, M. R., Broering, J. M., and Carroll, P. R. (2010). Time trends and local variation in primary treatment of localized prostate cancer. *J. Clin. Oncol.* 28, 1117–1123. doi: 10.1200/JCO.2009.26.0133

Cremer, T., and Cremer, C. (2001). Chromosome territories, nuclear architecture and gene regulation in mammalian cells. *Nat. Rev. Genet.* 2, 292–301. doi: 10.1038/35066075

Croft, J. A., Bridger, J. M., Boyle, S., Perry, P., Teague, P., and Bickmore, W. A. (1999). Differences in the localization and morphology of chromosomes in the human nucleus. *J. Cell Biol.* 145, 1119–1131. doi: 10.1083/jcb.145.6.1119

D'Amico, A. V., Whittington, R., Malkowicz, S. B., Schultz, D., Blank, K., Broderick, G. A., et al. (1998). Biochemical outcome after radical prostatectomy, external beam radiation therapy, or interstitial radiation therapy for clinically localized prostate cancer. *JAMA* 280, 969–974. doi: 10.1001/jama.280.11.969

Dittmer, T. A., and Misteli, T. (2011). The lamin protein family. *Genome Biol.* 12, 222. doi: 10.1186/gb-2011-12-5-222

Dundr, M., Ospina, J. K., Sung, M. H., John, S., Upender, M., Ried, T., et al. (2007). Actin-dependent intranuclear repositioning of an active gene locus *in vivo*. *J. Cell Biol.* 179, 1095–1103. doi: 10.1083/jcb.200710058

Epstein, J. I. (2018). Prostate cancer grading: a decade after the 2005 modified system. *Mod. Pathol.* 31, S47–S63. doi: 10.1038/modpathol.2017.133

Epstein, J. I., Allsbrook, W. C., Jr., Amin, M. B., Egevad, L. L., and Committee, I. G. (2005). The 2005 International Society of Urological Pathology (ISUP) Consensus conference on gleason grading of prostatic carcinoma. *Am. J. Surg. Pathol.* 29, 1228–1242. doi: 10.1097/01.pas.0000173646.99337.b1

Falk, M., Feodorova, Y., Naumova, N., Imakaev, M., Lajoie, B. R., Leonhardt, H., et al. (2019). Heterochromatin drives compartmentalization of inverted and conventional nuclei. *Nature* 570, 395–399. doi: 10.1038/s41586-019-1275-3

Federico, C., Owoka, T., Ragusa, D., Sturiale, V., Caponnetto, D., Leotta, C. G., et al. (2019). Deletions of Chromosome 7q affect nuclear organization and HLXB9Gene expression in hematological disorders. *Cancers (Basel)* 11, 585. doi: 10.3390/cancers11040585

Flavahan, W. A., Gaskell, E., and Bernstein, B. E. (2017). Epigenetic plasticity and the hallmarks of cancer. *Science* 357. doi: 10.1126/science.aal2380

Harewood, L., Schutz, F., Boyle, S., Perry, P., Delorenzi, M., Bickmore, W. A., et al. (2010). The effect of translocation-induced nuclear reorganization on gene expression. *Genome Res.* 20, 554–564. doi: 10.1101/gr.103622.109

Harr, J. C., Gonzalez-Sandoval, A., and Gasser, S. M. (2016). Histones and histone modifications in perinuclear chromatin anchoring: from yeast to man. *EMBO Rep.* 17, 139–155. doi: 10.15252/embr.201541809

Hiratani, I., Ryba, T., Itoh, M., Yokochi, T., Schwaiger, M., Chang, C. W., et al. (2008). Global reorganization of replication domains during embryonic stem cell differentiation. *PLoS Biol.* 6, e245. doi: 10.1371/journal.pbio.0060245

Hveem, T. S., Kleppe, A., Vlatkovic, L., Ersvaer, E., Waehre, H., Nielsen, B., et al. (2016). Chromatin changes predict recurrence after radical prostatectomy. *Br. J. Cancer* 114, 1243–1250. doi: 10.1038/bjc.2016.96

Knecht, H., Kongruttanachok, N., Sawan, B., Brossard, J., Prevost, S., Turcotte, E., et al. (2012). Three-dimensional telomere signatures of hodgkin- and reed-sternberg cells at diagnosis identify patients with poor response to conventional chemotherapy. *Transl. Oncol.* 5, 269–277. doi: 10.1593/tlo.12142

Knight, M., Ittiprasert, W., Odoemelam, E. C., Adema, C. M., Miller, A., Raghavan, N., et al. (2011). Non-random organization of the Biomphalaria glabrata genome in interphase Bge cells and the spatial repositioning of activated genes in cells co-cultured with Schistosoma mansoni. *Int. J. Parasitol.* 41, 61–70. doi: 10.1016/j.ijpara.2010.07.015

Kohwi-Shigematsu, T., Poterlowicz, K., Ordinario, E., Han, H. J., Botchkarev, V. A., and Kohwi, Y. (2013). Genome organizing function of SATB1 in tumor progression. *Semin. Cancer Biol.* 23, 72–79. doi: 10.1016/j.semcancer.2012.06.009

Kong, L., Schafer, G., Bu, H., Zhang, Y., Zhang, Y., and Klocker, H. (2012). Lamin A/C protein is overexpressed in tissue-invading prostate cancer and promotes prostate cancer cell growth, migration and invasion through the PI3K/AKT/PTEN pathway. *Carcinogenesis* 33, 751–759. doi: 10.1093/carcin/bgs022

Kornberg, Z., Cooperberg, M. R., Spratt, D. E., and Feng, F. Y. (2018). Genomic biomarkers in prostate cancer. *Transl. Androl. Urol.* 7, 459–471. doi: 10.21037/tau.2018.06.02

Kumaran, R. I., and Spector, D. L. (2008). A genetic locus targeted to the nuclear periphery in living cells maintains its transcriptional competence. *J. Cell Biol.* 180, 51–65. doi: 10.1083/jcb.200706060

Lallemand-Breitenbach, V., and de The, H. (2010). PML nuclear bodies. *Cold Spring Harb. Perspect. Biol.* 2, a000661. doi: 10.1101/cshperspect.a000661

Laverty, H. G., Wakefield, L. M., Occleston, N. L., O'Kane, S., and Ferguson, M. W. (2009). TGF-beta3 and cancer: a review. *Cytokine Growth Factor Rev.* 20, 305–317. doi: 10.1016/j.cytogfr.2009.07.002

Leshner, M., Devine, M., Roloff, G. W., True, L. D., Misteli, T., and Meaburn, K. J. (2016). Locus-specific gene repositioning in prostate cancer. *Mol. Biol. Cell* 27, 236–246. doi: 10.1091/mbc.e15-05-0280

Li, C., Shi, Z., Zhang, L., Huang, Y., Liu, A., Jin, Y., et al. (2010). Dynamic changes of territories 17 and 18 during EBV-infection of human lymphocytes. *Mol. Biol. Rep.* 37, 2347–2354. doi: 10.1007/s11033-009-9740-y

Mai, S. (2018). The three-dimensional cancer nucleus. *Genes Chromosomes Cancer* 58, 462–473. doi: 10.1002/gcc.22720

Mao, L., Yang, C., Wang, J., Li, W., Wen, R., Chen, J., et al. (2013). SATB1 is overexpressed in metastatic prostate cancer and promotes prostate cancer cell growth and invasion. *J. Transl. Med.* 11, 111. doi: 10.1186/1479-5876-11-111

Massague, J. (2008). TGFbeta in Cancer. *Cell* 134, 215–230. doi: 10.1016/j.cell.2008.07.001

Meaburn, K. J. (2010). Fluorescence *in situ* hybridization on 3D cultures of tumor cells. *Methods Mol. Biol.* 659, 323–336. doi: 10.1007/978-1-60761-789-1_25

Meaburn, K. J. (2016). Spatial genome organization and its emerging role as a potential diagnosis tool. *Front. Genet.* 7, 134. doi: 10.3389/fgene.2016.00134

Meaburn, K. J., Agunloye, O., Devine, M., Leshner, M., Roloff, G. W., True, L. D., et al. (2016). Tissue-of-origin-specific gene repositioning in breast and prostate cancer. *Histochem. Cell Biol.* 145, 433–446. doi: 10.1007/s00418-015-1401-8

Meaburn, K. J., Cabuy, E., Bonne, G., Levy, N., Morris, G. E., Novelli, G., et al. (2007). Primary laminopathy fibroblasts display altered genome organization and apoptosis. *Aging Cell* 6, 139–153. doi: 10.1111/j.1474-9726.2007.00270.x

Meaburn, K. J., Gudla, P. R., Khan, S., Lockett, S. J., and Misteli, T. (2009). Disease-specific gene repositioning in breast cancer. *J. Cell Biol.* 187, 801–812. doi: 10.1083/jcb.200909127

Meaburn, K. J., and Misteli, T. (2008). Locus-specific and activity-independent gene repositioning during early tumorigenesis. *J. Cell Biol.* 180, 39–50. doi: 10.1083/jcb.200708204

Mewborn, S. K., Puckelwartz, M. J., Abuisneineh, F., Fahrenbach, J. P., Zhang, Y., MacLeod, H., et al. (2010). Altered chromosomal positioning, compaction, and gene expression with a lamin A/C gene mutation. *PLoS One* 5, e14342. doi: 10.1371/journal.pone.0014342

Montironi, R., Mazzuccheli, R., Scarpelli, M., Lopez-Beltran, A., Fellegara, G., and Algaba, F. (2005). Gleason grading of prostate cancer in needle biopsies or radical prostatectomy specimens: contemporary approach, current clinical significance and sources of pathology discrepancies. *BJU Int.* 95, 1146–1152. doi: 10.1111/j.1464-410X.2005.05540.x

Naik, R., and Galande, S. (2019). SATB family chromatin organizers as master regulators of tumor progression. *Oncogene* 38, 1989–2004. doi: 10.1038/s41388-018-0541-4

Parada, L., McQueen, P., and Misteli, T. (2004). Tissue-specific spatial organization of genomes. *Genome Biol.* 7, R44. doi: 10.1186/gb-2004-5-7-r44

Paz, N., Felipe-Blanco, I., Royo, F., Zabala, A., Guerra-Merino, I., Garcia-Orad, A., et al. (2015). Expression of the DYRK1A gene correlates with its 3D positioning in the interphase nucleus of Down syndrome cells. *Chromosome Res.* 23, 285–298. doi: 10.1007/s10577-015-9467-7

Peric-Hupkes, D., Meuleman, W., Pagie, L., Bruggeman, S. W., Solovei, I., Brugman, W., et al. (2010). Molecular maps of the reorganization of genome-nuclear lamina interactions during differentiation. *Mol. Cell* 38, 603–613. doi: 10.1016/j.molcel.2010.03.016

Pound, C. R., Partin, A. W., Eisenberger, M. A., Chan, D. W., Pearson, J. D., and Walsh, P. C. (1999). Natural history of progression after PSA elevation following radical prostatectomy. *JAMA* 281, 1591–1597. doi: 10.1001/jama.281.17.1591

Punnen, S., and Cooperberg, M. R. (2013). The epidemiology of high-risk prostate cancer. *Curr. Opin. Urol.* 23, 331–336. doi: 10.1097/MOU.0b013e328361d48e

Randise-Hinchliff, C., Coukos, R., Sood, V., Sumner, M. C., Zdraljevic, S., Meldi Sholl, L., et al. (2016). Strategies to regulate transcription factor-mediated gene positioning and interchromosomal clustering at the nuclear periphery. *J. vCell Biol.* 212, 633–646. doi: 10.1083/jcb.201508068

Saarinen, I., Mirtti, T., Seikkula, H., Bostrom, P. J., and Taimen, P. (2015). Differential predictive roles of A- and B-type nuclear lamins in prostate cancer progression. *PLoS One* 10, e0140671. doi: 10.1371/journal.pone.0140671

Sandhu, G. S., and Andriole, G. L. (2012). Overdiagnosis of prostate cancer. *J. Natl. Cancer Inst. Monogr.* 2012, 146–151. doi: 10.1093/jncimonographs/lgs031

Scheuermann, M. O., Tajbakhsh, J., Kurz, A., Saracoglu, K., Eils, R., and Lichter, P. (2004). Topology of genes and nontranscribed sequences in human interphase nuclei. *Exp. Cell Res.* 301, 266–279. doi: 10.1016/j.yexcr.2004.08.031

Shachar, S., Voss, T. C., Pegoraro, G., Sciascia, N., and Misteli, T. (2015). Identification of gene positioning factors using high-throughput imaging mapping. *Cell* 162, 911–923. doi: 10.1016/j.cell.2015.07.035

Shukla, S., Sharma, H., Abbas, A., MacLennan, G. T., Fu, P., Danielpour, D., et al. (2013). Upregulation of SATB1 is associated with prostate cancer aggressiveness and disease progression. *PLoS One* 8, e53527. doi: 10.1371/journal.pone.0053527

Skvortsov, S., Schafer, G., Stasyk, T., Fuchsberger, C., Bonn, G. K., Bartsch, G., et al. (2011). Proteomics profiling of microdissected low- and high-grade prostate tumors identifies Lamin A as a discriminatory biomarker. *J. Proteome Res.* 10, 259–268. doi: 10.1021/pr100921j

Solovei, I., Wang, A. S., Thanisch, K., Schmidt, C. S., Krebs, S., Zwerger, M., et al. (2013). LBR and lamin A/C sequentially tether peripheral heterochromatin and inversely regulate differentiation. *Cell* 152, 584–598. doi: 10.1016/j.cell.2013.01.009

Takizawa, T., Gudla, P. R., Guo, L., Lockett, S., and Misteli, T. (2008a). Allele-specific nuclear positioning of the monoallelically expressed astrocyte marker GFAP. *Genes Dev.* 22, 489–498. doi: 10.1101/gad.1634608

Takizawa, T., Meaburn, K. J., and Misteli, T. (2008b). The meaning of gene positioning. *Cell* 135, 9–13. doi: 10.1016/j.cell.2008.09.026

Taslerova, R., Kozubek, S., Lukasova, E., Jirsova, P., Bartova, E., and Kozubek, M. (2003). Arrangement of chromosome 11 and 22 territories, EWSR1 and FLI1 genes, and other genetic elements of these chromosomes in human lymphocytes and Ewing sarcoma cells. *Hum. Genet.* 112, 143–155. doi: 10.1007/s00439-002-0847-7

Therizols, P., Illingworth, R. S., Courilleau, C., Boyle, S., Wood, A. J., and Bickmore, W. A. (2014). Chromatin decondensation is sufficient to alter nuclear organization in embryonic stem cells. *Science* 346, 1238–1242. doi: 10.1126/science.1259587

Thompson, I., Thrasher, J. B., Aus, G., Burnett, A. L., Canby-Hagino, E. D., Cookson, M. S., et al. (2007). Guideline for the management of clinically localized prostate cancer: 2007 update. *J. Urol.* 177, 2106–2131. doi: 10.1016/j.juro.2007.03.003

Tian, X., Wang, Y., Zhao, F., Liu, J., Yin, J., Chen, D., et al. (2015). A new classification of interphase nuclei based on spatial organizations of chromosome 8 and 21 for t(8;21) (q22;q22) acute myeloid leukemia by three-dimensional fluorescence *in situ* hybridization. *Leuk. Res.* 39, 1414–1420. doi: 10.1016/j.leukres.2015.09.013

Towbin, B. D., Gonzalez-Aguilera, C., Sack, R., Gaidatzis, D., Kalck, V., Meister, P., et al. (2012). Step-wise methylation of histone H3K9 positions heterochromatin at the nuclear periphery. *Cell* 150, 934–947. doi: 10.1016/j.cell.2012.06.051

Veltri, R. W., and Christudass, C. S. (2014). Nuclear morphometry, epigenetic changes, and clinical relevance in prostate cancer. *Adv. Exp. Med. Biol.* 773, 77–99. doi: 10.1007/978-1-4899-8032-8_4

Wang, L. Y., Cui, J. J., Zhu, T., Shao, W. H., Zhao, Y., Wang, S., et al. (2017). Biomarkers identified for prostate cancer patients through genome-scale screening. *Oncotarget* 8, 92055–92063. doi: 10.18632/oncotarget.20739

Welch, H. G., and Black, W. C. (2010). Overdiagnosis in cancer. *J. Natl. Cancer Inst.* 102, 605–613. doi: 10.1093/jnci/djq099

Williams, R. R., Azuara, V., Perry, P., Sauer, S., Dvorkina, M., Jorgensen, H., et al. (2006). Neural induction promotes large-scale chromatin reorganisation of the Mash1 locus. *J. Cell Sci.* 119, 132–140. doi: 10.1242/jcs.02727

Zink, D., Fische, A. H., and Nickerson, J. A. (2004). Nuclear structure in cancer cells. *Nat. Rev. Cancer* 4, 677–687. doi: 10.1038/nrc1430

Zuleger, N., Boyle, S., Kelly, D. A., de Las Heras, J. I., Lazou, V., Korfali, N., et al. (2013). Specific nuclear envelope transmembrane proteins can promote the location of chromosomes to and from the nuclear periphery. *Genome Biol.* 14, R14. doi: 10.1186/gb-2013-14-2-r14

Conflict of Interest: The authors declare that the research was conducted in the absence of any commercial or financial relationships that could be construed as a potential conflict of interest.

frontiers in Genetics

HYPOTHESIS AND THEORY
published: 21 November 2019
doi: 10.3389/fgene.2019.01179

Nucleolar Sequestration: Remodeling Nucleoli Into Amyloid Bodies

Miling Wang[1,2], *Michael Bokros*[1,2], *Phaedra Rebecca Theodoridis*[1,2] *and Stephen Lee*[1,2,3]*

[1] Department of Biochemistry and Molecular Biology, Miller School of Medicine, University of Miami, Miami, FL, United States, [2] Sylvester Comprehensive Cancer Center, Miller School of Medicine, University of Miami, Miami, FL, United States, [3] Department of Urology, Miller School of Medicine, University of Miami, FL, United States

This year marks the 20th anniversary of the discovery that the nucleolus can temporarily immobilize proteins, a process known as nucleolar sequestration. This review reflects on the progress made to understand the physiological roles of nucleolar sequestration and the mechanisms involved in the immobilization of proteins. We discuss how protein immobilization can occur through a highly choreographed amyloidogenic program that converts the nucleolus into a large fibrous organelle with amyloid-like characteristics called the amyloid body (A-body). We propose a working model of A-body biogenesis that includes a role for low-complexity ribosomal intergenic spacer RNA (rIGSRNA) and a discrete peptide sequence, the amyloid-converting motif (ACM), found in many proteins that undergo immobilization. Amyloid bodies provide a unique model to study the multistep assembly of a membraneless compartment and may provide alternative insights into the pathological amyloidogenesis involved in neurological disorders.

Keywords: heat shock (HS), acidosis, architectural RNA (arcRNA), Alzheimer's disease, cellular dormancy, physiological amyloidogenesis, beta-amyloid protein

OPEN ACCESS

Edited by:
Michael E. Symonds, University of Nottingham, United Kingdom

Reviewed by:
Alexander Kouzmenko, Tokiwa Foundation, Japan
Janine M. LaSalle, University of California, Davis, United States

***Correspondence:**
Stephen Lee
Stephenlee@med.miami.edu

Specialty section:
This article was submitted to Epigenomics and Epigenetics, a section of the journal Frontiers in Genetics

Received: *20 July 2019*
Accepted: *24 October 2019*
Published: *21 November 2019*

Citation:
Wang M, Bokros M, Theodoridis PR and Lee S (2019) Nucleolar Sequestration: Remodeling Nucleoli Into Amyloid Bodies. Front. Genet. 10:1179. doi: 10.3389/fgene.2019.01179

NUCLEOLAR SEQUESTRATION: VISITORS TO THE NUCLEOLUS

The role of the nucleolus as the site of ribosome biosynthesis has been established since the mid-1960s (Perry, 1960; Perry, 1962; Miller and Beatty, 1969). Nucleoli are built around tandem repeats of ribosomal DNA (rDNA) in nucleolar organizing regions (NORs) and structurally dependent on active transcription of rDNA (Hernandez-Verdun, 2006; Raska et al., 2006). Each nucleolus consists of a tripartite organization which is classically defined by their different appearances under electron microscopy (EM) (Pederson, 2011): the fibrillar center (FC), where the RNA polymerase I machinery is active; the dense fibrillar component (DFC) that is enriched in fibrillarin (FIB1); and the granular component (GC) that harbors B23. RNA polymerase I activity is believed to occur at the interface between the FC and the DFC, while processing of newly synthesized ribosomal RNA (rRNA) and assembly with ribosomal proteins occur within the GC (Scheer and Hock, 1999; Thiry and Lafontaine, 2005). The traditional role of the nucleolus as a hub of rRNA synthesis and ribosome assembly has been the subject of many excellent literature surveys (Boisvert, 2007; Pederson, 2011; Nemeth and Grummt, 2018). This review focuses on a lesser known phenomenon originally coined "nucleolar sequestration," which describes the ability of the nucleolus to sequester regulatory proteins in response to cellular cues (Emmott and Hiscox, 2009; Pederson and Tsai, 2009; Boulon, 2010).

2019 marks 20 years since nucleolar sequestration was first hypothesized (Bachant and Elledge, 1999) following the discoveries that cell cycle regulator Cdc14 phosphatase and E3 ubiquitin ligase MDM2 could be temporarily localized in nucleoli to affect cell cycle progression (Shou et al., 1999; Visintin et al., 1999; Weber, 1999; Lohrum, 2000; Bernardi et al., 2004). In *Saccharomyces cerevisiae*,

Cdc14 is sequestered in the nucleolus by Cfi1/Net1 until anaphase onset when it is released to promote exit from mitosis (Shou et al., 1999; Visintin et al., 1999). In mammalian cells, nucleolar sequestration of MDM2 prevents it from binding and exporting p53 into the cytoplasm for degradation (Weber, 1999; Lohrum, 2000; Bernardi et al., 2004). This stabilizes p53 in the nucleus, where it acts as a transcription factor that promotes growth arrest or apoptosis. The E3 ubiquitin ligase von Hippel–Lindau protein (VHL) is another example of nucleolar sequestration (Mekhail, 2004). VHL promotes the degradation of the transcription factor hypoxia-inducible factor (HIF) under normal oxygen conditions. Low extracellular pH triggers nucleolar sequestration of VHL, enabling HIF to evade degradation and promote transcription of target genes involved in oxygen homeostasis. **Table 1** summarizes the reports of nucleolar sequestration that have been observed for many other proteins under various cellular conditions. Taken together, these underscore a fundamental cellular strategy that uses the nucleolus to regulate protein dynamics in response to cellular cues.

NUCLEOLAR SEQUESTRATION: A CASE OF PROTEIN IMMOBILIZATION

The Nucleolar Detention Centers

Pioneering work by Phair and Misteli (2000) showed that proteins are highly mobile and rapidly exchange between affinity interactions and the cellular milieu. The nucleolus is considered a dynamic droplet, assembled by demixing of its three sub-structural liquid phases (i.e., FC, DFC, and GC), which are composed of highly mobile proteins (Brangwynne et al., 2011; Feric et al., 2016; Hult et al., 2017; Sawyer et al., 2019). It is remarkable, then, that proteins undergoing nucleolar sequestration are non-dynamic or immobile (Mekhail, 2004; Mekhail, 2005; Audas et al., 2012; Jacob, 2013). This has been demonstrated for Cdc14 (Tomson et al., 2009), MDM2 (Audas et al., 2012), VHL (Mekhail, 2005), RNF8 (Mekhail, 2007), DNMT1 (Audas et al., 2012), and Piwi (Mikhaleva, 2018), amongst other proteins. Even resident nucleolar proteins such as RNA polymerase I subunit RPA16, Pescadillo, and SENP3 can undergo cycles of mobility/immobility (Jacob, 2013). For example, VHL switches from a highly dynamic, uniform distribution under standard growth conditions (21% O_2, pH 7.4) to an immobilized state in the nucleolus on exposure to extracellular acidosis (1% O_2, pH 6.0) (Mekhail, 2005). Only upon neutralization of extracellular pH is VHL released from the nucleolus to return to its original distribution and mobility (Mekhail, 2005). These nuclear foci that contain sequestered/immobile proteins were originally called "nucleolar detention centers," as targets are both localized and detained within the nucleolus, unable to freely diffuse elsewhere (Mekhail, 2005; Audas et al., 2012b; Jacob, 2013). From this perspective, the function of nucleolar detention or immobilization is to temporarily inactivate relevant proteins, inhibiting their access to downstream effectors. Just as possible, though, is that the clustering of detained proteins may render an enzymatic reaction more efficient. For example, immobilized nucleolar Cdc14 maintains Spo12 dephosphorylation to regulate cell cycle progression (Tomson et al., 2009). In addition, Piwi switches from its canonical role as a non-nucleolar transposable element repressor to a rDNA-specific repressor when it is

TABLE 1 | List of the proteins whose activities have been reported to be regulated by nucleolar sequestration.

Protein symbol	Full name	Stimulus	Nucleolar response	Model system	Reference
Cdc14	Cell division cycle 14	Anaphase	Release	*S. cerevisiae*	(Shou, 1999) (Visintin et al., 1999)
Pch2	Pachytene checkpoint 2	Meiotic prophase arrest	Release	*S. cerevisiae*	(San-Segundo and Roeder, 1999)
MDM2	Murine double minute 2 homolog	Ribosomal stress DNA damage	Capture	Mammalian	(Weber, 1999) (Lohrum, 2000) (Bernardi, 2004)
hTERT	Human telomerase reverse transcriptase	Transformation, DNA damage Ionizing radiation	Release Capture	Mammalian	(Wong et al., 2002)
c-Myc	Proto-oncogene c-Myc	Proteasomal stress	Capture	Mammalian	(Arabi, 2003)
ADAR2	Adenosine deaminase that acts on RNA 2	Inhibition of rRNA synthesis	Release	Mammalian	(Sansam et al., 2003)
VHL	von Hippel Lindau tumor suppressor	Extracellular acidosis	Capture	Mammalian	(Mekhail, 2004)
RelA	p65 subunit of transcription factor NF-κB	Aspirin, serum withdrawal, UV-C radiation	Capture	Mammalian	(Stark and Dunlop, 2005) (Chen and Stark, 2017)
Polycomb	Polycomb	Cell differentiation	Capture	*D. melanogaster*	(Chen, 2005)
Hand1	Heart and neural crest derivatives expressed 1	Cell differentiation	Capture/Release	Mammalian	(Martindill et al., 2007)
Hsc70	Heat shock chaperone 70	Recovery from heat shock	Capture	Mammalian	(Banski, 2010)
Ulp1	Small ubiquitin-related modifier (SUMO) protease	Alcohol	Capture	*S. cerevisiae*	(Sydorskyy et al., 2010)
p53	Cell cycle regulator; tumor suppressor	Proteasomal inhibition (MG132)	Capture	Mammalian	(Kruger and Scheer, 2010) (Latonen, 2011)
Piwi	piRNA binding protein	Heat shock	Capture	*D. melanogaster*	(Mikhaleva, 2018)

sequestered in the nucleolus (Mikhaleva, 2018). From these studies, it is clear that cells have evolved a strategy to regulate molecular networks by reversibly switching proteins between a mobile and an immobile state. Whether nucleolar sequestration represents a loss- or gain-of-function might depend on the proteins undergoing immobilization.

Mechanisms of Nucleolar Sequestration

The ability of the nucleolus to sequester a wide variety of proteins in various cellular contexts suggests multiple mechanisms for nucleolar sequestration. Pathway analysis of interactions between resident nucleolar proteins and visitor proteins indicates that sequestered proteins interact either directly or indirectly, with the same small subset of "hub" nucleolar proteins, which primarily includes B23/NPM and Nucleolin (Emmott and Hiscox, 2009). Nucleolar retention of highly dynamic proteins through interactions with less mobile "hub" nucleolar partner(s) anchored by multivalent protein and RNA interactions contribute to nucleolar plasticity (Mitrea et al., 2016). Cdc14 is anchored in the nucleolus for most of the cell cycle through its association with Cfi1/Net1 (Shou et al., 1999; Visintin et al., 1999). During anaphase onset, a signaling cascade of phosphorylation inhibits the interaction of Cdc14 with Net1, releasing it to act as a mitotic exit activator (Azzam et al., 2004). ARF binding to MDM2 unmasks a cryptic nucleolar localization signal (NoLS) within its C-terminal RING domain, which is essential for MDM2 nucleolar sequestration (Tao and Levine, 1999; Weber, 1999; Lohrum, 2000; Weber et al., 2000). During DNA damage and acidosis, MDM2 is shuttled into the nucleolus by direct binding to PML (promyelocytic leukemia protein) (Bernardi et al., 2004), itself a target of nucleolar sequestration (Mattsson, 2001). MDM2 can also be sequestered in nucleoli by binding to ATP, independently of ARF (Poyurovsky et al., 2003). Alternatively, MDM2 binds ribosomal proteins (e.g., RPL5 and RPL11) that are released into the nucleoplasm during ribosomal stress, which stabilizes p53 (Boulon, 2010; Liu et al., 2016). Mapping analysis of VHL identified an approximately 30-amino acid fragment referred to as a nucleolar detention signal (NoDS) that is necessary and sufficient to immobilize proteins in nucleoli (Mekhail, 2007). The NoDS is composed of an arginine/histidine-rich sequence followed by two or more hydrophobic LXV motifs where X can be any hydrophobic residue (e.g., LWL, LLV, LFV, and LQV). A survey of proteins containing NoDS identified many candidates harboring this motif, including DNA methyltransferase I DNMT1, PML, and DNA polymerase delta catalytic subunit POLD1, all shown to be immobilized in nucleoli under extracellular acidosis (Mekhail, 2007; Audas et al., 2012a). The NoDS interacts with inducible long noncoding RNA derived from the ribosomal intergenic spacer (rIGSRNA) (Audas et al., 2012a). Silencing of rIGSRNA is sufficient to prevent both the formation of nucleolar detention centers and immobilization of NoDS-containing proteins (Audas et al., 2012a). The identification of the NoDS in many proteins provided evidence that nucleolar sequestration is a common cellular strategy to regulate protein function (Mekhail, 2007).

BIOCHEMICAL PROPERTIES OF NUCLEOLAR DETENTION CENTERS

Nucleolar Detention Centers Display Amyloidogenic-Like Characteristics

In various physiological settings, proteins with limited mobility often display amyloid-like properties (Kayatekin et al., 2014; Berchowitz et al., 2015). Amyloidogenesis is the process whereby soluble proteins assemble into aggregates known as amyloid fibrils (Knowles et al., 2014). Because of their association to neurodegenerative disorders, including Alzheimer's and Parkinson's disease, amyloids were classically perceived as exclusively toxic protein aggregates (Schnabel, 2010; Knowles et al., 2014). The discovery of functional amyloid Pmel17 in 2006 challenged the notion that the amyloid state is merely pathological (Fowler, 2006). Since then, several groups have reported the existence of functional/physiological amyloids in different organisms (Chiti and Dobson, 2006; Fowler, 2007; Maji et al., 2009; Falabella et al., 2012; Fowler and Kelly, 2012; Li et al., 2012; Kayatekin et al., 2014; Berchowitz et al., 2015; Tang et al., 2015; Saad, 2017; Cereghetti, 2018). Nucleolar detention centers composed of proteins such as VHL, MDM2, POLD1, etc., share many properties beyond immobility that are associated with the amyloid state. First, these nuclear foci stained positive with amyloidophilic dyes such as Congo red, Thioflavin S/T, and Amylo-Glo, all of which recognize different biochemical features of amyloids (Audas et al., 2016). Second, the nucleolar detention centers stain positive for the OC fibril antibody that specifically targets the amyloid fibril conformation (Kayed et al., 2007). Third, immobilized proteins found in these nuclear foci displayed biochemical properties associated with amyloids, including resistance to proteinase K, insolubility in common detergents, and can only be dissociated into monomers by SDS/high temperature (Audas et al., 2016). Arguably the utmost unique feature of amyloid bodies is their electron-dense fibrillar organization, which would be as predicted for a condensate enriched in amylogenic proteins (Jacob, 2013; Audas et al., 2016). Consequently, the terms "nucleolar detention centers" and NoDS were replaced with "amyloid bodies" (A-bodies) and "amyloid-converting motif" (ACM), respectively, to reflect the transformation of the nucleolus into an A-body, a molecular prison of proteins in their amyloid-like state. **Figure 1A** shows an example of this dramatic and reversible transformation of the tripartite nucleolus into the fibrillar A-body in cells responding to stimuli.

Amyloid Bodies Are Distinct From Liquid-Like Biomolecular Condensates and Other Nucleolar Organizations

Purification and mass spectrometry analysis have identified hundreds of cellular proteins that are captured in A-bodies, many of which were shown to undergo immobilization by photobleaching experiments (Mekhail, 2007; Audas et al., 2012a; Audas et al., 2016). Because A-bodies contain an array of immobilized proteins in an amyloid-like state, we suggested the term "systemic physiological amyloidogenesis" to describe A-body biogenesis, in keeping with the original terminology to describe functional amyloids (Chiti and Dobson, 2006; Fowler, 2007; Maji et al., 2009). Other laboratories have also proposed that A-body formation represents an amyloidogenic

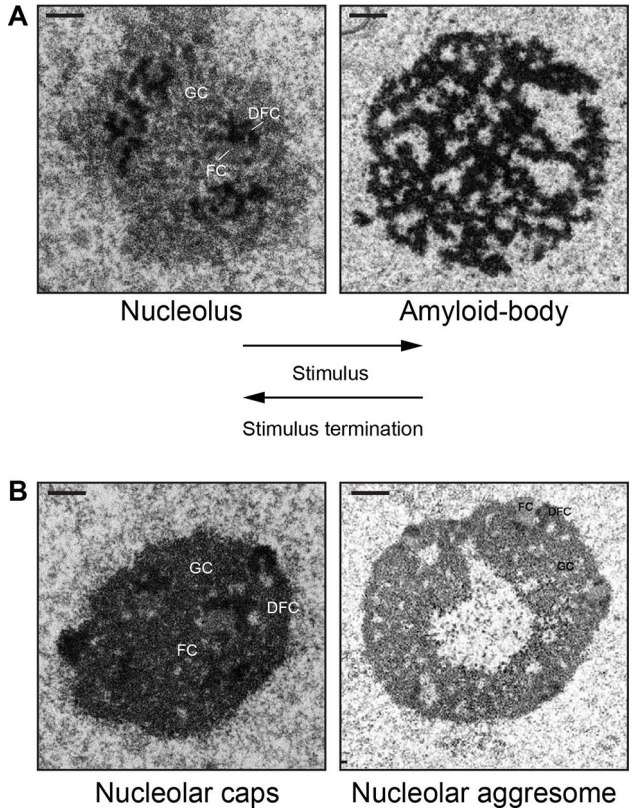

FIGURE 1 | Nucleolar sequestration: the reversible remodeling of the nucleolus into an amyloid body. **(A)** During stimuli (heat shock or extracellular acidosis), the tripartite nucleolus undergoes a dramatic transformation into electron-dense fibrillar organization that characterizes an amyloid body. The fibers contain immobilized proteins in an amyloid-like state. After stimuli termination, an amyloid body is disaggregated and transforms back into the tripartite nucleolus. **(B)** The fibrillar amyloid bodies are distinct from the amorphous, electron-dense nucleolar caps (16 h cisplatin) or the electron-light nucleolar aggresomes (16 h MG132). *FC,* fibrillar component; *DFC,* dense fibrillar component; *GC,* granular component. Scale represents 1 μm. Amyloid body and nucleolar aggresome taken from (Audas, 2016) and (Kruger and Scheer, 2010), with permission.

liquid-to-solid phase transition (Lyons and Anderson, 2016; Latonen, 2019; Hall et al., 2019) and used the terms "solid," "solid-like," or "non-dynamic" biomolecular condensates to describe this membraneless organelle (Lyons and Anderson, 2016; Weber, 2017; Cereghetti, 2018; Holehouse and Pappu, 2018; Woodruff et al., 2018; Itakura et al., 2018; Fay and Anderson, 2018; Latonen, 2019). Prior to the discovery of A-bodies, the terms "liquid-to-solid phase transition" and "solid" had been reserved to describe the formation of pathological aggregates (Patel et al., 2015; Murakami et al., 2015; Jain and Vale, 2017; Mateju et al., 2017; Peskett, 2018; Posey et al., 2018). Other physiological examples of "solid-like" structures include Balbiani bodies observed in *Xenopus* (Boke et al, 2016) and pH-regulated fluid-to-solid transition of the cytoplasm in yeast (Munder et al, 2016). The fibrous, amyloid-like characteristic of the A-body differentiates it from other biomolecular condensates that display liquid-like properties (Brangwynne et al., 2009; Brangwynne et al., 2011; Weber and Brangwynne, 2012; Zhu and Brangwynne, 2015; Banani, 2017; Shin and Brangwynne, 2017), such as stress granules, nucleoli, and paraspeckles, amongst others (Hodges, 1998; Gall, 2000; Lamond and Spector, 2003; Rizzi et al., 2004; Dellaire and Bazett-Jones, 2004; Valgardsdottir, 2005; Parker and Sheth, 2007; Sasaki and Hirose, 2009; Bond and Fox, 2009; Machyna et al., 2013; Pederson, 2011; Protter and Parker, 2016). Liquid-like biomolecular condensates are dynamic, their constituents are mobile, they do not form fibers detectable by EM nor do they typically stain with amyloidophilic dyes (Phair and Misteli, 2000; Shin and Brangwynne, 2017; Weber, 2017). The biochemical and biophysical differences between dynamic, liquid-like, and non-dynamic or solid-like condensates are summarized within **Table 2**.

A-bodies may also be contrasted from other stress-induced nucleolar structures, namely, nucleolar caps (Shav-Tal et al., 2005) and nucleolar aggresomes (Latonen, 2011; Latonen, 2011; Latonen, 2019) (**Figure 1B**). Transcriptional inhibition of Pol I results in nucleolar segregation, in which the FC and GC phases separate, perhaps as a consequence of changes in surface tension (Shin and

TABLE 2 | Biochemical, biophysical, and dynamic properties of liquid-like condensates or solid-like condensates with amyloid characteristics.

	Liquid-like condensates	**Solid-like condensates**
Examples	Cytoplasm stress granules (Protter and Parker, 2016) P-bodies (Parker and Sheth, 2007) Nuclear stress granules (Rizzi et al., 2004; Valgardsdottir et al., 2005) Cajal bodies (Gall, 2000; Machyna et al., 2013) Nuclear speckles (Lamond and Spector, 2003) Nuclear paraspeckles (Bond and Fox, 2009; Sasaki and Hirose, 2009) Nucleoli (Pederson, 2011) PML nuclear bodies (Hodges et al., 1998; Dellaire and Bazett-Jones, 2004)	Amyloid bodies (Audas, 2016) Balbiani bodies (Boke, 2016)
Protein mobility	Proteins are mobile; continuously exchanging with the structure and the surrounding milieu	Proteins are immobile; engaged in strong intermolecular interactions
Shape	Spherical	Spherical or fibrous
Biochemical and biophysical characteristics	• Structure is dynamic; exhibiting properties of water droplets:Fluid • Cycles of fusion (coalescence) and fission • Wetting behavior • Flows under shear force	• Structure is non-dynamic; exhibiting properties of amyloids:Static • Fibrillar organization • Positive staining with amyloidophilic dyes (e.g., Congo red) • Resistant to proteinase K • Insoluble in common detergents • Cross-β diffraction pattern
Material properties	Viscous	Elastic
Function	Biochemical reactions	Cell dormancy
Mechanism	Liquid–liquid phase separation	Liquid-to-solid phase transition

Brangwynne, 2017) resulting in the formation of perinucleolar caps that surround the segregated nucleolus (Shav-Tal et al., 2005). Proteasomal inhibition induces nucleolar inclusions called nucleolar aggresomes that contain proteins marked for degradation, and various RNAs (Latonen, 2011). By EM, A-bodies have a unique fibrillar organization characteristic of amyloids, whereas nucleolar caps appear as electron-dense amorphous structures and nucleolar aggresomes are cavernous, occupying a large electron-light central space of the nucleolus (Kruger and Scheer, 2010) (**Figure 1B**). Interestingly, while the formation of nucleolar caps and A-bodies is accompanied by a redistribution of nucleolar components and subsequent arrest of ribosomal biogenesis (Shav-Tal et al., 2005; Mekhail, 2006; Jacob, 2013), nucleolar aggresomes require transcriptionally active nucleoli to form (Latonen, 2011; Latonen, 2011), with all nucleolar components intact and visible by EM. Additionally, proteins are dynamically sorted into nucleolar caps and remain mobile (Shav-Tal et al., 2005), while several proteins in A-bodies and nucleolar aggresomes are immobile (Mekhail, 2005; Audas et al., 2012a; Jacob, 2013; Audas et al., 2016). Another recently identified nucleolar stress body, nucleolar amyloid bodies (NoABs), is induced by prematurely terminated peptides that diffuse through the nuclear pores and aggregate within the nucleolus (Mediani et al., 2019). EM has not been reported for NoABs. It remains to be tested if NoABs are rIGSRNA-dependent, as are A-bodies, and if prematurely terminated peptides are involved in nucleolar sequestration of full-length proteins. While there are definitive similarities between the different stress-induced nucleolar organizations and that proteins can undergo sequestration in nucleolar aggresomes (both are discussed in (Latonen, 2019), A-bodies represent a unique nucleolar structure based on their fibrous properties and dependency on rIGSRNA.

PROTEIN IMMOBILIZATION INTO A-BODIES: A CHOREOGRAPHED MULTISTEP PATHWAY

How membraneless subcellular condensates maintain their unique identities and how proteins and/or RNA are sorted into these condensates remain subjects of active research. New insights into the biophysical properties of biomolecular condensates have demonstrated unexpected links between the sequence-encoded information in protein and RNA components of compartments and the material properties they impart (Kato et al., 2012; Altmeyer et al., 2015; Brangwynne et al., 2015; Elbaum-Garfinkle et al., 2015; Molliex et al., 2015; Nott et al., 2015; Pak et al., 2016; Shin and Brangwynne, 2017; Weber, 2017; Langdon, 2018). Recent studies demonstrated the importance of RNA-binding proteins with prion-like, low-complexity domains in forming biomolecular condensates. Equally as exciting has been the work done to uncover the specific sequences or structural elements embedded in architectural RNA that dictate the biophysical properties of biomolecular condensates (Chujo, 2017; Chujo and Hirose, 2017; Yamazaki et al., 2018; Hirose et al., 2019). With these new tools, we have begun to understand how specific elements within RNA and proteins are involved in condensate biogenesis.

A Working Model of A-Body Biogenesis

Figure 2 proposes a stepwise working model of A-body biogenesis that integrates different opinions in the literature, showcasing this process as a precisely choreographed multistep routine rather than simply a random aggregation of misfolded proteins. The first step in the formation of A-bodies is the appearance of several transient foci that are distinct from known nucleolar layers (Wang et al., 2018). These foci are spherical, contain mobile proteins, and can undergo fusion, thereby displaying some of the properties associated with dynamic condensates. An interesting feature of the inducible nucleolar foci is that they stain positive for 1-anilino-8-naphthalenesulfonate (ANS), a dye specific for hydrophobic regions of proteins and used *in vitro* to detect the molten globule state, a precursor of amyloid fibrils (Booth, 1997). EM revealed that ANS-positive foci correspond to electron-dense, amorphous aggregates concomitant with loss of the typical tripartite organization of transcriptionally active nucleoli. In the second step, the stimulus-induced foci

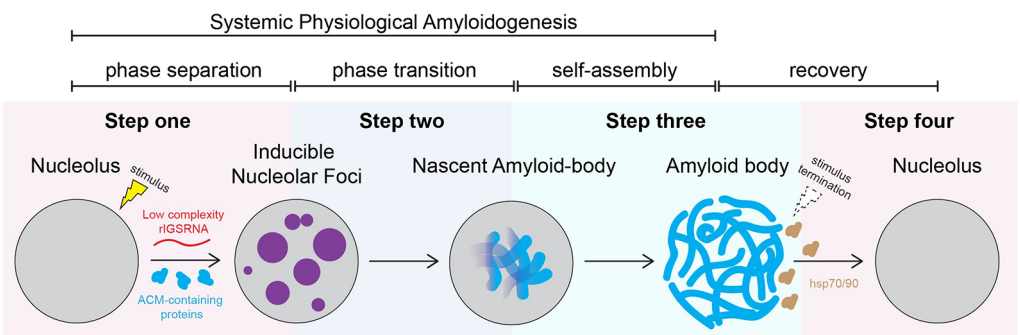

FIGURE 2 | Working model: amyloid body biogenesis is a precisely choreographed routine. We propose that, on stimulus, low-complexity ribosomal intergenic spacer RNA (rIGSRNA) derived from the rDNA intergenic spacer accumulate in the nucleolus. Step 1: Low-complexity rIGSRNA interact with short cationic peptides, such as the R/H-rich sequence of the ACM (formally NoDS), to form nucleolar liquid-like foci. Step 2: Local concentration of proteins with amyloidogenic propensity in the foci triggers physiological amyloidogenesis and generates nascent amyloid bodies (A-bodies). Step 3: Once seeded, nascent A-bodies self-assemble into fibrillar, solid-like A-bodies. A-bodies enable cells to rapidly and reversibly store a large array of proteins and enter cellular dormancy in response to stress. Step 4: Upon recovery/stimulus termination, A-body disaggregation is mediated by heat shock protein (hsp) chaperones 70 and 90. Through these steps, A-body biogenesis may represent a physiological liquid-to-solid phase transition.

rapidly mature into Congo red-positive aggregates that contain immobilized proteins, limiting their ability to diffuse within the nucleolus. We coined these maturing foci "nascent A-bodies." Photobleaching analysis showed that, once formed, nascent A-bodies expand by directly capturing and immobilizing free proteins (step 3) (Wang et al, 2018). Maturation of A-bodies terminates once the pools of cellular mobile proteins have been depleted, culminating in a distinct fibrous organization. Disassembly of A-bodies occurs within 1–2 h after stimulus termination, a process that requires heat shock proteins hsp70 and hsp90 (step 4) (Audas et al., 2016).

Low-Complexity rIGSRNA Drive Formation of Inducible Nucleolar Foci

In mammals, the nucleolus is organized around a scaffold of ~400 rDNA tandem repeats of 43 kb, of which approximately half are transcriptionally active (Nemeth and Grummt, 2018; Sharifi and Bierhoff, 2018). Each repeat consists of an rDNA enhancer/promoter located directly upstream of rRNA genes separated by a ribosomal intergenic spacer (rIGS) of variable length and organization (Gonzalez and Sylvester, 1995; Smirnov, 2016) (**Figure 3A**). The rIGS is an enigmatic region of the human genome historically, and erroneously, called the "non-transcribed region" (Smirnov, 2016). Interestingly, in recent years, species conservation (Agrawal and Ganley, 2018) and functional studies have demonstrated that these regions of the genome are transcriptionally active, generating various non-coding RNA (ncRNA) (Jacob, 2012; Audas and Lee, 2016). These ncRNA from the rIGS are involved in regulating rRNA expression (Mayer, 2006; Mayer et al., 2008; Schmitz, 2010; Zhao, 2016; Zhao, 2018) and thereby responsible for maintaining a significant fraction of the rDNA cassettes in a heterochromatic, transcriptionally silent chromatin structure (Grummt and Pikaard, 2003; Santoro, 2005), controlling PTBP1-regulated alternative splicing (Yap, 2018), and assembling A-bodies (Audas et al., 2012a; Jacob, 2013; Audas et al., 2016; Wang et al., 2018) (**Figure 3A**). The various rIGS ncRNA appear to be products of RNA polymerase I (Mayer, 2006; Audas et al., 2012a), except for the antisense PAPAS, which is transcribed by RNA polymerase II (Zhao, 2016).

The appearance of nucleolar foci under stress coincides with the induction of $rIGS_{28}$RNA in acidosis, and $rIGS_{16}$RNA and $rIGS_{22}$RNA in heat shock (**Figure 3**). Recent work suggests that low-complexity dinucleotide repetitive sequences operate as the architectural determinants of rIGSRNA to recruit proteins to A-bodies (Wang et al., 2018) (**Figure 3B**). Live cell imaging and *in vitro* assays indicated that positively charged R/H-rich peptide domains of the ACM (**Figure 4**) co-assemble more efficiently with the negatively charged low-complexity sequences of rIGSRNA than with flanking high-complexity RNA sequences to form the inducible nucleolar foci (Wang et al., 2018). The rIGSRNA/ACM interactions *in vitro* and *in vivo* are particularly sensitive to even the slightest increase in salt concentration. This contrasts other phase-separated compartments of the nucleolus, which are disrupted at considerably higher salt concentrations. Thus, the interactions between low-complexity RNA and the R/H-rich region of the ACM characteristic of step 1 in A-body biogenesis (**Figure 2**) appear to be electrostatic in nature and are likely driven by complex coacervation, a charge-based form of liquid–liquid phase separation that has been

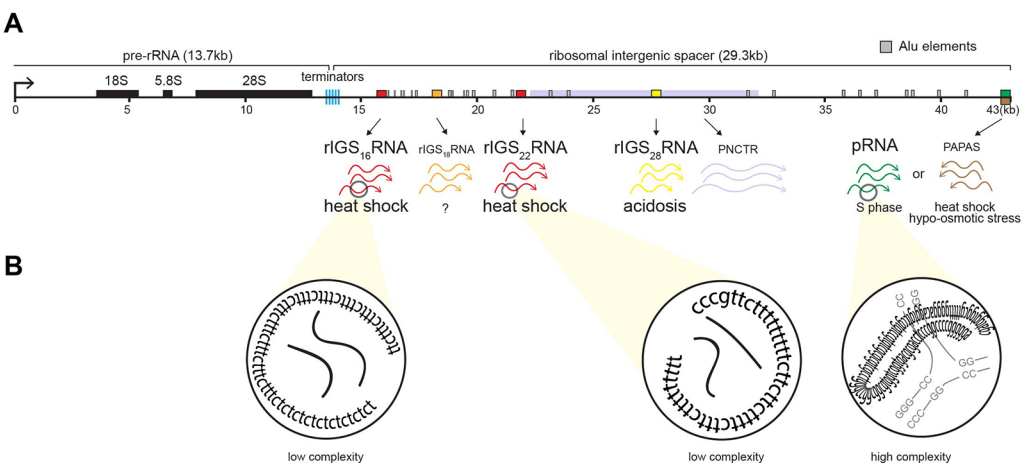

FIGURE 3 | Induction of non-coding RNA (ncRNA) from the ribosomal cassette. **(A)** Schematic of a single human rDNA repeat unit, which is composed of a ~13-kb pre-rRNA coding region flanked by a ~30-kb intergenic spacer (rIGS). The rIGS transcribes several functional non-coding RNA. Stimuli-specific loci of rIGS produce ribosomal intergenic spacer RNA (rIGSRNA) required for A-body formation. $rIGS_{28}$RNA and $rIGS_{16}$RNA/$rIGS_{22}$RNA are produced under acidotic (*yellow*) and heat shock (*red*) conditions, respectively. No function has been ascribed to $rIGS_{18}$RNA yet. Other ncRNA found in the rIGS include a >10-kb transcript called PNCTR (pyrimidine-rich non-coding transcript) involved in PTBP1 binding (purple), *pRNA* (green), and antisense PAPAS (brown) involved in rRNA regulation, as well as Alu element-derived (gray boxes) RNA involved in nucleolar architecture. **(B)** rIGSRNA contain low-complexity sequences comprising of long dinucleotide repeats, as determined by RNA sequencing, RT cloning, and RNA-FISH. This is in contrast to other ncRNA that display high complexity, i.e., possess secondary structure, such as pRNA.

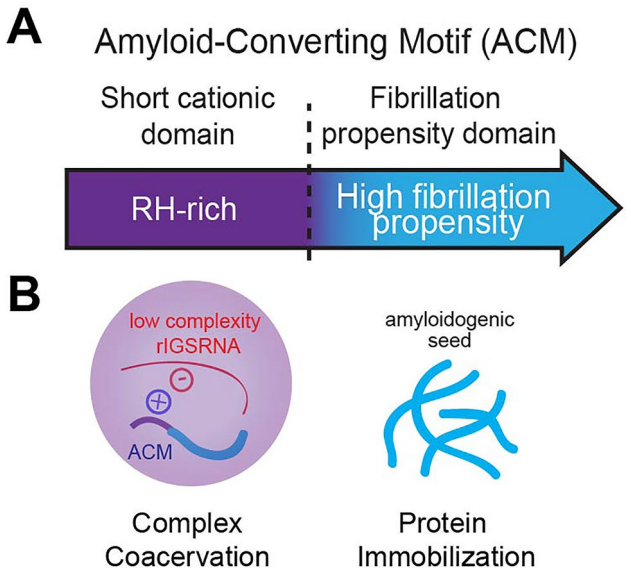

FIGURE 4 | The amyloid-converting motif (ACM). **(A)** The ACM is necessary and sufficient to target and immobilize proteins in amyloid bodies (A-bodies). It consists of a R/H-rich short cationic domain flanking a high fibrillation propensity domain (determined by Rosetta energy of less than −23 kcal/mol). **(B)** We propose that it is its bipartite nature that allows the ACM to traverse phase boundaries. Complex coacervation of short cationic domains and low-complexity rIGSRNA (liquid–liquid phase separation) concentrates fibrillation propensity domains to activate a liquid-to-solid phase transition to form A-bodies.

observed in other cellular settings *in vivo* (Altmeyer et al., 2015; Pak et al., 2016).

Amyloidogenic Properties of the ACM Trigger Protein Immobilization

In principle, A-bodies and Balbiani bodies should be composed of proteins that possess fibrillation propensity, i.e., increased likelihood of forming fibrils. Bioinformatic analysis of the consensus ACM revealed the hydrophobic LXV motifs make up a region of high fibrillation propensity, as predicted by a Rosetta energy score of less than −23 kcal/mol (Goldschmidt, 2010) (**Figure 4A**). As a whole, the ACM bears a striking resemblance to that of the prototypical pathological β-amyloid, historically associated with Alzheimer's disease, in which a R/H-rich sequence is in close proximity to a region of high fibrillation propensity referred to in literature as the P3 fragment (**Figure 4A**) (Dulin et al., 2008). The ACM exhibits classic amyloidogenic properties previously observed for β-amyloid, namely, the cross-β X-ray diffraction pattern *in vivo* and the ability to form fibrils *in vitro* (Audas et al., 2016).

It has been proposed that the function of the initial liquid state is to locally concentrate proteins with fibrillation propensity that would otherwise be at levels below the critical threshold in the cell (Knowles et al., 2014). Concentration-dependent activation of protein fibrillation has been well-documented *in vitro* (Eisenberg and Jucker, 2012; Knowles et al., 2014). Indeed, markers of early or nascent A-bodies include ANS and A11 staining (Wang et al., 2018) that are typically used *in vitro* to indicate accumulating pre-amyloidogenic structures (Booth, 1997; Kayed et al., 2007; Hawe et al., 2008; Tang et al., 2015). In addition, photobleaching analyses revealed that the core of nucleolar foci contain immobile proteins. Nascent A-bodies expand by self-assembly, during which soluble proteins are added directly and autonomously to the growing amyloid structure (**Figure 2**) (Wang et al., 2018).

The ACM Traverses Across Phase Boundaries to Confer A-Body Identity

As described above, low-complexity RNA sequences are important in conferring A-bodies their unique identity (Wang et al., 2018), adding to the list of architectural determinants, which includes sequence-specific RNA (Yamazaki et al., 2018), mRNA secondary structure (Jain and Vale, 2017; Langdon, 2018), and short unstructured RNA *in vitro* (Nott et al., 2016). The low-complexity rIGSRNA-mediated foci themselves appear immiscible from the three canonical compartments of the nucleolus (Feric et al., 2016; Wang et al., 2018), suggesting they exhibit distinct properties that may exclude mixing. Ultimately, it is the bipartite nature of the ACM that confers A-body identity and differentiates the ACM from other motifs. One possibility is that the R/H-rich "short cationic domain" mediates complex coacervation while the "fibrillation propensity domain" initiates amyloidogenesis to immobilize proteins in A-bodies (Audas et al., 2016; Wang et al., 2018) (**Figure 4B**). In this model, proteins without a region of high fibrillation propensity are unlikely to be incorporated into A-bodies. In other words, while many proteins containing positively charged domains can form transient rIGSRNA-dependent nucleolar foci, only the ones that harbor high fibrillation propensity sequences will be found immobilized in A-bodies. The balance of positive to negative charge ratio, presence of polar and/or aromatic residues, and modifications (Aumiller and Keating, 2016; Monahan et a.l, 2017) will affect how ACM engage in intermolecular interactions with other proteins and low-complexity RNA. Therefore, the ACM is versatile as it can physiologically transition proteins across phase boundaries.

PHYSIOLOGICAL AMYLOIDS PROMOTE CELL DORMANCY

Endogenous A-bodies have been found in primary cultures and cell lines exposed to various stimuli, the cores of human tumors, and subsets of cells in normal human and mouse tissues (Audas et al., 2016). So, while A-bodies share structural features with pathological amyloids, their ubiquitous and reversible nature is indicative of a physiological function. Pathway enrichment analysis determined that many of the proteins sequestered in A-bodies are involved in cell cycle regulation and DNA synthesis, such as CDK1, POLD1, and DNMT1 (Audas et al., 2016). By temporarily detaining key factors from their sites of activity into A-bodies, major molecular networks

are disrupted, suppressing metabolic activity (Mekhail, 2006) and arresting proliferation/DNA synthesis (Audas et al., 2016). This is different from the quiescent state (G0) in the cell cycle where cells arrest proliferation but remain metabolically active. Therefore, the biological role of A-body formation is to promote cellular dormancy as an adaptive response to environmental stressors. These findings are consistent with reports that show Balbiani bodies (Boke et al., 2016) and fluid-to-solid transitions in yeast (Munder et al, 2016) promote dormancy, reinforcing the concept that cells utilize different states of matter to perform various biological functions (**Table 2**). The material properties of "solid-like" systems—non-dynamic, amyloid-like—result in loss of metabolic activity and promote cellular dormancy, while those of "liquid-like" systems—dynamic, fluid-like—concentrate and facilitate biochemical reactions.

A-BODIES AS TARGETS FOR THERAPEUTIC DISCOVERY

Implications for Pathological Amyloids

A-bodies that are physiologically produced remain confined within the nucleus and are considered non-toxic amyloids (Wang et al., 2017). How the nuclear environment alters the interaction properties of aggregation-prone proteins to prevent toxicity (Woerner et al., 2016; Maharana, 2018) compared to the cytoplasm is unclear. These results imply the cell tightly regulates the induction and degradation of low-complexity rIGSRNA within the nucleolus in response to stimuli. It is interesting that the pathological β-amyloid involved in Alzheimer's disease is an ACM and undergoes immobilization in A-bodies. Mutations that decrease the fibrillation potential of β-amyloid prevent its immobilization in A-bodies, providing a link between β-amyloid fibrillation and A-body biogenesis. It is tempting to speculate that disruptions of A-body biogenesis, for example by cell death, may provide the initial seeds for pathological amyloidogenesis. Whether aberrant production or localization of low-complexity RNA or exposure of A-bodies to the extracellular environment is involved in amyloid pathologies such as Alzheimer's and Huntington's diseases will be the subject of future studies.

Implications for Tumor Cell Dormancy and Metastasis

Given the evidence that A-bodies are observed in the cores of tumors and promote cell dormancy (Audas et al., 2016), perhaps there is a link between A-body formation and tumor cell dormancy. This could allow cancer cells to adapt to the harsh hypoxic/acidotic conditions of the tumor microenvironment. Such a connection has pertinent implications for chemotherapeutic resistance and metastasis (Li, 2014; Li, 2015). With major metabolic pathways shut down and key drug targets stored away in A-bodies, a small population of dormant tumor cells may be resistant to treatment, survive for a prolonged period of time, and contribute to disease recurrence or metastasis upon their metabolic reactivation. Preventing cancer cells from forming A-bodies and going dormant or, more realistically, preventing cancer cells from reactivating may become a viable treatment option.

An interesting avenue of research that may offer a more effective cancer treatment strategy involves manipulating the proteins that evade capture into A-bodies. Interestingly, proteins that remain active to sustain basal metabolism and viability under stress tend to be devoid of fibrillation propensity domains and evade capture into A-bodies. These proteins would be more susceptible to manipulation and serve as better chemotherapeutic targets than proteins captured in A-bodies.

DISCUSSION

Twenty years after its discovery, the study of nucleolar sequestration has led to important conceptual and mechanistical advances in our understanding of the role of membraneless bodies and how they are constructed. The ability of cells to reversibly cycle proteins from a mobile to immobile state in A-bodies represents an effective posttranslational mechanism to regulate molecular networks. In this review, we propose a stepwise working model of A-body biogenesis that highlights this process as a precisely choreographed multistep routine rather than a random aggregation of misfolded proteins. This also makes A-bodies unique from the liquid compartments that populate the cell. A-bodies are characterized by electron-dense fibers composed of an array of immobilized proteins that stain positive with various amyloidogenic dyes. Liquid condensates do not display amyloidogenic features and generally contain mobile proteins. Obviously, this raises the key question of why liquid condensates typically do not mature into bodies with amyloidogenic properties. One possibility is that the clusters of low-complexity rIGSRNA are able to recruit sufficient quantity of proteins by simple electrostatic interactions, thereby reaching the critical concentration threshold to trigger amyloidogenesis (Knowles et al., 2014). This model is supported by the observation of electron-dense material early on in A-body biogenesis. The bipartite nature of the ACM, which can both electrostatically interact with low-complexity rIGSRNA and contains a high fibrillation propensity domain necessary for immobilization, may also explain the maturation of A-bodies. Perhaps the architectural determinants of RNA that seed various liquid bodies are too restrictive to certain binding partners to reach a concentration threshold required for amyloidogenesis. Additionally, there is evidence that suggests high nuclear RNA concentration acts as a buffer to prevent condensates from becoming amyloidogenic (Maharana et al., 2018). Indeed, mutated proteins with increased propensity to form amyloids are preferentially formed in the cytoplasm, which has low RNA concentration. While this appears to be the case for cytoplasmic stress granules enriched in amyloidogenic mutant proteins, this likely does not explain A-body maturation as the nucleolus is highly enriched in rRNA. How A-bodies progress from liquid-like condensates to solid-like condensates is a major question in the field of condensate biology, which we are actively pursuing. We are also keen to explore other stimuli,

particularly those that alter nucleolar architecture, that may promote the accumulation of rIGSRNA and the formation of A-bodies, including viral infection (Wang, 2010), inflammation, and diurnal cycles of metabolism. Diurnal oscillations in nucleolar size and abundance of nucleolar RNAs have been seen in mammalian systems (Sinturel et al., 2017; Aitken and Semple, 2017), as well as an emerging connection between circadian disturbances and Alzheimer's disease (Musiek, 2015). Despite most proteins having inherent fibrillation propensity, the dominant view remains that amyloids are inherently toxic, rather than a physiological fold exploited by cells to regulate various peptide functions. The challenge will be to decipher fundamental differences between A-bodies and other physiological or pathological membraneless compartments that could inform our understanding on how to prevent, detect, and treat amyloid-based diseases.

AUTHOR CONTRIBUTIONS

MW, MB, PT, and SL designed the manuscript, discussed the conceptual implications, wrote the paper, and made the figures.

FUNDING

This work was supported by grants from the National Institute of General Medical Sciences (R01GM115342) (SL), the National Cancer Institute (R01CA200676) of the NIH, and the Sylvester Comprehensive Cancer Center (SL).

REFERENCES

Agrawal, S., and Ganley, A. R. D. (2018). The conservation landscape of the human ribosomal RNA gene repeats. *PloS One* 13 (12), e0207531. doi: 10.1371/journal.pone.0207531

Aitken, S., and Semple, C. A. (2017). The circadian dynamics of small nucleolar RNA in the mouse liver. *J. R. Soc. Interface* 14 (130). doi: 10.1098/rsif.2017.0034

Altmeyer, M., Neelsen, K. J., Teloni, F., Pozdnyakova, I., Pellegrino, S., Grofte, M., et al. (2015). Liquid demixing of intrinsically disordered proteins is seeded by poly(ADP-ribose). *Nat. Commun.* 6, 8088. doi: 10.1038/ncomms9088

Arabi, A. (2003). Accumulation of c-Myc and proteasomes at the nucleoli of cells containing elevated c-Myc protein levels. *J. Cell Sci.* 116 (9), 1707–1717. doi: 10.1242/jcs.00370

Audas, T. E., Audas, D. E., Jacob, M. D., Ho, J. J., Khacho, M., Wang, M., et al. (2016). Stressing out over long noncoding RNA. *Biochim. Biophys. Acta* 1859 (1), 184–191. doi: 10.1016/j.bbagrm.2015.06.010

Audas, T. E., Jacob, M. D., and Lee, S. (2012a). Immobilization of proteins in the nucleolus by ribosomal intergenic spacer noncoding RNA. *Mol. Cell* 45 (2), 147–157. doi: 10.1016/j.molcel.2011.12.012

Audas, T. E., Jacob, M. D., and Lee, S. (2012b). The nucleolar detention pathway: a cellular strategy for regulating molecular networks. *Cell Cycle* 11 (11), 2059–2062. doi: 10.4161/cc.20140

Audas, T. E. (2016). Adaptation to stressors by systemic protein Amyloidogenesis. *Dev. Cell* 39 (2), 155–168. doi: 10.1016/j.devcel.2016.09.002

Audas, T.E., and Lee, S. (2016). Stressing out over long noncoding rna. *Biochim. Biophys. Acta* 1859, 184–191.

Aumiller, W. M. Jr., and Keating, C. D. (2016). Phosphorylation-mediated RNA/peptide complex coacervation as a model for intracellular liquid organelles. *Nat. Chem.* 8 (2), 129–137. doi: 10.1038/nchem.2414

Azzam, R., Chen, S. L., Shou, W., Mah, A. S., Alexandru, G., Nasmyth, K., et al. (2004). Phosphorylation by cyclin B-Cdk underlies release of mitotic exit activator Cdc14 from the nucleolus. *Science* 305 (5683), 516–519. doi: 10.1126/science.1099402

Bachant, J. B., and Elledge, S. J. (1999). Mitotic treasures in the nucleolus. *Nature* 398 (6730), 757–758. doi: 10.1038/19641

Banani, S. F., Lee, H. O., Hyman, A. A., and Rosen, M. K. (2017). Biomolecular condensates: organizers of cellular biochemistry. *Nat. Rev. Mol. Cell Biol.* 18 (5), 285–298. doi: 10.1038/nrm.2017.7

Banski, P., Mahboubi, H., Kodiha, M., Shrivastava, S., Kanagaratham, C., and Stochaj, U. (2010). Nucleolar targeting of the chaperone hsc70 is regulated by stress, cell signaling, and a composite targeting signal which is controlled by autoinhibition. *J. Biol. Chem.* 285 (28), 21858–21867. doi: 10.1074/jbc.M110.117291

Berchowitz, L. E., Kabachinski, G., Walker, M. R., Carlile, T. M., Gilbert, W. V., Schwartz, T. U., et al. (2015). Regulated formation of an Amyloid-like translational repressor governs gametogenesis. *Cell* 163 (2), 406–418. doi: 10.1016/j.cell.2015.08.060

Bernardi, R., Scaglioni, P. P., Bergmann, S., Horn, H. F., Vousden, K. H., and Pandolfi, P. P. (2004). PML regulates p53 stability by sequestering Mdm2 to the nucleolus. *Nat. Cell Biol.* 6 (7), 665–672. doi: 10.1038/ncb1147

Boisvert, F. M., van Koningsbruggen, S., Navascues, J., and Lamond, A. I. (2007). The multifunctional nucleolus. *Nat. Rev. Mol. Cell Biol.* 8 (7), 574–585. doi: 10.1038/nrm2184

Boke, E., Ruer, M., Wuhr, M., Coughlin, M., Lemaitre, R., Gygi, S. P., et al. (2016). Amyloid-like self-assembly of a cellular compartment. *Cell* 166 (3), 637–650. doi: 10.1016/j.cell.2016.06.051

Bond, C. S., and Fox, A. H. (2009). Paraspeckles: nuclear bodies built on long noncoding RNA. *J. Cell Biol.* 186 (5), 637–644. doi: 10.1083/jcb.200906113

Booth, D. R., Sunde, M., Bellotti, V., Robinson, C. V., Hutchinson, W. L., Fraser, P. E., et al. (1997). Instability, unfolding and aggregation of human lysozyme variants underlying amyloid fibrillogenesis. *Nature* 385 (6619), 787–793. doi: 10.1038/385787a0

Boulon, S., Westman, B. J., Hutten, S., Boisvert, F. M., and Lamond, A. I. (2010). The nucleolus under stress. *Mol. Cell* 40 (2), 216–227. doi: 10.1016/j.molcel.2010.09.024

Brangwynne, C. P., Eckmann, C. R., Courson, D. S., Rybarska, A., Hoege, C., Gharakhani, J., et al. (2009). Germline P granules are liquid droplets that localize by controlled dissolution/condensation. *Science* 324 (5935), 1729–1732. doi: 10.1126/science.1172046

Brangwynne, C. P., Mitchison, T. J., and Hyman, A. A. (2011). Active liquid-like behavior of nucleoli determines their size and shape in Xenopus laevis oocytes. *Proc. Natl. Acad. Sci. U.S.A.* 108 (11), 4334–4339. doi: 10.1073/pnas.1017150108

Brangwynne, C. P., Tompa, P., and Pappu, Rohit V. (2015). Polymer physics of intracellular phase transitions. *Nat. Phys.* 11 (11), 899–904. doi: 10.1038/nphys3532

Cereghetti, G., Saad, S., Dechant, R., and Peter, M. (2018). Reversible, functional amyloids: towards an understanding of their regulation in yeast and humans. *Cell Cycle* 17 (13), 1545–1558. doi: 10.1080/15384101.2018.1480220

Chen, J., and Stark, L. A. (2017). Aspirin prevention of colorectal cancer: focus on NF-kappaB signalling and the nucleolus. *Biomedicines* 5 (3). doi: 10.3390/biomedicines5030043

Chen, X., Hiller, M., Sancak, Y., and Fuller, M. T. (2005). Tissue-specific TAFs counteract Polycomb to turn on terminal differentiation. *Science* 310 (5749), 869–872. doi: 10.1126/science.1118101

Chiti, F., and Dobson, C. M. (2006). Protein misfolding, functional amyloid, and human disease. *Annu. Rev. Biochem.* 75, 333–366. doi: 10.1146/annurev.biochem.75.101304.123901

Chujo, T., and Hirose, T. (2017). Nuclear bodies built on architectural long noncoding RNAs: unifying principles of their construction and function. *Mol. Cells* 40 (12), 889–896. doi: 10.14348/molcells.2017.0263

Chujo, T., Yamazaki, T., Kawaguchi, T., Kurosaka, S., Takumi, T., Nakagawa, S., et al. (2017). Unusual semi-extractability as a hallmark of nuclear body-associated architectural noncoding RNAs. *EMBO J.* 36 (10), 1447–1462. doi: 10.15252/embj.201695848

Dellaire, G., and Bazett-Jones, D. P. (2004). PML nuclear bodies: dynamic sensors of DNA damage and cellular stress. *Bioessays* 26 (9), 963–977. doi: 10.1002/bies.20089

Dulin, F., Leveille, F., Ortega, J. B., Mornon, J. P., Buisson, A., Callebaut, I., et al. (2008). P3 peptide, a truncated form of A beta devoid of synaptotoxic effect, does not assemble into soluble oligomers. *FEBS Lett.* 582 (13), 1865–1870. doi: 10.1016/j.febslet.2008.05.002

Eisenberg, D., and Jucker, M. (2012). The amyloid state of proteins in human diseases. *Cell* 148 (6), 1188–1203. doi: 10.1016/j.cell.2012.02.022

Elbaum-Garfinkle, S., Kim, Y., Szczepaniak, K., Chen, C. C., Eckmann, C. R., Myong, S., et al. (2015). The disordered P granule protein LAF-1 drives phase separation into droplets with tunable viscosity and dynamics. *Proc. Natl. Acad. Sci. U.S.A.* 112 (23), 7189–7194. doi: 10.1073/pnas.1504822112

Emmott, E., and Hiscox, J. A. (2009). Nucleolar targeting: the hub of the matter. *EMBO Rep.* 10 (3), 231–238. doi: 10.1038/embor.2009.14

Falabella, P., Riviello, L., Pascale, M., Lelio, I. D., Tettamanti, G., Grimaldi, A., et al. (2012). Functional amyloids in insect immune response. *Insect Biochem. Mol. Biol.* 42 (3), 203–211. doi: 10.1016/j.ibmb.2011.11.011

Fay, M. M., and Anderson, P. J. (2018). The role of RNA in biological phase separations. *J. Mol. Biol.* 430 (23), 4685–4701. doi: 10.1016/j.jmb.2018.05.003

Feric, M., Vaidya, N., Harmon, T. S., Mitrea, D. M., Zhu, L., Richardson, T. M., et al. (2016). Coexisting liquid phases underlie nucleolar subcompartments. *Cell* 165 (7), 1686–1697. doi: 10.1016/j.cell.2016.04.047

Fowler, D. M., and Kelly, J. W. (2012). Functional amyloidogenesis and cytotoxicity-insights into biology and pathology. *PloS Biol.* 10 (12), e1001459. doi: 10.1371/journal.pbio.1001459

Fowler, D. M. Koulov, A. V., Alory-Jost, C., Marks, M. S., Balch, W. E., and Kelly, J. W. (2006). Functional amyloid formation within mammalian tissue. *PloS Biol.* 4 (1), e6. doi: 10.1371/journal.pbio.0040006

Fowler, D. M., Koulov, A. V., Balch, W. E., and Kelly, J. W. (2007). Functional amyloid–from bacteria to humans. *Trends Biochem. Sci.* 32 (5), 217–224. doi: 10.1016/j.tibs.2007.03.003

Gall, J. G. (2000). Cajal bodies: the first 100 years. *Annu. Rev. Cell Dev. Biol.* 16, 273–300. doi: 10.1146/annurev.cellbio.16.1.273

Goldschmidt, L., Teng, P. K., Riek, R., and Eisenberg, D. (2010). Identifying the amylome, proteins capable of forming amyloid-like fibrils. *Proc. Natl. Acad. Sci. U. S. A.* 107 (8), 3487–3492. doi: 10.1073/pnas.0915166107

Gonzalez, I. L., and Sylvester, J. E. (1995). Complete sequence of the 43-kb human ribosomal DNA repeat: analysis of the intergenic spacer. *Genomics* 27 (2), 320–328. doi: 10.1006/geno.1995.1049

Grummt, I., and Pikaard, C. S. (2003). Epigenetic silencing of RNA polymerase I transcription. *Nat. Rev. Mol. Cell Biol.* 4 (8), 641–649. doi: 10.1038/nrm1171

Hall, A. C., Ostrowski, L. A., and Mekhail, K. (2019). Phase separation as a melting pot for DNA repeats. *Trends Genet.* doi: 10.1016/j.tig.2019.05.001

Hawe, A., Sutter, M., and Jiskoot, W. (2008). Extrinsic fluorescent dyes as tools for protein characterization. *Pharm. Res.* 25 (7), 1487–1499. doi: 10.1007/s11095-007-9516-9

Hernandez-Verdun, D. (2006). Nucleolus: from structure to dynamics. *Histochem. Cell Biol.* 125 (1–2), 127–137. doi: 10.1007/s00418-005-0046-4

Hirose, T., Yamazaki, T., and Nakagawa, S. (2019). Molecular anatomy of the architectural NEAT1 noncoding RNA: The domains, interactors, and biogenesis pathway required to build phase-separated nuclear paraspeckles. *Wiley Interdiscip. Rev. RNA*, e1545. doi: 10.1002/wrna.1545

Hodges, M., Tissot, C., Howe, K., Grimwade, D., and Freemont, P. S. (1998). Structure, organization, and dynamics of promyelocytic leukemia protein nuclear bodies. *Am. J. Hum. Genet.* 63 (2), 297–304. doi: 10.1086/301991

Holehouse, A. S., and Pappu, R. V. (2018). Functional Implications of Intracellular Phase Transitions. *Biochemistry* 57 (17), 2415–2423. doi: 10.1021/acs.biochem.7b01136

Hult, C., Adalsteinsson, D., Vasquez, P. A., Lawrimore, J., Bennett, M., York, A., et al. (2017). Enrichment of dynamic chromosomal crosslinks drive phase separation of the nucleolus. *Nucleic Acids Res.* 45 (19), 11159–11173. doi: 10.1093/nar/gkx741

Itakura, A. K., Futia, R. A., and Jarosz, D. F. (2018). It pays to be in phase. *Biochemistry* 57 (17), 2520–2529. doi: 10.1021/acs.biochem.8b00205

Jacob, M. D., Audas, T. E., Mullineux, S. T., and Lee, S. (2012). Where no RNA polymerase has gone before: novel functional transcripts derived from the ribosomal intergenic spacer. *Nucleus* 3 (4), 315–319. doi: 10.4161/nucl.20585

Jacob, M. D., Audas, T. E., Uniacke, J., Trinkle-Mulcahy, L., and Lee, S. (2013). Environmental cues induce a long noncoding RNA-dependent remodeling of the nucleolus. *Mol. Biol. Cell* 24 (18), 2943–2953. doi: 10.1091/mbc.e13-04-0223

Jain, A., and Vale, R. D. (2017). RNA phase transitions in repeat expansion disorders. *Nature* 546 (7657), 243–247. doi: 10.1038/nature22386

Kato, M., Han, T. W., Xie, S., Shi, K., Du, X., Wu, L. C., et al. (2012). Cell-free formation of RNA granules: low complexity sequence domains form dynamic fibers within hydrogels. *Cell* 149 (4), 753–767. doi: 10.1016/j.cell.2012.04.017

Kayatekin, C., Matlack, K. E., Hesse, W. R., Guan, Y., Chakrabortee, S., Russ, J., et al. (2014). Prion-like proteins sequester and suppress the toxicity of huntingtin exon 1. *Proc. Natl. Acad. Sci. U. S. A.* 111 (33), 12085–12090. doi: 10.1073/pnas.1412504111

Kayed, R., Head, E., Sarsoza, F., Saing, T., Cotman, C. W., Necula, M., et al. (2007). Fibril specific, conformation dependent antibodies recognize a generic epitope common to amyloid fibrils and fibrillar oligomers that is absent in prefibrillar oligomers. *Mol. Neurodegener.* 2, 18. doi: 10.1186/1750-1326-2-18

Knowles, T. P., Vendruscolo, M., and Dobson, C. M. (2014). The amyloid state and its association with protein misfolding diseases. *Nat. Rev. Mol. Cell Biol.* 15 (6), 384–396. doi: 10.1038/nrm3810

Kruger, T., and Scheer, U. (2010). p53 localizes to intranucleolar regions distinct from the ribosome production compartments. *J. Cell Sci.* 123 (Pt 8), 1203–1208. doi: 10.1242/jcs.062398

Lamond, A. I., and Spector, D. L. (2003). Nuclear speckles: a model for nuclear organelles. *Nat. Rev. Mol. Cell Biol.* 4 (8), 605–612. doi: 10.1038/nrm1172

Langdon, E. M., Qiu, Y., Ghanbari Niaki, A., McLaughlin, G. A., Weidmann, C. A., Gerbich, T. M. (2018). mRNA structure determines specificity of a polyQ-driven phase separation. *Science* 360 (6391), 922–927. doi: 10.1126/science.aar7432

Latonen, L. (2011). Nucleolar aggresomes as counterparts of cytoplasmic aggresomes in proteotoxic stress. Proteasome inhibitors induce nuclear ribonucleoprotein inclusions that accumulate several key factors of neurodegenerative diseases and cancer. *Bioessays* 33 (5), 386–395. doi: 10.1002/bies.201100008

Latonen, L. (2019). Phase-to-phase with nucleoli - stress responses, protein aggregation and novel roles of RNA. *Front. Cell Neurosci.* 13, 151. doi: 10.3389/fncel.2019.00151

Latonen, L. Moore, H. M., Bai, B., Jaamaa, S., and Laiho, M. (2011). Proteasome inhibitors induce nucleolar aggregation of proteasome target proteins and polyadenylated RNA by altering ubiquitin availability. *Oncogene* 30 (7), 790–805. doi: 10.1038/onc.2010.469

Li, J., McQuade, T., Siemer, A. B., Napetschnig, J., Moriwaki, K., Hsiao, Y. S., et al. (2012). The RIP1/RIP3 necrosome forms a functional amyloid signaling complex required for programmed necrosis. *Cell* 150 (2), 339–350. doi: 10.1016/j.cell.2012.06.019

Li, J., Jiang, E., Wang, X., Shangguan, A. J., Zhang, L., and Yu, Z. (2015). Dormant Cells: the original cause of tumor recurrence and metastasis. *Cell Biochem. Biophys.* 72 (2), 317–320. doi: 10.1007/s12013-014-0477-4

Li, S., Kennedy, M., Payne, S., Kennedy, K., Seewaldt, V. L., Pizzo, S. V., et al. (2014). Model of tumor dormancy/recurrence after short-term chemotherapy. *PloS One* 9 (5), e98021. doi: 10.1371/journal.pone.0098021

Liu, Y., Deisenroth, C., and Zhang, Y. (2016). RP-MDM2-p53 pathway: linking ribosomal biogenesis and tumor surveillance. *Trends Cancer* 2 (4), 191–204. doi: 10.1016/j.trecan.2016.03.002

Lohrum, M. A., Ashcroft, M., Kubbutat, M. H., and Vousden, K. H. (2000). Identification of a cryptic nucleolar-localization signal in MDM2. *Nat. Cell Biol.* 2 (3), 179–181. doi: 10.1038/35004057

Lyons, S. M., and Anderson, P. (2016). RNA-Seeded functional amyloids balance growth and survival. *Dev. Cell* 39 (2), 131–132. doi: 10.1016/j.devcel.2016.10.005

Machyna, M., Heyn, P., and Neugebauer, K. M. (2013). Cajal bodies: where form meets function. *Wiley Interdiscip. Rev. RNA* 4 (1), 17–34. doi: 10.1002/wrna.1139

Maharana, S., Wang, J., Papadopoulos, D. K., Richter, D., Pozniakovsky, A., Poser, I., et al. (2018). RNA buffers the phase separation behavior of prion-like RNA binding proteins. *Science* 360 (6391), 918–921. doi: 10.1126/science.aar7366

Maji, S. K., Perrin, M. H., Sawaya, M. R., Jessberger, S., Vadodaria, K., Rissman, R. A., et al. (2009). Functional amyloids as natural storage of peptide hormones in pituitary secretory granules. *Science* 325 (5938), 328–332. doi: 10.1126/science.1173155

Martindill, D. M., Risebro, C. A., Smart, N., Franco-Viseras Mdel, M., Rosario, C. O., Swallow, C. J., et al. (2007). Nucleolar release of Hand1 acts as a molecular switch to determine cell fate. *Nat. Cell Biol.* 9 (10), 1131–1141. doi: 10.1038/ncb1633

Mateju, D., Franzmann, T. M., Patel, A., Kopach, A., Boczek, E. E., Maharana, S., et al. (2017). An aberrant phase transition of stress granules triggered by misfolded protein and prevented by chaperone function. *EMBO J.* 36 (12), 1669–1687. doi: 10.15252/embj.201695957

Mattsson, K., Pokrovskaja, K., Kiss, C., Klein, G., and Szekely, L. (2001). Proteins associated with the promyelocytic leukemia gene product (PML)-containing nuclear body move to the nucleolus upon inhibition of proteasome-dependent protein degradation. *Proc. Natl. Acad. Sci. U.S.A.* 98 (3), 1012–1017. doi: 10.1073/pnas.98.3.1012

Mayer, C., Neubert, M., and Grummt, I. (2008). The structure of NoRC-associated RNA is crucial for targeting the chromatin remodelling complex NoRC to the nucleolus. *EMBO Rep.* 9 (8), 774–780. doi: 10.1038/embor.2008.109

Mayer, C., Schmitz, K. M., Li, J., Grummt, I., and Santoro, R. (2006). Intergenic transcripts regulate the epigenetic state of rRNA genes. *Mol. Cell* 22 (3), 351–361. doi: 10.1016/j.molcel.2006.03.028

Mediani, L., Guillen-Boixet, J., Vinet, J., Franzmann, T. M., Bigi, I., Mateju, D., et al. (2019). Defective ribosomal products challenge nuclear function by impairing nuclear condensate dynamics and immobilizing ubiquitin. *EMBO J.*, e101341. doi: 10.15252/embj.2018101341

Mekhail, K., Gunaratnam, L., Bonicalzi, M. E., and Lee, S. (2004). HIF activation by pH-dependent nucleolar sequestration of VHL. *Nat. Cell Biol.* 6 (7), 642–647. doi: 10.1038/ncb1144

Mekhail, K. Khacho, M., Carrigan, A., Hache, R. R., Gunaratnam, L., and Lee, S. (2005). Regulation of ubiquitin ligase dynamics by the nucleolus. *J. Cell Biol.* 170 (5), 733–744. doi: 10.1083/jcb.200506030

Mekhail, K. Rivero-Lopez, L., Khacho, M., and Lee, S. (2006). Restriction of rRNA synthesis by VHL maintains energy equilibrium under hypoxia. *Cell Cycle* 5 (20), 2401–2413. doi: 10.4161/cc.5.20.3387

Mekhail, K. Rivero-Lopez, L., Al-Masri, A., Brandon, C., Khacho, M., and Lee, S. (2007). Identification of a common subnuclear localization signal. *Mol. Biol. Cell* 18 (10), 3966–3977. doi: 10.1091/mbc.e07-03-0295

Mikhaleva, E. A., Leinsoo, T. A., Ishizu, H., Gvozdev, V. A., and Klenov, M. S. (2018). The nucleolar transcriptome regulates Piwi shuttling between the nucleolus and the nucleoplasm. *Chromosome Res.* doi: 10.1007/s10577-018-9595-y

Miller, O. L. Jr., and Beatty, B. R. (1969). Visualization of nucleolar genes. *Science* 164 (3882), 955–957. doi: 10.1126/science.164.3882.955

Mitrea, D. M. Cika, J. A., Guy, C. S., Ban, D., Banerjee, P. R., Stanley, C. B., et al. (2016). Nucleophosmin integrates within the nucleolus via multi-modal interactions with proteins displaying R-rich linear motifs and rRNA. *Elife* 5. doi: 10.7554/eLife.13571

Molliex, A., Temirov, J., Lee, J., Coughlin, M., Kanagaraj, A. P., Kim, H. J., et al. (2015). Phase separation by low complexity domains promotes stress granule assembly and drives pathological fibrillization. *Cell* 163 (1), 123–133. doi: 10.1016/j.cell.2015.09.015

Monahan, Z., Ryan, V. H., Janke, A. M., Burke, K. A., Rhoads, S. N., Zerze, G. H., et al. (2017). Phosphorylation of the FUS low-complexity domain disrupts phase separation, aggregation, and toxicity. *EMBO J.* 36 (20), 2951–2967. doi: 10.15252/embj.201696394

Munder, M. C. Midtvedt, D., Franzmann, T., Nuske, E., Otto, O., Herbig, M., et al. (2016). A pH-driven transition of the cytoplasm from a fluid- to a solid-like state promotes entry into dormancy. *Elife* 5. doi: 10.7554/eLife.09347

Murakami, T., Qamar, S., Lin, J. Q., Schierle, G. S., Rees, E., Miyashita, A. et al. (2015). ALS/FTD mutation-induced phase transition of FUS liquid droplets and reversible hydrogels into irreversible hydrogels impairs RNP granule function. *Neuron* 88 (4), 678–690. doi: 10.1016/j.neuron.2015.10.030

Musiek, E. S. (2015). Circadian clock disruption in neurodegenerative diseases: cause and effect? *Front. Pharmacol.* 6, 29. doi: 10.3389/fphar.2015.00029

Nemeth, A., and Grummt, I. (2018). Dynamic regulation of nucleolar architecture. *Curr. Opin. Cell Biol.* 52, 105–111. doi: 10.1016/j.ceb.2018.02.013

Nott, T. J., Craggs, T. D., and Baldwin, A. J. (2016). Membraneless organelles can melt nucleic acid duplexes and act as biomolecular filters. *Nat. Chem.* 8 (6), 569–575. doi: 10.1038/nchem.2519

Nott, T. J., Petsalaki, E., Farber, P., Jervis, D., Fussner, E., Plochowietz, A., et al. (2015). Phase transition of a disordered nuage protein generates environmentally responsive membraneless organelles. *Mol. Cell* 57 (5), 936–947. doi: 10.1016/j.molcel.2015.01.013

Pak, C. W., Kosno, M., Holehouse, A. S., Padrick, S. B., Mittal, A., Ali, R., et al. (2016). Sequence determinants of intracellular phase separation by complex coacervation of a disordered protein. *Mol. Cell* 63 (1), 72–85. doi: 10.1016/j.molcel.2016.05.042

Parker, R., and Sheth, U. (2007). P bodies and the control of mRNA translation and degradation. *Mol. Cell* 25 (5), 635–646. doi: 10.1016/j.molcel.2007.02.011

Patel, A., Lee, H.O., Jawerth, L., Maharana, S., Jahnel, M., Hein, M. Y., et al. (2015). A liquid-to-solid phase transition of the ALS protein FUS accelerated by disease mutation. *Cell* 162 (5), 1066–1077. doi: 10.1016/j.cell.2015.07.047

Pederson, T., and Tsai, R. Y. (2009). In search of nonribosomal nucleolar protein function and regulation. *J. Cell Biol.* 184 (6), 771–776. doi: 10.1083/jcb.200812014

Pederson, T. (2011). The nucleolus. *Cold Spring Harb Perspect. Biol.* 3 (3). doi: 10.1101/cshperspect.a000638

Perry, R. P. (1960). On the nucleolar and nuclear dependence of cytoplasmic RNA synthesis in HeLa cells. *Exp. Cell Res.* 20, 216–220. doi: 10.1016/0014-4827(60)90240-8

Perry, R. P. (1962). The cellular sites of synthesis of Ribosomal and 4s Rna. *Proc. Natl. Acad. Sci. U. S. A.* 48 (12), 2179–2186. doi: 10.1073/pnas.48.12.2179

Peskett, T. R., Rau, F., O'Driscoll, J., Patani, R., Lowe, A. R., and Saibil, H. R. (2018). A liquid to solid phase transition underlying pathological huntingtin Exon1 aggregation. *Mol. Cell* 70 (4), 588–601, e6. doi: 10.1016/j.molcel.2018.04.007

Phair, R. D., and Misteli, T. (2000). High mobility of proteins in the mammalian cell nucleus. *Nature* 404 (6778), 604–609. doi: 10.1038/35007077

Posey, A. E., Ruff, K. M., Harmon, T. S., Crick, S. L., Li, A., Diamond, M. I., et al. (2018). Profilin reduces aggregation and phase separation of huntingtin N-terminal fragments by preferentially binding to soluble monomers and oligomers. *J. Biol. Chem.* 293 (10), 3734–3746. doi: 10.1074/jbc.RA117.000357

Poyurovsky, M. V., Jacq, X., Ma, C., Karni-Schmidt, O., Parker, P. J., Chalfie, M., et al. (2003). Nucleotide binding by the Mdm2 RING domain facilitates Arf-independent Mdm2 nucleolar localization. *Mol. Cell* 12 (4), 875–887. doi: 10.1016/S1097-2765(03)00400-3

Protter, D. S., and Parker, R. (2016). Principles and properties of stress granules. *Trends Cell Biol.* 26 (9), 668–679. doi: 10.1016/j.tcb.2016.05.004

Raska, I., Shaw, P. J., and Cmarko, D. (2006). Structure and function of the nucleolus in the spotlight. *Curr. Opin. Cell Biol.* 18 (3), 325–334. doi: 10.1016/j.ceb.2006.04.008

Rizzi, N., Denegri, M., Chiodi, I., Corioni, M., Valgardsdottir, R., Cobianchi, F., et al. (2004). Transcriptional activation of a constitutive heterochromatic domain of the human genome in response to heat shock. *Mol. Biol. Cell* 15 (2), 543–551. doi: 10.1091/mbc.e03-07-0487

Saad, S., Cereghetti, G., Feng, Y., Picotti, P., Peter, M., and Dechant, R. (2017). Reversible protein aggregation is a protective mechanism to ensure cell cycle restart after stress. *Nat. Cell Biol.* 19 (10), 1202–1213. doi: 10.1038/ncb3600

Sansam, C. L., Wells, K. S., and Emeson, R. B. (2003). Modulation of RNA editing by functional nucleolar sequestration of ADAR2. *Proc. Natl. Acad. Sci. U. S. A.* 100 (24), 14018–14023. doi: 10.1073/pnas.2336131100

San-Segundo, P. A., and Roeder, G. S. (1999). Pch2 links chromatin silencing to meiotic checkpoint control. *Cell* 97 (3), 313–324. doi: 10.1016/S0092-8674(00)80741-2

Santoro, R. (2005). The silence of the ribosomal RNA genes. *Cell Mol. Life Sci.* 62 (18), 2067–2079. doi: 10.1007/s00018-005-5110-7

Sasaki, Y. T., and Hirose, T. (2009). How to build a paraspeckle. *Genome Biol.* 10 (7), 227. doi: 10.1186/gb-2009-10-7-227

Sawyer, I. A., Sturgill, D., and Dundr, M. (2019). Membraneless nuclear organelles and the search for phases within phases. *Wiley Interdiscip. Rev. RNA* 10 (2), e1514. doi: 10.1002/wrna.1514

Scheer, U., and Hock, R. (1999). Structure and function of the nucleolus. *Curr. Opin. Cell Biol.* 11 (3), 385–390. doi: 10.1016/S0955-0674(99)80054-4

Schmitz, K. M., Mayer, C., Postepska, A., and Grummt, I. (2010). Interaction of noncoding RNA with the rDNA promoter mediates recruitment of DNMT3b and silencing of rRNA genes. *Genes Dev.* 24 (20), 2264–2269. doi: 10.1101/gad.590910

Schnabel, J. (2010). Protein folding: the dark side of proteins. *Nature* 464 (7290), 828–829. doi: 10.1038/464828a

Sharifi, S., and Bierhoff, H. (2018). Regulation of RNA Polymerase I transcription in development, disease, and aging. *Annu. Rev. Biochem.* doi: 10.1146/annurev-biochem-062917-012612

Shav-Tal, Y., Blechman, J., Darzacq, X., Montagna, C., Dye, B. T., Patton, J. G., et al. (2005). Dynamic sorting of nuclear components into distinct nucleolar caps during transcriptional inhibition. *Mol. Biol. Cell* 16 (5), 2395–2413. doi: 10.1091/mbc.e04-11-0992

Shin, Y., and Brangwynne, C. P. (2017). Liquid phase condensation in cell physiology and disease. *Science* 357 (6357). doi: 10.1126/science.aaf4382

Shou, W., Seol, J. H., Shevchenko, A., Baskerville, C., Moazed, D., Chen, Z. W., et al. (1999). Exit from mitosis is triggered by Tem1-dependent release of the protein phosphatase Cdc14 from nucleolar RENT complex. *Cell* 97 (2), 233–244. doi: 10.1016/S0092-8674(00)80733-3

Sinturel, F., Gerber, A., Mauvoisin, D., Wang, J., Gatfield, D., Stubblefield, J. J., et al. (2017). Diurnal oscillations in liver mass and cell size accompany ribosome assembly cycles. *Cell* 169 (4), 651–663 e14. doi: 10.1016/j.cell.2017.04.015

Smirnov, E., Cmarko, D., Mazel, T., Hornacek, M., and Raska, I. (2016). Nucleolar DNA: the host and the guests. *Histochem Cell Biol.* 145 (4), 359–372. doi: 10.1007/s00418-016-1407-x

Stark, L. A., and Dunlop, M. G. (2005). Nucleolar sequestration of RelA (p65) regulates NF-kappaB-driven transcription and apoptosis. *Mol. Cell Biol.* 25 (14), 5985–6004. doi: 10.1128/MCB.25.14.5985-6004.2005

Sydorskyy, Y., Srikumar, T., Jeram, S. M., Wheaton, S., Vizeacoumar, F. J., Makhnevych, T., et al. (2010). A novel mechanism for SUMO system control: regulated Ulp1 nucleolar sequestration. *Mol. Cell Biol.* 30 (18), 4452–4462. doi: 10.1128/MCB.00335-10

Tang, Z., Dai, S., He, Y., Doty, R. A., Shultz, L. D., Sampson, S. B., et al. (2015). MEK guards proteome stability and inhibits tumor-suppressive amyloidogenesis *via* HSF1. *Cell* 160 (4), 729–744. doi: 10.1016/j.cell.2015.01.028

Tao, W., and Levine, A. J. (1999). P19(ARF) stabilizes p53 by blocking nucleo-cytoplasmic shuttling of Mdm2. *Proc. Natl. Acad. Sci. U.S.A.* 96 (12), 6937–6941. doi: 10.1073/pnas.96.12.6937

Thiry, M., and Lafontaine, D. L. (2005). Birth of a nucleolus: the evolution of nucleolar compartments. *Trends Cell Biol.* 15 (4), 194–199. doi: 10.1016/j.tcb.2005.02.007

Tomson, B. N., Rahal, R., Reiser, V., Monje-Casas, F., Mekhail, K., Moazed, D., et al. (2009). Regulation of Spo12 phosphorylation and its essential role in the FEAR network. *Curr. Biol.* 19 (6), 449–460. doi: 10.1016/j.cub.2009.02.024

Valgardsdottir, R., Chiodi, I., Giordano, M., Cobianchi, F., Riva, S., and Biamonti, G. (2005). Structural and functional characterization of noncoding repetitive RNAs transcribed in stressed human cells. *Mol. Biol. Cell* 16 (6), 2597–2604. doi: 10.1091/mbc.e04-12-1078

Visintin, R., Hwang, E. S., and Amon, A. (1999). Cfi1 prevents premature exit from mitosis by anchoring Cdc14 phosphatase in the nucleolus. *Nature* 398 (6730), 818–823. doi: 10.1038/19775

Wang, L., Ren, X. M., Xing, J. J., and Zheng, A. C. (2010). The nucleolus and viral infection. *Virol. Sin.* 25 (3), 151–157. doi: 10.1007/s12250-010-3093-5

Wang, M., Audas, T. E., and Lee, S. (2017). Disentangling a bad reputation: changing perceptions of amyloids. *Trends Cell Biol.* 27 (7), 465–467. doi: 10.1016/j.tcb.2017.03.001

Wang, M., Tao, X., Jacob, M. D., Bennett, C. A., Ho, J. J. D., Gonzalgo, M. L., et al. (2018). Stress-induced low complexity rna activates physiological amyloidogenesis. *Cell Rep.* 241713-241721 (7), e4. doi: 10.1016/j.celrep.2018.07.040

Weber, S. C., and Brangwynne, C. P. (2012). Getting RNA and protein in phase. *Cell* 149 (6), 1188–1191. doi: 10.1016/j.cell.2012.05.022

Weber, J. D., Taylor, L. J., Roussel, M. F., Sherr, C. J., and Bar-Sagi, D. (1999). Nucleolar arf sequesters Mdm2 and activates p53. *Nat. Cell Biol.* 1 (1), 20–26. doi: 10.1038/8991

Weber, J. D., Kuo, M. L., Bothner, B., DiGiammarino, E. L., Kriwacki, R. W., Roussel, M. F., et al. (2000). Cooperative signals governing ARF-mdm2 interaction and nucleolar localization of the complex. *Mol. Cell Biol.* 20 (7), 2517–2528. doi: 10.1128/MCB.20.7.2517-2528.2000

Weber, S. C. (2017). Sequence-encoded material properties dictate the structure and function of nuclear bodies. *Curr. Opin. Cell Biol.* 46, 62–71. doi: 10.1016/j.ceb.2017.03.003

Woerner, A. C., Frottin, F., Hornburg, D., Feng, L. R., Meissner, F., Patra, M., et al. (2016). Cytoplasmic protein aggregates interfere with nucleocytoplasmic transport of protein and RNA. *Science* 351 (6269), 173–176. doi: 10.1126/science.aad2033

Wong, J. M., Kusdra, L., and Collins, K. (2002). Subnuclear shuttling of human telomerase induced by transformation and DNA damage. *Nat. Cell Biol.* 4 (9), 731–736. doi: 10.1038/ncb846

Woodruff, J. B., Hyman, A. A., and Boke, E. (2018). Organization and function of non-dynamic biomolecular condensates. *Trends Biochem. Sci.* 43 (2), 81–94. doi: 10.1016/j.tibs.2017.11.005

Yamazaki, T., Souquere, S., Chujo, T., Kobelke, S., Chong, Y. S., Fox, A. H., et al. (2018). Functional domains of NEAT1 architectural lncRNA induce paraspeckle assembly through phase separation. *Mol. Cell* 70 (6), 1038–1053 e7. doi: 10.1016/j.molcel.2018.05.019

Yap, K., Mukhina, S., Zhang, G., Tan, J. S. C., Ong, H. S., and Makeyev, E. V. (2018). A short tandem repeat-enriched RNA Assembles a nuclear compartment to control alternative splicing and promote cell survival. *Mol. Cell* 72 (3), 525–540 e13. doi: 10.1016/j.molcel.2018.08.041

Zhao, Z., Dammert, M. A., Grummt, I., and Bierhoff, H. (2016a). lncRNA-induced nucleosome repositioning reinforces transcriptional repression of rRNA genes upon hypotonic stress. *Cell Rep.* 14 (8), 1876–1882. doi: 10.1016/j.celrep.2016.01.073

Zhao, Z., Dammert, M. A., Hoppe, S., Bierhoff, H., and Grummt, I. (2016b). Heat shock represses rRNA synthesis by inactivation of TIF-IA and lncRNA-dependent changes in nucleosome positioning. *Nucleic Acids Res.* 44 (17), 8144–8152. doi: 10.1093/nar/gkw496

Zhao, Z., Senturk, N., Song, C., and Grummt, I. (2018). lncRNA PAPAS tethered to the rDNA enhancer recruits hypophosphorylated CHD4/NuRD to repress rRNA synthesis at elevated temperatures. *Genes Dev.* 32 (11–12), 836–848. doi: 10.1101/gad.311688.118

Zhu, L., and Brangwynne, C. P. (2015). Nuclear bodies: the emerging biophysics of nucleoplasmic phases. *Curr. Opin. Cell Biol.* 34, 23–30. doi: 10.1016/j.ceb.2015.04.003

Conflict of Interest: The authors declare that the research was conducted in the absence of any commercial or financial relationships that could be construed as a potential conflict of interest.

frontiers in Cell and Developmental Biology

REVIEW
published: 19 December 2019
doi: 10.3389/fcell.2019.00336

Roles for Non-coding RNAs in Spatial Genome Organization

Negin Khosraviani[1†], Lauren A. Ostrowski[1†] and Karim Mekhail[1,2]*

[1] Department of Laboratory Medicine and Pathobiology, MaRS Centre, Faculty of Medicine, University of Toronto, Toronto, ON, Canada, [2] Canada Research Chairs Program, Faculty of Medicine, University of Toronto, Toronto, ON, Canada

Genetic loci are non-randomly arranged in the nucleus of the cell. This order, which is important to overall genome expression and stability, is maintained by a growing number of factors including the nuclear envelope, various genetic elements and dedicated protein complexes. Here, we review evidence supporting roles for non-coding RNAs (ncRNAs) in the regulation of spatial genome organization and its impact on gene expression and cell survival. Specifically, we discuss how ncRNAs from single-copy and repetitive DNA loci contribute to spatial genome organization by impacting perinuclear chromosome tethering, major nuclear compartments, chromatin looping, and various chromosomal structures. Overall, our analysis of the literature highlights central functions for ncRNAs and their transcription in the modulation of spatial genome organization with connections to human health and disease.

Keywords: nuclear organization, non-coding RNA, DNA repeats, nucleolus, Cajal bodies (CBs)

OPEN ACCESS

Edited by:
Patrizio Dimitri,
Sapienza University of Rome, Italy

Reviewed by:
Igor V. Sharakhov,
Virginia Tech, United States
Maurizio D'Esposito,
Italian National Research Council (CNR), Italy

****Correspondence:***
Karim Mekhail
karim.mekhail@utoronto.ca

†ORCID:
Negin Khosraviani
orcid.org/0000-0003-0588-3618
Lauren A. Ostrowski
orcid.org/0000-0001-6922-6196

Specialty section:
This article was submitted to Epigenomics and Epigenetics, a section of the journal Frontiers in Cell and Developmental Biology

Received: *10 October 2019*
Accepted: *29 November 2019*
Published: *19 December 2019*

Citation:
Khosraviani N, Ostrowski LA and Mekhail K (2019) Roles for Non-coding RNAs in Spatial Genome Organization. Front. Cell Dev. Biol. 7:336. doi: 10.3389/fcell.2019.00336

INTRODUCTION

Spatial genome organization involves the 3D structure, positioning, and interactions of chromatin within the nucleus. This is a non-random process that is characterized by the regulation of various nuclear domains, topological associations, and epigenetic signatures. For example, decondensed euchromatin domains, which include active enhancer elements and are generally conducive to transcription, are found preferentially within the nuclear interior. On the other hand, heterochromatin domains are densely packed chromosome regions that are occupied by gene-silencing histone marks, which include histone H3 methylated on Lysine 27 (H3K27me3) or Lysine 9 (H3K9me2 and H3K9me3) (Rice and Allis, 2001; Richards and Elgin, 2002). Such heterochromatin domains are preferentially located near the nuclear periphery or a major nuclear compartment called the nucleolus.

In fact, the nuclear genome is generally arranged within several cytologically distinct compartments. In addition to the prominent nucleolus, other nuclear compartments include the Cajal bodies, speckles, paraspeckles, and histone locus bodies. Nuclear compartments generally form via dynamic self-organization of their different constituents at sites of gene clusters (Mao et al., 2011; Sleeman and Trinkle-Mulcahy, 2014; Wang et al., 2016). For example, nucleoli encompass the tandem ribosomal DNA (rDNA) repeats while histone locus bodies form around the histone-encoding gene clusters. Early studies identified a role for molecular crowding in the formation of some nuclear compartments (Richter et al., 2007; Cho and Kim, 2012). High concentrations of macromolecules in a local environment creates crowding and promotes formation of weak non-covalent bonds between the macromolecules, thereby forming membrane-less nuclear compartments. Consistent with this notion, the formation of several

nuclear compartments is driven by liquid-liquid phase separation (Zhu and Brangwynne, 2015; Hall et al., 2019). Importantly, the three-dimensional organization of chromatin into these nuclear compartments often underlies the expression and stability of the various genetic loci that are harbored within such nuclear bodies. For example, actively transcribed genes often associate with the periphery of nuclear speckles, which are sites of RNA processing (Hu et al., 2019). Disruption of nuclear speckles changes gene expression profiles by decreasing intrachromosomal interactions between active chromatin regions.

In addition to the formation of cytologically distinct nuclear compartments, the genome is organized into topologically associated domains (TADs) (Dixon et al., 2012), which can be viewed as three-dimensional building blocks of looped chromatin domains (Lieberman-Aiden et al., 2009; Dixon et al., 2012). TADs are present in the genomes of several eukaryotes including *Drosophila* (Sexton et al., 2012), mice (Krefting et al., 2018) and humans (Lieberman-Aiden et al., 2009), and are categorized into type A (active genes) and type B (inactive genes) compartments. TADs can regulate transcription by acting as insulators, preventing the spread of euchromatin or heterochromatin marks and regulating enhancer-promoter interactions.

Topologically associated domains are built or defined by their associated proteins, which include the cohesin complex, condensin complex and CCCTCF binding factor (CTCF) which binds DNA in a sequence-specific manner (Dixon et al., 2012; Zuin et al., 2014). Cohesin and condensin are ring-shaped protein complexes that bind chromatin independently of the DNA sequence and mediate chromatin looping, bringing distant DNA sequences along the linear genome into close proximity within the 3D space of the nucleus (Nuebler et al., 2018). The cohesin and condensin complexes, which are composed of structural maintenance of chromosome (SMC) proteins, extrude the DNA into loops through an ATP hydrolysis-dependent mechanism (Burmann et al., 2017; Diebold-Durand et al., 2017; Ganji et al., 2018). Cohesin loading onto chromatin is mediated by the loading factor NIPBL, the absence of which results in the loss of local TAD patterns (Schwarzer et al., 2017). The DNA is extruded until cohesin reaches a boundary element or insulator such as CTCF (Nuebler et al., 2018; Vian et al., 2018). CTCF is a DNA binding protein that mostly associates with TAD boundary regions, insulator sequences, and imprinting control regions (Rao et al., 2014; Sanborn et al., 2015). CTCF is responsible for the majority of chromatin loops across the human genome and is thus an important regulator of spatial genome organization.

Another regulator of spatial genome organization is the nuclear envelope, which harbors the inner nuclear membrane (INM) proteins and nuclear pore complexes (NPCs) and is lined by the nuclear lamina (NL), which is a meshwork of lamin and lamin-associated proteins. The nuclear lamins are important regulators of chromatin organization (Kind et al., 2015). Genes that are activated for transcription are commonly repositioned from the NL to either the nuclear interior or closer to NPCs. Regions of the chromatin that interact with the lamina are referred to as lamina associated domains (LADs), and this association is mediated by lamin-associated proteins. In mammals (Guelen et al., 2008), nematodes (Ikegami et al., 2010) and flies (Pickersgill et al., 2006; van Bemmel et al., 2010), LADs mostly harbor silent or weakly expressed genes, and contain heterochromatin marks such as H3K9me3 and H3K9me2 (Casolari et al., 2004; Wen et al., 2009), whereas budding yeast has no lamina or LADs and its genome is instead organized into gene crumples and directly tethered to INM or NPC proteins (Taddei et al., 2006; Mekhail et al., 2008; Hsieh et al., 2015). In *Drosophila* cells, NL disruption alters LAD composition such that there is more histone H3 acetylated on Lysine 9 (H3K9Ac) and less chromatin compaction (Ulianov et al., 2019). Furthermore, association of chromosomes with the nuclear lamina limits their mobility within the nucleus (Wang H. et al., 2018). In addition, studies in different organisms revealed that NPCs can regulate chromatin structure and function (Dilworth et al., 2005; Brown et al., 2008; Mekhail and Moazed, 2010). For example, the nucleoporins from which NPCs are built can associate with the promoters of active genes in yeast, thereby regulating gene expression (Schmid et al., 2006).

In addition to nuclear compartments, TADs/LADs, the nuclear envelope and their associated protein complexes, non-coding RNAs (ncRNAs) have emerged as major regulators of spatial genome organization. ncRNAs are RNA molecules that are not translated into proteins. ncRNAs are categorized based on their size – long (>200 bp) and short (<200 bp) – and are implicated in numerous cellular processes including transcription, mRNA splicing, and protein translation (Mortazavi et al., 2008; Khalil et al., 2009; Palazzo and Lee, 2015). ncRNAs emerging from within a given genetic locus can regulate transcription at the same locus (*cis*) or elsewhere in the genome (*trans*). Here we review ncRNAs that emerge from single-copy DNA loci or repetitive DNA loci and have diverse roles in spatial genome organization, thus impacting gene expression and stability. Collectively, ncRNAs impact spatial genome organization by modulating perinuclear chromosome tethering, the formation of major nuclear compartments, chromatin looping and various chromosomal structures. These roles of ncRNAs often intersect with various other regulators of genome structure and function.

NON-CODING RNA AT SINGLE COPY LOCI

Single copy loci include genes required for cell function and survival and can give rise to ncRNAs that regulate higher order chromatin structure and positioning (**Figure 1**). ncRNAs and their active transcription can mediate chromatin looping to bring distant DNA regions into close proximity and reposition genetic loci to regulate their expression. Nuclear bodies, such as Cajal bodies and paraspeckles, are formed by ncRNA transcription and can regulate the localization or sequestration of transcriptional regulators. Furthermore, ncRNAs play roles in organismal development by regulating the subnuclear positioning and transcriptional status of the X chromosome, HOX genes and *Kcnq1* genes. In this section we discuss roles for ncRNAs and their transcription in the control of spatial gene positioning, chromatin remodeling and nuclear compartmentalization.

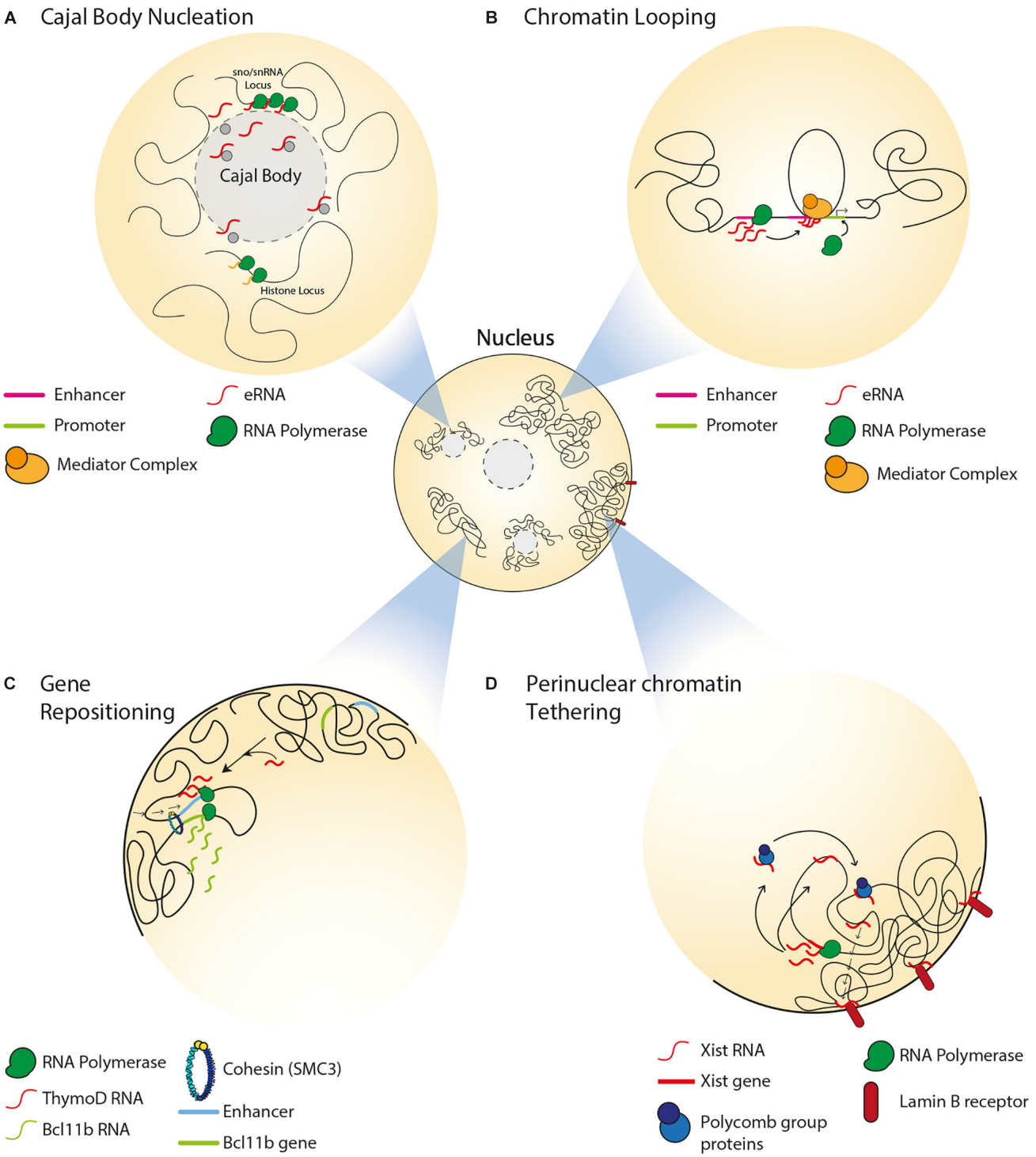

FIGURE 1 | Spatial organization of single copy loci by ncRNAs. **(A)** Transcription of snRNA genes and interaction between intron-encoded snoRNA/snRNAs with coilin mediate Cajal body formation. Cajal bodies associate with sn/snoRNA and histone gene loci and regulate their gene expression. **(B)** Transcription of an enhancer can produce eRNAs, which associate with the mediator complex and enable chromatin looping, thereby driving enhancer-promoter interaction. **(C)** In the absence of the *ThymoD* ncRNA, the enhancer for the *BCL11B* locus is at nuclear periphery. *ThymoD* ncRNA mediates enhancer repositioning away from the nuclear periphery and drives chromatin looping of the enhancer bringing it in close proximity to the *BCL11B* locus, thereby allowing for the transcriptional activation of this locus. **(D)** In the somatic tissues of placental mammals, *Xist* lncRNA tethers the inactive X chromosome to the nuclear lamina by interacting with lamin B receptor. *Xist* interacts with polycomb proteins to establish the heterochromatin state of the inactive X chromosome. *Xist* also mediates relocation of active genes from the surface of the X chromosome to its interior.

ncRNAs in the Formation and Maintenance of Nuclear Compartments

Non-coding RNAs can impact the structure and function of nuclear compartments such as Cajal bodies. The latter are involved in various processes including telomerase biogenesis, 3′-end processing of histone pre-mRNAs, as well as the processing, assembly and maturation of spliceosomal small nuclear ribonucleoproteins (snRNPs) (Sawyer et al., 2016). Cajal bodies associate with small nuclear and nucleolar RNA (sn/snoRNA) gene loci, such that these genes form intra- and inter-chromosomal clusters around the bodies (**Figure 1A**) (Wang et al., 2016). In fact, the formation of Cajal bodies is itself mediated by the transcription of snRNA genes (Kaiser et al., 2008) and by interactions between intron-encoded snoRNA/snRNAs and a protein called coilin (Kaiser et al., 2008; Machyna et al., 2014). This is in accordance with studies reporting the loss of Cajal bodies during mitosis and their reformation during early G1 upon the resumption of transcription (Carmo-Fonseca et al., 1993; Strzelecka et al., 2010). Furthermore, these ncRNA-dependent Cajal bodies are responsible for the spatial organization and expression of other types of genes, including those encoding for histones or pre-mRNA splicing factors (Sawyer et al., 2016; Wang et al., 2016; Wang H. et al., 2018).

Paraspeckles are nuclear bodies that form in response to environmental stress at and around the *NEAT1* gene (nuclear enriched abundant transcript 1), which is transcribed into the long ncRNAs (lncRNAs) *NEAT1_1* (Men ε) and *NEAT1_2* (Men β) (Sunwoo et al., 2009). These lncRNAs and their ongoing transcription are required for the nucleation and maintenance of these nuclear compartments (Shevtsov and Dundr, 2011). Transcriptional upregulation of *NEAT1* increases paraspeckle size and sequestration of paraspeckle-associated transcriptional regulators, such as the splicing factor proline/glutamine-rich (SFPQ) (Hirose et al., 2014). In contrast, repression of *NEAT1* disrupts paraspeckles, releases paraspeckle-associated proteins into the nucleoplasm and hyper-induces the transcription of various genes including *ADARB2* (adenosine deaminase RNA-specific B2), which is involved in RNA editing (Clemson et al., 2009; Mao et al., 2011; Hirose et al., 2014; Imamura et al., 2014).

NEAT1 can also regulate the subnuclear localization of growth control genes by associating with Polycomb 2 protein (Pc2), a key subunit of the chromatin-repressive PRC1 complex (Yang et al., 2011). Methylation/demethylation cycles of Pc2 dictate its association with two ncRNAs, *TUG1* (Taurine up-regulated 1) and *NEAT1*, which are found in two distinct nuclear bodies. Methylated Pc2 preferentially interacts with the *TUG1* ncRNA within the transcriptionally repressive Polycomb nuclear bodies, thereby silencing the Pc2-associated growth control genes. On the other hand, demethylation of Pc2 results in its preferential interaction with *NEAT1*, which relocates Pc2 together with its associated growth control genes to inter-chromosomal granules within which the genes can be actively transcribed.

NEAT1 is commonly induced upon viral infection and can regulate the transcriptional activation of various antiviral genes (Ma et al., 2017). The splicing factor SFPQ is a transcriptional repressor of the antiviral gene *IL-8*. Recently, *NEAT1* has been shown to mediate the relocation of SFPQ from the *IL-8* promoter to paraspeckles, thereby activating *IL-8* gene expression (Imamura et al., 2014). Paraspeckles and *NEAT1* have also been linked to cancer biology, where they can have both oncogenic and tumor suppressive roles. In some cancers, the upregulation of *NEAT1* and associated paraspeckles can be driven by tumor microenvironmental conditions and estrogen receptor stimulation, respectively (Chakravarty et al., 2014; Choudhry et al., 2015). This upregulation is associated with increases in active epigenetic marks and cellular proliferation. Surprisingly, in some types of cancer, upregulation of *NEAT1* and paraspeckles prevented cellular transformation and tumorigenesis (Adriaens et al., 2016). Overall, these findings highlight functional connections between ncRNAs and nuclear compartments. These studies also underscore the importance of understanding the exact roles that ncRNAs can exert within different biological and clinical settings.

ncRNAs and Chromatin Looping

Non-coding RNAs can regulate gene expression by mediating chromatin remodeling between enhancers and promoters. Transcription of enhancers in mammalian cells can give rise to a type of ncRNA that is referred to as enhancer RNA (eRNA), which can bring an enhancer and promoter in close proximity by mediating the formation of a DNA loop, and associate with mediator complexes to drive the expression of target genes (**Figure 1B**) (Kim et al., 2010; Orom et al., 2010). For example, activation of estrogen receptor-α induces the transcription of eRNAs that mediate chromatin looping, thereby driving transcription-inducing enhancer-promoter interactions at target genes (Li W. et al., 2013). Another class of ncRNAs, which is known as ncRNA-activating (ncRNA-a), has a function similar to that of eRNA (Lai et al., 2013; Li W. et al., 2013). These ncRNA-a species activate their neighboring genes by associating with the mediator complex and enabling chromatin looping in *cis*. This 3D chromatin configuration and gene expression are reduced upon disruption of ncRNA-a species or mediator, suggesting the dependence of chromatin loop structure and function on interactions between ncRNA-a and mediator.

The active transcription of ncRNAs can also result in the looping of DNA, bringing gene loci in close proximity or blocking transcription of distant genes. In the plant *Arabidopsis thaliana*, transcription of the ncRNA *APOLO* forms a chromatin loop encompassing the promoter of its neighboring gene, *PID* (Ariel et al., 2014), which is the key regulator of polar auxin transport and root development (Benjamins et al., 2001). This *APOLO*-mediated 3D chromatin configuration, which is also influenced by PRC1 and PRC2 (polycomb repressive complex 1 and 2), limits the access of Pol II to the *PID* promoter, thereby regulating the transcriptional activity of this gene (Ariel et al., 2014). Disruption of the *APOLO*-dependent expression of *PID* results in defects in root development, highlighting the importance of ncRNA-mediated chromatin remodeling to plant growth and development (Benjamins et al., 2001).

Intergenic transcription-driven chromatin looping is also implicated in lymphocyte development. In developing B cells,

V(D)J recombination is required for the assembly of antigen receptors (Alt et al., 1984; Sayegh et al., 2005). Importantly, V(D)J recombination requires changes to the 3D configuration of the immunoglobulin heavy locus (*Igh*) in order to bring the V_H, D_H and J_H genes in close proximity, which in turn allows the genetic rearrangements to occur (Kosak et al., 2002; Medvedovic et al., 2013). Prior to rearrangement, non-coding transcription at this locus occurs at the V_H intergenic region in the antisense orientation (Yancopoulos and Alt, 1985). This intergenic region contains Pax5-activated intergenic repeat (PAIR) elements (Fuxa et al., 2004), which are transcriptionally upregulated in the absence of CTCF (Degner et al., 2009). Antisense transcription of these PAIR elements in pro-B cells mediates long-distance interaction with the E_μ region on the *Igh* locus (Verma-Gaur et al., 2012). The resulting DNA looping brings the distal V_H into close proximity with DJ_H and allows for V_H to DJ_H recombination. These DNA loops are not observed in the absence of ncRNA transcription, highlighting the importance of active ncRNA transcription to V(D)J recombination and its role in B cell development.

In developing T cells, expression of BCL11B (BAF Chromatin Remodeling Complex Subunit BCL11B) promotes expression of T-lineage-specific genes and suppresses expression of the genes associated with alternative cell fates (Li et al., 2010). Activation of BCL11B expression is mediated by an enhancer that is located at the so-called intergenic control region (ICR) (Li L. et al., 2013). Repositioning of the enhancer from the nuclear lamina to the interior allows for the transcriptional activation of *BCL11B* (**Figure 1C**) (Isoda et al., 2017). Importantly, this relocation within nuclear space is mediated by transcription of the ncRNA *ThymoD* (thymocyte differentiation factor), which mediates DNA demethylation at CTCF binding sites and subsequent activation of CTCF/cohesin-dependent chromatin looping.

ncRNAs and X Chromosome Silencing and Positioning

One of the well-studied ncRNAs implicated in mammalian 3D genome organization is *Xist* (X inactive specific transcript), a 17 kb lncRNA that mediates inactivation of one of the X chromosomes during early female embryonic development (Brown et al., 1992). *Xist* is specifically transcribed from the inactive X chromosome. *Xist* occupies inactive regions of the X chromosome before spreading across transcriptionally active regions and initiating their inactivation. Subsequently, the inactive X chromosome forms a heterochromatic structure, which is referred to as Barr body and is found at the perinuclear and perinucleolar regions, where transcription silencing machineries are enriched (Zhang et al., 2007). Of note, tethering of the inactive X chromosome to the nuclear lamina is the result of interactions between *Xist* and the INM-embedded lamin B receptor (**Figure 1D**) (Chen et al., 2016). This interaction repositions transcriptionally active DNA regions of the X chromosome in close proximity with *Xist* and its transcriptional silencing domain, thereby promoting the spread of *Xist* across the chromosome. In female embryonic stem cells, the spreading of *Xist* along an X chromosome results in the establishment of polycomb group proteins-dependent heterochromatin and exclusion of transcription machineries (**Figure 1D**) (Plath et al., 2003; Okamoto et al., 2004; Chaumeil et al., 2006; Schoeftner et al., 2006). During this process, active genes that were once on the surface of the X chromosome relocate to the interior, forming *Xist*-containing transcriptionally silent domains (Chaumeil et al., 2006). Furthermore, *Xist* maintains this heterochromatic nuclear compartment by acting in *cis* to repel cohesin and other chromatin looping factors that typically facilitate gene expression (Minajigi et al., 2015). Consequently, compared to the active X chromosome, the inactive X chromosome is devoid of TADs, which can nonetheless be re-established upon depletion of *Xist* and restoration of cohesin loading (Nora et al., 2012). Taken together, these findings highlight how the *Xist* lncRNA mediates mammalian X chromosome inactivation through the formation of perinuclear heterochromatin domains and the exclusion of factors that can promote chromatin looping and gene expression.

The expression of *Xist* on the active X chromosome is regulated by another lncRNA, *Tsix*, which is transcribed antisense to *Xist* (Stavropoulos et al., 2001). Transcription of *Tsix* represses *Xist* expression in *cis* through epigenetic processes (Stavropoulos et al., 2001; Shibata and Lee, 2004). In mouse embryonic stem cells, the X chromosome lacking *Tsix* transcription was non-randomly inactivated (Lee and Lu, 1999; Luikenhuis et al., 2001), and induction of *Tsix* transcription resulted in targeted X chromosome activation (Luikenhuis et al., 2001). Therefore, *Tsix* and *Xist* play antagonistic roles in regulating X chromosome inactivation during embryonic stem cell differentiation.

In addition to *Xist* and *Tsix*, *Firre* (functional intergenic repeating element) is another lncRNA that is transcribed from a locus on the X chromosome (Hacisuleyman et al., 2014). *Firre* can maintain the silencing of the X chromosome by tethering it to the perinucleolar compartment (Yang et al., 2015). In addition, *Firre* interacts with the nuclear matrix factor hnRNPU and colocalizes with five distinct *trans*-chromosomal loci, which reside in spatial proximity to the *Firre* locus. This colocalization is lost in the absence of *Firre*, suggesting a role of this ncRNA in the establishment of higher order chromosomal architectures within nuclear space.

Typically, cells randomly choose whether the maternal or paternal X chromosome is inactivated. However, under certain circumstances, there can be bias toward one parental X chromosome. Such a bias is referred to as skewed X inactivation. In females, this can result in diseases such as Duchenne muscular dystrophy and hemophilia A (Yoshioka et al., 1998; Renault et al., 2007). Incomplete silencing of the X chromosome can also result in skewed X inactivation since some genes manage to evade silencing and remain therefore expressed. For example, escape of the steroid sulfatase locus from silencing can trigger X-linked ichthyosis, which is a group of diseases characterized by very dry skin (Hernandez-Martin et al., 1999). Thus, ncRNAs operate at the interface of spatial genome organization and epigenetic silencing to mediate X chromosome inactivation, the dysregulation of which underlies different human diseases.

ncRNAs and the Spatial Organization of Developmental Genes

During vertebrate development, ncRNAs can regulate the spatial organization of gene clusters, such as the *HOX* genes (Flyamer et al., 2017). *HOX* genes, which are homeotic genes involved in antero-posterior body axis development in vertebrates, are found on four spatially clustered chromosomal loci (*HOXA*, *HOXB*, *HOXC,* and *HOXD*). The genes are separated into distinct topological compartments based on their transcriptional profile, and during development, there exists a dynamic switch between these topological domains (Noordermeer et al., 2011). This higher order structure of the *HOX* gene clusters is regulated by intergenic ncRNAs (Wang et al., 2011). For example, the ncRNA *HOTTIP* (*HOXA* transcript at the distal tip) is transcribed from the 5′ edge of the *HOXA* locus and is required for maintaining the compartmentalization of the locus. *HOTTIP* can associate with and target the WD repeat mixed lineage leukemia (WDR-MLL) complex across the *HOXA* locus to yield active histone marks. This in return maintains the active state of some of the *HOXA* genes. *HOTTIP* also physically associates with CTCF, which can bind to six conserved binding sites at *HOXA* and serve as an insulator (Wang F. et al., 2018). This contributes to the discrete expression profile of genes across the *HOXA* locus. The dynamic 3D architecture of these gene clusters is important as it dictates the transcriptional profile of the *HOX* genes during development. Dysregulation of *HOX* gene expression can abrogate limb and skeletal development in murine and *Drosophila* embryos (Di-Poi et al., 2010; Andrey et al., 2013). Therefore, regulation of the spatial organization of HOX genes by ncRNAs is important for organismal development.

Another critical component of development is known as genetic imprinting, which consists of the silencing of one parental allele. Imprinted genes tend to spatially cluster and this allows for their coordinated regulation during development. lncRNAs have been shown to regulate the expression and large-scale chromatin structure of these genes through interaction with histone modifying proteins and chromatin looping (Umlauf et al., 2004; Terranova et al., 2008; Zhang et al., 2014). In early mammalian embryos, the *Kcnq1* genes cluster into a compact subnuclear compartment, devoid of transcriptional activity (Verona et al., 2003; Lewis et al., 2006). This nuclear compartment is enriched with repressive histone marks and silencing protein complexes such as polycomb proteins (Umlauf et al., 2004; Terranova et al., 2008). Formation of this higher order repressive domain and its localization within the perinucleolar compartment is mediated by the *Kcnq1ot1* ncRNA, which associates with the H3K9me3 repressive histone mark and polycomb proteins (Mohammad et al., 2008; Pandey et al., 2008; Terranova et al., 2008). *Kcnq1ot1* is an antisense ncRNA (∼100 kb) that is transcribed from the intronic region of the *Kcnq1* locus of one of the parental chromosomes. Deletion of *Kcnq1ot1* results in expression of the parental allele that is normally silent (Mancini-Dinardo et al., 2006). More recently, this ncRNA has been shown to directly interact with the chromosome, through its 5′ terminal region, in order to mediate intrachromosomal looping between the *Kcnq1* promoter and *Kcnq1ot1* promoter KvDMR (Zhang et al., 2014). These promoters are 200 kb apart in the linear genome (Zhang et al., 2014). However, promoter looping results in the imprinting of the *Kcnq1* cluster, or its allelic silencing. Deletion of KvDMR can result in biallelic expression of maternal-specific genes in the *Kcnq1* cluster and growth deficiency in mice (Fitzpatrick et al., 2002; Shin et al., 2008). In humans, loss of imprinting can lead to Beckwith–Wiedemann syndrome, which is associated with cancer growth and progression (Lee et al., 1999; Fitzpatrick et al., 2002; Valente et al., 2019). Therefore, regulation of the spatial organization of the *Kcnq1* gene cluster by *Kcnq1ot1* is important for mammalian genetic imprinting and healthy development. Overall, these findings suggest that ncRNAs play a role in regulating gene expression during development via establishment of nuclear compartments and regulation of locus positioning within nuclear space.

Taken together, ncRNAs from single-copy loci contribute to spatial genome organization through chromatin remodeling, nuclear compartmentalization and the subnuclear positioning of various genes within nuclear space. These roles of ncRNA help mediate cellular processes that are central to the proper control of gene expression, genome stability, development, and health.

NON-CODING RNA AT REPETITIVE DNA LOCI

Eukaryotic genomes are largely composed of repetitive DNA sequences that can be generally classified as tandem or interspersed repeats. Tandem repeats include satellite and minisatellite repeats (e.g., centromeres) as well as microsatellite repeats (telomeres). Interspersed repeats include transposable elements that are either retrotransposons or DNA transposons. Retrotransposons include LTR-retrotransposons such as HERV and non-LTR retrotransposons such as SINEs (e.g., Alu), LINEs (e.g., LINE-1) or SVAs. It is also important to note that some types of repeats such as human ribosomal DNA (rDNA) can be arranged in tandem repeats that are interspersed throughout the linear genome. Regardless of their relative genomic location, DNA repeats are often clustered within nuclear space. This can facilitate their transcriptional co-regulation, minimize their potential deleterious interaction with the rest of the genome and control their exposure to potentially genome-destabilizing DNA recombination and repair machineries.

Repetitive DNA sequences are non-randomly arranged within the nucleus. For example, rDNA repeats are physically sequestered in the nucleolar compartment of the nucleus. This sequestration can be driven by inter- or intra-chromosomal interactions, or even direct tethering to the nuclear envelope in some organisms (O'Sullivan et al., 2009; Mekhail and Moazed, 2010; Chan et al., 2011; Hult et al., 2017). Telomeres, which are at the ends of linear chromosomes, often colocalize within PML bodies (Chang et al., 2013) at the nuclear interior or within telomeric clusters or bouquets at the nuclear periphery (Gotta et al., 1996). In budding yeast, the Transposons of Yeast 1 (Ty1) retrotransposons cluster within or near nucleoli (O'Sullivan et al., 2009), while centromeres cluster at the

yeast spindle pole body (Jin et al., 2000). Importantly, several ncRNAs from repetitive DNA loci have emerged as major players that mediate crosstalk between spatial genome organization, expression and stability. Here were review such ncRNAs, which emerge from rDNA repeats, telomeric regions, transposable elements, and centromeres.

Non-coding RNAs in rDNA Structure and Function

Non-coding RNAs can play a role in the spatial organization and function of rDNA through the modulation of heterochromatin formation. Transcription of rDNA into ribosomal RNA (rRNA) molecules is dependent on the varying demand for protein synthesis that cells experience in response to intracellular signals or environmental stimuli. Therefore, despite the existence of 100s of rDNA repeats in eukaryotes, only a fraction of rDNA units are transcribed, while the remainder of the repeats is epigenetically silenced. Transcriptionally active rDNA units are marked by DNA hypomethylation, H4Ac and H3K4me2, whereas inactive rDNA units are marked by promoter hypermethylation, histone H4 hypoacetylation and methylation of H3K9, H3K27, and H4K20 (Santoro et al., 2002). Deposition of these marks is facilitated by the nucleolar remodeling complex (NoRC), which guides chromatin remodeling proteins to the rDNA and other loci. In mice, NoRC is recruited to nucleoli through interaction between the large subunit of NoRC (TIP5) and promoter-associated RNAs (pRNAs) that overlap the rDNA promoter (Mayer et al., 2006). A class of pRNAs termed PAPAS (promoter and pre-rRNA antisense) covers the rDNA promoter, and levels of PAPAS generally reflect the physiological state of the cell, such that there is an anti-correlation between PAPAS and pre-rRNA levels (**Figure 2A**) (Bierhoff et al., 2010). In quiescent mammalian cells, PAPAS is induced, binds to the histone methyltransferase Suv4-20h2, targets it to the rDNA promoter and downregulates rRNA transcription through enhanced H4K20me3 (Bierhoff et al., 2014). In addition, upon heat shock, upregulation of PAPAS attenuates pre-rRNA synthesis by recruiting another chromatin remodeling complex named CHD4/NuRD to the mammalian rDNA promoter (Zhao et al., 2018). On another front, in mammalian cells under hypotonic stress conditions, PAPAS upregulation recruits NuRD to reposition the rDNA promoter-bound nucleosome to the "off" position, thereby halting pre-rRNA synthesis (Zhao et al., 2016). Interestingly, pRNA-dependent heterochromatin formation at rDNA has also been shown to initiate the downstream establishment of heterochromatic structures at genomic regions that are in close proximity but lie outside of the murine nucleolus (Savic et al., 2014). Taken together, these studies reveal that under different environmental conditions, promoter-associated ncRNAs from repetitive loci can silence gene expression in *cis* through various processes. Future studies should explore how such ncRNAs are induced under different environmental conditions.

The nucleolus typically exhibits a phase separation-driven tripartite organization into a fibrillar centre (FC), dense fibrillar component (DFC), and granular component (GC) (Feric et al., 2016; Hall et al., 2019). Upon exposure to environmental stresses including heat shock or acidosis, a couple of ncRNAs induced from the mammalian rDNA intergenic spacer (IGS) dissolve this tripartite organization, structurally remodeling the nucleolus into a so-called "protein detention centre" (DC) (Mekhail et al., 2005; Jacob et al., 2013). The DC is suggested to be spatially, dynamically and biochemically distinct from the standard tripartite domains (Jacob et al., 2013). This structural remodeling of the mammalian nucleolus can arrest rRNA synthesis and create a hub for immobilized proteins, effectively mediating their nucleolar sequestration and functional inactivation (Audas et al., 2012). Upon removal of the environmental stressor, the ncRNAs are repressed, DC is dissolved and tripartite nucleolar organization is re-established (Jacob et al., 2013). Thus, ncRNAs spatially remodel the nucleolus during stress. Importantly, future studies should explore how cells control the generation and function of such intergenic ncRNAs under varying environmental conditions.

The organization of rDNA repeat regions into epigenetically silent chromatin structures is essential to proper cellular function and alterations in this organization may be associated with human disease. For example, rDNA hypermethylation is characteristic of early Alzheimer's disease (Pietrzak et al., 2011), upregulation of rRNA expression is characteristic of tumor cells (White, 2005; Montanaro et al., 2008; Bywater et al., 2013) and rRNA dysfunction is linked to a group of genetic diseases known as ribosomopathies (Narla and Ebert, 2010; Nakhoul et al., 2014). In addition, in yeast, the dysregulation of IGS ncRNAs at rDNA repeats has been associated with premature aging through three distinct mechanisms. First, loss of IGS silencing leads to the upregulation of IGS ncRNAs, which displace cohesin complexes, triggering rDNA instability and premature aging (Saka et al., 2013). Second, IGS ncRNAs are prone to the formation of DNA replication-blocking RNA–DNA hybrid-containing structures called R-loops (Salvi et al., 2014). When these structures accumulate, as in some yeast mutants, unequal sister chromatid exchange events occur within the rDNA repeats, leading to chromosome instability and premature cellular aging (Salvi et al., 2014). Lastly, in yeast genetic models of neurodegenerative diseases, hyper-reductions in IGS ncRNA levels can lead to rDNA copy number instability and premature cellular aging (Ostrowski et al., 2018). Thus, ncRNAs that play important roles in the epigenetic silencing and organization of rDNA repeats can impact processes underlying organismal health span.

Crosstalk Between Telomeric ncRNAs, Heterochromatin, and Subnuclear Positioning

The telomeres at the end of linear chromosomes are often heterochromatic. In vertebrates, telomeres are composed of hexameric 5′-TTAGGG-3′ repeats that are flanked by repetitive subtelomeric regions. Telomeric and subtelomeric repeats exhibit heterochromatic marks (H3K9me3, H4K20me3, and hypoacetylation of H3 and H4). Loss of heterochromatin disrupts telomere length control, increases telomeric recombination and promotes premature cellular senescence (Garcia-Cao et al., 2004; Benetti et al., 2007). Interestingly, the establishment

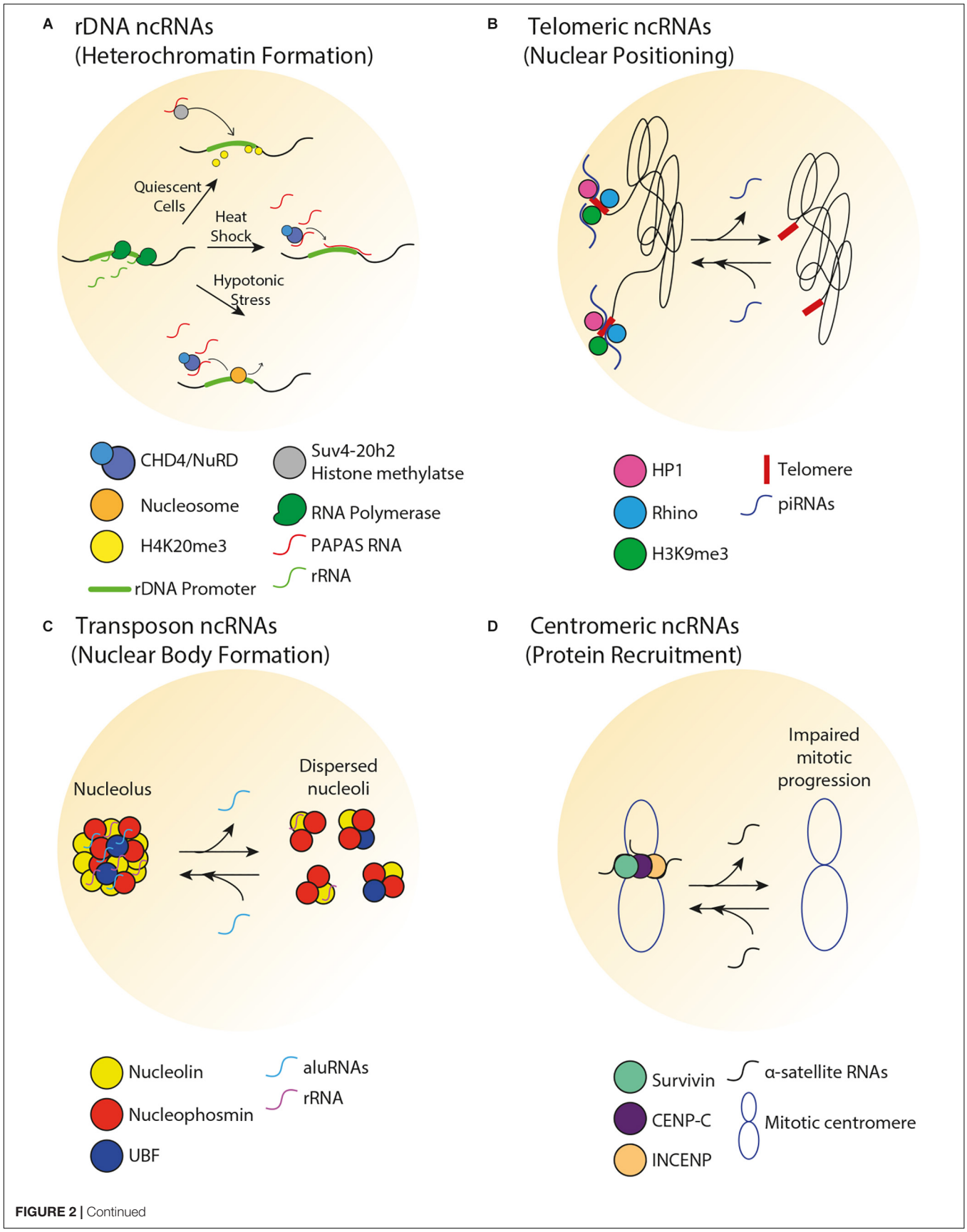

FIGURE 2 | Continued

FIGURE 2 | Spatial organization of repetitive DNA loci by ncRNA. **(A)** In human cells, there is an inverse correlation between PAPAS and pre-rRNA levels. In quiescent cells, PAPAS binds to the Suv4-20h2 histone methyltransferase and directs it to the rDNA promoter for H4K20me3-dependent repression. Upon heat shock, PAPAS hybridizes with the rDNA promoter and recruits the CHD4/NuRD complex, thereby preventing rDNA transcription. Upon hypotonic stress, upregulation of PAPAS recruits the CHD4/NuRD complex to reposition rDNA promoter-bound nucleosome to the off position, thereby halting pre-rRNA synthesis. **(B)** In germline tissues of flies, piRNAs transcribed from the telomeric region mediate perinuclear positioning of telomeres and promote HP1, Rhino, and H3K9me3 enrichments at telomeres. **(C)** In human cells, aluRNAs enriched in the nucleolus interact with nucleolin to maintain nucleolar structure and function. **(D)** In human cells, α-satellite RNAs associate with and promote the centromeric enrichment of Survivin, CENP-C, and INCENP in order to maintain centromere stability.

of telomeric heterochromatin is influenced by a type of ncRNA called telomeric repeat-containing RNA (TERRA), which is composed of UUAGGG repeats (Nergadze et al., 2009). TERRA transcription typically initiates from subtelomeric CpG islands and proceeds to chromosomal ends. Several lines of evidence support a role for TERRA in the regulation of heterochromatin and other structures near chromosome ends. First, TERRA associates with TIP5 and subsequently recruits NoRC and the histone-modifying enzymes Suv4-20h2 and SIRT6 to human telomeres (Postepska-Igielska et al., 2013). Second, loss of human TERRA decreases telomeric H3K9me3 and HP1 enrichments and induces the DNA damage response (Blasco, 2007; Deng et al., 2009). Third, TERRA facilitates heterochromatin-promoting interactions between the human Shelterin complex, HP1 and the origin recognition complex (Deng et al., 2009). Fourth, TERRA transcription initiates at subtelomeric CTCF-binding sites, tentatively suggesting that the transcription of TERRA is itself spatially regulated by chromosome looping (Beishline et al., 2017). ncRNAs also regulate telomeric heterochromatin formation in non-vertebrate species. For example, small ncRNAs are implicated in heterochromatin formation at fission yeast telomeres (Cao et al., 2009). Together, these studies highlight a role for telomeric ncRNAs in the promotion of local heterochromatin structures and consequent prevention of premature cellular senescence. Importantly, there is crosstalk between telomeric heterochromatin and the subnuclear positioning of telomeres. For example, in budding yeast, the constitutive co-localization of telomeres in a handful of clusters at the nuclear periphery increases the local concentration of chromatin silencing factors, reinforcing telomeric heterochromatin and limiting access to the potentially genome-destabilizing recombination machinery (Therizols et al., 2006; Schober et al., 2009; Chan et al., 2011). In the fly germline, loss of some PIWI-interacting RNAs (piRNAs) that are typically transcribed from telomeric regions decreased perinuclear telomere positioning and lowered the local enrichment of HP1, Rhino, and H3K9me3 (**Figure 2B**) (Radion et al., 2018).

Connections exist between telomere malfunction and disease. The aberrant loss of telomeric heterochromatin can trigger telomeric DNA damage responses and recombination events, which are associated with several diseases (Hagelstrom et al., 2010). The accumulation of TERRA-associated R-loops drives telomere instability in the rare autosomal recessive syndrome ICF (immunodeficiency, centromeric instability, and facial anomalies; Sagie et al., 2017). Similarly, in budding yeast, elevated TERRA levels can promote premature senescence (Wanat et al., 2018). On another front, various changes to TERRA levels are linked to cancer (Artandi and DePinho, 2010), dyskeratosis congenita (Armanios et al., 2009; Gu et al., 2009; Mason and Bessler, 2011) and aplastic anemia (Armanios et al., 2009; O'Sullivan and Karlseder, 2010; Armanios, 2012). We refer the reader elsewhere for a full review on the emerging connections between telomeric ncRNAs and disease (Maicher et al., 2012). Taken together, these studies suggest that telomeric ncRNAs modulate heterochromatin formation and subnuclear positioning at telomeres to promote health and longevity.

Transposable Elements

Similar to other repetitive DNA loci, transposable elements are often silenced by heterochromatin formation to limit the potentially deleterious effects of such elements (Slotkin and Martienssen, 2007). Transposable elements are silenced through a wide range of chromatin modifications, including DNA methylation, histone modifications (e.g., H3K9me and H4K20me) and chromatin condensation (Slotkin and Martienssen, 2007). Similar to PAPAS-dependent recruitment of Suv4-20h2 to the rDNA, in quiescent human cells, it was reported that ncRNAs from the transposable elements *IAP* and *LINE-1* recruit Suv4-20h2 to mediate H4K20me3 enrichment and condense chromatin at transposable elements (Bierhoff et al., 2014). Such elements are also silenced through the action of small ncRNAs. For example, murine piRNAs generated from retroelements are bound to the PIWI-like protein MIWI2 and translocated into the nucleus to silence retroelements through *de novo* DNA methylation (Aravin et al., 2008; De Fazio et al., 2011). Additionally, small RNAs generated from *LINE-1* and *IAP* retroelements can regulate their epigenetic state in mouse embryos (Fadloun et al., 2013). Taken together, these studies suggest that ncRNAs help establish the epigenetic states necessary to keep transposable elements in check.

In addition to regulating chromatin compaction at transposable elements, transposon-associated ncRNAs can modulate the spatial organization of the nucleolus. For example, in HeLa cells, transcripts originating from intronic *Alu* elements (*aluRNAs*) become enriched in the nucleolus, where they interact with the nucleolin (NCL) protein and contribute to the maintenance of nucleolar structure and function (**Figure 2C**) (Caudron-Herger et al., 2015). Similar processes were observed in human keratinocytes and fibroblasts for *aluRNAs*, and for the related *B1* transcripts in mice. Interestingly, *aluRNAs* can somehow target other genomic loci to the nucleolus (Caudron-Herger et al., 2015), tentatively suggesting that these ncRNAs may impact spatial genome organization by establishing physical links within and outside of the nucleolus.

Given the high mutagenic potential of transposable element activity, it is perhaps not surprising that these elements have been linked to disease (Belancio et al., 2009). Transposons can

promote disease through several processes including insertional mutations, deleterious non-allelic homologous recombination and the generation of *cis*-acting signals that modify gene expression (Belancio et al., 2009). It is estimated that ∼0.3% of human genetic diseases are caused by retroelements (Callinan and Batzer, 2006). For example, 15 human diseases are caused by Alu insertions while 18 germ-line diseases and 6 types of cancer are caused by unequal homologous recombination events between Alu repeats (Deininger and Batzer, 1999; Burns, 2017). In addition, *LINE-1* and *SVAs* are causative agents in numerous other human diseases (Belancio et al., 2009). In fact, the increased activity of transposable elements is a known contributing factor to neurodegenerative diseases such as Alzheimer's disease, Aicardi Goutières syndrome, multiple sclerosis, and amyotrophic lateral sclerosis (Guo et al., 2018; Tam et al., 2019). Elevated expression of transposable elements is also a potential mechanism underlying the pathogenic development of various mental disorders including schizophrenia, bipolar disorder, autism spectrum disorders, and major depression (Misiak et al., 2019). In the context of these various diseases, it is thought that loss of heterochromatin structures may be a major contributor to the increased transposable element activity and its deleterious impact. Together, the literature indicates that ncRNAs from transposable elements can positively contribute to spatial genome organization and stability, but that losing control of such elements can disrupt genome function and promote disease.

Centromeres

Centromeres are tandem repeats, which are largely assembled into heterochromatic structures and are important for kinetochore function and chromosome integrity. Centromeres are composed of centric and pericentric regions, which have different chromatin structures that are epigenetically established. CENP-A-containing centric chromatin is characterized by H3K4me3, while pericentric regions are enriched in H3K9me2, H3K9me3, H4K20, and HP1. Heterochromatin formation at centric and pericentric regions is mediated by NoRC, similar to heterochromatin formation at rDNA (Wong et al., 2007; Nemeth et al., 2010). In fact, the common positioning of centromeres near nucleoli may contribute to this dual role for NoRC at rDNA and centromeres (Wong et al., 2007; Nemeth et al., 2010).

Several classes of centromeric ncRNAs have been found to play a role in the establishment of centromeric heterochromatin and kinetochore function across a wide range of species. Importantly, centromeric heterochromatin is maintained by low levels of satellite repeat RNAs (Diaz et al., 1981; Trapitz et al., 1988; Rudert et al., 1995; Li and Kirby, 2003; Martens et al., 2005; Wong et al., 2007). In fission yeast, short-interfering RNAs produced by pericentromeric 'otr' ncRNAs help establish and maintain pericentric heterochromatin (Volpe et al., 2002), while in budding yeast, the expression of centromere-derived lncRNAs (cenRNAs) must be fine-tuned in order to maintain centromere function (Ling and Yuen, 2019). Increased cenRNA levels result in chromosome instability, aneuploidy and down-regulation of centromeric proteins while decreased cenRNA levels also result in chromosome instability. There is overwhelming evidence that centromeric- or pericentromeric-derived ncRNAs are important for the recruitment of centromeric proteins (**Figure 2D**) (Maison et al., 2002; Wong et al., 2007; Ferri et al., 2009; Chan et al., 2012). In *Drosophila*, centromeric SAT III ncRNAs act as a structural component of the kinetochore and are required for the recruitment of centromeric proteins (Rosic et al., 2014). In mice, lncRNAs produced from major pericentromeric satellite repeats recruit the SUMOylated form of HP1 through direct interaction with DNA at the site of their transcription (Maison et al., 2011). Murine major satellite-derived ncRNAs have also been shown to form RNA–DNA hybrids that promote the association of histone lysine methyltransferases Suv39h1 and Suv39h2 with polynucleosomes (Velazquez Camacho et al., 2017), suggesting a function for these ncRNAs in establishing heterochromatic structures. In human cells, single-stranded α-satellite RNAs are required for nucleolar localization of CENP-C and INCENP in interphase cells (Wong et al., 2007). Reducing or increasing centromeric transcription decreases the loading of several CENP proteins (Bergmann et al., 2011, 2012). In human cells and *X. laevis* egg extracts, loss of α-satellite ncRNAs reduces centromeric localization of the kinetochore protein Aurora-B and causes improper spindle attachment and chromosome misalignment (Ideue et al., 2014; Blower, 2016). Additionally, studies in maize, human cells and *X. laevis* suggest that centromeric ncRNAs stabilize CENP-C binding to DNA (Du et al., 2010; Grenfell et al., 2016; McNulty et al., 2017). Murine minor satellite repeat transcripts associate with CENP-A and regulate the structure and function of centromeres during stress and differentiation (Bouzinba-Segard et al., 2006; Ferri et al., 2009). Moreover, aberrant accumulation of these transcripts disrupts chromosome segregation, weakens sister chromatid cohesion, abrogates centromeric epigenetic signatures and results in the accumulation of micronuclei. Together, these studies reveal that the maintenance of an optimal level of centromeric ncRNAs may be important for centromeric function.

While mammalian centromeres can often co-localize with nucleoli in S phase cells, budding yeast centromeres cluster with each other at the spindle pole body, which is opposite the nucleolus (Mekhail and Moazed, 2010). Importantly, this co-localization may contribute to the cells' ability to survive DNA double strand breaks (DSBs). Specifically, it was proposed that centromeres are released from the spindle pole body upon DNA damage induction to allow for increased chromosome flexibility and facilitate donor-acceptor locus contacts necessary for homology-directed repair (Strecker et al., 2016). The release of centromeres also drove the formation of intranuclear microtubule filaments onto which damaged DNA was mobilized by motor proteins to repair-conducive nuclear neighborhoods (Chung et al., 2015; Oshidari et al., 2018, 2019). It will be important to test whether endogenous transcription of centromeric ncRNAs contributes to this increased genome flexibility and formation of intranuclear filaments mediating DNA repair. Consistent with this possibility, the forced expression of an inducible gene integrated within a single centromere was sufficient to trigger the formation of the intranuclear microtubule filaments that are typically only observed upon DNA damage induction (Oshidari et al., 2018).

Changes to the epigenetic state of centromeres has been linked to disease (Black and Giunta, 2018). Tandemly arranged satellite repeats are prone to recombination events that can lead to chromosome rearrangements, genetic abnormalities and karyotypic abnormalities that are hallmarks of cancer (Kim et al., 2013). In addition, a study examining epigenetic signatures in ICF patients reported that, in all of the patients studied, juxtacentromeric satellite II repeats exhibited hypomethylation, tentatively suggesting that this altered epigenetic feature may underlie the chromosome fragility observed in ICF patients (Miniou et al., 1994). Centromeric repeat-associated ncRNAs have been implicated in chromatin-related changes in age and age-related diseases. There is a correlation between centromeric instability and senescence, which is potentially explained by an age-related loss of CENP-A at centromeres (Lee et al., 2010; Maehara et al., 2010; Hedouin et al., 2017). Senescence-related loss of CENP-A may be mediated by alterations to the levels of centromeric repeat transcripts, due to the fact that constitutive pericentromeric heterochromatin is decondensed in senescent cells (Swanson et al., 2013; Giunta and Funabiki, 2017). It has been directly shown that high rates of centromeric transcription can cause CENP-A translocation and mitotic arrest (Hedouin et al., 2017). Interestingly, some forms of cancer are characterized by elevated levels of α-satellite and pericentromeric satellite ncRNAs (Ting et al., 2011). These ncRNAs can form deleterious R-loop structures, which have been suggested to contribute to pericentromeric instability in several cancers (Bersani et al., 2015).

Taken together, the literature reveals numerous intersections between various types of ncRNAs and spatial genome organization in the modulation of repetitive DNA loci and their broader impact on the genome and health.

CONCLUDING REMARKS

In this review we have highlighted roles of ncRNAs and intergenic transcription from single copy and repetitive DNA loci in the regulation of spatial genome organization. Several ncRNAs participate in spatial genome organization through several common mechanisms of action, such as chromatin looping and heterochromatin formation, while others operate through distinct pathways such as perinuclear tethering. Deregulation of spatial genome organization is associated with developmental and age-related diseases including cancer. Although aberrant expression of ncRNAs has been implicated in disease, more direct or causal links between such ncRNAs, spatial genome organization and pathobiology should be established (Palazzo and Lee, 2015). Future studies should aim to identify the exact molecular switches that induce ncRNA-dependent changes to spatial genome organization, and whether these regulatory mechanisms are conserved across evolution. Furthermore, we expect future studies to identify novel processes through which ncRNAs can regulate the relationship between genome structure and function.

AUTHOR CONTRIBUTIONS

NK and LO wrote the manuscript and prepared the figures. The manuscript was edited and updated by KM.

FUNDING

NK was supported by a scholarship from the Canadian Institutes of Health Research (CIHR). LO was supported by a scholarship from the Ontario Graduate Studies (OGS) Program. This work was supported by CIHR grants (#388041 and #399687) to KM, who holds the Canada Research Chair (CRC, #950-230661) in Spatial Genome Organization.

ACKNOWLEDGMENTS

We thank members of the Mekhail lab for fruitful discussions.

REFERENCES

Adriaens, C., Standaert, L., Barra, J., Latil, M., Verfaillie, A., Kalev, P., et al. (2016). p53 induces formation of NEAT1 lncRNA-containing paraspeckles that modulate replication stress response and chemosensitivity. *Nat. Med.* 22, 861–868. doi: 10.1038/nm.4135

Alt, F. W., Yancopoulos, G. D., Blackwell, T. K., Wood, C., Thomas, E., Boss, M., et al. (1984). Ordered rearrangement of immunoglobulin heavy chain variable region segments. *EMBO J.* 3, 1209–1219. doi: 10.1002/j.1460-2075.1984.tb01955.x

Andrey, G., Montavon, T., Mascrez, B., Gonzalez, F., Noordermeer, D., Leleu, M., et al. (2013). A switch between topological domains underlies HoxD genes collinearity in mouse limbs. *Science* 340:1234167. doi: 10.1126/science.1234167

Aravin, A. A., Sachidanandam, R., Bourc'his, D., Schaefer, C., Pezic, D., Toth, K. F., et al. (2008). A piRNA pathway primed by individual transposons is linked to de novo DNA methylation in mice. *Mol. Cell.* 31, 785–799. doi: 10.1016/j.molcel.2008.09.003

Ariel, F., Jegu, T., Latrasse, D., Romero-Barrios, N., Christ, A., Benhamed, M., et al. (2014). Noncoding transcription by alternative RNA polymerases dynamically regulates an auxin-driven chromatin loop. *Mol. Cell.* 55, 383–396. doi: 10.1016/j.molcel.2014.06.011

Armanios, M. (2012). Telomerase and idiopathic pulmonary fibrosis. *Mutat. Res.* 730, 52–58. doi: 10.1016/j.mrfmmm.2011.10.013

Armanios, M., Alder, J. K., Parry, E. M., Karim, B., Strong, M. A., and Greider, C. W. (2009). Short telomeres are sufficient to cause the degenerative defects associated with aging. *Am. J. Hum. Genet.* 85, 823–832. doi: 10.1016/j.ajhg.2009.10.028

Artandi, S. E., and DePinho, R. A. (2010). Telomeres and telomerase in cancer. *Carcinogenesis* 31, 9–18. doi: 10.1093/carcin/bgp268

Audas, T. E., Jacob, M. D., and Lee, S. (2012). Immobilization of proteins in the nucleolus by ribosomal intergenic spacer noncoding RNA. *Mol. Cell.* 45, 147–157. doi: 10.1016/j.molcel.2011.12.012

Beishline, K., Vladimirova, O., Tutton, S., Wang, Z., Deng, Z., and Lieberman, P. M. (2017). CTCF driven TERRA transcription facilitates completion of telomere DNA replication. *Nat. Commun.* 8:2114. doi: 10.1038/s41467-017-02212-w

Belancio, V. P., Deininger, P. L., and Roy-Engel, A. M. (2009). LINE dancing in the human genome: transposable elements and disease. *Genome Med.* 1:97. doi: 10.1186/gm97

Benetti, R., Gonzalo, S., Jaco, I., Schotta, G., Klatt, P., Jenuwein, T., et al. (2007). Suv4-20h deficiency results in telomere elongation and derepression of telomere recombination. *J. Cell Biol.* 178, 925–936. doi: 10.1083/jcb.200703081

Benjamins, R., Quint, A., Weijers, D., Hooykaas, P., and Offringa, R. (2001). The PINOID protein kinase regulates organ development in Arabidopsis by enhancing polar auxin transport. *Development* 128, 4057–4067.

Bergmann, J. H., Jakubsche, J. N., Martins, N. M., Kagansky, A., Nakano, M., Kimura, H., et al. (2012). Epigenetic engineering: histone H3K9 acetylation is compatible with kinetochore structure and function. *J. Cell Sci.* 125(Pt 2), 411–421. doi: 10.1242/jcs.090639

Bergmann, J. H., Rodriguez, M. G., Martins, N. M., Kimura, H., Kelly, D. A., Masumoto, H., et al. (2011). Epigenetic engineering shows H3K4me2 is required for HJURP targeting and CENP-A assembly on a synthetic human kinetochore. *EMBO J.* 30, 328–340. doi: 10.1038/emboj.2010.329

Bersani, F., Lee, E., Kharchenko, P. V., Xu, A. W., Liu, M., Xega, K., et al. (2015). Pericentromeric satellite repeat expansions through RNA-derived DNA intermediates in cancer. *Proc. Natl. Acad. Sci. U.S.A.* 112, 15148–15153. doi: 10.1073/pnas.1518008112

Bierhoff, H., Dammert, M. A., Brocks, D., Dambacher, S., Schotta, G., and Grummt, I. (2014). Quiescence-induced LncRNAs trigger H4K20 trimethylation and transcriptional silencing. *Mol. Cell.* 54, 675–682. doi: 10.1016/j.molcel.2014.03.032

Bierhoff, H., Schmitz, K., Maass, F., Ye, J., and Grummt, I. (2010). Noncoding transcripts in sense and antisense orientation regulate the epigenetic state of ribosomal RNA genes. *Cold. Spring Harb. Symp. Quant. Biol* 75, 357–364. doi: 10.1101/sqb.2010.75.060

Black, E. M., and Giunta, S. (2018). Repetitive fragile sites: centromere satellite DNA as a source of genome instability in human diseases. *Genes* 9:E615. doi: 10.3390/genes9120615

Blasco, M. A. (2007). The epigenetic regulation of mammalian telomeres. *Nat. Rev. Genet.* 8, 299–309. doi: 10.1038/nrg2047

Blower, M. D. (2016). Centromeric transcription regulates aurora-B localization and activation. *Cell Rep.* 15, 1624–1633. doi: 10.1016/j.celrep.2016.04.054

Bouzinba-Segard, H., Guais, A., and Francastel, C. (2006). Accumulation of small murine minor satellite transcripts leads to impaired centromeric architecture and function. *Proc. Natl. Acad. Sci. U.S.A.* 103, 8709–8714. doi: 10.1073/pnas.0508006103

Brown, C. J., Hendrich, B. D., Rupert, J. L., Lafreniere, R. G., Xing, Y., Lawrence, J., et al. (1992). The human XIST gene: analysis of a 17 kb inactive X-specific RNA that contains conserved repeats and is highly localized within the nucleus. *Cell* 71, 527–542. doi: 10.1016/0092-8674(92)90520-m

Brown, C. R., Kennedy, C. J., Delmar, V. A., Forbes, D. J., and Silver, P. A. (2008). Global histone acetylation induces functional genomic reorganization at mammalian nuclear pore complexes. *Genes Dev.* 22, 627–639. doi: 10.1101/gad.1632708

Burmann, F., Basfeld, A., Vazquez Nunez, R., Diebold-Durand, M. L., Wilhelm, L., and Gruber, S. (2017). Tuned SMC arms drive chromosomal loading of prokaryotic condensin. *Mol. Cell.* 65, 861.e–872.e. doi: 10.1016/j.molcel.2017.01.026

Burns, K. H. (2017). Transposable elements in cancer. *Nat. Rev. Cancer* 17, 415–424. doi: 10.1038/nrc.2017.35

Bywater, M. J., Pearson, R. B., McArthur, G. A., and Hannan, R. D. (2013). Dysregulation of the basal RNA polymerase transcription apparatus in cancer. *Nat. Rev. Cancer* 13, 299–314. doi: 10.1038/nrc3496

Callinan, P. A., and Batzer, M. A. (2006). Retrotransposable elements and human disease. *Genome Dyn.* 1, 104–115. doi: 10.1159/000092503

Cao, F., Li, X., Hiew, S., Brady, H., Liu, Y., and Dou, Y. (2009). Dicer independent small RNAs associate with telomeric heterochromatin. *RNA* 15, 1274–1281. doi: 10.1261/rna.1423309

Carmo-Fonseca, M., Ferreira, J., and Lamond, A. I. (1993). Assembly of snRNP-containing coiled bodies is regulated in interphase and mitosis–evidence that the coiled body is a kinetic nuclear structure. *J. Cell Biol.* 120, 841–852. doi: 10.1083/jcb.120.4.841

Casolari, J. M., Brown, C. R., Komili, S., West, J., Hieronymus, H., and Silver, P. A. (2004). Genome-wide localization of the nuclear transport machinery couples transcriptional status and nuclear organization. *Cell* 117, 427–439. doi: 10.1016/s0092-8674(04)00448-9

Caudron-Herger, M., Pankert, T., Seiler, J., Nemeth, A., Voit, R., Grummt, I., et al. (2015). Alu element-containing RNAs maintain nucleolar structure and function. *EMBO J.* 34, 2758–2774. doi: 10.15252/embj.201591458

Chakravarty, D., Sboner, A., Nair, S. S., Giannopoulou, E., Li, R., Hennig, S., et al. (2014). The oestrogen receptor alpha-regulated lncRNA NEAT1 is a critical modulator of prostate cancer. *Nat. Commun.* 5:5383. doi: 10.1038/ncomms6383

Chan, F. L., Marshall, O. J., Saffery, R., Kim, B. W., Earle, E., Choo, K. H., et al. (2012). Active transcription and essential role of RNA polymerase II at the centromere during mitosis. *Proc. Natl. Acad. Sci. U.S.A.* 109, 1979–1984. doi: 10.1073/pnas.1108705109

Chan, J. N., Poon, B. P., Salvi, J., Olsen, J. B., Emili, A., and Mekhail, K. (2011). Perinuclear cohibin complexes maintain replicative life span via roles at distinct silent chromatin domains. *Dev. Cell* 20, 867–879. doi: 10.1016/j.devcel.2011.05.014

Chang, F. T., McGhie, J. D., Chan, F. L., Tang, M. C., Anderson, M. A., Mann, J. R., et al. (2013). PML bodies provide an important platform for the maintenance of telomeric chromatin integrity in embryonic stem cells. *Nucleic Acids Res.* 41, 4447–4458. doi: 10.1093/nar/gkt114

Chaumeil, J., Le Baccon, P., Wutz, A., and Heard, E. (2006). A novel role for Xist RNA in the formation of a repressive nuclear compartment into which genes are recruited when silenced. *Genes Dev.* 20, 2223–2237. doi: 10.1101/gad.380906

Chen, C. K., Blanco, M., Jackson, C., Aznauryan, E., Ollikainen, N., Surka, C., et al. (2016). Xist recruits the X chromosome to the nuclear lamina to enable chromosome-wide silencing. *Science* 354, 468–472. doi: 10.1126/science.aae0047

Cho, E. J., and Kim, J. S. (2012). Crowding effects on the formation and maintenance of nuclear bodies: insights from molecular-dynamics simulations of simple spherical model particles. *Biophys. J.* 103, 424–433. doi: 10.1016/j.bpj.2012.07.007

Choudhry, H., Albukhari, A., Morotti, M., Haider, S., Moralli, D., Smythies, J., et al. (2015). Tumor hypoxia induces nuclear paraspeckle formation through HIF-2alpha dependent transcriptional activation of NEAT1 leading to cancer cell survival. *Oncogene* 34, 4482–4490. doi: 10.1038/onc.2014.378

Chung, D. K., Chan, J. N., Strecker, J., Zhang, W., Ebrahimi-Ardebili, S., Lu, T., et al. (2015). Perinuclear tethers license telomeric DSBs for a broad kinesin- and NPC-dependent DNA repair process. *Nat. Commun.* 6:7742. doi: 10.1038/ncomms8742

Clemson, C. M., Hutchinson, J. N., Sara, S. A., Ensminger, A. W., Fox, A. H., Chess, A., et al. (2009). An architectural role for a nuclear noncoding RNA: NEAT1 RNA is essential for the structure of paraspeckles. *Mol. Cell.* 33, 717–726. doi: 10.1016/j.molcel.2009.01.026

De Fazio, S., Bartonicek, N., Di Giacomo, M., Abreu-Goodger, C., Sankar, A., Funaya, C., et al. (2011). The endonuclease activity of Mili fuels piRNA amplification that silences LINE1 elements. *Nature* 480, 259–263. doi: 10.1038/nature10547

Degner, S. C., Wong, T. P., Jankevicius, G., and Feeney, A. J. (2009). Cutting edge: developmental stage-specific recruitment of cohesin to CTCF sites throughout immunoglobulin loci during B lymphocyte development. *J. Immunol.* 182, 44–48. doi: 10.4049/jimmunol.182.1.44

Deininger, P. L., and Batzer, M. A. (1999). Alu repeats and human disease. *Mol. Genet. Metab.* 67, 183–193. doi: 10.1006/mgme.1999.2864

Deng, Z., Norseen, J., Wiedmer, A., Riethman, H., and Lieberman, P. M. (2009). TERRA RNA binding to TRF2 facilitates heterochromatin formation and ORC recruitment at telomeres. *Mol. Cell.* 35, 403–413. doi: 10.1016/j.molcel.2009.06.025

Diaz, M. O., Barsacchi-Pilone, G., Mahon, K. A., and Gall, J. G. (1981). Transcripts from both strands of a satellite DNA occur on lampbrush chromosome loops of the newt *Notophthalmus*. *Cell* 24, 649–659. doi: 10.1016/0092-8674(81)90091-x

Diebold-Durand, M. L., Lee, H., Ruiz Avila, L. B., Noh, H., Shin, H. C., Im, H., et al. (2017). Structure of full-length SMC and rearrangements required for chromosome organization. *Mol. Cell* 67, 334.e5–347.e5. doi: 10.1016/j.molcel.2017.06.010

Dilworth, D. J., Tackett, A. J., Rogers, R. S., Yi, E. C., Christmas, R. H., Smith, J. J., et al. (2005). The mobile nucleoporin Nup2p and chromatin-bound Prp20p function in endogenous NPC-mediated transcriptional control. *J. Cell Biol.* 171, 955–965. doi: 10.1083/jcb.200509061

Di-Poi, N., Montoya-Burgos, J. I., Miller, H., Pourquie, O., Milinkovitch, M. C., and Duboule, D. (2010). Changes in Hox genes' structure and function during the evolution of the squamate body plan. *Nature* 464, 99–103. doi: 10.1038/nature08789

Dixon, J. R., Selvaraj, S., Yue, F., Kim, A., Li, Y., Shen, Y., et al. (2012). Topological domains in mammalian genomes identified by analysis of chromatin interactions. *Nature* 485, 376–380. doi: 10.1038/nature11082

Du, Y., Topp, C. N., and Dawe, R. K. (2010). DNA binding of centromere protein C (CENPC) is stabilized by single-stranded RNA. *PLoS Genet.* 6:e1000835. doi: 10.1371/journal.pgen.1000835

Fadloun, A., Le Gras, S., Jost, B., Ziegler-Birling, C., Takahashi, H., Gorab, E., et al. (2013). Chromatin signatures and retrotransposon profiling in mouse embryos reveal regulation of LINE-1 by RNA. *Nat. Struct. Mol. Biol.* 20, 332–338. doi: 10.1038/nsmb.2495

Feric, M., Vaidya, N., Harmon, T. S., Mitrea, D. M., Zhu, L., Richardson, T. M., et al. (2016). Coexisting liquid phases underlie nucleolar subcompartments. *Cell* 165, 1686–1697. doi: 10.1016/j.cell.2016.04.047

Ferri, F., Bouzinba-Segard, H., Velasco, G., Hube, F., and Francastel, C. (2009). Non-coding murine centromeric transcripts associate with and potentiate Aurora B kinase. *Nucleic Acids Res.* 37, 5071–5080. doi: 10.1093/nar/gkp529

Fitzpatrick, G. V., Soloway, P. D., and Higgins, M. J. (2002). Regional loss of imprinting and growth deficiency in mice with a targeted deletion of KvDMR1. *Nat. Genet.* 32, 426–431. doi: 10.1038/ng988

Flyamer, I. M., Gassler, J., Imakaev, M., Brandao, H. B., Ulianov, S. V., Abdennur, N., et al. (2017). Single-nucleus Hi-C reveals unique chromatin reorganization at oocyte-to-zygote transition. *Nature* 544, 110–114. doi: 10.1038/nature21711

Fuxa, M., Skok, J., Souabni, A., Salvagiotto, G., Roldan, E., and Busslinger, M. (2004). Pax5 induces V-to-DJ rearrangements and locus contraction of the immunoglobulin heavy-chain gene. *Genes Dev.* 18, 411–422. doi: 10.1101/gad.291504

Ganji, M., Shaltiel, I. A., Bisht, S., Kim, E., Kalichava, A., Haering, C. H., et al. (2018). Real-time imaging of DNA loop extrusion by condensin. *Science* 360, 102–105. doi: 10.1126/science.aar7831

Garcia-Cao, M., O'Sullivan, R., Peters, A. H., Jenuwein, T., and Blasco, M. A. (2004). Epigenetic regulation of telomere length in mammalian cells by the Suv39h1 and Suv39h2 histone methyltransferases. *Nat. Genet.* 36, 94–99. doi: 10.1038/ng1278

Giunta, S., and Funabiki, H. (2017). Integrity of the human centromere DNA repeats is protected by CENP-A, CENP-C, and CENP-T. *Proc. Natl. Acad. Sci. U.S.A.* 114, 1928–1933. doi: 10.1073/pnas.1615133114

Gotta, M., Laroche, T., Formenton, A., Maillet, L., Scherthan, H., and Gasser, S. M. (1996). The clustering of telomeres and colocalization with Rap1, Sir3, and Sir4 proteins in wild-type *Saccharomyces cerevisiae*. *J. Cell Biol.* 134, 1349–1363. doi: 10.1083/jcb.134.6.1349

Grenfell, A. W., Heald, R., and Strzelecka, M. (2016). Mitotic noncoding RNA processing promotes kinetochore and spindle assembly in *Xenopus*. *J. Cell Biol.* 214, 133–141. doi: 10.1083/jcb.201604029

Gu, B., Bessler, M., and Mason, P. J. (2009). Dyskerin, telomerase and the DNA damage response. *Cell Cycle* 8, 6–10. doi: 10.4161/cc.8.1.7265

Guelen, L., Pagie, L., Brasset, E., Meuleman, W., Faza, M. B., Talhout, W., et al. (2008). Domain organization of human chromosomes revealed by mapping of nuclear lamina interactions. *Nature* 453, 948–951. doi: 10.1038/nature06947

Guo, C., Jeong, H. H., Hsieh, Y. C., Klein, H. U., Bennett, D. A., De Jager, P. L., et al. (2018). Tau activates transposable elements in Alzheimer's Disease. *Cell Rep.* 23, 2874–2880. doi: 10.1016/j.celrep.2018.05.004

Hacisuleyman, E., Goff, L. A., Trapnell, C., Williams, A., Henao-Mejia, J., Sun, L., et al. (2014). Topological organization of multichromosomal regions by the long intergenic noncoding RNA Firre. *Nat. Struct. Mol. Biol.* 21, 198–206. doi: 10.1038/nsmb.2764

Hagelstrom, R. T., Blagoev, K. B., Niedernhofer, L. J., Goodwin, E. H., and Bailey, S. M. (2010). Hyper telomere recombination accelerates replicative senescence and may promote premature aging. *Proc. Natl. Acad. Sci. U.S.A.* 107, 15768–15773. doi: 10.1073/pnas.1006338107

Hall, A. C., Ostrowski, L. A., and Mekhail, K. (2019). Phase separation as a melting pot for DNA repeats. *Trends Genet.* 35, 589–600. doi: 10.1016/j.tig.2019.05.001

Hedouin, S., Grillo, G., Ivkovic, I., Velasco, G., and Francastel, C. (2017). CENP-A chromatin disassembly in stressed and senescent murine cells. *Sci. Rep.* 7:42520. doi: 10.1038/srep42520

Hernandez-Martin, A., Gonzalez-Sarmiento, R., and De Unamuno, P. (1999). X-linked ichthyosis: an update. *Br. J. Dermatol.* 141, 617–627. doi: 10.1046/j.1365-2133.1999.03098.x

Hirose, T., Virnicchi, G., Tanigawa, A., Naganuma, T., Li, R., Kimura, H., et al. (2014). NEAT1 long noncoding RNA regulates transcription via protein sequestration within subnuclear bodies. *Mol. Biol. Cell* 25, 169–183. doi: 10.1091/mbc.E13-09-0558

Hsieh, T. H., Weiner, A., Lajoie, B., Dekker, J., Friedman, N., and Rando, O. J. (2015). Mapping nucleosome resolution chromosome folding in yeast by micro-C. *Cell* 162, 108–119. doi: 10.1016/j.cell.2015.05.048

Hu, S., Lv, P., Yan, Z., and Wen, B. (2019). Disruption of nuclear speckles reduces chromatin interactions in active compartments. *Epigenetics Chromatin* 12:43. doi: 10.1186/s13072-019-0289-2

Hult, C., Adalsteinsson, D., Vasquez, P. A., Lawrimore, J., Bennett, M., York, A., et al. (2017). Enrichment of dynamic chromosomal crosslinks drive phase separation of the nucleolus. *Nucleic Acids Res.* 45, 11159–11173. doi: 10.1093/nar/gkx741

Ideue, T., Cho, Y., Nishimura, K., and Tani, T. (2014). Involvement of satellite I noncoding RNA in regulation of chromosome segregation. *Genes Cells* 19, 528–538. doi: 10.1111/gtc.12149

Ikegami, K., Egelhofer, T. A., Strome, S., and Lieb, J. D. (2010). Caenorhabditis elegans chromosome arms are anchored to the nuclear membrane via discontinuous association with LEM-2. *Genome Biol.* 11:R120. doi: 10.1186/gb-2010-11-12-r120

Imamura, K., Imamachi, N., Akizuki, G., Kumakura, M., Kawaguchi, A., Nagata, K., et al. (2014). Long noncoding RNA NEAT1-dependent SFPQ relocation from promoter region to paraspeckle mediates IL8 expression upon immune stimuli. *Mol. Cell.* 53, 393–406. doi: 10.1016/j.molcel.2014.01.009

Isoda, T., Moore, A. J., He, Z., Chandra, V., Aida, M., Denholtz, M., et al. (2017). Non-coding transcription instructs chromatin folding and compartmentalization to dictate enhancer-promoter communication and t cell fate. *Cell* 171, 103.e18–119.e18. doi: 10.1016/j.cell.2017.09.001

Jacob, M. D., Audas, T. E., Uniacke, J., Trinkle-Mulcahy, L., and Lee, S. (2013). Environmental cues induce a long noncoding RNA-dependent remodeling of the nucleolus. *Mol. Biol. Cell* 24, 2943–2953. doi: 10.1091/mbc.E13-04-0223

Jin, Q. W., Fuchs, J., and Loidl, J. (2000). Centromere clustering is a major determinant of yeast interphase nuclear organization. *J. Cell Sci.* 113(Pt 11), 1903–1912.

Kaiser, T. E., Intine, R. V., and Dundr, M. (2008). De novo formation of a subnuclear body. *Science* 322, 1713–1717. doi: 10.1126/science.1165216

Khalil, A. M., Guttman, M., Huarte, M., Garber, M., Raj, A., Rivea Morales, D., et al. (2009). Many human large intergenic noncoding RNAs associate with chromatin-modifying complexes and affect gene expression. *Proc. Natl. Acad. Sci. U.S.A.* 106, 11667–11672. doi: 10.1073/pnas.0904715106

Kim, T. K., Hemberg, M., Gray, J. M., Costa, A. M., Bear, D. M., Wu, J., et al. (2010). Widespread transcription at neuronal activity-regulated enhancers. *Nature* 465, 182–187. doi: 10.1038/nature09033

Kim, T. M., Xi, R., Luquette, L. J., Park, R. W., Johnson, M. D., and Park, P. J. (2013). Functional genomic analysis of chromosomal aberrations in a compendium of 8000 cancer genomes. *Genome Res.* 23, 217–227. doi: 10.1101/gr.140301.112

Kind, J., Pagie, L., de Vries, S. S., Nahidiazar, L., Dey, S. S., Bienko, M., et al. (2015). Genome-wide maps of nuclear lamina interactions in single human cells. *Cell* 163, 134–147. doi: 10.1016/j.cell.2015.08.040

Kosak, S. T., Skok, J. A., Medina, K. L., Riblet, R., Le Beau, M. M., Fisher, A. G., et al. (2002). Subnuclear compartmentalization of immunoglobulin loci during lymphocyte development. *Science* 296, 158–162. doi: 10.1126/science.1068768

Krefting, J., Andrade-Navarro, M. A., and Ibn-Salem, J. (2018). Evolutionary stability of topologically associating domains is associated with conserved gene regulation. *BMC Biol.* 16:87. doi: 10.1186/s12915-018-0556-x

Lai, F., Orom, U. A., Cesaroni, M., Beringer, M., Taatjes, D. J., Blobel, G. A., et al. (2013). Activating RNAs associate with Mediator to enhance chromatin architecture and transcription. *Nature* 494, 497–501. doi: 10.1038/nature11884

Lee, J. T., and Lu, N. (1999). Targeted mutagenesis of Tsix leads to nonrandom X inactivation. *Cell* 99, 47–57. doi: 10.1016/s0092-8674(00)80061-6

Lee, M. P., DeBaun, M. R., Mitsuya, K., Galonek, H. L., Brandenburg, S., Oshimura, M., et al. (1999). Loss of imprinting of a paternally expressed transcript, with antisense orientation to KVLQT1, occurs frequently in Beckwith-Wiedemann syndrome and is independent of insulin-like growth factor II imprinting. *Proc. Natl. Acad. Sci. U.S.A.* 96, 5203–5208. doi: 10.1073/pnas.96.9.5203

Lee, S. H., Itkin-Ansari, P., and Levine, F. (2010). CENP-A, a protein required for chromosome segregation in mitosis, declines with age in islet but not exocrine cells. *Aging* 2, 785–790. doi: 10.18632/aging.100220

Lewis, A., Green, K., Dawson, C., Redrup, L., Huynh, K. D., Lee, J. T., et al. (2006). Epigenetic dynamics of the Kcnq1 imprinted domain in the early embryo. *Development* 133, 4203–4210. doi: 10.1242/dev.02612

Li, L., Leid, M., and Rothenberg, E. V. (2010). An early T cell lineage commitment checkpoint dependent on the transcription factor Bcl11b. *Science* 329, 89–93. doi: 10.1126/science.1188989

Li, L., Zhang, J. A., Dose, M., Kueh, H. Y., Mosadeghi, R., Gounari, F., et al. (2013). A far downstream enhancer for murine Bcl11b controls its T-cell specific expression. *Blood* 122, 902–911. doi: 10.1182/blood-2012-08-447839

Li, W., Notani, D., Ma, Q., Tanasa, B., Nunez, E., Chen, A. Y., et al. (2013). Functional roles of enhancer RNAs for oestrogen-dependent transcriptional activation. *Nature* 498, 516–520. doi: 10.1038/nature12210

Li, Y. X., and Kirby, M. L. (2003). Coordinated and conserved expression of alphoid repeat and alphoid repeat-tagged coding sequences. *Dev. Dyn.* 228, 72–81. doi: 10.1002/dvdy.10355

Lieberman-Aiden, E., van Berkum, N. L., Williams, L., Imakaev, M., Ragoczy, T., Telling, A., et al. (2009). Comprehensive mapping of long-range interactions reveals folding principles of the human genome. *Science* 326, 289–293. doi: 10.1126/science.1181369

Ling, Y. H., and Yuen, K. W. Y. (2019). Point centromere activity requires an optimal level of centromeric noncoding RNA. *Proc. Natl. Acad. Sci. U.S.A.* 116, 6270–6279. doi: 10.1073/pnas.1821384116

Luikenhuis, S., Wutz, A., and Jaenisch, R. (2001). Antisense transcription through the Xist locus mediates Tsix function in embryonic stem cells. *Mol. Cell. Biol.* 21, 8512–8520. doi: 10.1128/MCB.21.24.8512-8520.2001

Ma, H., Han, P., Ye, W., Chen, H., Zheng, X., Cheng, L., et al. (2017). The long noncoding RNA NEAT1 exerts antihantaviral effects by acting as positive feedback for RIG-I signaling. *J. Virol.* 91:e2250-16. doi: 10.1128/JVI.02250-16

Machyna, M., Kehr, S., Straube, K., Kappei, D., Buchholz, F., Butter, F., et al. (2014). The coilin interactome identifies hundreds of small noncoding RNAs that traffic through Cajal bodies. *Mol. Cell.* 56, 389–399. doi: 10.1016/j.molcel.2014.10.004

Maehara, K., Takahashi, K., and Saitoh, S. (2010). CENP-A reduction induces a p53-dependent cellular senescence response to protect cells from executing defective mitoses. *Mol. Cell. Biol.* 30, 2090–2104. doi: 10.1128/MCB.01318-09

Maicher, A., Kastner, L., and Luke, B. (2012). Telomeres and disease: enter TERRA. *RNA Biol.* 9, 843–849. doi: 10.4161/rna.20330

Maison, C., Bailly, D., Peters, A. H., Quivy, J. P., Roche, D., Taddei, A., et al. (2002). Higher-order structure in pericentric heterochromatin involves a distinct pattern of histone modification and an RNA component. *Nat. Genet.* 30, 329–334. doi: 10.1038/ng843

Maison, C., Bailly, D., Roche, D., Montes de Oca, R., Probst, A. V., Vassias, I., et al. (2011). SUMOylation promotes de novo targeting of HP1alpha to pericentric heterochromatin. *Nat. Genet.* 43, 220–227. doi: 10.1038/ng.765

Mancini-Dinardo, D., Steele, S. J., Levorse, J. M., Ingram, R. S., and Tilghman, S. M. (2006). Elongation of the Kcnq1ot1 transcript is required for genomic imprinting of neighboring genes. *Genes Dev.* 20, 1268–1282. doi: 10.1101/gad.1416906

Mao, Y. S., Zhang, B., and Spector, D. L. (2011). Biogenesis and function of nuclear bodies. *Trends Genet.* 27, 295–306. doi: 10.1016/j.tig.2011.05.006

Martens, J. H., O'Sullivan, R. J., Braunschweig, U., Opravil, S., Radolf, M., Steinlein, P., et al. (2005). The profile of repeat-associated histone lysine methylation states in the mouse epigenome. *EMBO J.* 24, 800–812. doi: 10.1038/sj.emboj.7600545

Mason, P. J., and Bessler, M. (2011). The genetics of dyskeratosis congenita. *Cancer Genet.* 204, 635–645. doi: 10.1016/j.cancergen.2011.11.002

Mayer, C., Schmitz, K. M., Li, J., Grummt, I., and Santoro, R. (2006). Intergenic transcripts regulate the epigenetic state of rRNA genes. *Mol. Cell.* 22, 351–361. doi: 10.1016/j.molcel.2006.03.028

McNulty, S. M., Sullivan, L. L., and Sullivan, B. A. (2017). Human centromeres produce chromosome-specific and array-specific alpha satellite transcripts that are complexed with CENP-A and CENP-C. *Dev. Cell* 42, 226.e6–240.e6. doi: 10.1016/j.devcel.2017.07.001

Medvedovic, J., Ebert, A., Tagoh, H., Tamir, I. M., Schwickert, T. A., Novatchkova, M., et al. (2013). Flexible long-range loops in the VH gene region of the Igh locus facilitate the generation of a diverse antibody repertoire. *Immunity* 39, 229–244. doi: 10.1016/j.immuni.2013.08.011

Mekhail, K., Khacho, M., Carrigan, A., Hache, R. R., Gunaratnam, L., and Lee, S. (2005). Regulation of ubiquitin ligase dynamics by the nucleolus. *J. Cell Biol.* 170, 733–744. doi: 10.1083/jcb.200506030

Mekhail, K., and Moazed, D. (2010). The nuclear envelope in genome organization, expression and stability. *Nat. Rev. Mol. Cell Biol.* 11, 317–328. doi: 10.1038/nrm2894

Mekhail, K., Seebacher, J., Gygi, S. P., and Moazed, D. (2008). Role for perinuclear chromosome tethering in maintenance of genome stability. *Nature* 456, 667–670. doi: 10.1038/nature07460

Minajigi, A., Froberg, J., Wei, C., Sunwoo, H., Kesner, B., Colognori, D., et al. (2015). Chromosomes. A comprehensive Xist interactome reveals cohesin repulsion and an RNA-directed chromosome conformation. *Science* 349:aab2276. doi: 10.1126/science.aab2276

Miniou, P., Jeanpierre, M., Blanquet, V., Sibella, V., Bonneau, D., Herbelin, C., et al. (1994). Abnormal methylation pattern in constitutive and facultative (X inactive chromosome) heterochromatin of ICF patients. *Hum. Mol. Genet.* 3, 2093–2102. doi: 10.1093/hmg/3.12.2093

Misiak, B., Ricceri, L., and Sasiadek, M. M. (2019). Transposable elements and their epigenetic regulation in mental disorders: current evidence in the field. *Front. Genet.* 10:580. doi: 10.3389/fgene.2019.00580

Mohammad, F., Pandey, R. R., Nagano, T., Chakalova, L., Mondal, T., Fraser, P., et al. (2008). Kcnq1ot1/Lit1 noncoding RNA mediates transcriptional silencing by targeting to the perinucleolar region. *Mol. Cell. Biol.* 28, 3713–3728. doi: 10.1128/MCB.02263-07

Montanaro, L., Trere, D., and Derenzini, M. (2008). Nucleolus, ribosomes, and cancer. *Am. J. Pathol.* 173, 301–310. doi: 10.2353/ajpath.2008.070752

Mortazavi, A., Williams, B. A., McCue, K., Schaeffer, L., and Wold, B. (2008). Mapping and quantifying mammalian transcriptomes by RNA-Seq. *Nat. Methods* 5, 621–628. doi: 10.1038/nmeth.1226

Nakhoul, H., Ke, J., Zhou, X., Liao, W., Zeng, S. X., and Lu, H. (2014). Ribosomopathies: mechanisms of disease. *Clin. Med. Insights Blood Disord.* 7, 7–16. doi: 10.4137/CMBD.S16952

Narla, A., and Ebert, B. L. (2010). Ribosomopathies: human disorders of ribosome dysfunction. *Blood* 115, 3196–3205. doi: 10.1182/blood-2009-10-178129

Nemeth, A., Conesa, A., Santoyo-Lopez, J., Medina, I., Montaner, D., Peterfia, B., et al. (2010). Initial genomics of the human nucleolus. *PLoS Genet.* 6:e1000889. doi: 10.1371/journal.pgen.1000889

Nergadze, S. G., Farnung, B. O., Wischnewski, H., Khoriauli, L., Vitelli, V., Chawla, R., et al. (2009). CpG-island promoters drive transcription of human telomeres. *RNA* 15, 2186–2194. doi: 10.1261/rna.1748309

Noordermeer, D., Leleu, M., Splinter, E., Rougemont, J., De Laat, W., and Duboule, D. (2011). The dynamic architecture of Hox gene clusters. *Science* 334, 222–225. doi: 10.1126/science.1207194

Nora, E. P., Lajoie, B. R., Schulz, E. G., Giorgetti, L., Okamoto, I., Servant, N., et al. (2012). Spatial partitioning of the regulatory landscape of the X-inactivation centre. *Nature* 485, 381–385. doi: 10.1038/nature11049

Nuebler, J., Fudenberg, G., Imakaev, M., Abdennur, N., and Mirny, L. A. (2018). Chromatin organization by an interplay of loop extrusion and compartmental segregation. *Proc. Natl. Acad. Sci. U.S.A.* 115, E6697–E6706. doi: 10.1073/pnas.1717730115

Okamoto, I., Otte, A. P., Allis, C. D., Reinberg, D., and Heard, E. (2004). Epigenetic dynamics of imprinted X inactivation during early mouse development. *Science* 303, 644–649. doi: 10.1126/science.1092727

Orom, U. A., Derrien, T., Beringer, M., Gumireddy, K., Gardini, A., Bussotti, G., et al. (2010). Long noncoding RNAs with enhancer-like function in human cells. *Cell* 143, 46–58. doi: 10.1016/j.cell.2010.09.001

Oshidari, R., Huang, R., Medghalchi, M., Elizabeth, Y. W., Ashgriz, N., Lee, H. O., et al. (2019). DNA repair by Rad52 liquid droplets. *bioRxiv* [Preprint]. doi: 10.1101/768119

Oshidari, R., Strecker, J., Chung, D. K. C., Abraham, K. J., Chan, J. N. Y., Damaren, C. J., et al. (2018). Nuclear microtubule filaments mediate non-linear directional motion of chromatin and promote DNA repair. *Nat. Commun.* 9:2567. doi: 10.1038/s41467-018-05009-7

Ostrowski, L. A., Hall, A. C., Szafranski, K. J., Oshidari, R., Abraham, K. J., Chan, J. N. Y., et al. (2018). Conserved Pbp1/Ataxin-2 regulates retrotransposon activity and connects polyglutamine expansion-driven protein aggregation to

lifespan-controlling rDNA repeats. *Commun. Biol.* 1:187. doi: 10.1038/s42003-018-0187-3

O'Sullivan, J. M., Sontam, D. M., Grierson, R., and Jones, B. (2009). Repeated elements coordinate the spatial organization of the yeast genome. *Yeast* 26, 125–138. doi: 10.1002/yea.1657

O'Sullivan, R. J., and Karlseder, J. (2010). Telomeres: protecting chromosomes against genome instability. *Nat. Rev. Mol. Cell Biol.* 11, 171–181. doi: 10.1038/nrm2848

Palazzo, A. F., and Lee, E. S. (2015). Non-coding RNA: what is functional and what is junk? *Front. Genet.* 6:2. doi: 10.3389/fgene.2015.00002

Pandey, R. R., Mondal, T., Mohammad, F., Enroth, S., Redrup, L., Komorowski, J., et al. (2008). Kcnq1ot1 antisense noncoding RNA mediates lineage-specific transcriptional silencing through chromatin-level regulation. *Mol. Cell.* 32, 232–246. doi: 10.1016/j.molcel.2008.08.022

Pickersgill, H., Kalverda, B., de Wit, E., Talhout, W., Fornerod, M., and van Steensel, B. (2006). Characterization of the *Drosophila melanogaster* genome at the nuclear lamina. *Nat. Genet.* 38, 1005–1014. doi: 10.1038/ng1852

Pietrzak, M., Rempala, G., Nelson, P. T., Zheng, J. J., and Hetman, M. (2011). Epigenetic silencing of nucleolar rRNA genes in Alzheimer's disease. *PLoS One* 6:e22585. doi: 10.1371/journal.pone.0022585

Plath, K., Fang, J., Mlynarczyk-Evans, S. K., Cao, R., Worringer, K. A., Wang, H., et al. (2003). Role of histone H3 lysine 27 methylation in X inactivation. *Science* 300, 131–135. doi: 10.1126/science.1084274

Postepska-Igielska, A., Krunic, D., Schmitt, N., Greulich-Bode, K. M., Boukamp, P., and Grummt, I. (2013). The chromatin remodelling complex NoRC safeguards genome stability by heterochromatin formation at telomeres and centromeres. *EMBO Rep.* 14, 704–710. doi: 10.1038/embor.2013.87

Radion, E., Morgunova, V., Ryazansky, S., Akulenko, N., Lavrov, S., Abramov, Y., et al. (2018). Key role of piRNAs in telomeric chromatin maintenance and telomere nuclear positioning in *Drosophila germline*. *Epigenetics Chromatin* 11:40. doi: 10.1186/s13072-018-0210-4

Rao, S. S., Huntley, M. H., Durand, N. C., Stamenova, E. K., Bochkov, I. D., Robinson, J. T., et al. (2014). A 3D map of the human genome at kilobase resolution reveals principles of chromatin looping. *Cell* 159, 1665–1680. doi: 10.1016/j.cell.2014.11.021

Renault, N. K., Dyack, S., Dobson, M. J., Costa, T., Lam, W. L., and Greer, W. L. (2007). Heritable skewed X-chromosome inactivation leads to haemophilia A expression in heterozygous females. *Eur. J. Hum. Genet.* 15, 628–637. doi: 10.1038/sj.ejhg.5201799

Rice, J. C., and Allis, C. D. (2001). Histone methylation versus histone acetylation: new insights into epigenetic regulation. *Curr. Opin. Cell Biol.* 13, 263–273. doi: 10.1016/s0955-0674(00)00208-8

Richards, E. J., and Elgin, S. C. (2002). Epigenetic codes for heterochromatin formation and silencing: rounding up the usual suspects. *Cell* 108, 489–500. doi: 10.1016/s0092-8674(02)00644-x

Richter, K., Nessling, M., and Lichter, P. (2007). Experimental evidence for the influence of molecular crowding on nuclear architecture. *J. Cell Sci.* 120(Pt 9), 1673–1680. doi: 10.1242/jcs.03440

Rosic, S., Kohler, F., and Erhardt, S. (2014). Repetitive centromeric satellite RNA is essential for kinetochore formation and cell division. *J. Cell Biol.* 207, 335–349. doi: 10.1083/jcb.201404097

Rudert, F., Bronner, S., Garnier, J. M., and Dolle, P. (1995). Transcripts from opposite strands of gamma satellite DNA are differentially expressed during mouse development. *Mamm. Genome* 6, 76–83. doi: 10.1007/bf00303248

Sagie, S., Toubiana, S., Hartono, S. R., Katzir, H., Tzur-Gilat, A., Havazelet, S., et al. (2017). Telomeres in ICF syndrome cells are vulnerable to DNA damage due to elevated DNA:RNA hybrids. *Nat. Commun.* 8:14015. doi: 10.1038/ncomms14015

Saka, K., Ide, S., Ganley, A. R., and Kobayashi, T. (2013). Cellular senescence in yeast is regulated by rDNA noncoding transcription. *Curr. Biol.* 23, 1794–1798. doi: 10.1016/j.cub.2013.07.048

Salvi, J. S., Chan, J. N., Szafranski, K., Liu, T. T., Wu, J. D., Olsen, J. B., et al. (2014). Roles for Pbp1 and caloric restriction in genome and lifespan maintenance via suppression of RNA-DNA hybrids. *Dev. Cell* 30, 177–191. doi: 10.1016/j.devcel.2014.05.013

Sanborn, A. L., Rao, S. S., Huang, S. C., Durand, N. C., Huntley, M. H., Jewett, A. I., et al. (2015). Chromatin extrusion explains key features of loop and domain formation in wild-type and engineered genomes. *Proc. Natl. Acad. Sci. U.S.A.* 112, E6456–E6465. doi: 10.1073/pnas.1518552112

Santoro, R., Li, J., and Grummt, I. (2002). The nucleolar remodeling complex NoRC mediates heterochromatin formation and silencing of ribosomal gene transcription. *Nat. Genet.* 32, 393–396. doi: 10.1038/ng1010

Savic, N., Bar, D., Leone, S., Frommel, S. C., Weber, F. A., Vollenweider, E., et al. (2014). lncRNA maturation to initiate heterochromatin formation in the nucleolus is required for exit from pluripotency in ESCs. *Cell Stem Cell* 15, 720–734. doi: 10.1016/j.stem.2014.10.005

Sawyer, I. A., Sturgill, D., Sung, M. H., Hager, G. L., and Dundr, M. (2016). Cajal body function in genome organization and transcriptome diversity. *Bioessays* 38, 1197–1208. doi: 10.1002/bies.201600144

Sayegh, C. E., Jhunjhunwala, S., Riblet, R., and Murre, C. (2005). Visualization of looping involving the immunoglobulin heavy-chain locus in developing B cells. *Genes Dev.* 19, 322–327. doi: 10.1101/gad.1254305

Schmid, M., Arib, G., Laemmli, C., Nishikawa, J., Durussel, T., and Laemmli, U. K. (2006). Nup-PI: the nucleopore-promoter interaction of genes in yeast. *Mol. Cell.* 21, 379–391. doi: 10.1016/j.molcel.2005.12.012

Schober, H., Ferreira, H., Kalck, V., Gehlen, L. R., and Gasser, S. M. (2009). Yeast telomerase and the SUN domain protein Mps3 anchor telomeres and repress subtelomeric recombination. *Genes Dev.* 23, 928–938. doi: 10.1101/gad.1787509

Schoeftner, S., Sengupta, A. K., Kubicek, S., Mechtler, K., Spahn, L., Koseki, H., et al. (2006). Recruitment of PRC1 function at the initiation of X inactivation independent of PRC2 and silencing. *EMBO J.* 25, 3110–3122. doi: 10.1038/sj.emboj.7601187

Schwarzer, W., Abdennur, N., Goloborodko, A., Pekowska, A., Fudenberg, G., Loe-Mie, Y., et al. (2017). Two independent modes of chromatin organization revealed by cohesin removal. *Nature* 551, 51–56. doi: 10.1038/nature24281

Sexton, T., Yaffe, E., Kenigsberg, E., Bantignies, F., Leblanc, B., Hoichman, M., et al. (2012). Three-dimensional folding and functional organization principles of the *Drosophila genome*. *Cell* 148, 458–472. doi: 10.1016/j.cell.2012.01.010

Shevtsov, S. P., and Dundr, M. (2011). Nucleation of nuclear bodies by RNA. *Nat. Cell Biol.* 13, 167–173. doi: 10.1038/ncb2157

Shibata, S., and Lee, J. T. (2004). Tsix transcription- versus RNA-based mechanisms in Xist repression and epigenetic choice. *Curr. Biol.* 14, 1747–1754. doi: 10.1016/j.cub.2004.09.053

Shin, J. Y., Fitzpatrick, G. V., and Higgins, M. J. (2008). Two distinct mechanisms of silencing by the KvDMR1 imprinting control region. *EMBO J.* 27, 168–178. doi: 10.1038/sj.emboj.7601960

Sleeman, J. E., and Trinkle-Mulcahy, L. (2014). Nuclear bodies: new insights into assembly/dynamics and disease relevance. *Curr. Opin. Cell Biol.* 28, 76–83. doi: 10.1016/j.ceb.2014.03.004

Slotkin, R. K., and Martienssen, R. (2007). Transposable elements and the epigenetic regulation of the genome. *Nat. Rev. Genet.* 8, 272–285. doi: 10.1038/nrg2072

Stavropoulos, N., Lu, N., and Lee, J. T. (2001). A functional role for Tsix transcription in blocking Xist RNA accumulation but not in X-chromosome choice. *Proc. Natl. Acad. Sci. U.S.A.* 98, 10232–10237. doi: 10.1073/pnas.171243598

Strecker, J., Gupta, G. D., Zhang, W., Bashkurov, M., Landry, M. C., Pelletier, L., et al. (2016). DNA damage signalling targets the kinetochore to promote chromatin mobility. *Nat. Cell Biol.* 18, 281–290. doi: 10.1038/ncb3308

Strzelecka, M., Oates, A. C., and Neugebauer, K. M. (2010). Dynamic control of Cajal body number during zebrafish embryogenesis. *Nucleus* 1, 96–108. doi: 10.4161/nucl.1.1.10680

Sunwoo, H., Dinger, M. E., Wilusz, J. E., Amaral, P. P., Mattick, J. S., and Spector, D. L. (2009). MEN epsilon/beta nuclear-retained non-coding RNAs are up-regulated upon muscle differentiation and are essential components of paraspeckles. *Genome Res.* 19, 347–359. doi: 10.1101/gr.087775.108

Swanson, E. C., Manning, B., Zhang, H., and Lawrence, J. B. (2013). Higher-order unfolding of satellite heterochromatin is a consistent and early event in cell senescence. *J. Cell Biol.* 203, 929–942. doi: 10.1083/jcb.201306073

Taddei, A., Van Houwe, G., Hediger, F., Kalck, V., Cubizolles, F., Schober, H., et al. (2006). Nuclear pore association confers optimal expression levels for an inducible yeast gene. *Nature* 441, 774–778. doi: 10.1038/nature04845

Tam, O. H., Ostrow, L. W., and Gale Hammell, M. (2019). Diseases of the nERVous system: retrotransposon activity in neurodegenerative disease. *Mob DNA* 10:32. doi: 10.1186/s13100-019-0176-1

Terranova, R., Yokobayashi, S., Stadler, M. B., Otte, A. P., van Lohuizen, M., Orkin, S. H., et al. (2008). Polycomb group proteins Ezh2 and Rnf2 direct genomic

contraction and imprinted repression in early mouse embryos. *Dev. Cell* 15, 668–679. doi: 10.1016/j.devcel.2008.08.015

Therizols, P., Fairhead, C., Cabal, G. G., Genovesio, A., Olivo-Marin, J. C., Dujon, B., et al. (2006). Telomere tethering at the nuclear periphery is essential for efficient DNA double strand break repair in subtelomeric region. *J. Cell Biol.* 172, 189–199. doi: 10.1083/jcb.200505159

Ting, D. T., Lipson, D., Paul, S., Brannigan, B. W., Akhavanfard, S., Coffman, E. J., et al. (2011). Aberrant overexpression of satellite repeats in pancreatic and other epithelial cancers. *Science* 331, 593–596. doi: 10.1126/science.1200801

Trapitz, P., Wlaschek, M., and Bunemann, H. (1988). Structure and function of Y chromosomal DNA. II. Analysis of lampbrush loop associated transcripts in nuclei of primary spermatocytes of *Drosophila* hydei by in situ hybridization using asymmetric RNA probes of four different families of repetitive DNA. *Chromosoma* 96, 159–170. doi: 10.1007/bf00331048

Ulianov, S. V., Doronin, S. A., Khrameeva, E. E., Kos, P. I., Luzhin, A. V., Starikov, S. S., et al. (2019). Nuclear lamina integrity is required for proper spatial organization of chromatin in *Drosophila*. *Nat. Commun.* 10, 1176. doi: 10.1038/s41467-019-09185-y

Umlauf, D., Goto, Y., Cao, R., Cerqueira, F., Wagschal, A., Zhang, Y., et al. (2004). Imprinting along the Kcnq1 domain on mouse chromosome 7 involves repressive histone methylation and recruitment of Polycomb group complexes. *Nat. Genet.* 36, 1296–1300. doi: 10.1038/ng1467

Valente, F. M., Sparago, A., Freschi, A., Hill-Harfe, K., Maas, S. M., Frints, S. G. M., et al. (2019). Transcription alterations of KCNQ1 associated with imprinted methylation defects in the Beckwith-Wiedemann locus. *Genet. Med.* 21, 1808–1820. doi: 10.1038/s41436-018-0416-7

van Bemmel, J. G., Pagie, L., Braunschweig, U., Brugman, W., Meuleman, W., Kerkhoven, R. M., et al. (2010). The insulator protein SU(HW) fine-tunes nuclear lamina interactions of the *Drosophila genome*. *PLoS One* 5:e15013. doi: 10.1371/journal.pone.0015013

Velazquez Camacho, O., Galan, C., Swist-Rosowska, K., Ching, R., Gamalinda, M., Karabiber, F., et al. (2017). Major satellite repeat RNA stabilize heterochromatin retention of Suv39h enzymes by RNA-nucleosome association and RNA:DNA hybrid formation. *eLife* 6:e25293. doi: 10.7554/eLife.25293

Verma-Gaur, J., Torkamani, A., Schaffer, L., Head, S. R., Schork, N. J., and Feeney, A. J. (2012). Noncoding transcription within the Igh distal V(H) region at PAIR elements affects the 3D structure of the Igh locus in pro-B cells. *Proc. Natl. Acad. Sci. U.S.A.* 109, 17004–17009. doi: 10.1073/pnas.1208398109

Verona, R. I., Mann, M. R., and Bartolomei, M. S. (2003). Genomic imprinting: intricacies of epigenetic regulation in clusters. *Annu. Rev. Cell Dev. Biol.* 19, 237–259. doi: 10.1146/annurev.cellbio.19.111401.092717

Vian, L., Pekowska, A., Rao, S. S. P., Kieffer-Kwon, K. R., Jung, S., Baranello, L., et al. (2018). The energetics and physiological impact of cohesin extrusion. *Cell* 173, 1165.e20–1178.e20. doi: 10.1016/j.cell.2018.03.072

Volpe, T. A., Kidner, C., Hall, I. M., Teng, G., Grewal, S. I., and Martienssen, R. A. (2002). Regulation of heterochromatic silencing and histone H3 lysine-9 methylation by RNAi. *Science* 297, 1833–1837. doi: 10.1126/science.1074973

Wanat, J. J., Logsdon, G. A., Driskill, J. H., Deng, Z., Lieberman, P. M., and Johnson, F. B. (2018). TERRA and the histone methyltransferase Dot1 cooperate to regulate senescence in budding yeast. *PLoS One* 13:e0195698. doi: 10.1371/journal.pone.0195698

Wang, F., Tang, Z., Shao, H., Guo, J., Tan, T., Dong, Y., et al. (2018). Long noncoding RNA HOTTIP cooperates with CCCTC-binding factor to coordinate HOXA gene expression. *Biochem. Biophys. Res. Commun.* 500, 852–859. doi: 10.1016/j.bbrc.2018.04.173

Wang, H., Xu, X., Nguyen, C. M., Liu, Y., Gao, Y., Lin, X., et al. (2018). CRISPR-mediated programmable 3D genome positioning and nuclear organization. *Cell* 175, 1405.e14–1417.e14. doi: 10.1016/j.cell.2018.09.013

Wang, K. C., Yang, Y. W., Liu, B., Sanyal, A., Corces-Zimmerman, R., Chen, Y., et al. (2011). A long noncoding RNA maintains active chromatin to coordinate homeotic gene expression. *Nature* 472, 120–124. doi: 10.1038/nature09819

Wang, Q., Sawyer, I. A., Sung, M. H., Sturgill, D., Shevtsov, S. P., Pegoraro, G., et al. (2016). Cajal bodies are linked to genome conformation. *Nat. Commun.* 7:10966. doi: 10.1038/ncomms10966

Wen, B., Wu, H., Shinkai, Y., Irizarry, R. A., and Feinberg, A. P. (2009). Large histone H3 lysine 9 dimethylated chromatin blocks distinguish differentiated from embryonic stem cells. *Nat. Genet.* 41, 246–250. doi: 10.1038/ng.297

White, R. J. (2005). RNA polymerases I and III, growth control and cancer. *Nat. Rev. Mol. Cell Biol.* 6, 69–78. doi: 10.1038/nrm1551

Wong, L. H., Brettingham-Moore, K. H., Chan, L., Quach, J. M., Anderson, M. A., Northrop, E. L., et al. (2007). Centromere RNA is a key component for the assembly of nucleoproteins at the nucleolus and centromere. *Genome Res.* 17, 1146–1160. doi: 10.1101/gr.6022807

Yancopoulos, G. D., and Alt, F. W. (1985). Developmentally controlled and tissue-specific expression of unrearranged VH gene segments. *Cell* 40, 271–281. doi: 10.1016/0092-8674(85)90141-2

Yang, F., Deng, X., Ma, W., Berletch, J. B., Rabaia, N., Wei, G., et al. (2015). The lncRNA Firre anchors the inactive X chromosome to the nucleolus by binding CTCF and maintains H3K27me3 methylation. *Genome Biol.* 16:52. doi: 10.1186/s13059-015-0618-0

Yang, L., Lin, C., Liu, W., Zhang, J., Ohgi, K. A., Grinstein, J. D., et al. (2011). ncRNA- and Pc2 methylation-dependent gene relocation between nuclear structures mediates gene activation programs. *Cell* 147, 773–788. doi: 10.1016/j.cell.2011.08.054

Yoshioka, M., Yorifuji, T., and Mituyoshi, I. (1998). Skewed X inactivation in manifesting carriers of Duchenne muscular dystrophy. *Clin. Genet.* 53, 102–107. doi: 10.1111/j.1399-0004.1998.tb02655.x

Zhang, H., Zeitz, M. J., Wang, H., Niu, B., Ge, S., Li, W., et al. (2014). Long noncoding RNA-mediated intrachromosomal interactions promote imprinting at the Kcnq1 locus. *J. Cell Biol.* 204, 61–75. doi: 10.1083/jcb.201304152

Zhang, L. F., Huynh, K. D., and Lee, J. T. (2007). Perinucleolar targeting of the inactive X during S phase: evidence for a role in the maintenance of silencing. *Cell* 129, 693–706. doi: 10.1016/j.cell.2007.03.036

Zhao, Z., Dammert, M. A., Grummt, I., and Bierhoff, H. (2016). lncRNA-induced nucleosome repositioning reinforces transcriptional repression of rRNA genes upon hypotonic stress. *Cell Rep.* 14, 1876–1882. doi: 10.1016/j.celrep.2016.01.073

Zhao, Z., Senturk, N., Song, C., and Grummt, I. (2018). lncRNA PAPAS tethered to the rDNA enhancer recruits hypophosphorylated CHD4/NuRD to repress rRNA synthesis at elevated temperatures. *Genes Dev.* 32, 836–848. doi: 10.1101/gad.311688.118

Zhu, L., and Brangwynne, C. P. (2015). Nuclear bodies: the emerging biophysics of nucleoplasmic phases. *Curr. Opin. Cell Biol.* 34, 23–30. doi: 10.1016/j.ceb.2015.04.003

Zuin, J., Dixon, J. R., van der Reijden, M. I., Ye, Z., Kolovos, P., Brouwer, R. W., et al. (2014). Cohesin and CTCF differentially affect chromatin architecture and gene expression in human cells. *Proc. Natl. Acad. Sci. U.S.A.* 111, 996–1001. doi: 10.1073/pnas.1317788111

Conflict of Interest: The authors declare that the research was conducted in the absence of any commercial or financial relationships that could be construed as a potential conflict of interest.

frontiers in Genetics

MINI REVIEW
published: 08 January 2020
doi: 10.3389/fgene.2019.01301

Modulation of Cell Identity by Modification of Nuclear Pore Complexes

Mercè Gomar-Alba [1,2,3,4] *and Manuel Mendoza* [1,2,3,4]*

[1] Institut de Génétique et de Biologie Moléculaire et Cellulaire, Illkirch, France, [2] Centre National de la Recherche Scientifique, Illkirch, France, [3] Institut National de la Santé et de la Recherche Médicale, Illkirch, France, [4] Université de Strasbourg, Strasbourg, France

Nuclear pore complexes (NPCs) are protein assemblies that form channels across the nuclear envelope to mediate communication between the nucleus and the cytoplasm. Additionally, NPCs interact with chromatin and influence the position and expression of multiple genes. Interestingly, the composition of NPCs can vary in different cell-types, tissues, and developmental states. Here, we review recent findings suggesting that modifications of NPC composition, including post-translational modifications, play an instructive role in cell fate establishment. In particular, we focus on the role of cell-specific NPC deacetylation in asymmetrically dividing budding yeast, which modulates transport-dependent and transport-independent NPC functions to determine the time of commitment to a new division cycle in daughter cells. By modulating protein localization and gene expression, NPCs are therefore emerging as central regulators of cell identity.

Keywords: nuclear pore complex, cell differentiation, deacetylase, budding yeast, Hos3

OPEN ACCESS

Edited by:
Karim Mekhail,
University of Toronto, Canada

Reviewed by:
Charlene Boumendil,
Institut Jacques Monod (IJM), France
Maya Capelson,
University of Pennsylvania, United States

***Correspondence:**
Manuel Mendoza
mendozam@igbmc.fr

Specialty section:
This article was submitted to Epigenomics and Epigenetics, a section of the journal Frontiers in Genetics

Received: *14 October 2019*
Accepted: *26 November 2019*
Published: *08 January 2020*

Citation:
Gomar-Alba M and Mendoza M (2020) Modulation of Cell Identity by Modification of Nuclear Pore Complexes. Front. Genet. 10:1301. doi: 10.3389/fgene.2019.01301

INTRODUCTION

Complex organisms develop through the generation of cellular diversity from a single undifferentiated cell. How are the main cellular components modulated to produce different types of cells? Understanding the answer to this question is one of the fundamental problems in biology. One way to generate different cell types after division is through the partitioning of regulatory molecules to only one of the progeny cells. In the simplest scenario, the asymmetrically partitioned molecule (or "cell fate determinant") directs transcription of genes that are important for differentiation of the receiving cell (Li, 2013). Much of the knowledge on this topic has come from the study of simple organisms that exhibit basic forms of cell differentiation. One of the best characterized is the budding yeast *Saccharomyces cerevisiae*. This organism divides asymmetrically, giving rise to mother and daughter cells that differ in their identity and behavior. Indeed, newborn daughter cells have different gene expression patterns than their mothers, which affect cell-type-specific processes such as cell separation, mating-type switching, and cell cycle progression (Colman-Lerner et al., 2001; Di Talia et al., 2009; Haber, 2012).

Recent work from our laboratory revealed that in budding yeast, an enzyme that deacetylates nuclear pore complexes acts as a cell fate determinant in daughter cells (Kumar et al., 2018). Nuclear pore complexes (NPCs) are multi-protein assemblies that forms channels in the nuclear envelope thus connecting the nucleus and cytoplasm. We found that deacetylation of NPCs in daughter cells modulates their gene expression program by multiple mechanisms. These findings established that

NPCs are biochemically and functionally different in budding yeast mother and daughter cells. Because NPCs are major regulators of nuclear composition and gene expression in eukaryotes, the discovery of cell-type-specific acetylation of NPCs in yeast opens the possibility that similar mechanisms may regulate cell differentiation in multicellular organisms. Here we will briefly describe the structure and function of NPCs, summarize the main mechanisms by which they regulate gene expression and differentiation in yeast and animal cells, and discuss how modulation of NPC acetylation may shape cell identity in eukaryotes.

NUCLEAR PORE COMPLEXES: ROLES IN NUCLEO-CYTOPLASMIC TRANSPORT

Since their initial description as components of the "porous layer" in the nuclear envelope of amphibian oocytes (Callan et al., 1949; Callan and Tomlin, 1950), NPCs were proposed to facilitate the transport of molecules between the nucleus and cytoplasm. Structural studies revealed that NPCs are macromolecular assemblies composed of approximately 30–50 different nucleoporins (Nups) that form a channel across the nuclear envelope (NE). The NPC structure is based on an eightfold radial symmetry and contains specific sub-structures (for recent reviews, see Knockenhauer and Schwartz, 2016; Beck and Hurt, 2017; Lin and Hoelz, 2019). These include the central ring, which lays across the NE; the cytoplasmic and nuclear rings, which are anchored at opposite sides of the central ring; and the cytoplasmic filaments and nuclear basket, associated with the cytoplasmic and nuclear rings, respectively. Although this general structure is highly conserved among eukaryotes, NPCs display significant variability across biological species in terms of size and composition, ranging in size from ~60 MDa in yeast to ~90–120 MDa in humans (Maimon et al., 2012; Lin and Hoelz, 2019). As discussed later, some variability in NPC composition is also present between different cell types in yeast and animal cells.

Functionally, NPCs operate as a selective barrier that allows compartmentalization between nucleus and cytoplasm. Small molecules (below approximately 30 KDa in mass, or 3 nm in diameter) such as ions and metabolites can freely diffuse through the NPC in human cells (Mohr et al., 2009). In contrast, transport of larger molecules including most proteins and RNAs requires assistance of specific transport receptors that translocate their cargo through the NPC channel and deliver it to the other side. Transport of most proteins and some RNA species such as tRNA, rRNA, and micro-RNAs is assisted by proteins of the karyopherin family (reviewed in Köhler and Hurt, 2007). Transport directionality is established by cargo release from karyopherins in either the nuclear or cytoplasmic side of the channel, achieved by the Ran GTPase system (Görlich et al., 2003). In contrast, export of messenger RNA (mRNA) is independent of karyopherins and Ran, and involves a dedicated heterodimeric transport receptor (Nxf1/Nxt1 in mammalian cells, and Mtr2/Mex67 in yeast) (Natalizio and Wente, 2013).

ROLE OF NUCLEAR PORE COMPLEXES IN GENOME ORGANIZATION AND GENE EXPRESSION

The function of NPCs in transport is linked to gene expression, since the nuclear concentration of transcriptional regulators and the rate of mRNA export are dependent on nucleo-cytoplasmic transport. In addition, NPCs directly impact gene expression by interacting with chromatin. The nuclear periphery plays a key role in the non-random distribution of chromatin inside the nucleus (Akhtar and Gasser, 2007; Cremer and Cremer, 2010) and is generally considered a repressive environment for transcription in yeast and metazoans (Taddei and Gasser, 2012; Steglich et al., 2013). Early visualization of the nuclear membrane showed heterochromatin preferentially associated with the nuclear periphery, with the exception of areas near nuclear pores (Aaronson and Blobel, 1975). These observations led to the idea that association of active genes with NPCs would facilitate the nuclear export of their transcripts, and conversely, that increased transcription may lead to targeting of active genes to nuclear pores. NPCs would therefore shape chromatin spatial organization and act as platforms to couple transcription and mRNA export—the "gene gating" hypothesis (Blobel, 1985). Supporting this idea, yeast genome-wide studies demonstrate that certain Nups and NPC-associated transport factors (e.g., karyopherins) bind preferentially highly transcribed genes (Casolari et al., 2004) and the existence of a vast number of interactions between gene promoters and components of the nuclear pore basket (Schmid et al., 2006).

In yeast, the best-characterized examples of transcriptionally active genes that associate with NPCs are inducible genes, which are highly expressed under specific environmental conditions. Multiple genes, including *GAL1, HXK1, INO1, HSP104,* and *TSA2* localize in the nuclear interior when repressed, and are recruited to the nuclear pores when induced (Brickner and Walter, 2004; Casolari et al., 2004; Casolari et al., 2005; Dieppois et al., 2006; Taddei et al., 2006; Brickner et al., 2007; Ahmed et al., 2010). Specifically, nuclear pore basket nups, such as Nup2, Nup1, Nup60, or Mlp2 are required for perinuclear localization of the active *GAL1* locus (Brickner et al., 2007; Brickner et al., 2016). Other important factors for the association of *GAL1* to NPCs are components of the Spt-Ada-Gcn5 acetyltransferase (SAGA) complex, and the transcription and mRNA export complex 2 (TREX-2) (Casolari et al., 2004; Cabal et al., 2006; Dieppois et al., 2006; Schmid et al., 2006; Luthra et al., 2007; Dultz et al., 2016). Thus, targeting of active genes to NPCs is promoted by basket nups and mRNA elongation and export factors; interestingly, NPC tethering may be mediated by RNA for some but not all active genes (Casolari et al., 2005; Brickner et al., 2007). Additionally, NPC recruitment of inducible yeast genes relies on specific gene recruitment sequences (GRS) in their promoters, which are necessary and sufficient to drive the gene to the NPCs and for their optimal expression (Ahmed et al., 2010). Strikingly, at least some of these genes remain associated with NPCs for several hours after withdrawal of the stimulus and transcriptional repression. This is linked to their faster reactivation upon a

second round of induction—a phenomenon known as "transcriptional memory" that requires Nup100 and the histone variant H2A.Z (Brickner et al., 2007; Light et al., 2010).

In animal cells, NPCs have been shown to modulate both chromatin organization and gene expression. As examples of the role of NPCs in chromatin organization, the nuclear basket protein Tpr is required for the exclusion of perinuclear heterochromatin from NPC-associated areas in HeLa cells infected with poliovirus (Krull et al., 2010), influences HIV integration sites by maintaining an open chromatin architecture near the NPC (Lelek et al., 2015; Wong et al., 2015), and promotes the formation and maintenance of senescence-associated heterochromatin foci in the nuclear interior in Ras-induced senescent cells (Boumendil et al., 2019). NPCs modulate gene expression by associating not only with gene promoters, but also with enhancers and super-enhancers to promote enhancer-promoter interactions through chromatin loops (Ibarra et al., 2016; Pascual-Garcia et al., 2017). In animal cells, Nup98 (homologue of yeast Nup100), Nup93, and Nup153 modulate gene expression through binding to chromatin either at the nucleoplasm or at NPCs (Kalverda et al., 2010; Ibarra et al., 2016; Liu et al., 2017; Pascual-Garcia and Capelson, 2019). Moreover, the role of NPCs in transcriptional memory is also conserved in animal cells. Nup98 mediates enhancer-promoter loop formation to ensure faster and higher expression of hormone inducible genes upon repeated activation in Drosophila (Pascual-Garcia et al., 2017), and promotes transcriptional memory after treatment with interferon gamma in human cells (Light et al., 2013). Thus, the role of Nup98 in transcriptional memory is conserved in yeast, flies, and humans (Tan-Wong et al., 2009; Light and Brickner, 2013; D'Urso and Brickner, 2017).

NPC-dependent mechanisms of gene expression involve their interaction with transcription factors (TFs) and histone-modifying enzymes including acetyl-transferases, deacetylases, and ubiquitin-transferases. For example, in human cells exposed to proliferative signals, MYC is recruited to the nuclear pore basket where it interacts with the nups Tpr and Nup153, promoting the formation of a complex that includes the SAGA acetyltransferase component Gcn5, and regulating the expression of mitogen-stimulated genes (Su et al., 2018). In mouse embryonic stem cells, Nup153 represses developmental genes by recruiting the polycomb-repressive complex 1 (PRC1) subunit RING1B, which catalyzes ubiquitination of histone H2A (Jacinto et al., 2015). Finally, in cardiomyocytes, the histone deacetylase HDAC4 interacts with Nup155 at NPCs, and prevents the association of sarcomeric and calcium signaling genes to the NPCs to negatively regulate their expression (Kehat et al., 2011; D'Angelo, 2018).

NUCLEAR PORE PLASTICITY DURING CELLULAR DIFFERENTIATION

Although the overall structure of NPCs is conserved across species and within cell types, recent evidence indicates that NPCs display cell-type specific variability in their protein composition, which in some cases can affect their gene regulatory functions. Early proteomics studies have revealed that the levels of nups including Nup50, Tpr, Nup214, Nup210, Pom121, and Nup37 showed significant variability across cancer cell lines and human tissues (Guan et al., 2000; Cho et al., 2009; Ori et al., 2013). This opened the possibility that tissue-specific expression levels of certain nups could mediate protein transport and/or gene expression changes during development. This may be the case for murine Nup133, which is predominantly expressed in embryonic progenitors and is required for efficient neural differentiation in ESC and neuronal progenitors (Lupu et al., 2008).

Changes in the levels of specific Nups can affect cellular differentiation by regulating the transcription of developmental genes in specific cell types. A well-characterized example is the transmembrane ring NPC component Nup210. The expression of Nup210 is cell-type specific during mouse organogenesis (Olsson et al., 2004). In an *in vitro* myogenic model, Nup210 levels are low in proliferative myoblasts, but increase during myogenic differentiation (D'Angelo et al., 2012). Interestingly, Nup210 depletion inhibits myotube formation. While absence of Nup210 had no detectable defects in protein import or export, it resulted in downregulation of genes involved in myogenesis and other developmental genes (D'Angelo et al., 2012). Nup210 promotes myoblast differentiation through the recruitment to NPCs of Mef2C, a TF key for the regulation of skeletal and cardiac muscle developmental genes at the nuclear periphery (Raices et al., 2017).

Whereas Nup210 levels increase during myogenic differentiation, the levels of the nuclear basket component Nup153 decrease during neural differentiation (Jacinto et al., 2015; Toda et al., 2017). Thus, Nup153 levels correlate with the degree of cellular plasticity, and evidence suggests that Nup153 promotes the maintenance of an undifferentiated cellular state. In mESCs, Nup153 binds to silenced developmental genes at NPCs and also in the nucleoplasm. Loss of Nup153 causes early neuronal differentiation, probably by deficient recruitment of polycomb repressive complexes to developmental genes (Jacinto et al., 2015). Consistent with a role in repressing differentiation, in rat neural progenitor cells, Nup153 is necessary for maintaining the expression of genes distinctive of the neural progenitor cells specific transcriptional program. Nup153 interacts with the neural progenitor TF Sox2 and together, both factors regulate gene expression through their association with promoters and with 3' gene regions, possibly to mediate transcription and repression, respectively (Toda et al., 2017).

Two important conclusions emerge from these studies. First, Nup levels and thus NPCs composition can vary in the different developmental stages. Second, by modulating gene expression through specific nucleoporins, NPCs can either promote or prevent cell differentiation. This has led to the proposal that specialized NPCs with different characteristics may ultimately lead to cell-specific functions (Raices and D'Angelo, 2012). How differences in NPC composition arise during development in animal cells remains unclear.

NUCLEAR PORE DEACETYLATION REGULATES GENE EXPRESSION IN BUDDING YEAST DAUGHTER CELLS

A new link between changes in NPC composition and cell differentiation was revealed by studies of asymmetric division

in budding yeast. Yeast cells proliferate by first growing a bud on the surface of the mother cell; DNA replication is then followed by transport of one of the newly generated nuclei across the mother-bud neck and into the future daughter cell. Cytokinesis produces mother and daughter cells that differ not only in size (at the time of birth, buds are generally smaller than their mothers) but also in their age and transcriptional activity (Li, 2013). This is due to asymmetric partitioning of ageing and cell fate determinants during cell division (Long et al., 1997; Sinclair and Guarente, 1997). The lysine deacetylase Hos3 is a new cell fate determinant that modifies NPCs in newborn daughter cells (**Figure 1A**). Hos3 binds to the daughter-cell side of the septin ring, a cytoskeletal structure that assembles at the bud neck (Wang and Collins, 2014). Hos3 then transiently associates with the periphery of the daughter cell nucleus during anaphase chromosome segregation (Kumar et al., 2018). Since the yeast NE does not disassemble during mitosis, NPCs destined to the bud are in close proximity with the bud neck during anaphase. This suggests that Hos3 transfers from the septin ring to NPCs as they transit through the bud neck. Recruitment of Hos3 to the nuclear periphery is associated with Hos3 association with the nuclear pore basket, and deacetylation of nups at both the central channel (including Nup49, Nup53, and Nup57) and nuclear basket (Nup60). Thus, Hos3 establishes biochemical differences in NPCs between mother and daughter cells: NPCs that are retained in mother cells are acetylated, whereas NPCs transmitted to daughter cells are hypo-acetylated (Kumar et al., 2018). What are the physiological consequences of these differences in NPC acetylation?

Commitment to a new division cycle is regulated asymmetrically in *S. cerevisiae*: daughter cells have a longer G1 phase, and thus start a new cycle later than mother cells. This is due to a cell size-dependent delay that prolongs G1 until daughter cells reach the critical cell size needed to enter in a new round of cell division (Hartwell and Unger, 1977; Turner et al., 2012) and to a size-independent daughter-specific delay of the G1/S transition (Laabs et al., 2003; Di Talia et al., 2009). We found that deacetylation of daughter nucleoporins inhibits cell cycle entry in a manner that is independent of cell size, through regulation of transport-dependent and transport-independent NPC functions in daughter cells (**Figure 1B**). The transport-dependent pathway may act by modulating the nuclear concentration of cell cycle regulators, such as the transcriptional repressor Whi5 (homologue of the retinoblastoma tumor suppressor protein, pRb). The concentration of Whi5 at the start of the cell cycle is highly predictive of G1 duration, and is higher in daughter than in mother cells (Schmoller et al., 2015). We found that higher nuclear concentration of Whi5 in daughter cells requires Hos3-dependent deacetylation of central pore channel nucleoporins (including Nup49) and to a lesser extent, of the basket nup Nup60 in daughter cells (Kumar et al., 2018). How NPC acetylation modulates the nuclear concentration of Whi5 is unclear, but may involve changes in its nuclear transport dynamics. Supporting this possibility, NPC deacetylation reduces the nuclear levels of the karyopherins responsible for Whi5 nuclear import and export (Kap95 and Msn5), raising the possibly that deacetylation of nups in the central channel inhibits their affinity for Whi5 transport receptors. Since Kap95 and Msn5 transport multiple cargoes in addition to Whi5, NPC deacetylation may impact the asymmetric distribution of a plethora of nuclear proteins.

Deacetylation of NPCs also modulates G1 duration independently of nuclear transport. Indeed, deacetylation of the nuclear basket promotes the perinuclear tethering and silencing of at least one key cell cycle control gene, encoding the G1/S cyclin Cln2 (homologue of mammalian Cyclin E). We found that in daughter cells, the *CLN2* locus localizes to the nuclear periphery and associates with the nuclear basket component Nup60 (homologue of mammalian Nup153) during G1, when it is repressed. *CLN2* then moves away from NPCs during S phase, when it is expressed. Artificial targeting of *CLN2* to the nuclear periphery leads to longer G1 phase, suggesting that association with NPCs leads to *CLN2* repression. The daughter-cell-specific recruitment of *CLN2* to NPCs is independent of Whi5 but depends on deacetylation of Nup60 or Nup49 by Hos3 (Kumar et al., 2018). The molecular mechanisms mediating *CLN2* repression at NPCs remain to be elucidated.

In summary, deacetylation of NPCs in daughter cells establishes a key aspect of their identity, inhibiting commitment to a new round of cell division. It is interesting to note that in addition to the putative Hos3 substrates studied so far, additional nups are acetylated in yeast (**Figure 2**); the function of these modifications, and the identity of the responsible acetylases and deacetylases, are not known (Henriksen et al., 2012). Thus, deacetylation of NPCs in yeast daughter cells may have other functions in addition to inhibiting the G1/S transition.

FUTURE PERSPECTIVES

Yeast cells have devised an elaborate mechanism to ensure deacetylation of NPCs in daughter cells and not in mother cells, by coupling inheritance of a Nup deacetylase with passage of the nucleus through the bud neck during mitosis (Kumar et al., 2018). Although this inheritance mechanism may be unique to budding yeast, it remains possible that modulation of NPC acetylation may also impact proliferation and differentiation of animal cells. Although evidence for this is currently lacking, several observations suggest that this possibility warrants investigation. Firstly, as is the case in yeast, human nucleoporins are acetylated, including nups in the central channel (Nup98), nuclear basket (Nup153, Nup50, and Tpr), cytoplasmic filaments (Nup214, Nup358), and inner ring (Nup188, Nup205) (Choudhary et al., 2009; Henriksen et al., 2012) (**Figure 2**). The physiological relevance of these modifications, if any, remains to be explored. Secondly, nucleoporins associate with acetylases and deacetylases both during normal development (Kehat et al., 2011; Su et al., 2018) and in pathological contexts. Indeed, when fused to DNA binding proteins after cancer-induced translocations, nucleoporins such as Nup98 can act as potent transcriptional trans-activators or repressors by recruiting acetylases and deacetylases (Kasper et al., 1999; Bai et al., 2006; Wang et al., 2007).

As we have seen, NPC composition can change during cell differentiation and the mechanisms mediating NPC compositional

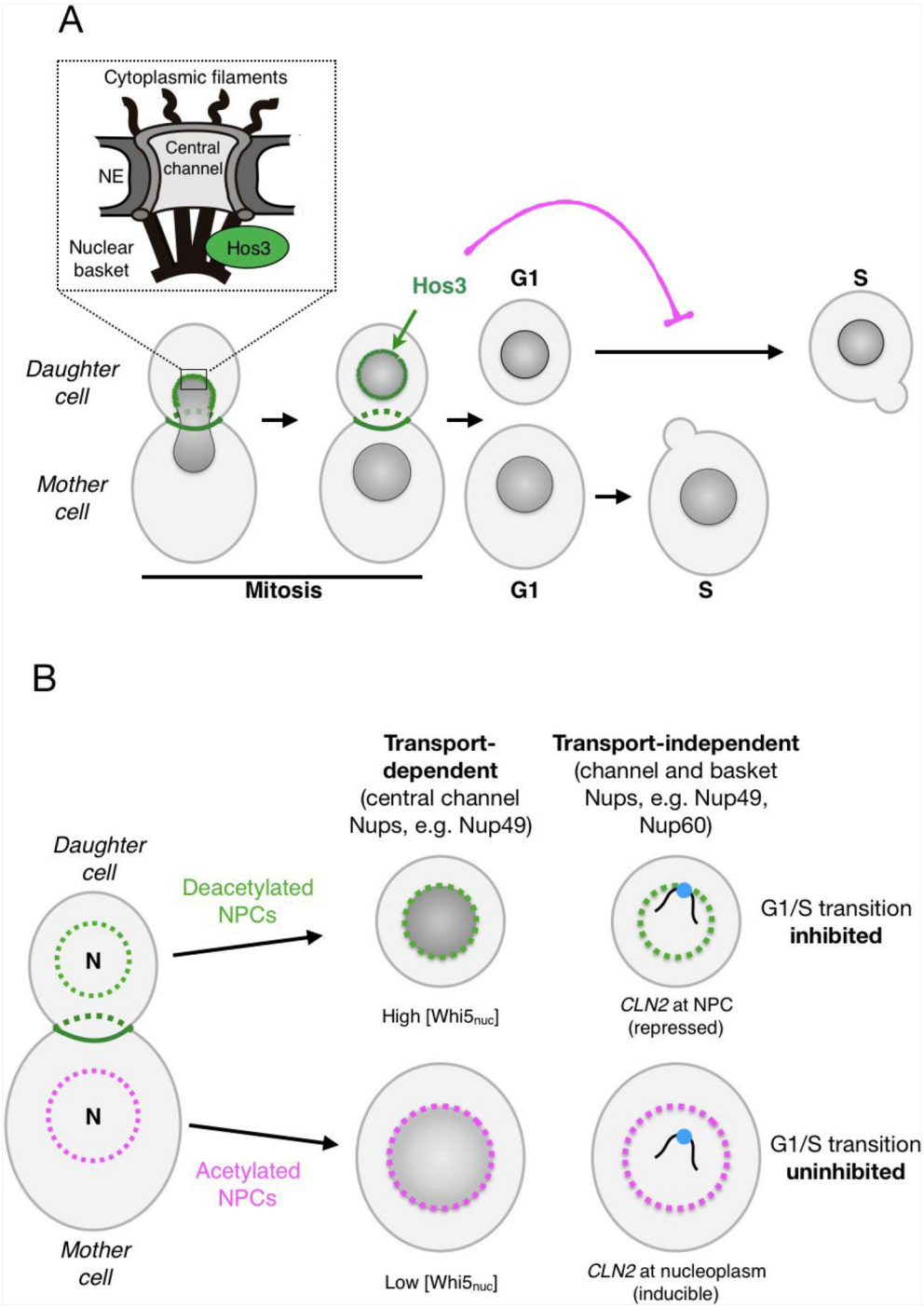

FIGURE 1 | Daughter-cell-specific deacetylation of nuclear pore complexes (NPCs) modulates cell cycle identity in budding yeast. **(A)** During mitotic division, the deacetylase Hos3 (in green) associates with the bud neck and with daughter-cell NPCs during nuclear migration into the bud. Deacetylated NPCs delay the G1/S transition in daughter cells. The inset depicts the main architectural elements of NPCs. **(B)** NPC deacetylation (left) inhibits the G1/S transition in daughter cells through two major mechanisms: nuclear transport of the transcriptional repressor Whi5 (middle) and NPC-mediated repression of the G1/S cyclin gene *CLN2* (right). See text for details.

variability remain unclear (Lupu et al., 2008; D'Angelo et al., 2012; Toda et al., 2017). It is possible that acetylation of specific Nups may affect the ability of NPCs to incorporate additional subunits during development. Nup acetylation may also regulate their ability to interact with gene regulatory factors involved in transcription and/or RNA export. Notably, the ortholog of yeast Nup60 (which is deacetylated to allow for repression of the *CLN2* gene) is Nup153, which as mentioned earlier is essential for repression of developmental genes in rat neural progenitors (Jacinto et al., 2015; Toda et al., 2017). It would be of interest to investigate if

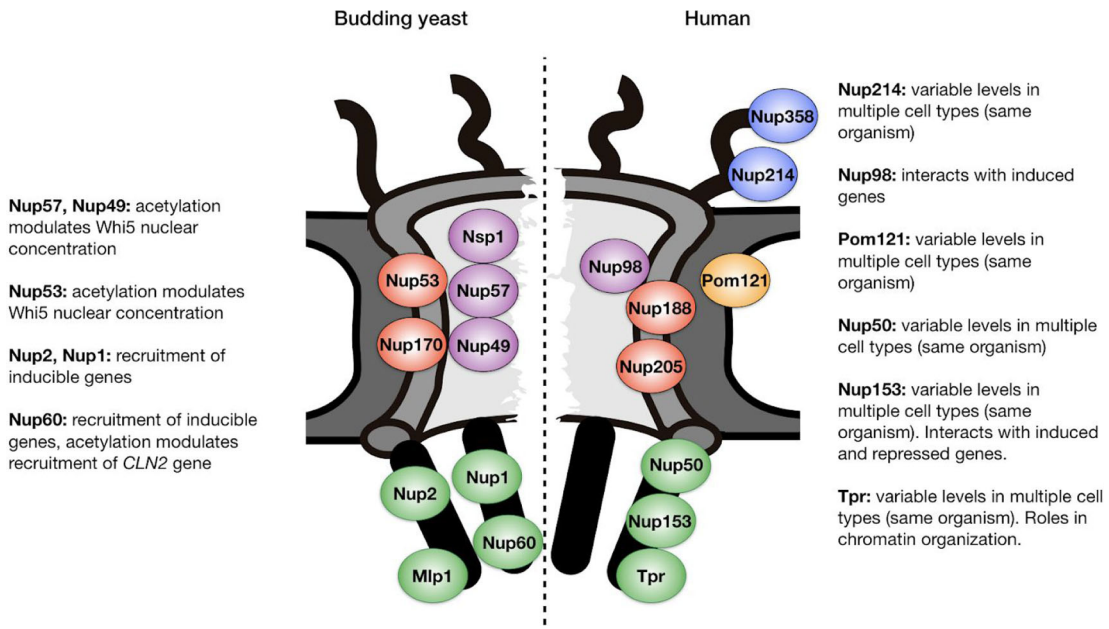

FIGURE 2 | Position within the nuclear pore complex of acetylated nucleoporins in yeast and human cells. Examples of acetylated Nups are based on (Choudhary et al., 2009; Henriksen et al., 2012) and are located in the central channel (purple), inner ring (red), transmembrane ring (orange), cytoplasmic filaments (blue), and nuclear basket (green). Functions relevant to cell identity establishment are annotated. See text for details and references.

Nup153 acetylation or deacetylation is important for its roles in cell fate specification.

Notably, perinuclear deacetylation is important to maintain spatial chromatin organization relative to NPCs, as observed after inhibition of histone deacetylase (HDAC) activity in HeLa cells (Brown et al., 2008). Perinuclear HDACs are thought to regulate gene expression and possibly chromatin-NPC interactions through their well-documented role in deacetylation of histones near promoter regions (Seto and Yoshida, 2014). However, our findings in yeast suggest that nucleoporins may represent a novel category of HDAC substrates with important roles in gene expression and nuclear organization. Interestingly, mammalian deacetylases such as HDAC3 and HDAC4 are enriched in the nuclear periphery and regulate gene expression through regulation of chromatin interactions with the nuclear periphery and/or nuclear pores (Kehat et al., 2011; Poleshko et al., 2017). Identification of the molecular mechanisms by which perinuclear HDACs regulate gene expression, whether by deacetylation of histone or non-histone proteins such as nucleoporins, will be an important future challenge.

AUTHOR CONTRIBUTIONS

MG-A and MM wrote the manuscript.

FUNDING

This work has benefitted from support provided by the University of Strasbourg Institute for Advanced Study (USIAS) for a Fellowship, within the French national program "Investment for the future" (IdEx-Unistra). Research in our laboratory is supported by grant from "La Ligue Contre le Cancer," and "Fondation ARC pour la Recherche sur le Cancer" PJA20181208052 to MM, and grant ANR-10-LABX-0030-INRT, which is a French State fund managed by the Agence Nationale de la Recherche under the frame Programme Investissements d'Avenir ANR-10-IDEX-0002-02 to the Institut de Génétique et de Biologie Moléculaire et Cellulaire (IGBMC). MG-A is a recipient of a Postdoctoral Fellowship APOSTD/2017/094 from the Generalitat Valenciana.

REFERENCES

Aaronson, R. P., and Blobel, G. (1975). Isolation of nuclear pore complexes in association with a lamina. *Proc. Natl. Acad. Sci. U. S. A.* 72, 1007–1011. doi: 10.1073/pnas.72.3.1007

Ahmed, S., Brickner, D. G., Light, W. H., Cajigas, I., McDonough, M., Froyshteter, A. B., et al. (2010). DNA zip codes control an ancient mechanism for gene targeting to the nuclear periphery. *Nat. Cell Biol.* 12, 111–118. doi: 10.1038/ncb2011

Akhtar, A., and Gasser, S. M. (2007). The nuclear envelope and transcriptional control. *Nat. Rev. Genet.* 8, 507–517. doi: 10.1038/nrg2122

Bai, X.-T., Gu, B.-W., Yin, T., Niu, C., Xi, X.-D., Zhang, J., et al. (2006). Trans-repressive effect of NUP98-PMX1 on PMX1-regulated c-FOS gene through recruitment of histone deacetylase 1 by FG repeats. *Cancer Res.* 66, 4584–4590. doi: 10.1158/0008-5472.CAN-05-3101

Beck, M., and Hurt, E. (2017). The nuclear pore complex: understanding its function through structural insight. *Nat. Rev. Mol. Cell Biol.* 18, 73–89. doi: 10.1038/nrm.2016.147

Blobel, G. (1985). Gene gating: a hypothesis. *Proc. Natl. Acad. Sci. U. S. A.* 82, 8527–8529. doi: 10.1073/pnas.82.24.8527

Boumendil, C., Hari, P., Olsen, K. C. F., Acosta, J. C., and Bickmore, W. A. (2019). Nuclear pore density controls heterochromatin reorganization during senescence. *Genes Dev.* 33, 144–149. doi: 10.1101/gad.321117.118

Brickner, J. H., and Walter, P. (2004). Gene recruitment of the activated INO1 locus to the nuclear membrane. *PLoS Biol.* 2, e342. doi: 10.1371/journal.pbio.0020342

Brickner, D. G., Cajigas, I., Fondufe-Mittendorf, Y., Ahmed, S., Lee, P.-C., Widom, J., et al. (2007). H2A.Z-mediated localization of genes at the nuclear periphery confers epigenetic memory of previous transcriptional state. *PLoS Biol.* 5, e81. doi: 10.1371/journal.pbio.0050081

Brickner, D. G., Sood, V., Tutucci, E., Coukos, R., Viets, K., Singer, R. H., et al. (2016). Subnuclear positioning and interchromosomal clustering of the GAL1-10 locus are controlled by separable, interdependent mechanisms. *Mol. Biol. Cell* 27, 2980–2993. doi: 10.1091/mbc.E16-03-0174

Brown, C. R., Kennedy, C. J., Delmar, V. A., Forbes, D. J., and Silver, P. A. (2008). Global histone acetylation induces functional genomic reorganization at mammalian nuclear pore complexes. *Genes Dev.* 22, 627–639. doi: 10.1101/gad.1632708

Cabal, G. G., Genovesio, A., Rodriguez-Navarro, S., Zimmer, C., Gadal, O., Lesne, A., et al. (2006). SAGA interacting factors confine sub-diffusion of transcribed genes to the nuclear envelope. *Nature* 441, 770–773. doi: 10.1038/nature04752

Callan, H. G., and Tomlin, S. G. (1950). Experimental studies on amphibian oocyte nuclei. I. Investigation of the structure of the nuclear membrane by means of the electron microscope. *Proc. R. Soc Lond. B Biol. Sci.* 137, 367–378. doi: 10.1038/163280a0

Callan, H. G., Randall, J. T., and Tomlin, S. G. (1949). An electron microscope study of the nuclear membrane. *Nature* 163, 280.

Casolari, J. M., Brown, C. R., Komili, S., West, J., Hieronymus, H., and Silver, P. A. (2004). Genome-wide localization of the nuclear transport machinery couples transcriptional status and nuclear organization. *Cell* 117, 427–439. doi: 10.1016/s0092-8674(04)00448-9

Casolari, J. M., Brown, C. R., Drubin, D. A., Rando, O. J., and Silver, P. A. (2005). Developmentally induced changes in transcriptional program alter spatial organization across chromosomes. *Genes Dev.* 19, 1188–1198. doi: 10.1101/gad.1307205

Cho, A. R., Yang, K. J., Bae, Y., Bahk, Y. Y., Kim, E., Lee, H., et al. (2009). Tissue-specific expression and subcellular localization of ALADIN, the absence of which causes human triple A syndrome. *Exp. Mol. Med.* 41, 381–386. doi: 10.3858/emm.2009.41.6.043

Choudhary, C., Kumar, C., Gnad, F., Nielsen, M. L., Rehman, M., Walther, T. C., et al. (2009). Lysine acetylation targets protein complexes and co-regulates major cellular functions. *Science* 325, 834–840. doi: 10.1126/science.1175371

Colman-Lerner, A., Chin, T. E., and Brent, R. (2001). Yeast Cbk1 and Mob2 activate daughter-specific genetic programs to induce asymmetric cell fates. *Cell* 107, 739–750. doi: 10.1016/s0092-8674(01)00596-7

Cremer, T., and Cremer, M. (2010). Chromosome territories. *Cold Spring Harb. Perspect. Biol.* 2, a003889. doi: 10.1101/cshperspect.a003889

D'Angelo, M. A., Gomez-Cavazos, J. S., Mei, A., Lackner, D. H., and Hetzer, M. W. (2012). A change in nuclear pore complex composition regulates cell differentiation. *Dev. Cell* 22, 446–458. doi: 10.1016/j.devcel.2011.11.021

D'Angelo, M. A. (2018). Nuclear pore complexes as hubs for gene regulation. *Nucleus* 9, 142–148. doi: 10.1080/19491034.2017.1395542

D'Urso, A., and Brickner, J. H. (2017). Epigenetic transcriptional memory. *Curr. Genet.* 63, 435–439. doi: 10.1007/s00294-016-0661-8

Di Talia, S., Wang, H., Skotheim, J. M., Rosebrock, A. P., Futcher, B., and Cross, F. R. (2009). Daughter-specific transcription factors regulate cell size control in budding yeast. *PLoS Biol.* 7, e1000221. doi: 10.1371/journal.pbio.1000221

Dieppois, G., Iglesias, N., and Stutz, F. (2006). Cotranscriptional recruitment to the mRNA export receptor Mex67p contributes to nuclear pore anchoring of activated genes. *Mol. Cell. Biol.* 26, 7858–7870. doi: 10.1128/MCB.00870-06

Dultz, E., Tjong, H., Weider, E., Herzog, M., Young, B., Brune, C., et al. (2016). Global reorganization of budding yeast chromosome conformation in different physiological conditions. *J. Cell Biol.* 212, 321–334. doi: 10.1083/jcb.201507069

Görlich, D., Seewald, M. J., and Ribbeck, K. (2003). Characterization of Ran-driven cargo transport and the RanGTPase system by kinetic measurements and computer simulation. *EMBO J.* 22, 1088–1100. doi: 10.1093/emboj/cdg113

Guan, T., Kehlenbach, R. H., Schirmer, E. C., Kehlenbach, A., Fan, F., Clurman, B. E., et al. (2000). Nup50, a nucleoplasmically oriented nucleoporin with a role in nuclear protein export. *Mol. Cell. Biol.* 20, 5619–5630. doi: 10.1128/mcb.20.15.5619-5630.2000

Haber, J. E. (2012). Mating-type genes and MAT switching in Saccharomyces cerevisiae. *Genetics* 191, 33–64. doi: 10.1534/genetics.111.134577

Hartwell, L. H., and Unger, M. W. (1977). Unequal division in Saccharomyces cerevisiae and its implications for the control of cell division. *J. Cell Biol.* 75, 422–435. doi: 10.1083/jcb.75.2.422

Henriksen, P., Wagner, S. A., Weinert, B. T., Sharma, S., Bacinskaja, G., Rehman, M., et al. (2012). Proteome-wide analysis of lysine acetylation suggests its broad regulatory scope in Saccharomyces cerevisiae. *Mol. Cell. Proteomics* 11, 1510–1522. doi: 10.1074/mcp.M112.017251

Ibarra, A., Benner, C., Tyagi, S., Cool, J., and Hetzer, M. W. (2016). Nucleoporin-mediated regulation of cell identity genes. *Genes Dev.* 30, 2253–2258. doi: 10.1101/gad.287417.116

Jacinto, F. V., Benner, C., and Hetzer, M. W. (2015). The nucleoporin Nup153 regulates embryonic stem cell pluripotency through gene silencing. *Genes Dev.* 29, 1224–1238. doi: 10.1101/gad.260919.115

Kalverda, B., Pickersgill, H., Shloma, V. V., and Fornerod, M. (2010). Nucleoporins directly stimulate expression of developmental and cell-cycle genes inside the nucleoplasm. *Cell* 140, 360–371. doi: 10.1016/j.cell.2010.01.011

Kasper, L. H., Brindle, P. K., Schnabel, C. A., Pritchard, C. E., Cleary, M. L., and van Deursen, J. M. (1999). CREB binding protein interacts with nucleoporin-specific FG repeats that activate transcription and mediate NUP98-HOXA9 oncogenicity. *Mol. Cell. Biol.* 19, 764–776. doi: 10.1128/mcb.19.1.764

Kehat, I., Accornero, F., Aronow, B. J., and Molkentin, J. D. (2011). Modulation of chromatin position and gene expression by HDAC4 interaction with nucleoporins. *J. Cell Biol.* 193, 21–29. doi: 10.1083/jcb.201101046

Knockenhauer, K. E., and Schwartz, T. U. (2016). The nuclear pore complex as a flexible and dynamic gate. *Cell* 164, 1162–1171. doi: 10.1016/j.cell.2016.01.034

Köhler, A., and Hurt, E. (2007). Exporting RNA from the nucleus to the cytoplasm. *Nat. Rev. Mol. Cell Biol.* 8, 761–773. doi: 10.1038/nrm2255

Krull, S., Dörries, J., Boysen, B., Reidenbach, S., Magnius, L., Norder, H., et al. (2010). Protein Tpr is required for establishing nuclear pore-associated zones of heterochromatin exclusion. *EMBO J.* 29, 1659–1673. doi: 10.1038/emboj.2010.54

Kumar, A., Sharma, P., Gomar-Alba, M., Shcheprova, Z., Daulny, A., Sanmartín, T., et al. (2018). Daughter-cell-specific modulation of nuclear pore complexes controls cell cycle entry during asymmetric division. *Nat. Cell Biol.* 20, 432–442. doi: 10.1038/s41556-018-0056-9

Laabs, T. L., Markwardt, D. D., Slattery, M. G., Newcomb, L. L., Stillman, D. J., and Heideman, W. (2003). ACE2 is required for daughter cell-specific G1 delay in Saccharomyces cerevisiae. *Proc. Natl. Acad. Sci. U. S. A.* 100, 10275–10280. doi: 10.1073/pnas.1833999100

Lelek, M., Casartelli, N., Pellin, D., Rizzi, E., Souque, P., Severgnini, M., et al. (2015). Chromatin organization at the nuclear pore favours HIV replication. *Nat. Commun.* 6, 6483. doi: 10.1038/ncomms7483

Li, R. (2013). The art of choreographing asymmetric cell division. *Dev. Cell* 25, 439–450. doi: 10.1016/j.devcel.2013.05.003

Light, W. H., and Brickner, J. H. (2013). Nuclear pore proteins regulate chromatin structure and transcriptional memory by a conserved mechanism. *Nucleus* 4, 357–360. doi: 10.4161/nucl.26209

Light, W. H., Brickner, D. G., Brand, V. R., and Brickner, J. H. (2010). Interaction of a DNA zip code with the nuclear pore complex promotes H2A.Z incorporation and INO1 transcriptional memory. *Mol. Cell* 40, 112–125. doi: 10.1016/j.molcel.2010.09.007

Light, W. H., Freaney, J., Sood, V., Thompson, A., D'Urso, A., Horvath, C. M., et al. (2013). A conserved role for human Nup98 in altering chromatin structure and promoting epigenetic transcriptional memory. *PloS Biol.* 11, e1001524. doi: 10.1371/journal.pbio.1001524

Lin, D. H., and Hoelz, A. (2019). The Structure of the Nuclear Pore Complex (An Update). *Annu. Rev. Biochem.* 88, 725–783. doi: 10.1146/annurev-biochem-062917-011901

Liu, X., Zhang, Y., Chen, Y., Li, M., Zhou, F., Li, K., et al. (2017). In situ capture of chromatin interactions by biotinylated dCas9. *Cell* 170, 1028–1043.e19. doi: 10.1016/j.cell.2017.08.003

Long, R. M., Singer, R. H., Meng, X., Gonzalez, I., Nasmyth, K., and Jansen, R. P. (1997). Mating type switching in yeast controlled by asymmetric localization of ASH1 mRNA. *Science* 277, 383–387. doi: 10.1126/science.277.5324.383

Lupu, F., Alves, A., Anderson, K., Doye, V., and Lacy, E. (2008). Nuclear pore composition regulates neural stem/progenitor cell differentiation in the mouse embryo. *Dev. Cell* 14, 831–842. doi: 10.1016/j.devcel.2008.03.011

Luthra, R., Kerr, S. C., Harreman, M. T., Apponi, L. H., Fasken, M. B., Ramineni, S., et al. (2007). Actively transcribed GAL genes can be physically linked to the nuclear pore by the SAGA chromatin modifying complex. *J. Biol. Chem.* 282, 3042–3049. doi: 10.1074/jbc.M608741200

Maimon, T., Elad, N., Dahan, I., and Medalia, O. (2012). The human nuclear pore complex as revealed by cryo-electron tomography. *Structure* 20, 998–1006. doi: 10.1016/j.str.2012.03.025

Mohr, D., Frey, S., Fischer, T., Güttler, T., and Görlich, D. (2009). Characterisation of the passive permeability barrier of nuclear pore complexes. *EMBO J.* 28, 2541–2553. doi: 10.1038/emboj.2009.200

Natalizio, B. J., and Wente, S. R. (2013). Postage for the messenger: designating routes for nuclear mRNA export. *Trends Cell Biol.* 23, 365–373. doi: 10.1016/j.tcb.2013.03.006

Olsson, M., Schéele, S., and Ekblom, P. (2004). Limited expression of nuclear pore membrane glycoprotein 210 in cell lines and tissues suggests cell-type specific nuclear pores in metazoans. *Exp. Cell Res.* 292, 359–370. doi: 10.1016/j.yexcr.2003.09.014

Ori, A., Banterle, N., Iskar, M., Andrés-Pons, A., Escher, C., Khanh Bui, H., et al. (2013). Cell type-specific nuclear pores: a case in point for context-dependent stoichiometry of molecular machines. *Mol. Syst. Biol.* 9, 648. doi: 10.1038/msb.2013.4

Pascual-Garcia, P., and Capelson, M. (2019). Nuclear pores in genome architecture and enhancer function. *Curr. Opin. Cell Biol.* 58, 126–133. doi: 10.1016/j.ceb.2019.04.001

Pascual-Garcia, P., Debo, B., Aleman, J. R., Talamas, J. A., Lan, Y., Nguyen, N. H., et al. (2017). Metazoan nuclear pores provide a scaffold for poised genes and mediate induced enhancer-promoter contacts. *Mol. Cell* 66, 63–76.e6. doi: 10.1016/j.molcel.2017.02.020

Poleshko, A., Shah, P. P., Gupta, M., Babu, A., Morley, M. P., Manderfield, L. J., et al. (2017). Genome-nuclear lamina interactions regulate cardiac stem cell lineage restriction. *Cell* 171, 573–587.e14. doi: 10.1016/j.cell.2017.09.018

Raices, M., and D'Angelo, M. A. (2012). Nuclear pore complex composition: a new regulator of tissue-specific and developmental functions. *Nat. Rev. Mol. Cell Biol.* 13, 687–699. doi: 10.1038/nrm3461

Raices, M., Bukata, L., Sakuma, S., Borlido, J., Hernandez, L. S., Hart, D. O., et al. (2017). Nuclear pores regulate muscle development and maintenance by assembling a localized Mef2C complex. *Dev. Cell* 41, 540–554.e7. doi: 10.1016/j.devcel.2017.05.007

Schmid, M., Arib, G., Laemmli, C., Nishikawa, J., Durussel, T., and Laemmli, U. K. (2006). Nup-PI: the nucleopore-promoter interaction of genes in yeast. *Mol. Cell* 21, 379–391. doi: 10.1016/j.molcel.2005.12.012

Schmoller, K. M., Turner, J. J., Kõivomägi, M., and Skotheim, J. M. (2015). Dilution of the cell cycle inhibitor Whi5 controls budding-yeast cell size. *Nature.* 526, 268–272. doi: 10.1038/nature14908

Seto, E., and Yoshida, M. (2014). Erasers of histone acetylation: the histone deacetylase enzymes. *Cold Spring Harb. Perspect. Biol.* 6, a018713. doi: 10.1101/cshperspect.a018713

Sinclair, D. A., and Guarente, L. (1997). Extrachromosomal rDNA circles—a cause of aging in yeast. *Cell* 91, 1033–1042.

Steglich, B., Sazer, S., and Ekwall, K. (2013). Transcriptional regulation at the yeast nuclear envelope. *Nucleus* 4, 379–389. doi: 10.4161/nucl.26394

Su, Y., Pelz, C., Huang, T., Torkenczy, K., Wang, X., Cherry, A., et al. (2018). Post-translational modification localizes MYC to the nuclear pore basket to regulate a subset of target genes involved in cellular responses to environmental signals. *Genes Dev.* 32, 1398–1419. doi: 10.1101/gad.314377.118

Taddei, A., and Gasser, S. M. (2012). Structure and function in the budding yeast nucleus. *Genetics* 192, 107–129. doi: 10.1534/genetics.112.140608

Taddei, A., Van Houwe, G., Hediger, F., Kalck, V., Cubizolles, F., Schober, H., et al. (2006). Nuclear pore association confers optimal expression levels for an inducible yeast gene. *Nature* 441, 774–778. doi: 10.1038/nature04845

Tan-Wong, S. M., Wijayatilake, H. D., and Proudfoot, N. J. (2009). Gene loops function to maintain transcriptional memory through interaction with the nuclear pore complex. *Genes Dev.* 23, 2610–2624. doi: 10.1101/gad.1823209

Toda, T., Hsu, J. Y., Linker, S. B., Hu, L., Schafer, S. T., Mertens, J., et al. (2017). Nup153 interacts with Sox2 to enable bimodal gene regulation and maintenance of neural progenitor cells. *Cell Stem Cell* 21, 618–634.e7. doi: 10.1016/j.stem.2017.08.012

Turner, J. J., Ewald, J. C., and Skotheim, J. M. (2012). Cell Size Control in Yeast. *Curr. Biol.* 22, R350–R359. doi: 10.1016/j.cub.2012.02.041

Wang, M., and Collins, R. N. (2014). A lysine deacetylase Hos3 is targeted to the bud neck and involved in the spindle position checkpoint. *Mol. Biol. Cell* 25, 2720–2734. doi: 10.1091/mbc.E13-10-0619

Wang, G. G., Cai, L., Pasillas, M. P., and Kamps, M. P. (2007). NUP98-NSD1 links H3K36 methylation to Hox-A gene activation and leukaemogenesis. *Nat. Cell Biol.* 9, 804–812. doi: 10.1038/ncb1608

Wong, R. W., Mamede, J. I., and Hope, T. J. (2015). Impact of nucleoporin-mediated chromatin localization and nuclear architecture on HIV integration site selection. *J. Virol.* 89, 9702–9705. doi: 10.1128/JVI.01669-15

Conflict of Interest: The authors declare that the research was conducted in the absence of any commercial or financial relationships that could be construed as a potential conflict of interest.

frontiers in Genetics

TECHNOLOGY AND CODE
published: 21 January 2020
doi: 10.3389/fgene.2019.01372

4See: A Flexible Browser to Explore 4C Data

Yousra Ben Zouari[1,2,3,4], *Angeliki Platania*[1,2,3,4], *Anne M. Molitor*[1,2,3,4] *and Tom Sexton*[1,2,3,4]*

[1] Institute of Genetics and Molecular and Cellular Biology (IGBMC), Illkirch, France, [2] CNRS UMR7104, Illkirch, France, [3] INSERM U1258, Illkirch, France, [4] University of Strasbourg, Illkirch, France

It is established that transcription of many metazoan genes is regulated by distal regulatory sequences beyond the promoter. Enhancers have been identified at up to megabase distances from their regulated genes, and/or proximal to or within the introns of unregulated genes. The unambiguous identification of the target genes of newly identified regulatory elements can thus be challenging. Well-studied enhancers have been found to come into direct physical proximity with regulated genes, presumably by the formation of chromatin loops. Chromosome conformation capture (3C) derivatives that assess the frequency of proximity between different genetic elements is thus a popular method for exploring gene regulation by distal regulatory elements. For studies of chromatin loops and promoter-enhancer communication, 4C (circular chromosome conformation capture) is one of the methods of choice, optimizing cost (required sequencing depth), throughput, and resolution. For ease of visual inspection of 4C data we present 4See, a versatile and user-friendly browser. 4See allows 4C profiles from the same bait to be flexibly plotted together, allowing biological replicates to either be compared, or pooled for comparisons between different cell types or experimental conditions. 4C profiles can be integrated with gene tracks, linear epigenomic profiles, and annotated regions of interest, such as called significant interactions, allowing rapid data exploration with limited computational resources or bioinformatics expertise.

Keywords: 4C, epigenomics, browser, chromatin loops, quantile normalization, biological replicates

OPEN ACCESS

Edited by:
Karim Mekhail,
University of Toronto, Canada

Reviewed by:
Mikhail Spivakov,
Babraham Institute (BBSRC), United Kingdom
Alexander Kouzmenko,
Tokiwa Foundation, Japan

***Correspondence:**
Tom Sexton
sexton@igbmc.fr

Specialty section:
This article was submitted to Epigenomics and Epigenetics, a section of the journal Frontiers in Genetics

Received: *23 September 2019*
Accepted: *16 December 2019*
Published: *21 January 2020*

Citation:
Ben Zouari Y, Platania A, Molitor AM and Sexton T (2020) 4See: A Flexible Browser to Explore 4C Data. Front. Genet. 10:1372. doi: 10.3389/fgene.2019.01372

INTRODUCTION

Since early transgenic studies it has been clear that promoter sequences are insufficient to regulate the spatiotemporal expression patterns of many developmental genes. "Remote control" is additionally conferred by distal activating sequences, termed enhancers, which have been intensively studied over the last years (Schoenfelder and Fraser, 2019). Genome-wide profiling of histone modifications and protein binding sites by ChIP-seq have uncovered a general chromatin signature of enhancer regions: DNase-hypersensitive, bound by the transcriptional coactivator p300, and marked by the monomethylation of lysine-4 of histone H3 (H3K4me1) (Heintzman et al., 2009). Follow-on studies refined these findings further by identifying chromatin features that were characteristic of different enhancer properties. For example, the strongest-acting enhancers are also accompanied by acetylation of lysine-27 of histone H3 (H3K27ac) (Creyghton et al., 2010;

Rada-Iglesias et al., 2011) and/or acetylation on globular histone domains (Pradeepa et al., 2016), recruit RNA polymerase II, and general transcriptional machinery (Koch et al., 2011), and are even transcriptionally active, producing non-coding RNA (eRNAs) (Kim et al., 2010). Enhancers lacking these extra features, and sometimes even encompassing repressive marks, such as H3K27 trimethylation (H3K27me3), are proposed to be "poised" enhancers, which may become activated at later developmental stages. Interestingly, the chromatin states at enhancer sequences vary much more across cell types than those of gene promoters (Roadmap Epigenomics et al., 2015), suggesting that much of the regulatory potential is epigenetically carried by enhancers. However despite advances in identifying enhancers genome-wide, both through epigenomic profiling and high-throughput reporter assays (Arnold et al., 2013; Roadmap Epigenomics et al., 2015), unambiguous identification of their target genes is still a major challenge. Important developmental enhancers have been found at megabase distances from target genes, and/or within the introns of unregulated genes (Lettice et al., 2003; Amano et al., 2009; Herranz et al., 2014); previous studies estimate that up to ~90% of enhancers may indeed skip the closest genes on the linear chromosome fiber (Sanyal et al., 2012; Schoenfelder et al., 2015).

Since the advent of the chromosome conformation capture method (3C) (Dekker et al., 2002) and its variants to measure relative spatial proximity of pairwise genomic regions, many enhancers have been found to physically interact with their target genes, often with "looping out" of the intervening chromatin (Palstra et al., 2003); the resultant "active chromatin hub" has been proposed to provide the permissive regulatory environment for transcription initiation, although the exact mechanism remains unclear. In many studied cases, looping is concomitant with transcriptional induction, whereas in others, the loop is pre-formed to poise the gene for subsequent activation (Schoenfelder and Fraser, 2019). Recent reports using microscopy methods have also been made of enhancers and promoters being well separated on gene activation (Alexander et al., 2019; Benabdallah et al., 2019), although enhancer-promoter interactions were previously reported in the studied loci, raising questions as to whether interactions may completely precede transcription and/or be very transient events. In any case, physical proximity measured by 3C-based methods is becoming a popular means of ascribing target genes to otherwise cryptic distal regulatory elements, or of identifying novel candidate regulatory regions of specific genes of interest. For example, intergenic sequence variants associated with diseases have been better characterized once their target genes were identified by 3C-based approaches (Herranz et al., 2014; Schoenfelder and Fraser, 2019).

With the advent of next-generation sequencing, several higher throughput variants of 3C have been developed to obtain genome-wide chromatin interaction maps. Hi-C is an "all-to-all" method, systematically assessing all pairwise chromatin contacts (Lieberman-Aiden et al., 2009). However, due to the great complexity of the sequenced material, calling specific looping interactions requires prohibitively expensive sequencing depth (Rao et al., 2014; Bonev et al., 2017), and Hi-C loop calling algorithms have been demonstrated to not be very robust (Forcato et al., 2017). A recent modification, Capture Hi-C, incorporates capture with a pool of thousands of oligonucleotides, allowing the complexity of sequenced Hi-C material to be reduced sufficiently to assess the chromatin looping interactions with all promoters (Hughes et al., 2014; Sahlen et al., 2015; Schoenfelder et al., 2015). However, capture libraries can be expensive, and their design still represents a trade-off between coverage of assessed promoters and resolution of the identified loops. For the highest resolution profiling of smaller numbers of candidate regions, the method of choice is the "one-to-all" 4C (circular chromosome conformation capture), which assesses all the chromatin interactions with one specific bait of interest (Simonis et al., 2006; van de Werken et al., 2012) (**Figure 1A**). In brief, nuclei are fixed in their native topologies with formaldehyde, digested with a restriction enzyme and re-ligated, as for 3C, such that chimeric DNA sequences are generated between restriction fragments which may be unlinked on the linear chromosome fiber but are physically proximal at the time of fixation. The purified DNA is then circularized by digestion with a secondary restriction enzyme and re-ligation under dilute conditions, allowing an inverse PCR strategy to amplify all the chimeric DNA linked to a specific bait restriction fragment of interest. The much reduced complexity of a 4C library, compared to that of Hi-C, means that promoter interactomes can be reliably profiled with just a few million sequence reads, and ~20 baits can readily be multiplexed into a sequencing run, making it a much more cost-effective method (van de Werken et al., 2012). The major limitations of 4C are the relatively small throughput in baits that can be assessed at a time, and that the direct sequencing of PCR products confounds results with large numbers of PCR duplicates that cannot be distinguished from counts of true 3C ligation events. However, *in silico* approaches can minimize the impact of PCR duplicates (de Wit et al., 2015), and "unique molecular identifier" variants of 4C have also been developed (Schwartzman et al., 2016).

Due to the growing popularity of 4C experiments, several algorithms have been developed to call significant interactions (van de Werken et al., 2012; Thongjuea et al., 2013; Williams et al., 2014; Klein et al., 2015; Raviram et al., 2016; Geeven et al., 2018); recent benchmarking shows that all methods work well on simulated data, but no single method is optimum for all experimental setups (Walter et al., 2019). However, whereas most of these methods has an in-built tool to plot the static results after data processing, a simple, flexible browser allowing a user to rapidly visualize their 4C results is currently lacking (see **Figure 2** and summary of the different plotting options currently available in **Table 1**). Moreover, while some methods allowed raw and/or smoothed 4C data to be exported as files that can be opened and visualized alongside epigenomic profiles on genome browsers, they offered no flexibility in plotting the epigenomic profiles directly alongside the 4C plot while different smoothing or peak calling parameters are being trialed. We recently developed ChiCMaxima, a suite of tools to analyze Capture Hi-C data, which includes a GUI (graphical user interface) to flexibly visualize data sets alongside gene annotations and epigenomic profiles (Ben Zouari et al., 2019). Here we report

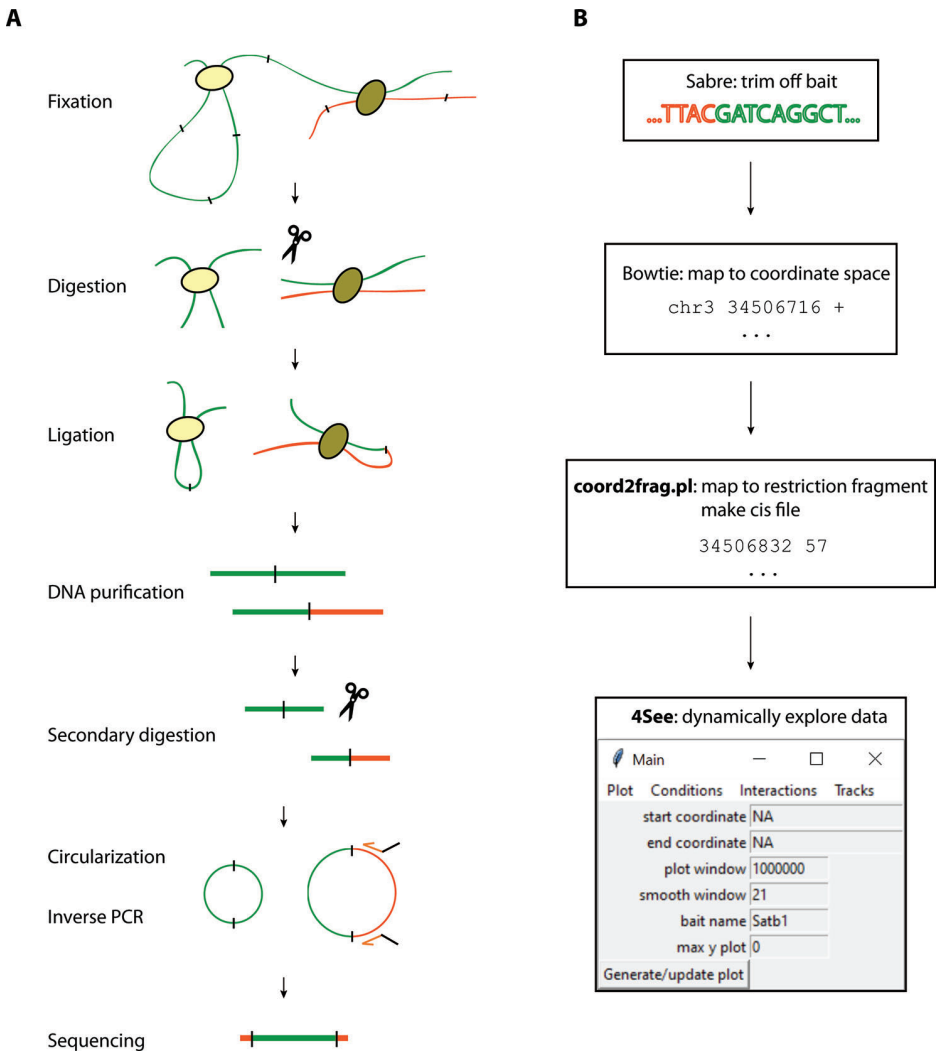

FIGURE 1 | Overview of the 4C method and analysis. **(A)** The 4C method entails chromatin fixation, restriction digestion and re-ligation to generate hybrid sequences between fragments that were physically proximal during fixation. The DNA is purified, digested with a secondary restriction enzyme and re-ligated under dilute conditions to generate DNA circles. Chimeric products linked to a specific bait fragment of interest (orange) are amplified by inverse PCR with bait-specific primers (orange arrows) flanked by Illumina sequencing adapters (black overhangs). The PCR products are then directly loaded onto Illumina flow-cells for high-throughput sequencing. **(B)** Pre-processing steps before 4See; tools denoted in bold accompany this manuscript. The fastq sequences are first trimmed to remove bait restriction fragment sequence (orange), leaving just the prey DNA sequence (green) for mapping to the reference genome with Bowtie. The mapped genomic coordinates are converted to restriction fragment space by a custom perl script, which counts the total number of reads mapping to each fragment on the same chromosome as the bait. This "cis" file can then be directly input into 4See.

4See, the adaptation of ChiCMaxima tools for the user-friendly integrative exploration of 4C data sets. 4See provides flexibility to compare different replicates side by side, or to average them together when comparing experimental conditions, and to visualize 4C profiles at different smoothing window sizes, necessary to identify putative interactions at different distances from the bait, without the need to reload or re-process the initial data. 4See utilizes quantile normalization to allow different plotted profiles to be fairly compared during the visualization. 4See also allows 4C profiles to be easily plotted alongside gene annotations and linear epigenomic tracks, as well as for specific regions (e.g. interactions called by other algorithms) to be highlighted. We anticipate that 4See will be a useful tool to the community for quick and easy exploration of 4C data, particularly when used in conjunction with existing interaction calling tools.

MATERIALS AND METHODS

Pre-Processing

4C

J1 mouse embryonic stem (ES) cells were grown on gamma-irradiated mouse embryonic fibroblast cells under standard

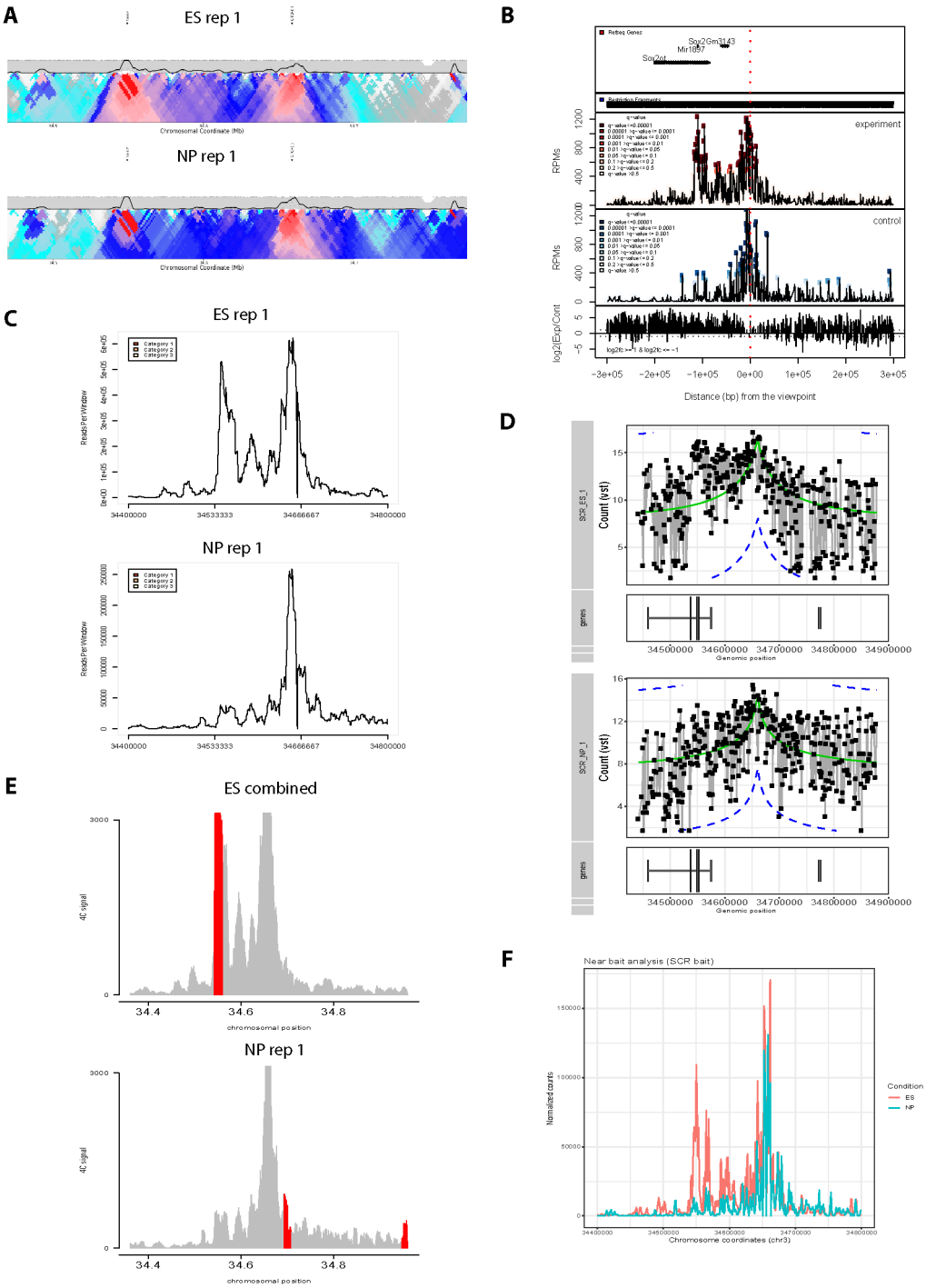

FIGURE 2 | Overview of graphing options from existing 4C analysis methods. All methods have been applied to two ES replicates and one NPC 4C data set for the *Sox2* SCR bait (see also **Figure 3**). **(A)** 4Cseqpipe (van de Werken et al., 2012) results shown independently for one ES replicate and the NPC data set. Running median scores are plotted as a line graph (5 kb resolution), with domainograms plotted underneath as a heat map for median scores at steadily increasing window sizes. Positions of the CTCF site within the SCR and the *Sox2* gene are indicated by arrows. Note that the independent normalization means that the SCR-*Sox2* interaction differences between the two cell types is not evident, compared to other methods. **(B)** r3Cseq (Thongjuea et al., 2013) results for the combined three data sets, showing panels, from top to bottom: positions of Refseq genes; restriction fragment coverage; averaged profile for the "experiment" (ES) condition, with called interactions at different confidence levels highlighted; profile for the "control" (NPC) condition, with called interactions at different confidence levels highlighted; plot of the log2-ratio of experiment vs control 4C signal. The position of the SCR bait is indicated by a red dashed line. Note that r3Cseq appears to call a very large number of

(*continued*)

FIGURE 2 | interactions. **(C)** fourSig (Williams et al., 2014) results shown independently for one ES and one NPC replicate, showing smoothed 4C plots (21-fragment windows). Called interactions ("Categories" 1, 2 or 3, for different confidence levels) would be highlighted on the plot, but none were called by fourSig. **(D)** FourCSeq (Klein et al., 2015) results shown independently for one ES and one NPC replicate, showing normalized and processed 4C signal plots (gray line graphs and black points), alongside the positions of known genes. The green line indicates the centralized 4C value, and the dashed blue lines indicate the threshold values for a z-score difference > 2. Significant interactions would be highlighted, but were not detected by FourCSeq. Note that differences between the two cell types is not so evident, compared to most other methods. **(E)** peakC (Geeven et al., 2018) results shown for the combined analysis of the two ES replicates, independently of the NP replicate, giving smoothed 4C plots (21-fragment windows) as histograms. The red regions indicate called interactions. **(F)** 4C-ker (Raviram et al., 2016) results shown for the combined analysis, with line plots of combined ES (red) and NPC (blue) 4C signal. Note that many interactions were called by 4C-ker within the plotted window for both ES and NP, but that the documentation did not provide a means to plot them alongside the shown line plots.

conditions (4.5 g/L glucose-DMEN, 15% FCS, 0.1 mM non-essential amino acids, 0.1 mM beta-mercaptoethanol, 1 mM glutamine, 500 U/mL LIF, gentamicin), then passaged onto feeder-free 0.2% gelatin-coated plates for at least two passages to remove feeder cells. For *in vitro* differentiation to neural precursor cells (NPCs), F1 ES cells were cultured in the same medium supplemented with 1 μM PD03259010 and 3 μM CHIR99021 ("2i" conditions) and without feeders. The cells were then cultured for six days with medium without LIF or 2i and with 10% FCS, and with 5 μM retinoic acid for the final four days, to generate embryoid bodies (Bibel et al., 2007). J1/F1 ES or differentiated cells were detached with trypsin, then washed by centrifugation in PBS before fixation. Mouse $CD4^+$ $CD8^+$ double-positive (DP) thymocytes were obtained from 4 week old mouse thymus by FACS with anti-CD4-PE and anti-CD8a-FITC antibodies (eBioScience). Both cell preparations were fixed with 2% formaldehyde in mES culture medium for 10 min at 23°C. The fixation was quenched with cold glycine at a final concentration of 125 mM, then cells were washed with PBS and permeabilized on ice for 1 h with 10 mM Tris-HCl, pH 8, 100 mM NaCl, 0.1% NP-40, and protease inhibitors. Nuclei were resuspended in *Dpn*II restriction buffer at 10 million nuclei/mL concentration, and 5 million nuclei aliquots were further permeabilized by treatment for either 1 h with 0.4% SDS at 37°C (ES cells), or for 20 min with 0.7% SDS at 65°C, then for 40 min at 37°C (DP cells). The SDS was then neutralized by incubating for a further 1 h with either 2.6% (ES) or 3.3% (DP) Triton-X100 at 37°C. Nuclei were digested overnight with 1000 U *Dpn*II at 37°C, then washed twice by centrifuging and resuspending in T4 DNA ligase buffer. *In situ* ligation was performed in 400 μL T4 DNA ligase buffer with 20,000 U T4 DNA ligase overnight at 16°C. DNA was purified by reverse cross-linking with an overnight incubation at 65°C with proteinase K, followed by RNase A digestion, phenol/chloroform extraction, and isopropanol precipitation. The DNA was digested with 5 U/μg *Csp*6I at 37°C overnight, then re-purified by phenol/chloroform extraction and isopropanol precipitation. The DNA was then circularized by ligation with 200 U/μg T4 DNA ligase under dilute conditions (5 ng/μL DNA), and purified by phenol/chloroform extraction and isopropanol precipitation. 50 ng aliquots of this DNA were used as template for PCR with bait-specific primers containing Illumina adapter termini (primer sequences and optimal PCR conditions available on request). PCR reactions were pooled, primers removed by washing with 1.8× AMPure XP beads, then quantified on a Bioanalyzer (Agilent) before sequencing with a HiSeq 4000 (Illumina).

Pre-Processing 4C Data for 4See

All bait sequence (including and downstream of the primer sequence, up to but not including the GATC *Dpn*II site) are trimmed by the demultiplexing Sabre tool (https://github.com/najoshi/sabre), allowing two mismatches, before mapping to the mm9 genome with Bowtie (Langmead et al., 2009) (**Figure 1B**). Interaction calling was done with peakC (Geeven et al., 2018) with different window sizes as specified by the parameter wSize.

TABLE 1 | Comparison of graphing options from existing 4C analysis methods.

Method	GUI	Preprocessing	Handles conditions/replicates	Plotting options	Annotations
4Cseqpipe	No	Several custom scripts to convert fastq files to multiple formats and intermediate files. These failed for test data and intermediate files had to be made manually.	No	Can alter trendline resolution and plotting window (coordinate space); domainogram parameters fixed	Limited: manually curated bed file gives arrows on plot
r3Cseq	No	Processes bam files directly	Yes, but restricted to pairwise comparison of "experiment" and "control" conditions	Can only alter plotting window	RefSeq genes
fourSig	No	Custom script converts bam to input format	No	Can only alter plotting window	None
FourCSeq	No	Need to set up metadata table in R, which points to processed bam files	Handled in one combined object, but default is to plot each data set individually, and documentation does not say how to do otherwise.	Can only alter plotting window	Positions of genes from transcriptome (unlabeled)
4C-ker	No	Requires bed file of restriction fragments and bedgraph of 4C coverage per observed fragment. Custom scripts to generate from sam files failed and input files had to be made manually.	Yes	In principle, many settings can be changed in the R command prompt (ggplot2 call settings), but is not documented or user-friendly	None
peakC	No	Essentially the same as this manuscript, but utility scripts not provided	Handles replicates but not different conditions	Can only alter plotting window	None

For previously published 4C results (Narendra et al., 2015), fastq files were downloaded from the Gene Expression Omnibus and processed just like the other data sets.

Analysis and Plotting of 4C Data Sets by Other Methods

Three 4C data sets (two replicates from ES cells; one replicate from *in vitro* differentiation of ES cells towards NPCs) were analyzed and plotted by 4Cseqpipe (van de Werken et al., 2012), r3Cseq (Thongjuea et al., 2013), fourSig (Williams et al., 2014), FourCSeq (Klein et al., 2015), 4C-ker (Raviram et al., 2016), and peakC (Geeven et al., 2018), using the default or recommended parameters given within the documentation accompanying the tools.

4See

System Requirements

4See is a GUI written in R (version > = 3.2), with the following packages (and their dependencies) additionally required, found on Bioconductor and/or CRAN: tcltk2, tkrplot, limma, caTools, rtracklayer. All scripts and test data are available under the terms of the GNU General Public License, version 3, on Github: https://github.com/TomSexton00/4See. The GUI is launched by sourcing the main script, 4See.r, from within an R environment. From then on, all manipulation is performed from a windows interface, and does not require use of command prompts. A full user manual in pdf format is also found with the scripts on Github, and is provided as **Supplementary Data**.

Input Format

4See deals with a simple text format, which we term the "cis" format, entailing a header with three tab-delimited fields (data set name, bait chromosome, bait coordinate) followed by a two-column table, denoting the coordinate of the mid-point of every restriction fragment found on the same chromosome as the bait, and its corresponding number of supporting sequence reads. The cis format is generated by a perl script, coord2frag.pl, provided with 4See, which maps the genomic coordinates of 4C sequencing results into their corresponding restriction fragments and then counts the number of reads for each fragment. The perl script accepts any non-headed text format for sequences, as long as a column for chromosome, coordinate, and strand can be specified. The restriction fragment information is provided by "frag" tables, headed four-column tables, giving a unique integer identifier, the chromosome, coordinate, and fragment length for each restriction fragment. These in turn are generated by a provided perl script, makefrags.pl, requiring a user input for the sequence of the primary restriction enzyme cutting site, and a folder containing the sequences in fasta format for each chromosome of the genome assembly used. The header of the cis file provides the required information on the bait location and 4C data set name, but is also used to ensure that only 4C data sets for the same bait (with identical bait chromosome and coordinate) are treated together.

Managing Conditions and Replicates

After loading one or more cis files, 4See opens a dialog box allowing the user to determine how to handle different conditions and replicates by assigning a value to each data set (**Figures 3A, C**). All 4C data sets assigned a non-zero integer are quantile normalized for fairer comparison across data sets (Ritchie et al., 2015). Data sets given the same value are averaged together before plotting; those assigned zero are omitted from normalization and plotting. Additional options allow the plotting color and data label to be specified by the user, and these can be re-run *via* the "Conditions" drop-down menu. Thus a user can rapidly compare different replicates side by side, or average them into one plot for comparison with different cell types or conditions, without needing to reload the data (**Figures 3B, D**).

Plot Settings

4C profiles and the chromatin interactions they uncover differ with bait and experimental condition. In particular, the ease of distinguishing peaks of 4C signal above background depends on the distance of the interaction, since background signal of random chromosome collisions is much higher at shorter ranges (Dekker et al., 2002; Lieberman-Aiden et al., 2009). Other factors, such as whether the interaction is sharp with a single regulatory element, or is broadened across larger regions, such as "super-enhancers", or the extent to which very short-range contacts dominate the plot and hide longer-range loops (which may be a consequence of the 4C digestion efficiency and/or relative compaction of the assessed locus), mean that features of chromatin topology are often overlooked with one fixed plot setting. The control panel of 4See includes options for the user to alter the region plotted, up to ± 1.5 Mb of the bait position, and to set a maximum plotted value on the y-axis (4C signal), to better visualize certain aspects of the 4C profile (**Figure 4A**). However a major confounding factor in visualizing 4C data is the need to smooth the plots, since "spikes" from spurious PCR duplicates make them appear very noisy at single restriction fragment resolution. Most analytical approaches counter this by taking running means (or medians) of sliding windows, but the results can be heavily influenced by the choice of window size. Reflecting this challenge, some 4C analytical tools adopt a "domainogram" approach, whereby averages are taken over many sliding windows of many different sizes, and the results are pooled together in a heat map (de Wit et al., 2008; van de Werken et al., 2012; see also **Figure 2A**), although the visual interpretation of these results is often challenging. To aid user choice in setting appropriate parameters for their particular 4C profile, 4See allows the window size (in numbers of restriction fragments) to be altered, and the appropriate running mean is calculated on the quantile normalized (and averaged, if replicates are pooled) data before plotting. In this manner, different aspects of chromosome topology can be readily explored (**Figures 4B, C**).

Annotations

To put the 4C profiles into a wider biological context, 4See supports the inclusion of three different types of annotations:

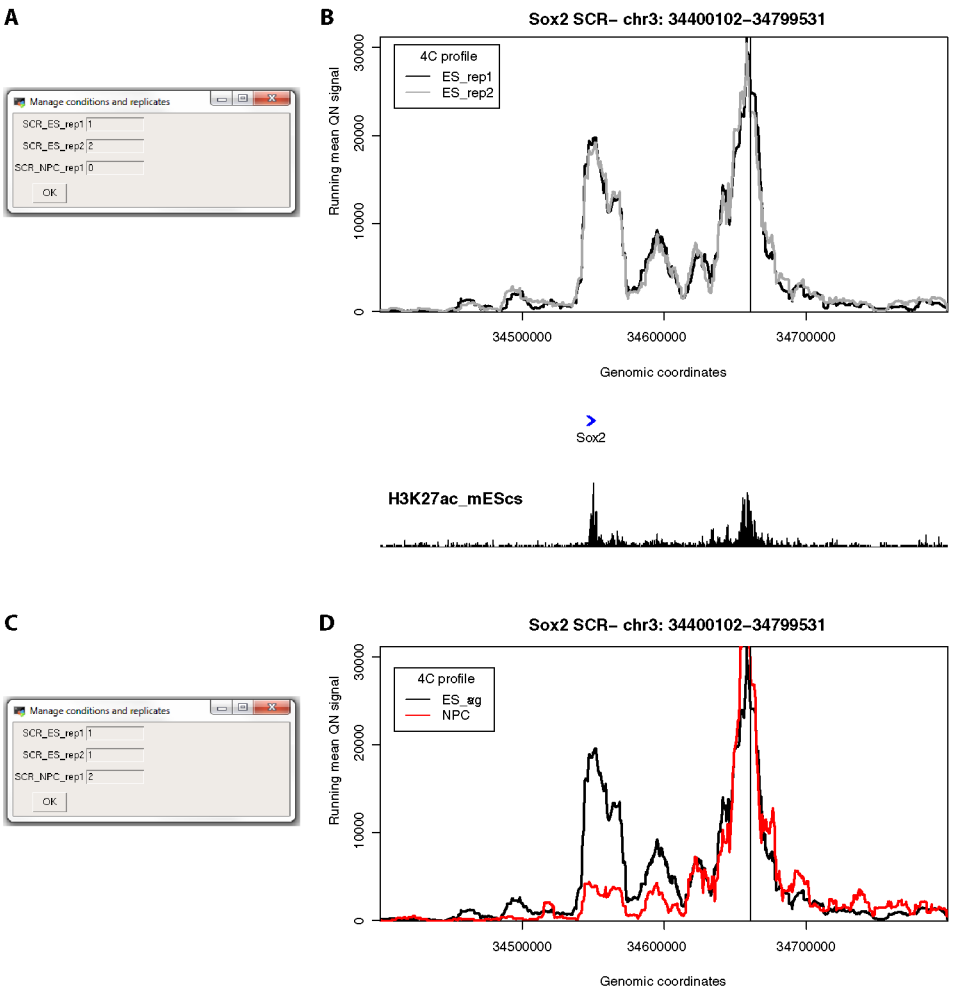

FIGURE 3 | 4See provides flexibility in handling multiple replicates and/or experimental conditions. **(A)** The 4See dialog box for conditions settings automatically opens when cis files are first loaded, in this instance two ES replicates and one NPC 4C data set for the *Sox2* SCR bait. The two ES replicates have been assigned different integers to be treated independently, and the NPC data set has been omitted by assigning it 0. **(B)** The resultant 4See plot from the conditions set in **(A)**, whereby the two ES 4C replicates are quantile normalized and plotted separately, one in black, the other gray. The plot has normalized 4C signal as the y-axis and genomic coordinate of the interacting fragment as the x-axis. The position of the SCR bait is denoted by a black vertical line, and gene position (blue arrows) and the ES H3K27ac ChIP-seq profile (black) is shown underneath the 4C plot. The profiles are highly consistent between replicates, with a strong interaction peak centered on the *Sox2* gene; note that both the gene and enhancer have a strong enrichment for H3K27ac. **(C)** As for **(A)**, but in this case the two ES replicates are given the same value to be averaged together, and the NPC data set is included as a different integer to the ES data sets. **(D)** As for **(B)**, but with the settings conditions of **(C)**, and the redundant gene and H3K27ac tracks omitted. The averaged ES 4C plot is given in black and the NPC 4C plot in red, showing a strong perturbation of the SCR-*Sox2* interaction on differentiation.

genes, linear epigenomic profiles (termed "tracks") and called interactions. Gene information is provided as a tab-delimited headed text file with the following fields: Name, Chr (with the prefix "chr"), Start, End, Strand (as "+" or "–"). When selected, the gene track is plotted in blue directly underneath the 4C profile. Only one gene track can be loaded at a time. Management of epigenomic profiles is more flexible. Any format supported by the *import* function of the rtracklayer package can be supported, but for running time efficiency we recommend loading bigWig files. As for the 4C profiles, the color and plotting level for each individual track can be altered by the user in an automatically loaded dialog box. As before, the plotting levels can be 0 (not plotted), or consecutive, positive integers. When tracks have the same level, their plots are auto-scaled to the maximum value of all of the included data sets within the plotted window. This feature allows fairer comparison for the same epigenetic mark across different conditions/tissue types (**Figure 5**). Technically, the numbers of tracks that can be loaded is only limited by system memory, although the plots become difficult to visually interpret after more than four tracks are loaded at a time.

To better highlight interactions called by existing peak-calling methods, or indeed to test how different methods and/or their parameters perform on specific 4C profiles, interactions (as bed

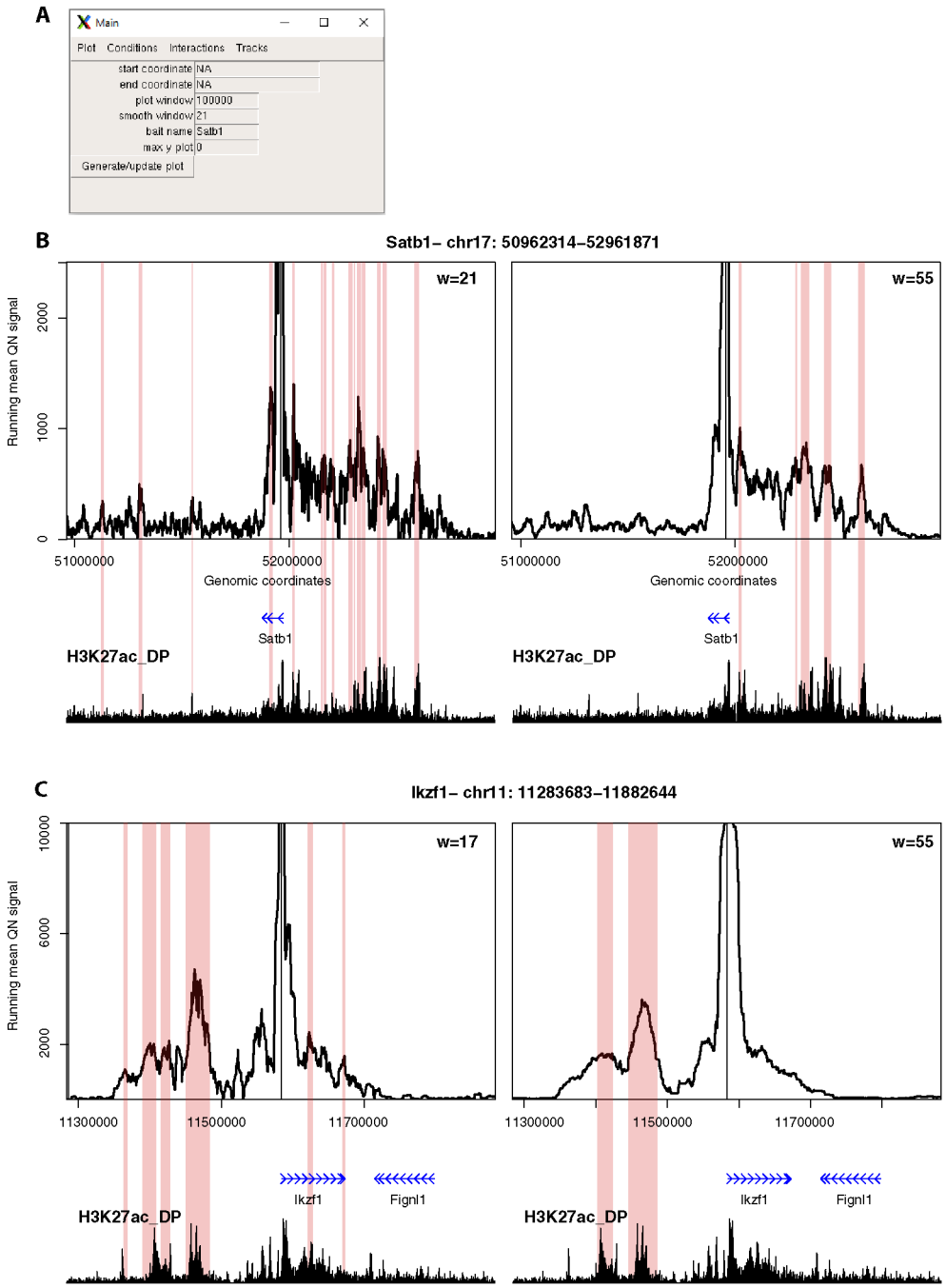

FIGURE 4 | 4See provides flexibility in running mean window sizes. **(A)** The main control panel of 4See, including options to set the x-axis ("start coordinate," "end coordinate," and "plot window") and y-axis ("max y plot") plot limits, to choose a bait name for the plot title ("bait name"), and to set the running mean window size ("smooth window") in number of restriction fragments. **(B)** 4See plots for a 4C data set in DP thymocytes with the *Satb1* gene promoter as bait. Two instances of the same x- and y-axis limits are shown, with a running mean window of 21 (left) or 55 (right) fragments. The position of the *Satb1* bait is denoted by a black vertical line, and gene position (blue arrows) and the DP H3K27ac ChIP-seq profile (black) is shown underneath the 4C plots. Pink rectangles denote regions called as interacting by peakC for the equivalent window size as the plot. For the long-range interaction, the smaller window size appears to have more spurious called interactions, less evidently linked to H3K27ac peaks; the link is better seen with greater smoothing from a larger window size. **(C)** As for **(B)**, but with the *Ikzf1* gene promoter as bait. In this case, the smaller window size (17 fragments) seems to give better resolution of specific interactions with distinct putative enhancers, which are merged into one at larger window sizes.

files or similar, with headed "chr", "start," and "end" columns) can also be loaded, and these are represented as rectangles flanking the relevant region on the 4C profile (**Figures 4B, C**). A dialog box allows the user to alter the color of the annotation and to check whether or not it is plotted. The latter feature is useful since simultaneous plotting of more than one interactions set, which often overlap, can be difficult to visually interpret. Note that whereas these are labeled "Interactions" by 4See, any region described by a bed file can be highlighted in this manner. The user can thus use this setting to highlight any feature of interest, such as called differential interactions between two 4C data sets, or the presence of specific sequence motifs (e.g. CTCF) that may be expected to be enriched at interactions.

Exporting 4See Results

Once the user settings have been finalized, a pull-down menu option allows the plot to be saved in.eps format, where it can be further processed in preparation of a figure for publication or presentation. Alternatively, the data that are actually plotted in the current 4See window (one or more quantile-normalized 4C profiles with a running mean of a specified window size applied) can be exported as bedGraph files, ready for integration into other browsers, such as local instances of UCSC (Kent et al., 2002) or IGV (Robinson et al., 2011).

RESULTS

We demonstrate the usefulness of 4See on different original and previously published 4C data sets. First, we investigate the interaction between the mouse *Sox2* gene and an established cluster of enhancers (the "SCR", or *Sox2* control region), which has been shown to be essential for *Sox2* expression in pluripotent cells (Zhou et al., 2014). Using bait primers at the SCR, we generated two biological replicates for ES cells and one after *in vitro* differentiation ("NPC"; **Figure 3**). As expected, we observed a strong interaction with the *Sox2* gene which is greatly reduced on differentiation. After loading the three data sets into the 4See browser, only changing the options within one dialog box is required to switch the view from plotting the two ES biological replicates side by side (omitting the differentiated data set) to confirm that they have consistent profiles, to comparing the averaged ES profile with the differentiated one.

Second, we explored different distance ranges of promoter-enhancer interactions at key developmental genes in mouse $CD4^+/CD8^+$ (double-positive, DP) thymocytes, namely the distal (~500 kb) enhancer cluster for *Satb1*, and the shorter-range (~50 kb) enhancer for *Ikzf1* (**Figure 4**). Comparing 4C plots at different running mean window sizes, it is apparent that different insights can be gained, and that no one window size is optimum for all profiles. For *Satb1*, shorter window sizes create what appear to be noisy profiles at the large genomic span assessed, and specific interactions are harder to discern. When the running mean window size is increased, the profile becomes smoother, and apparent peaks line up well with putative enhancers, as denoted by the presence of H3K27ac. Conversely, at the shorter distances assessed at the *Ikzf1* locus, a smaller window size allows interactions with specific enhancers to be resolved, whereas they merge into one large peak at larger window sizes. In support of this observation, we called interactions using the peakC algorithm (Geeven et al., 2018) at different window sizes, and found a good visual corroboration between discernible peaks and called interactions. 4See allows rapid re-plotting of 4C profiles with different window sizes, and also has the functionalities for adding the epigenomic profile and highlighting called interactions directly on the plot.

Third, we compared the same *Satb1* promoter-enhancer interaction between DP thymocytes, where the gene is highly expressed, and ES cells, where the gene is silent (**Figure 5**). As expected, the gene does not make any specific contacts with the thymocyte enhancer in ES cells. This locus is largely devoid of H3K27ac in ES cells, but a common problem with some browsers is that an automatic scaling creates some apparent peaks from noise on a small range of the y-axis (**Figure 5B**). 4See counters this by providing flexibility with how the epigenomic tracks are handled. By coercing the two tracks to the same scale, the difference between the two tissues is much more evident (**Figure 5C**).

Finally, we used 4See to re-analyze published 4C data, namely comparing profiles from the *Hoxa5* gene between wild-type ES cells and those where one or more key CTCF insulator sites have been deleted (Narendra et al., 2015). In this study, the authors reported that CTCF site loss caused topological defects during differentiation to neurons, with inappropriate spreading of H3K27me3. However, their analyses concluded that the topology of the *Hoxa* locus was largely unchanged in pluripotent cells (**Figure 6A**). Plotting the same data with 4See, it appears that ectopic looping interactions are formed between *Hoxa5* and more caudal regions of the locus (**Figure 6B**). Different loop calling algorithms with different parameter choices were inconsistent in calling these apparent interactions as "significant", and only one biological replicate was available, so the importance of this observation is yet to be confirmed. In any case, the CTCF site deletion did not alter H3K27me3 patterning or *Hoxa* gene expression within undifferentiated ES cells (Narendra et al., 2015), so any potential topological changes do not appear to be borne out in other phenotypes. However, we wish to use this example to highlight how the use of a flexible browser like 4See facilitates exploration of the data, potentially identifying new features that "one size fits all" algorithms may overlook.

DISCUSSION

Using novel and previously published data sets for demonstration, we have shown the flexibility and utility of 4See in exploring 4C data. With limited processing of sequencing results, and one line of code in the R prompt, a user-friendly windows-based interface is available for a broader community to explore chromatin interaction profiles. As a consequence, we envisage that 4See will be of great use to the

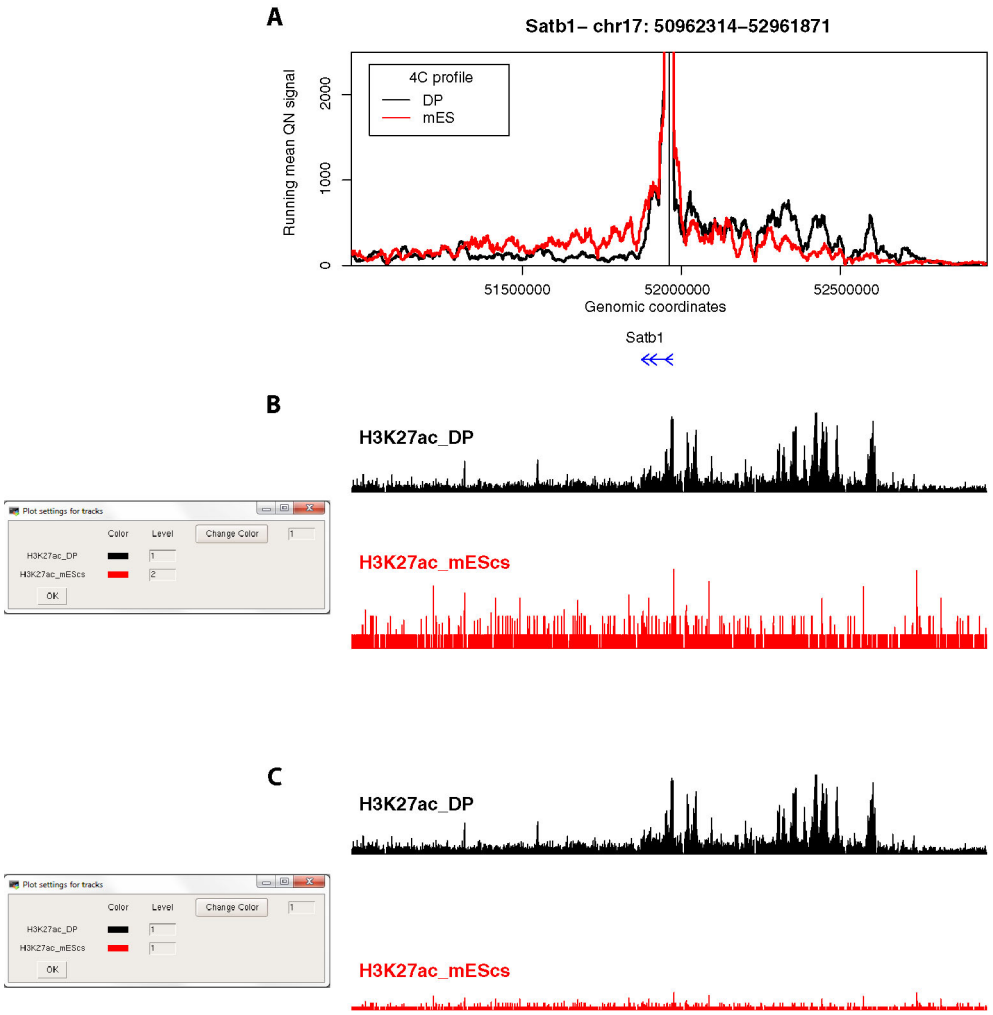

FIGURE 5 | 4See provides flexibility in handling epigenomic track scales. **(A)** The same 4C profile as **Figure 4B** (55-fragment window size; black) is plotted alongside the 4C profile for ES cells, where the locus is silent, and thymocyte enhancer interactions are not evident. **(B)** The 4See dialog box for managing epigenomic tracks defines how the different tracks are scaled. In this case, the ChIP-seq tracks for H3K27ac in ES and DP cells are treated independently, so the autoscaling of the ES track creates some spurious peaks from noise above background. **(C)** As for **(B)**, but this time the two H3K27ac tracks have been set the same integer, making the lower ES signal much more visually apparent in the plot.

chromatin field. The input cis files are not very large (~ 4 MB for mouse or human), so the browser can be run on most desktop computers and laptops. The major systems limitation comes from the importing of epigenomic tracks (which can be >500 MB) with the rtracklayer package, which is the slowest step and may overload some standalone computers if too many tracks are imported at once. If the user is interested in only a specific set of baits, the system load can be reduced by restricting imports to chromosome-specific tracks. Due to the reliance of 4See plotting on quantile normalization, which is confounded by an excessive number of zeros or very small values, 4See is not an appropriate tool for visualizing very long-range (>1.5 Mb) or interchromosomal interactions; although their built-in graphical capabilities are more limited, the tools linked to algorithms such as fourSig should be used instead (Williams et al., 2014; Walter et al., 2019). It should also be noted that 4See does not replace the existing suite of interaction calling algorithms (Walter et al., 2019). Indeed, due to its capacity to incorporate these algorithms' results into the plots, 4See should be viewed as a complementary tool for comprehensive 4C analysis, whereby the results of the algorithms can be readily visualized and compared to epigenomic tracks for validation and obtaining biological insight. Overall, 4See, in conjunction with other analytical tools, promises to facilitate chromatin interaction exploration, and will thus be of use to the epigenetics community.

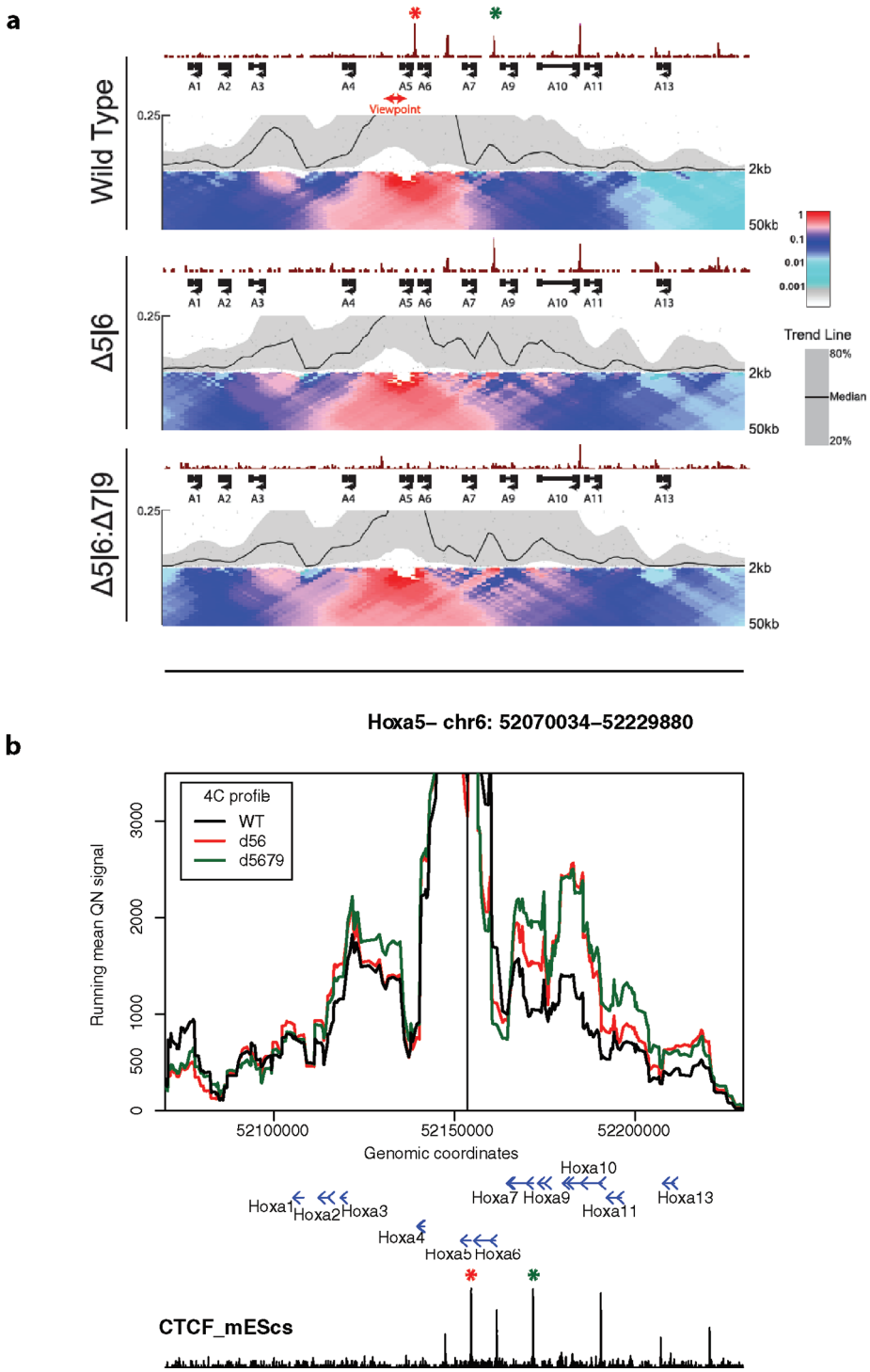

FIGURE 6 | 4See exploration can uncover previously overlooked features of chromatin topology. **(A)** Reproduced Supplemental Fig 7A from Narendra et al. (2015), used with permission. 4C profiles from the *Hoxa5* bait are shown as domainogram heat maps for wild-type ES cells (top), as well as lines that have had deletions of one CTCF site (middle; site of deletion denoted by red asterisk) or two (bottom; additional deletion site denoted by green asterisk). The CTCF ChIP-seq profile is shown above the 4C sets. No chromatin topology differences are apparent between these cell lines, and the original study concluded that spatial phenotypes only occurred on cell differentiation (Narendra et al., 2015). **(B)** The same data, processed and plotted using 4See. The position of the *Hoxa5* bait is denoted by a black vertical line, and gene position (blue arrows) and the ES CTCF ChIP-seq profile (black) is shown underneath the 4C plots. Red and green asterisks denote the positions of the single and double CTCF site deletions, as for **(A)**. In this plot, CTCF-dependent restriction of interactions between *Hoxa5* and more caudal regions (e.g. the gene body of *Hoxa10*) seems apparent.

DATA AVAILABILITY STATEMENT

Raw 4C data and the processed cis files first described here are available on GEO (GSE137417); previously published 4C results (Narendra et al., 2015) are available as data set GSE60240. ChIP-seq tracks were obtained from GEO for mouse ES (Shen et al., 2012) (CTCF and H3K27ac; GSE29218) and DP cells (Vanhille et al., 2015) (H3K27ac; GSE63732).

AUTHOR CONTRIBUTIONS

YBZ and TS designed and wrote the 4See code and accompanying scripts. AP and AM performed 4C experiments and preprocessing. TS wrote the manuscript, with continuous feedback from all authors.

FUNDING

This study was supported by funds from the European Research Council (ERC) under the European Union's Horizon 2020 research and innovation program (Starting Grant 678624-CHROMTOPOLOGY), the ATIP-Avenir program, and the grant ANR-10-LABX-0030-INRT, a French State fund managed by the Agence Nationale de la Recherche under the frame program Investissements d'Avenir ANR-10-IDEX-0002-02. YBZ is supported by funds from LabEX INRT, la Region Grand Est and the ERC. AP is supported by funds from LabEX INRT, the ERC, and the Ligue Nationale Contre le Cancer. AM is supported by funds from IDEX (University of Strasbourg) and the Institut National du Cancer. TS is supported by INSERM.

ACKNOWLEDGMENTS

Sequencing was performed by the IGBMC GenomEast platform, a member of the France Genomique consortium (ANR-10-INBS-0009). We thank Claudine Ebel and Muriel Philipps for their support within the flow cytometry platform.

SUPPLEMENTARY MATERIAL

The Supplementary Material for this article can be found online at: https://www.frontiersin.org/articles/10.3389/fgene.2019.01372/full#supplementary-material

REFERENCES

Alexander, J. M., Guan, J., Li, B., Maliskova, L., Song, M., Shen, Y., et al. (2019). Live-cell imaging reveals enhancer-dependent Sox2 transcription in the absence of enhancer proximity. *Elife* 8, e41769. doi: 10.7554/eLife.41769

Amano, T., Sagai, T., Tanabe, H., Mizushina, Y., Nakazawa, H., and Shiroishi, T. (2009). Chromosomal dynamics at the Shh locus: limb bud-specific differential regulation of competence and active transcription. *Dev. Cell* 16 (1), 47–57. doi: 10.1016/j.devcel.2008.11.011

Arnold, C. D., Gerlach, D., Stelzer, C., Boryn, L. M., Rath, M., and Stark, A. (2013). Genome-wide quantitative enhancer activity maps identified by STARR-seq. *Science* 339 (6123), 1074–1077. doi: 10.1126/science.1232542

Ben Zouari, Y., Molitor, A. M., Sikorska, N., Pancaldi, V., and Sexton, T. (2019). ChiCMaxima: a robust and simple pipeline for detection and visualization of chromatin looping in Capture Hi-C. *Genome Biol.* 20 (1), 102. doi: 10.1186/s13059-019-1706-3

Benabdallah, N. S., Williamson, I., Illingworth, R. S., Kane, L., Boyle, S., Sengupta, D., et al. (2019). Decreased enhancer-promoter proximity accompanying enhancer activation. *Mol. Cell.* 76 (3), 473–484. doi: 10.1016/j.molcel.2019.07.038

Bibel, M., Richter, J., Lacroix, E., and Barde, Y. A. (2007). Generation of a defined and uniform population of CNS progenitors and neurons from mouse embryonic stem cells. *Nat. Protoc.* 2 (5), 1034–1043. doi: 10.1038/nprot.2007.147

Bonev, B., Mendelson Cohen, N., Szabo, Q., Fritsch, L., Papadopoulos, G. L., Lubling, Y., et al. (2017). Multiscale 3D genome rewiring during mouse neural development. *Cell* 171 (3), 557–572 e524. doi: 10.1016/j.cell.2017.09.043

Creyghton, M. P., Cheng, A. W., Welstead, G. G., Kooistra, T., Carey, B. W., Steine, E. J., et al. (2010).). Histone H3K27ac separates active from poised enhancers and predicts developmental state. *Proc. Natl. Acad. Sci. U.S.A.* 107 (50), 21931–21936. doi: 10.1073/pnas.1016071107

de Wit, E., Braunschweig, U., Greil, F., Bussemaker, H. J., and van Steensel, B. (2008). Global chromatin domain organization of the Drosophila genome. *PloS Genet.* 4 (3), e1000045. doi: 10.1371/journal.pgen.1000045

de Wit, E., Vos, E. S., Holwerda, S. J., Valdes-Quezada, C., Verstegen, M. J., Teunissen, H., et al. (2015). CTCF binding polarity determines chromatin looping. *Mol. Cell* 60 (4), 676–684. doi: 10.1016/j.molcel.2015.09.023

Dekker, J., Rippe, K., Dekker, M., and Kleckner, N. (2002). Capturing chromosome conformation. *Science* 295 (5558), 1306–1311. doi: 10.1126/science.1067799

Forcato, M., Nicoletti, C., Pal, K., Livi, C. M., Ferrari, F., and Bicciato, S. (2017). Comparison of computational methods for Hi-C data analysis. *Nat. Methods* 14 (7), 679–685. doi: 10.1038/nmeth.4325

Geeven, G., Teunissen, H., de Laat, W., and de Wit, E. (2018). peakC: a flexible, non-parametric peak calling package for 4C and Capture-C data. *Nucleic Acids Res.* 46 (15), e91. doi: 10.1093/nar/gky443

Heintzman, N. D., Hon, G. C., Hawkins, R. D., Kheradpour, P., Stark, A., Harp, L. F., et al. (2009). Histone modifications at human enhancers reflect global cell-type-specific gene expression. *Nature* 459 (7243), 108–112. doi: 10.1038/nature07829

Herranz, D., Ambesi-Impiombato, A., Palomero, T., Schnell, S. A., Belver, L., Wendorff, A. A., et al. (2014). A NOTCH1-driven MYC enhancer promotes T cell development, transformation and acute lymphoblastic leukemia. *Nat. Med.* 20 (10), 1130–1137. doi: 10.1038/nm.3665

Hughes, J. R., Roberts, N., McGowan, S., Hay, D., Giannoulatou, E., Lynch, M., et al. (2014). Analysis of hundreds of cis-regulatory landscapes at high resolution in a single, high-throughput experiment. *Nat. Genet.* 46 (2), 205–212. doi: 10.1038/ng.2871

Kent, W. J., Sugnet, C. W., Furey, T. S., Roskin, K. M., Pringle, T. H., Zahler, A. M., et al. (2002). The human genome browser at UCSC. *Genome Res.* 12 (6), 996–1006. doi: 10.1101/gr.229102

Kim, T. K., Hemberg, M., Gray, J. M., Costa, A. M., Bear, D. M., Wu, J., et al. (2010). Widespread transcription at neuronal activity-regulated enhancers. *Nature* 465 (7295), 182–187. doi: 10.1038/nature09033

Klein, F. A., Pakozdi, T., Anders, S., Ghavi-Helm, Y., Furlong, E. E., and Huber, W. (2015). FourCSeq: analysis of 4C sequencing data. *Bioinformatics* 31 (19), 3085–3091. doi: 10.1093/bioinformatics/btv335

Koch, F., Fenouil, R., Gut, M., Cauchy, P., Albert, T. K., Zacarias-Cabeza, J., et al. (2011). Transcription initiation platforms and GTF recruitment at tissue-specific enhancers and promoters. *Nat. Struct. Mol. Biol.* 18 (8), 956–963. doi: 10.1038/nsmb.2085

Langmead, B., Trapnell, C., Pop, M., and Salzberg, S. L. (2009). Ultrafast and memory-efficient alignment of short DNA sequences to the human genome. *Genome Biol.* 10 (3), R25. doi: 10.1186/gb-2009-10-3-r25

Lettice, L. A., Heaney, S. J., Purdie, L. A., Li, L., de Beer, P., Oostra, B. A., et al. (2003). A long-range Shh enhancer regulates expression in the developing limb and fin and is associated with preaxial polydactyly. *Hum. Mol. Genet.* 12 (14), 1725–1735. doi: 10.1093/hmg/ddg180

Lieberman-Aiden, E., van Berkum, N. L., Williams, L., Imakaev, M., Ragoczy, T., Telling, A., et al. (2009). Comprehensive mapping of long-range interactions reveals folding principles of the human genome. *Science* 326 (5950), 289–293. doi: 10.1126/science.1181369

Narendra, V., Rocha, P. P., An, D., Raviram, R., Skok, J. A., Mazzoni, E. O., et al. (2015). CTCF establishes discrete functional chromatin domains at the Hox clusters during differentiation. *Science* 347 (6225), 1017–1021. doi: 10.1126/science.1262088

Palstra, R. J., Tolhuis, B., Splinter, E., Nijmeijer, R., Grosveld, F., and de Laat, W. (2003). The beta-globin nuclear compartment in development and erythroid differentiation. *Nat. Genet.* 35 (2), 190–194. doi: 10.1038/ng1244

Pradeepa, M. M., Grimes, G. R., Kumar, Y., Olley, G., Taylor, G. C., Schneider, R., et al. (2016). Histone H3 globular domain acetylation identifies a new class of enhancers. *Nat. Genet.* 48 (6), 681–686. doi: 10.1038/ng.3550

Rada-Iglesias, A., Bajpai, R., Swigut, T., Brugmann, S. A., Flynn, R. A., and Wysocka, J. (2011). A unique chromatin signature uncovers early developmental enhancers in humans. *Nature* 470 (7333), 279–283. doi: 10.1038/nature09692

Rao, S. S., Huntley, M. H., Durand, N. C., Stamenova, E. K., Bochkov, I. D., Robinson, J. T., et al. (2014). A 3D map of the human genome at kilobase resolution reveals principles of chromatin looping. *Cell* 159 (7), 1665–1680. doi: 10.1016/j.cell.2014.11.021

Raviram, R., Rocha, P. P., Muller, C. L., Miraldi, E. R., Badri, S., Fu, Y., et al. (2016). 4C-ker: A Method to Reproducibly Identify Genome-Wide Interactions Captured by 4C-Seq Experiments. *PloS Comput. Biol.* 12 (3), e1004780. doi: 10.1371/journal.pcbi.1004780

Ritchie, M. E., Phipson, B., Wu, D., Hu, Y., Law, C. W., Shi, W., et al. (2015). limma powers differential expression analyses for RNA-sequencing and microarray studies. *Nucleic Acids Res.* 43 (7), e47. doi: 10.1093/nar/gkv007

Roadmap Epigenomics, C., Kundaje, A., Meuleman, W., Ernst, J., Bilenky, M., Yen, A., et al. (2015). Integrative analysis of 111 reference human epigenomes. *Nature* 518 (7539), 317–330. doi: 10.1038/nature14248

Robinson, J. T., Thorvaldsdóttir, H., Winckler, W., Guttman, M., Lander, E. S., Getz, G., et al. (2011). Integrative genomics viewer. *Nat. Biotech.* 29 (1), 24–26. doi: 10.1038/nbt.1754

Sahlen, P., Abdullayev, I., Ramskold, D., Matskova, L., Rilakovic, N., Lotstedt, B., et al. (2015). Genome-wide mapping of promoter-anchored interactions with close to single-enhancer resolution. *Genome Biol.* 16, 156. doi: 10.1186/s13059-015-0727-9

Sanyal, A., Lajoie, B. R., Jain, G., and Dekker, J. (2012). The long-range interaction landscape of gene promoters. *Nature* 489 (7414), 109–113. doi: 10.1038/nature11279

Schoenfelder, S., and Fraser, P. (2019). Long-range enhancer-promoter contacts in gene expression control. *Nat. Rev. Genet.* 20 (8), 437–455. doi: 10.1038/s41576-019-0128-0

Schoenfelder, S., Furlan-Magaril, M., Mifsud, B., Tavares-Cadete, F., Sugar, R., Javierre, B. M., et al. (2015). The pluripotent regulatory circuitry connecting promoters to their long-range interacting elements. *Genome Res.* 25 (4), 582–597. doi: 10.1101/gr.185272.114

Schwartzman, O., Mukamel, Z., Oded-Elkayam, N., Olivares-Chauvet, P., Lubling, Y., Landan, G., et al. (2016). UMI-4C for quantitative and targeted chromosomal contact profiling. *Nat. Methods* 13 (8), 685–691. doi: 10.1038/nmeth.3922

Shen, Y., Yue, F., McCleary, D. F., Ye, Z., Edsall, L., Kuan, S., et al. (2012). A map of the cis-regulatory sequences in the mouse genome. *Nature* 488 (7409), 116–120. doi: 10.1038/nature11243

Simonis, M., Klous, P., Splinter, E., Moshkin, Y., Willemsen, R., de Wit, E., et al. (2006). Nuclear organization of active and inactive chromatin domains uncovered by chromosome conformation capture-on-chip (4C). *Nat. Genet.* 38 (11), 1348–1354. doi: 10.1038/ng1896

Thongjuea, S., Stadhouders, R., Grosveld, F. G., Soler, E., and Lenhard, B. (2013). r3Cseq: an R/Bioconductor package for the discovery of long-range genomic interactions from chromosome conformation capture and next-generation sequencing data. *Nucleic Acids Res.* 41 (13), e132. doi: 10.1093/nar/gkt373

van de Werken, H. J., Landan, G., Holwerda, S. J., Hoichman, M., Klous, P., Chachik, R., et al. (2012). Robust 4C-seq data analysis to screen for regulatory DNA interactions. *Nat. Methods* 9 (10), 969–972. doi: 10.1038/nmeth.2173

Vanhille, L., Griffon, A., Maqbool, M. A., Zacarias-Cabeza, J., Dao, L. T., Fernandez, N., et al. (2015). High-throughput and quantitative assessment of enhancer activity in mammals by CapStarr-seq. *Nat. Commun.* 6, 6905. doi: 10.1038/ncomms7905

Walter, C., Schuetzmann, D., Rosenbauer, F., and Dugas, M. (2019). Benchmarking of 4C-seq pipelines based on real and simulated data. *Bioinformatics* 35 (23), 4938–4945. doi: 10.1093/bioinformatics/btz426

Williams, R. L. Jr., Starmer, J., Mugford, J. W., Calabrese, J. M., Mieczkowski, P., Yee, D., et al. (2014). fourSig: a method for determining chromosomal interactions in 4C-Seq data. *Nucleic Acids Res.* 42 (8), e68. doi: 10.1093/nar/gku156

Zhou, H. Y., Katsman, Y., Dhaliwal, N. K., Davidson, S., Macpherson, N. N., Sakthidevi, M., et al. (2014). A Sox2 distal enhancer cluster regulates embryonic stem cell differentiation potential. *Genes Dev.* 28 (24), 2699–2711. doi: 10.1101/gad.248526.114

Conflict of Interest: The authors declare that the research was conducted in the absence of any commercial or financial relationships that could be construed as a potential conflict of interest.

frontiers in Genetics

MINI REVIEW
published: 12 February 2020
doi: 10.3389/fgene.2020.00033

Radial Organization in the Mammalian Nucleus

Nicola Crosetto and Magda Bienko *

Science for Life Laboratory, Department of Medical Biochemistry and Biophysics, Karolinska Institutet, Stockholm, Sweden

In eukaryotic cells, most of the genetic material is contained within a highly specialized organelle—the nucleus. A large body of evidence indicates that, within the nucleus, chromatinized DNA is spatially organized at multiple length scales. The higher-order organization of chromatin is crucial for proper execution of multiple genome functions, including DNA replication and transcription. Here, we review our current knowledge on the spatial organization of chromatin in the nucleus of mammalian cells, focusing in particular on how chromatin is radially arranged with respect to the nuclear lamina. We then discuss the possible mechanisms by which the radial organization of chromatin in the cell nucleus is established. Lastly, we propose a unifying model of nuclear spatial organization, and suggest novel approaches to test it.

Keywords: 3D chromatin architecture, gene expression regulation, nucleus, genome organization, chromosoma

OPEN ACCESS

Edited by:
Evi Soutoglou,
INSERM U964 Institut de Génétique et de Biologie Moléculaire et Cellulaire (IGBMC), France

Reviewed by:
Vladimir B. Teif,
University of Essex, United Kingdom
Richard Alan Katz,
Fox Chase Cancer Center, United States

***Correspondence:**
Magda Bienko
magda.bienko@ki.se

Specialty section:
This article was submitted to Epigenomics and Epigenetics, a section of the journal Frontiers in Genetics

Received: *11 October 2019*
Accepted: *10 January 2020*
Published: *12 February 2020*

Citation:
Crosetto N and Bienko M (2020) Radial Organization in the Mammalian Nucleus. Front. Genet. 11:33. doi: 10.3389/fgene.2020.00033

THE BUILDING BLOCKS OF NUCLEAR ARCHITECTURE

The nucleus is a sub-cellular organelle that has evolved to enable the storage, preservation, reading, and duplication of the information encoded in the DNA sequence. Evidence collected over the past 50 years strongly suggests that this functional specialization is made possible by a multi-level spatial organization that manifests itself at various length scales. The nuclear space is filled by both chromatin and sub-nuclear structures—including nucleoli (Németh and Längst, 2011), nuclear speckles (Spector and Lamond, 2011), and various types of nuclear bodies (Mao et al., 2011)—that contribute to orchestrate genomic functions in various ways. The linear genomic sequence is organized into structural domains that form the building blocks of the higher-order three-dimensional (3D) architecture of the genome. Chromosomes typically condense into distinct masses known as chromosome territories (CTs), whose existence was proposed already more than a century ago by the Austrian anatomist Carl Rabl and the German biologist Theodor Boveri (Strickfaden et al., 2010), and later confirmed in multiple cell types and species (Cremer and Cremer, 2001; Cremer et al., 2006). At the sub-chromosomal level, structural domains comprise megabase (Mb)-sized cytobands visible in metaphase chromosomes, and A/B compartments identified by Hi-C (Lieberman-Aiden et al., 2009), as well as smaller domains spanning from several kilobases (kb) up to a few Mb, including topologically associating domains (TADs) (Dixon et al., 2012) and long-range chromatin loops (Rao et al., 2014). A and B compartments are defined as genomic regions that tend to engage in homotypic (A-A and B-B) rather than heterotypic (A-B) contacts, and largely overlap with euchromatic and heterochromatic cytobands, respectively (Lieberman-Aiden et al., 2009). Each A/B compartment consists, in turn, of a variable number of TADs, defined computationally as clusters of increased contacts between adjacent parts of the same chromosome in the Hi-C data matrix (Dixon et al., 2012). TADs represent hubs of *cis*-interactions often contained within chromatin loops anchored by CCCTC-binding factors (CTCF)

(Rao et al., 2014), which facilitate specific enhancer-promoter contacts, while preventing unspecific and potentially detrimental interactions (Rowley and Corces, 2018). Accordingly, disruption of specific TAD borders and chromatin loops results in aberrant gene expression and can cause a variety of disease conditions, including developmental defects and cancer (Corces and Corces, 2016; Spielmann et al., 2018). TAD borders are highly conserved across metazoans and tend to coincide with dense clusters of conserved noncoding elements (Harmston et al., 2017), whereas A/B compartments appear to be less conserved across cell types and species (Schmitt et al., 2016a; Szabo et al., 2019; Yang et al., 2019). B compartments overlap, to a large extent, with lamina-associated domains (LADs), defined as genomic regions that frequently contact the nuclear lamina (Guelen et al., 2008). Depending on the cell type, LADs may comprise up to one third of the whole genomic sequence, and many LADs overlap with nucleoli-associated domains (NADs) (Németh et al., 2010) as well as with pericentromeric heterochromatin-associated domains (PADs) (Wijchers et al., 2015), suggesting that a substantial part of the genome is either localized at the nuclear periphery, close to the lamina, or in the inner part of the nucleus, around nucleoli. Unlike CTs, A/B compartments, TADs, and LADs were originally identified using bulk assays that average the signal over millions or even billions of cells. However, the recent development of single-cell Hi-C (Nagano et al., 2013; Flyamer et al., 2017; Ramani et al., 2017; Stevens et al., 2017; Ramani et al., 2020), Dip-C (Tan et al., 2018), and single-cell DamID (Kind et al., 2015), together with super-resolution microscopy assays (Boettiger et al., 2016; Wang et al., 2016; Bintu et al., 2018; Nir et al., 2018), have made it possible to confirm the existence of these sub-chromosomal domains in single cells. Another important consideration is that, although A/B compartments, TADs, and LADs have been observed in different cell types and species, all of the studies conducted so far have used either *in vitro* cultured cells or cells freshly dissociated from their tissue of origin. Therefore, we still lack a comprehensive portrait of the sub-chromosomal organization in cells directly embedded in their tissue context. Achieving this will require the development of novel assays combining high-throughput sequencing with preservation of spatial information.

Independently of the length scale at which chromatin domains are observed, studying how they are spatially arranged in the cell nucleus requires the definition of a reference system of coordinates. Since individual nuclei have different shapes and lack defined symmetry axes, one approach is to measure the distance of different chromatin domains from each other or from well-defined sub-nuclear structures serving as reference, such as the nuclear lamina. This has been classically achieved through the use of microscopy techniques, such as DNA fluorescence *in situ* hybridization (FISH), which allows measuring the distance of chromosomes or individual genomic loci from each other or from defined nuclear structures, in single cells. More recently, a new method named TSA-seq was developed to infer the relative distance from nuclear speckles of thousands of genomic loci simultaneously, based on next-generation sequencing (Chen et al., 2018). However, unlike DNA FISH, TSA-seq is a bulk assay that averages the signal over millions of cells, and thus, at least in its current design, cannot provide spatial information at the single-cell level.

In this review, we primarily focus on studies that have assessed the radial position of individual chromosomes or smaller chromatin domains relative to the nuclear periphery and center—which we here refer to as "chromatin radiality." For a detailed description of the folding principles of chromatin in the nucleus, of the available methods for mapping 3D genome architecture, and of the role of 3D genome organization in physiological and pathological processes, we instead refer the reader to many excellent recent reviews that have extensively covered these topics (Bonev and Cavalli, 2016; Corces and Corces, 2016; Dekker and Mirny, 2016; Schmitt et al., 2016b; Rowley and Corces, 2018; Zheng and Xie, 2019).

Radial Arrangement of Chromosomes

One of the best studied aspects of chromatin radiality is how individual CTs or selected gene loci are arranged with respect to the nuclear lamina. Early studies that examined the location of chromosomes in metaphase spreads prepared from cultured human fibroblasts, found that larger chromosomes were generally more peripherally located compared to smaller ones (Ockey, 1969; Hoo and Cramer, 1971). These observations were subsequently recapitulated in interphase nuclei of different human cell types, in which the nuclear lamina is preserved, revealing that the radial position of CTs with respect to the lamina is associated with the size of the chromosomes in base-pairs, but also with the density of genes along each chromosome (Manuelidis, 1985; Lichter et al., 1988; Nagele et al., 1999; Bridger et al., 2000; Sun et al., 2000; Boyle et al., 2001; Mahy et al., 2002; Weierich et al., 2003; Bolzer et al., 2005; Wiblin et al., 2005; Grasser et al., 2008; Jowhar et al., 2018a). Accordingly, despite having a very similar size, chromosomes (chr) 18 and 19 are mostly localized at the periphery and center of human interphase nuclei, respectively (Croft et al., 1999). Similar findings were also reported for primates (Tanabe et al., 2002; Tanabe et al., 2005; Mora et al., 2006), mouse (Parada et al., 2004; Mayer et al., 2005), and other vertebrate species (Federico et al., 2006; Skinner et al., 2009). In contrast, the radial position of CTs appears less defined in plant cells (Pecinka et al., 2004), although a tendency for centromeres to be closer to the nuclear lamina and telomeres to be more central was observed (Schubert et al., 2012; Schubert et al., 2014), which is reminiscent of the pattern of centromeres and telomeres in human and mouse cells (Weierich et al., 2003). In dividing cells, the 3D genome architecture is massively remodeled at every mitosis, and then re-established at the onset of the subsequent G1-phase, remaining relatively stable until the next mitosis (Manders et al., 1999; Edelmann et al., 2001; Lucas and Cervantes, 2002; Walter et al., 2003; Nagano et al., 2017; Gibcus et al., 2018). However, changes in the radial position of CTs and individual gene loci can occur in a variety of physiological conditions, including cell differentiation (Kuroda et al., 2004; Stadler et al., 2004; Marella et al., 2009a; Sehgal et al., 2016; Orsztynowicz et al., 2017), gametogenesis (Scherthan et al., 1998; Mudrak et al., 2009), signaling in response to extra-cellular stimuli (Branco et al., 2008; Mehta et al., 2010; Mourad et al., 2014; Ioannou et al.,

2015), as well as following DNA damage (Spitkovsky et al., 2002; Mehta et al., 2013; Schwarz-Finsterle et al., 2013; Kulashreshtha et al., 2016). Importantly, the radial placement of CTs in the nucleus is often altered in cancer cells (Cremer et al., 2003; Murata et al., 2007; Marella et al., 2009b; Timme et al., 2011) and in the presence of chromosomal translocations and aneuploidies associated with cancer (Taslerová et al., 2003; Taslerová et al., 2006; Harewood et al., 2010; Allinne et al., 2014) or congenital disorders (Jowhar et al., 2018b; Kemeny et al., 2018). Altogether, these findings suggest that the non-random radial arrangement of chromosomes and sub-chromosomal regions with respect to the nuclear lamina is a universal feature of nuclear architecture, which is conserved across species and whose alteration is associated with a variety of disease conditions. It should be noted, however, that the observation that CTs and gene loci have a preferred radial location must be interpreted probabilistically, meaning that a given chromosome or locus will never be found at the same radial distance from the nuclear lamina and have the same shape or orientation in all the cells examined. Indeed, a recent study based on high-throughput DNA FISH, which measured the position of hundreds of genomic loci in thousands of human fibroblast cells, revealed that the radial distance of the same locus from the nuclear lamina is highly variable across cells (Finn et al., 2019). Thus, although individual CTs and specific gene loci have a clear propensity for being localized closer or farther from the nuclear lamina, there is a high cell-to-cell variability in the radial placement of chromatin in the nucleus. Another important consideration is that, although the non-random radial organization of CTs has been well documented in many cell types and different species, until recently only a few studies have examined CTs in cells in their natural tissue context (Solovei, 2010; Kernohan and Bérubé, 2014; Fields et al., 2019). In the future, it will be important to extend these studies to explore how the spatial arrangement of chromosomes in the nucleus is affected by cell identity, nuclear shape, surrounding cell types, and the geometry of the tissue, in different tissues and organs.

In addition to being radially arranged, several lines of evidence indicate that CTs have a non-random internal structure that is also radially organized. Early studies by DNA FISH in cultured human, mouse, and Chinese hamster cells, showed that CTs have a polarized structure, with gene-rich regions more centrally located compared to gene-poor parts of the same chromosome (Sadoni et al., 1999; Küpper et al., 2007). In human lymphocytes, telomeres were found to be, on average, closer to the nuclear center compared to centromeres, and q-telomeres were more central compared to the p-telomeres of the same chromosome (Amrichová et al., 2003). More recently, the existence of a polarized structure of individual CTs was confirmed in two studies that used DNA FISH to visualize either multiple TADs or LADs together with inter-LAD regions belonging to the same chromosome (Wang et al., 2016; Luperchio et al., 2018). These single-cell studies revealed that TADs belonging to A and B compartments (A- and B-TADs, respectively) were spatially polarized in most of the cells analyzed (Wang et al., 2016), and that, within the same chromosome, LADs and inter-LAD (iLAD) regions were clearly radially separated (Luperchio et al., 2018). One limitation of these studies is that only a few chromosomes were investigated in cultured cells of a single cell type (mouse embryonic fibroblasts in (Luperchio et al., 2018) and human fibroblasts in (Wang et al., 2016)). In the future, application of high-throughput FISH techniques, together with novel ways for visualizing the internal structure of CTs, such as 'chromosome spotting' (Gelali et al., 2019), will enable us to draw a refined portrait of the internal radial organization of all chromosomes, in many different cell types.

Nuclear Periphery *vs*. Center

Aside from the notion that CTs are radially positioned in the nucleus and have a polarized internal structure, the only other aspect of chromatin radiality that is relatively well understood is the fact that the chromatin adjacent to the nuclear lamina is structurally and functionally different from the chromatin found in more centrally located parts of the nucleus. Early investigations of the nuclear structure of chicken erythrocytes by electron microscopy revealed the presence of large blocks of electron-dense material aligned all along the nuclear lamina, whereas more interior regions appeared significantly less dense (Davies, 1968; Everid et al., 1970). The electron-dense chromatin in the nuclear periphery corresponds to the LADs identified in human fibroblasts using lamin DamID (Guelen et al., 2008), and is enriched in LINE repeats and several histone marks of transcriptionally inactive chromatin, such as lysine nine di- and tri-methylated histone H3 (H3K9me2 and H3K9me3) (Guelen et al., 2008; Wen et al., 2009). The peripheral chromatin immediately adjacent to the nuclear envelope is known as "epichromatin" and can be visualized in cells from different species using a special bivalent mouse monoclonal anti-nucleosome antibody (mAb PL2-6), which binds to the acidic patch on nucleosomes (Olins and Olins, 2018). This suggests that the chromatin close to the nuclear lamina not only has a peculiar composition, but additionally harbors a unique nucleosome structure that is not seen elsewhere in the nucleus. In contrast, more central parts of the nucleus contain chromatin enriched in histone marks of transcriptionally active or permissive chromatin, such as lysine 4 tri-methylated histone H3 (H3K4me3) and lysine 27 acetylated histone H3 (H3K27Ac), which mark iLADs (van Steensel and Belmont, 2017). Although this radial arrangement of chromatin has been observed in many cell types of different species, exceptions also exist. For example, the rod cells of nocturnal animals have the opposite pattern, with more open and active chromatin close to the nuclear lamina, and compact and transcriptionally inactive chromatin amassed in the nuclear center (Solovei et al., 2009). This inverted chromatin arrangement is believed to redirect photons toward the light-sensing outer segments of the rods, thus facilitating vision in darkness (Solovei et al., 2009).

Altogether, the above observations can be summarized in a simplified binary model of radial chromatin organization, which we name "periphery *vs.* center" or "P-C" model (**Figure 1A**). According to the P-C model, the nuclear periphery consists of largely inactive chromatin domains, such as LADs, B compartments, and their constituent B-TADs, which are localized mainly close to the nuclear lamina, but also around nucleoli. On the

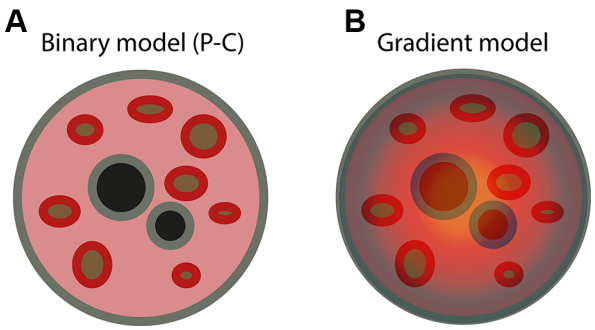

FIGURE 1 | Two different models of radial organization in the mammalian nucleus. **(A)** Binary model of radial nuclear organization ("periphery vs. center" or "P-C" model). According to the P-C model, inactive chromatin (gray) is localized along the nuclear lamina (the "nuclear periphery") and around nucleoli (black), whereas active chromatin (pink) is distributed in the intervening space (the "nuclear center"), without any specific radial order. Hubs of active chromatin (red) are positioned around speckles (brown), as revealed by TSA-seq (Chen et al., 2018). **(B)** We propose instead a gradient model of radial nuclear organization, according to which both active and inactive chromatin form a continuous gradient along the nuclear radius, with inactive chromatin concentrated near the nuclear lamina and around nucleoli, and active chromatin increasing in concentration toward the nuclear center and around speckles. In the gradient model, every genomic locus has a preferred radial location, which is determined by a "radial ZIP code," although the exact position can vary from cell to cell. The gradient model also postulates that the content of sub-nuclear structures, such as speckles and nucleoli, as well as the inter-chromatin space, are also radially arranged along a similar gradient.

other hand, the nuclear center is composed of more active chromatin regions, including iLADs, A compartments, and A-TADs, which are distributed in the remaining nuclear space. Although the P-C model provides a simplified framework for spatially organizing various chromatin domains with distinct functional properties, the division between nuclear periphery and center is rather artificial, because it is not clear where the boundary between the two compartments lies (if there exists one). Furthermore, while it is relatively easy to define the nuclear periphery using the lamina as reference, the definition of the nuclear center is more problematic: strictly geometrically speaking, only spheroidal nuclei have a defined center, while for ellipsoidal nuclei, such as those of fibroblasts, the definition is less clear. This ambiguity in distinguishing between nuclear periphery and center is also highlighted by the fact that the same LADs can be found both close to the nuclear lamina, as well as in more interior parts of the nucleus, around nucleoli (Kind et al., 2013). Indeed, a comparison between LADs identified in human fibroblasts (Guelen et al., 2008) and NADs identified in HeLa cells by sequencing the nucleoli-associated portions of the genome (Németh et al., 2010), showed that LADs tend to overlap with NADs. Thus, although it is clear that different types of chromatin are differentially positioned with respect to the nuclear lamina and peri-nucleolar space, a detailed map of the radial organization of chromatin in the cell nucleus is still missing.

One important limitation of the P-C model described above is that it does not explain how active regions are spatially arranged between nucleoli and the lamina. In an attempt to answer this question, two sequencing-based methods were recently developed: TSA-seq (Chen et al., 2018) and SPRITE (Quinodoz et al., 2018). In TSA-seq, the chromatin proximal to a defined sub-nuclear structure, such as nuclear speckles (Spector and Lamond, 2011), is targeted by a specific antibody and subsequently biotinylated using a tyramide reaction. The amount of biotin that gets covalently bound to DNA decreases exponentially as the distance from the sub-nuclear structure targeted by the antibody increases. By sequencing the resulting biotinylated DNA, the parts of the genome that are in close physical proximity to the targeted sub-nuclear structure can be distinguished from the genomic regions that are farther away (Chen et al., 2018). Using TSA-seq, it was shown that, in K562 human chronic myeloid leukemia cells, transcriptionally active genomic regions tend to form two distinct hubs, one localized in a range of a few nanometers around speckles, and the other more dispersed in the space between speckles and the nuclear lamina (Chen et al., 2018). Unlike TSA-seq, SPRITE measures chromosome contacts as well as DNA-RNA interactions without the use of proximity ligation, in contrast to Hi-C (Quinodoz et al., 2018). Using SPRITE, a hub of inter-chromosomal interactions involving transcriptionally active genes was found to be organized around speckles, whereas inter-chromosomal interactions involving inactive regions were organized around nucleoli, in both mouse embryonic stem and human lymphoblastoid cells (Quinodoz et al., 2018). Although these studies were the first to reveal the importance of sub-nuclear structures in shaping the higher-order spatial organization of chromatin in the nucleus, they still do not answer the question of whether the repertoire of genomic loci that speckles and nucleoli contact varies depending on the radial distance of these sub-nuclear structures from the lamina.

What Shapes Chromatin Radiality?

The studies summarized above clearly indicate that the nucleus of mammalian cells is characterized by some level of radial organization. However, the forces and molecular mechanisms that shape this radial organization remain largely elusive. The primary reason for this is the fact that, until now, it has been extremely challenging to selectively perturb the radial position of defined genomic regions or even entire chromosomes in a controlled fashion, followed by assessing the effect of such perturbations on the global nuclear architecture. Even more limiting has been the lack of genome-wide methods capable of measuring the distance from the nuclear lamina of thousands of genomic loci simultaneously. So far, the strongest evidence pointing to the existence of specific mechanisms that shape chromatin radiality comes from experiments in which specific protein components of the nuclear lamina were genetically ablated. In post-mitotic mouse cells, simultaneous knockout of lamin A and C isoforms and of the lamin B receptor (LBR)—the three major constituents of the nuclear lamina—led to condensation of heterochromatin in the nuclear interior (Solovei et al., 2013). The resulting pattern was reminiscent of the inverted chromatin arrangement seen in mouse rod cells, which indeed lack expression of both lamin A/C and LBR (Solovei et al., 2013). In mouse embryonic stem cells, loss of

lamins caused the detachment of certain LADs from the nuclear lamina, and disrupted 3D chromatin contacts in the nuclear interior (Zheng et al., 2018). Similarly, knockdown of emerin in human primary epidermal keratinocytes—another protein component of the nuclear lamina—resulted in chromosome repositioning inside the nucleus and reduction of H3K9me3 levels and distribution (Le et al., 2016). These findings are in line with the observation that, in humans carrying congenital mutations of lamin genes, the radial location of certain chromosomes is altered, which in turn is associated with changes in gene expression (Malhas et al., 2007; Mewborn et al., 2010; Puckelwartz et al., 2011). In addition to components of the nuclear lamina, histone modifications might also play a role in shaping chromatin radiality. For example, treatment of human adenocarcinoma HT29 cells with a histone deacetylase inhibitor resulted in increased levels of acetylated histone H3K9 and, concurrently, in relocation of multiple loci from the nuclear periphery toward the center (Strasák et al., 2009). Using a different approach combining RNA interference with high-throughput DNA FISH, 50 different factors were found to be involved in determining the radial position of three different genes in hTERT immortalized CRL-1474 human skin fibroblasts (Shachar et al., 2015). These radial positioning factors included chromatin remodelers, histone modifiers, as well as components of the nuclear pore and envelope (Shachar et al., 2015). Although this study assessed the radial position of only three genes, it was the first to establish that multiple factors, in addition to nuclear lamina components, can contribute to the radial arrangement of specific gene loci in the nucleus. Changes in the radial position of a gene locus can also be induced by selectively perturbing its transcriptional activity. For instance, tethering a viral transcriptional activator to a transgene constitutively localized close to the nuclear lamina caused the relocation of the transgene toward the nuclear interior in Chinese hamster ovary cells (Chuang et al., 2006). Similarly, targeting of a transcriptional activation domain to the promoters of genes in facultative LADs modified their radial position, moving them toward the nuclear center in mouse embryonic stem cells (Therizols et al., 2014). Notably, in the same cell type, a local change in chromatin condensation, without transcriptional activation, was sufficient to reposition these genes from the nuclear periphery to the center (Therizols et al., 2014). Thus, it is possible that the landscape of chromatin compaction, coupled with the action of specific tethers such as lamins, act as the primary forces that shape the radial organization of chromatin in the nucleus. However, it cannot be ruled out that transcription *per se* contributes to shape the global arrangement of chromatin, perhaps by locally modulating its compaction. In fact, based on a biophysical model of chromatin folding, it was recently proposed that transcriptional activity, rather than gene density, represents the dominant force that orchestrates the radial arrangement of chromatin in the nucleus (Cook and Marenduzzo, 2018).

In addition to specific nuclear proteins, histone modifications, and transcription, other factors have been suggested to contribute to shaping chromatin radiality. Genome-intrinsic features, such as chromosome size, guanine-cytosine (GC)-content, gene density, as well as the type and density of repetitive elements along the genome have long been associated with the radial arrangement of chromatin in the nucleus, in different human and mouse cell types (Bridger et al., 2000; Boyle et al., 2001; Mayer et al., 2005). Indeed, computer simulations of the formation of CTs at the onset of the G1-phase have suggested that the radial arrangement of chromosomes in interphase nuclei is predominantly dictated by the density of genes along each chromosome (Kreth et al., 2004). Gene density and GC-content have also been related to the topology of individual CTs, as gene-rich chromosomes, such as chr11, 17, and 19, were shown to have a more irregular shape, at least in WI38 human fibroblasts (Sehgal et al., 2014). A potentially important, yet largely neglected, factor that might contribute to dictate how chromatin is radially organized is nuclear shape. The shape and size of the nucleus are ultimately determined by a complex interplay between cytoskeletal forces and chromatin compaction inside the nucleus (Mukherjee et al., 2016). A recent study showed that experimental perturbations of the nuclear geometry in NIH 3T3 fibroblasts resulted in chromosome repositioning and changes in gene expression (Wang et al., 2017). Notably, alterations in nuclear shape and size are a defining feature of cancer cells (Uhler and Shivashankar, 2018), but how exactly chromatin is radially arranged in cancer nuclei with different shapes remains to be investigated.

An emerging concept in the field of genome organization is that hydrophobic interactions between intrinsically disordered domains of certain nuclear proteins, such as transcription factors, can induce liquid-liquid phase separation between different genomic regions, thus contributing to spatially organize chromatin in the nucleus (Cramer, 2019). Similarly, homotypic interactions between certain repetitive elements, such as short interspersed nuclear elements (SINEs) and long interspersed nuclear elements (LINEs), have been proposed to drive the physical separation between euchromatin and heterochromatin in the nucleus (Solovei et al., 2016). Along the same line, a model named "dog-on-a-lead" was proposed, according to which the radial arrangement of chromatin in the nucleus is dictated by repetitive genomic sequences, including ribosomal RNA genes and centromeric repeats (Krijger and de Laat, 2013). Homotypic interactions between DNA repeats might be either direct or mediated by proteins (*e.g.*, chromatin-bound factors and/or histone modifications) or by long non-coding RNAs (lncRNAs). Indeed, several lncRNAs have been implicated in reorganizing genome architecture and initiating the formation of nuclear compartments (Engreitz et al., 2016), including the lncRNA *Xist* that mediates X chromosome inactivation (Jégu et al., 2017).

In addition to phase separation, sub-nuclear compartments, such as nucleoli (Németh and Längst, 2011) and speckles (Spector and Lamond, 2011), have recently come into the spotlight as possible organizers of the higher-order structure of chromatin in the nucleus. As discussed above, hubs of inter-chromosome contacts are formed around nucleoli and speckles (Quinodoz et al., 2018), and most of the actively transcribed genes were found to be localized either around speckles or in the intervening

space between them and the nuclear lamina, in both mouse embryonic stem and human lymphoblastoid cells (Chen et al., 2018). In addition to sub-nuclear structures, specific gene loci or clusters of genes might, under certain conditions, contribute to the radial arrangement of chromatin in the nucleus, by acting as "nucleators" that pull transcriptionally active chromatin toward the nuclear interior. For instance, in mouse embryonic stem cells, the pluripotency factors Oct4 and Nanog were shown to organize clusters of pluripotency factor-binding sites, and thus contribute to the unique higher-order chromatin organization of these cells (de Wit et al., 2013). In conclusion, multiple forces are likely in place to shape the final blueprint of radial chromatin organization in a given cell. Teasing apart the relative contribution of different forces and their mechanism of action will, however, require the design of sophisticated experiments, in which each of them is perturbed separately, and the effect on radial organization is quantified genome-wide.

Toward a Unified Model of Spatial Nuclear Organization

In this review, we have summarized the existing evidence that chromosomes and the underlying sub-chromosomal domains are non-randomly arranged with respect to the nuclear lamina. However, many questions still await an answer before we can reach a thorough understanding of this fundamental aspect of cell biology: *Is chromatin randomly placed between the lamina and nucleoli, or is there a preferred radial location for every gene? If so, can we identify a "radial ZIP code" that specifies where a given locus will be preferentially radially located? Does radial organization only apply to chromatin or also to proteins and RNA in the inter-chromatin space? What are the forces that build and maintain the radial architecture of the nucleus after each cell division? Is radial nuclear organization disrupted by genomic rearrangements that occur, for instance, during tumorigenesis? If so, does disruption of radial nuclear organization contribute to cancer progression?* Answering these questions will require drawing comprehensive maps of radial nuclear organization in many cell and tissue types, as well as in different disease conditions.

The P-C model described above (**Figure 1A**) recapitulates many of the observations on radial chromatin organization that have been reported so far. However, one key limitation of this model is that it does not specify whether any locus along a given genome has a defined probability of being located at a specific radial location, or whether it is either peripherally (close to the lamina) or centrally located. We propose instead a gradient model of spatial nuclear organization, according to which every genomic locus has a preferred radial location (a "radial ZIP code") that is dependent on the type, differentiation, and functional state of the cell in which it is present (**Figure 1B**). This model does not only apply to DNA, as we envisage that the entire inter-chromatin space may also be radially organized, with different probabilities of finding specific protein complexes, lncRNAs, and nuclear bodies at defined radial positions. Notably, a gradient model of chromatin organization was already proposed 26 years ago, based on how the radial arrangement of chromatin in the nucleus changes during chondrogenesis in chicken embryos (Erenpreisa and Zhukotsky, 1993). Testing the validity of the gradient model, which we propose here, will require developing new methods that can probe the radial location of DNA, RNA, and proteins throughout the nuclear space, and not just close to the nuclear lamina, as done by lamin DamID (Guelen et al., 2008). The recent development of SPRITE (Quinodoz et al., 2018) and TSA-seq (Chen et al., 2018) are important steps in this direction, and, in our lab, we are also developing new methodologies for probing the radial position of genomic loci and proteins all along the nuclear radius. Ideally, these methodologies should, one day, be able to probe genome-wide radial locations in single cells, allowing us to quantify the extent of cell-to-cell variability in nuclear radial organization, and relate it to gene expression variability. In addition to developing novel methodologies, testing the gradient model that we have proposed here, will require devising ways to experimentally perturb the radial location of large chromatin domains, and possibly entire chromosomes, by changing their sequence, epigenetic status, or transcriptional activity, in a controlled fashion. Finally, we will need to develop spatially resolved methods enabling us to explore chromatin organization directly in cells embedded in their natural tissue context, in order to fully understand how different tissue and organ architectures cross-talk with organization within the cell nucleus. Whatever it takes to get there, we anticipate that obtaining a comprehensive portrait of the radial architecture of the cell nucleus will bring us closer to fully understand how this essential cellular organelle functions in health and disease.

AUTHOR CONTRIBUTIONS

Both authors equally contributed to writing this mini-review.

FUNDING

This work was supported by grants from the Swedish Research Council (521-2014-2866), the Swedish Cancer Research Foundation (CAN 2015/585), the Ragnar Söderberg Foundation (Fellows in Medicine 2016), and the Strategic Research Programme in Cancer (StratCan) at Karolinska Institutet to NC; and by grants from the Science for Life Laboratory, the Karolinska Institutet KID Funding Program, the Swedish Research Council (621-2014-5503), the Human Frontier Science Program (CDA-00033/2016-C), the Ragnar Söderberg Foundation (Fellows in Medicine 2016), and the European Research Council under the European Union's Horizon 2020 research and innovation programme (StG-2016_GENOMIS_715727) to MB.

ACKNOWLEDGMENTS

We thank Britta Bouwman from our lab for critically reading the manuscript and for providing valuable suggestions.

REFERENCES

Allinne, J., Pichugin, A., Iarovaia, O., Klibi, M., Barat, A., Zlotek-Zlotkiewicz, E., et al. (2014). Perinucleolar relocalization and nucleolin as crucial events in the transcriptional activation of key genes in mantle cell lymphoma. *Blood* 123, 2044–2053. doi: 10.1182/blood-2013-06-510511

Amrichová, J., Lukásová, E., Kozubek, S., and Kozubek, M. (2003). Nuclear and territorial topography of chromosome telomeres in human lymphocytes. *Exp. Cell Res.* 289, 11–26. doi: 10.1016/S0014-4827(03)00208-8

Bintu, B., Mateo, L. J., Su, J.-H., Sinnott-Armstrong, N. A., Parker, M., Kinrot, S., et al. (2018). Super-resolution chromatin tracing reveals domains and cooperative interactions in single cells. *Science* 362, 6413. doi: 10.1126/science.aau1783

Boettiger, A. N., Bintu, B., Moffitt, J. R., Wang, S., Beliveau, B. J., Fudenberg, G., et al. (2016). Super-resolution imaging reveals distinct chromatin folding for different epigenetic states. *Nature* 529, 418–422. doi: 10.1038/nature16496

Bolzer, A., Kreth, G., Solovei, I., Koehler, D., Saracoglu, K., Fauth, C., et al. (2005). Three-dimensional maps of all chromosomes in human male fibroblast nuclei and prometaphase rosettes. *PloS Biol.* 3, e157. doi: 10.1371/journal.pbio.0030157

Bonev, B., and Cavalli, G. (2016). Organization and function of the 3D genome. *Nat. Rev. Genet.* 17, 661–678. doi: 10.1038/nrg.2016.112

Boyle, S., Gilchrist, S., Bridger, J. M., Mahy, N. L., Ellis, J. A., and Bickmore, W. A. (2001). The spatial organization of human chromosomes within the nuclei of normal and emerin-mutant cells. *Hum. Mol. Genet.* 10, 211–219. doi: 10.1093/hmg/10.3.211

Branco, M. R., Branco, T., Ramirez, F., and Pombo, A. (2008). Changes in chromosome organization during PHA-activation of resting human lymphocytes measured by cryo-FISH. *Chromosome Res. Int. J. Mol. Supramol. Evol. Asp. Chromosome Biol.* 16, 413–426. doi: 10.1007/s10577-008-1230-x

Bridger, J. M., Boyle, S., Kill, I. R., and Bickmore, W. A. (2000). Re-modelling of nuclear architecture in quiescent and senescent human fibroblasts. *Curr. Biol. CB* 10, 149–152. doi: 10.1016/S0960-9822(00)00312-2

Chen, Y., Zhang, Y., Wang, Y., Zhang, L., Brinkman, E. K., Adam, S. A., et al. (2018). Mapping 3D genome organization relative to nuclear compartments using TSA-Seq as a cytological ruler. *J. Cell Biol.* 217, 4025–4048. doi: 10.1083/jcb.201807108

Chuang, C.-H., Carpenter, A. E., Fuchsova, B., Johnson, T., de Lanerolle, P., and Belmont, A. S. (2006). Long-range directional movement of an interphase chromosome site. *Curr. Biol. CB* 16, 825–831. doi: 10.1016/j.cub.2006.03.059

Cook, P. R., and Marenduzzo, D. (2018). Transcription-driven genome organization: a model for chromosome structure and the regulation of gene expression tested through simulations. *Nucleic Acids Res.* 46, 9895–9906. doi: 10.1093/nar/gky763

Corces, M. R., and Corces, V. G. (2016). The three-dimensional cancer genome. *Curr. Opin. Genet. Dev.* 36, 1–7. doi: 10.1016/j.gde.2016.01.002

Cramer, P. (2019). Organization and regulation of gene transcription. *Nature* 573, 45–54. doi: 10.1038/s41586-019-1517-4

Cremer, T., and Cremer, C. (2001). Chromosome territories, nuclear architecture and gene regulation in mammalian cells. *Nat. Rev. Genet.* 2, 292–301. doi: 10.1038/35066075

Cremer, M., Küpper, K., Wagler, B., Wizelman, L., von Hase, J., Weiland, Y., et al. (2003). Inheritance of gene density-related higher order chromatin arrangements in normal and tumor cell nuclei. *J. Cell Biol.* 162, 809–820. doi: 10.1083/jcb.200304096

Cremer, T., Cremer, M., Dietzel, S., Müller, S., Solovei, I., and Fakan, S. (2006). Chromosome territories–a functional nuclear landscape. *Curr. Opin. Cell Biol.* 18, 307–316. doi: 10.1016/j.ceb.2006.04.007

Croft, J. A., Bridger, J. M., Boyle, S., Perry, P., Teague, P., and Bickmore, W. A. (1999). Differences in the localization and morphology of chromosomes in the human nucleus. *J. Cell Biol.* 145, 1119–1131. doi: 10.1083/jcb.145.6.1119

Davies, H. G. (1968). Electron-microscope observations on the organization of heterochromatin in certain cells. *J. Cell Sci.* 3 (1), 129–50.

de Wit, E., Bouwman, B. A. M., Zhu, Y., Klous, P., Splinter, E., Verstegen, M. J. A. M., et al. (2013). The pluripotent genome in three dimensions is shaped around pluripotency factors. *Nature* 501, 227–231. doi: 10.1038/nature12420

Dekker, J., and Mirny, L. (2016). The 3D genome as moderator of chromosomal communication. *Cell* 164, 1110–1121. doi: 10.1016/j.cell.2016.02.007

Dixon, J. R., Selvaraj, S., Yue, F., Kim, A., Li, Y., Shen, Y., et al. (2012). Topological domains in mammalian genomes identified by analysis of chromatin interactions. *Nature* 485, 376–380. doi: 10.1038/nature11082

Edelmann, P., Bornfleth, H., Zink, D., Cremer, T., and Cremer, C. (2001). Morphology and dynamics of chromosome territories in living cells. *Biochim. Biophys. Acta* 1551, M29–M39. doi: 10.1016/S0304-419X(01)00023-3

Engreitz, J. M., Ollikainen, N., and Guttman, M. (2016). Long non-coding RNAs: spatial amplifiers that control nuclear structure and gene expression. *Nat. Rev. Mol. Cell Biol.* 17, 756–770. doi: 10.1038/nrm.2016.126

Erenpreisa, J., and Zhukotsky, A. (1993). Interphase genome as the active space: chromatin dynamics during chick embryo chondrogenesis. *Mech. Ageing Dev.* 67, 21–32. doi: 10.1016/0047-6374(93)90109-5

Everid, A. C., Small, J. V., and Davies, H. G. (1970). Electron-microscope observations on the structure of condensed chromatin: evidence for orderly arrays of unit threads on the surface of chicken erythrocyte nuclei. *J. Cell Sci.* 7, 35–48.

Federico, C., Scavo, C., Cantarella, C. D., Motta, S., Saccone, S., and Bernardi, G. (2006). Gene-rich and gene-poor chromosomal regions have different locations in the interphase nuclei of cold-blooded vertebrates. *Chromosoma* 115, 123–128. doi: 10.1007/s00412-005-0039-z

Fields, B. D., Nguyen, S. C., Nir, G., and Kennedy, S. (2019). A multiplexed DNA FISH strategy for assessing genome architecture in Caenorhabditis elegans. *ELife* 8. doi: 10.7554/eLife.42823.030

Finn, E. H., Pegoraro, G., Brandão, H. B., Valton, A.-L., Oomen, M. E., Dekker, J., et al. (2019). Extensive heterogeneity and intrinsic variation in spatial genome organization. *Cell* 176, 1502–1515.e10. doi: 10.1016/j.cell.2019.01.020

Flyamer, I. M., Gassler, J., Imakaev, M., Brandão, H. B., Ulianov, S. V., Abdennur, N., et al. (2017). Single-nucleus Hi-C reveals unique chromatin reorganization at oocyte-to-zygote transition. *Nature* 544, 110–114. doi: 10.1038/nature21711

Gelali, E., Girelli, G., Matsumoto, M., Wernersson, E., Custodio, J., Mota, A., et al. (2019). iFISH is a publically available resource enabling versatile DNA FISH to study genome architecture. *Nat. Commun.* 10, 1636. doi: 10.1038/s41467-019-09616-w

Gibcus, J. H., Samejima, K., Goloborodko, A., Samejima, I., Naumova, N., Nuebler, J., et al. (2018). A pathway for mitotic chromosome formation. *Science* 359, 6376. doi: 10.1126/science.aao6135

Grasser, F., Neusser, M., Fiegler, H., Thormeyer, T., Cremer, M., Carter, N. P., et al. (2008). Replication-timing-correlated spatial chromatin arrangements in cancer and in primate interphase nuclei. *J. Cell Sci.* 121, 1876–1886. doi: 10.1242/jcs.026989

Guelen, L., Pagie, L., Brasset, E., Meuleman, W., Faza, M. B., Talhout, W., et al. (2008). Domain organization of human chromosomes revealed by mapping of nuclear lamina interactions. *Nature* 453, 948–951. doi: 10.1038/nature06947

Harewood, L., Schütz, F., Boyle, S., Perry, P., Delorenzi, M., Bickmore, W. A., et al. (2010). The effect of translocation-induced nuclear reorganization on gene expression. *Genome Res.* 20, 554–564. doi: 10.1101/gr.103622.109

Harmston, N., Ing-Simmons, E., Tan, G., Perry, M., Merkenschlager, M., and Lenhard, B. (2017). Topologically associating domains are ancient features that coincide with Metazoan clusters of extreme noncoding conservation. *Nat. Commun.* 8, 441. doi: 10.1038/s41467-017-00524-5

Hoo, J. J., and Cramer, H. (1971). On the position of chromosomes in prepared mitosis figures of human fibroblasts. *Humangenetik* 13, 166–170. doi: 10.1007/BF00295800

Ioannou, D., Kandukuri, L., Simpson, J. L., and Tempest, H. G. (2015). Chromosome territory repositioning induced by PHA-activation of lymphocytes: a 2D and 3D appraisal. *Mol. Cytogenet.* 8, 47. doi: 10.1186/s13039-015-0146-3

Jégu, T., Aeby, E., and Lee, J. T. (2017). The X chromosome in space. *Nat. Rev. Genet.* 18, 377–389. doi: 10.1038/nrg.2017.17

Jowhar, Z., Gudla, P. R., Shachar, S., Wangsa, D., Russ, J. L., Pegoraro, G., et al. (2018a). HiCTMap: detection and analysis of chromosome territory structure and position by high-throughput imaging. *Methods San Diego Calif* 142, 30–38. doi: 10.1016/j.ymeth.2018.01.013

Jowhar, Z., Shachar, S., Gudla, P. R., Wangsa, D., Torres, E., Russ, J. L., et al. (2018b). Effects of human sex chromosome dosage on spatial chromosome organization. *Mol. Biol. Cell* 29, 2458–2469. doi: 10.1091/mbc.E18-06-0359

Küpper, K., Kölbl, A., Biener, D., Dittrich, S., von Hase, J., Thormeyer, T., et al. (2007). Radial chromatin positioning is shaped by local gene density, not by gene expression. *Chromosoma* 116, 285–306. doi: 10.1007/s00412-007-0098-4

Kemeny, S., Tatout, C., Salaun, G., Pebrel-Richard, C., Goumy, C., Ollier, N., et al. (2018). Spatial organization of chromosome territories in the interphase nucleus of trisomy 21 cells. *Chromosoma* 127, 247–259. doi: 10.1007/s00412-017-0653-6

Kernohan, K. D., and Bérubé, N. G. (2014). Three dimensional dual labelled DNA fluorescent *in situ* hybridization analysis in fixed tissue sections. *MethodsX* 1, 30–35. doi: 10.1016/j.mex.2014.04.001

Kind, J., Pagie, L., Ortabozkoyun, H., Boyle, S., de Vries, S. S., Janssen, H., et al. (2013). Single-cell dynamics of genome-nuclear lamina interactions. *Cell* 153, 178–192. doi: 10.1016/j.cell.2013.02.028

Kind, J., Pagie, L., de Vries, S. S., Nahidiazar, L., Dey, S. S., Bienko, M., et al. (2015). Genome-wide maps of nuclear lamina interactions in single human cells. *Cell* 163, 134–147. doi: 10.1016/j.cell.2015.08.040

Kreth, G., Finsterle, J., von Hase, J., Cremer, M., and Cremer, C. (2004). Radial arrangement of chromosome territories in human cell nuclei: a computer model approach based on gene density indicates a probabilistic global positioning code. *Biophys. J.* 86, 2803–2812. doi: 10.1016/S0006-3495(04)74333-7

Krijger, P. H. L., and de Laat, W. (2013). Identical cells with different 3D genomes; cause and consequences? *Curr. Opin. Genet. Dev.* 23, 191–196. doi: 10.1016/j.gde.2012.12.010

Kulashreshtha, M., Mehta, I. S., Kumar, P., and Rao, B. J. (2016). Chromosome territory relocation during DNA repair requires nuclear myosin 1 recruitment to chromatin mediated by ϒ-H2AX signaling. *Nucleic Acids Res.* 44, 8272–8291. doi: 10.1093/nar/gkw573

Kuroda, M., Tanabe, H., Yoshida, K., Oikawa, K., Saito, A., Kiyuna, T., et al. (2004). Alteration of chromosome positioning during adipocyte differentiation. *J. Cell Sci.* 117, 5897–5903. doi: 10.1242/jcs.01508

Le, H. Q., Ghatak, S., Yeung, C.-Y. C., Tellkamp, F., Günschmann, C., Dieterich, C., et al. (2016). Mechanical regulation of transcription controls Polycomb-mediated gene silencing during lineage commitment. *Nat. Cell Biol.* 18, 864–875. doi: 10.1038/ncb3387

Lichter, P., Cremer, T., Borden, J., Manuelidis, L., and Ward, D. C. (1988). Delineation of individual human chromosomes in metaphase and interphase cells by *in situ* suppression hybridization using recombinant DNA libraries. *Hum. Genet.* 80, 224–234. doi: 10.1007/BF01790090

Lieberman-Aiden, E., van Berkum, N. L., Williams, L., Imakaev, M., Ragoczy, T., Telling, A., et al. (2009). Comprehensive mapping of long range interactions reveals folding principles of the human genome. *Science* 326, 289–293. doi: 10.1126/science.1181369

Lucas, J. N., and Cervantes, E. (2002). Significant large-scale chromosome territory movement occurs as a result of mitosis, but not during interphase. *Int. J. Radiat. Biol.* 78, 449–455. doi: 10.1080/09553000110097190

Luperchio, T., Sauria, M., Hoskins, V., Wong, X., DeBoy, E., Gaillard, M.-C., et al. (2018). The repressive genome compartment is established early in the cell cycle before forming the lamina associated domains. *BioRxiv* 481598. doi: 10.1101/481598

Mahy, N. L., Perry, P. E., and Bickmore, W. A. (2002).). Gene density and transcription influence the localization of chromatin outside of chromosome territories detectable by FISH. *J. Cell Biol.* 159, 753–763. doi: 10.1083/jcb.200207115

Malhas, A., Lee, C. F., Sanders, R., Saunders, N. J., and Vaux, D. J. (2007). Defects in lamin B1 expression or processing affect interphase chromosome position and gene expression. *J. Cell Biol.* 176, 593–603. doi: 10.1083/jcb.200607054

Manders, E. M., Kimura, H., and Cook, P. R. (1999). Direct imaging of DNA in living cells reveals the dynamics of chromosome formation. *J. Cell Biol.* 144, 813–821. doi: 10.1083/jcb.144.5.813

Manuelidis, L. (1985). Individual interphase chromosome domains revealed by *in situ* hybridization. *Hum. Genet.* 71, 288–293. doi: 10.1007/BF00388453

Mao, Y. S., Zhang, B., and Spector, D. L. (2011). Biogenesis and function of nuclear bodies. *Trends Genet. TIG* 27, 295–306. doi: 10.1016/j.tig.2011.05.006

Marella, N. V., Seifert, B., Nagarajan, P., Sinha, S., and Berezney, R. (2009a). Chromosomal rearrangements during human epidermal keratinocyte differentiation. *J. Cell. Physiol.* 221, 139–146. doi: 10.1002/jcp.21855

Marella, N. V., Bhattacharya, S., Mukherjee, L., Xu, J., and Berezney, R. (2009b). Cell type specific chromosome territory organization in the interphase nucleus of normal and cancer cells. *J. Cell. Physiol.* 221, 130–138. doi: 10.1002/jcp.21836

Mayer, R., Brero, A., von Hase, J., Schroeder, T., Cremer, T., and Dietzel, S. (2005). Common themes and cell type specific variations of higher order chromatin arrangements in the mouse. *BMC Cell Biol.* 6, 44. doi: 10.1186/1471-2121-6-44

Mehta, I. S., Amira, M., Harvey, A. J., and Bridger, J. M. (2010). Rapid chromosome territory relocation by nuclear motor activity in response to serum removal in primary human fibroblasts. *Genome Biol.* 11, R5. doi: 10.1186/gb-2010-11-1-r5

Mehta, I. S., Kulashreshtha, M., Chakraborty, S., Kolthur-Seetharam, U., and Rao, B. J. (2013). Chromosome territories reposition during DNA damage-repair response. *Genome Biol.* 14, R135. doi: 10.1186/gb-2013-14-12-r135

Mewborn, S. K., Puckelwartz, M. J., Abuisneineh, F., Fahrenbach, J. P., Zhang, Y., MacLeod, H., et al. (2010). Altered chromosomal positioning, compaction, and gene expression with a lamin A/C gene mutation. *PloS One* 5, e14342. doi: 10.1371/journal.pone.0014342

Mora, L., Sánchez, I., Garcia, M., and Ponsà, M. (2006). Chromosome territory positioning of conserved homologous chromosomes in different primate species. *Chromosoma* 115, 367–375. doi: 10.1007/s00412-006-0064-6

Mourad, R., Hsu, P.-Y., Juan, L., Shen, C., Koneru, P., Lin, H., et al. (2014). Estrogen induces global reorganization of chromatin structure in human breast cancer cells. *PloS One* 9, e113354. doi: 10.1371/journal.pone.0113354

Mudrak, O., Chandra, R., Jones, E., Godfrey, E., and Zalensky, A. (2009). Reorganisation of human sperm nuclear architecture during formation of pronuclei in a model system. *Reprod. Fertil. Dev.* 21, 665–671. doi: 10.1071/RD08269

Mukherjee, R. N., Chen, P., and Levy, D. L. (2016). Recent advances in understanding nuclear size and shape. *Nucl. Austin Tex* 7, 167–186. doi: 10.1080/19491034.2016.1162933

Murata, S.-I., Nakazawa, T., Ohno, N., Terada, N., Iwashina, M., Mochizuki, K., et al. (2007). Conservation and alteration of chromosome territory arrangements in thyroid carcinoma cell nuclei. *Thyroid Off. J. Am. Thyroid Assoc.* 17, 489–496. doi: 10.1089/thy.2006.0328

Németh, A., and Längst, G. (2011). Genome organization in and around the nucleolus. *Trends Genet. TIG* 27, 149–156. doi: 10.1016/j.tig.2011.01.002

Németh, A., Conesa, A., Santoyo-Lopez, J., Medina, I., Montaner, D., Péterfia, B., et al. (2010). Initial genomics of the human nucleolus. *PloS Genet.* 6, 3. doi: 10.1371/journal.pgen.1000889

Nagano, T., Lubling, Y., Stevens, T. J., Schoenfelder, S., Yaffe, E., Dean, W., et al. (2013). Single-cell Hi-C reveals cell-to-cell variability in chromosome structure. *Nature* 502, 59–64. doi: 10.1038/nature12593

Nagano, T., Lubling, Y., Várnai, C., Dudley, C., Leung, W., Baran, Y., et al. (2017). Cell-cycle dynamics of chromosomal organization at single-cell resolution. *Nature* 547, 61–67. doi: 10.1038/nature23001

Nagele, R. G., Freeman, T., McMorrow, L., Thomson, Z., Kitson-Wind, K., and Lee, H. y (1999). Chromosomes exhibit preferential positioning in nuclei of quiescent human cells. *J. Cell Sci.* 112 (Pt 4), 525–535.

Nir, G., Farabella, I., Pérez Estrada, C., Ebeling, C. G., Beliveau, B. J., Sasaki, H. M., et al. (2018). Walking along chromosomes with super-resolution imaging, contact maps, and integrative modeling. *PloS Genet.* 14, e1007872. doi: 10.1371/journal.pgen.1007872

Ockey, C. H. (1969). Human chromosome identification and the pattern of DNA replication in fibroblasts from an XXY male. a quantitative autoradiographic study of early and late synthesis. *Cytogenetics* 8, 272–295. doi: 10.1159/000130039

Olins, D. E., and Olins, A. L. (2018). Epichromatin and chromomeres: a "fuzzy" perspective. *Open Biol.* 8, 6. doi: 10.1098/rsob.180058

Orsztynowicz, M., Lechniak, D., Pawlak, P., Kociucka, B., Kubickova, S., Cernohorska, H., et al. (2017). Changes in chromosome territory position within the nucleus reflect alternations in gene expression related to embryonic lineage specification. *PloS One* 12, e0182398. doi: 10.1371/journal.pone.0182398

Parada, L. A., McQueen, P. G., and Misteli, T. (2004). Tissue-specific spatial organization of genomes. *Genome Biol.* 5, R44. doi: 10.1186/gb-2004-5-7-r44

Pecinka, A., Schubert, V., Meister, A., Kreth, G., Klatte, M., Lysak, M. A., et al. (2004). Chromosome territory arrangement and homologous pairing in nuclei

of Arabidopsis thaliana are predominantly random except for NOR-bearing chromosomes. *Chromosoma* 113, 258–269. doi: 10.1007/s00412-004-0316-2

Puckelwartz, M. J., Depreux, F. F., and McNally, E. M. (2011). Gene expression, chromosome position and lamin A/C mutations. *Nucl. Austin Tex* 2, 162–167. doi: 10.4161/nucl.2.3.16003

Quinodoz, S. A., Ollikainen, N., Tabak, B., Palla, A., Schmidt, J. M., Detmar, E., et al. (2018). Higher-order inter-chromosomal hubs shape 3d genome organization in the nucleus. *Cell* 174, 744–757.e24. doi: 10.1016/j.cell.2018.05.024

Ramani, V., Deng, X., Qiu, R., Gunderson, K. L., Steemers, F. J., Disteche, C. M., et al. (2017). Massively multiplex single-cell Hi-C. *Nat. Methods* 14, 263–266. doi: 10.1038/nmeth.4155

Ramani, V., Deng, X., Qiu, R., Lee, C., Disteche, C. M., Noble, W. S., et al. (2020). Sci-Hi-C: a single-cell Hi-C method for mapping 3D genome organization in large number of single cells. *Methods* 170, 61–68. doi: 10.1016/j.ymeth.2019.09.012

Rao, S. S. P., Huntley, M. H., Durand, N. C., Stamenova, E. K., Bochkov, I. D., Robinson, J. T., et al. (2014). A 3D map of the human genome at kilobase resolution reveals principles of chromatin looping. *Cell* 159, 1665–1680. doi: 10.1016/j.cell.2014.11.021

Rowley, M. J., and Corces, V. G. (2018). Organizational principles of 3D genome architecture. *Nat. Rev. Genet.* 19, 789–800. doi: 10.1038/s41576-018-0060-8

Sadoni, N., Langer, S., Fauth, C., Bernardi, G., Cremer, T., Turner, B. M., et al. (1999). Nuclear organization of mammalian genomes. Polar chromosome territories build up functionally distinct higher order compartments. *J. Cell Biol.* 146, 1211–1226. doi: 10.1083/jcb.146.6.1211

Scherthan, H., Eils, R., Trelles-Sticken, E., Dietzel, S., Cremer, T., Walt, H., et al. (1998). Aspects of three-dimensional chromosome reorganization during the onset of human male meiotic prophase. *J. Cell Sci.* 111 (Pt 16), 2337–2351.

Schmitt, A. D., Hu, M., Jung, I., Xu, Z., Qiu, Y., Tan, C. L., et al. (2016a). A compendium of chromatin contact maps reveals spatially active regions in the human genome. *Cell Rep.* 17, 2042–2059. doi: 10.1016/j.celrep.2016.10.061

Schmitt, A. D., Hu, M., and Ren, B. (2016b). Genome-wide mapping and analysis of chromosome architecture. *Nat. Rev. Mol. Cell Biol.* 17, 743–755. doi: 10.1038/nrm.2016.104

Schubert, V., Berr, A., and Meister, A. (2012). Interphase chromatin organisation in Arabidopsis nuclei: constraints versus randomness. *Chromosoma* 121, 369–387. doi: 10.1007/s00412-012-0367-8

Schubert, V., Rudnik, R., and Schubert, I. (2014). Chromatin associations in Arabidopsis interphase nuclei. *Front. Genet.* 5, 389. doi: 10.3389/fgene.2014.00389

Schwarz-Finsterle, J., Scherthan, H., Huna, A., González, P., Mueller, P., Schmitt, E., et al. (2013). Volume increase and spatial shifts of chromosome territories in nuclei of radiation-induced polyploidizing tumour cells. *Mutat. Res.* 756, 56–65. doi: 10.1016/j.mrgentox.2013.05.004

Sehgal, N., Fritz, A. J., Morris, K., Torres, I., Chen, Z., Xu, J., et al. (2014). Gene density and chromosome territory shape. *Chromosoma* 123, 499–513. doi: 10.1007/s00412-014-0480-y

Sehgal, N., Seifert, B., Ding, H., Chen, Z., Stojkovic, B., Bhattacharya, S., et al. (2016). Reorganization of the interchromosomal network during keratinocyte differentiation. *Chromosoma* 125, 389–403. doi: 10.1007/s00412-015-0546-5

Shachar, S., Voss, T. C., Pegoraro, G., Sciascia, N., and Misteli, T. (2015). Identification of gene positioning factors using high-throughput imaging mapping. *Cell* 162, 911–923. doi: 10.1016/j.cell.2015.07.035

Skinner, B. M., Völker, M., Ellis, M., and Griffin, D. K. (2009). An appraisal of nuclear organisation in interphase embryonic fibroblasts of chicken, turkey and duck. *Cytogenet. Genome Res.* 126, 156–164. doi: 10.1159/000245915

Solovei, I., Kreysing, M., Lanctôt, C., Kösem, S., Peichl, L., Cremer, T., et al. (2009). Nuclear architecture of rod photoreceptor cells adapts to vision in mammalian evolution. *Cell* 137, 356–368. doi: 10.1016/j.cell.2009.01.052

Solovei, I., Wang, A. S., Thanisch, K., Schmidt, C. S., Krebs, S., Zwerger, M., et al. (2013). LBR and lamin A/C sequentially tether peripheral heterochromatin and inversely regulate differentiation. *Cell* 152, 584–598. doi: 10.1016/j.cell.2013.01.009

Solovei, I., Thanisch, K., and Feodorova, Y. (2016). How to rule the nucleus: divide et impera. *Curr. Opin. Cell Biol.* 40, 47–59. doi: 10.1016/j.ceb.2016.02.014

Solovei, I. (2010). Fluorescence *in situ* hybridization (FISH) on tissue cryosections. *Methods Mol. Biol. Clifton NJ* 659, 71–82. doi: 10.1007/978-1-60761-789-1_5

Spector, D. L., and Lamond, A. I. (2011). Nuclear Speckles. *Cold Spring Harb. Perspect. Biol.* 3, 2. doi: 10.1101/cshperspect.a000646

Spielmann, M., Lupiáñez, D. G., and Mundlos, S. (2018). Structural variation in the 3D genome. *Nat. Rev. Genet.* 19, 453–467. doi: 10.1038/s41576-018-0007-0

Spitkovsky, D. M., Kuzmina, I. V., Makarenkov, A. S., Terekhov, S. M., and Karpukhin, A. V. (2002). Interphase chromosome locus displacement induced by low-doses of radiation. *Radiats. Biol. Radioecol.* 42, 604–607.

Stadler, S., Schnapp, V., Mayer, R., Stein, S., Cremer, C., Bonifer, C., et al. (2004). The architecture of chicken chromosome territories changes during differentiation. *BMC Cell Biol.* 5, 44. doi: 10.1186/1471-2121-5-44

Stevens, T. J., Lando, D., Basu, S., Atkinson, L. P., Cao, Y., Lee, S. F., et al. (2017). 3D structures of individual mammalian genomes studied by single-cell Hi-C. *Nature* 544, 59–64. doi: 10.1038/nature21429

Strasák, L., Bártová, E., Harnicarová, A., Galiová, G., Krejcí, J., and Kozubek, S. (2009). H3K9 acetylation and radial chromatin positioning. *J. Cell. Physiol.* 220, 91–101. doi: 10.1002/jcp.21734

Strickfaden, H., Zunhammer, A., van Koningsbruggen, S., Köhler, D., and Cremer, T. (2010). 4D chromatin dynamics in cycling cells: Theodor Boveri's hypotheses revisited. *Nucl. Austin Tex* 1, 284–297. doi: 10.4161/nucl.11969

Sun, H. B., Shen, J., and Yokota, H. (2000). Size-dependent positioning of human chromosomes in interphase nuclei. *Biophys. J.* 79, 184–190. doi: 10.1016/S0006-3495(00)76282-5

Szabo, Q., Bantignies, F., and Cavalli, G. (2019). Principles of genome folding into topologically associating domains. *Sci. Adv.* 5, eaaw1668. doi: 10.1126/sciadv.aaw1668

Tan, L., Xing, D., Chang, C.-H., Li, H., and Xie, X. S. (2018). Three-dimensional genome structures of single diploid human cells. *Science* 361, 924–928. doi: 10.1126/science.aat5641

Tanabe, H., Müller, S., Neusser, M., von Hase, J., Calcagno, E., Cremer, M., et al. (2002). Evolutionary conservation of chromosome territory arrangements in cell nuclei from higher primates. *Proc. Natl. Acad. Sci. U. S. A.* 99, 4424–4429. doi: 10.1073/pnas.072618599

Tanabe, H., Küpper, K., Ishida, T., Neusser, M., and Mizusawa, H. (2005). Inter- and intra-specific gene-density-correlated radial chromosome territory arrangements are conserved in Old World monkeys. *Cytogenet. Genome Res.* 108, 255–261. doi: 10.1159/000080824

Taslerová, R., Kozubek, S., Lukásová, E., Jirsová, P., Bártová, E., and Kozubek, M. (2003). Arrangement of chromosome 11 and 22 territories, EWSR1 and FLI1 genes, and other genetic elements of these chromosomes in human lymphocytes and Ewing sarcoma cells. *Hum. Genet.* 112, 143–155. doi: 10.1007/s00439-002-0847-7

Taslerová, R., Kozubek, S., Bártová, E., Gajdusková, P., Kodet, R., and Kozubek, M. (2006). Localization of genetic elements of intact and derivative chromosome 11 and 22 territories in nuclei of Ewing sarcoma cells. *J. Struct. Biol.* 155, 493–504. doi: 10.1016/j.jsb.2006.05.005

Therizols, P., Illingworth, R. S., Courilleau, C., Boyle, S., Wood, A. J., and Bickmore, W. A. (2014). Chromatin decondensation is sufficient to alter nuclear organization in embryonic stem cells. *Science* 346, 1238–1242. doi: 10.1126/science.1259587

Timme, S., Schmitt, E., Stein, S., Schwarz-Finsterle, J., Wagner, J., Walch, A., et al. (2011). Nuclear position and shape deformation of chromosome 8 territories in pancreatic ductal adenocarcinoma. *Anal. Cell. Pathol. Amst.* 34, 21–33. doi: 10.1155/2011/840696

Uhler, C., and Shivashankar, G. V. (2018). Nuclear Mechanopathology and cancer diagnosis. *Trends Cancer* 4, 320–331. doi: 10.1016/j.trecan.2018.02.009

van Steensel, B., and Belmont, A. S. (2017). Lamina-associated domains: links with chromosome architecture, heterochromatin, and gene repression. *Cell* 169, 780–791. doi: 10.1016/j.cell.2017.04.022

Walter, J., Schermelleh, L., Cremer, M., Tashiro, S., and Cremer, T. (2003). Chromosome order in HeLa cells changes during mitosis and early G1, but is stably maintained during subsequent interphase stages. *J. Cell Biol.* 160, 685–697. doi: 10.1083/jcb.200211103

Wang, S., Su, J.-H., Beliveau, B. J., Bintu, B., Moffitt, J. R., Wu, C., et al. (2016). Spatial organization of chromatin domains and compartments in single chromosomes. *Science* 353, 598–602. doi: 10.1126/science.aaf8084

Wang, Y., Nagarajan, M., Uhler, C., and Shivashankar, G. V. (2017). Orientation and repositioning of chromosomes correlate with cell geometry-dependent gene expression. *Mol. Biol. Cell* 28, 1997–2009. doi: 10.1091/mbc.e16-12-0825

Weierich, C., Brero, A., Stein, S., von Hase, J., Cremer, C., Cremer, T., et al. (2003). Three-dimensional arrangements of centromeres and telomeres in nuclei of human and murine lymphocytes. *Chromosome Res. Int. J. Mol. Supramol. Evol. Asp. Chromosome Biol.* 11, 485–502. doi: 10.1023/A:1025016828544

Wen, B., Wu, H., Shinkai, Y., Irizarry, R. A., and Feinberg, A. P. (2009). Large histone H3 lysine 9 dimethylated chromatin blocks distinguish differentiated from embryonic stem cells. *Nat. Genet.* 41, 246–250. doi: 10.1038/ng.297

Wiblin, A. E., Cui, W., Clark, A. J., and Bickmore, W. A. (2005). Distinctive nuclear organisation of centromeres and regions involved in pluripotency in human embryonic stem cells. *J. Cell Sci.* 118, 3861–3868. doi: 10.1242/jcs.02500

Wijchers, P. J., Geeven, G., Eyres, M., Bergsma, A. J., Janssen, M., Verstegen, M., et al. (2015). Characterization and dynamics of pericentromere-associated domains in mice. *Genome Res.* 25, 958–969. doi: 10.1101/gr.186643.114

Yang, Y., Zhang, Y., Ren, B., Dixon, J. R., and Ma, J. (2019). Comparing 3D genome organization in multiple species using phylo-HMRF. *Cell Syst.* 8, 494–505.e14. doi: 10.1016/j.cels.2019.05.011

Zheng, H., and Xie, W. (2019). The role of 3D genome organization in development and cell differentiation. *Nat. Rev. Mol. Cell Biol.* 20, 535–550. doi: 10.1038/s41580-019-0132-4

Zheng, X., Hu, J., Yue, S., Kristiani, L., Kim, M., Sauria, M., et al. (2018). Lamins organize the global three-dimensional genome from the nuclear periphery. *Mol. Cell* 71, 802–815.e7. doi: 10.1016/j.molcel.2018.05.017

Conflict of Interest: The authors declare that the research was conducted in the absence of any commercial or financial relationships that could be construed as a potential conflict of interest.

frontiers in Genetics

REVIEW
published: 28 February 2020
doi: 10.3389/fgene.2020.00136

SUNny Ways: The Role of the SUN-Domain Protein Mps3 Bridging Yeast Nuclear Organization and Lipid Homeostasis

Maria Laura Sosa Ponce[1,2], *Sarah Moradi-Fard*[1], *Vanina Zaremberg*[2] *and Jennifer A. Cobb*[1]*

[1] Departments of Biochemistry & Molecular Biology and Oncology, Robson DNA Science Centre, Arnie Charbonneau Cancer Institute, Cumming School of Medicine, Calgary, AB, Canada, [2] Department of Biological Sciences, University of Calgary, Calgary, AB, Canada

OPEN ACCESS

Edited by:
Kyoko Yokomori, University of California, Irvine, United States

Reviewed by:
Akira Shinohara, Osaka University, Japan
Michael Klutstein, Hebrew University of Jerusalem, Israel
Laure Crabbe, UMR5088 Laboratoire de Biologie Cellulaire et Moléculaire du Contrôle de la Prolifération (LBCMCP), France

***Correspondence:**
Jennifer A. Cobb
jcobb@ucalgary.ca

Specialty section:
This article was submitted to Epigenomics and Epigenetics, a section of the journal Frontiers in Genetics

Received: *14 October 2019*
Accepted: *04 February 2020*
Published: *28 February 2020*

Citation:
Sosa Ponce ML, Moradi-Fard S, Zaremberg V and Cobb JA (2020) SUNny Ways: The Role of the SUN-Domain Protein Mps3 Bridging Yeast Nuclear Organization and Lipid Homeostasis. Front. Genet. 11:136. doi: 10.3389/fgene.2020.00136

Mps3 is a SUN (Sad1-UNC-84) domain-containing protein that is located in the inner nuclear membrane (INM). Genetic screens with multiple Mps3 mutants have suggested that distinct regions of Mps3 function in relative isolation and underscore the broad involvement of Mps3 in multiple pathways including mitotic spindle formation, telomere maintenance, and lipid metabolism. These pathways have largely been characterized in isolation, without a holistic consideration for how key regulatory events within one pathway might impinge on other aspects of biology at the nuclear membrane. Mps3 is uniquely positioned to function in these multiple pathways as its N- terminus is in the nucleoplasm, where it is important for telomere anchoring at the nuclear periphery, and its C-terminus is in the lumen, where it has links with lipid metabolic processes. Emerging work suggests that the role of Mps3 in nuclear organization and lipid homeostasis are not independent, but more connected. For example, a failure in regulating Mps3 levels through the cell cycle leads to nuclear morphological abnormalities and loss of viability, suggesting a link between the N-terminal domain of Mps3 and nuclear envelope homeostasis. We will highlight work suggesting that Mps3 is pivotal factor in communicating events between the nucleus and the lipid bilayer.

Keywords: telomeres, lipid metabolism, transcription, nuclear envelope, SUN-domain proteins

The Wind and the Sun (Æsop Fables (Sixth century B.C.). The Harvard Classics. 1909–14.

THE WIND and the SUN were disputing which was the stronger. Suddenly they saw a traveller coming down the road, and the Sun said: "I see a way to decide our dispute. Whichever of us can cause that traveller to take off his cloak shall be regarded as the stronger. You begin." So the Sun retired behind a cloud, and the Wind began to blow as hard as it could upon the traveller. But the harder he blew the more closely did the traveller wrap his cloak round him, till at last the Wind had to give up in despair. Then the Sun came out and shone in all his glory upon the traveller, who soon found it too hot to walk with his cloak on.

"KINDNESS EFFECTS MORE THAN SEVERITY."

MPS3 IS A STRUCTURAL COMPONENT OF THE NUCLEAR ENVELOPE

The nucleus of a eukaryotic cell is demarcated by the nuclear envelope (NE), a double lipid bilayer structure composed of an inner nuclear membrane (INM) and an outer nuclear membrane (ONM). While the ONM is continuous with the endoplasmic reticulum (ER) and is very similar in protein and lipid composition, the composition of the INM is quite distinct (Schirmer and Gerace, 2005). The ONM and INM are joined throughout the NE by nuclear pore complexes (NPCs), which serve as gateways of transportation between the cytoplasm and nucleoplasm. The contribution of the NPC to NE structure has been reviewed extensively elsewhere and will not be discussed here (Knockenhauer and Schwartz, 2016; Beck and Hurt, 2017; Goldberg, 2017).

In higher eukaryotes, the structure of the nucleus is largely maintained by the nuclear lamina, a network of lamin proteins associated with the nucleoplasmic side of the INM (Shimi et al., 2010; Romero-Bueno et al., 2019) and Sad1-UNC-84 (SUN)-domain containing proteins first discovered from an ~150 amino-acid region of homology between Sad1 in *Schizosaccharomyces pombe* and UNC-84 in *Caenorhabditis elegans* (Hagan and Yanagida, 1995; Malone et al., 1999). SUN-domain containing proteins in higher eukaryotes interact with lamin and also contribute to NE structure by their involvement in the linker of nucleo-skeleton and cytoskeleton (LINC) complex. The LINC complex includes a SUN domain protein in the INM and a KASH (Klarsicht-Anc-1-Syne-1) domain protein in the ONM that interact with one another in the lumen of the NE (Crisp et al., 2006; Razafsky and Hodzic, 2009).

The SUN-domain containing protein in *Saccharomyces cerevisiae* is called Monopolar spindle 3 (Mps3). However, a canonical LINC complex has not been detected in budding yeast because a *bona fide* KASH domain-containing protein has not yet been identified (Friederichs et al., 2012). Csm4 was proposed to function as a 'KASH' partner during chromosome segregation in meiosis because it binds Mps3 and localizes to the ONM (Burri and Lithgow, 2004; Koszul and Kleckner, 2009; Morillo-Huesca et al., 2019). More recently, a Csm4 paralogue called Mps2 was identified as a KASH-like protein and shown to form a non-canonical SUN-KASH complex with Mps3 (Chen et al., 2019).

The structural organization of Mps3 is multifaceted (**Figure 1**). SUN-domain proteins typically form trimers that span the INM (Zhou et al., 2012; Nie et al., 2016). Consistently, Mps3 has been shown to oligomerize in yeast (Li et al., 2017). Each Mps3 monomer contains an N-terminal region (1–150 aa) extending into the nucleoplasm, a transmembrane domain (154–181 aa) spanning the INM, and many functional domains oriented within the perinuclear space, including an ATP binding P-loop (187–194 aa), coiled-coil domains (242–260 aa and 366–390 aa) and a SUN domain (427–616 aa) (Jaspersen et al., 2002; Jaspersen et al., 2006; Bupp et al., 2007). Based on work with mammalian Sun2, the SUN domain of Mps3 folds into a series of β-sheets (Sosa et al., 2012; Burke, 2018).

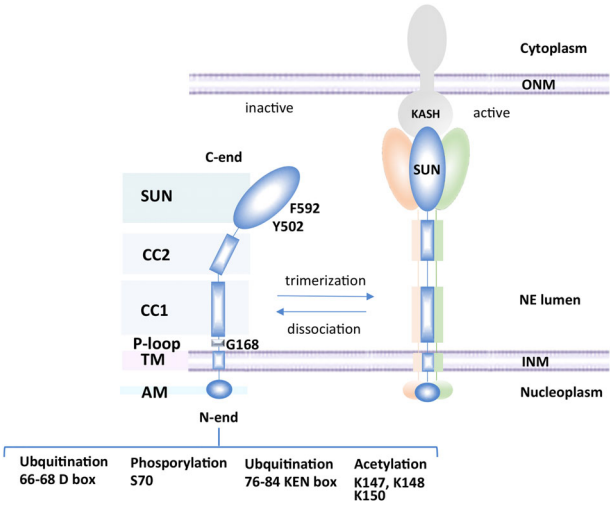

FIGURE 1 | Schematic of Mps3 domains. Mps3 consists of an N-terminal nucleoplasmic region (1–150 aa), a transmembrane domain (154–181 aa), a P-loop (187–194 aa), two coiled-coil domains (242–260 and 366–390) and a SUN domain (427–616). SUN domains typically associate with KASH domain proteins in the outer nuclear membrane after trimerization of the SUN-domain protein. Mps3 can be modified by acetylation, ubiquitination or phosphorylation.

Mutations in the SUN domain disrupt spindle pole body (SPB) organization, which is a major function of Mps3 in mitosis (Jaspersen et al., 2002; Nishikawa et al., 2003).

The cell cycle turnover of Mps3 is regulated by ubiquitination and degradation by Cdh1, which acts in late mitosis and early G1 (Koch et al., 2019). The regulated turnover of Mps3 depends on phosphorylation of S70, which is located between two anaphase-promoting complex (APC) destruction motifs in the N-terminal domain of Mps3, a KEN box (66–68 aa) and a D box (76–84 aa) (**Figure 1**) (Glotzer et al., 1991; Pfleger and Kirschner, 2000; Koch et al., 2019). The degradation of Mps3 in late mitosis likely contributes to spindle pole body disassembly. Failure to degrade Mps3 leads to its accumulation in the INM, aberrant nuclear envelope expansion, and an impairment in cell cycle progression (Friederichs et al., 2011; Li et al., 2017; Koch et al., 2019). Similarly, mutations in conserved residues in the SUN domain, like *mps3*-Y502H and *mps3*-F592S, show mitotic arrest as well as synthetic sickness or lethality in combination with the deletion of factors involved in lipid metabolism (Friederichs et al., 2012). Thus, two distinct regions of Mps3, which function in separate compartments, the N-terminal domain in the nucleoplasm and the SUN domain in the lumen, are implicated in mitotic progression and in NE proliferation. However, a genetic screen predicted that the distinct domains of Mps3 function in relative isolation, impacting pathways such as mitotic spindle formation, NPC insertion, chromatin organization, and lipid homeostasis (Friederichs et al., 2012). The role of Mps3 in SPB and NPC insertion has been reviewed elsewhere (Jaspersen and Ghosh, 2012) and there are multiple comprehensive reviews on the

LINC complex and SUN-KASH interactions; we direct readers to these for details (Rothballer et al., 2013; Tapley and Starr, 2013; Hieda, 2017; Hao and Starr, 2019). In this mini-review, we will cover emerging evidence supporting a role for Mps3 in balancing lipid metabolism and NE homeostasis and links with telomere organization.

MPS3 AND LIPID METABOLISM

Although no KASH proteins have been confirmed in *S. cerevisiae,* several tail-anchored proteins known to localize to the ER have been shown to physically interact with Mps3 and could equally be considered KASH-like partners (Burri and Lithgow, 2004; Bommi et al., 2019). One of these ONM proteins is Scs2, which has been linked to telomere silencing (Craven and Petes, 2001; Cuperus and Shore, 2002). Scs2 is a type II integral membrane protein, member of the VAP (VAMP/synaptobrevin-associated protein) family that localizes to the nuclear membrane, where it regulates phospholipid biosynthesis and lipid traffic (Loewen et al., 2003). Scs2 interacts with proteins containing FFAT motifs (two phenylalanines (FF) in an Acidic Tract). Among these is the transcriptional corepressor of phospholipid biosynthetic gene Opi1 (Loewen et al., 2003). The interaction between Scs2 and Opi1 favors binding of the transcriptional regulator to phosphatidic acid (PA) at the nuclear membrane and expression of lipid biosynthetic genes. Conditions that result in PA consumption favor the release of Opi1 from the ONM, allowing its translocation to the nucleus and subsequent repression of its target genes (Kliewe et al., 2017). Investigating a link between Scs2 and Mps3 could connect lipid homeostasis at the ONM with telomere silencing at the INM through known functions of Mps3, Scs2 or both.

Considering the potential for Mps3 to affect lipid homeostasis through Scs2, it is interesting to note that several Mps3 mutants have been shown to affect lipid levels (Friederichs et al., 2011; Ohsaki et al., 2016). In order to understand the effect of these mutants on nuclear structure, one must have a concept of the lipid metabolic pathway. In brief, PA is the precursor for all glycerolipids, and represents a branching point between membrane synthesis and energy storage pathways. In yeast, conversion of PA to CDP-diacylglycerol (CDP-DAG) channels metabolism towards phospholipid biosynthesis (**Figure 2A**). Conversion of PA to DAG by the PA phosphatase Pah1 diverts the metabolic pathway towards the synthesis of the storage lipid triacylglycerol (TAG), based on the cellular demand for energy storage during cessation of growth [**Figure 2A**; reviewed in (Siniossoglou, 2013)]. Synthesis of TAG leads to the emergence of lipid droplets (LDs), which are micellar organelles that store and metabolize neutral lipids (Walther et al., 2017). LDs serve as energy reservoirs that are consumed during resumption of growth.

It has been postulated that maintaining a balance between DAG and PA levels is important for the maintenance of NE structure (Barbosa et al., 2015). This has been shown in cells that undergo mitotic arrest or accumulate PA, which develop an extension of the NE known as a "nuclear flare" (Campbell et al., 2006; Witkin et al., 2012; Barbosa et al., 2015). Therefore, lipid levels are important for the maintenance of nuclear shape. Importantly, LDs were recently discovered to be synthesized in the nucleoplasm and may contribute to NE maintenance by regulating DAG levels (Layerenza et al., 2013; Uzbekov and Roingeard, 2013; Cartwright et al., 2015; Grippa et al., 2015; Wolinski et al., 2015; Ohsaki et al., 2016; Romanauska and Köhler, 2018).

In mammalian hepatocyte lines, knockdown of SUN proteins increased nuclear lipid droplet formation, suggesting SUN proteins can influence membrane lipid composition and the DAG : PA balance (Ohsaki et al., 2016). In *S. cerevisiae, MPS3* can be completely deleted if the nuclear pore complex biogenesis factor *POM152* is also deleted (Rout et al., 2000; Fernandez-Martinez and Rout, 2009; Witkin et al., 2010). In this genetic background, deletion of *MPS3* showed an increase in DAG and ergosterol levels compared to the *pom152Δ* mutant alone (Friederichs et al., 2011), which is consistent with the increase in neutral lipids seen in mammalian hepatocytes. This same synthetic viable double *pom152Δ mps3Δ* mutant showed a more than two-fold increase in both TAG and phospholipid levels (Friederichs et al., 2011). Additionally, there is evidence that Mps3 promotes membrane rigidity. Overexpression of Mps3 at cold temperatures was found to be lethal and multiple *mps3* point mutations showed sensitivity to membrane fluidizing agents (Friederichs et al., 2011). Based on these observations, Mps3 mutants are likely to affect nuclear LD formation through changes in DAG and TAG levels. This would be an interesting avenue for future investigations.

A screen for point mutations in the ATP-binding P-loop of Mps3 created the lethal mutant Mps3-G186K (Friederichs et al., 2011). Galactose-induced expression of this mutant, integrated in the genome and in an otherwise wild type background, led to nuclear membrane expansion. Cells exhibited up to eight additional bilayers when the mutant was expressed, but not when the wild type was induced (Friederichs et al., 2011). The G186K mutation also exhibited a halt in mitotic progression suggestive of SPB duplication failure, which has been shown to cause nuclear flare formation elsewhere (Friederichs et al., 2011; Witkin et al., 2012). Interestingly, deletion of the acyl-coA synthetase, *FAA3,* rescued the Mps3-G186K phenotype (Friederichs et al., 2011). Faa3 prefers C16:0-C18:0 long-chain fatty acids, which are the most abundant saturated acyl tails found in yeast glycerophospholipids (Knoll et al., 1994; Grillitsch et al., 2011). Faa3 has also been identified as part of the yeast LD proteome (Grillitsch et al., 2011) and collaborates with the DAG acyltransferase Dga1 in the synthesis of TAG (Kamisaka et al., 2007). Interestingly, Dga1 was immuno-affinity purified using antibodies directed towards Mps3-FLAG protein (Bommi et al., 2019). Taken together, a model emerges whereby lipid metabolic enzymes and structural membrane proteins like Mps3 cooperate in lipid and NE homeostasis. Future work should aim to explore how the P-loop of Mps3 relates to membrane proliferation.

MPS3 LINKS LIPID METABOLISM AND TELOMERE ORGANIZATION AT THE NUCLEAR PERIPHERY

Yeast telomeres are spatially organized within the nucleus: 32 telomeres in haploid cells cluster in 3 to 8 foci at the NE (Palladino et al., 1993). The nucleoplasmic N-terminal domain of Mps3 contains an acidic motif (75–150) that is important for tethering of telomeres in S-phase (Bupp et al., 2007). Consistently, ectopic expression of the N-terminal fragment (1–153) of Msp3, Mps3-N', out-competes the N-terminus of endogenously expressed full-length Mps3 for binding to telomeres (Schober et al., 2009). The N-terminus of Mps3 physically interacts with the PAD domain of the silent information regulator protein Sir4 and this interaction is required for telomere tethering (Bupp et al., 2007). The Sir4 protein is essential for telomere clustering and anchoring across the cell cycle. In addition, Sir4 is important for the initiation of sub-telomeric transcriptional silencing by its direct interaction with double-stranded DNA binding protein Rap1 at telomeres and subsequent recruitment of additional SIR factors (Sir2 and Sir3) (reviewed in Grunstein and Gasser, 2013). The SIR complex nucleates along sub-telomeres leading to deacetylation of lysine residues on the tails of histone H3 and H4, repressing transcription (Hardy et al., 1992; Moretti et al., 1994; Wotton and Shore, 1997). The dispersion of SIR proteins from telomeres has been shown to induce transcriptional changes in the euchromatin (Taddei et al., 2009). Although telomere tethering per se is not required for transcriptional repression at telomeres (Mondoux et al., 2007), the pool of SIR factors concentrated at clustered telomeres, partly through Mps3, promotes telomere silencing (**Figure 2A**). Interestingly, and in line with the importance of Mps3-linked telomere tethering, *mps3*Δ75 to 150 shows telomere silencing defects (Bupp et al., 2007). In a second, Sir4-independent pathway, Mps3 interacts with telomere-bound yKu70/80 through Est1 (ever shorter telomeres) (Antoniacci et al., 2007), a non-catalytic subunit of telomerase. In this pathway, yKu80 interacts with Tlc1, the RNA template subunit of telomerase, and therefore, physically connects telomere regulation to Mps3 at the nuclear periphery (**Figure 2A**) (Schober et al., 2009). Importantly, Ikeda et al. showed that inhibition of sphingolipid synthesis by treatment with aureobasidin A or by disrupting *LCB1*, the enzyme which regulates the first committed step in sphingolipid synthesis, decreased telomere clustering. Using microarray analysis, the authors also showed that reducing sphingolipid synthesis by inhibiting inositol incorporation reduced expression of genes involved in telomere homeostasis, including Est1, Est2 and Est3 (Antoniacci et al., 2007; Ikeda et al., 2015). It is tempting to speculate that Mps3 is the intermediary between changes in sphingolipid levels and changes in telomere clustering.

Furthermore, and consistent with the S phase tethering function of Mps3, tethering of telomeres was decreased in the *mps3*-K-R mutant (Ghosh et al., 2012). This mutant has three

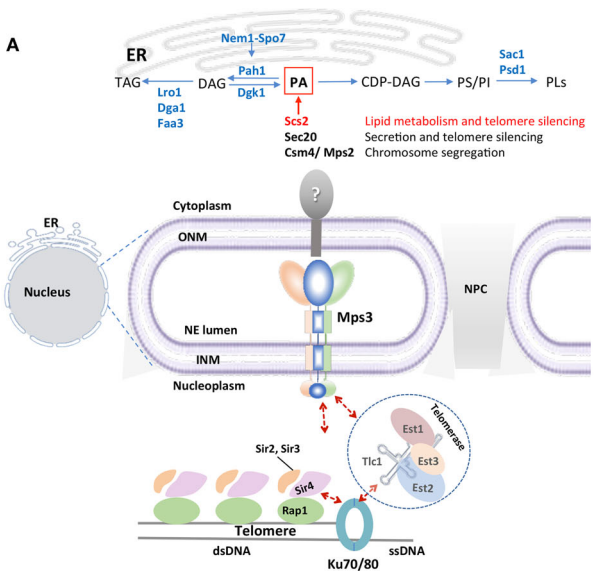

B

Deletion	Function	Mps3 mutation	Interaction
APQ12	NE and lipid homeostasis; Negative genetic interactions with *SIR2* and *YKU70*.	F592S	Lethal
DEP1	Component of the Rpd3L histone deacetylase complex that regulates phospholipid biosynthesis. Negative interactions with *YKU80*.	Y502H G186K	Sick Synthetic rescue
FAA3	Long chain (C16:0-C18:0) fatty acyl-CoA synthetase	G186K	Synthetic rescue
NEM1	Catalytic subunit of Nem1p-Spo7p phosphatase; regulates nuclear growth by controlling phospholipid biosynthesis; activates Pah1. Genetic rescue of telomere defects in *cdc13*-1 mutants.	Y502H	Sick
PSD1	Phosphatidylserine decarboxylase of the mitochondrial inner membrane. Synthetic growth defect with *EST1*	F592S	Sick
SAC1	Phosphatidylinositol phosphate phosphatase; Physically interacts with Scs2; Negative genetic interactions with *YKU70*.	F592S	Lethal

FIGURE 2 | Mps3 is at the crossroads of lipid metabolism and telomere organization. **(A)** Mps3 participates in tethering of telomeres through interactions with Sir4 and Est1. These interactions facilitate maintenance of telomere length, telomere clustering, and telomere silencing. The position of Mps3 in the nuclear membrane makes it a potential sensor to communicate changes in membrane composition to the nucleus, potentially affecting telomere regulation. Potential KASH-like binding partners of Mps3 like Scs2 (red), Sec20, and Csm4/Mps2 are indicated, as well as enzymes related to lipid metabolism mentioned in the text. DAG, diacylglycerol; PA, phosphatidic acid; PI, phosphatidylinositol; PS, phosphatidylserine; PLs, phospholipids; TAG, triacylglycerol. **(B)** Summary of the genetic interactions between mps3 mutants and genes involved in lipid biosynthesis regulation.

lysine residues (K147, K148, and K150) mutated to arginine in the acid region of Mps3 (**Figure 1**), which are acetylated by the sister chromatid cohesion regulator Eco1 (Ghosh et al., 2012). The *mps3*-K-R mutant did not alter SPB duplication or Mps3 integration in the INM, but did disrupt nuclear morphology and the interaction of Mps3 with telomeres (Bupp et al., 2007; Ghosh et al., 2012). Consistently, deletion of the acidic motif of Mps3 had no effect on cell viability and showed no impact on spindle pole body (SPB) structure or organization (Bupp et al., 2007).

Acetylation of Mps3 by Eco1 may represent a point of regulation with lipid metabolic pathways, as lipid biosynthesis and degradation have been shown to alter nuclear acetyl-CoA pools impacting the epigenome (Berger and Sassone-Corsi, 2016; Etchegaray and Mostoslavsky, 2016; McDonnell et al., 2016; Su et al., 2016; van der Knaap and Verrijzer, 2016; Sivanand et al., 2018). Decreased fatty acid synthesis in yeast acetyl-CoA carboxylase mutants coincides with increased global histone acetylation levels (Galdieri and Vancura, 2012; Papsdorf and Brunet, 2019). The increase in histone H3 and H4 acetylation contributed to increased expression of genes known to be regulated by histone deacetylases (Galdieri and Vancura, 2012). Additionally, in cell cultures, acetyl-CoA derived from fatty acid breakdown was shown to account for 90% of the carbon source used in histone acetylation, directly upregulating genes involved in fatty acid metabolic processes (McDonnell et al., 2016). This strongly suggests a conserved mechanism of communication between the nucleus and lipid metabolism, which may be mediated by SUN proteins like Mps3.

Based on these connections, changes in NE composition could have downstream effects on gene expression regulation, particularly of non-essential genes silenced at sub-telomeres that are expressed upon environmental changes (Grunstein, 1997; Brown et al., 2010; Kueng et al., 2013). One function of Mps3 might involve organizing the genome, *via* telomere anchoring, such that the nucleus is poised for a transcriptional response through the cell cycle and under stress. Consistently, it was postulated that the repression of ribosomal protein genes in response to secretory stress is mediated by Mps3 (Mizuta and Warner, 1994; Mizuta et al., 1998; Yabuki et al., 2017).

GENETIC INTERACTIONS OF MPS3

Based on the role of Mps3 in maintaining NE integrity and its role in telomere organization, we speculate that Mps3 serves to link NE membrane status to genome organization. Notably, telomere organization and telomere binding factors have genetic and physical interactions with factors regulating lipid homeostasis. For example, Est1 physically interacts with Lro1, a TAG synthesis enzyme (Lin et al., 2015). Lro1 was recently shown to localize to the INM under normal growth conditions and relocate in PA biosynthesis mutants, suggesting a physiological role for Lro1 in LD formation and in preservation of NE integrity through maintenance of DAG levels (Barbosa et al., 2019). Cells without *EST1* have short telomeres and positive genetic interactions with *pah1Δ* and negative interactions with loss of *OPI1* (Chang et al., 2011; Kyriakou et al., 2016). Conversely, cells lacking *RAP1* have longer telomeres and have negative genetic interactions with the loss of *LRO1* (Costanzo et al., 2016). The interactions between Est1 and PA metabolizing proteins warrant nuclear envelope studies in cells lacking *EST1*.

Lastly, to emphasize the functional interplay between telomere organization and lipid homeostasis, many of the proteins involved in lipid metabolism that have genetic interactions with Mps3 also show genetic interactions with factors at telomeres (**Figure 2B**). The Mps3–Y502H SUN domain mutant is synthetic sick with loss of *DEP1* and *NEM1*, two proteins involved in phospholipid biosynthesis. Loss of *DEP1* results in shorter telomeres and has negative interactions with the loss of *YKu80* (Costanzo et al., 2016), whereas loss of *NEM1* rescues end-protection defects in *cdc13-1*, a ts mutant for telomere specific single stranded binding factor that regulates telomerase (Addinall et al., 2008). The *mps3*-F592S mutation in the SUN domain is synthetic lethal with the loss of *SAC1*. Sac1 is a PI4P phosphatase that physically interacts with Scs2 (Manford et al., 2012). Moreover, it negatively interacts with telomere binding factors involved in silencing including yKu70 (Schuldiner et al., 2005; Addinall et al., 2011). The mps3-F592S variant is also synthetic lethal with loss of *APQ12*, an ER/NE integral membrane protein involved in lipid homeostasis and nuclear morphology, which itself has negative genetic interactions with loss of *SIR2* and *YKU70* (Friederichs et al., 2012). Finally, *mps3*-F592S also displayed synthetic growth defects with the deletion of *PSD1*. The Psd1 enzyme converts phosphatidylserine to phosphatidylethanolamine and its loss also displayed synthetic growth defects and lethality with deletions in *SAC1* and *EST1* respectively (Costanzo et al., 2010; Chang et al., 2011; Hoppins et al., 2011; Kuroda et al., 2011). Further characterization of these mutants will provide mechanistic insight into how Mps3's "SUNny way" integrates lipid metabolic cues with nuclear envelope architecture and telomere association.

AUTHOR CONTRIBUTIONS

MLSP, SM-F, VZ, and JC all contributed to writing.

FUNDING

MLSP is supported by a Queen Elizabeth II graduate award, SM-F holds a Alberta Cancer Board fellowship. VZ is supported by a Discovery grant and a Discovery Accelerator from NSERC. JC is supported by a Discovery grant from NSERC and an operating grant from CIHR.

REFERENCES

Addinall, S. G., Downey, M., Yu, M., Zubko, M. K., Dewar, J., Leake, A., et al. (2008). A genomewide suppressor and enhancer analysis of cdc13-1 reveals varied cellular processes influencing telomere capping in Saccharomyces cerevisiae. *Genetics* 180, 2251–2266. doi: 10.1534/genetics.108.092577

Addinall, S. G., Holstein, E. M., Lawless, C., Yu, M., Chapman, K., Banks, A. P., et al. (2011). Quantitative fitness analysis shows that NMD proteins and many other protein complexes suppress or enhance distinct telomere cap defects. *PloS Genet.* 7, e1001362. doi: 10.1371/journal.pgen.1001362

Antoniacci, L. M., Kenna, M., and Skibbens, R. V. (2007). The nuclear envelope and spindle pole body-associated Mps3 protein bind telomere regulators and function in telomere clustering. *Cell Cycle* 6, 75–79. doi: 10.4161/cc.6.1.3647

Barbosa, A. D., Sembongi, H., Su, W.-M., Abreu, S., Reggiori, F., Carman, G. M., et al. (2015). Lipid partitioning at the nuclear envelope controls membrane biogenesis. *Mol. Biol. Cell* 26, 3641–3657. doi: 10.1091/mbc.E15-03-0173

Barbosa, A. D., Lim, K., Mari, M., Edgar, J. R., Gal, L., Sterk, P., et al. (2019). Compartmentalized synthesis of triacylglycerol at the inner nuclear membrane regulates nuclear organization. *Dev. Cell.* 50, 755–766.e6. doi: 10.1016/J.DEVCEL.2019.07.009

Beck, M., and Hurt, E. (2017). The nuclear pore complex: understanding its function through structural insight. *Nat. Rev. Mol. Cell Biol.* 18, 73–89. doi: 10.1038/nrm.2016.147

Berger, S. L., and Sassone-Corsi, P. (2016). Metabolic signaling to chromatin. *Cold Spring Harb. Perspect. Biol.* 8, a019463. doi: 10.1101/cshperspect.a019463

Bommi, J. R., Rao, H. B. D. P., Challa, K., Higashide, M., Shinmyozu, K., Nakayama, J. I., et al. (2019). Meiosis-specific cohesin component, Rec8, promotes the localization of Mps3 SUN domain protein on the nuclear envelope. *Genes Cells* 24, 94–106. doi: 10.1111/gtc.12653

Brown, C. A., Murray, A. W., and Verstrepen, K. J. (2010). Rapid expansion and functional divergence of subtelomeric gene families in yeasts. *Curr. Biol.* 20, 895–903. doi: 10.1016/j.cub.2010.04.027

Bupp, J. M., Martin, A. E., Stensrud, E. S., and Jaspersen, S. L. (2007). Telomere anchoring at the nuclear periphery requires the budding yeast Sad1-UNC-84 domain protein Mps3. *J. Cell Biol.* 179, 845–854. doi: 10.1083/jcb.200706040

Burke, B. (2018). LINC complexes as regulators of meiosis. *Curr. Opin. Cell Biol.* 52, 22–29. doi: 10.1016/J.CEB.2018.01.005

Burri, L., and Lithgow, T. (2004). A complete set of SNAREs in yeast. *Traffic* 5, 45–52. doi: 10.1046/j.1600-0854.2003.00151.x

Campbell, J. L., Lorenz, A., Witkin, K. L., Hays, T., Loidl, J., and Cohen-Fix, O. (2006). Yeast nuclear envelope subdomains with distinct abilities to resist membrane expansion. *Mol. Biol. Cell* 17, 1768–1778. doi: 10.1091/mbc.E05-09-0839

Cartwright, B. R., Binns, D. D., Hilton, C. L., Han, S., Gao, Q., and Goodman, J. M. (2015). Seipin performs dissectible functions in promoting lipid droplet biogenesis and regulating droplet morphology. *Mol. Biol. Cell* 26, 726–739. doi: 10.1091/mbc.E14-08-1303

Chang, H. Y., Lawless, C., Addinall, S. G., Oexle, S., Taschuk, M., Wipat, A., et al. (2011). Genome-wide analysis to identify pathways affecting telomere-initiated senescence in budding yeast. *G3 Genes Genomes Genet.* 1, 197–208. doi: 10.1534/g3.111.000216

Chen, J., Gardner, J. M., Yu, Z., Smith, S. E., McKinney, S., Slaughter, B. D., et al. (2019). Yeast centrosome components form a noncanonical LINC complex at the nuclear envelope insertion site. *J. Cell Biol.* 218, 1478–1490. doi: 10.1083/jcb.201809045

Costanzo, M., Baryshnikova, A., Bellay, J., Kim, Y., Spear, E. D., Sevier, C. S., et al. (2010). The genetic landscape of a cell. *Sci. (80-.).* 327, 425–431. doi: 10.1126/science.1180823

Costanzo, M., VanderSluis, B., Koch, E. N., Baryshnikova, A., Pons, C., Tan, G., et al. (2016). A global genetic interaction network maps a wiring diagram of cellular function. *Sci. (80-.)* , 353. doi: 10.1126/science.aaf1420

Craven, R. J., and Petes, T. D. (2001). The Saccharomyces cerevisiae suppressor of choline sensitivity (SCS2) gene is a multicopy Suppressor of mec1 telomeric silencing defects. *Genetics* 158, 145–154. [Accessed November 12, 2019].

Crisp, M., Liu, Q., Roux, K., Rattner, J. B., Shanahan, C., Burke, B., et al. (2006). Coupling of the nucleus and cytoplasm: role of the LINC complex. *J. Cell Biol.* 172, 41–53. doi: 10.1083/jcb.200509124

Cuperus, G., and Shore, D. (2002). Restoration of silencing in Saccharomyces cerevisiae by tethering of a novel Sir2-interacting protein, Esc8. *Genetics* 162, 633–645. [Accessed November 12, 2019].

Etchegaray, J. P., and Mostoslavsky, R. (2016). Interplay between metabolism and epigenetics: a nuclear adaptation to environmental changes. *Mol. Cell* 62, 695–711. doi: 10.1016/j.molcel.2016.05.029

Fernandez-Martinez, J., and Rout, M. P. (2009). Nuclear pore complex biogenesis. *Curr. Opin. Cell Biol.* 21, 603–612. doi: 10.1016/j.ceb.2009.05.001

Friederichs, J. M., Ghosh, S., Smoyer, C. J., McCroskey, S., Miller, B. D., Weaver, K. J., et al. (2011). The SUN protein Mps3 is required for spindle pole body insertion into the nuclear membrane and nuclear envelope homeostasis. *PloS Genet.* 7, e1002365. doi: 10.1371/journal.pgen.1002365

Friederichs, J. M., Gardner, J. M., Smoyer, C. J., Whetstine, C. R., Gogol, M., Slaughter, B. D., et al. (2012). Genetic analysis of Mps3 SUN domain mutants in Saccharomyces cerevisiae reveals an interaction with the SUN-like protein Slp1. *G3 Genes Genomes Genet.* 2, 1703–1718. doi: 10.1534/g3.112.004614

Galdieri, L., and Vancura, A. (2012). Acetyl-CoA carboxylase regulates global histone acetylation. *J. Biol. Chem.* 287, 23865–23876. doi: 10.1074/jbc.M112.380519

Ghosh, S., Gardner, J. M., Smoyer, C. J., Friederichs, J. M., Unruh, J. R., Slaughter, B. D., et al. (2012). Acetylation of the SUN protein Mps3 by Eco1 regulates its function in nuclear organization. *Mol. Biol. Cell* 23, 2546–2559. doi: 10.1091/mbc.E11-07-0600

Glotzer, M., Murray, A. W., and Kirschner, M. W. (1991). Cyclin is degraded by the ubiquitin pathway. *Nature* 349, 132–138. doi: 10.1038/349132a0

Goldberg, M. W. (2017). Nuclear pore complex tethers to the cytoskeleton. *Semin. Cell Dev. Biol.* 68, 52–58. doi: 10.1016/j.semcdb.2017.06.017

Grillitsch, K., Connerth, M., Köfeler, H., Arrey, T. N., Rietschel, B., Wagner, B., et al. (2011). Lipid particles/droplets of the yeast Saccharomyces cerevisiae revisited: lipidome meets proteome. *Biochim. Biophys. Acta - Mol. Cell Biol. Lipids* 1811, 1165–1176. doi: 10.1016/j.bbalip.2011.07.015

Grippa, A., Buxó, L., Mora, G., Funaya, C., Idrissi, F.-Z., Mancuso, F., et al. (2015). The seipin complex Fld1/Ldb16 stabilizes ER-lipid droplet contact sites. *J. Cell Biol.* 211, 829–844. doi: 10.1083/jcb.201502070

Grunstein, M., and Gasser, S. M. (2013). Epigenetics in Saccharomyces cerevisiae. *Cold Spring Harb. Perspect. Biol.* 5, a017491. doi: 10.1101/cshperspect.a017491

Grunstein, M. (1997). Histone acetylation in chromatin structure and transcription. *Nature* 389, 349–352. doi: 10.1038/38664

Hagan, I., and Yanagida, M. (1995). The product of the spindle formation gene sad1+ associates with the fission yeast spindle pole body and is essential for viability. *J. Cell Biol.* 129, 1033–1047. doi: 10.1083/jcb.129.4.1033

Hao, H., and Starr, D. A. (2019). SUN/KASH interactions facilitate force transmission across the nuclear envelope. *Nucleus* 10, 73–80. doi: 10.1080/19491034.2019.1595313

Hardy, C. F. J., Sussel, L., and Shore, D. (1992). A RAP1-interacting protein involved in transcriptional silencing and telomere length regulation. *Genes Dev.* 6, 801–814. doi: 10.1101/gad.6.5.801

Hieda, M. (2017). Implications for diverse functions of the LINC complexes based on the structure. *Cells* 6, 3. doi: 10.3390/cells6010003

Hoppins, S., Collins, S. R., Cassidy-Stone, A., Hummel, E., DeVay, R. M., Lackner, L. L., et al. (2011). A mitochondrial-focused genetic interaction map reveals a scaffold-like complex required for inner membrane organization in mitochondria. *J. Cell Biol.* 195, 323–340. doi: 10.1083/jcb.201107053

Ikeda, A., Muneoka, T., Murakami, S., Hirota, A., Yabuki, Y., Karashima, T., et al. (2015). Sphingolipids regulate telomere clustering by affecting the transcription of genes involved in telomere homeostasis. *J. Cell Sci.* 128, 2454–2467. doi: 10.1242/jcs.164160

Jaspersen, S. L., and Ghosh, S. (2012). Nuclear envelope insertion of spindle pole bodies and nuclear pore complexes. *Nucleus (United States)* 3, 226–236. doi: 10.4161/nucl.20148

Jaspersen, S. L., Giddings, T. H., and Winey, M. (2002). Mps3p is a novel component of the yeast spindle pole body that interacts with the yeast centrin homologue Cdc31p. *J. Cell Biol.* 159, 945–956. doi: 10.1083/jcb.200208169

Jaspersen, S. L., Martin, A. E., Glazko, G., Giddings, T. H., Morgan, G., Mushegian, A., et al. (2006). The Sad1-UNC-84 homology domain in Mps3 interacts with Mps2 to connect the spindle pole body with the nuclear envelope. *J. Cell Biol.* 174, 665–675. doi: 10.1083/jcb.200601062

Kamisaka, Y., Tomita, N., Kimura, K., Kainou, K., and Uemura, H. (2007). DGA1 (diacylglycerol acyltransferase gene) overexpression and leucine biosynthesis significantly increase lipid accumulation in the Δsnf2 disruptant of Saccharomyces cerevisiae. *Biochem. J.* 408, 61–68. doi: 10.1042/BJ20070449

Kliewe, F., Kumme, J., Grigat, M., Hintze, S., and Schüller, H. J. (2017). Opi1 mediates repression of phospholipid biosynthesis by phosphate limitation in the yeast Saccharomyces cerevisiae. *Yeast* 34, 67–81. doi: 10.1002/yea.3215

Knockenhauer, K. E., and Schwartz, T. U. (2016). The nuclear pore complex as a flexible and dynamic gate. *Cell* 164, 1162–1171. doi: 10.1016/j.cell.2016.01.034

Knoll, L. J., Johnson, D. R., and Gordon, J. I. (1994). Biochemical studies of three Saccharomyces cerevisiae acyl-CoA synthetases, Faa1p, Faa2p, and Faa3p. *J. Biol. Chem.* 269, 16348–16356.

Koch, B. A., Jin, H., Tomko, R. J., and Yu, H.-G. (2019). The anaphase-promoting complex regulates the degradation of the inner nuclear membrane protein Mps3. *J. Cell Biol.* 218, 839–854. doi: 10.1083/jcb.201808024

Koszul, R., and Kleckner, N. (2009). Dynamic chromosome movements during meiosis: a way to eliminate unwanted connections? *Trends Cell Biol.* 19, 716–724. doi: 10.1016/j.tcb.2009.09.007

Kueng, S., Oppikofer, M., and Gasser, S. M. (2013). SIR proteins and the assembly of silent chromatin in budding yeast. *Annu. Rev. Genet.* 47, 275–306. doi: 10.1146/annurev-genet-021313-173730

Kuroda, T., Tani, M., Moriguchi, A., Tokunaga, S., Higuchi, T., Kitada, S., et al. (2011). FMP30 is required for the maintenance of a normal cardiolipin level and mitochondrial morphology in the absence of mitochondrial phosphatidylethanolamine synthesis. *Mol. Microbiol.* 80, 248–265. doi: 10.1111/j.1365-2958.2011.07569.x

Kyriakou, D., Stavrou, E., Demosthenous, P., Angelidou, G., San Luis, B.-J., Boone, C., et al. (2016). Functional characterisation of long intergenic non-coding RNAs through genetic interaction profiling in Saccharomyces cerevisiae. *BMC Biol.* 14, 106. doi: 10.1186/s12915-016-0325-7

Layerenza, J. P., González, P., García de Bravo, M. M., Polo, M. P., Sisti, M. S., and Ves-Losada, A. (2013). Nuclear lipid droplets: a novel nuclear domain. *Biochim. Biophys. Acta - Mol. Cell Biol. Lipids* 1831, 327–340. doi: 10.1016/J.BBALIP.2012.10.005

Li, P., Jin, H., Koch, B. A., Abblett, R. L., Han, X., Yates, J. R., et al. (2017). Cleavage of the SUN-domain protein Mps3 at its N-terminus regulates centrosome disjunction in budding yeast meiosis. *PloS Genet.* 13, e1006830. doi: 10.1371/journal.pgen.1006830

Lin, K. W., McDonald, K. R., Guise, A. J., Chan, A., Cristea, I. M., and Zakian, V. A. (2015). Proteomics of yeast telomerase identified Cdc48-Npl4-Ufd1 and Ufd4 as regulators of Est1 and telomere length. *Nat. Commun.* 6 (8290), 1–14. doi: 10.1038/ncomms9290

Loewen, C. J. R., Roy, A., and Levine, T. P. (2003). A conserved ER targeting motif in three families of lipid binding proteins and in Opi1p binds VAP. *EMBO J.* 22, 2025–2035. doi: 10.1093/emboj/cdg201

Malone, C. J., Fixsen, W. D., Horvitz, H. R., and Han, M. (1999). UNC-84 localizes to the nuclear envelope and is required for nuclear migration and anchoring during C. elegans development. *Development* 126, 3171–3181.

Manford, A. G., Stefan, C. J., Yuan, H. L., MacGurn, J. A., and Emr, S. D. (2012). ER-to-plasma membrane tethering proteins regulate cell signaling and ER morphology. *Dev. Cell* 23, 1129–1140. doi: 10.1016/j.devcel.2012.11.004

McDonnell, E., Crown, S. B., Fox, D. B., Kitir, B., Ilkayeva, O. R., Olsen, C. A., et al. (2016). Lipids reprogram metabolism to become a major carbon source for histone acetylation. *Cell Rep.* 17, 1463–1472. doi: 10.1016/j.celrep.2016.10.012

Mizuta, K., and Warner, J. R. (1994). Continued functioning of the secretory pathway is essential for ribosome synthesis. *Mol. Cell. Biol.* 14, 2493–2502. doi: 10.1128/MCB.14.4.2493

Mizuta, K., Tsujii, R., Warner, J. R., and Nishiyama, M. (1998). The C-terminal silencing domain of Rap1p is essential for the repression of ribosomal protein genes in response to a defect in the secretory pathway. *Nucleic Acids Res.* 26, 1063–1069. doi: 10.1093/nar/26.4.1063

Mondoux, M. A., Scaife, J. G., and Zakian, V. A. (2007). Differential nuclear localization does not determine the silencing status of Saccharomyces cerevisiae telomeres. *Genetics* 177, 2019–2029. doi: 10.1534/genetics.107.079848

Moretti, P., Freeman, K., Coodly, L., and Shore, D. (1994). Evidence that a complex of SIR proteins interacts with the silencer and telomere-binding protein RAP1. *Genes Dev.* 8, 2257–2269. doi: 10.1101/gad.8.19.2257

Morillo-Huesca, M., Murillo-Pineda, M., Barrientos-Moreno, M., Gómez-Marín, E., Clemente-Ruiz, M., and Prado, F. (2019). Actin and nuclear envelope components influence ectopic recombination in the absence of Swr1. *Genetics.* 213, 819–834. doi: 10.1534/genetics.119.302580

Nie, S., Ke, H., Gao, F., Ren, J., Wang, M., Huo, L., et al. (2016). Coiled-coil domains of SUN proteins as intrinsic dynamic regulators. *Structure* 24, 80–91. doi: 10.1016/j.str.2015.10.024

Nishikawa, S.-I., Terazawa, Y., Nakayama, T., Hirata, A., Makio, T., and Endo, T. (2003). Nep98p is a component of the yeast spindle pole body and essential for nuclear division and fusion. *J. Biol. Chem.* 278, 9938–9943. doi: 10.1074/jbc.M210934200

Ohsaki, Y., Kawai, T., Yoshikawa, Y., Cheng, J., Jokitalo, E., and Fujimoto, T. (2016). PML isoform II plays a critical role in nuclear lipid droplet formation. *J. Cell Biol.* 212, 29–38. doi: 10.1083/jcb.201507122

Palladino, F., Laroche, T., Gilson, E., Axelrod, A., Pillus, L., and Gasser, S. M. (1993). SIR3 and SIR4 proteins are required for the positioning and integrity of yeast telomeres. *Cell* 75, 543–555. doi: 10.1016/0092-8674(93)90388-7

Papsdorf, K., and Brunet, A. (2019). Linking lipid metabolism to chromatin regulation in aging. *Trends Cell Biol.* 29, 97–116. doi: 10.1016/j.tcb.2018.09.004

Pfleger, C. M., and Kirschner, M. W. (2000). The KEN box: an APC recognition signal distinct from the D box targeted by Cdh1. *Genes Dev.* 14, 655–665. doi: 10.1101/gad.14.6.655

Razafsky, D., and Hodzic, D. (2009). Bringing KASH under the SUN: the many faces of nucleo-cytoskeletal connections. *J. Cell Biol.* 186, 461–472. doi: 10.1083/jcb.200906068

Romanauska, A., and Köhler, A. (2018). The inner nuclear membrane is a metabolically active territory that generates nuclear lipid droplets. *Cell* 174, 700–715.e18. doi: 10.1016/j.cell.2018.05.047

Romero-Bueno, R., de la Cruz Ruiz, P., Artal-Sanz, M., Askjaer, P., and Dobrzynska, A. (2019). Nuclear organization in stress and aging. *Cells* 8, 664. doi: 10.3390/cells8070664

Rothballer, A., Schwartz, T. U., and Kutay, U. (2013). LINCing complex functions at the nuclear envelope what the molecular architecture of the LINC complex can reveal about its function. *Nucleus (United States)* 4, 1–8. doi: 10.4161/nucl.23387

Rout, M. P., Aitchison, J. D., Suprapto, A., Hjertaas, K., Zhao, Y., and Chait, B. T. (2000). The yeast nuclear pore complex: composition, architecture, transport mechanism. *J. Cell Biol.* 148, 635–651. doi: 10.1083/jcb.148.4.635

Schirmer, E. C., and Gerace, L. (2005). The nuclear membrane proteome: extending the envelope. *Trends Biochem. Sci.* 30, 551–558. doi: 10.1016/j.tibs.2005.08.003

Schober, H., Ferreira, H., Kalck, V., Gehlen, L. R., and Gasser, S. M. (2009). Yeast telomerase and the SUN domain protein Mps3 anchor telomeres and repress subtelomeric recombination. *Genes Dev.* 23, 928–938. doi: 10.1101/gad.1787509

Schuldiner, M., Collins, S. R., Thompson, N. J., Denic, V., Bhamidipati, A., Punna, T., et al. (2005). Exploration of the function and organization of the yeast early secretory pathway through an epistatic miniarray profile. *Cell* 123, 507–519. doi: 10.1016/j.cell.2005.08.031

Shimi, T., Butin-Israeli, V., Adam, S. A., and Goldman, R. D. (2010). Nuclear lamins in cell regulation and disease. *Cold Spring Harb. Symp. Quant. Biol.* 75, 525–531. doi: 10.1101/sqb.2010.75.045

Siniossoglou, S. (2013). Phospholipid metabolism and nuclear function: roles of the lipin family of phosphatidic acid phosphatases. *Biochim. Biophys. Acta - Mol. Cell Biol. Lipids* 1831, 575–581. doi: 10.1016/j.bbalip.2012.09.014

Sivanand, S., Viney, I., and Wellen, K. E. (2018). Spatiotemporal control of acetyl-CoA metabolism in chromatin regulation. *Trends Biochem. Sci.* 43, 61–74. doi: 10.1016/j.tibs.2017.11.004

Sosa, B. A., Rothballer, A., Kutay, U., and Schwartz, T. U. (2012). LINC complexes form by binding of three KASH peptides to domain interfaces of trimeric SUN proteins. *Cell* 149, 1035–1047. doi: 10.1016/j.cell.2012.03.046

Su, X., Wellen, K. E., and Rabinowitz, J. D. (2016). Metabolic control of methylation and acetylation. *Curr. Opin. Chem. Biol.* 30, 52–60. doi: 10.1016/j.cbpa.2015.10.030

Taddei, A., Van Houwe, G., Nagai, S., Erb, L., Van Nimwegen, E., and Gasser, S. M. (2009). The functional importance of telomere clustering: Global changes in gene expression result from SIR factor dispersion. *Genome Res.* 19, 611–625. doi: 10.1101/gr.083881.108

Tapley, E. C., and Starr, D. A. (2013). Connecting the nucleus to the cytoskeleton by SUN-KASH bridges across the nuclear envelope. *Curr. Opin. Cell Biol.* 25, 57–62. doi: 10.1016/j.ceb.2012.10.014

Uzbekov, R., and Roingeard, P. (2013). Nuclear lipid droplets identified by electron microscopy of serial sections. *BMC Res. Notes* 6, 386. doi: 10.1186/1756-0500-6-386

van der Knaap, J. A., and Verrijzer, C. P. (2016). Undercover: gene control by metabolites and metabolic enzymes. *Genes Dev.* 30, 2345–2369. doi: 10.1101/gad.289140.116

Walther, T. C., Chung, J., and Farese, R. V. (2017). Lipid droplet biogenesis. *Annu. Rev. Cell Dev. Biol.* 33, 491–510. doi: 10.1146/annurev-cellbio-100616-060608

Witkin, K. L., Friederichs, J. M., Cohen-Fix, O., and Jaspersen, S. L. (2010). Changes in the nuclear envelope environment affect spindle pole body duplication in Saccharomyces cerevisiae. *Genetics* 186, 867–883. doi: 10.1534/genetics.110.119149

Witkin, K. L., Chong, Y., Shao, S., Webster, M. T., Lahiri, S., Walters, A. D., et al. (2012). The budding yeast nuclear envelope adjacent to the nucleolus serves as a membrane sink during mitotic delay. *Curr. Biol.* 22, 1128–1133. doi: 10.1016/j.cub.2012.04.022

Wolinski, H., Hofbauer, H. F., Hellauer, K., Cristobal-Sarramian, A., Kolb, D., Radulovic, M., et al. (2015). Seipin is involved in the regulation of phosphatidic acid metabolism at a subdomain of the nuclear envelope in yeast. *Biochim. Biophys. Acta - Mol. Cell Biol. Lipids* 1851, 1450–1464. doi: 10.1016/J.BBALIP.2015.08.003

Wotton, D., and Shore, D. (1997). A novel Rap1p-interacting factor, Rif2p, cooperates with Rif1p to regulate telomere length in Saccharomyces cerevisiae. *Genes Dev.* 11, 748–760. doi: 10.1101/gad.11.6.748

Yabuki, Y., Katayama, M., Kodama, Y., Sakamoto, A., Yatsuhashi, A., Funato, K., et al. (2017). Arp2/3 complex and Mps3 are required for regulation of ribosome biosynthesis in the secretory stress response. *Yeast* 34, 155–163. doi: 10.1002/yea.3221

Zhou, Z., Du, X., Cai, Z., Song, X., Zhang, H., Mizuno, T., et al. (2012). Structure of Sad1-UNC84 homology (SUN) domain defines features of molecular bridge in nuclear envelope. *J. Biol. Chem.* 287, 5317–5326. doi: 10.1074/jbc.M111.304543

Conflict of Interest: The authors declare that the research was conducted in the absence of any commercial or financial relationships that could be construed as a potential conflict of interest.

frontiers in Genetics

ORIGINAL RESEARCH
published: 06 March 2020
doi: 10.3389/fgene.2020.00174

Recruitment of an Activated Gene to the Yeast Nuclear Pore Complex Requires Sumoylation

Natasha O. Saik[1†], Nogi Park[1,2†], Christopher Ptak[1†], Neil Adames[1,3], John D. Aitchison[4] and Richard W. Wozniak[1]*

[1] Department of Cell Biology, University of Alberta, Edmonton, AB, Canada, [2] Department of Basic Sciences, College of Veterinary Medicine, Mississippi State University, Starkville, MS, United States, [3] New Culture, San Francisco, CA, United States, [4] Seattle Children's Research Institute, Seattle, WA, United States

In addition to their role in regulating transport across the nuclear envelope, increasing evidence suggests nuclear pore complexes (NPCs) function in regulating gene expression. For example, the induction of certain genes (e.g., yeast *INO1*) is accompanied by their movement from the nuclear interior to NPCs. As sumoylation has been linked to the regulation of chromatin spatial organization and transcriptional activity, we investigated the role of sumoylation in the expression and NPC recruitment of the *INO1* gene. We observed that induction of *INO1* is accompanied by both increased and decreased sumoylation of proteins associated with specific regions along the *INO1* locus. Furthermore, we show that the E3 ligase Siz2/Nfi1 is required for targeting the *INO1* locus to the NPC where it interacts with the SUMO isopeptidase Ulp1. Our data suggest that this interaction is required for both the association of *INO1* with the NPC and for its normal expression. These results imply that sumoylation is a key regulator of *INO1* targeting to the NPC, and a cycle of sumoylation and NPC-associated desumoylation events contribute to the regulation of *INO1* expression.

Keywords: nuclear pore complex, gene positioning, gene expression, sumoylation, *INO1*, Ulp1, Siz2

OPEN ACCESS

Edited by:
Karim Mekhail, University of Toronto, Canada

Reviewed by:
Aishwarya Swaminathan, University of Massachusetts Medical School, United States
Michael Lisby, University of Copenhagen, Denmark
Marc Gartenberg, Robert Wood Johnson Medical School, United States

***Correspondence:**
Richard W. Wozniak
rick.wozniak@ualberta.ca

[†] These authors have contributed equally to this work

Specialty section:
This article was submitted to Epigenomics and Epigenetics, a section of the journal Frontiers in Genetics

Received: *16 October 2019*
Accepted: *13 February 2020*
Published: *06 March 2020*

Citation:
Saik NO, Park N, Ptak C, Adames N, Aitchison JD and Wozniak RW (2020) Recruitment of an Activated Gene to the Yeast Nuclear Pore Complex Requires Sumoylation. Front. Genet. 11:174. doi: 10.3389/fgene.2020.00174

INTRODUCTION

Small ubiquitin-related modifier (SUMO) is an ubiquitin-like peptide that is covalently attached to certain lysines in proteins. Sumoylation of proteins can result in changes to protein stability, subcellular localization, or interactions with other proteins. The vast majority of proteins modified by sumoylation are nuclear proteins and sumoylation and desumoylation events have been linked to the regulation of diverse group of nuclear processes including DNA replication, transcriptional control, and the spatial organization of the genome (Jentsch and Psakhye, 2013; Texari and Stutz, 2015; Zhao, 2018; Rosonina, 2019).

In *Saccharomyces cerevisiae*, the SUMO polypeptide is encoded by a single gene, *SMT3*. SUMO is translated with a C-terminal extension and later cleaved at a di-glycine motif by a SUMO peptidase to yield mature SUMO (Li and Hochstrasser, 1999). Like ubiquitination, SUMO conjugation is accomplished by a series of enzymes that first activate the mature peptide via ATP-dependent formation of a thioester bond (E1 enzyme, Aos1/Uba2 heterodimer in *S. cerevisiae*). Activated SUMO is subsequently handed-off to an active site cysteine in the E2 conjugating enzyme Ubc9. Ubc9 functions to directly transfer SUMO to a lysine in the target protein. In most cases, an E3 ligase aids SUMO-substrate specificity by mediating or stabilizing target interactions with the E2 (Geiss-Friedlander and Melchior, 2007). There are four known SUMO ligases in yeast, Zip3,

Mms21, Siz1, and Siz2, the former functioning during meiosis while the latter three function in actively growing cells (Johnson, 2004; Jentsch and Psakhye, 2013). There is a significant overlap and redundancy in E3 ligase targets; however, E3 ligases have also been shown to have specific and independent functions (Makhnevych et al., 2007; Ferreira et al., 2011; Hannan et al., 2015). The SUMO conjugating system components are primarily present in the nucleoplasm (Srikumar et al., 2013) as are the vast majority of proteins modified by sumoylation (Panse et al., 2004; Wohlschlegel et al., 2004; Zhao et al., 2004; Zhou et al., 2004; Hannich et al., 2005; Wykoff and O'Shea, 2005).

Sumoylation is a reversible process. In budding yeast, there are two functionally distinct isopeptidases, Ulp1 and Ulp2. Both Ulp1 and Ulp2 deconjugate SUMO from target proteins; however, Ulp2 also suppresses poly-SUMO chain accumulation (Bylebyl et al., 2003), while Ulp1 carries out the essential role of processing pre-SUMO to mature SUMO (Li and Hochstrasser, 1999; Mossessova and Lima, 2000). *ulp1-ts* and *ulp2*Δ mutants exhibit very different overall sumoylation patterns (Li and Hochstrasser, 2000), and the desumoylation of specific sumoylated targets have been shown to be dependent on specific isopeptidases (Makhnevych et al., 2007; Felberbaum et al., 2012), indicating that each enzyme has distinct substrates. Ulp1 and Ulp2 also have distinct locations in the cell; Ulp2 is distributed throughout the nucleoplasm, while Ulp1 is associated with the nucleoplasmic face of nuclear pore complexes (NPCs) (Li and Hochstrasser, 2000; Panse et al., 2003).

The Ulp1 catalytic domain resides in its C-terminus, whereas several N-terminal domains of Ulp1 contribute to its association with NPCs (Li and Hochstrasser, 2003; Panse et al., 2003; Makhnevych et al., 2007). The N-terminal regions also bind to nuclear transport factors; residues 1–150 bind the import karyopherin Kap121, residues 150–340 bind the import karyopherin heterodimer Kap95/Kap60, and residues 340–403 contain a nuclear export signal that appears to interact with the export factor Xpo1 (Panse et al., 2003). Binding of Ulp1 to the NPC appears dependent on structures positioned on the nucleoplasmic face of the NPC, including proteins such as Mlp1, Mlp2, Nup60, and Nup2 (Zhao et al., 2004; Palancade et al., 2007; Srikumar et al., 2013). However, the molecular basis for these interactions has not been established.

The association of Ulp1 with NPCs is particularly intriguing and has led to the analysis of its role in various processes performed by NPCs, including the regulation of nuclear transport (Stade et al., 2002; Panse et al., 2006; Lewis et al., 2007), certain DNA repair pathways (Zhao et al., 2004; Palancade et al., 2007; Freudenreich and Su, 2016), and the regulation of gene expression (Texari et al., 2013; Bonnet et al., 2015; Abraham and Mishra, 2018). Among the various mechanisms by which NPCs can influence gene expression is their direct interactions with chromatin. NPCs interact with both transcriptionally repressed and active genes through interactions that appear to be mediated by transcription factors (TFs) of various types that bind specific chromatin sites and interact with different sets of Nups (Brickner et al., 2007; Ahmed et al., 2010; Light et al., 2010; Ruben et al., 2011; Van de Vosse et al., 2013; Brickner et al., 2019). These interactions influence both the spatial organization of associated genes and contribute to transcriptional state.

In yeast, numerous studies have examined the relocalization to NPCs of inducible genes following activation. Several genes have been shown to reside in the nuclear interior when repressed, but move to NPCs when induced. Well studied among these is the *INO1* locus (Brickner and Walter, 2004; Cabal et al., 2006; Brickner et al., 2007; Ahmed et al., 2010; Light et al., 2010). In the presence of inositol (repressive conditions), *INO1* is bound by the repressors Opi1 and Ume6, and the Rpd3(L) histone deacetylase complex, which repress *INO1* expression and association with the NPC. Following induction (inositol starvation), Opi1, presumably with Ume6 and Rpd3(L), dissociates from *INO1*. This is thought to be followed by the binding of TFs (Put3 and Cbf1) to cis-acting DNA elements (termed gene GRS1 and GRS2), which exhibit redundant functions in targeting *INO1* to an NPC (Loewen et al., 2003; Brickner and Walter, 2004; Shetty and Lopes, 2010; Brickner and Brickner, 2012; Randise-Hinchliff et al., 2016; Brickner et al., 2019). The SAGA complex (involved in transcription initiation) also appears to contribute to the association of active *INO1* with the NPC (Lo et al., 2001, 2005). Here, specific NPC components contribute to the efficient binding to *INO1* (Light et al., 2010). These interactions have been proposed to promote optimal transcription and mRNA export. However, our current lack of knowledge on the molecular basis for the interactions of *INO1*, and other active genes, with the NPC has limited our understanding of its significance.

Several Nups that play a role in the NPC-association of *INO1* also functionally interact with Ulp1 suggesting it is positioned at or near the site of gene association. Furthermore, alterations in sumoylation events have been shown to impact *INO1* transcription (Felberbaum et al., 2012). Consistent with this idea, Ulp1 has been previously shown to contribute to the activation and NPC-binding of the *GAL1* gene (Cabal et al., 2006; Texari et al., 2013). These observations and others implicating sumoylation in chromatin association with the NE and the regulation of gene expression has led us to investigate the role of sumoylation and desumoylation in the localization and expression of *INO1*. Our analysis of the roles of the SUMO ligase Siz2 and Ulp1 have revealed functions for sumoylation and desumoylation events in the NPC targeting and expression of activated *INO1*. We show that induction of *INO1* is accompanied by Siz2-dependent sumoylation of proteins associated with the *INO1* locus and propose that these modifications are required for targeting the gene to the NPC. Once at an NPC, Ulp1 interacts with sumoylated proteins associated with the induced *INO1* gene, primarily within its ORF. We propose that subsequent Ulp1-mediated desumoylation promotes expression and NPC association of activated *INO1*.

MATERIALS AND METHODS

Media, Yeast Strains, and Plasmids

Saccharomyces cerevisiae strains used in this study were derived from YEF473A (Bi and Pringle, 1996) and are listed in **Supplementary Table S1**. Strains were grown in either fully

supplemented synthetic media (SC media) (0.17% yeast nitrogen base, 0.5% ammonium sulfate, 2% glucose) or in synthetic media lacking inositol (INO^- media) or were grown in YPD (1% yeast extract, 2% bactopeptone, and 2% glucose). Plasmid bearing strains were grown in the appropriate synthetic dropout media (0.8% dropout powder, 0.17% yeast nitrogen base, 0.5% ammonium sulfate, 2% glucose) that either contained or lacked inositol.

Strain construction employed genome modifications performed using a one-step genomic integration method (Longtine et al., 1998), in which a DNA cassette was transformed into an appropriate strain using the lithium acetate/polyethylene glycol method (Gietz and Woods, 2002). DNA cassettes used to produce C-terminal Protein A, GFP, RFP, and mCherry gene fusions were made using a plasmid/PCR-based method (Longtine et al., 1998). DNA cassettes encoding the various *ulp1*Δ mutants were made by ligating together PCR generated DNA segments modified with specific restriction enzyme sites. For $ulp1\Delta_{1-150}$ and $ulp1\Delta_{1-340}$, these DNA cassettes (bracketed) and restriction sites include: (*ULP1* 5′UTR)-*Eco*RI-(*ULP1* nucleotides from 451 within the ORF to 26 after the stop codon for $ulp1\Delta_{1-150}$ and nucleotides from 1021 within the ORF to 26 after the stop codon for $ulp1\Delta_{1-340}$)-*Bam*HI-(marker gene: *NATMX* for $ulp1\Delta_{1-150}$ and *KANMX* for $ulp1\Delta_{1-340}$)-*Spe*I-(*ULP1* 3′UTR). The *Eco*RI site introduces Glu-Phe codons after the Met start codon. The $ulp1\Delta_{150-340}$ cassette consisted of (*ULP1* 5′UTR to *ULP1* nucleotide 450 within the ORF)-*Bss*HII-(*ULP1* nucleotides 1021–1861 within the ORF)-*Spe*I-(*ULP1* nucleotides 2–26 after the stop codon)-*Bam*HI-(marker gene *NATMX*)-*Spe*I-(*ULP1* 3′UTR). The *Bss*HII restriction site introduces Ala-Arg codons, while the *Spe*I restriction site at the 3′ end of $ulp1\Delta_{150-340}$ overlaps with the stop codon and introduces a Lys to Asn codon substitution at the 3′ end of the ORF. PCR-based generation of DNA cassettes also introduced a point mutation in, $ulp1\Delta_{1-340}$ resulting in an F610S amino acid residue substitution, and in $ulp1\Delta_{150-340}$ resulting in an E409G residue substitution, that have no apparent effect on the relative function of these deletion derivatives. The *NUP53-ulp*$^{340-621}$ DNA cassette consisted of (*ULP1* 5′UTR)-*Nde*I-(*NUP53*)-*Sal*I-(*ULP1* nucleotides from 1018 within the ORF to 26 after the stop codon)-*Spe*I-(*ULP1* nucleotides 2–26 after the stop codon)-*Bam*HI-(marker gene *NATMX*)-*Spe*I-(*ULP1* 3′UTR). The *Sal*I restriction site adds Val-Asp codons at the fusion point between *NUP53* and *ulp1*$^{340-621}$. The *Spe*I restriction site at the 3′ end of *ulp*$^{340-621}$ overlaps with the stop codon and introduces a Lys to Asn codon substitution at the 3′ end of the ORF. PCR-based generation of *NUP53-ulp*$^{340-621}$ introduced point mutations resulting in an E409G, and V584A amino acid substitutions in *ulp*$^{340-621}$ that have no apparent effect on the relative function of this fusion.

To visualize *INO1* gene localization, a previously described genomic tagging system was employed (Straight et al., 1996). *GFP-lacI-HIS* was integrated at the *his-Δ200* locus using the pAFS78 plasmid (Robinett et al., 1996). To tag the *INO1* locus, the plasmid pAFS52.*INO1* was made by cloning PCR amplified *INO1*, containing *Xho*I sites at its 5′ and 3′ ends, into pAFS52 (Straight et al., 1996). *Bgl*II digested pAFS52.*INO1* was then transformed into yeast to integrate the $lacO_{256}$-*TRP* array. This resulted in a duplication of the *INO1* locus with $lacO_{256}$-*TRP* found between the duplicates.

Plasmids used here are derivatives of pRS315 (pEMPTY) (Sikorski and Hieter, 1989) and include pRS315.Ulp1-GFP and pRS315.ulp1^{CSDN}-GFP (Elmore et al., 2011), as well as pRS315.Ulp1 and pRS315.ulp1^{CSDN} (this work).

INO1 Gene Induction

To induce *INO1* gene expression, cell cultures were grown overnight at room temperature in SC media, diluted into fresh SC media to an OD_{600} = 0.2, and then grown at 30°C until the cultures reached mid-log phase (OD_{600} = ∼0.8). A sample of these cultures was then taken as the uninduced control, and processed as required. A second sample of cells from these cultures were collected by centrifugation, washed once with water, and then resuspended in INO^- media to an OD_{600} = 0.5 to induce INO1 expression. These cultures were then grown at 30°C. Cells were collected at the stated time points and processed as indicated.

qRT-PCR for *INO1* Gene Expression

INO1 induction was carried out as described above and, at each time point, an OD_{600} = 10 equivalent of cells was pelleted and processed. RNA preparation from these cells and subsequent real-time qRT-PCRs were performed as previously described (Wan et al., 2009). cDNA was amplified using 2 μg of DNAse-treated RNA that was reverse transcribed using 200 units of Superscript II reverse transcriptase (Invitrogen) at 42°C for 50 min and the resulting cDNAs were diluted 100-fold. Reactions were assembled using SYBR green super mix (Quanta), as per the manufacturer's protocol, and included sense (S) and antisense (AS) primers against *ACT1* (S-GGATTCCGGTGATG GTGTTA, AS-TCAAATCTCTACCGGCCAAA) and *INO1* (S-CACCAT GGAAAACCTCTTGC, AS-GGGGACACCTTCCAAGATAGA) as previously described (Brickner et al., 2007). Reactions were carried out on an Mx3000P QPCR System (Agilent Technologies). *INO1* mRNA levels were normalized relative to *ACT1* mRNA levels from three independent qRT-PCR analyses.

ChIP for Protein Localization at *INO1*

INO1 induction was carried out as described above and, at each time point, an OD_{600} = 50 equivalent of cells was pelleted and processed. Chromatin immunoprecipitation experiments were performed as previously described (Wan et al., 2009). For immunoprecipitation, 4 μl of rabbit polyclonal anti-PrA (Sigma) antibody or 4 μl of rabbit polyclonal anti-Smt3 (SUMO) antibody (Wozniak lab) was prebound to 100 μl of Protein G Dynabeads (Invitrogen). Immunoprecipitated DNA was recovered and analyzed by qRT-PCR as described above. Sense (S) and antisense (AS) primers used for qRT-PCR included: Chromosome V intergenic region (S-ACATTCTTGGAAA CCCATCG, AS-TCGTATCATGATTTAGCGTCGT); *INO1* regions: *GRS1* (S-TC GTTCCTTTTGTTC TTCACG, AS-GCCTCCGCATATTTCA CATT), *A* (S-AAATGCGGCATGTGAAAAGT, AS-AGAG GTG CGCTTTCTCTGC), *B* (S-AGAGAAAGCGCACCTCTGC, AS-(AGGAACCCGACAACAGAACA), *C* (S-CGACAAGTGCACG TACAAGG, AS-CAGTGGGCGTTACATCGAA), *D* (S-CTTC

GGCTCC ATGACTCAAT, AS-GCTAACCATGGGCAACAG AG), *E* (S-GGACTCAAAAGTGGCAATGG, AS-TCAAGGGC GTAGCCAGTAAA), *F* (S-CGTCTTAAAAGGGGCGTTTT, AS-TTTACTGAGG TGGCCCTTGA). To quantify the ChIP experiments, we first expressed the amount of *INO1* or Chromosome V intergenic region sequence immunoprecipitated as a percentage of total input (% of input). Using these values, we calculated ratios comparing the% of input from each region of the *INO1* gene to the% of input for the Chromosome V intergenic region for both uninduced (cells grown in the presence of inositol) and induced (cells grown in the absence of inositol for 1 and 3 h) samples. Relative fold change for the induced samples was then calculated by dividing the induced ratio determined for a given region of the *INO1* gene by the uninduced ratio for that same region.

Fluorescence Microscopy

To image the GFP-lacI/lacO_{256} tagged *INO1* locus, cell cultures were treated as described above for *INO1* gene induction. Cells from 1 ml of culture were pelleted by centrifugation, washed once with the appropriate synthetic media, and then resuspended in the same media; 1.5 μl of cells was then spotted onto a microscope slide for live-cell image acquisition. Epifluorescence images were acquired on a DeltaVision Elite imaging system (GE Healthcare Life Sciences) at 60x magnification using a 1.42 NA oil, Plan Apo N objective (Olympus). Images were collected and saved as 15 × 0.2 μm z-stacks using SoftWoRx software (version 6.5.2, GE Healthcare Life Sciences), then rendered and analyzed using Image J (NIH). *INO1* localization (GFP-lacI signal) was assessed relative the nuclear periphery (Nup49-mRFP signal) and was considered to colocalize with NPCs when the GFP-lacI focus fully or partially overlapped with Nup49-mRFP, similar to the previously described method (Brickner and Walter, 2004; Brickner and Brickner, 2010).

To assess the localization of the various Ulp1-GFP and Ulp1-mCherrry derivatives, strains producing these derivatives were grown in YPD media at 30°C to mid-log phase; 1 ml of cells from each culture was then pelleted by centrifugation, washed once with 1 ml of SC media, and resuspended in 20 μl of SC media; 1.5 μl was then spotted onto a microscope slide for epifluorescence imaging. Images were acquired using an Axio Observer.Z1 microscope (Carl Zeiss, Inc.), equipped with an UPlanS-Apochromat 100x/1.40 NA oil objective lens (Carl Zeiss, Inc.) and an AxioCam MRm digital camera with a charge-coupled device (Carl Zeiss, Inc.). Images were acquired in a single focal plane through the center of nuclei. Images were saved using AxioVision (Carl Zeiss, Inc.) software and rendered for display using Image J (NIH) software.

Western Blot

Ulp1-GFP and various ulp1Δ-GFP derivatives were detected using western blot. Proteins from cells lysates were separated by SDS-PAGE and then transferred to nitrocellulose membranes. Membranes were incubated in blocking buffer (TBS containing 0.1% Tween-20 and 5% milk powder) for at least 1 h at room temperature. Blocking buffer was then removed and replaced with fresh blocking buffer supplemented with rabbit polyclonal antibodies directed against GFP, GSP1, or SUMO (Makhnevych et al., 2007) then incubated overnight at 4°C. Membranes were then washed three times using 0.1% Tween-20 in TBS, followed by incubation in blocking buffer supplemented with goat anti-rabbit HRP conjugated antibody (BioRad) at a 1:10,000 dilution for at least 1 h at room temperature. Membranes were then washed three times using 0.1% Tween-20 in TBS. Bound anti-rabbit HRP conjugated antibody was detected by chemiluminescence (Amersham) using an ImageQuant LAS 4000 (GE) imaging system.

RESULTS

Activation of the *INO1* Gene Is Accompanied by Sumoylation of Associated Proteins

Following their activation, numerous yeast genes are repositioned from the nuclear interior to the nuclear envelope (Brickner and Walter, 2004; Texari et al., 2013; Brickner et al., 2019). A well-studied example is the *INO1* gene. When cells are switched from medium containing inositol to medium lacking this carbon source, the *INO1* gene is induced and the gene locus is targeted to NPCs (Brickner and Walter, 2004; Cabal et al., 2006; Brickner et al., 2007; Ahmed et al., 2010; Light et al., 2010). Since changes in the expression of genes are often accompanied by changes in the levels of sumoylation of associated TFs and other chromatin-associated proteins, we examined whether the induction of *INO1* alters the sumoylation state of proteins associated with the *INO1* locus. To test this, antibodies directed against SUMO were used in ChIP analysis targeting the *INO1* gene prior to and following induction. For these experiments, various sets of oligonucleotides were used to detect interacting regions along the *INO1* gene (**Figure 1A**). Prior to induction, the sumoylation state of chromatin associated proteins within the *GRS1* and ORF regions of the *INO1* gene were higher than that detected in a control intergenic region (**Supplementary Figure S1B**). Following induction, we observed significant changes in the levels of sumoylated proteins associated with specific regions of the gene (**Figure 1B**). In a 5′ region containing the previously identified *INO1* gene recruitment sequence 1 (GRS I), we observed a decrease in sumoylation of associated proteins while adjacent regions containing the transcriptional start site showed increases. Downstream regions within the ORF and the 3′ regions showed little or no change in the levels of associated sumoylated proteins.

The SUMO Ligase Siz2 Is Required for Recruitment of the *INO1* Locus to the NE

Our observations that the levels of sumoylated proteins bound to the *INO1* locus, in particular those associated with 5' regions containing the GRS1 sequence, changed upon induction led us to investigate the role of sumoylation in the NPC association of *INO1*. As the SUMO ligase Siz2 had been previously shown to play a role in the nuclear envelope association of telomeres (Ferreira et al., 2011; Churikov et al., 2016; Lapetina et al., 2017),

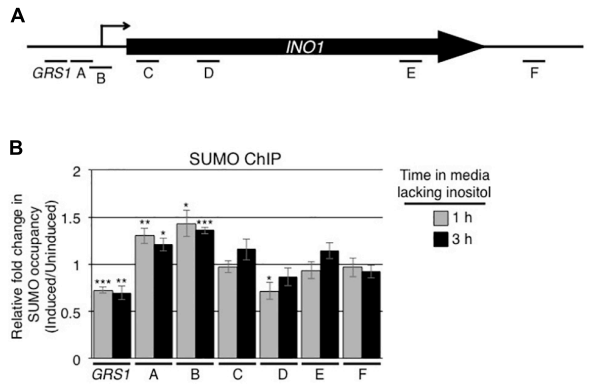

FIGURE 1 | Induction of *INO1* leads to changes in the sumoylation of *INO1*-associated proteins. **(A)** Diagram of the *INO1* locus showing the relative positions of the transcriptional start site (arrow), the *GRS1* sequence, the open reading frame, and regions targeted for the ChIP analysis shown in **B**. **(B)** WT cells were grown in medium containing inositol (repressing/uninduced conditions) to an OD_{600} of ∼0.8, washed, and transferred to medium lacking inositol (inducing conditions). Cells were then subjected to ChIP analysis using antibodies directed against the SUMO polypeptide (anti-SUMO antibody) prior to and at 1 and 3 h post induction of *INO1*. qRT-PCR was used to quantify levels of DNA corresponding to the various regions of *INO1* (see **A**) bound to sumoylated proteins. Shown is the relative fold change in the occupancy of sumoylated proteins associated with the various regions of *INO1* at the indicated times after induction relative to the uninduced samples (see section "Materials and Methods"). Results are the means ± SEM of five biological replicates. Asterisks indicate a significant difference relative to uninduced as determined by a Student's paired *t*-test. $^{*}p < 0.05$, $^{**}p < 0.01$, $^{***}p < 0.001$.

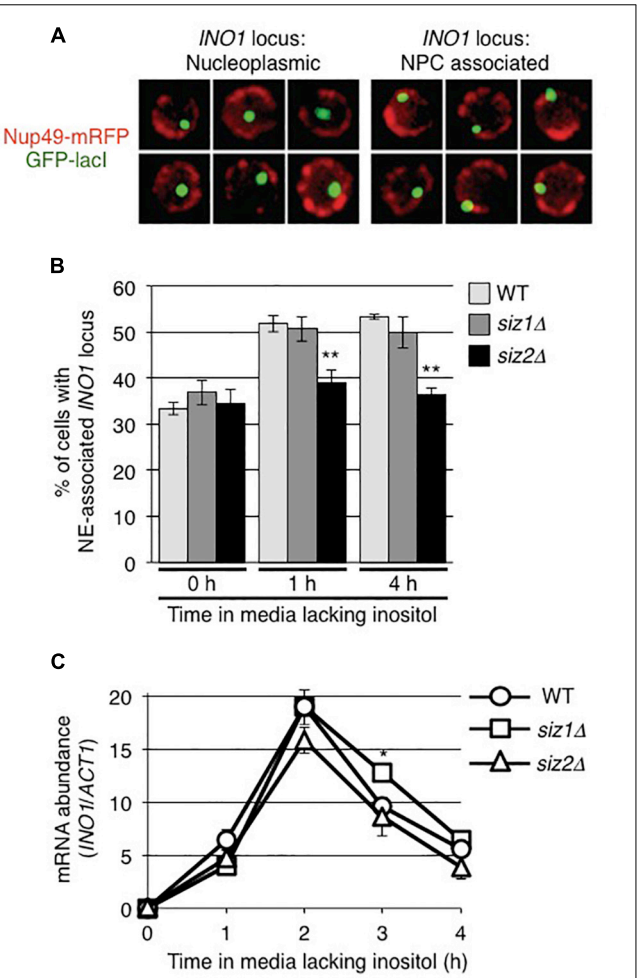

FIGURE 2 | The SUMO ligase Siz2 is required for NE-association, but not transcription, of induced *INO1*. Localization of the *INO1* locus prior to and following *INO1* induction was examined in cells containing the *INO1-lacO*$_{256}$ construct and producing GFP-lacI (green). The position of the nuclear envelope (NE) in these cells relative to the *INO1-lacO* locus was determined using Nup49-RFP (red). **(A)** Examples of cell nuclei in which the *INO1* locus (green) was (left panels) or was not (right panels) associated with the nuclear periphery (red) are shown. *INO1* was scored to be NE-associated if the GFP-lacI signal fully or partially overlapped with the Nup49-mRFP signal. **(B)** The percentage of cells showing NE-association of *INO1-lacO* prior to (0 h) or at 1 and 4 h after induction was determined in the indicated strains. Results are the means ± SD of three biological replicates. At least 100 cells were counted for each sample. **(C)** Levels of *INO1* mRNA were examined in the indicated strains. Cell cultures were grown in medium containing inositol (repressing conditions) to an OD_{600} of ∼0.8 and then washed and placed in medium lacking inositol (inducing conditions) for the indicated times. Levels of mRNA encoded by the *INO1* gene were evaluated by qRT-PCR and their abundance relative to *ACT1* mRNA was determined. Results are the means ± SEM of three biological replicates. Asterisks indicate a significant difference from WT as indicated by Student's unpaired *t*-test, $^{*}p < 0.05$, $^{**}p < 0.01$.

we examined the role of Siz2, and the related SUMO ligase Siz1, in *INO1* localization following its induction. The position of *INO1* was monitored by tagging with an adjacent *lacO*$_{256}$ cassette in cells producing the GFP-lacI protein (Brickner and Walter, 2004; Ahmed et al., 2010; see **Figure 2A**). Induction of *INO1* led to a rapid (within 1 h) accumulation of *INO1:lacO*$_{256}$/GFP-lacI foci at the nuclear periphery in WT cells and those lacking Siz1 (*siz1*Δ) (**Figure 2B**). By contrast, we observed that in cells lacking Siz2 (*siz2*Δ), *INO1* recruitment to the NE was not observed following induction. We also measured *INO1* mRNA levels following induction in these various strains, and observed no differences in the induction profiles (**Figure 2C**). These results suggest that Siz2 is required for *INO1* binding to the nuclear periphery upon induction, but its loss has no significant effect on *INO1* expression.

The requirement of Siz2 for the binding of induced *INO1* to the NE led us to examine whether Siz2 contributed to sumoylation at the *INO1* locus. To test this idea, we examined levels of sumoylated proteins at the *INO1* locus in the *siz2*Δ mutant. In contrast to WT cells, the *siz2*Δ mutant cells showed reduced levels of sumoylation within the ORF of the *INO1* locus in uninduced cells. Moreover, induction of *INO1* did not significantly alter sumoylated proteins levels along the INO1 locus (**Supplementary Figure S1C**). These results are consistent with Siz2 functioning in the sumoylation of proteins associated with regions of the *INO1* locus prior to and following *INO1* activation.

We also examined whether Siz2 physically interacted with the *INO1* locus upon activation of the *INO1* gene. Using protein A tagged Siz2 (Siz2-PrA) and ChIP analysis, we examined the binding of Siz2-PrA along the *INO1* locus prior to and

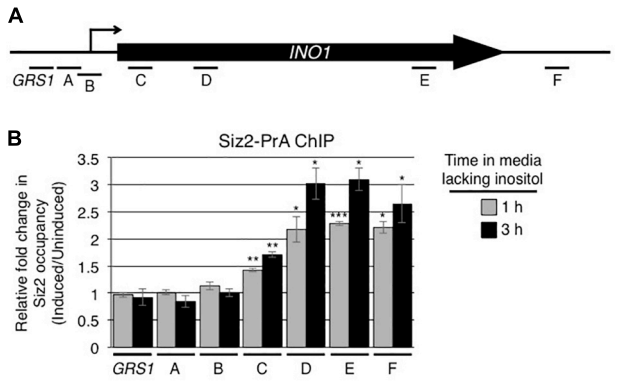

FIGURE 3 | Induction of *INO1* is accompanied by recruitment of Siz2 to the *INO1* locus. **(A)** Diagram of the *INO1* locus and regions detected by ChIP analysis (see **Figure 1A**) in **B**. **(B)** Cells expressing protein A tagged Siz2 (Siz2-PrA) were grown as described in the **Figure 1** legend, and harvested at 0, 1, and 3 h after *INO1* induction. Changes in Siz2-PrA occupancy along the *INO1* locus following induction were examined by ChIP and qRT-PCR using primer pairs that amplify regions of *INO1* indicated in **A**. Relative fold change in Siz2-PrA binding was determined as described for SUMO binding in **Figure 1**. Results are the means ± SEM of at least three biological replicates. Asterisks indicate a significant difference relative to uninduced as determined by a Student's paired *t*-test. $^{*}p < 0.05$, $^{**}p < 0.01$, $^{***}p < 0.001$.

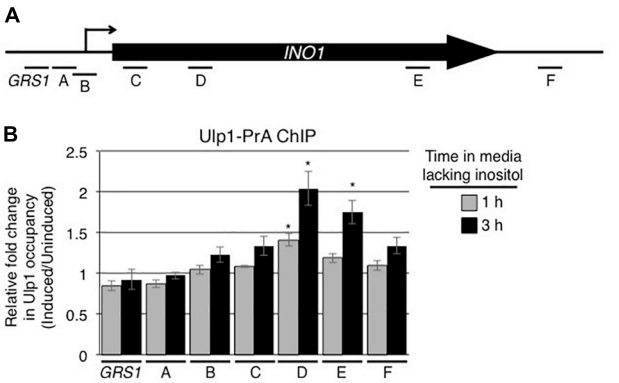

FIGURE 4 | Ulp1 interacts with the induced *INO1* gene. **(A)** Diagram of the *INO1* locus and regions detected by ChIP analysis (see **Figure 1A**). **(B)** Cells producing protein A tagged Ulp1 (Ulp1-PrA) were grown as described in the **Figure 1** legend, and harvested at 0, 1, and 3 h after *INO1* induction. Changes in Ulp1-PrA occupancy throughout the *INO1* locus upon induction were examined by ChIP and qRT-PCR using primer pairs that amplify regions of *INO1* indicated in **A**. Relative fold change in Ulp1-PrA binding was determined as described for SUMO binding in **Figure 1**. Results are the means ± SEM of three biological replicates. Asterisks indicate a significant difference relative to uninduced as determined by a Student's paired *t*-test. $^{*}p < 0.05$.

following 1 and 3 h induction (**Supplementary Figure S2** and **Figure 3B**). In uninduced cells, we detected significantly higher levels of Siz2-PrA bound to the *GRS1*-containing region relative to the intergenic control, while other regions show no enrichment (**Supplementary Figure S2**). Upon induction of *INO1*, we observed no significant change in Siz2-PrA binding within 5′ regions of *INO1* locus (from site GRS I to site B, see **Figure 3A** for map). However, Siz2-PrA occupancy within the *INO1* ORF (region C to F) increased markedly upon induction (**Figure 3B**). These results are consistent with Siz2 functioning in the sumoylation of proteins associated with various regions of the *INO1* locus both prior to (upstream of the ORF) or in response to *INO1* activation (within the ORF).

INO1 Interacts With Ulp1 Following Induction

The association of activated genes with NPCs is thought to occur through interactions between the transcriptional machinery and proteins located on the nuclear face of the NPC. Among these, Nup60 and the related proteins Mlp1/Mlp2 are required for *INO1* association with NPCs (Brickner et al., 2007; Ahmed et al., 2010; Light et al., 2010; Brickner et al., 2019). These NPC proteins are also required for the association of the desumoylase Ulp1 with NPCs (Zhao et al., 2004; Palancade et al., 2007; Srikumar et al., 2013). As Ulp1 is an important regulator of protein sumoylation, we investigated its role in the expression and NPC targeting of the induced *INO1* gene. We tested whether the *INO1* gene physically interacts with Ulp1. Using ChIP, no significant enrichment of Ulp1-pA was detected along the *INO1* locus prior to induction (**Supplementary Figure S2C**). However, following activation, we observed that Ulp1 occupancy significantly increased specifically within the *INO1* ORF (**Figure 4**). By contrast, no detectable change was observed in regions upstream of the ORF. These results suggest that induction of *INO1* is followed by the association of Ulp1 with specific regions of the *INO1* gene.

NPC Recruitment and Expression of *INO1* Require NPC-Associated Ulp1

To evaluate the role of Ulp1 in the recruitment of activated *INO1* to NPCs, we examined whether *ulp1* mutants that lacked domains required for Ulp1 association with NPCs altered the localization of the *INO1* gene. Our strategy was to uncouple Ulp1 from NPCs without altering its catalytic domain (contained within amino-acid residues 403-621) and its essential function in SUMO maturation (Li and Hochstrasser, 2003). Mutants lacking either of the two of previously described NPC binding domains of Ulp1, residues 1–150 (ulp1Δ_{1-150}) or 150–340 (ulp1$\Delta_{150-340}$), were previously shown to still bind to NPCs (Li and Hochstrasser, 2003; Panse et al., 2003). However, a mutant lacking both domains, i.e., residues 1–340 (ulp1Δ_{1-340}), showed greatly reduced levels of NPC association (Panse et al., 2003). Each of these truncation mutations was integrated within the context of the endogenous *ULP1* locus by replacing the endogenous ORF and thus retaining the endogenous promoter and single copy number of the gene. This approach reduces the potential for artifacts arising from elevated levels of Ulp1 derived from plasmid-encoded genes. An examination of the integrated GFP-tagged versions of these mutants revealed similar protein levels to WT (**Supplementary Figure S3B**) and a localization pattern consistent with previous reports, with both the ulp1Δ_{1-150}-GFP and the ulp1$\Delta_{150-340}$-GFP

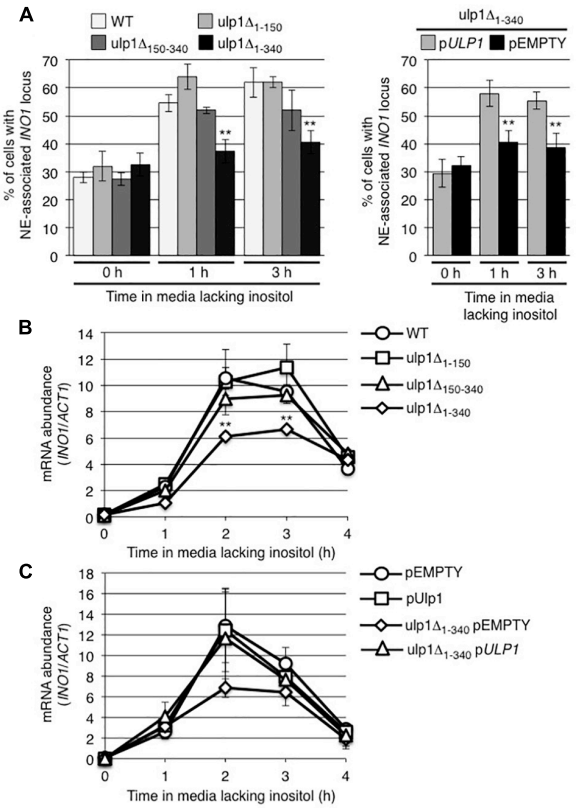

FIGURE 5 | Ulp1 is required for *INO1* expression and NE-association following induction. **(A)** The percentage of cells showing NE-association of *INO1-lacO*$_{256}$ was determined as described in **Figure 2** prior to (0 h) and at 1 and 3 h post induction in WT and the indicated *ulp1* mutant strain backgrounds. Shown on the right are the results of similar experiments performed on a *ulp1*$\Delta_{1\text{-}340}$ strain transformed with either an empty plasmid (pEMPTY) or a plasmid containing a version of WT *ULP1* (p*ULP1*). Results are the means ± SD of three or more biological replicates. At least 50 cells were counted for each sample. **(B,C)** Levels of mRNA encoded by the *INO1* gene were evaluated by qRT-PCR as described in **Figure 2** following induction for the specified times in the indicated strains. Results are the means ± SEM of three biological replicates. Note, **C** shows data from the indicated strains transformed with either an empty plasmid (pEMPTY) or a plasmid containing a version of WT *ULP1* (p*ULP1*). Asterisks indicate a significant difference from WT as indicated by a Student's unpaired *t*-test, $^{**}p < 0.01$.

showing NE levels similar to WT Ulp1, while ulp1Δ_{1-340}-GFP showed low levels of NE-association with a concomitant increase in cytoplasmic and nucleoplasmic localization relative to WT Ulp1-GFP (**Supplementary Figure S3A**). Similarly, sumoylation patterns in the ulp1Δ_{1-150} and the ulp1$\Delta_{150-340}$ mutants appeared largely similar to WT cells. However, levels of sumoylated proteins are slightly reduced in the ulp1Δ_{1-340} mutant (**Supplementary Figure S3C**).

We examined the effects of *ulp1* truncation mutants on the inducible recruitment of *INO1* to NPCs (**Figure 5A**). Induction of *INO1* led to a rapid (within 1 h) accumulation of *INO1* foci at the nuclear periphery in cells producing the ulp1Δ_{1-150} or ulp1$\Delta_{150-340}$ truncation, similar to that observed in WT cells. By contrast, cells producing the ulp1Δ_{1-340} mutant showed no localization of *INO1* to the NE following induction. Furthermore, in monitoring mRNA levels at various times post induction, we found that *INO1* transcript levels were reduced in the *ulp1*Δ_{1-340} mutant and failed to reach levels detected in the *ulp1*Δ_{1-150}, *ulp1*$\Delta_{150-340}$, or WT strains (**Figure 5B**). Importantly, both the recruitment of *INO1* to the NE and WT levels of *INO1* mRNA levels could be restored in the *ulp1*Δ_{1-340} mutant by the introduction of WT *ULP1* (**Figures 5A,C**), suggesting the phenotype detected in *ulp1*Δ_{1-340} mutant arises from the loss of Ulp1 at NPCs, and not the presence of the ulp1Δ_{1-340} mutant protein outside of the NPC.

The effects of the *ulp1*Δ_{1-340} mutant on the *INO1* localization and expression could occur as a consequence of the loss of functions linked to its N-terminal domain (residues 1–340) or the loss of Ulp1 isopeptidase activity at the NPC. To investigate these possibilities, we examined the effects of expressing a *ulp1* double point mutant (*ulp1*^{CSDN}) that abrogates SUMO binding and isopeptidase activity (Mossessova and Lima, 2000; Elmore et al., 2011) but does not alter its N-terminal domain or targeting to NPCs. This catalytically dead *ulp1*^{CSDN} does not support cell viability in the absence of WT Ulp1 (Elmore et al., 2011), thus we expressed the *ulp1*^{CSDN} mutant in WT cells and assessed whether the mutant exhibited dominant negative phenotypes. As shown in **Figure 6A**, ulp1^{CSDN}-GFP localizes to NPCs, consistent with the known functionality of its N-terminus. Levels of the mutant protein at the nuclear periphery varied between cells, likely due to cell-to-cell variations in the amount of ulp1^{CSDN}-GFP (arising from cell-to-cell variation in the plasmid encoded gene). Inspection of these cells revealed that the amount of ulp1^{CSDN}-GFP at the NE appeared inversely proportional to the amount of endogenous WT Ulp1p at the same locale, suggesting the mutant protein was capable of competing with the WT protein for NPC binding sites (**Figure 6B**).

The expression of the *ulp1*^{CSDN} mutant had little effect on cell growth and no striking changes were seen in global protein sumoylation patterns (**Supplementary Figures S4A,B**). However, when we examined the localization of *INO1* following induction, the presence of the ulp1^{CSDN} mutant protein inhibited the *INO1* locus from relocating to the NE (**Figure 6C**). By contrast, plasmid-borne *ULP1* did not alter induction-dependent *INO1* association with the NE. These results led us to conclude that the association of Ulp1 catalytic activity at the NPC is required for recruitment of the *INO1* locus. However, cells producing the ulp1^{CSDN}-GFP mutant did not exhibit altered *INO1* expression following induction (**Figure 6D**), suggesting that the mutant may not exhibit a dominant negative phenotype with respect to *INO1* expression.

Our analysis of the *ulp1*^{CSDN} mutant suggests a role for the Ulp1 catalytic activity in the association of induced *INO1* with NPCs; however, these data provided no insight into its function in *INO1* expression. Therefore, we asked whether positioning of the Ulp1 catalytic domain at NPCs would be sufficient for *INO1* expression. To do this, we constructed a chimeric gene encoding the Ulp1 catalytic domain (residues 340–621) fused to the C-terminus of the nucleoporin Nup53 (**Figure 7A**). The Nup53-ulp1$^{340-621}$ fusion protein showed a similar localization pattern to that observed for nucleoporins, consistent with its association

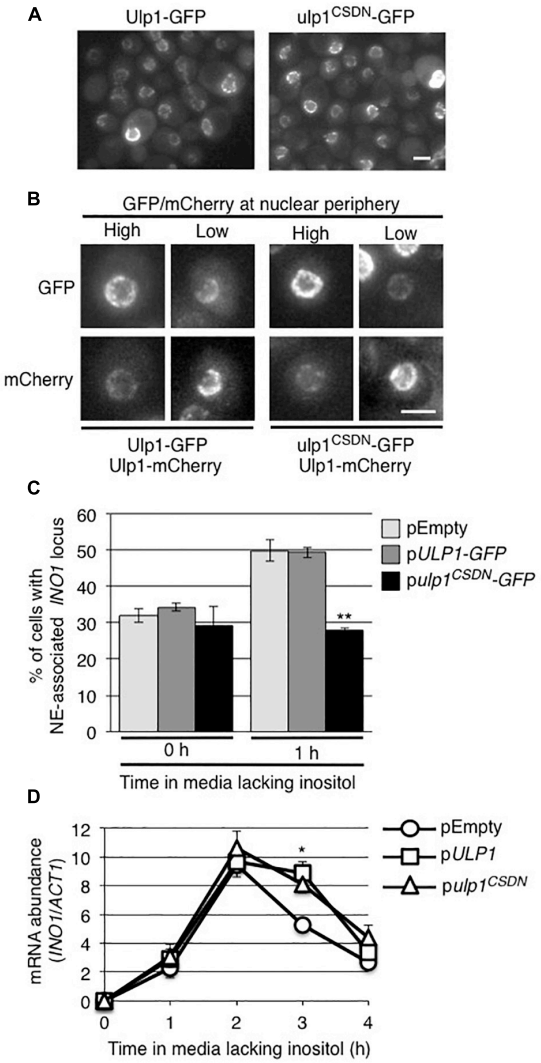

FIGURE 6 | The *ulp1-CSDN* mutant inhibits *INO1* targeting to the NE. **(A)** Shown are images of WT cells producing exogenously expressed, plasmid-encoded Ulp1-GFP or Ulp1^{CSDN}-GFP. **(B)** The localization of plasmid-encoded Ulp1-GFP or Ulp1^{CSDN}-GFP in cells producing mCherry-tagged endogenous wild-type Ulp1 (Ulp1-mCherry) was examined. Shown are cells containing relatively high or low levels of the GFP fusion, likely stemming from cell to cell variability in plasmid copy number. Competition of NE-associated binding between the plasmid-encoded Ulp1-GFP or Ulp1^{CSDN}-GFP and endogenous Ulp1-mCherry proteins is indicated by the relative GFP and mCherry signal intensities at the NE. Scale bars = 2 μm. **(C)** Recruitment of *INO1* to the NPCs was measured as in **Figure 2** in a WT strain containing *INO1-lacO*$_{256}$/GFP-lacI and the indicated plasmid. Results are the means ± SD of three or more biological replicates. At least 50 cells were counted for each sample. **(D)** Levels of mRNA encoded by the *INO1* gene were evaluated by qRT-PCR as described in **Figure 2** following induction for the specified times in the indicated strains. Asterisks indicate a significant difference from WT (pEMPTY) as indicated by a Student's unpaired *t*-test, $^{*}p < 0.05$, $^{**}p < 0.01$.

with NPCs (**Figure 7B**). Moreover, cells producing the Nup53-ulp1$^{340-621}$ protein, and lacking endogenous Ulp1, grew similar to WT cells (**Supplementary Figure S4C**), suggesting that the Ulp1 catalytic domain of the fusion protein could replace the essential function of WT Ulp1. In these Nup53-ulp1$^{340-621}$ producing cells, we observed levels of *INO1* mRNA production following induction similar to that detected in WT cells, and analysis of *INO1* localization showed its recruitment to the NE was comparable to that seen in WT cells (**Figures 7C,D**). Thus, positioning of the Ulp1 catalytic domain at NPCs was sufficient to support *INO1* expression and NPC association.

Several *nup* mutants have been previously shown to inhibit post-induction *INO1* association with the NE, including a strain lacking Nup60 (*nup60*Δ) or Nup2 (*nup2*Δ) (Ahmed et al., 2010; Light et al., 2010; also see **Figure 7E**). Both Nup60 and Nup2 are functionally linked to Ulp1; the loss of Nup60 results in decreased cellular levels of Ulp1 (Palancade et al., 2007) and Nup2 has been reported as a SUMO target and a Ulp1 interacting partner (Hannich et al., 2005; Srikumar et al., 2013; Folz et al., 2019). Therefore, we tested whether the Nup53-ulp1$^{340-621}$ protein could rescue the *INO1* targeting defects in the *nup60*Δ and *nup2*Δ mutants. In these mutants, the Nup53-ulp1$^{340-621}$-GFP fusion was visible at the NE in a characteristic NPC pattern (**Figure 7B**). Importantly, we observed that production of the Nup53-ulp1$^{340-621}$ protein in the *nup60*Δ and *nup2*Δ mutants rescued inducible *INO1* recruitment to the NPC (**Figure 7E**). Moreover, an examination of the expression of the *INO1* gene in these strains revealed that they produced WT levels of *INO1* mRNA (**Figure 7F**). On the basis of these data, we conclude that the defects previously detected in the *nup60*Δ and *nup2*Δ mutants are functionally linked to Ulp1.

NPC-Associated Ulp1 Regulates Sumoylation Levels of Proteins Associated With the *INO1* ORF

Since the C-terminal domain of Ulp1 (residues 340–621) possesses both SUMO binding and desumoylase activity, we examined the effects of removing this domain of Ulp1 from the NPC on the sumoylation state of *INO1* bound proteins. To test this, we examined SUMO occupancy along the induced *INO1* locus in the *ulp1*Δ$_{1-340}$ mutant. In this mutant, we observed an increase in sumoylation of proteins in regions A and B of the *INO1* gene (adjacent to and containing the transcriptional start site) after induction (**Figure 8B**) similar to that seen in WT cells (**Figure 1B**). However unlike WT cells, the *ulp1*Δ$_{1-340}$ mutant showed no decrease in sumoylation in the GRS1 region and generally higher levels of protein sumoylation within *INO1* ORF (**Figure 1B**) where we detected Ulp1 binding in WT cells (**Figure 4B**). These data led us to conclude that Ulp1, within the context of the NPCs, functions to bind and desumoylate proteins associated with the induced *INO1* GRS1 and ORF.

DISCUSSION

Numerous observations have established that the spatial organization of the yeast genome is dynamic, and the positioning of numerous yeast genes within the nucleoplasm has been shown to be altered by their expression status. For example, transcriptional activation of the *INO1* gene, induced by a lack

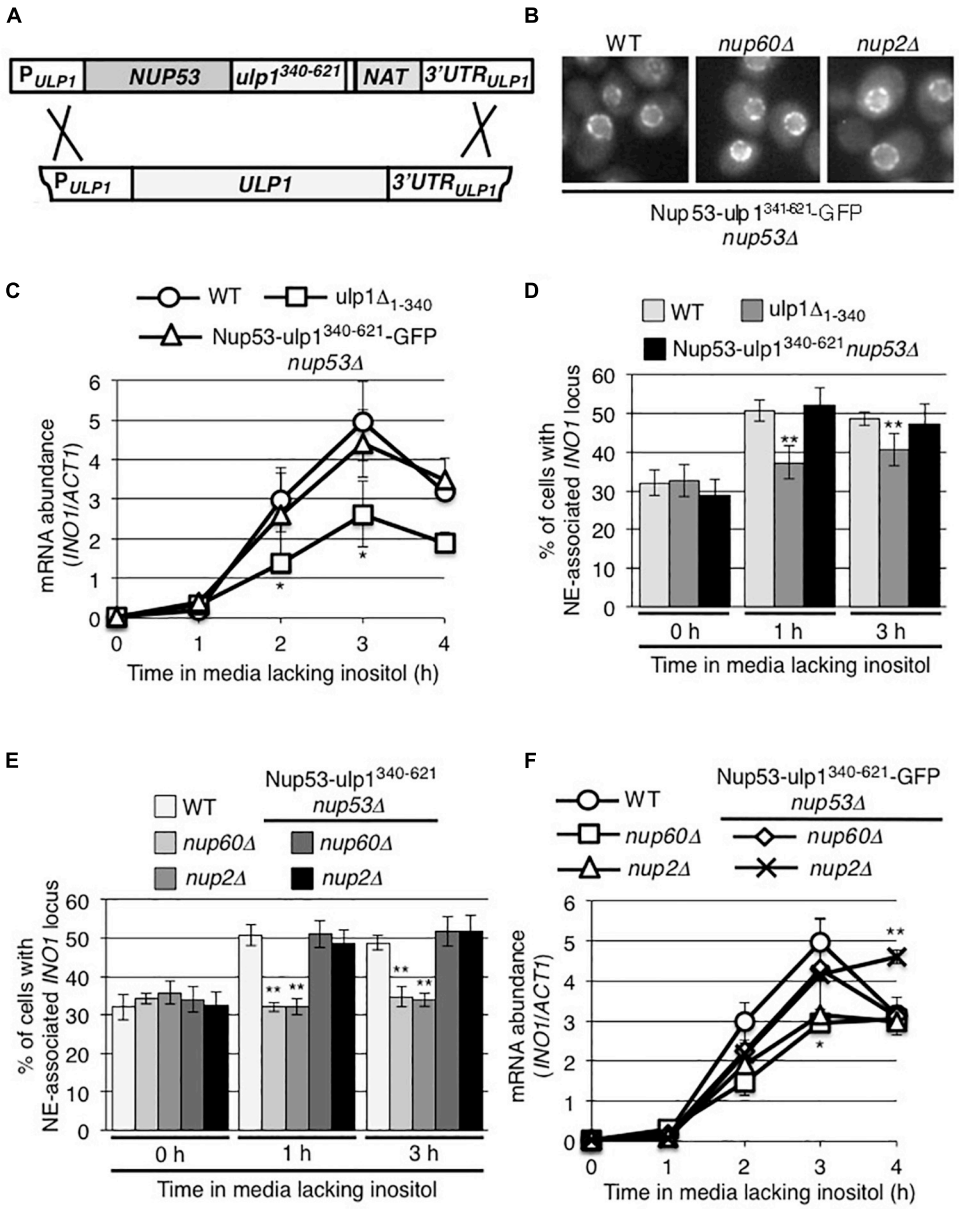

FIGURE 7 | The NPC association of the C-terminal domain of Ulp1 is sufficient to support recruitment of induced *INO1*. **(A)** Endogenous *ULP1* was replaced by a *NUP53-ulp1*$^{340\text{-}621}$ chimera under the control of the *ULP1* promoter in a haploid yeast strain. A schematic representation of the construction of this chimeric gene is shown. **(B)** Localization of the Nup53-ulp1$^{340\text{-}621}$ fusion protein C-terminally tagged with GFP was examined in an otherwise WT background or in strains lacking *NUP60* or *NUP2*. **(C,F)** Levels of mRNA encoded by the *INO1* gene were evaluated by qRT-PCR following induction for the indicated times; **(C)** in WT, *NUP53-ulp1*$^{340\text{-}621}$, and *ulp1*$\Delta_{1\text{-}340}$ strains and **(F)** in WT, *nup60*Δ, *nup2*Δ, *NUP53-ulp1*$^{340\text{-}621}$ *nup60*Δ, *and NUP53-ulp1*$^{340\text{-}621}$ *nup2*Δ strains as described in **Figure 2**. Results are the means ± SEM of three biological replicates. **(D,E)** Localization of the *INO1-lacO*$_{256}$ locus was examined prior to (0 h) or at 1 and 3 h after induction in the indicated strain backgrounds. Note that the data shown here for *ulp1*$\Delta_{1\text{-}340}$ in **D** are the same as that in **Figure 5A** and are shown here for comparison. Localization of *INO1-lacO*$_{256}$ locus was assessed as described in **Figure 2**. Results are the means ± SD of at least three biological replicates. For **D** and **E**, at least 100 cells were counted for each replicate. Asterisks indicate a significant difference from WT samples at the corresponding time points as indicated by Student's unpaired *t*-test. $^{*}p < 0.05$, $^{**}p < 0.01$.

of inositol, is accompanied by its relocalization from the nuclear interior to an NPC. Here we report that these events are dependent on specific regulators of sumoylation, suggesting a role for sumoylation in the expression of the *INO1* gene and its targeting to the NPC. Conditions that induce expression of *INO1* lead to changes in the sumoylation of proteins associated with the *INO1* gene. These sumoylation events are largely mediated by the SUMO ligase Siz2, and, importantly, Siz2 is essential for the relocalization of activated *INO1* from the nucleoplasm to the NE. Concomitant with relocalization, *INO1* also interacts

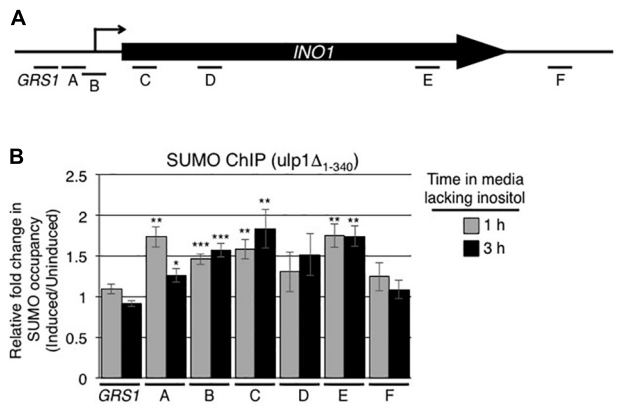

FIGURE 8 | Ulp1 regulates sumoylation levels of proteins associated with the *INO1* ORF. **(A)** Diagram of the *INO1* locus and regions detected by ChIP analysis (see **Figure 1A**). **(B)** *ulp*Δ_{1-340} cells were subjected to ChIP analysis using antibodies directed against the SUMO polypeptide (anti-SUMO antibody) prior to and at 1 and 3 h post induction of *INO1*. qRT-PCR was used to quantify levels of DNA corresponding to the various regions of *INO1* (see panel **A**) bound to sumoylated proteins. Shown are the relative fold changes in the occupancy of sumoylated proteins associated with the various regions of *INO1* at the indicated times after induction relative to the uninduced samples. Results are the means ± SEM of five biological replicates. Asterisks indicate a significant difference relative to uninduced as determined by a Student's paired *t*-test. $^{*}p < 0.05$, $^{**}p < 0.01$, $^{***}p < 0.001$.

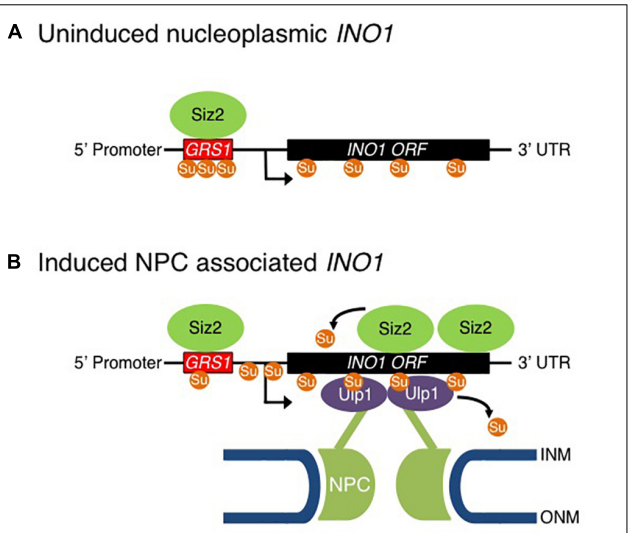

FIGURE 9 | Model for Sumo-mediated recruitment of *INO1* to the NPC. Shown is model for the proposed role of sumoylation in the NPC targeting and transcriptional activation of the *INO1* gene. **(A)** In a repressed state, *INO1* is positioned in the nucleoplasm. **(B)** Reducing levels of inositol in the medium leads to recruitment of Siz2 to the *INO1* locus and increased Siz2-mediated sumoylation of *INO1*-associated proteins. These events are required for the targeting of the *INO1* locus to the NPC where it interacts with NPC-associated Ulp1. Ulp1 supports the association of *INO1* with the NPC and functions to desumoylation of *INO1* bound proteins in regions containing the GRS1 and the ORF. Desumoylation of *INO1*-associated proteins is proposed to promote *INO1* transcription.

with NPC-associated Ulp1. Our data suggest that this interaction desumoylates *INO1*-associated proteins and is required for both targeting of the *INO1* locus to an NPC and normal induction of *INO1* expression. These results imply that a cycle of sumoylation and NPC-associated desumoylation contribute to *INO1* targeting to the NPC and its expression.

The observation that a gene locus relocalizes from the nucleoplasm to an NPC following activation was first described in yeast for the *INO1* gene, and it represents one of the most well studied of a growing list of genes exhibiting this behavior (Egecioglu and Brickner, 2011; Randise-Hinchliff and Brickner, 2016). Several factors required for *INO1* targeting to the NPC have been identified. Two cis-acting DNA elements 5′ to the *INO1* ORF are involved in *INO1* recruitment to NPCs following long-term repression (Ahmed et al., 2010; Light et al., 2010; Randise-Hinchliff et al., 2016). Both sites bind TFs, GRS-I binds Put3 and GRS-II binds Cbf1, and each TF is required for directing GRS-containing DNA elements to NPCs (Shetty and Lopes, 2010; Brickner and Brickner, 2012; Randise-Hinchliff et al., 2016; Brickner et al., 2019). Notably, while TFs may be required for NPC association of activated genes (Randise-Hinchliff et al., 2016; Brickner et al., 2019), RNA polymerase II-mediated transcription is not necessarily required, as shown for both *GAL1* and *INO1* (Schmid et al., 2006; Brickner et al., 2007, 2016).

The functions of Put3 and Cbf1 are not unique as various other TFs, including those functioning in inducible and constitutive expression, or acting as transcriptional regulators (including repressors), also have the potential to target genes to NPCs (Randise-Hinchliff et al., 2016; Brickner et al., 2019). Whether these various factors interact directly or indirectly with Nups is not clear, but it does appear that specific subsets of Nups are required for genes to interact with NPCs. For example, the binding of multiple TFs to NPCs requires Nup2 and Nup100 (Dilworth et al., 2005; Brickner et al., 2019). These and additional Nups positioned on the nucleoplasmic face of NPCs, including Nup60 and Nup1, have been linked to the NPC association of induced *INO1* (Brickner et al., 2007; Ahmed et al., 2010; Light et al., 2010). Of note, this function of Nup1 appears to require its phosphorylation by Cdc28 (Brickner et al., 2007; Brickner and Brickner, 2010). This and related observations support the idea that NPC association of activated *INO1* is cell cycle regulated, being lost during S-phase and reestablished during G2/M-phase where it primarily resides until the following S-phase (Brickner and Brickner, 2010).

Built upon the various requirements previously established for the expression and NPC-targeting of *INO1*, our data have led us to conclude that a cycle of sumoylation and desumoylation is essential for the expression and NPC targeting of activated *INO1*. We envisage a model for these processes that includes multiple steps that we assume initiate in the nucleoplasm (**Figure 9**). Prior to induction, Siz2 is bound to the *GRS1*-containing region of *INO1* (**Supplementary Figure S2B**) and Siz2-dependent sumoylation of proteins associated with the ORF is detected (**Supplementary Figure S1C**). Following induction, Siz2 binding increases within the *INO1* ORF (**Figure 3B**), as does sumoylation of targets associated with the 5′ region of the locus, including the *INO1* transcriptional start site (**Figure 1**,

regions A and B). These increases in sumoylation are Siz2 dependent (**Supplementary Figure S1C**). While we have yet to identify the exact targets of Siz2 sumoylation prior to or following activation of INO1, considering their location within the *INO1* gene, it seems likely that these would include TFs that function in *INO1* targeting to the NPC, including Put3, which contains consensus sumoylation sites (Zhao et al., 2014), and Cbf1, which has previously been shown to be sumoylated (Wohlschlegel et al., 2004; Denison et al., 2005).

Siz2-mediated sumoylation events at the *INO1* locus may perform several functions. In some contexts, sumoylation of TFs and histones has been shown to contribute to transcriptional repression; whereas, in others, sumoylation has been linked to activation of gene transcription (Rosonina et al., 2010; Chymkowitch et al., 2015). Interestingly, previous reports have also implicated sumoylation in both repression and activation of certain genes, suggesting that the effects of sumoylation at a given gene are dependent on the target proteins bound to the locus. For example, analysis of the expression of the inducible *GAL1* gene suggests that it is maintained in a repressed state by sumoylation of two corepressors, Tup1 and Ssn6, that are desumoylated upon activation, reportedly by Ulp1 (Smith and Johnson, 2000; Zhang and Reese, 2004; Texari et al., 2013). Paradoxically, activation of the *GAL1* gene is also accompanied by the recruitment of the SUMO conjugating enzyme Ubc9 to the gene locus and increased levels of SUMO-modified proteins within the promoter region (Rosonina et al., 2010).

Similarly, activation of *INO1* is accompanied by both increased and decreased levels of bound SUMO-modified proteins at distinct regions of the gene (**Figure 1B**). In addition to increased sumoylation in regions A and B containing the transcriptional start site, *INO1* induction is accompanied by decreased sumoylation levels in the Put3-binding GRS1 region (**Figure 1**). These events raise the possibility that desumoylation of proteins associated with the GRS1 region contribute to increased *INO1* expression. In this regard, increased levels of Siz2-dependent sumoylation within the *INO1* gene observed in the $ulp1\Delta_{1-340}$ mutant (**Figure 8B**) are coincident with reduced levels of *INO1* mRNA accumulation following induction (**Figure 5B**). Whether Siz2 sumoylation may play a repressive role in *INO1* expression will require further analysis.

Siz2 is required for targeting the activated *INO1* locus to the NE (**Figure 2B**). This could involve Siz2 directly mediating the binding of *INO1* to Nups. However, several observations have led us to conclude that Siz2-mediated sumoylation events direct *INO1* relocation to the NPC, including, for example, sumoylation of proteins bound to regions of *INO1* such as those near the transcriptional start site (**Figure 1B**). We speculate that the SUMO polypeptide may function as the NPC targeting signal. This idea is consistent with our observation that Ulp1, a SUMO binding protein, is required for the NE localization of *INO1* (**Figure 5A**). Specifically, we showed that the C-terminal domain of Ulp1, which contains SUMO binding sites within the catalytic pocket and a SIM domain, when alone anchored to the NPC, is sufficient for the accumulation of the activated *INO1* gene at the NPC (**Figure 7D**). Moreover, Ulp1 binds to the *INO1* ORF and is required for the desumoylation of Siz2-mediated sumoylation sites positioned within the ORF (**Figures 4B**, **8B**). Finally, we observed that a $ulp1^{CSDN}$ mutant protein, which exhibits reduced SUMO binding and no isopeptidase activity (Elmore et al., 2011) but binds to the NPC and competes with endogenous Ulp1 for NPC-binding (**Figure 6B**), also inhibits NE localization of *INO1* (**Figure 6C**). Each of these observations is consistent with a role for SUMO, and its association with Ulp1, in the targeting of *INO1* to the NPC (see **Figure 9**).

The requirement for NPC-bound Ulp1 in the targeting of activated *INO1* to the NPC provides further insight into previously described defects associated with certain *nup* mutations, including several encoding Nups positioned on the nucleoplasmic face of the NPC (Ahmed et al., 2010; Light et al., 2010). These include Nup60 and Nup2, both of which physically and functionally interact with Ulp1 (Zhao et al., 2004; Srikumar et al., 2013) and have been shown to play a role in the association of Ulp1 with the NPC. Here we have shown that the *INO1* localization defects associated with *nup60* and *nup2* null mutants can be rescued by positioning the Ulp1 C-terminal catalytic domain at the NPC as part of a fusion protein with Nup53 (Nup53-$ulp1^{340-621}$; **Figure 7**) suggesting the role Nup2 and Nup60 play in this process is to position Ulp1 at the NPC.

The positioning of Ulp1 at the NPC is also essential for normal expression of *INO1*. In cells where NPC association of Ulp1 is inhibited, such as in the $ulp1\Delta_{1-340}$ mutant, levels of *INO1* mRNA are reduced (**Figures 5A**, **7D**). Importantly, placing the Ulp1 C-terminal catalytic domain at the NPC using Nup53-$ulp1^{340-621}$ fusion rescued *INO1* expression defects in an otherwise WT background, as well as in the *nup60* and *nup2* null mutants (**Figures 7D,F**).

Cumulatively, our observations support a model in which induction of *INO1* is followed by increased binding of Siz2 to regions within the *INO1* ORF and its 3′ end. We propose that the sumoylation events that arise from the Siz2 binding facilitate binding of the *INO1* locus to NPC-bound Ulp1 and desumoylation of ORF-associated targets. The continuous presence of both Siz2 and Ulp1 bound to the *INO1* ORF (during the 3 h period of induction examined) may support a cycle of sumoylation and desumoylation of as yet unidentified target proteins that retains these proteins and the associated *INO1* gene at the NPC. Furthermore, Ulp1 binding and desumoylation of proteins associated with the *GRS1* region are also predicted to facilitate *INO1* binding to the NPC and potentially facilitate *INO1* transcription. Interestingly, Ulp1 bound near the 3′-end of the *INO1* gene might facilitate desumoylation of *GRS1* associated proteins as a consequence of *INO1* gene looping, which has been previously shown to occur following induction (Kaderi et al., 2009). Such a mechanism could also support Siz2 sumoylation of proteins within the 5′ region of *INO1*. We envisage that these steps in the NPC targeting and expression of *INO1* are built upon other key requirements previously reported for these processes, including specific DNA sequences, TFs, nuclear transport factors, and Nups (Chen et al., 2007; Light and Brickner, 2013; Randise-Hinchliff and Brickner, 2016).

The concepts described here for SUMO-mediated regulation of *INO1* localization and expression are likely to apply to

other inducible genes. Of note, previous observations made in the analysis of the *GAL1* gene revealed sumoylation processes that occur during its activation that parallel events we have observed for *INO1*. For example, induction of the *GAL1* gene is accompanied by sumoylation of associated proteins (Rosonina et al., 2010), and NPC association of activated *GAL1* was inhibited when Ulp1 association with NPCs was reduced (Texari et al., 2013). It will be of interest to further test the broader impact of sumoylation and NPC-associated desumoylation.

DATA AVAILABILITY STATEMENT

The raw data supporting the conclusions of this article will be made available by the authors, without undue reservation, to any qualified researcher.

AUTHOR CONTRIBUTIONS

NP, NS, and CP performed the experiments. All authors contributed to the conception and design of the study, manuscript revision, and read and approved the submitted version. Figures were assembled by NS, NP, and CP. RW wrote the first draft of the manuscript.

FUNDING

Funding for this work was supported by the Canadian Institutes of Health Research (MOP 106502 and 36519) to RW and the National Institutes of Health, United States (NCDIR: 2P41GM109824-06 and R01: 2R01GM112108-05) to JA. The authors declare no competing financial interests.

ACKNOWLEDGMENTS

We thank Dr. Ben Montpetit (University of California, Davis), Michael Hendzel (University of Alberta), and members of the Wozniak lab for helpful discussions.

SUPPLEMENTARY MATERIAL

The Supplementary Material for this article can be found online at: https://www.frontiersin.org/articles/10.3389/fgene.2020.00174/full#supplementary-material

FIGURE S1 | Sumoylation of proteins at the uninduced *INO1* locus. **(A)** Diagram of the *INO1* locus and regions detected by ChIP analysis (see **Figure 1A**). **(B,C)** The graphs show the relative fold enrichment of SUMO modified proteins at each position along the *INO1* gene relative to the level of SUMO modified proteins at an intergenic region within chromosome V as assessed by ChIP. **B** shows ChIP results for uninduced WT samples while **C** shows results comparing uninduced WT samples (WT 0 h) to samples derived from *siz2*Δ cells at the indicated times after *INO1* induction. Results are the means ± SEM of at least three biological replicates.

FIGURE S2 | Siz2 associates with the *GRS1* region of the uninduced *INO1* locus. **(A)** Diagram of the *INO1* locus and regions detected by ChIP analysis (see **Figure 1A**). The graph shows the relative fold enrichment of Siz2-PrA **(B)** or Ulp1-PrA **(C)** at each position along the *INO1* gene relative to the level at an intergenic region within chromosome V as assessed by ChIP. Results are the means ± SEM of at least three biological replicates.

FIGURE S3 | Characterization of chromosomally encoded *ulp1* truncation mutants. **(A)** Shown are cells producing Ulp1-GFP or the indicated truncation mutants (ulp1Δ_{1-150}-GFP, ulp1$\Delta_{150-340}$-GFP, and ulp1Δ_{1-340}-GFP) encoded by integrated and *ULP1* promoter-controlled mutant genes. Camera exposure times are equivalent for each strain. Scale bars = 2 μm. **(B)** Truncation mutants showed similar expression levels with that of full length Ulp1-GFP. Whole cell lysates of the indicated strains were tested by Western blotting with an anti-GFP antibody. For the loading control, the levels of Gsp1 were tested with an anti-Gsp1p antibody. **(C)** Whole cell lysates, derived from cultures of the indicated strains, were examined by Western blotting using an anti-Smt3 (SUMO) or an anti-Gsp1 (loading control) antibody. The positions of molecular mass markers are indicated in kilodaltons.

FIGURE S4 | Growth of strains producing ulp1^{CSDN} and Nup53-ulp1$^{341-621}$. **(A)** WT cells transformed with an empty plasmid (pEMPTY), a plasmid encoding WT Ulp1 (p*ULP1*), or a plasmid encoding the ulp1^{CSDN} mutant (p*ulp1*^{CSDN}) were grown to mid-log phase in synthetic drop out liquid culture. Tenfold serial dilutions of each culture were made and cells from each dilution spotted onto synthetic drop out plates. Total cells plated ranged between 10^5 and 10^2 cells per spot. Plates were then incubated at 30°C for 2 days prior to imaging. **(B)** Cell lysates, derived from the same cultures described in **A**, were examined by Western blotting using an anti-Smt3 (SUMO) or an anti-Gsp1 (loading control) antibody. The positions of molecular mass markers are indicated in kilodaltons. **(C)** WT and *NUP53-ulp1*$^{341-621}$ cells were grown in YPD liquid culture to mid-log phase and cells from each culture analyzed as described in **A**.

TABLE S1 | Yeast strains used in this study.

REFERENCES

Abraham, N. M., and Mishra, K. (2018). Elevated dosage of Ulp1 disrupts telomeric silencing in *Saccharomyces cerevisiae*. *Mol. Biol. Rep.* 45, 2481–2489. doi: 10.1007/s11033-018-4415-1

Ahmed, S., Brickner, D. G., Light, W. H., Cajigas, I., McDonough, M., Froyshteter, A. B., et al. (2010). DNA zip codes control an ancient mechanism for gene targeting to the nuclear periphery. *Nat. Cell Biol.* 12, 111–118. doi: 10.1038/ncb2011

Bi, E., and Pringle, J. R. (1996). ZDS1 and ZDS2, genes whose products may regulate Cdc42p in *Saccharomyces cerevisiae*. *Mol. Cell. Biol.* 16, 5264–5275. doi: 10.1128/mcb.16.10.5264

Bonnet, A., Bretes, H., and Palancade, B. (2015). Nuclear pore components affect distinct stages of intron-containing gene expression. *Nucleic Acids Res.* 43, 4249–4261. doi: 10.1093/nar/gkv280

Brickner, D. G., and Brickner, J. H. (2010). Cdk phosphorylation of a nucleoporin controls localization of active genes through the cell cycle. *Mol. Biol. Cell* 21, 3421–3432. doi: 10.1091/mbc.e10-01-0065

Brickner, D. G., and Brickner, J. H. (2012). Interchromosomal clustering of active genes at the nuclear pore complex. *Nucleus* 3, 487–492. doi: 10.4161/nucl.22663

Brickner, D. G., Cajigas, I., Fondufe-Mittendorf, Y., Ahmed, S., Lee, P. C., Widom, J., et al. (2007). H2A.Z-mediated localization of genes at the nuclear periphery confers epigenetic memory of previous transcriptional state. *PLoS Biol.* 5:e81. doi: 10.1371/journal.pbio.0050081

Brickner, D. G., Randise-Hinchliff, C., Lebrun Corbin, M., Liang, J. M., Kim, S., Sump, B., et al. (2019). The role of transcription factors and nuclear pore proteins in controlling the spatial organization of the yeast genome. *Dev. Cell* 49, 936–947.

Brickner, D. G., Sood, V., Tutucci, E., Coukos, R., Viets, K., Singer, R. H., et al. (2016). Subnuclear positioning and interchromosomal clustering of the GAL1-10 locus are controlled by separable, interdependent mechanisms. *Mol. Biol. Cell* 27, 2980–2993. doi: 10.1091/mbc.e16-03-0174

Brickner, J. H., and Walter, P. (2004). Gene recruitment of the activated INO1 locus to the nuclear membrane. *PLoS Biol.* 2:e342. doi: 10.1371/journal.pbio.0020342

Bylebyl, G. R., Belichenko, I., and Johnson, E. S. (2003). The SUMO isopeptidase Ulp2 prevents accumulation of SUMO chains in yeast. *J. Biol. Chem.* 278, 44113–44120. doi: 10.1074/jbc.m308357200

Cabal, G. G., Genovesio, A., Rodriguez-Navarro, S., Zimmer, C., Gadal, O., Lesne, A., et al. (2006). SAGA interacting factors confine sub-diffusion of transcribed genes to the nuclear envelope. *Nature* 441, 770–773. doi: 10.1038/nature04752

Chen, M., Hancock, L. C., and Lopes, J. M. (2007). Transcriptional regulation of yeast phospholipid biosynthetic genes. *Biochim. Biophys. Acta* 1771, 310–321. doi: 10.1016/j.bbalip.2006.05.017

Churikov, D., Charifi, F., Eckert-Boulet, N., Silva, S., Simon, M.-N., Lisby, M., et al. (2016). SUMO-Dependent relocalization of eroded telomeres to nuclear pore complexes controls telomere recombination. *Cell Rep.* 15, 1242–1253. doi: 10.1016/j.celrep.2016.04.008

Chymkowitch, P., Nguea, P. A., and Enserink, J. M. (2015). SUMO-regulated transcription: challenging the dogma. *Bioessays* 37, 1095–1105. doi: 10.1002/bies.201500065

Denison, C., Rudner, A. D., Gerber, S. A., Bakalarski, C. E., Moazed, D., and Gygi, S. P. (2005). A proteomic strategy for gaining insights into protein sumoylation in yeast. *Mol. Cell. Proteom.* 4, 246–254. doi: 10.1074/mcp.m400154-mcp200

Dilworth, D. J., Tackett, A. J., Rogers, R. S., Yi, E. C., Christmas, R. H., Smith, J. J., et al. (2005). The mobile nucleoporin Nup2p and chromatin-bound Prp20p function in endogenous NPC-mediated transcriptional control. *J. Cell. Biol.* 171, 955–965. doi: 10.1083/jcb.200509061

Egecioglu, D., and Brickner, J. H. (2011). Gene positioning and expression. *Curr. Opin. Cell Biol.* 23, 338–345. doi: 10.1016/j.ceb.2011.01.001

Elmore, Z. C., Donaher, M., Matson, B. C., Murphy, H., Westerbeck, J. W., and Kerscher, O. (2011). Sumo-dependent substrate targeting of the SUMO protease Ulp1. *BMC Biol.* 9:74. doi: 10.1186/1741-7007-9-74

Felberbaum, R., Wilson, N. R., Cheng, D., Peng, J., and Hochstrasser, M. (2012). Desumoylation of the endoplasmic reticulum membrane VAP family protein Scs2 by Ulp1 and SUMO regulation of the inositol synthesis pathway. *Mol. Cell. Biol.* 32, 64–75. doi: 10.1128/mcb.05878-11

Ferreira, H. C., Luke, B., Schober, H., Kalck, V., Lingner, J., and Gasser, S. M. (2011). The PIAS homologue Siz2 regulates perinuclear telomere position and telomerase activity in budding yeast. *Nat. Cell Biol.* 13, 867–874. doi: 10.1038/ncb2263

Folz, H., Nino, C. A., Taranum, S., Caesar, S., Lorenz, L., Waharte, F., et al. (2019). SUMOylation of the nuclear pore complex basket is involved in sensing cellular stresses. *J. Cell Sci.* 132:jcs224279. doi: 10.1242/jcs.224279

Freudenreich, C. H., and Su, X. A. (2016). Relocalization of DNA lesions to the nuclear pore complex. *FEMS Yeast Res.* 16:fow095. doi: 10.1093/femsyr/fow095

Geiss-Friedlander, R., and Melchior, F. (2007). Concepts in sumoylation: a decade on. *Nat. Rev. Mol. Cell Biol.* 8, 947–956. doi: 10.1038/nrm2293

Gietz, R. D., and Woods, R. A. (2002). Transformation of yeast by lithium acetate/single-stranded carrier DNA/polyethylene glycol method. *Methods Enzymol.* 350, 87–96. doi: 10.1016/s0076-6879(02)50957-5

Hannan, A., Abraham, N. M., Goyal, S., Jamir, I., Priyakumar, U. D., and Mishra, K. (2015). Sumoylation of Sir2 differentially regulates transcriptional silencing in yeast. *Nucleic Acids Res.* 43, 10213–10226.

Hannich, J. T., Lewis, A., Kroetz, M. B., Li, S. J., Heide, H., Emili, A., et al. (2005). Defining the SUMO-modified proteome by multiple approaches in *Saccharomyces cerevisiae*. *J. Biol. Chem.* 280, 4102–4110. doi: 10.1074/jbc.m413209200

Jentsch, S., and Psakhye, I. (2013). Control of nuclear activities by substrate-selective and protein-group SUMOylation. *Annu. Rev. Genet.* 47, 167–186. doi: 10.1146/annurev-genet-111212-133453

Johnson, E. S. (2004). Protein modification by SUMO. *Annu. Rev. Bioch.* 73, 355–382. doi: 10.1146/annurev.biochem.73.011303.074118

Kaderi, E. B., Medler, S., Raghunayakula, S., and Ansari, A. (2009). Gene looping is conferred by activator-dependent interaction of transcription initiation and termination machineries. *J. Biol. Chem.* 284, 25015–25025. doi: 10.1074/jbc.m109.007948

Lapetina, D. L., Ptak, C., Roesner, U. K., and Wozniak, R. W. (2017). Yeast silencing factor Sir4 and a subset of nucleoporins form a complex distinct from nuclear pore complexes. *J. Cell. Biol.* 16, 3145–3159. doi: 10.1083/jcb.201609049

Lewis, A., Felberbaum, R., and Hochstrasser, M. (2007). A nuclear envelope protein linking nuclear pore basket assembly, SUMO protease regulation, and mRNA surveillance. *J. Cell. Biol.* 178, 813–827. doi: 10.1083/jcb.200702154

Li, S. J., and Hochstrasser, M. (1999). A new protease required for cell-cycle progression in yeast. *Nature* 398, 246–251. doi: 10.1038/18457

Li, S. J., and Hochstrasser, M. (2000). The yeast ULP2 (SMT4) gene encodes a novel protease specific for the ubiquitin-like Smt3 protein. *Mol. Cell Biol.* 20, 2367–2377. doi: 10.1128/mcb.20.7.2367-2377.2000

Li, S. J., and Hochstrasser, M. (2003). The Ulp1 SUMO isopeptidase: distinct domains required for viability, nuclear envelope localization, and substrate specificity. *J. Cell. Biol.* 160, 1069–1081.

Light, W. H., Brickner, D. G., Brand, V. R., and Brickner, J. H. (2010). Interaction of a DNA zip code with the nuclear pore complex promotes H2A.Z incorporation and INO1 transcriptional memory. *Mol. Cell* 40, 112–125. doi: 10.1016/j.molcel.2010.09.007

Light, W. H., and Brickner, J. H. (2013). Nuclear pore proteins regulate chromatin structure and transcriptional memory by a conserved mechanism. *Nucleus* 4, 357–360. doi: 10.4161/nucl.26209

Lo, W. S., Duggan, L., Emre, N. C., Belotserkovskya, R., Lane, W. S., and Shiekhattar, R. (2001). Snf1 – a histone kinase that works in concert with the histone acetyltransferase Gcn5 to regulate transcription. *Science* 293, 1142–1146. doi: 10.1126/science.1062322

Lo, W. S., Gamache, E. R., Henry, K. W., Yang, D., Pillus, L., and Berger, S. L. (2005). Histone H3 phosphorylation can promote TBP recruitment through distinct promoter-specific mechanisms. *EMBO J.* 24, 997–1008. doi: 10.1038/sj.emboj.7600577

Loewen, C. J., Roy, A., and Levine, T. P. (2003). A conserved ER targeting motif in three families of lipid binding proteins and in Opi1p binds VAP. *EMBO J.* 22, 2025–2035. doi: 10.1093/emboj/cdg201

Longtine, M. S., McKenzie, A., Demarini, D. J., Shah, N. G., Wach, A., Brachat, A., et al. (1998). Additional modules for versatile and economical PCR-based gene deletion and modification in *Saccharomyces cerevisiae*. *Yeast* 14, 953–961. doi: 10.1002/(sici)1097-0061(199807)14:10<953::aid-yea293>3.0.co;2-u

Makhnevych, T., Ptak, C., Lusk, C. P., Aitchison, J. D., and Wozniak, R. W. (2007). The role of karyopherins in the regulated sumoylation of septins. *J. Cell Biol.* 177, 39–49. doi: 10.1083/jcb.200608066

Mossessova, E., and Lima, C. D. (2000). Ulp1-SUMO crystal structure and genetic analysis reveal conserved interactions and a regulatory element essential for cell growth in yeast. *Mol. Cell* 5, 865–876. doi: 10.1016/s1097-2765(00)80326-3

Palancade, B., Liu, X., Garcia-Rubio, M., Aguilera, A., Zhao, X., and Doye, V. (2007). Nucleoporins prevent DNA damage accumulation by modulating Ulp1-dependent sumoylation processes. *Mol. Biol. Cell* 18, 2912–2923. doi: 10.1091/mbc.e07-02-0123

Panse, V. G., Hardeland, U., Werner, T., Kuster, B., and Hurt, E. (2004). A proteome-wide approach identifies sumoylated substrate proteins in yeast. *J. Biol. Chem.* 279, 41346–41351. doi: 10.1074/jbc.m407950200

Panse, V. G., Kressler, D., Pauli, A., Petfalski, E., Gnädig, M., Tollervey, D., et al. (2006). Formation and nuclear export of preribosomes are functionally linked to the small-ubiquitin-related modifier pathway. *Traffic* 7, 1311–1321. doi: 10.1111/j.1600-0854.2006.00471.x

Panse, V. G., Kuster, B., Gerstberger, T., and Hurt, E. (2003). Unconventional tethering of Ulp1 to the transport channel of the nuclear pore complex by karyopherins. *Nat. Cell Biol.* 5, 21–27. doi: 10.1038/ncb893

Randise-Hinchliff, C., and Brickner, J. H. (2016). Transcription factors dynamically control the spatial organization of the yeast genome. *Nucleus* 7, 369–374. doi: 10.1080/19491034.2016.1212797

Randise-Hinchliff, C., Coukos, R., Sood, V., Sumner, M. C., Zdraljevic, S., Meldi Sholl, L., et al. (2016). Strategies to regulate transcription factor–mediated gene positioning and interchromosomal clustering at the nuclear periphery. *J. Cell Biol.* 212, 633–646. doi: 10.1083/jcb.201508068

Robinett, C. C., Straight, A. F., Li, G., Willhelm, C., Sudlow, G., Murray, A. W., et al. (1996). In vivo localization of DNA sequences and visualization of large-scale chromatin organization using lac operator/repressor recognition. *J. Cell Biol.* 135, 1685–1700. doi: 10.1083/jcb.135.6.1685

Rosonina, E. (2019). A conserved role for transcription factor sumoylation in binding-site selection. *Curr. Genet.* 65, 1307–1312. doi: 10.1007/s00294-019-00992-w

Rosonina, E., Duncan, S. M., and Manley, J. L. (2010). SUMO functions in constitutive transcription and during activation of inducible genes in yeast. *Genes Dev.* 24, 1242–1252. doi: 10.1101/gad.1917910

Ruben, G. J., Kirkland, J. G., MacDonough, T., Chen, M., Dubey, R. N., Gartenberg, M. R., et al. (2011). Nucleoporin mediated nuclear positioning and silencing of HMR. *PLoS ONE* 6:e21923. doi: 10.1371/journal.pone.0021923

Schmid, M., Arib, G., Laemmli, C., Nishikawa, J., Durussel, T., and Laemmli, U. K. (2006). Nup-PI: the nucleopore-promoter interaction of genes in yeast. *Mol. Cell.* 21, 379–391. doi: 10.1016/j.molcel.2005.12.012

Shetty, A., and Lopes, J. M. (2010). Derepression of INO1 transcription requires cooperation between the Ino2p-Ino4p heterodimer and Cbf1p and recruitment of the ISW2 chromatin-remodeling complex. *Eukaryot. Cell* 9, 1845–1855. doi: 10.1128/ec.00144-10

Sikorski, R. S., and Hieter, P. (1989). A system of shuttle vectors and yeast host strains designed for efficient manipulation of DNA in *Saccharomyces cerevisiae*. *Genetics* 122, 19–27.

Smith, R. L., and Johnson, A. D. (2000). Turning genes off by Ssn-Tup1: a conserved system of transcriptional repression in eukaryotes. *Trends Biochem. Sci.* 25, 325–330. doi: 10.1016/s0968-0004(00)01592-9

Srikumar, T., Lewicki, M. C., and Raught, B. (2013). A global *S. cerevisiae* small ubiquitin-related modifier (SUMO) system interactome. *Mol. Syst. Biol.* 9:668. doi: 10.1038/msb.2013.23

Stade, K., Vogel, F., Schwienhorst, I., Meusser, B., Volkwein, C., Nentwig, B., et al. (2002). A lack of SUMO conjugation affects cNLS-dependent nuclear protein import in yeast. *J. Biol. Chem.* 277, 49554–49561. doi: 10.1074/jbc.m207991200

Straight, A. F., Belmont, A. S., Robinett, C. C., and Murray, A. W. (1996). GFP tagging of budding yeast chromosomes reveals that protein-protein interactions can mediate sister chromatid cohesion. *Curr. Biol.* 6, 1599–1608. doi: 10.1016/s0960-9822(02)70783-5

Texari, L., Dieppois, G., Vinciguerra, P., Contreras, M. P., Groner, A., Letourneau, A., et al. (2013). The nuclear pore regulates GAL1 gene transcription by controlling the localization of the SUMO protease Ulp1. *Mol. Cell* 51, 807–818. doi: 10.1016/j.molcel.2013.08.047

Texari, L., and Stutz, F. (2015). Sumoylation and transcription regulation at nuclear pores. *Chromosoma* 124, 45–56. doi: 10.1007/s00412-014-0481-x

Van de Vosse, D. W., Wan, Y., Lapetina, D. L., Chen, W. M., Chiang, J. H., Aitchison, J. D., et al. (2013). A role for the nucleoporin Nup170p in chromatin structure and gene silencing. *Cell* 152, 969–983. doi: 10.1016/j.cell.2013.01.049

Wan, Y., Saleem, R. A., Ratushny, A. V., Roda, O., Smith, J. J., Lin, C. H., et al. (2009). Role of the histone variant H2A.Z/*Htz*1p in TBP recruitment, chromatin dynamics, and regulated expression of oleate-responsive genes. *Mol. Cell Biol.* 29, 2346–2358. doi: 10.1128/mcb.01233-08

Wohlschlegel, J. A., Johnson, E. S., Reed, S. I., and Yates, J. R. III (2004). Global analysis of protein sumoylation in *Saccharomyces cerevisiae*. *J. Biol. Chem.* 279, 45662–45668. doi: 10.1074/jbc.m409203200

Wykoff, D. D., and O'Shea, E. K. (2005). Identification of sumoylated proteins by systematic immunoprecipitation of the budding yeast proteome. *Mol. Cell. Proteomics* 4, 73–83. doi: 10.1074/mcp.m400166-mcp200

Zhang, Z., and Reese, J. C. (2004). Redundant mechansims are used by Ssn6-Tup1 in repressing chromosomal gene transcription in *Saccharomyces cerevisiae*. *J. Biol. Chem.* 279, 39240–39250. doi: 10.1074/jbc.m407159200

Zhao, Q., Xie, Y., Zheng, Y., Jiang, S., Liu, W., Mu, W., et al. (2014). GPS-SUMO: a tool for the prediction of sumoylation sites and SUMO-interaction motifs. *Nucleic Acids Res.* 42, W325–W330. doi: 10.1093/nar/gku383

Zhao, X. (2018). SUMO-mediated regulation of nuclear functions and signaling processes. *Mol. Cell* 71, 409–418. doi: 10.1016/j.molcel.2018.07.027

Zhao, X., Wu, C. Y., and Blobel, G. (2004). Mlp-dependent anchorage and stabilization of a desumoylating enzyme is required to prevent clonal lethality. *J. Cell Biol.* 167, 605–611. doi: 10.1083/jcb.200405168

Zhou, W., Ryan, J. J., and Zhou, H. (2004). Global analyses of sumoylated proteins in *Saccharomyces cerevisiae*. Induction of protein sumoylation by cellular stresses. *J. Biol. Chem.* 279, 32262–32268. doi: 10.1074/jbc.m404173200

Conflict of Interest: The authors declare that the research was conducted in the absence of any commercial or financial relationships that could be construed as a potential conflict of interest.

frontiers in Genetics

MINI REVIEW
published: 27 August 2020
doi: 10.3389/fgene.2020.00800

Complex Chromatin Motions for DNA Repair

Judith Miné-Hattab[1,2]* *and Irene Chiolo*[3]*

[1] UMR 3664, CNRS, Institut Curie, PSL Research University, Paris, France, [2] UMR 3664, CNRS, Institut Curie, Sorbonne Université, Paris, France, [3] Molecular and Computational Biology Department, University of Southern California, Los Angeles, CA, United States

A number of studies across different model systems revealed that chromatin undergoes significant changes in dynamics in response to DNA damage. These include local motion changes at damage sites, increased nuclear exploration of both damaged and undamaged loci, and directed motions to new nuclear locations associated with certain repair pathways. These studies also revealed the need for new analytical methods to identify directed motions in a context of mixed trajectories, and the importance of investigating nuclear dynamics over different time scales to identify diffusion regimes. Here we provide an overview of the current understanding of this field, including imaging and analytical methods developed to investigate nuclear dynamics in different contexts. These dynamics are essential for genome integrity. Identifying the molecular mechanisms responsible for these movements is key to understanding how their misregulation contributes to cancer and other genome instability disorders.

Keywords: chromatin motions, double-strand break repair, homologous recombination, mean square displacement, directed motion, multi-scale motion

OPEN ACCESS

Edited by:
Karim Mekhail,
University of Toronto, Canada

Reviewed by:
Jean-Yves Masson,
Laval University, Canada
Jean Gautier,
Columbia University Irving Medical Center, United States

***Correspondence:**
Judith Miné-Hattab
judith.mine@curie.fr
Irene Chiolo
chiolo@usc.edu

Specialty section:
This article was submitted to Epigenomics and Epigenetics, a section of the journal Frontiers in Genetics

Received: *25 March 2020*
Accepted: *06 July 2020*
Published: *27 August 2020*

Citation:
Miné-Hattab J and Chiolo I (2020) Complex Chromatin Motions for DNA Repair. Front. Genet. 11:800. doi: 10.3389/fgene.2020.00800

INTRODUCTION: CHROMATIN EXPLORES A LARGER NUCLEAR VOLUME IN RESPONSE TO DNA DAMAGE

A significant number of studies in the past decade have identified essential roles for nuclear dynamics in DNA repair, particularly during homologous recombination (HR) repair of double-strand breaks (DSBs) (**Figures 1A–D**). First, a larger nuclear volume explored by repair sites is typically detected during inter-homolog recombination (**Figure 1A**) (Miné-Hattab and Rothstein, 2012; Neumann et al., 2012; Cho et al., 2014; Miné-Hattab et al., 2017) (reviewed in Dion and Gasser, 2013; Mine-Hattab and Rothstein, 2013). This change in chromatin mobility in response to DNA damage likely reflects the exploration of the nuclear space during "homology search" (Kalocsay et al., 2009; Dion et al., 2012; Miné-Hattab and Rothstein, 2012; Neumann et al., 2012; Agmon et al., 2013; Cho et al., 2014; Saad et al., 2014; Herbert et al., 2017; Miné-Hattab et al., 2017), i.e., the process where a resected DSB covered by a Rad51 nucleoprotein filament scans the genome in search of a homologous donor. Second, undamaged chromatin also becomes more dynamic during DSB repair, albeit to a lesser extent than repair sites (**Figure 1B**) (Chiolo et al., 2011; Krawczyk et al., 2012; Miné-Hattab and Rothstein, 2012; Seeber et al., 2013; Lottersberger et al., 2015; Strecker et al., 2016; Herbert et al., 2017; Lawrimore et al., 2017; Miné-Hattab et al., 2017; Caridi et al., 2018a; Smith et al., 2019; Zada et al., 2019). The significance of the genome-wide increase in nuclear exploration is still under debate, but this response might increase the frequency of DNA contacts to facilitate homology search (Gehen et al., 2011; Neumann et al., 2012; Mine-Hattab and Rothstein, 2013; Amitai and Holcman, 2018), or reflect chromatin relaxation to promote access for repair (Kruhlak et al., 2006; Ziv et al., 2006;

Seeber et al., 2013; Delabaere and Chiolo, 2016). Third, repair sites undergoing HR aggregate into larger units, or "clusters" (**Figure 1C**) (Lisby et al., 2003; Aten et al., 2004; Kruhlak et al., 2006; Chiolo et al., 2011, 2013; Krawczyk et al., 2012; Neumaier et al., 2012; Cho et al., 2014; Caron et al., 2015; Aymard et al., 2017; Caridi et al., 2018a; Schrank et al., 2018; Oshidari et al., 2019a; Waterman et al., 2019) (reviewed in Chiolo et al., 2013; Guénolé and Legube, 2017; Schrank and Gautier, 2019), likely to facilitate DSB signaling and resection, e.g., by increasing the local concentration of checkpoint and repair proteins (Chiolo et al., 2013; Schrank et al., 2018; Kilic et al., 2019; Oshidari et al., 2019a; Schrank and Gautier, 2019). This response also occurs in G1 in human cells (Aten et al., 2004; Aymard et al., 2017), where HR cannot be completed with the sister chromatid, and clustering might temporarily sequester breaks that will be repaired in S phase (Aymard et al., 2017). Clustering can also be deleterious, as increasing the proximity of DSBs on different chromosomes promotes chromosomal translocations (Agmon et al., 2013; Roukos et al., 2013; Lee et al., 2016; Cohen et al., 2018). Fourth, DSBs relocalize to specific subnuclear compartments when the lesion occurs in DNA regions that are difficult to repair. Specifically, DSBs in pericentromeric heterochromatin relocalize to the nuclear periphery in *Drosophila* cells (**Figure 1D**) (Chiolo et al., 2011; Ryu et al., 2015, 2016; Janssen et al., 2016, 2019; Caridi et al., 2018a), and to the periphery of heterochromatin "domains" (or "chromocenters") in mouse cells (Jakob et al., 2011; Chiolo et al., 2013; Tsouroula et al., 2016; Caridi et al., 2018a). rDNA sequences move to the nuclear periphery in budding yeast (Torres-Rosell et al., 2007; Horigome et al., 2019) and to nucleolar caps in mammalian cells (Harding et al., 2015; van Sluis and McStay, 2015; Korsholm et al., 2019; Marnef et al., 2019). Relocalization of repair sites to the nuclear periphery is also a response to damaged CAG repeats in budding yeast (Su et al., 2015; Aguilera et al., 2020; Whalen et al., 2020), collapsed replication forks in yeast and mammalian cells (Nagai et al., 2008; Su et al., 2015; Lamm et al., 2018; Aguilera et al., 2020; Whalen et al., 2020), and damaged telomeric or subtelomeric sequences in yeast (Therizols et al., 2006; Khadaroo et al., 2009; Cho et al., 2014; Chung et al., 2015; Churikov et al., 2016; Oshidari et al., 2018; Aguilera et al., 2020). Similar relocalization occurs as a result of persistent/unrepairable DSBs (Nagai et al., 2008; Kalocsay et al., 2009; Oza et al., 2009; Horigome et al., 2014, 2016; Swartz et al., 2014; Marcomini et al., 2018). In these contexts, relocalization appears to prevent aberrant recombination with ectopic repeated sequences (Torres-Rosell et al., 2007; Chiolo et al., 2011; Ryu et al., 2015, 2016; Su et al., 2015; Caridi et al., 2018a; Dialynas et al., 2019; Aguilera et al., 2020) and/or promote alternative repair mechanisms (Therizols et al., 2006; Nagai et al., 2008; Khadaroo et al., 2009; Oza et al., 2009; Horigome et al., 2014, 2016; Churikov et al., 2016; Aguilera et al., 2020) (reviewed in Amaral et al., 2017; Caridi et al., 2017, 2019; Rawal et al., 2019). Further dynamics have been associated with other repair pathways. For example, deprotected telomeres are mobilized in mouse cells to promote non-homologous end-joining (NHEJ) (Dimitrova et al., 2008; Lottersberger et al., 2015). Additionally, a few chromosome territories reposition in response to damage in human fibroblasts, perhaps reflecting large-scale changes in chromatin organization (Mehta et al., 2010; Kulashreshtha et al., 2016). Several molecular mechanisms governing chromatin dynamics in response to DSBs have been identified, and specialized pathways appear to participate in different contexts [reviewed in Amaral et al. (2017); Caridi et al. (2017); Zimmer (2018); Oshidari et al. (2019b)]. Together, these studies revealed important roles for nuclear dynamics in DSB repair, particularly for homology search and for isolating repeated DNA sequences at high risk for aberrant recombination, enabling "safe" repair or alternative rescue pathways.

METHODS TO CHARACTERIZE NUCLEAR DYNAMICS DURING DSB REPAIR

Several techniques have been applied to study the nuclear dynamics of DSBs in different organisms, with "gold standard" approaches relying on damage induction with endonucleases or ionizing radiation (IR), and on monitoring repair sites with *lacO/tetO* arrays and fluorescent-tagged HR repair components (**Figures 1E–G**).

A widely used approach relies on the induction of site-specific DSBs with an endonuclease (e.g., I-*Sce*I, or HO), which recognizes a target sequence proximal to *tetO* or *lacO* arrays (**Figure 1E**). The position of the damage site is monitored using fluorescent-tagged TetR or LacI proteins that bind to the arrays, resulting in bright nuclear spots (or *foci*) (Robinett et al., 1996). Given that endonucleases can digest both sister chromatids, the sister is mostly unavailable as a template for repair, promoting inter-homolog exchanges (Miné-Hattab and Rothstein, 2012). In yeast, this approach enabled the study of nuclear dynamics associated with inter-homologous recombination (Miné-Hattab and Rothstein, 2012; Neumann et al., 2012; Miné-Hattab et al., 2017), unrepairable DSBs (Nagai et al., 2008; Kalocsay et al., 2009; Dion et al., 2012; Horigome et al., 2014, 2016; Saad et al., 2014; Herbert et al., 2017), sub-telomeric breaks (Khadaroo et al., 2009; Chung et al., 2015; Churikov et al., 2016; Oshidari et al., 2019b), and rDNA lesions (Torres-Rosell et al., 2005). Similar systems have been used to characterize DSB clustering in budding yeast and human cells (Lisby et al., 2003; Roukos et al., 2013; Waterman et al., 2019). A variant of this approach employs a *lacO* array close to the cut site and a *tetO* array on a different chromosome, enabling the simultaneous tracking of both damaged and undamaged loci (Miné-Hattab and Rothstein, 2012; Miné-Hattab et al., 2017). These studies and others (Seeber et al., 2013; Herbert et al., 2017) revealed that not only damaged sites, but also undamaged chromatin explores a larger nuclear volume in response to DSB formation. An alternative system employed sequence-based tethering of oligomerizing fluorescent proteins that spread along the DNA, to study the dynamics of resected DNA (Saad et al., 2014). Here, resection results in loss of DNA-associated proteins and reduced signal at repair sites, and correlates with a local reduction in focus dynamics (Saad et al., 2014). These approaches are very powerful, but also limited to the site targeted by the endonuclease. Given that repair responses and relocalization pathways are affected by

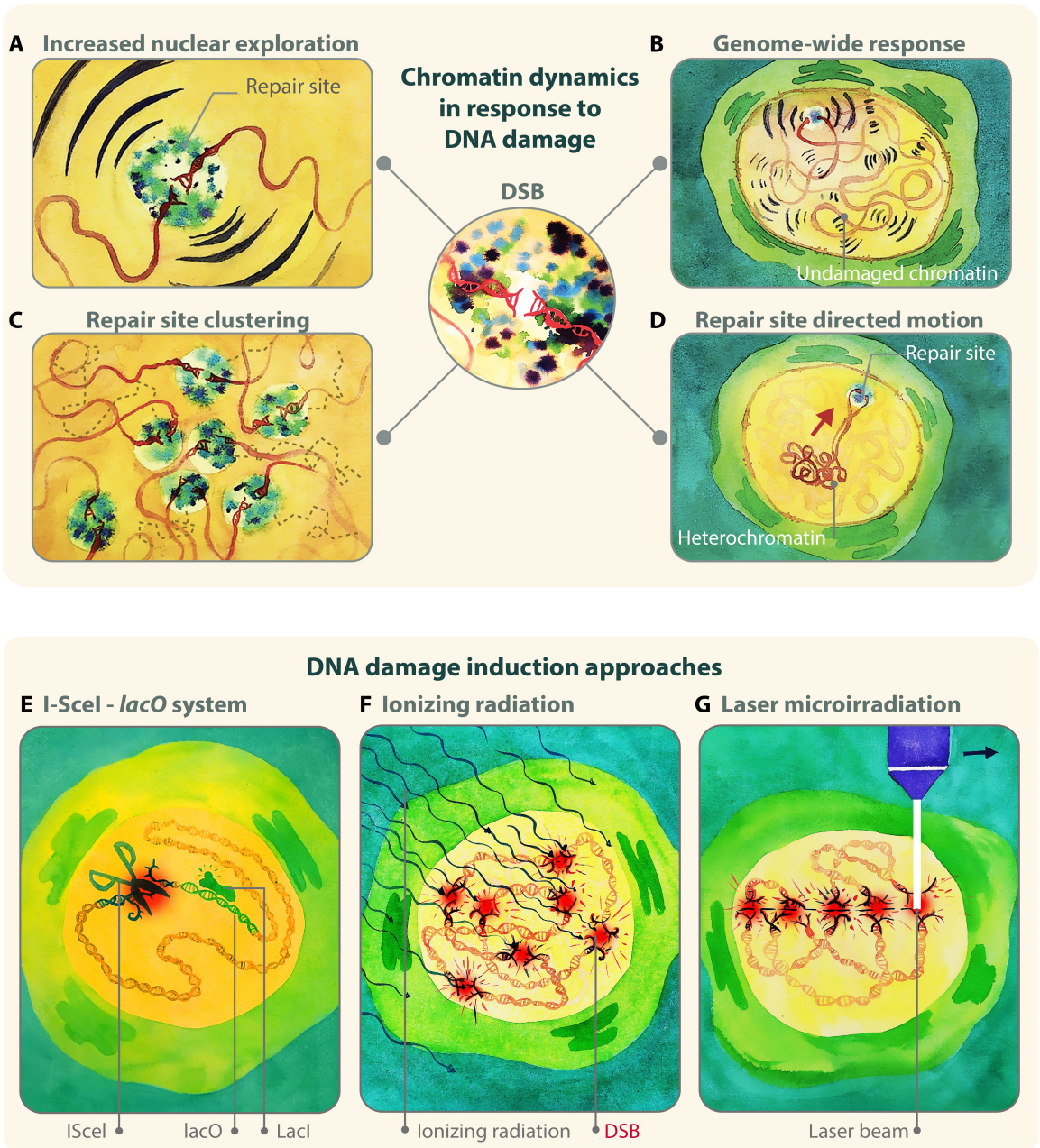

FIGURE 1 | Examples of damage-induced changes in chromatin dynamics. **(A)** A damaged chromatin site explores a larger nuclear volume during HR repair of DSBs. **(B)** Larger nuclear exploration is also observed for undamaged chromatin sites, indicating that the change in chromatin mobility is a genome-wide response. **(C)** Multiple DSB repair sites cluster together. **(D)** Damaged heterochromatic sites relocalize to the nuclear periphery with directed motions in Drosophila cells. **(E,F)** Three main approaches to study nuclear dynamics in response to DSBs rely on: **(E)** enzymatic digestion to induce damage and lacO or tetO arrays to follow damage sites; **(F)** IR to induce damage and fluorescent tagging of repair proteins to detect repair foci; **(G)** laser, alpha particles, or heavy ions, to induce damage along linear tracks where repair protein recruitment is detectable by live imaging or immunofluorescence. Illustration by Olga Markova.

chromatin state (Delabaere and Chiolo, 2016; Hauer and Gasser, 2017), nuclear positioning (Lemaitre et al., 2014), and the phase separated nature of nuclear subdomains (Altmeyer et al., 2015; Kilic et al., 2019; Lenzken et al., 2019; Oshidari et al., 2019a; Pessina et al., 2019) (reviewed in Clouaire and Legube, 2019; Rawal et al., 2019), the endonuclease-based approach would need to be applied to a large number of sites to provide a comprehensive understanding of the mechanisms responsible for these dynamics in different contexts.

Site-specific endonucleases have also been used to induce DSBs in highly repeated DNA sequences. For example, studies using Cas9 targeting heterochromatic satellites (Tsouroula et al.,

2016) or PpoI or Cas9 recognizing rDNA sequences (Harding et al., 2015; van Sluis and McStay, 2015; Korsholm et al., 2019; Marnef et al., 2019) revealed the dynamics of these sites in mammalian cells. It is important to consider that Cas9 affects the processing of repair intermediates (Richardson et al., 2016, 2018; Brinkman et al., 2018), potentially affecting outcomes and dynamics of repair.

Another commonly used approach relies on inducing damage with ionizing radiation (IR), and detecting repair sites using fluorescent-tagged HR components (**Figure 1F**). This has been an invaluable approach to characterize focus mobility relative to other nuclear structures, such as the heterochromatin domain, the nuclear periphery, or other repair foci (Kruhlak et al., 2006; Falk et al., 2007; Miné-Hattab and Rothstein, 2012; Chiolo et al., 2013; Lottersberger et al., 2015; Ryu et al., 2015, 2016; Caridi et al., 2018a,b; Schrank et al., 2018; Dialynas et al., 2019; Oshidari et al., 2019a; See et al., 2020). These studies established, for example, that heterochromatic DSBs move to the nuclear periphery to continue repair in *Drosophila* cells (Chiolo et al., 2011, 2013; Ryu et al., 2015, 2016; Caridi et al., 2018a). A major advantage of inducing DSBs with IR, relative to using chemical treatments or enzymatic digestion, is that IR-induced DSBs form within a very tight time window. This enables synchronous responses, and an easier characterization of focus dynamics and kinetics at the population level, including in animal tissues (see for example: Lisby et al., 2004; Delabaere et al., 2017; Caridi et al., 2018b; See et al., 2020). Further, IR treatments are well suited to damaging chromatin that is difficult to access with enzymatic digestion, such as heterochromatin (Goodarzi et al., 2008; Iacovoni et al., 2010; Chiolo et al., 2011; Ryu et al., 2015, 2016; Caridi et al., 2018a,b). A potential limitation of this approach is that tracking several sites in the nuclei requires frequent time points to minimize ambiguous tracks, which increases the potential for photobleaching and phototoxicity effects in long kinetics (Caridi et al., 2018b; See et al., 2020).

Alternative approaches employed lasers, alpha-particles, or heavy ions to induce damage along linear tracks in the nucleus of mammalian cells (**Figure 1G**), and repositioning of damage sites is monitored relative to these tracks and specific nuclear compartments (Aten et al., 2004; Chiolo et al., 2011; Jakob et al., 2011; Reynolds et al., 2013). These approaches revealed, for example, that repair foci cluster over time (Aten et al., 2004), and that damage in pericentric heterochromatin results in relocalization of repair sites to outside the chromocenters in mouse cells (Jakob et al., 2011). Using laser beams mounted on a microscope is also an effective method to investigate early damage responses (Bekker-Jensen et al., 2006). However, the high energy associated with some of these damage sources might also impair the chromatin state and repair outcomes (Singleton et al., 2002; Lukas et al., 2005; Reynolds et al., 2013; Kong et al., 2018), and even directly affect relocalization mechanisms (Chiolo et al., 2011).

Thus, several approaches have been developed to characterize the dynamics of repair foci. The preferred method depends on the type of question and the features of the motion under investigation.

MSD ANALYSIS

A traditional approach to characterize the dynamics of damaged DNA is the mean-square displacement (MSD) analysis of the positional data of repair sites (reviewed in Spichal and Fabre, 2017; Caridi et al., 2018b). The MSD curve represents the amount of space a locus explores in the nucleus, and its shape has been used to describe the nature of the movement (Michalet and Berglund, 2012; Oswald et al., 2014; Spichal and Fabre, 2017; Caridi et al., 2018b; **Figure 2**). The time-averaged MSD of a single trajectory is calculated using the following equation:

$$\mathrm{MSD}\,(n\cdot\Delta t)=\frac{1}{N-n}\sum_{i=1}^{N-n}\left[(x_{i+n}-x_i)^2+(y_{i+n}-y_i)^2+(z_{i+n}-z_i)^2\right]$$

where N is the number of points in the trajectory, (x, y, z) the coordinates of the locus in 3-dimensions, and Δt the time interval of the acquisition. MSDs are typically calculated for several trajectories across distinct nuclei, and averaged to extract a time-ensemble-averaged MSD. The data are then fitted to a curve to characterize the type of diffusion. In the following sections, we present different models used in the literature to fit averaged MSD curves.

Brownian Motion

When a molecule freely diffuses, its MSD curve is linear at increased time intervals and its motion is called Brownian (**Figure 2A**). In this case, the MSD follows:

$$\mathrm{MSD}\,(\Delta t)=2dD\Delta t$$

where d is the dimension of the movement, D is the diffusion coefficient of the locus, and Δt is the time interval. The term $2\mathrm{dD}\Delta t$ is the theoretical MSD for Brownian motion in the absence of any experimental noise. However, when measuring the position of a molecule in living cells, the experimental location accuracy can strongly affect the experimental MSD. The error in location for molecules detected by live imaging can be divided into two components (**Supplementary Table S1**):

- Error in the determination of the position due to convolution of the sample with the point spread function (PSF). This depends on imaging conditions and microscope features (e.g., the numerical aperture of the objective, the number of photons collected by the camera, and the wavelength of light). This error is higher at short acquisition times since the number of photons collected is small.
- Error due to the movement of the spot during the acquisition. This error, referred as "motion blur" is higher at longer exposure times.

Experimental MSD curves for Brownian motion, taking into account the location errors, can be fitted by Michalet (2010):

$$\mathrm{MSD}\;(\Delta t)=2dD\Delta t+\sigma_0^2\left(1+\frac{Dt_{\mathrm{Exp}}}{s_0^2}\right)-\frac{4}{3}t_{\mathrm{Exp}}$$

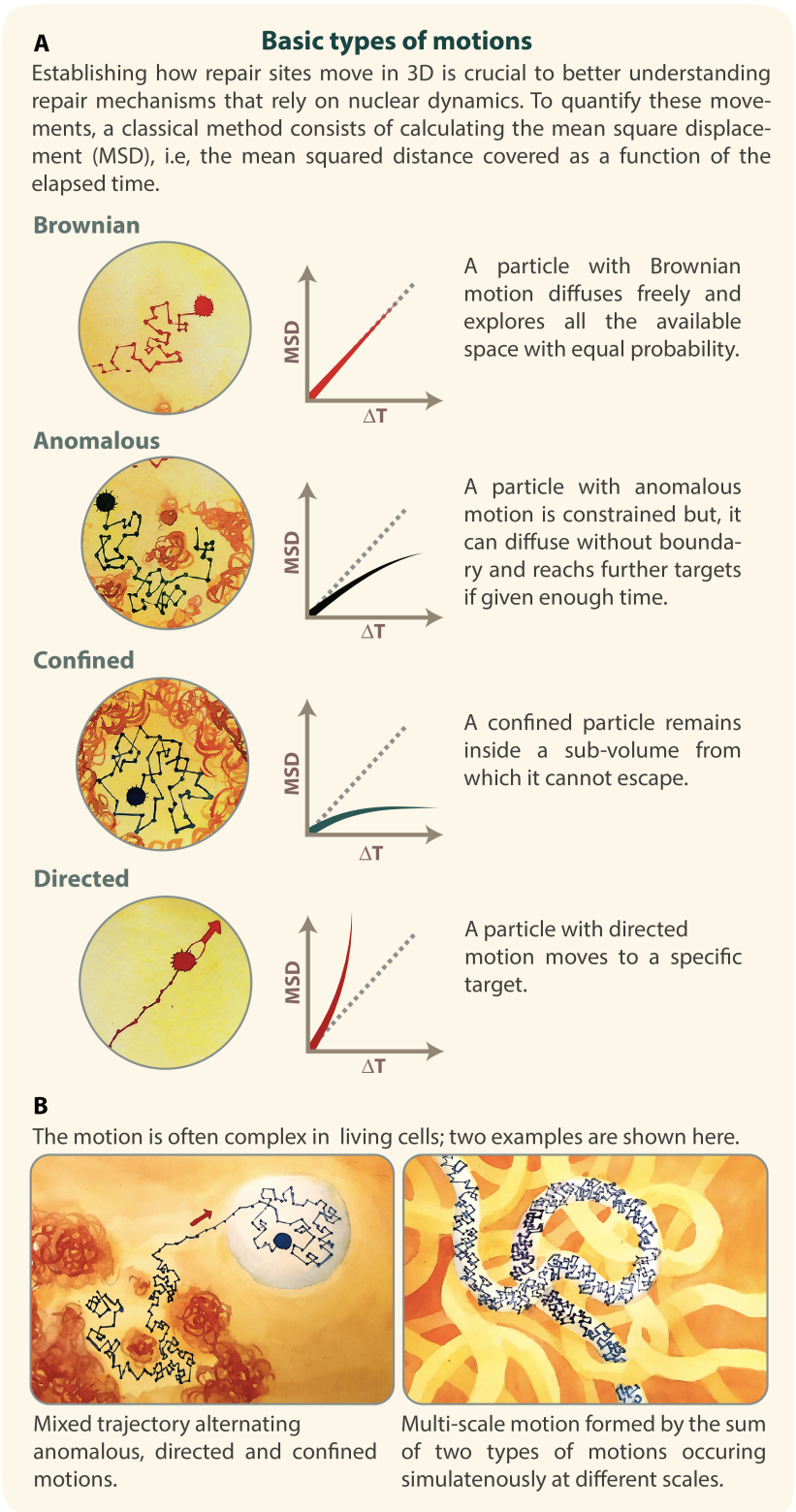

FIGURE 2 | MSD curves identify different types of motions. **(A)** Illustration of Brownian, anomalous, confined and directed motions, with corresponding MSD curves. **(B)** Examples of complex motion. Left: a mixed trajectory alternating anomalous, directed, and confined motion. Right: a motion of a site characterized by a diffusion coefficient Amicro, in a region that itself diffuses with a diffusion coefficient Amacro. Inspired by De Gennes's reptation model (Gennes, 1982). Illustration by Olga Markova.

where σ_0^2 is the localization accuracy of an immobile particle;
s_0^2 is the variance of the PSF;
t_{Exp} is the exposure time of the camera.

Sub-diffusive Motion

In living cells, DNA motion is often slower than Brownian and is called "sub-diffusive" (Barkai et al., 2012). This is due to the existence of constraints that limit chromatin movement, including the polymeric nature of the chromatin, chromatin compaction, molecular crowding, phase separation, and anchoring to subnuclear compartments (Marshall et al., 1997; Spichal and Fabre, 2017; Caridi et al., 2018b). Two types of sub-diffusive motions have been described: confined sub-diffusion and anomalous sub-diffusion.

Confined Sub-diffusion

When a chromosomal locus stays confined inside a sub-volume of the nucleus, its motion is called confined sub-diffusion (**Figure 2A**). The MSD exhibits a plateau (Marshall et al., 1997) and follows the equation:

$$\mathrm{MSD}\,(\Delta t) = R_\infty^2(1 - e^{-2dD\Delta t/R_\infty^2}) + \varepsilon$$

where R_∞ is the measured plateau of the MSD, D is the diffusion coefficient of the locus and ε is the noise due to the experimental measurements. The confinement radius (Rc) of the motion is given by the relation: $R_c = R_\infty\sqrt{(d+2)/d}$, where d is the dimension of the motion. It refers to the radius of a sphere inside which the motion is contained. The MSD curve starts to bend at time $t_c = R_c^2/(2\mathrm{dD})$, representing the characteristic equilibration time after which the effect of boundaries appears.

Anomalous Sub-diffusion

When the force or structure that restricts the motion is not a simple confinement but is modulated in time and space with scaling properties, the motion is called anomalous sub-diffusion (Barkai et al., 2012; Metzler et al., 2014) (**Figure 2A**). In this case, sub-diffusive loci are constrained, but, unlike confined loci, they can diffuse without boundary and thus reach further targets if given enough time. For sub-diffusive motion, the MSD exhibits a power law,

$$\mathrm{MSD}\,(\Delta t) = A\Delta t^\alpha + \varepsilon$$

where α, the anomalous exponent, is smaller than 1.

The anomalous exponent α is linked to the degree of recurrence of DNA exploration, i.e., the number of times a locus reiteratively scans neighboring regions before reaching a distant position (Ben-Avraham, 2000). When α is small, the locus recurrently explores the same environment for a long time, while a large α indicates that the locus is able to explore new environments often. The anomalous diffusion coefficient A represents the amplitude of the motion; it is proportional to the diffusion coefficient only in the case of normal diffusion (when α = 1), which is rarely observed in biological systems (Barkai et al., 2012).

Experimental noise ε can strongly affect MSD measurements also in the case of anomalous sub-diffusion. The exact formula to fit the MSD curves of anomalous diffusion, including localization accuracy, is given by the formula:

$$\mathrm{MSD}\,(\Delta t) = A\Delta t^\alpha + \sigma_0^2\,(1 + \frac{At_{Exp}^\alpha}{4s_0^2}) - \frac{A\alpha(1-\alpha)t_{Exp}^2}{12\Delta t^2}\Delta t^\alpha - \frac{2A}{(\alpha+1)(\alpha+2)}$$

which has been calculated and used to characterize chromatin mobility at multiple time scales (Miné-Hattab et al., 2017).

Directed Motion

Recent studies of chromatin mobility in the context of DNA repair have revealed the existence of transient directed motion in living cells (Cho et al., 2014; Caridi et al., 2018a,b; Lamm et al., 2018; Oshidari et al., 2018) (**Figure 2A**). For directed motion, MSD values rapidly increase at higher time intervals, as follows:

$$\mathrm{MSD}\,(\Delta t) = 2dD\Delta t + \nu^2\Delta t^2 + \varepsilon$$

where D is the diffusion coefficient, ν is the velocity of the directed motion and ε is the noise due to the experimental measurements.

MSD ANALYSES REVEAL INCREASED NUCLEAR EXPLORATION OF DAMAGED AND UNDAMAGED CHROMATIN IN RESPONSE TO DSBs

MSD analyses have been used to characterize the dynamics of repair sites in different contexts, from yeast to mammalian cells, deriving descriptive parameters like diffusion coefficient and confinement radius. In yeast, for example, MSD analyses of repair sites in response to *ISceI*-induced breaks revealed that resected DSBs explore a nuclear volume up to ten times larger than before damage (Dion et al., 2012; Miné-Hattab and Rothstein, 2012). This response depends on resection, chromatin remodeling, checkpoint activation, the strand invasion component Rad51 (Oza et al., 2009; Dion et al., 2012; Miné-Hattab and Rothstein, 2012; Neumann et al., 2012; Horigome et al., 2014; Saad et al., 2014; Amitai et al., 2017; Miné-Hattab et al., 2017; Smith et al., 2018), and it has been linked to homology search (Dion et al., 2012; Miné-Hattab and Rothstein, 2012; Neumann et al., 2012; Miné-Hattab et al., 2017). This process is exceptionally efficient. For example, in *S. cerevisiae*, a single recipient locus and a single donor locus that share as little as 1.2 kb of homology will find each other in the 15,000 kb of genome, and engage in repair with 90% efficiency within 2 h after DSB formation (Aylon et al., 2003; Miné-Hattab and Rothstein, 2012). Increased nuclear exploration is more pronounced in diploid than in haploid cells (Dion et al., 2012; Miné-Hattab and Rothstein, 2012), potentially reflecting a more active search when the homologous partner is available (Mine-Hattab and Rothstein, 2013). Indeed, HR repair with the sister chromatid, which is kept in close proximity through cohesion, is not associated with extensive dynamics

(Dion et al., 2012, 2013), further linking nuclear exploration with inter-homologous repair in yeast.

Importantly, studies in yeast revealed that undamaged loci also become more dynamic in response to damage, exploring a nuclear volume up to four times larger, and more DSBs induce larger nuclear exploration (Miné-Hattab and Rothstein, 2012; Seeber et al., 2013; Herbert et al., 2017; Lawrimore et al., 2017; Miné-Hattab et al., 2017). Changes in chromatin mobility are thus a general feature of the cellular response to DSBs affecting the whole genome. Experimental and theoretical studies suggest that changes in chromatin mobility of both damaged and undamaged loci increase the probability of contact between distant loci, thus promoting the kinetics of homologous pairing (Miné-Hattab and Rothstein, 2012; Guerin et al., 2016; Miné-Hattab et al., 2017; Amitai and Holcman, 2018).

Increased nuclear exploration of damaged sites during HR repair is also observed in mammalian and *Drosophila* cells (Chiolo et al., 2011; Krawczyk et al., 2012; Becker et al., 2014; Cho et al., 2014; Lottersberger et al., 2015; Ryu et al., 2015; Caridi et al., 2018a,b; Schrank et al., 2018). Studies of Rad52 foci in S phase of human cells revealed significant dynamics even when the sister chromatid is used as a template, and linked it to clustering of repair sites (Schrank et al., 2018) (**Supplementary Table S1**). Notably, in human cells NHEJ appears to operate more frequently than HR (Beucher et al., 2009), and does not require extensive movement (Krawczyk et al., 2012; Aymard et al., 2017; Schrank et al., 2018; Schrank and Gautier, 2019), except at unprotected telomeres (Dimitrova et al., 2008; Lottersberger et al., 2015). This might explain why repair focus dynamics have not been detected in early studies (Nelms et al., 1998; Soutoglou et al., 2007; Jakob et al., 2009). Further, studies in *Drosophila* cells treated with IR, revealed that both euchromatic and heterochromatic repair foci are mobilized (Caridi et al., 2018a), with the most extensive nuclear exploration associated with heterochromatic sites that relocalize to the nuclear periphery (Ryu et al., 2015; Caridi et al., 2018a).

Although the movement of undamaged sites has not been consistently tracked in these systems, the dynamics of other (undamaged) chromosomal loci (e.g., telomeres and centromeres) before and after damage suggest that global chromatin mobilization is also conserved (Lottersberger et al., 2015; Caridi et al., 2018a).

What promotes the dynamics of undamaged loci in response to DSBs? Different contributing mechanisms have been identified: (i) the release of structures that anchor chromosomal loci to the nuclear periphery, (ii) repair and checkpoint proteins; (iii) the transfer of cytoplasmic forces to the chromatin through the LINC complex; and (iv) global chromatin modifications. Specifically, anchoring of centromeres, telomeres and the nucleolus to the nuclear envelope provides constraints to the motion of interphase chromosomes in budding yeast, limiting chromosome dynamics (Berger et al., 2008; Therizols et al., 2010; Wong et al., 2012; Agmon et al., 2013; Verdaasdonk et al., 2013; Strecker et al., 2016; Lawrimore et al., 2017). Releasing telomere and centromere attachments reproduces chromatin mobility observed in response to DSBs (Strecker et al., 2016; Lawrimore et al., 2017). These studies also identified a Mec1-dependent phosphorylation of the kinetocore protein Cep3 as an essential player in global chromatin mobilization (Strecker et al., 2016). In addition to checkpoint kinases, Rad51 and Rad52 HR proteins are required to facilitate global chromatin dynamics (Seeber et al., 2013; Miné-Hattab et al., 2017; Smith et al., 2018, 2019). Further, studies in yeast and mammalian cells suggest that cytoplasmic actin and microtubules induce a global chromatin "shake-up" in response to DSB formation (Lottersberger et al., 2015; Spichal et al., 2016; Amitai et al., 2017; Lawrimore et al., 2017). Finally, intrinsic modifications of chromatin properties following DSBs, such as chromatin decondensation and changes in chromatin stiffness, appear to contribute to the global increase in chromatin dynamics. Global chromatin decondensation in response to DNA damage has been described across different model systems and likely results from histone modifications, chromatin remodeling, and histone loss (Ziv et al., 2006; Ayoub et al., 2008; Chiolo et al., 2011; Luijsterburg et al., 2012; Seeber et al., 2013; Strecker et al., 2016; Amitai et al., 2017; Hauer et al., 2017). These modifications might promote nuclear exploration by reducing chromatin compaction and increasing its flexibility. Additional studies applied numerical simulation of chromatin dynamics, mainly based on Rouse-like models (Arbona et al., 2017), to predict chromatin mobility in response to DSBs both at the damaged site and genome-wide (Herbert et al., 2017; Lawrimore et al., 2017; Miné-Hattab et al., 2017). For example, β-polymer modeling and simulations suggest that local chromatin expansion is sufficient to drive extrusion of the damage site from its local domain, affecting longer-range dynamics (Amitai et al., 2017). However, multi-scale tracking of chromatin (see: *Multi-scale motion* section, below) and polymer simulations also suggest the importance of chromatin stiffening in local and global chromatin dynamics (Herbert et al., 2017; Lawrimore et al., 2017; Miné-Hattab et al., 2017). This is potentially in contradiction with the role of chromatin relaxation in the same responses, and might reflect a different extent of relaxation/stiffening across distinct loci or time points following damage formation. Thus, more studies are needed to establish the relative contribution of chromatin stiffening and relaxation to increased chromatin exploration, toward an integrated model for damage-induced chromatin dynamics.

Of note, studies in yeast revealed that increased nuclear exploration does not correlate with higher speed of locus movement. In fact, the diffusion coefficient does not significantly change in response to damage, both at damaged and undamaged loci (Miné-Hattab and Rothstein, 2012; Mine-Hattab and Rothstein, 2013). In other words, changes in mobility allow chromatin to go further but not faster.

Overall, MSD analyses have been an invaluable tool for identifying damage-induced nuclear dynamics, revealing a significant increase of nuclear exploration in response to DSBs for both damaged and undamaged chromatin, and identifying several molecular mechanisms responsible for these dynamics.

LIMITATIONS OF MSD ANALYSES

Recent studies of chromatin trajectories in response to DNA damage revealed that MSD analyses also suffer from several limitations, and can even mask the existence of certain

characteristics of the motion. First, MSDs are typically calculated as time-ensemble-averaged values over several trajectories to obtain a precise estimate of the parameters describing the motion (e.g., confinement radius and diffusion coefficient). This is in part to compensate for the location measurement errors mentioned above, and in part to enable the use of relatively short trajectories limited by photo-bleaching and photo-toxicity effects. However, averaging the behavior of several trajectories affects the ability to detect the differences between them, i.e., it does not account for heterogeneity across different cells and break sites. Second, MSD calculations assume that each site undergoes homogenous motion during the time of acquisition, which is rarely the case. For example: (i) repair sites can be transiently bound to the nuclear periphery or other nuclear structures; (ii) their motion can be different inside or outside phase separated domains; and (iii) directed motions can occur for limited time periods (**Figure 2B**, left). A locus can also undergo distinct diffusion regimes at different time scales, which simultaneously contribute to the motion of a particle. For example, a locus can exhibit a subdiffusive motion characterized by A_{micro}, in a region that itself moves with a diffusion coefficient A_{macro} (**Figure 2B**, right). Additionally, chromatin motion is not purely sub-diffusive even in the absence of DNA damage; studies in budding yeast (Heun et al., 2001) and Chinese hamster ovary cells (Levi et al., 2005) showed that chromatin undergoes confined random motion alternating with rare fast jumps that likely reflect rare events of active diffusion.

Accordingly, simulations of a particle moving with different types of motions: confined, directed, and a combination of confined and directed (mixed trajectory), show how MSD curves can mask the presence of directed motions (**Figure 3** and **Supplementary Movies S1–S3**) (Bacher et al., 2004; Masedunskas et al., 2017). The simulation of a mixed trajectory accounts for asynchronous motion, where the starting point of directed motion and its duration is different for each particle as observed experimentally. While MSD curves for confined and directed motions display the expected shapes (**Figures 4A,B**), the MSD graph for mixed trajectories resembles that describing a subdiffusive confined motion (**Figure 4C**), confirming that the MSD approach is not suitable to describe heterogenous and asynchronous motions.

In the following sections, we will illustrate two major types of complex motions occurring in response to DNA damage (**Figure 4**), and we will discuss experimental approaches and analytical methods that enabled their characterization beyond simple MSD analyses.

MIXED TRAJECTORIES

A major question in the field of nuclear dynamics is whether repair focus motion is driven by active forces, or alternatively subdiffusive motions followed by anchoring to subnuclear structures are sufficient to generate these dynamics. Recent studies revealed the existence of directed motions in a context of mixed trajectories for at least some damage-induced responses (reviewed in Caridi et al., 2019).

First, IR-induced heterochromatic repair foci that relocalize to the nuclear periphery in *Drosophila* cells, are characterized by directed motion driven by transient nuclear actin filaments (F-actin) and myosins (Caridi et al., 2018a; Dialynas et al., 2019; See et al., 2020) (reviewed in Caridi et al., 2019) (**Figure 4A**, left). Repair foci slide along the filaments, and focus movement requires myosins' ability to walk along filaments, suggesting that nuclear F-actin provides "highways" for the relocalization of repair sites *via* myosin motors (Caridi et al., 2018a). Myosins and the actin nucleator Arp2/3 associate with the heterochromatin repair component Smc5/6 in response to damage, suggesting Smc5/6 as a physical link between heterochromatic repair sites and the motor system (Caridi et al., 2018a). Smc5/6 also recruits the myosin activator Unc45 to repair sites, inducing chromatin mobilization (Caridi et al., 2018a). Further, relocalization requires SUMOylation, checkpoint and resection proteins, similar to other relocalization pathways (Chiolo et al., 2011; Ryu et al., 2015, 2016; Amaral et al., 2017; Caridi et al., 2018a). Defective relocalization results in unrepaired or misrepaired DSBs, revealing the importance of this pathway for "safe" HR in heterochromatin (Chiolo et al., 2011; Ryu et al., 2015, 2016; Caridi et al., 2018a; Dialynas et al., 2019). Notably, in this context, directed motions primarily occur between the periphery of the heterochromatin domain [a distinct structure in *Drosophila* cells (Chiolo et al., 2011; Li et al., 2017)] and the nuclear periphery, which is where most nuclear actin filaments are organized (Caridi et al., 2018a). Directed motions typically last 24 min, corresponding to the average time required for repair sites to reach the nuclear periphery and the average duration of nuclear actin filaments (Caridi et al., 2018a). However, time points coinciding with the initial movement of repair sites from inside the heterochromatin domain to its periphery are characterized by confined diffusion (Caridi et al., 2018a; Rawal et al., 2019), similar to the rest of undamaged heterochromatin that behaves like a phase separated domain (Larson et al., 2017; Strom et al., 2017). Time points following focus association with the nuclear periphery also display confined diffusion (Ryu et al., 2015; Caridi et al., 2018a; Rawal et al., 2019). In this context where directed motions alternate with diffusive motions, and initiate asynchronously in the population of foci, directed motions are not detected in a simple time-ensemble MSD analysis (Ryu et al., 2015; Caridi et al., 2018a,b) (**Supplementary Table S1**). Time points characterized by directed motions were identified using an analytical method that scans the trajectory of each focus at variable time windows and initiation times, and detects time windows in which MSD graphs displays upward curvature (Caridi et al., 2018a,b) (**Supplementary Table S1**). Isolating these time points also required imaging techniques that minimize cell movement and correct for modest rotational and translational motion of the nuclei (Amitai et al., 2017), removing a significant amount of noise from the system (Caridi et al., 2018b; See et al., 2020) (**Supplementary Table S1**). Additionally, given the long time span along which these motions occur, optimizing imaging conditions for long time imaging and sufficiently spaced time intervals is essential for their detection (Ryu et al., 2015; Caridi et al., 2018a,b; See et al., 2020).

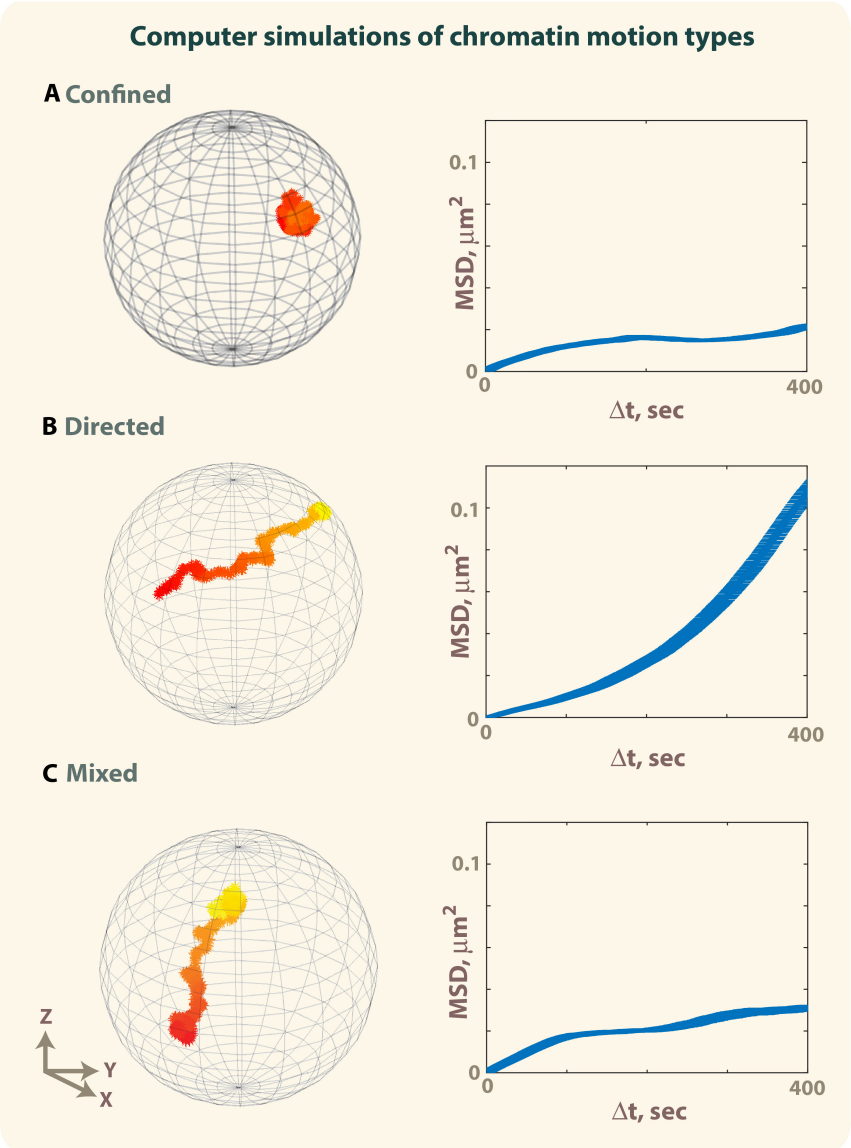

FIGURE 3 | Simulation of confined motion, directed motion and mixed trajectories. The motion of a particle in a sphere of 1 μm radius was simulated using 1,000 iterations (Bacher et al., 2004; Masedunskas et al., 2017). Early timepoints are colored in red, late timepoints in yellow. **(A)** Example of a trajectory obtained by simulating a confined motion (D = 0.005 μm^2/s, Rc = 0.3 μm) (see also corresponding **Supplementary Movie S1**). **(B)** Example of a trajectory obtained by simulating directed motion until the particle reaches the surface of the sphere (D = 0.005 μm^2/s, ν = 1 μm) (see also corresponding **Supplementary Movie S2**). **(C)** Example of a mixed trajectory characterized by confined motion (D = 0.005 μm^2/s, Rc = 0.3 μm) lasting 200 timepoints, followed by directed motion (D = 0.005 μm^2/s, ν = 1 μm for t = 201–400) and confined motion for the last 600 time points (D = 0.005 μm^2/s, Rc = 0.3 μm. Time-ensemble MSDs were calculated over 10 trajectories. For panel **(C)**, each trajectory is characterized by a different time point when the directed motion starts, and different duration of the directed motion (see also **Supplementary Movie S3**).

Notably, these studies also established that the average speed of focus motion associated with the relocalization of heterochromatic DSBs is not higher at time points characterized by directed motion relative to time points characterized by confined diffusion (Caridi et al., 2018a; Rawal et al., 2019). This is consistent with a model where actin filaments and motors do not increase motion speed. Rather, they provide directionality and counteract other forces that might limit the release of repair foci from the heterochromatin domain (e.g., chromatin compaction and/or phase separation) (Rawal et al., 2019).

Second, in a study currently in preprint, application of similar analysis methods identified short time points characterized by directed motions for damaged replication forks in human cells, which also correlate with the formation of nuclear actin filaments and the restart of stalled forks (Lamm et al., 2018).

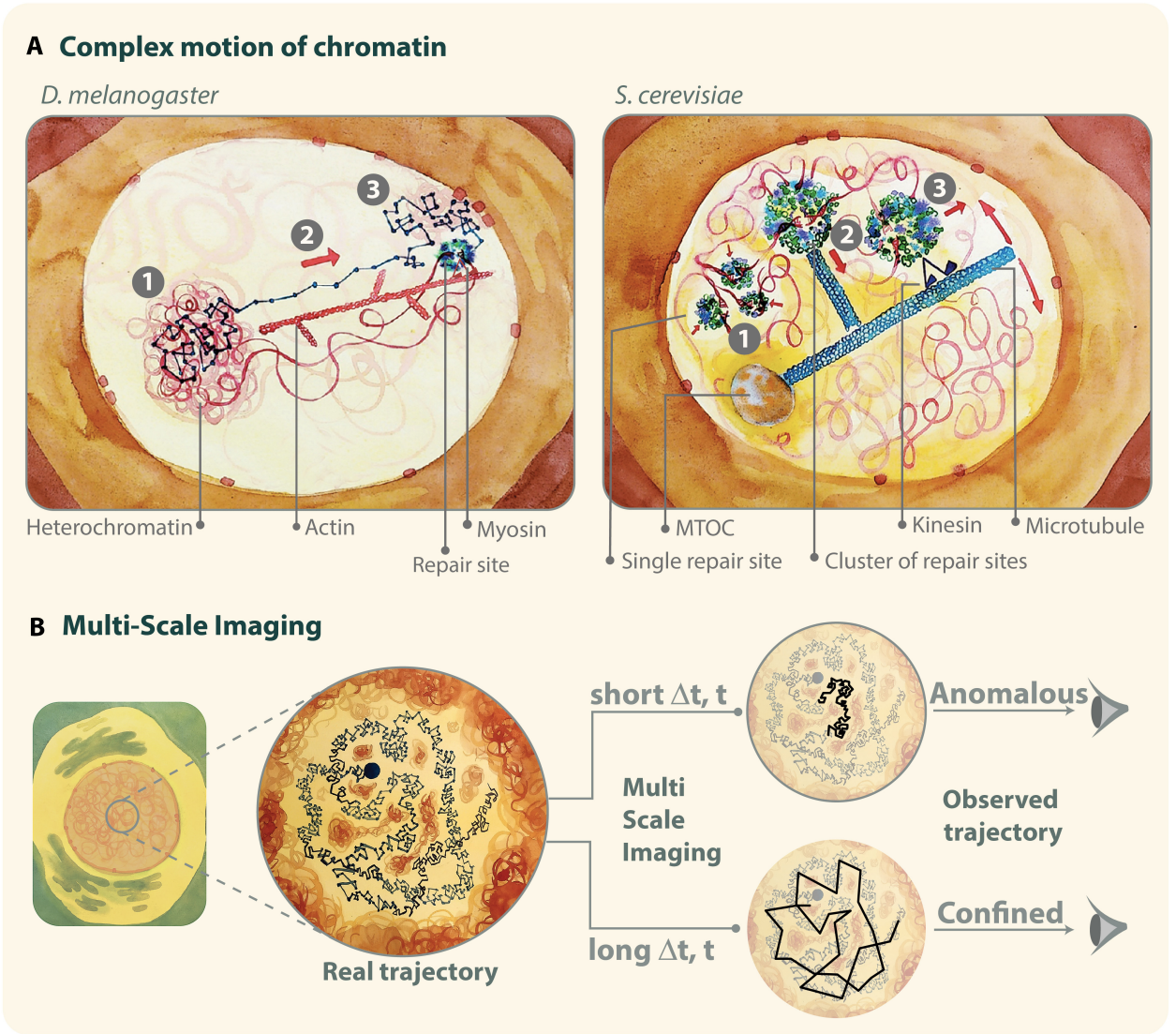

FIGURE 4 | (A) Illustration of examples of mixed trajectories. Left: in Drosophila cells, the motion of DSBs leaving the heterochromatin domain and reaching the nuclear periphery is characterized by: (1) confined diffusion inside the heterochromatin domain; (2) myosin-driven directed motion along actin filaments between the heterochromatin domain periphery and the nuclear periphery; and (3) confined diffusion at the nuclear periphery. Right: in budding yeast, repair sites: (1) cluster into larger foci; (2) are "captured"i by short microtubules; and (3) move by kinesin-driven directed motions along long nuclear microtubules that pivot around the microtubule organizing center (MTOC). **(B)** Illustration of multi-scale motion. Chromatin imaging at different time scales reveals anomalous diffusion at short time intervals (Δt) and confined diffusion at longer time intervals. It is important to keep in mind that experiments reveal only the mobility of molecules accessible with the specific imaging conditions used during the acquisition. Thus, different imaging settings can shed light on different diffusive behaviors, which are visible only at certain time scales. Illustration by Olga Markova.

Third, directed motions have been detected during homology search for HR repair of telomeres in ALT human cells (Cho et al., 2014), which might also potentially include C-circles released from telomeres (Henson et al., 2009; Schrank and Gautier, 2019; Zhang et al., 2019). In this case, time-ensemble-average MSD graphs were characterized by $\alpha > 1$ when calculated at selected time points preceding telomere-telomere association for ALT repair, effectively limiting the analysis to time points when the motion is homogeneous (**Supplementary Table S1**).

Fourth, directed motions have been described for subtelomeric DSBs repaired by the HR sub-pathway break-induced replication (BIR) in *S. cerevisiae* (Oshidari et al., 2018) (**Figure 4A**, right). These damage sites move along a single nuclear microtubule but directed motions are not easily detectable using canonical MSD analyses because of two major confounding effects: (i) DSB movement along microtubules is transient; and (ii) microtubules pivot around the microtubule organizing center (MTOC), resulting in non-linear directed motions (Oshidari et al., 2018). In this case, directed motions

were identified by directional change distribution (DCD) analysis, which measures changes in the angle of a trajectory and can reveal broader motion profiles by increasing the temporal coarse graining (Oshidari et al., 2018) (reviewed in Oshidari et al., 2019b) (**Supplementary Table S1**). This study also identified a role for Kar3 in kinesin-dependent directed motions and BIR completion (Oshidari et al., 2018). Notably, loss of Kar3 does not affect the average speed of motion (Oshidari et al., 2018), suggesting that also in this context, filaments and motors have a role in providing directionality to the repair site motion rather than affecting speed. In addition to these functions, short nuclear microtubules have been proposed to generate a flow that facilitates clustering of repair foci, and additional short filaments departing from these clusters promote the capturing of repair centers by the main microtubule (Oshidari et al., 2019a).

Fifth, application of the DCD analysis also identified directed motions for persistent DSBs that move to the nuclear periphery in budding yeast (Oshidari et al., 2018), reverting the previous conclusion that these are characterized by diffusive motion followed by nuclear periphery anchoring (Amitai et al., 2017).

Finally, Arp2/3 and nuclear actin polymerization contributes to repair focus clustering and HR repair in *Drosophila* and mammalian cells (Caridi et al., 2018a; Schrank et al., 2018), and short actin filaments travel with repair foci in human cells (Schrank et al., 2018), suggesting a direct role of these structures in mobilizing damage sites. While directed motions have not been directly investigated in this context, and myosins do not seem to be involved (Caridi et al., 2018a), the requirement of nuclear filaments suggest that directed motions might also contribute to these dynamics (Caridi et al., 2019).

It is worth noting that, in addition to heterochromatin, other membraneless -or phase separated- compartments exist in the nucleus, including nucleoli and repair foci *per se* (Altmeyer et al., 2015; Frottin et al., 2019; Kilic et al., 2019; Min et al., 2019; Singatulina et al., 2019) (reviewed in Mine-Hattab and Taddei, 2019; Rawal et al., 2019), which can affect the dynamics of repair foci at different levels. Phase separation of a nuclear domain might promote diffusion of repair sites inside the domain, while limiting release from the domain due to surface tension (Hyman et al., 2014). Phase separation properties of repair components might also contribute to the clustering of repair foci into larger structures, promoting local dynamics (Altmeyer et al., 2015; Kilic et al., 2019; Oshidari et al., 2019a). Notably, as repair sites move from one domain to another, their motion is likely to change properties exhibiting successive diffusion regimes, which cannot be detected with time-ensemble MSD analyses (**Figure 4A**, right). In all these cases, dedicated analytical methods should be applied to characterize the diffusion regimes involved.

Further, damage-induced nuclear dynamics can occur in the context of a dynamic nucleus, which adds rotational motion to the system. In yeast, removal of nuclear rotations *via* Latrunculin treatment enabled the identification of modes of diffusion that are otherwise masked by the nuclear rotational movement (Amitai et al., 2017). In mouse and *Drosophila* cells, these rotational movements were corrected by registering the nuclei relative to repair foci prior to tracking repair sites to establish repair locus trajectories (Ryu et al., 2015; Caridi et al., 2018a,b; See et al., 2020) (**Supplementary Table S1**).

These studies point to the importance of applying dedicated imaging approaches, image processing methods, and analytical tools to identify directed motions. They also suggest that nuclear structures and motors contribute to repositioning repair sites in more situations than initially thought, including where diffusive motions appear to prevail. More studies are needed to identify repair contexts relying on directed movements and the structural/motor components mediating these dynamics, and more methods need to be developed to account for different types of mixed trajectories.

MULTI-SCALE MOTION

Chromatin presents several levels of organization, which translates into different scales of chromatin mobility (Mine-Hattab and Darzacq, 2018). These different modes of diffusion can be unraveled by imaging the chromatin at different time-scales (**Figure 4B** and **Supplementary Table S1**). For example, in the absence of DNA damage, chromatin undergoes anomalous diffusion when observed at short time intervals (10-ms to 1-s) (Maeshima et al., 2010; Weber et al., 2010; Burnecki et al., 2012; Hajjoul et al., 2013; Lucas et al., 2014; Backlund et al., 2015; Amitai et al., 2017; Miné-Hattab et al., 2017). However, at longer time scales, MSD exhibits a plateau characteristic of confined diffusion, consistent with the chromatin remaining confined inside a sub-volume of the nucleus (Marshall et al., 1997; Heun et al., 2001; Maeshima et al., 2010; Masui et al., 2011; Miné-Hattab and Rothstein, 2012; Backlund et al., 2015).

Several recent studies applied multi scale imaging to characterize chromatin mobility in response to DSBs. Increased exploration of the nuclear space is detected in response to I-SceI-induced DSBs when imaging is done at 1.5s or longer time intervals (Dion et al., 2012; Miné-Hattab and Rothstein, 2012). However, remarkably, imaging at 100 ms time intervals or faster reveals lower mobility of the damaged site relative to undamaged conditions (Miné-Hattab et al., 2017). Given that a shorter time scale for data collection investigates chromatin motion on a smaller temporal and spatial scale, the low mobility observed at short time scales reflects reduced local mobility of the cut site (Miné-Hattab et al., 2017). These dynamics can be modeled assuming that chromatin persistence length (a measure of the bending stiffness of a polymer) globally increases (Herbert et al., 2017; Miné-Hattab et al., 2017). At the damaged sites, such response likely results from the recruitment of the repair machinery that increases chromatin stiffness (Mine et al., 2007). Accordingly, reduced local mobility has been associated with resected DNA and requires Rad51 (Saad et al., 2014; Miné-Hattab et al., 2017).

The reduced mobility detected at lower time scales also characterizes undamaged chromatin, consistent with a global increase in chromatin stiffness that spreads beyond the damaged

loci (Herbert et al., 2017; Miné-Hattab et al., 2017). This might depend on H2A phosphorylation, which spreads for kilobases to megabases from the cut site (Rogakou et al., 1999), and introduces negative charges into the chromatin (Herbert et al., 2017). As a consequence of a global increase in chromatin stiffness, intrachromosomal loci become more distant and their dynamics change, as observed experimentally in yeast (Herbert et al., 2017; Miné-Hattab et al., 2017).

It has been proposed that increased rigidity of the chromatin facilitates the movement of the cut site through the dense nucleoplasm (Miné-Hattab et al., 2017). In other words, a stiffer chromatin (with more rigidity associated with the break site) would enable resected DNA to navigate through adjacent obstacles more efficiently, thus allowing it to reach farther targets. The stiffer chromatin would act like a needle to help move damaged DNA through the chromatin mesh, likened to a "ball of yarn" (Miné-Hattab et al., 2017). Of note, there is currently no method to directly measure chromatin flexibility in living cells. The two studies referred to here (Herbert et al., 2017; Miné-Hattab et al., 2017) use indirect methods to assess chromatin stiffness, by comparing conformation and dynamics of tagged chromosomal loci with polymer simulation.

These studies emphasize the importance of interrogating different spatiotemporal scales to understand chromatin motions, potentially revealing distinct dynamic processes and regulatory mechanisms. Additionally, more sophisticated and refined mathematical tools are necessary to account for the composite nature of chromatin motion, and for example to distinguish between the local diffusion of a locus in a region that itself moves with a different mode of diffusion.

CONCLUSION AND PERSPECTIVES

A large number of studies in the past decade have shown that DSBs trigger a larger exploration of the nucleus for damaged and undamaged chromatin sites, and this response is conserved from yeast to mammalian cells. Increasing chromatin confinement radius, or changing the nature of its motion, dramatically enhances the ability of a locus to sample neighboring DNA sequences during homology search. In addition to this response, recent studies have shown that chromatin motion is more complex than initially anticipated. Relocalization of repair sites *via* molecular motors typically results in mixed trajectories, where directed motions occur in alternation with subdiffusive regimes. Further, the transient directed movement of repair sites along oscillating structures (e.g., nuclear microtubules), nuclear flows, and phase separation of nuclear domains, add complexity to the trajectories. Additionally, distinct diffusion regimes typically occur at different time scales, likely reflecting different level of chromatin organization. A simple MSD analysis is not adapted for such composite motions, as it assumes a homogenous mode of diffusion during the acquisition. Additionally, time-ensemble MSD analyses mix different type of motions that start asynchronously and occur for different durations. New analytical methods enabled the dissection of some of these dynamics. To reveal the existence of several diffusion regimes, multi-scale tracking, simulations, and mathematical models of complex motions need to be performed. The identification of several contexts where nuclear dynamics is dependent on nuclear actin filaments or microtubules, and characterized by short or long tracts of directed motions, suggests the existence of forces that drive the motion in more situations than initially thought. The development of new dedicated analytical methods started unlocking the door toward a deeper understanding of these dynamics, and the discovery of the molecular mechanisms responsible for their regulation. Nuclear dynamics facilitate DNA repair in different contexts, but nuclear exploration of damaged sequences is also responsible for chromosome rearrangements (Neumann et al., 2012; Roukos et al., 2013; Marcomini et al., 2018). Defects in relocalization pathways also result in genome instability (Torres-Rosell et al., 2007; Chiolo et al., 2011; Ryu et al., 2015, 2016; Su et al., 2015; Caridi et al., 2018a; Dialynas et al., 2019; Aguilera et al., 2020) (reviewed in Caridi et al., 2017; Caridi et al., 2019; Schrank and Gautier, 2019), and establishing the mechanisms responsible for these dynamics is a necessary step to understand how their misregulation contributes to cancer and other genome instability disorders.

AUTHOR CONTRIBUTIONS

Both authors equally contributed to this review and approved the submitted version.

FUNDING

This work was supported by NIH R01GM117376 and NSF Career 1751197 to IC and ANR (Agence Nationale pour la Recherche), the Labex DEEP (ANR-11-LABX-0044-DEEP and ANR-10-IDEX-0001-02 PSL), ANR-18-CE12-0015-03, the FRM (Fondation pour la Recherche Médicale), the PIC3i (Program Interdisciplinaire Curie), and the Q-Life program to JM-H and her team.

ACKNOWLEDGMENTS

We thank Scott Keagy and Mathias Heltberg for critical reading of the manuscript and Olga Markova for the artwork.

SUPPLEMENTARY MATERIAL

The Supplementary Material for this article can be found online at: https://www.frontiersin.org/articles/10.3389/fgene.2020.00800/full#supplementary-material

REFERENCES

Agmon, N., Liefshitz, B., Zimmer, C., Fabre, E., and Kupiec, M. (2013). Effect of nuclear architecture on the efficiency of double-strand break repair. *Nat. Cell Biol.* 15, 694–699. doi: 10.1038/ncb2745

Aguilera, P., Whalen, J., Minguet, C., Churikov, D., Freudenreich, C., Simon, M. N., et al. (2020). The nuclear pore complex prevents sister chromatid recombination during replicative senescence. *Nat. Commun.* 11:160.

Altmeyer, M., Neelsen, K. J., Teloni, F., Pozdnyakova, I., Pellegrino, S., Grofte, M., et al. (2015). Liquid demixing of intrinsically disordered proteins is seeded by poly(ADP-ribose). *Nat. Commun.* 6:8088.

Amaral, N., Ryu, T., Li, X., and Chiolo, I. (2017). Nuclear Dynamics of Heterochromatin Repair. *Trends Genet.* 33, 86–100. doi: 10.1016/j.tig.2016.12.004

Amitai, A., and Holcman, D. (2018). Encounter times of chromatin loci influenced by polymer decondensation. *Phys. Rev. E* 97:032417.

Amitai, A., Seeber, A., Gasser, S. M., and Holcman, D. (2017). Visualization of Chromatin Decompaction and Break Site Extrusion as Predicted by Statistical Polymer Modeling of Single-Locus Trajectories. *Cell Rep.* 18, 1200–1214. doi: 10.1016/j.celrep.2017.01.018

Arbona, J. M., Herbert, S., Fabre, E., and Zimmer, C. (2017). Inferring the physical properties of yeast chromatin through Bayesian analysis of whole nucleus simulations. *Genome Biol.* 18:81.

Aten, J. A., Stap, J., Krawczyk, P. M., van Oven, C. H., Hoebe, R. A., Essers, J., et al. (2004). Dynamics of DNA double-strand breaks revealed by clustering of damaged chromosome domains. *Science* 303, 92–95. doi: 10.1126/science.1088845

Aylon, Y., Liefshitz, B., Bitan-Banin, G., and Kupiec, M. (2003). Molecular dissection of mitotic recombination in the yeast Saccharomyces cerevisiae. *Mol. Cell Biol.* 23, 1403–1417. doi: 10.1128/mcb.23.4.1403-1417.2003

Aymard, F., Aguirrebengoa, M., Guillou, E., Javierre, B. M., Bugler, B., Arnould, C., et al. (2017). Genome-wide mapping of long-range contacts unveils clustering of DNA double-strand breaks at damaged active genes. *Nat. Struct. Mol. Biol.* 24, 353–361. doi: 10.1038/nsmb.3387

Ayoub, N., Jeyasekharan, A. D., Bernal, J. A., and Venkitaraman, A. R. (2008). HP1-beta mobilization promotes chromatin changes that initiate the DNA damage response. *Nature* 453, 682–686. doi: 10.1038/nature06875

Bacher, C. P., Reichenzeller, M., Athale, C., Herrmann, H., and Eils, R. (2004). 4-D single particle tracking of synthetic and proteinaceous microspheres reveals preferential movement of nuclear particles along chromatin - poor tracks. *BMC Cell Biol.* 5:45. doi: 10.1186/1471-2121-5-45

Backlund, M. P., Joyner, R., and Moerner, W. E. (2015). Chromosomal locus tracking with proper accounting of static and dynamic errors. *Phys. Rev. E Stat. Nonlin. Soft. Matter. Phys.* 91:062716.

Barkai, E., Garini, Y., and Metzler, R. (2012). Strange kinetics of single molecules in living cells. *Phys. Today* 65, 29–35. doi: 10.1063/pt.3.1677

Becker, A., Durante, M., Taucher-Scholz, G., and Jakob, B. (2014). ATM alters the otherwise robust chromatin mobility at sites of DNA double-strand breaks (DSBs) in human cells. *PLoS One* 9:e92640. doi: 10.1371/journal.pone.0092640

Bekker-Jensen, S., Lukas, C., Kitagawa, R., Melander, F., Kastan, M. B., Bartek, J., et al. (2006). Spatial organization of the mammalian genome surveillance machinery in response to DNA strand breaks. *J. Cell Biol.* 173, 195–206. doi: 10.1083/jcb.200510130

Ben-Avraham, D. H. (2000). *Diffusion and Reactions in Fractals and Disordered Systems*. Cambridge: Cambridge University Press.

Berger, A. B., Cabal, G. G., Fabre, E., Duong, T., Buc, H., Nehrbass, U., et al. (2008). High-resolution statistical mapping reveals gene territories in live yeast. *Nat. Methods* 5, 1031–1037. doi: 10.1038/nmeth.1266

Beucher, A., Birraux, J., Tchouandong, L., Barton, O., Shibata, A., Conrad, S., et al. (2009). ATM and Artemis promote homologous recombination of radiation-induced DNA double-strand breaks in G2. *EMBO J.* 28, 3413–3427. doi: 10.1038/emboj.2009.276

Brinkman, E. K., Chen, T., de Haas, M., Holland, H. A., Akhtar, W., and van Steensel, B. (2018). Kinetics and Fidelity of the Repair of Cas9-Induced Double-Strand DNA Breaks. *Mol. Cell* 70, 801–813.e6. doi: 10.1016/j.molcel.2018.04.016

Bronstein, I., Israel, Y., Kepten, E., Mai, S., Shav-Tal, Y., Barkai, E., et al. (2009). Transient anomalous diffusion of telomeres in the nucleus of mammalian cells. *Phys. Rev. Lett.* 103:018102.

Burnecki, K., Kepten, E., Janczura, J., Bronshtein, I., Garini, Y., and Weron, A. (2012). Universal algorithm for identification of fractional Brownian motion. A case of telomere subdiffusion. *Biophys. J.* 103, 1839–1847. doi: 10.1016/j.bpj.2012.09.040

Bystricky, K., Laroche, T., van Houwe, G., Blaszczyk, M., and Gasser, S. M. (2005). Chromosome looping in yeast: telomere pairing and coordinated movement reflect anchoring efficiency and territorial organization. *J. Cell Biol.* 168, 375–387.

Caridi, C. P., D'Agostino, C., Ryu, T., Zapotoczny, G., Delabaere, L., Li, X., et al. (2018a). Nuclear F-actin and myosins drive relocalization of heterochromatic breaks. *Nature* 559, 54–60. doi: 10.1038/s41586-018-0242-8

Caridi, C. P., Delabaere, L., Tjong, H., Hopp, H., Das, D., Alber, F., et al. (2018b). Quantitative Methods to Investigate the 4D Dynamics of Heterochromatic Repair Sites in Drosophila Cells. *Methods Enzymol.* 601, 359–389. doi: 10.1016/bs.mie.2017.11.033

Caridi, C. P., Plessner, M., Grosse, R., and Chiolo, I. (2019). Nuclear actin filaments in DNA repair dynamics. *Nat. Cell Biol.* 21, 1068–1077. doi: 10.1038/s41556-019-0379-1

Caridi, P. C., Delabaere, L., Zapotoczny, G., and Chiolo, I. (2017). And yet, it moves: nuclear and chromatin dynamics of a heterochromatic double-strand break. *Philos. Trans. R. Soc. Lond. B Biol. Sci.* 372:20160291. doi: 10.1098/rstb.2016.0291

Caron, P., Choudjaye, J., Clouaire, T., Bugler, B., Daburon, V., Aguirrebengoa, M., et al. (2015). Non-redundant Functions of ATM and DNA-PKcs in Response to DNA Double-Strand Breaks. *Cell Rep.* 13, 1598–1609. doi: 10.1016/j.celrep.2015.10.024

Chiolo, I., Minoda, A., Colmenares, S. U., Polyzos, A., Costes, S. V., and Karpen, G. H. (2011). Double-strand breaks in heterochromatin move outside of a dynamic HP1a domain to complete recombinational repair. *Cell* 144, 732–744. doi: 10.1016/j.cell.2011.02.012

Chiolo, I., Tang, J., Georgescu, W., and Costes, S. V. (2013). Nuclear dynamics of radiation-induced foci in euchromatin and heterochromatin. *Mutat. Res.* 750, 56–66. doi: 10.1016/j.mrfmmm.2013.08.001

Cho, N. W., Dilley, R. L., Lampson, M. A., and Greenberg, R. A. (2014). Interchromosomal homology searches drive directional ALT telomere movement and synapsis. *Cell* 159, 108–121. doi: 10.1016/j.cell.2014.08.030

Chung, D. K., Chan, J. N., Strecker, J., Zhang, W., Ebrahimi-Ardebili, S., Lu, T., et al. (2015). Perinuclear tethers license telomeric DSBs for a broad kinesin- and NPC-dependent DNA repair process. *Nat. Commun.* 6:7742.

Churikov, D., Charifi, F., Eckert-Boulet, N., Silva, S., Simon, M. N., Lisby, M., et al. (2016). SUMO-Dependent Relocalization of Eroded Telomeres to Nuclear Pore Complexes Controls Telomere Recombination. *Cell Rep.* 15, 1242–1253. doi: 10.1016/j.celrep.2016.04.008

Clouaire, T., and Legube, G. (2019). A Snapshot on the Cis Chromatin Response to DNA Double-Strand Breaks. *Trends Genet.* 35, 330–345. doi: 10.1016/j.tig.2019.02.003

Cohen, S., Puget, N., Lin, Y. L., Clouaire, T., Aguirrebengoa, M., Rocher, V., et al. (2018). Senataxin resolves RNA:DNA hybrids forming at DNA double-strand breaks to prevent translocations. *Nat. Commun.* 9:533.

Delabaere, L., and Chiolo, I. (2016). ReiNF4rcing repair pathway choice during cell cycle. *Cell Cycle* 15, 1182–1183. doi: 10.1080/15384101.2016.1159108

Delabaere, L., Ertl, H. A., Massey, D. J., Hofley, C. M., Sohail, F., and Bienenstock, E. J. (2017). Aging impairs double-strand break repair by homologous recombination in Drosophila germ cells. *Aging Cell* 16, 320–328. doi: 10.1111/acel.12556

Dialynas, G., Delabaere, L., and Chiolo, I. (2019). Arp2/3 and Unc45 maintain heterochromatin stability in Drosophila polytene chromosomes. *Exp. Biol. Med.* 244, 1362–1371. doi: 10.1177/1535370219862282

Dimitrova, N., Chen, Y. C., Spector, D. L., and de Lange, T. (2008). 53BP1 promotes non-homologous end joining of telomeres by increasing chromatin mobility. *Nature* 456, 524–528. doi: 10.1038/nature07433

Dion, V., and Gasser, S. M. (2013). Chromatin movement in the maintenance of genome stability. *Cell* 152, 1355–1364. doi: 10.1016/j.cell.2013.02.010

Dion, V., Kalck, V., Horigome, C., Towbin, B. D., and Gasser, S. M. (2012). Increased mobility of double-strand breaks requires Mec1, Rad9 and the homologous recombination machinery. *Nat. Cell Biol.* 14, 502–509. doi: 10.1038/ncb2465

Dion, V., Kalck, V., Seeber, A., Schleker, T., and Gasser, S. M. (2013). Cohesin and the nucleolus constrain the mobility of spontaneous repair foci. *EMBO Rep.* 14, 984–991. doi: 10.1038/embor.2013.142

Eckert-Boulet, N., Rothstein, R., and Lisby, M. (2011). Cell biology of homologous recombination in yeast. *Methods Mol. Biol.* 745, 523–536. doi: 10.1007/978-1-61779-129-1_30

Falk, M., Lukasova, E., Gabrielova, B., Ondrej, V., and Kozubek, S. (2007). Chromatin dynamics during DSB repair. *Biochim. Biophys. Acta* 1773, 1534–1545. doi: 10.1016/j.bbamcr.2007.07.002

Frottin, F., Schueder, F., Tiwary, S., Gupta, R., Korner, R., Schlichthaerle, T., et al. (2019). The nucleolus functions as a phase-separated protein quality control compartment. *Science* 365, 342–347. doi: 10.1126/science.aaw9157

Gehen, L. R., Gasser, S. M., and Dion, V. (2011). How Broken DNA Finds Its Template for Repair: A Computational Approach. *Progre. Theor. Phys. Suppl.* 191, 20–28.

Gennes, P. G. D. (1982). Kinetics of diffusion-controlled processes in dense polymer systems. II. Effects of entanglements. *J. Chem. Phys.* 76, 3322–3326. doi: 10.1063/1.443329

Goodarzi, A. A., Noon, A. T., Deckbar, D., Ziv, Y., Shiloh, Y., Lobrich, M., et al. (2008). ATM signaling facilitates repair of DNA double-strand breaks associated with heterochromatin. *Mol. Cell* 31, 167–177. doi: 10.1016/j.molcel.2008.05.017

Guénolé, A., and Legube, G. (2017). *A Meeting at Risk: Unrepaired DSBs Go for Broke*. Milton Park: Taylor & Francis, 1–12.

Guerin, T., Levernier, N., Benichou, O., and Voituriez, R. (2016). Mean first-passage times of non-Markovian random walkers in confinement. *Nature* 534, 356–359. doi: 10.1038/nature18272

Hajjoul, H., Mathon, J., Ranchon, H., Goiffon, I., Mozziconacci, J., Albert, B., et al. (2013). High-throughput chromatin motion tracking in living yeast reveals the flexibility of the fiber throughout the genome. *Genome Res.* 23, 1829–1838. doi: 10.1101/gr.157008.113

Harding, S. M., Boiarsky, J. A., and Greenberg, R. A. (2015). ATM Dependent Silencing Links Nucleolar Chromatin Reorganization to DNA Damage Recognition. *Cell Rep.* 13, 251–259. doi: 10.1016/j.celrep.2015.08.085

Hauer, M. H., and Gasser, S. M. (2017). Chromatin and nucleosome dynamics in DNA damage and repair. *Genes Dev.* 31, 2204–2221. doi: 10.1101/gad.307702.117

Hauer, M. H., Seeber, A., Singh, V., Thierry, R., Sack, R., Amitai, A., et al. (2017). Histone degradation in response to DNA damage enhances chromatin dynamics and recombination rates. *Nat. Struct. Mol. Biol.* 24, 99–107. doi: 10.1038/nsmb.3347

Henson, J. D., Cao, Y., Huschtscha, L. I., Chang, A. C., Au, A. Y., Pickett, H. A., et al. (2009). DNA C-circles are specific and quantifiable markers of alternative-lengthening-of-telomeres activity. *Nat. Biotechnol.* 27, 1181–1185. doi: 10.1038/nbt.1587

Herbert, S., Brion, A., Arbona, J. M., Lelek, M., Veillet, A., Lelandais, B., et al. (2017). Chromatin stiffening underlies enhanced locus mobility after DNA damage in budding yeast. *EMBO J.* 36, 2595–2608. doi: 10.15252/embj.201695842

Heun, P., Laroche, T., Shimada, K., Furrer, P., and Gasser, S. M. (2001). Chromosome dynamics in the yeast interphase nucleus. *Science* 294, 2181–2186. doi: 10.1126/science.1065366

Horigome, C., Bustard, D. E., Marcomini, I., Delgoshaie, N., Tsai-Pflugfelder, M., Cobb, J. A., et al. (2016). PolySUMOylation by Siz2 and Mms21 triggers relocation of DNA breaks to nuclear pores through the Slx5/Slx8 STUbL. *Genes Dev.* 30, 931–945. doi: 10.1101/gad.277665.116

Horigome, C., Oma, Y., Konishi, T., Schmid, R., Marcomini, I., Hauer, M. H., et al. (2014). SWR1 and INO80 Chromatin Remodelers Contribute to DNA Double-Strand Break Perinuclear Anchorage Site Choice. *Mol. Cell* 55, 626–639. doi: 10.1016/j.molcel.2014.06.027

Horigome, C., Unozawa, E., Ooki, T., and Kobayashi, T. (2019). Ribosomal RNA gene repeats associate with the nuclear pore complex for maintenance after DNA damage. *PLoS Genet.* 15:e1008103. doi: 10.1371/journal.pgen.1008103

Hyman, A. A., Weber, C. A., and Julicher, F. (2014). Liquid-liquid phase separation in biology. *Annu. Rev. Cell Dev. Biol.* 30, 39–58.

Iacovoni, J. S., Caron, P., Lassadi, I., Nicolas, E., Massip, L., Trouche, D., et al. (2010). High-resolution profiling of gammaH2AX around DNA double strand breaks in the mammalian genome. *EMBO J.* 29, 1446–1457. doi: 10.1038/emboj.2010.38

Jakob, B., Splinter, J., Conrad, S., Voss, K. O., Zink, D., Durante, M., et al. (2011). DNA double-strand breaks in heterochromatin elicit fast repair protein recruitment, histone H2AX phosphorylation and relocation to euchromatin. *Nucleic Acids Res.* 39, 6489–6499. doi: 10.1093/nar/gkr230

Jakob, B., Splinter, J., Durante, M., and Taucher-Scholz, G. (2009). Live cell microscopy analysis of radiation-induced DNA double-strand break motion. *Proc. Natl. Acad. Sci. U.S.A.* 106, 3172–3177. doi: 10.1073/pnas.0810987106

Janssen, A., Breuer, G. A., Brinkman, E. K., van der Meulen, A. I., Borden, S. V., van Steensel, B., et al. (2016). A single double-strand break system reveals repair dynamics and mechanisms in heterochromatin and euchromatin. *Genes Dev.* 30, 1645–1657. doi: 10.1101/gad.283028.116

Janssen, A., Colmenares, S. U., Lee, T., and Karpen, G. H. (2019). Timely double-strand break repair and pathway choice in pericentromeric heterochromatin depend on the histone demethylase dKDM4A. *Genes Dev.* 33, 103–115. doi: 10.1101/gad.317537.118

Kalocsay, M., Hiller, N. J., and Jentsch, S. (2009). Chromosome-wide Rad51 spreading and SUMO-H2A.Z-dependent chromosome fixation in response to a persistent DNA double-strand break. *Mol. Cell* 33, 335–343. doi: 10.1016/j.molcel.2009.01.016

Khadaroo, B., Teixeira, M. T., Luciano, P., Eckert-Boulet, N., Germann, S. M., Simon, M. N., et al. (2009). The DNA damage response at eroded telomeres and tethering to the nuclear pore complex. *Nat. Cell Biol.* 11, 980–987. doi: 10.1038/ncb1910

Kilic, S., Lezaja, A., Gatti, M., Bianco, E., Michelena, J., Imhof, R., et al. (2019). Phase separation of 53BP1 determines liquid-like behavior of DNA repair compartments. *EMBO J.* 38:e101379.

Kong, X., Cruz, G. M. S., Silva, B. A., Wakida, N. M., Khatibzadeh, N., Berns, M. W., et al. (2018). Laser Microirradiation to Study In Vivo Cellular Responses to Simple and Complex DNA Damage. *J. Vis. Exp.* 131:56213.

Korsholm, L. M., Gal, Z., Lin, L., Quevedo, O., Ahmad, D. A., Dulina, E., et al. (2019). Double-strand breaks in ribosomal RNA genes activate a distinct signaling and chromatin response to facilitate nucleolar restructuring and repair. *Nucleic Acids Res.* 47, 8019–8035. doi: 10.1093/nar/gkz518

Krawczyk, P. M., Borovski, T., Stap, J., Cijsouw, T., ten Cate, R., Medema, J. P., et al. (2012). Chromatin mobility is increased at sites of DNA double-strand breaks. *J. Cell Sci.* 125(Pt 9), 2127–2133. doi: 10.1242/jcs.089847

Kruhlak, M. J., Celeste, A., Dellaire, G., Fernandez-Capetillo, O., Müller, W. G., McNally, J. G., et al. (2006). Changes in chromatin structure and mobility in living cells at sites of DNA double-strand breaks. *J. Cell Biol.* 172, 823–834. doi: 10.1083/jcb.200510015

Kulashreshtha, M., Mehta, I. S., Kumar, P., and Rao, B. J. (2016). Chromosome territory relocation during DNA repair requires nuclear myosin 1 recruitment to chromatin mediated by Upsilon-H2AX signaling. *Nucleic Acids Res.* 44, 8272–8291. doi: 10.1093/nar/gkw573

Lamm, N., Masamsetti, V. P., Read, M. N., Biro, M., and Cesare, A. J. (2018). ATR and mTOR regulate F-actin to alter nuclear architecture and repair replication stress. *bioRxiv [Preprint]* doi: 10.1101/451708v3.full

Larson, A. G., Elnatan, D., Keenen, M. M., Trnka, M. J., Johnston, J. B., Burlingame, A. L., et al. (2017). Liquid droplet formation by HP1alpha suggests a role for phase separation in heterochromatin. *Nature* 547, 236–240. doi: 10.1038/nature22822

Lawrimore, J., Barry, T. M., Barry, R. M., York, A. C., Friedman, B., Cook, D. M., et al. (2017). Microtubule dynamics drive enhanced chromatin motion and mobilize telomeres in response to DNA damage. *Mol. Biol. Cell* 28, 1701–1711. doi: 10.1091/mbc.e16-12-0846

Lee, C. S., Wang, R. W., Chang, H. H., Capurso, D., Segal, M. R., and Haber, J. E. (2016). Chromosome position determines the success

of double-strand break repair. *Proc. Natl. Acad. Sci. U.S.A.* 113, E146–E154.

Lemaitre, C., Grabarz, A., Tsouroula, K., Andronov, L., Furst, A., Pankotai, T., et al. (2014). Nuclear position dictates DNA repair pathway choice. *Genes Dev.* 28, 2450–2463. doi: 10.1101/gad.248369.114

Lenzken, S. C., Levone, B. R., Filosa, G., Antonaci, M., Conte, F., Kizilirmak, C., et al. (2019). FUS-dependent phase separation initiates double-strand break repair. *bioRxiv [Preprint]* doi: 10.1101/798884v1?rss=1

Levi, V., Ruan, Q., and Gratton, E. (2005). 3-D particle tracking in a two-photon microscope: application to the study of molecular dynamics in cells. *Biophys. J.* 88, 2919–2928. doi: 10.1529/biophysj.104.044230

Li, Q., Tjong, H., Li, X., Gong, K., Zhou, X. J., Chiolo, I., et al. (2017). The three-dimensional genome organization of Drosophila melanogaster through data integration. *Genome Biol.* 18:145.

Lisby, M., Barlow, J. H., Burgess, R. C., and Rothstein, R. (2004). Choreography of the DNA damage response: spatiotemporal relationships among checkpoint and repair proteins. *Cell* 118, 699–713.

Lisby, M., Mortensen, U. H., and Rothstein, R. (2003). Colocalization of multiple DNA double-strand breaks at a single Rad52 repair centre. *Nat. Cell Biol.* 5, 572–577. doi: 10.1038/ncb997

Lottersberger, F., Karssemeijer, R. A., Dimitrova, N., and de Lange, T. (2015). 53BP1 and the LINC Complex Promote Microtubule-Dependent DSB Mobility and DNA Repair. *Cell* 163, 880–893. doi: 10.1016/j.cell.2015.09.057

Lucas, J. S., Zhang, Y., Dudko, O. K., and Murre, C. (2014). 3D trajectories adopted by coding and regulatory DNA elements: first-passage times for genomic interactions. *Cell* 158, 339–352. doi: 10.1016/j.cell.2014.05.036

Luijsterburg, M. S., Lindh, M., Acs, K., Vrouwe, M. G., Pines, A., van Attikum, H., et al. (2012). DDB2 promotes chromatin decondensation at UV-induced DNA damage. *J. Cell Biol.* 197, 267–281. doi: 10.1083/jcb.201106074

Lukas, C., Bartek, J., and Lukas, J. (2005). Imaging of protein movement induced by chromosomal breakage: tiny 'local' lesions pose great 'global' challenges. *Chromosoma* 114, 146–154. doi: 10.1007/s00412-005-0011-y

Maeshima, K., Hihara, S., and Eltsov, M. (2010). Chromatin structure: does the 30-nm fibre exist in vivo? *Curr. Opin. Cell Biol.* 22, 291–297. doi: 10.1016/j.ceb.2010.03.001

Marcomini, I., Shimada, K., Delgoshaie, N., Yamamoto, I., Seeber, A., Cheblal, A., et al. (2018). Asymmetric Processing of DNA Ends at a Double-Strand Break Leads to Unconstrained Dynamics and Ectopic Translocation. *Cell Rep.* 24, 2614–2628e4.

Marnef, A., Finoux, A. L., Arnould, C., Guillou, E., Daburon, V., Rocher, V., et al. (2019). A cohesin/HUSH- and LINC-dependent pathway controls ribosomal DNA double-strand break repair. *Genes Dev.* 33, 1175–1190. doi: 10.1101/gad.324012.119

Marshall, W. F., Straight, A., Marko, J. F., Swedlow, J., Dernburg, A., Belmont, A., et al. (1997). Interphase chromosomes undergo constrained diffusional motion in living cells. *Curr. Biol.* 7, 930–939. doi: 10.1016/s0960-9822(06)00412-x

Masedunskas, A., Chen, Y., Stussman, R., Weigert, R., and Mather, I. H. (2017). Kinetics of milk lipid droplet transport, growth, and secretion revealed by intravital imaging: lipid droplet release is intermittently stimulated by oxytocin. *Mol. Biol. Cell* 28, 935–946. doi: 10.1091/mbc.e16-11-0776

Masui, O., Bonnet, I., Baccon, P. Le, Brito, I., Pollex, T., Murphy, N., et al. (2011). Live-cell chromosome dynamics and outcome of X chromosome pairing events during ES cell differentiation. *Cell* 145, 447–458. doi: 10.1016/j.cell.2011.03.032

Mehta, I. S., Amira, M., Harvey, A. J., and Bridger, J. M. (2010). Rapid chromosome territory relocation by nuclear motor activity in response to serum removal in primary human fibroblasts. *Genome Biol.* 11:R5.

Metzler, R., Jeon, J. H., Cherstvy, A. G., and Barkai, E. (2014). Anomalous diffusion models and their properties: non-stationarity, non-ergodicity, and ageing at the centenary of single particle tracking. *Phys. Chem. Chem. Phys.* 16, 24128–24164. doi: 10.1039/c4cp03465a

Michalet, X. (2010). Mean square displacement analysis of single-particle trajectories with localization error: brownian motion in an isotropic medium. *Phys. Rev. E Stat. Nonlin Soft. Matter. Phys.* 82(4 Pt 1):041914.

Michalet, X., and Berglund, A. J. (2012). Optimal diffusion coefficient estimation in single-particle tracking. *Phys. Rev. E Stat. Nonlin. Soft. Matter. Phys.* 85(6 Pt 1):061916.

Min, J., Wright, W. E., and Shay, J. W. (2019). Clustered telomeres in phase-separated nuclear condensates engage mitotic DNA synthesis through BLM and RAD52. *Genes Dev.* 33, 814–827. doi: 10.1101/gad.324905.119

Mine, J., Disseau, L., Takahashi, M., Cappello, G., Dutreix, M., and Viovy, J. L. (2007). Real-time measurements of the nucleation, growth and dissociation of single Rad51-DNA nucleoprotein filaments. *Nucleic Acids Res.* 35, 7171–7187. doi: 10.1093/nar/gkm752

Mine-Hattab, J., and Darzacq, X. (2018). Dynamique de la chromatine en réponse aux dommages de l'ADN. *Med. Sci.* 34, 778–781. doi: 10.1051/medsci/2018214

Miné-Hattab, J., Recamier, V., Izeddin, I., Rothstein, R., and Darzacq, X. (2017). Multi-scale tracking reveals scale-dependent chromatin dynamics after DNA damage. *Mol. Biol. Cell* 28, 3323–3332. doi: 10.1091/mbc.e17-05-0317

Miné-Hattab, J., and Rothstein, R. (2012). Increased chromosome mobility facilitates homology search during recombination. *Nat. Cell Biol.* 14, 510–517. doi: 10.1038/ncb2472

Mine-Hattab, J., and Rothstein, R. (2013). DNA in motion during double-strand break repair. *Trends Cell Biol.* 23, 529–536.

Mine-Hattab, J., and Taddei, A. (2019). Physical principles and functional consequences of nuclear compartmentalization in budding yeast. *Curr. Opin. Cell Biol.* 58, 105–113. doi: 10.1016/j.ceb.2019.02.005

Nagai, S., Dubrana, K., Tsai-Pflugfelder, M., Davidson, M. B., Roberts, T. M., Brown, G. W., et al. (2008). Functional targeting of DNA damage to a nuclear pore-associated SUMO-dependent ubiquitin ligase. *Science* 322, 597–602. doi: 10.1126/science.1162790

Nelms, B. E., Maser, R. S., MacKay, J. F., Lagally, M. G., and Petrini, J. H. (1998). In situ visualization of DNA double-strand break repair in human fibroblasts. *Science* 280, 590–592. doi: 10.1126/science.280.5363.590

Neumaier, T., Swenson, J., Pham, C., Polyzos, A., Lo, A. T., Yang, P., et al. (2012). Evidence for formation of DNA repair centers and dose-response nonlinearity in human cells. *Proc. Natl. Acad. Sci. U.S.A.* 109, 443–448. doi: 10.1073/pnas.1117849108

Neumann, F. R., Dion, V., Gehlen, L. R., Tsai-Pflugfelder, M., Schmid, R., Taddei, A., et al. (2012). Targeted INO80 enhances subnuclear chromatin movement and ectopic homologous recombination. *Genes Dev.* 26, 369–383. doi: 10.1101/gad.176156.111

Oshidari, R., Huang, R., Medghalchi, M., Tse, E. Y. W., Ashgriz, N., Lee, H. O., et al. (2019a). DNA repair by Rad52 liquid droplets. *bioRxiv [Preprint]* doi: 10.1101/768119v1

Oshidari, R., Mekhail, K., and Seeber, A. (2019b). Mobility and Repair of Damaged DNA: random or Directed?. *Trends Cell Biol.* 30, 144–156. doi: 10.1016/j.tcb.2019.11.003

Oshidari, R., Strecker, J., Chung, D. K. C., Abraham, K. J., Chan, J. N. Y., Damaren, C. J., et al. (2018). Nuclear microtubule filaments mediate non-linear directional motion of chromatin and promote DNA repair. *Nat. Commun.* 9:2567.

Oswald, F., Baa, L. M., Bollen, E. Y. J., and Peterman, E. J. (2014). Imaging and quantification of trans-membrane protein diffusion in living bacteria. *Phys. Chem. Chem. Phys.* 16, 12625–12634. doi: 10.1039/c4cp00299g

Oza, P., Jaspersen, S. L., Miele, A., Dekker, J., and Peterson, C. L. (2009). Mechanisms that regulate localization of a DNA double-strand break to the nuclear periphery. *Genes Dev.* 23, 912–927. doi: 10.1101/gad.1782209

Pessina, F., Giavazzi, F., Yin, Y., Gioia, U., Vitelli, V., Galbiati, A., et al. (2019). Functional transcription promoters at DNA double-strand breaks mediate RNA-driven phase separation of damage-response factors. *Nat. Cell Biol.* 21, 1286–1299. doi: 10.1038/s41556-019-0392-4

Rawal, C. C., Caridi, C. P., and Chiolo, I. (2019). Actin' between phase separated domains for heterochromatin repair. *DNA Repair* 81:102646. doi: 10.1016/j.dnarep.2019.102646

Reynolds, P., Botchway, S. W., Parker, A. W., and O'Neill, P. (2013). Spatiotemporal dynamics of DNA repair proteins following laser microbeam induced DNA damage - when is a DSB not a DSB? *Mutat. Res.* 756, 14–20. doi: 10.1016/j.mrgentox.2013.05.006

Richardson, C. D., Kazane, K. R., Feng, S. J., Zelin, E., Bray, N. L., and Schafer, A. J. (2018). CRISPR-Cas9 genome editing in human cells occurs via the *Fanconi anemia* pathway. *Nat. Genet.* 50, 1132–1139. doi: 10.1038/s41588-018-0174-0

Richardson, C. D., Ray, G. J., DeWitt, M. A., Curie, G. L., and Corn, J. E. (2016). Enhancing homology-directed genome editing by catalytically active

and inactive CRISPR-Cas9 using asymmetric donor DNA. *Nat. Biotechnol.* 34, 339–344. doi: 10.1038/nbt.3481

Robinett, C. C., Straight, A., Li, G., Willhelm, C., Sudlow, G., Murray, A., et al. (1996). In vivo localization of DNA sequences and visualization of large-scale chromatin organization using lac operator/repressor recognition. *J. Cell Biol.* 135(6 Pt 2), 1685–1700. doi: 10.1083/jcb.135.6.1685

Rogakou, E. P., Boon, C., Redon, C., and Bonner, W. M. (1999). Megabase chromatin domains involved in DNA double-strand breaks in vivo. *J. Cell Biol.* 146, 905–916. doi: 10.1083/jcb.146.5.905

Roukos, V., Voss, T. C., Schmidt, C. K., Lee, S., Wangsa, D., and Misteli, T. (2013). Spatial dynamics of chromosome translocations in living cells. *Science* 341, 660–664. doi: 10.1126/science.1237150

Ryu, T., Bonner, M. R., and Chiolo, I. (2016). Cervantes and Quijote protect heterochromatin from aberrant recombination and lead the way to the nuclear periphery. *Nucleus* 7, 485–497. doi: 10.1080/19491034.2016.1239683

Ryu, T., Spatola, B., Delabaere, L., Bowlin, K., Hopp, H., Kunitake, R., et al. (2015). Heterochromatic breaks move to the nuclear periphery to continue recombinational repair. *Nat. Cell Biol.* 17, 1401–1411. doi: 10.1038/ncb3258

Saad, H., Gallardo, F., Dalvai, M., Tanguy-le-Gac, N., Lane, D., and Bystricky, K. (2014). DNA dynamics during early double-strand break processing revealed by non-intrusive imaging of living cells. *PLoS Genet.* 10:e1004187. doi: 10.1371/journal.pgen.1004187

Schrank, B., and Gautier, J. (2019). Assembling nuclear domains: lessons from DNA repair. *J. Cell Biol.* 218, 2444–2455. doi: 10.1083/jcb.201904202

Schrank, B. R., Aparicio, T., Li, Y., Chang, W., Chait, B. T., Gundersen, G. G., et al. (2018). Nuclear ARP2/3 drives DNA break clustering for homology-directed repair. *Nature* 559, 61–66. doi: 10.1038/s41586-018-0237-5

See, C., Arya, D., Lin, E., and Chiolo, I. (2020). Live cell imaging of nuclear actin filaments and repair foci in Drosophila and mouse cells. *Methods Mol. Biol.* 7:e27900v1.

Seeber, A., Dion, V., and Gasser, S. M. (2013). Checkpoint kinases and the INO80 nucleosome remodeling complex enhance global chromatin mobility in response to DNA damage. *Genes Dev.* 27, 1999–2008. doi: 10.1101/gad.222992.113

Singatulina, A. S., Hamon, L., Sukhanova, M. V., Desforges, B., Joshi, V., Bouhss, A., et al. (2019). PARP-1 Activation Directs FUS to DNA Damage Sites to Form PARG-Reversible Compartments Enriched in Damaged DNA. *Cell Rep.* 27, 1809-1821.e5.

Singleton, B. K., Griffin, C. S., and Thacker, J. (2002). Clustered DNA damage leads to complex genetic changes in irradiated human cells. *Cancer Res.* 62, 6263–6269.

Smith, M. J., Bryant, E. E., Joseph, F. J., and Rothstein, R. (2019). DNA damage triggers increased mobility of chromosomes in G1-phase cells. *Mol. Biol. Cell* 30, 2620–2625. doi: 10.1091/mbc.e19-08-0469

Smith, M. J., Bryant, E. E., and Rothstein, R. (2018). Increased chromosomal mobility after DNA damage is controlled by interactions between the recombination machinery and the checkpoint. *Genes Dev.* 32, 1242–1251. doi: 10.1101/gad.317966.118

Soutoglou, E., Dorn, J. F., Sengupta, K., Jasin, M., Nussenzweig, A., Ried, T., et al. (2007). Positional stability of single double-strand breaks in mammalian cells. *Nat. Cell Biol.* 9, 675–682. doi: 10.1038/ncb1591

Spichal, M., Brion, A., Herbert, S., Cournac, A., Marbouty, M., Zimmer, C., et al. (2016). Evidence for a dual role of actin in regulating chromosome organization and dynamics in yeast. *J. Cell Sci.* 129, 681–692. doi: 10.1242/jcs.175745

Spichal, M., and Fabre, E. (2017). The emerging role of the cytoskeleton in chromosome dynamics. *Front. Genet.* 8:60. doi: 10.3389/fgene.2017.00060

Strecker, J., Gupta, G. D., Zhang, W., Bashkurov, M., Landry, M. C., Pelletier, L., et al. (2016). DNA damage signalling targets the kinetochore to promote chromatin mobility. *Nat. Cell Biol.* 18, 281–290. doi: 10.1038/ncb3308

Strom, A. R., Emelyanov, A. V., Mir, M., Fyodorov, D. V., Darzacq, X., and Karpen, G. H. (2017). Phase separation drives heterochromatin domain formation. *Nature* 547, 241–245. doi: 10.1038/nature22989

Su, X. A., Dion, V., Gasser, S. M., and Freudenreich, C. H. (2015). Regulation of recombination at yeast nuclear pores controls repair and triplet repeat stability. *Genes Dev.* 29, 1006–1017. doi: 10.1101/gad.256404.114

Swartz, R. K., Rodriguez, E. C., and King, M. C. (2014). A role for nuclear envelope-bridging complexes in homology-directed repair. *Mol. Biol. Cell* 25, 2461–2471. doi: 10.1091/mbc.e13-10-0569

Therizols, P., Duong, T., Dujon, B., Zimmer, C., and Fabre, E. (2010). Chromosome arm length and nuclear constraints determine the dynamic relationship of yeast subtelomeres. *Proc. Natl. Acad. Sci. U.S.A.* 107, 2025–2030. doi: 10.1073/pnas.0914187107

Therizols, P., Fairhead, C., Cabal, G. G., Genovesio, A., Olivo-Marin, J. C., Dujon, B., et al. (2006). Telomere tethering at the nuclear periphery is essential for efficient DNA double strand break repair in subtelomeric region. *J. Cell Biol.* 172, 189–199. doi: 10.1083/jcb.200505159

Torres-Rosell, J., Machin, F., Farmer, S., Jarmuz, A., Eydmann, T., Dalgaard, J. Z., et al. (2005). SMC5 and SMC6 genes are required for the segregation of repetitive chromosome regions. *Nat. Cell Biol.* 7, 412–419. doi: 10.1038/ncb1239

Torres-Rosell, J., Sunjevaric, I., Piccoli, G. De, Sacher, M., Eckert-Boulet, N., Reid, R., et al. (2007). The Smc5-Smc6 complex and SUMO modification of Rad52 regulates recombinational repair at the ribosomal gene locus. *Nat. Cell Biol.* 923–931. doi: 10.1038/ncb1619

Tsouroula, K., Furst, A., Rogier, M., Heyer, V., Maglott-Roth, A., Ferrand, A., et al. (2016). Temporal and Spatial Uncoupling of DNA Double Strand Break Repair Pathways within Mammalian Heterochromatin. *Mol. Cell* 63, 293–305. doi: 10.1016/j.molcel.2016.06.002

van Sluis, M., and McStay, B. (2015). A localized nucleolar DNA damage response facilitates recruitment of the homology-directed repair machinery independent of cell cycle stage. *Genes Dev.* 29, 1151–1163. doi: 10.1101/gad.260703.115

Verdaasdonk, J. S., Vasquez, P. A., Barry, R. M., Barry, T., Goodwin, S., Forest, M. G., et al. (2013). Centromere tethering confines chromosome domains. *Mol. Cell* 52, 819–831. doi: 10.1016/j.molcel.2013.10.021

Waterman, D. P., Zhou, F., Li, K., Lee, C. S., Tsabar, M., Eapen, V. V., et al. (2019). Live cell monitoring of double strand breaks in *S. cerevisiae*. *PLoS Genet.* 15:e1008001. doi: 10.1371/journal.pgen.1008001

Weber, S. C., Spakowitz, A. J., and Theriot, J. A. (2010). Bacterial chromosomal loci move subdiffusively through a viscoelastic cytoplasm. *Phys. Rev. Lett.* 104:238102.

Whalen, J. M., Dhingra, N., Wei, L., Zhao, X., and Freudenreich, C. (2020). Relocation of Collapsed Forks to the Nuclear Pore Complex Depends on Sumoylation of DNA Repair Proteins and Permits Rad51 Association. *Cell Rep.* 31:107635. doi: 10.2139/ssrn.3523272

Wong, H., Marie-Nelly, H., Herbert, S., Carrivain, P., Blanc, H., Koszul, R., et al. (2012). A predictive computational model of the dynamic 3D interphase yeast nucleus. *Curr. Biol.* 22, 1881–1890. doi: 10.1016/j.cub.2012.07.069

Zada, D., Bronshtein, I., Lerer-Goldshtein, T., Garini, Y., and Appelbaum, L. (2019). Sleep increases chromosome dynamics to enable reduction of accumulating DNA damage in single neurons. *Nat. Commun.* 10:895.

Zhang, T., Zhang, Z., Shengzhao, G., Li, X., Liu, H., and Zhao, Y. (2019). Strand break-induced replication fork collapse leads to C-circles, C-overhangs and telomeric recombination. *PLoS Genet.* 15:e1007925. doi: 10.1371/journal.pgen.1007925

Zimmer, C. (2018). "Chromatin mobility upon DNA damage: state of the art and remaining questions," in *Current Genetics*, Ed. M. Kupiec (Berlin: Springer), 0–0.

Ziv, Y., Bielopolski, D., Galanty, Y., Lukas, C., Taya, Y., Schultz, D. C., et al. (2006). Chromatin relaxation in response to DNA double-strand breaks is modulated by a novel ATM- and KAP-1 dependent pathway. *Nat. Cell Biol.* 8, 870–876. doi: 10.1038/ncb1446

Conflict of Interest: The authors declare that the research was conducted in the absence of any commercial or financial relationships that could be construed as a potential conflict of interest.

Advantages of publishing in Frontiers

OPEN ACCESS
Articles are free to read for greatest visibility and readership

FAST PUBLICATION
Around 90 days from submission to decision

HIGH QUALITY PEER-REVIEW
Rigorous, collaborative, and constructive peer-review

TRANSPARENT PEER-REVIEW
Editors and reviewers acknowledged by name on published articles

Frontiers
Avenue du Tribunal-Fédéral 34
1005 Lausanne | Switzerland

Visit us: www.frontiersin.org
Contact us: frontiersin.org/about/contact

REPRODUCIBILITY OF RESEARCH
Support open data and methods to enhance research reproducibility

DIGITAL PUBLISHING
Articles designed for optimal readership across devices

FOLLOW US
@frontiersin

IMPACT METRICS
Advanced article metrics track visibility across digital media

EXTENSIVE PROMOTION
Marketing and promotion of impactful research

LOOP RESEARCH NETWORK
Our network increases your article's readership